OSCCAR:
FUTURE OCCUPANT SAFETY FOR CRASHES IN CARS

Validation and Demonstration of Advanced Passenger Protection Principles

Document Type	Deliverable
Document Number	D2.5
Primary Author(s)	Sabine Compigne | TME Matthias Schiessler | BASt Michael Hamacher | FKA Richard Lancashire | Siemens Simon Dussinger | ESI Julian Becker | RWTH / IKA Genís Mensa | IDIADA
Document Version / Status	5.1 | Final
Distribution Level	CO (confidential – consortium only)

Project Acronym	OSCCAR
Project Title	FUTURE OCCUPANT SAFETY FOR CRASHES IN CARS
Project Website	www.osccarproject.eu
Project Coordinator	Werner Leitgeb | VIF | werner.leitgeb@v2c2.at
Grant Agreement Number	768947
Date of latest version of Annex I against which the assessment will be made	2021-05-02
Upload by coordinator:	First submitted: 2021-12-03 Re-submitted: 2022-04-11

OSCCAR has received funding from the European Union's Horizon 2020 research and innovation programme under grant agreement No 768947.

CONTRIBUTORS

Name	Organization	Name	Organization
Martin Östling	Autoliv	Genís Mensa	IDIADA
Krystoffer Mroz	Autoliv	Richard Lancashire	Siemens
Matthias Schiessler	BASt	Paul van Hooijdonk	Siemens
Andre Eggers	BASt	Shigeki Hayashi	TMC
Julian Ott	BASt	Mie Tokuyama	TMC
Simon Dussinger	ESI	Hiroshi Miyazaki	TMC
Gian Antonio D'Addetta	Bosch	Sabine Compigne	TME
Maja Wolkenstein	Bosch	Lotta Jakobsson	Volvo Cars
Michael Hamacher	FKA	Michael Sprenger	ZF
Julian Becker	RWTH / IKA	Swen Schaub	ZF

FORMAL REVIEWERS

Name	Organization	Date
Lotta Jakobsson	Volvo Cars	2021-06-25
Christoph Klein	VIF	2021-06-25

DOCUMENT HISTORY

Revision	Date	Author / Organization	Description
1	2021-06-18	Compigne / TME	First overall draft
2	2021-06-24	Compigne / TME Hamacher / FKA	Draft for internal review
3	2021-07-15	Compigne / TME	Reviewers' comments overall document
4	2021-07-19	Schiessler / BASt	Reviewers' comments Chapter 3.1
5	2021-08-31	Schiessler / BASt Compigne / TME Hamacher / FKA	Final version
5.1	2022-03-25	Hamacher / FKA	Updates after EU Review

TABLE OF CONTENTS

LIST OF FIGURES

LIST OF TABLES

ABBREVIATIONS AND DEFINITIONS

Term	Definition
AD	Automated Driving
AEB	Autonomous Emergency Braking
ASIS	Anterior Superior Iliac Spine
AHM	Active Human Model
ATD	Anthropomorphic Testing Device
BMI	Body Mass Index
CAD	Computer Aided Design
CLT	Crash Locking Tongue
COG	Centre of Gravity
CORA	Correlation and Analysis Method
Euro NCAP	European New Car assessment Programme
FEM	Finite Element Model
HBM	Human Body Model
LTAP	Left Turn Across Path
LTAP-OD	Left Turn Across Path - Opposite Direction
MBS	Multi-Body System
PP	Protection Principle
SCP	Straight Crossing Path
SOTA DLPT belt	State of the Art belt with Double Lap belt Pre-Tensioning
THOR	Test Device for Human Occupant Restraint
THUMS	Total Human Model for Safety
TMC	Toyota Motor Corporation
VPS	Virtual Performance Solution
WP	Work Package
WorldSID	Worldwide Harmonized Side Impact Dummy

Although this deliverable is of official confidentiality level CO, the OSCCAR General Assembly unanimously decided to make its contents publicly available. You can find it in its complete form on the OSCCAR webpage (https://www.osccarproject.eu/media/deliverables/) for your reference.

1 EXECUTIVE SUMMARY

This report presents the results of Task 2.4 on demonstration and validation of a homologation demonstrator test case as well as two advanced passenger protection principles (PPs). Several hardware test series were conducted in order to validate the homologation demonstrator simulation model used within OSCCAR Work Package 4 (WP4) and to demonstrate the functionality of PP2 and PP6, two exemplary protection principles from the six studied in Task 2.3 [7].

For the validation part, a homologation demonstrator was built and used in two test series, in addition to a simulation series using a virtual counterpart. The homologation demonstrator focuses on a reclined seating position and the challenges for the restraint system and the test devices associated with such a configuration. Two restraint systems were included; a state of the art 3-point belt (SOTA belt) and the SOTA belt equipped with a double lap belt pretensioning (SOTA DLPT belt) in order to avoid occupant submarining in such seating configurations, one of the issues investigated in PP3. With the purpose to provide input for Task 4.3 “Demonstration”, the test results were used to validate the numerical models of the homologation demonstrator, which were developed under three simulation codes (LS-Dyna, VPS and Madymo).

The first test series included seven test configurations in which the two restraint system configurations (SOTA belt / SOTA DLPT belt), two seatback angles (23° upright and 48° reclined seating position) and three crash test pulses were varied. In all test configurations submarining was avoided. Overall validation of the numerical models was good. However, missing bending stiffness of the belt and differences in pelvis modelling resulted in suboptimal pelvis-to-belt interaction and prediction of submarining by the FE-simulations in the reclined seating position without double lap belt pre-tensioning, although no submarining occurred in the tests. A second test series was performed repeating some of the upright and reclined configurations from the first series, but only for one of the crash pulses. This second test series confirmed the findings of the first test series. It also contributed with improved quantification of the test scatter by repeating the test of one configuration four times. The purpose of these tests was to define realistic validation tolerances. The results were provided to WP5 with regard to the environment validation procedure for Virtual Testing. The validation of the numerical models in relation to the second test series showed good results as well.

The functionality of PP2 was demonstrated by a physical demonstrator on a test sled for different types of occupants (Hybrid III ATDs from a 5th percentile female to an obese occupant) and footrest configurations. The seat was not actively rotated (as for PP1) but the rotation was initiated solely by an emergency braking prior to the crash with a simultaneous release of the seat, considering an optimised rotation axis. For all dummy sizes, a complete seat rotation from an initial seat angle of 30° inwards could be achieved within a total time of around 500 ms for a maximum brake deceleration of only 0.5 g. Besides the physical tests, corresponding simulations for the 50th percentile male occupant HIII dummy model as well as the Active Human Model (AHM) were conducted within the framework of a virtual demonstrator. Overall, the simulations showed comparable results to the physical demonstrator in terms of rotation duration, maximum rotation velocity and occupant upper body kinematics. All simulated rotation axis positions successfully rotated the 50th percentile occupant to the forward facing seating position. Despite various limitations of the hardware dummy as well as the dummy and seat simulation models with respect to the investigated load case, the physical and the virtual demonstrators showed the overall functionality of PP2 for a large variety of rotation axis positions and demonstrated that a fast seat rotation, caused only by brake deceleration, is possible.

Another physical demonstrator was used to study the performance of PP6. Different restraint system configurations as well as seat side supports were evaluated with a WorldSID ATD in a far-side load case (opposite side to the one that is struck in a side crash), representing a future crash scenario for vehicles with flexible interiors without the presence of a centre console. PP6 used a SOTA DLPT belt with variations adding either an in-board seat belt routing, seat side supports or a combination of both. Ten sled tests with a WorldSID ATD were performed using a generic simplified vehicle environment and adjusting it to integrate the seat-mounted anchorage points of the SOTA DLPT belt as well as the seat side supports. The combination of the SOTA DLPT belt and of the seat side supports gave the best compromise to control the occupant kinematics while mitigating the injury assessment values.

The numerical models of the SOTA DLPT belt and the other components of the PP6 environment were developed under LS-Dyna and Madymo. Simulation results were compared with test data, looking at dummy kinematics, kinetics and injury assessment values. In LS-Dyna, considering that the SOTA DLPT belt model was initially not validated for the far-side load case, good agreement between simulation results and test measurements was reached. The head excursion values of the model agreed well those of the tests despite some variations in the lap belt forces between the model and the tests. The dummy measurements matched the test data well. The Madymo model achieved a good match between the simulation and the test results. The modelling of the WorldSID Finite Element Model interaction with the shoulder belt needed special attention whereas for the multibody model AHM, a different kinematic load to the occupant could be observed for the configurations with the seat side supports due to the dummy model structure.

Keywords: occupant restraint, protection principles, reclined seating position, occupant repositioning, far-side load case, hardware demonstrator, virtual demonstrator, model validation

2 BACKGROUND AND OBJECTIVES

2.1 Background

This deliverable reports the Task 2.4 activities. The objective was on demonstration and validation. A physical homologation demonstrator, mainly as input for WP4 and WP5, was built up accompanied by the validation of corresponding simulation models for LS-Dyna, VPS and Madymo. Furthermore, in order to demonstrate the feasibility of selected protection principles (PPs) developed in Task 2.3, physical as well as virtual demonstrators were built up. The different PPs investigated within OSCCAR address future needs of car occupant protection in automated vehicles for Test Cases (combination of Crash Configuration, Occupant Use Case and Occupant Individual Variations) derived following the methodology defined in [1]. Relevant Crash Configurations for automated vehicles were identified from accident data and automated driving (AD) pre-crash simulations [2], and combined with Occupant Use Cases. The identified Test Cases are shown in Figure 1.

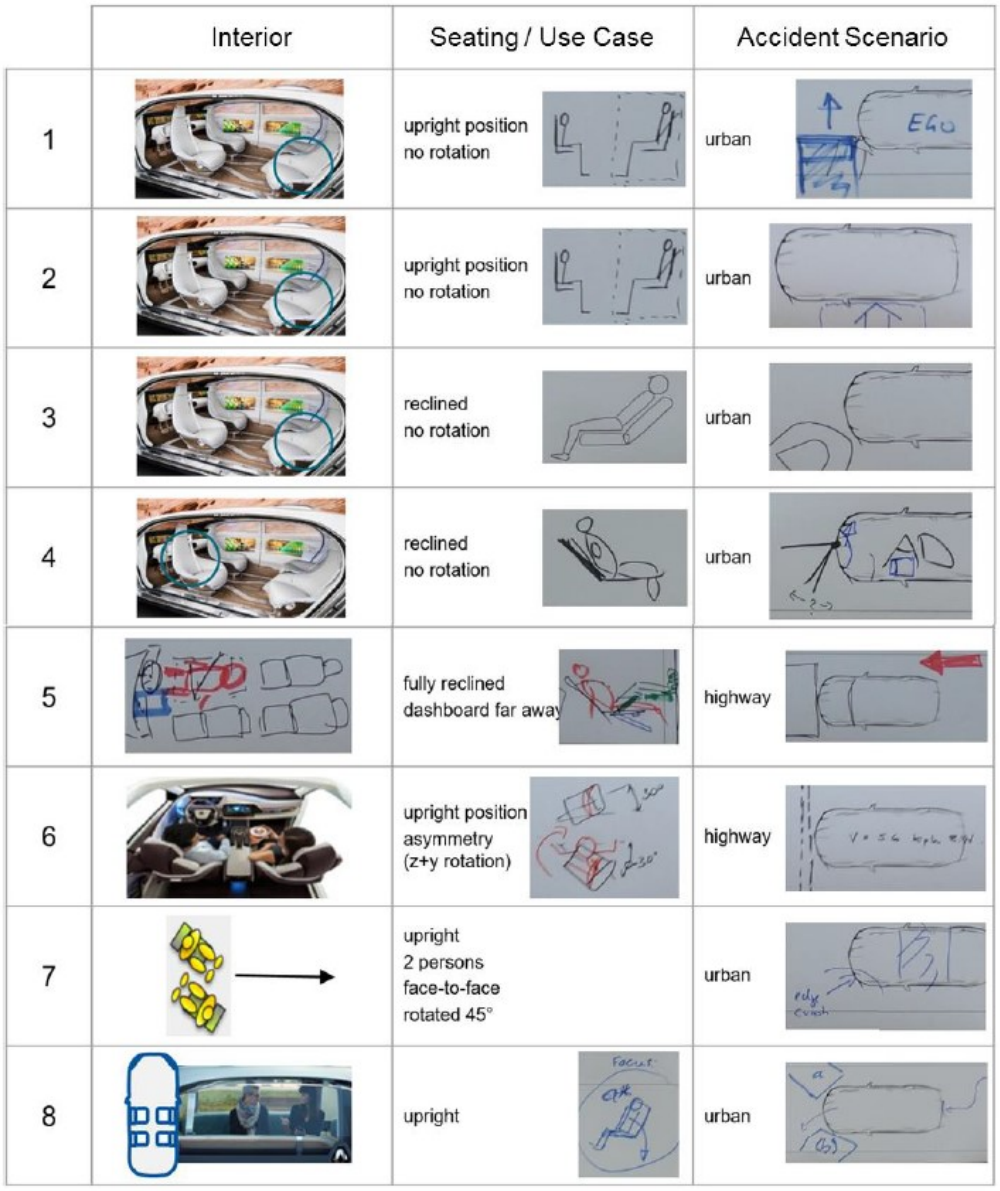

Figure 1 Selected occupant use cases and accident scenarios [4]

The main step for identifying and selecting the advanced passenger protection principles took place in an ideation workshop with involvement of almost all OSCCAR partners. Finally, six advanced protection principles were selected for further investigation. For the virtual conception and investigation of the advanced occupant protection principles addressing different seating positions and postures, different working groups were established. Both an adaptation of the restraint systems towards the new boundary conditions and a repositioning of the occupant into a conventional seating configuration prior to a crash were regarded, considering aspects like occupant variety and omnidirectional occupant loading. The respective working groups dealt with rotated seats, reclined seating positions, an advanced airbag design for a “living room” configuration (occupants facing each other) as well as occupant restraint in a future interior with regard to a side crash (Figure 2).

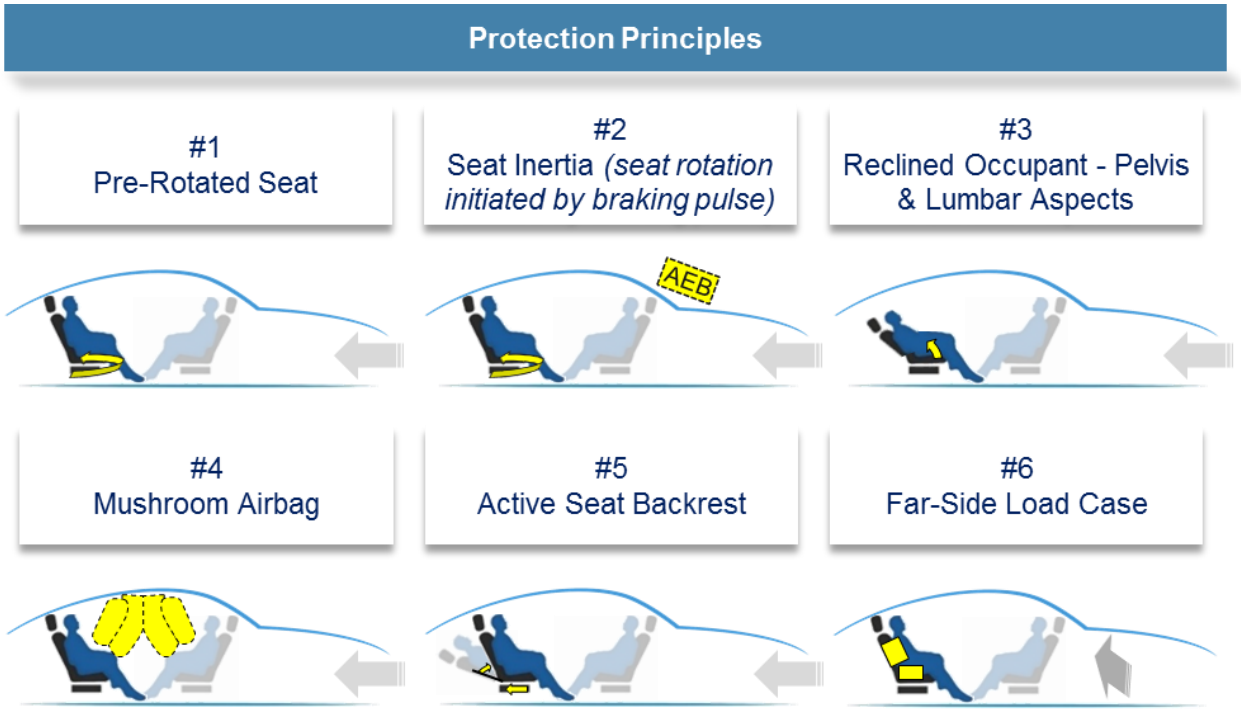

Figure 2 Protection principles analysed in OSCCAR WP2 [7]

With regard to the homologation demonstrator, the focus in Task 2.4 was on a reclined seating position and the challenges for the restraint system and the testing devices associated with such a configuration (also dealing with aspects considered within the framework of PP3). In this context, a state of the art 3-point belt (SOTA belt) was compared to a belt with double lap belt pre-tensioning (SOTA DLPT belt). Beside the homologation demonstrator, two PPs were selected for physical and virtual demonstration in Task 2.4, one was PP2 and the other was PP6. PP2 addresses an occupant who is sitting in a slightly rotated position (pointing away from the driving direction). If a crash is unavoidable, the seat is rotated in crash direction, only due to the inertia of seat and occupant by an active release of the seat. No actuator is needed, the seat rotation is initiated solely by an emergency braking prior to the crash. Another physical and virtual demonstrator was set up to study the performance of PP6. PP6 deals with different restraint system configurations as well as seat side supports in a far-side load case (opposite side to the one that is struck in a side crash), representing a future crash scenario for vehicles with flexible interiors without the presence of a centre console. While the homologation demonstrator already addressed a reclined seating position (PP3), the choice of PP2 and PP6 for the PP demonstrations allowed further aspects, i.e. a rotated seating position as well as a side crash, to be demonstrated with regard to future interiors. The test methods used are also suitable for demonstrating the other PPs (PP1, PP4 & PP5). However, a physical demonstration of PP4 would first require a hardware prototype of the Mushroom Airbag concept.

2.2 Objectives

Considering one of the OSCCAR general objectives to establish an integrated virtual assessment framework, Task 2.4 brought a major contribution by setting up a virtual as well as physical homologation demonstrator, providing according test data necessary for the development of such a virtual framework. Moreover, Task 2.4 demonstrated the feasibility of two of the six protection principles analysed in Task 2.3 (Figure 2) in order to conceptually address the challenges of new seating positions and car interiors envisaged in future highly automated vehicles. Again, physical as well as virtual demonstrators were built up for this purpose.

More precisely, the Task 2.4 objectives were twofold:

- Firstly, to demonstrate through the use of physical and virtual demonstrators the functionality of a state of the art 3-point belt (SOTA belt) equipped with double lap belt pretensioning (SOTA DLPT belt) in a reclined seating position (homologation demonstrator) and the functionality of PP2 as well as PP6. In Task 2.4 corresponding physical demonstrators were built and tested using crash test dummies:
    - The SOTA DLPT belt / homologation demonstrator was evaluated in sled tests carried out by BASt in collaboration with Autoliv. Full-width frontal and frontal-oblique load cases with a reclined seatback were used. It was checked whether the SOTA DLPT belt could prevent submarining and what would be the pelvis and lumbar spine loads in that case.
    - PP2 was demonstrated by ika and fka using a physical demonstrator on a test sled for different types of occupants and footrest configurations. The seat rotation was initiated solely by an emergency braking prior to the crash with a simultaneous release of the seat, considering different rotation axis positions. It was investigated whether seat and occupant could be rotated for different dummy sizes from an initial seat angle of 30° inwards back to the standard position within a total time of less than one second. Beside the physical demonstrator, also a virtual demonstrator was generated.
    - PP6 was evaluated in sled tests carried-out by IDIADA and CTAG-IDIADA in collaboration with TME and Autoliv. A far-side load case with an upright seatback was used. Different restraint system configurations as well as seat side supports were evaluated, representing a future crash scenario for vehicles with flexible interiors without the presence of a centre console. It was checked physically and virtually whether the PP6 countermeasures could limit the occupant excursion and what would be the rib deflections and the neck loads in that case.
- Secondly, to provide validated environment simulation models to WP4 that can serve as basis for the virtual homologation demonstrator. The SOTA DLPT belt and its environment were validated under different numerical codes (Finite Element solvers LS-Dyna and VPS, Multi-Body software Simcenter Madymo) with an equivalent validation level between the three codes. A first test series performed at BASt was used to validate the environment models. The validated model responses were compared with a second test series and the validation level could thus also be evaluated taking into account the test scatter. This latter data was provided to WP5, where it was used in the course of the development of environment validation procedures for Virtual Testing.

3 DESCRIPTION OF WORK

This section describes the homologation demonstrator and two PPs (PP2 & PP6), their vehicle interior environment and performances in laboratory tests. For the homologation demonstrator, the level of validation of the environment including the SOTA DLPT belt and the vehicle interiors were quantified and compared between the three numerical codes LS-Dyna, VPS and Madymo.

3.1 Homologation Demonstrator

This chapter describes the sled tests performed to evaluate the functionalities of the SOTA DLPT belt and the corresponding models developed and validated under LS-Dyna, VPS and Madymo.

The test configuration for the OSCCAR homologation demonstrator was based on a proposal by Autoliv. Additionally, Autoliv provided seatbelts (both test series), the semi-rigid seat (first test series) and the corresponding simulation models. BASt performed both test series including the analysis of the results and provided a THOR-50M ATD (both test series) as well as the semi-rigid seat (second test series). Furthermore, the corresponding LS-Dyna model was set-up, calibrated and validated by BASt. ESI and Siemens developed and validated the VPS and Madymo model respectively. Processing of results into plots and tables used to discuss the model's validation level was done by BASt. The presented test analysis and model validation were discussed by all companies mentioned as contributors to this report in Task 2.4 meetings.

3.1.1 Motivation and Background

The homologation demonstrator combined the most frequent future load case according to WP1 at intersections involving automated cars in mixed traffic and a use case where the occupant is in a forward-facing seat with a reclined backrest in a vehicle interior without knee restraints. The SOTA belt used in the tests was a seat-mounted 3-point belt equipped with a pretensioner in the shoulder retractor and with a crash locking tongue (CLT) at the buckle. The SOTA DLPT belt used for the 48° reclined seat was the same belt system as the SOTA belt except that lap belt pretensioners included at the anchorage and the buckle side were fired. The function of the SOTA DLPT belt is to limit pelvic excursion and pelvic loading and to reduce the risk of submarining due to the reclined backrest. In a first test series, the SOTA DLPT belt performance was compared to the SOTA belt and corresponding virtual demonstrators were validated under LS-Dyna, VPS and Madymo. In a second test series, test limitations identified after the first test series were addressed and the accuracy and robustness of the environment model validation was further checked.

The homologation demonstrator served the purpose of demonstrating within WP4 the potential and further work required to implement Virtual Testing in the homologation process. Furthermore, the test results and the validation of the homologation demonstrator were considered in WP5 as a practical example for the evaluation of the proposed validation methodology. As far as the virtual demonstrators are concerned, the LS-Dyna, VPS and Madymo models were developed and validated by means of the first test series.

3.1.1.1 Crash Pulses

The frontal-oblique load case was derived from WP1 where accident analysis and pre-crash simulations found out that this load case will be the predominant accident scenario in mixed traffic conditions at intersections. Two main configurations were extracted from this load case and used for the SOTA DLPT belt evaluation:

- The Straight Crossing Path configuration with an AD car impact velocity of 74 km/h and an opponent car impact velocity of 33 km/h (SCP1)
- The Left Turn Across Path Opposite Direction configuration with an AD car impact velocity of 53 km/h and an opponent car impact velocity of 35 km/h (LTAP OD2)

Full-vehicle model simulations were performed using above configurations in order to derive longitudinal and lateral vehicle pulses. Sled model simulations were then carried out to define the suitable sled angle that could best reproduce dummy kinematics from the full-vehicle model simulations as described in OSCCAR Deliverable D1.3 [3]. As a result, a sled angle of 15° in combination with a 31 km/h pulse and a 47 km/h pulse for SCP1 and LTAP OD2 respectively was defined [3] (Figure 3).

Additionally, the homologation demonstrator was tested using the 50 km/h full-frontal pulse of [5] to evaluate its performance under a particularly stringent pulse, similar to the current R137 regulation or Euro NCAP full-width frontal pulses (Figure 3).

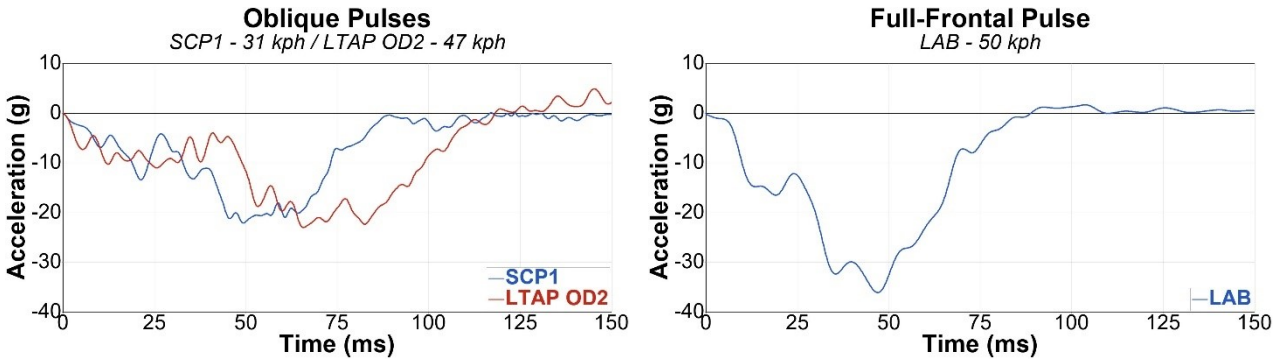

Figure 3 Pulses used for the homologation demonstrator

3.1.2 Physical Demonstrator

The OSCCAR homologation test case represents a reclined seating position in combination with a belt-in-seat restraint system and a generic semi-rigid seat developed by Uriot et al. [5]. Within OSCCAR WP2, tests of the physical demonstrator, as well as the corresponding simulations, were performed with the THOR-50M ATD, while simulations with different HBMs were performed in OSCCAR WP4.

3.1.2.1 Environment

The semi-rigid seat used for the physical demonstrator was initially used by [5] to assess the submarining behaviour in an upright seating position. Unlike generic rigid seats used in previous projects (e.g. [18],[19]), the seat pan and anti-submarining ramp were pivoted, hence better replicating the behaviour of production seats (Figure 4). Thereby, the rotary movement of the seat pan was counteracted by three springs (two on the side; one in the centre, which is loaded after approx. 8° of rotation), while the rotational motion of the anti-submarining ramp was transformed into linear motion via rack and pinion, here, the stiffness was characterised by two horizontal springs. The stiffness of the seat could be modified by changing the springs (front / rear seat set-up). For the OSCCAR homologation test case the front seat set-up [5] was used. Furthermore, two string potentiometers were used to measure the displacement of the seat pan and of the anti-submarining ramp.

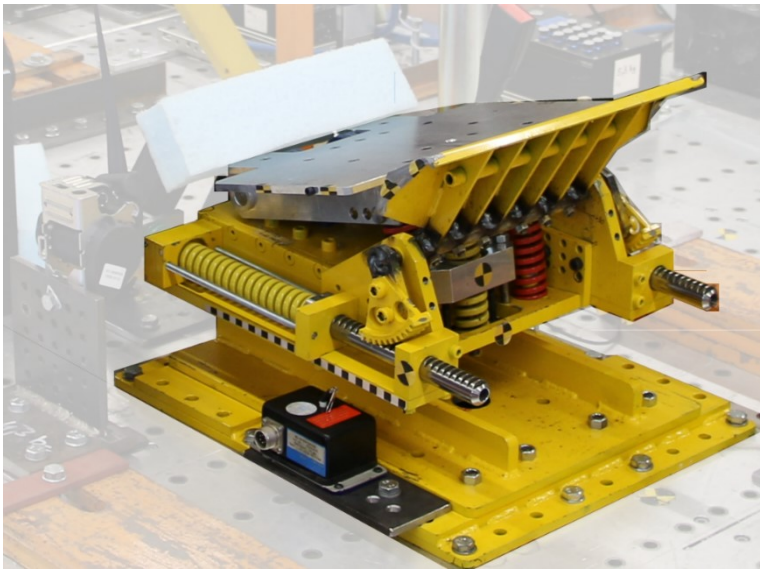

Figure 4 Semi-rigid seat by [5]

Two different versions of the semi-rigid seat were used in the OSCCAR project. In the first test series, the mechanical design was similar to the original design of [5], however, the seat pan was shortened by 20 mm. For the second test series, an updated version of the semi-rigid seat with a revised mechanical design was used. By that, the rebound of the springs was prevented by three dampers (one damper for the seat pan and two dampers for the anti-submarining ramp). For the new seat design the central spring of the seat pan was moved to a different position while the stiffness was adjusted accordingly. However, both versions of the semi-rigid seat should have a comparable stiffness. In Addition, the seat forces were measured by a 6-axis load cell. Table 1 compares the different mechanical designs and specifications of the semi-rigid seat as used within OSCCAR project.

Feature	First Test Series	Second Test Series
Springs Seat Pan Side (SS)	128 N/mm (×2)	128 N/mm (×2)
Springs Seat Pan Centre (CS)	379 N/mm (×1)	350 N/mm (×2)
Seat Pan Length	280 mm	300 mm
Design	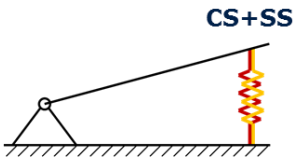	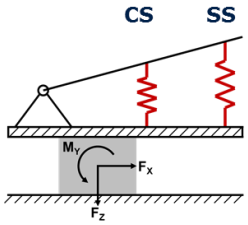
Load Cells	-	1
Springs Anti-Sub Ramp	132 N/mm (×2)	132 N/mm (×2)
Rebound Seat Pan	No	Yes (Damper)
Rebound Anti-Sub Ramp	No	Yes (Damper)

Table 1 Design & specifications of the semi-rigid seat

The restraint system combined two pretensioners at the lap belt anchorage and buckle (pyro-buckle) with a common 3-point belt system consisting of shoulder retractor (3.5 kN load limiter and 2 kN pretensioner) and crash locking tongue (CLT[1]). With the shoulder retractor ($t_{Shoulder}$ = 8 ms) only triggered, the restraint system corresponds to the SOTA belt. If in addition the pretensioners at the lap belt anchorage (t_{Lap} = 8 ms) and buckle (t_{Buckle} = 1 ms) were triggered, the restraint system corresponded with PP 3 (SOTA DLPT belt) from [7]. The three anchorage points of the seat-mounted 3-point belt replicated those from [15].

The back of the dummy was supported with a steel beam covered by foam. The rigid footrest from the SENIORS project was adapted to measure forces and moments. In order to avoid serious damages to the dummy in case of submarining, the legs were loosely fixed with a belt and the forces in the belt were measured.

3.1.2.2 THOR-M50 ATD

The THOR 50th percentile male dummy was used within the physical demonstrator. Thereby, the dummy corresponds to the Euro NCAP specifications with standard-build level B (SBL-B) and Hybrid III legs and was certified in accordance to Euro NCAP [16]. An In-Dummy Data Acquisition System was used to record the experiments, furthermore, a string potentiometer was added to measure the THOR pelvis forward motion with respect to the seat (blue dotted line in Figure 5).

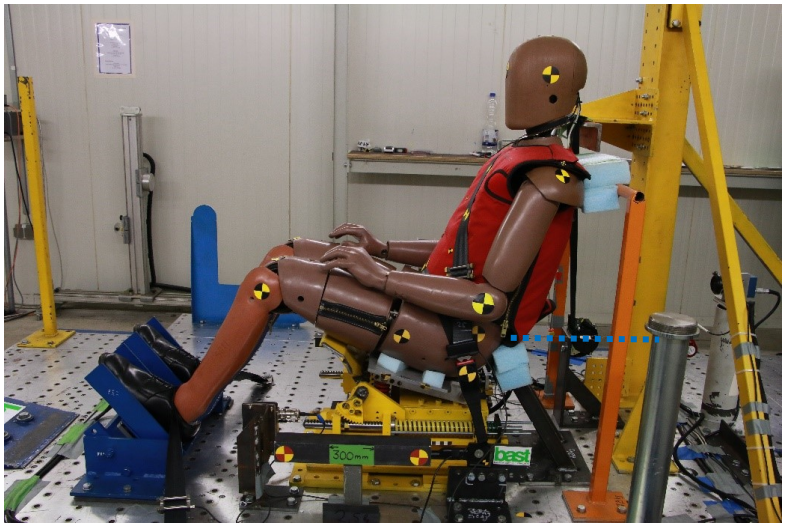

Figure 5 Seated dummy (upright seating position) with attached pelvis string potentiometer

3.1.2.3 Dummy Positioning and Belt Routing

The test configuration for the OSCCAR homologation test case as well as the dummy position were proposed by Autoliv. Thereby, the dummy H-point was approx. 123 mm forward of the origin of the coordinate system (Figure 6) while pelvic angles (Y) of 33° ± 2.5° for the upright seating position respectively 48° ± 2.5° for the reclined seating position were chosen. To ensure repeatability, the feet were lightly squeezed into the footrest. Position of the knees as well as femur and tibia angles

[1] During the pre-tensioning phase, webbing can be transported through the buckle tongue to eliminate belt slack in all belt portions. Afterwards belt forces increase until the phase of load limiting is reached. When the force differences between the diagonal belt and the lap belt increase, the locking tongue mechanism is activated, whereby the friction is first increased until the locking tongue reaches a very high friction value, quasi “locked”. Webbing transport is no longer possible. The locking tongue used in this study “locks” at a force difference of approximately 1.5 kN.

were consequently pre-defined by the H-point and feet. In addition, the knee distance, measured at the outboard metal surface, was set to 270 mm. The dummy torso position was changed with the T1 tilt angle sensor to 23° (upright) respectively 48° (reclined). Thereby, the lower thoracic pitch joint was set to the 'slouched' position which is equivalent to +9°. Shoulder joints were in a neutral position, while the upper arms were aligned parallel to the upper body and lower arms were placed on the thighs. The position of the head was not modified as it would return to its original position.

In general, the dummy was symmetric to the seat mid sagittal plane (tilt sensor (X) 0° ± 1°). Figure 6 shows the position of dummy head, torso and leg relative to the seat / origin of the coordinate system.

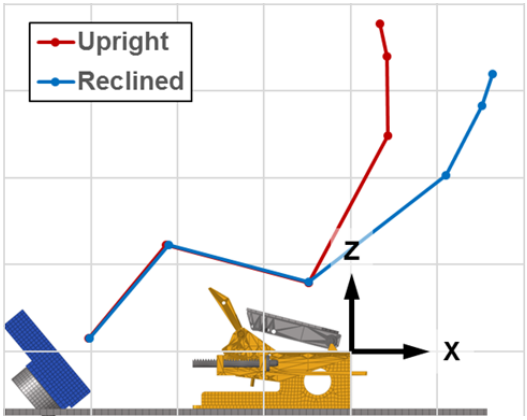

Measurement	Upright	Reclined
H-Point	x = -123 mm	
Pelvis Angle	y = 33°	y = 48°
Thorax Angle	y = 23°	y = 48°

Figure 6 Dummy seating position and some relevant measurements

For documentation and later positioning of the simulation models, the dummy position was measured using a 3D measurement arm. Furthermore, tilt sensors, tibia angles as well as hand joint and knee distances were documented.

The diagonal belt was positioned on the thorax relative to the chin (d = 120 mm), while for the lap belt the same z-coordinate relative to the seat was targeted. Load cells for measuring the seat belt forces were attached to the upper (B3) and lower (B4) diagonal belt and to the lap belt (B6). As for the dummy position, the belt routing was documented with a 3D measurement arm.

3.1.2.4 Cameras and Landmarks

Five stationary cameras and three on-board cameras were used in the first sled test series to record the dummy kinematics at a sampling rate of 1000 Hz (Figure 7).

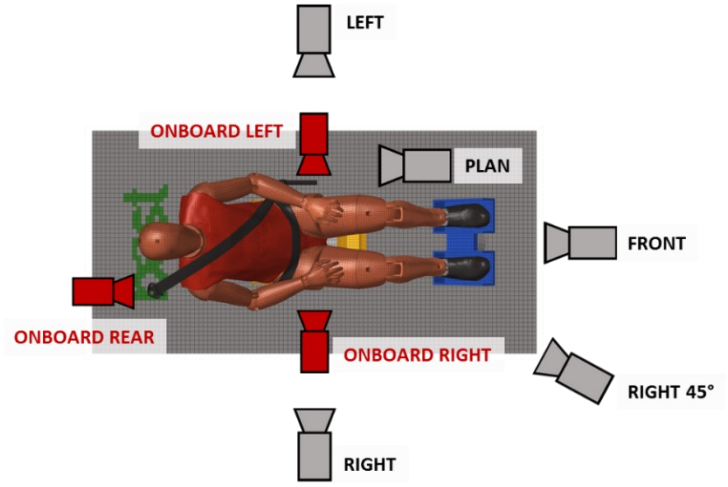

Figure 7 Camera positioning within the first test series relative to the sled

Kinematics were obtained from point tracking with FalCon eXtra software. Therefore, target points were attached each to the left and right head COG, shoulder, elbow, H-point holes, pelvis skin point at 200 mm forward of H-point and knee (Figure 8). Trajectories of hidden markers were, whenever reasonable, linearly interpolated.

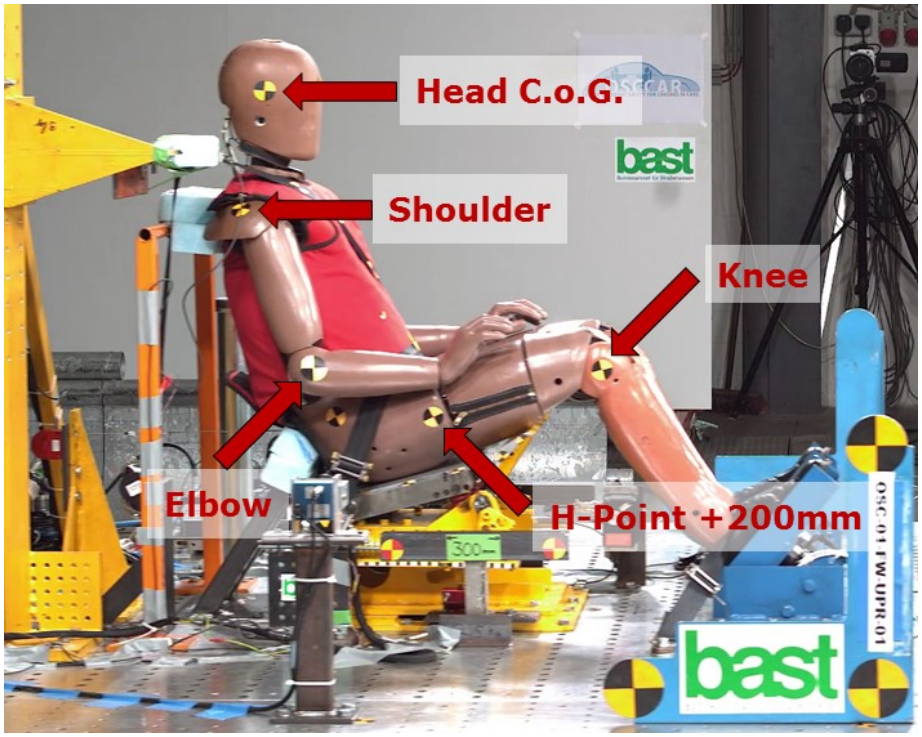

Figure 8 Seated dummy (upright position; right hand side) with targets

Belt pay-in/-out of the shoulder retractor was measured with a target, additional targets to document the belt routing were attached to the belt. On-board cameras on the left- and right-hand-side were used to measure the kinematics of the buckle and at external lap belt retractor. In addition, these cameras were used to observe the belt-to-pelvis interaction.

3.1.3 Physical Demonstrator – First Test Series Results

The first test series investigated the behaviour of occupants in reclined and upright seating positions. Whether new restraint systems, such as the protection principle developed in OSCCAR Deliverable D2.4 [7] (SOTA DLPT belt), were able to increase the occupant protection in reclined seating position and if the performance of the restraint system was still given for the oblique pulses developed in OSCCAR WP1 and reported in Deliverable D1.3 [3]. Results from the first test series were also used to calibrate and subsequently validate the simulation models (see Chapter 3.1.4), especially the generic interior, which was later used in OSCCAR WP4.

3.1.3.1 Test Matrix

Using the THOR-50M ATD, seven different configurations, varying the seating position, restraint system, pulse and sled angle were studied. In total, 13 tests were executed in the first test series, as shown in Table 2. All except one were repeated once.

#	Test No.	Pulse	Angle	Dummy	Restraint System	Comment
1	OSC-01-FW-UPR-01	LAB 50 km/h	0°	Upright	SOTA belt	-
2	OSC-01-FW-UPR-02	LAB 50 km/h	0°	Upright	SOTA belt	Repetition
3	OSC-02-FW-REC-01	LAB 50 km/h	0°	Reclined	SOTA belt	-
4	OSC-02-FW-REC-02	LAB 50 km/h	0°	Reclined	SOTA belt	Repetition
5	OSC-03-FW-REC-01	LAB 50 km/h	0°	Reclined	SOTA DLPT belt	-
6	OSC-03-FW-REC-02	LAB 50 km/h	0°	Reclined	SOTA DLPT belt	Repetition
7	OSC-05-OB-UPR-01	SCP1 31 km/h	15°	Upright	SOTA belt	-
8	OSC-05-OB-UPR-02	SCP1 31 km/h	15°	Upright	SOTA belt	Repetition
9	OSC-06-OB-REC-01	SCP1 31 km/h	15°	Reclined	SOTA DLPT belt	-
10	OSC-06-OB-REC-02	SCP1 31 km/h	15°	Reclined	SOTA DLPT belt	Repetition
11	OSC-08-OB-UPR-01	LTAP OD2 47 km/h	15°	Upright	SOTA belt	-
12	OSC-08-OB-UPR-02	LTAP OD2 47 km/h	15°	Upright	SOTA belt	Repetition
13	OSC-09-OB-REC-01	LTAP OD2 47 km/h	15°	Reclined	SOTA DLPT belt	-

Table 2 Test matrix of the first test series

3.1.3.2 Comparison of Reclined and Upright Seating Positions

To understand differences in occupant behaviour resulting from different seating positions, results of the reclined and upright seating position with the SOTA belt were compared.

Figure 9 shows the dummy kinematics for both seating positions. In the upright seating position, the dummy torso rotated forwards as it moved forwards and was fully erected after approx. 75 ms. Whereas the whole dummy in the reclined seating position moved (in its initial position) forwards into the belt and seat pan until approx. 60 ms. After these 60 ms the dummy started to rotate forwards from its reclined seating position, especially in the upper thorax, but never got fully erected. As a result, the belt slid towards the neck and became trapped between the neck and spine box (a.k.a. shoulder belt entrapment). In contrast, the shoulder to belt interaction in the upright seating position was stable – no shoulder belt entrapment was observed. Relative to the seat, the head forward displacement was greater in the upright seating position while the pelvis forward displacement was greater in the reclined seating position.

Figure 9 Dummy kinematics in upright and reclined seating positions with SOTA belt

Differences were also observed for the seat displacements and belt loadings (Figure 10). Thereby, the bigger pelvis forward displacement in the reclined seating position resulted in larger displacements of the anti-submarining ramp while seat pan displacements were comparable. The upper diagonal belt forces (B3) tended to be greater in the upright seating position. In the reclined seating position, the CLT and shoulder belt entrapment prevented the belt from slipping across the chest, which resulted in significantly increased lower diagonal belt forces (B4) when the dummy rotated into the belt (after approx. 90ms). Peak lap belt loading (B6) was about equal for both load cases, although the total belt loading was greater in the reclined seating position. Belt pay-in during pretensioning was comparable for both configurations, while the delayed dummy erection and less forward movement of the upper thorax in the reclined seating position resulted in smaller belt pay-out.

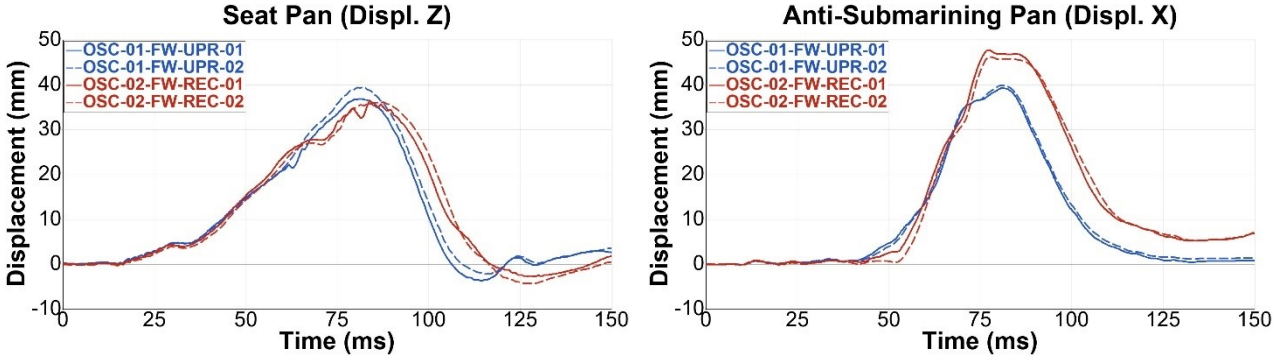

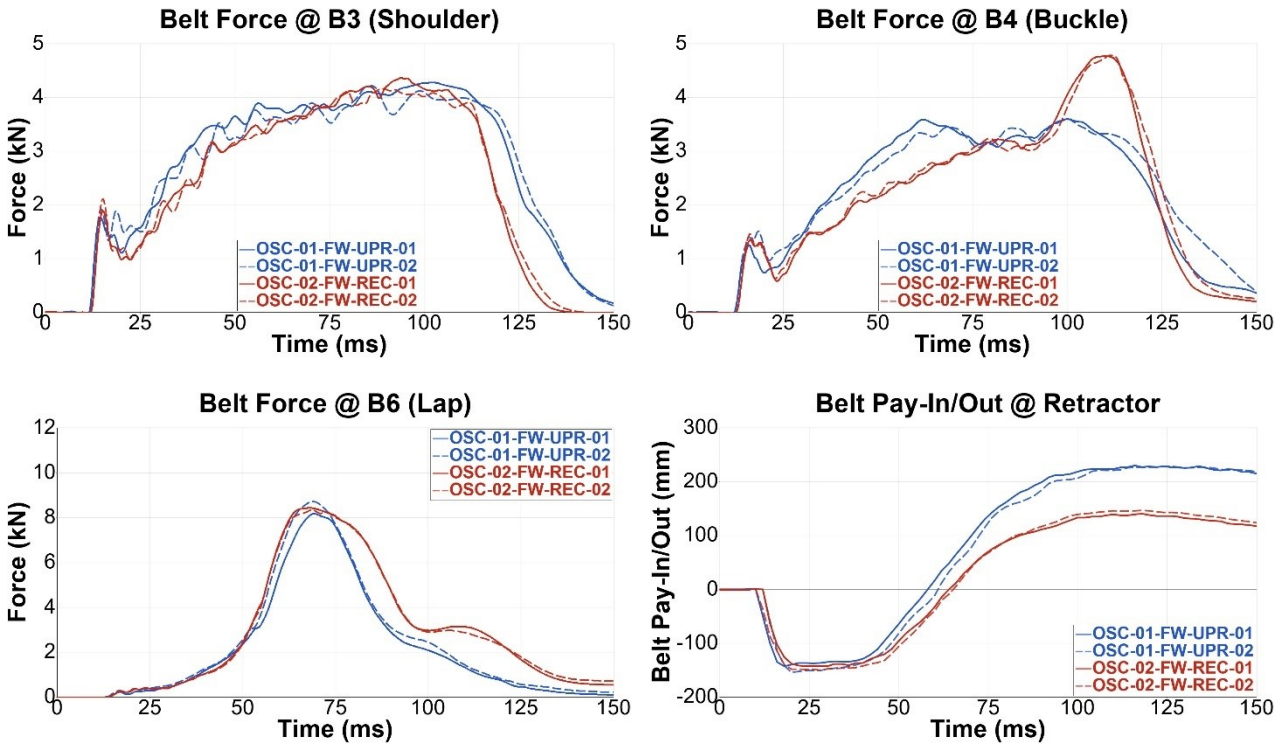

Figure 10 Seat displacements, belt forces & shoulder retractor belt pay-in/-out for upright (blue) & reclined (red) seating positions

For the upright seating position, lower thoracic spine accelerations in the x-direction were generally greater, while z-accelerations were greater for the reclined seating position (Figure 11). As a result, the compression loading (z-force) to the lower thoracic spine was also greater in the reclined seating position. Both can be explained with the initial seating position and resulting differences in the dummy kinematics (upright: early rotation of the torso; reclined: forward movement into the belt / seat, late rotation of the upper thorax). Differences in the y-moment were also a result of the different rotational behaviour of the upper thorax.

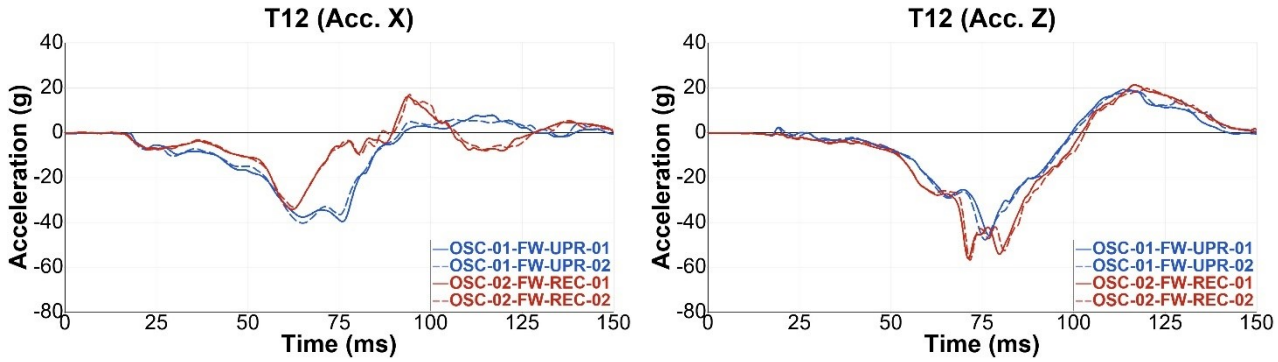

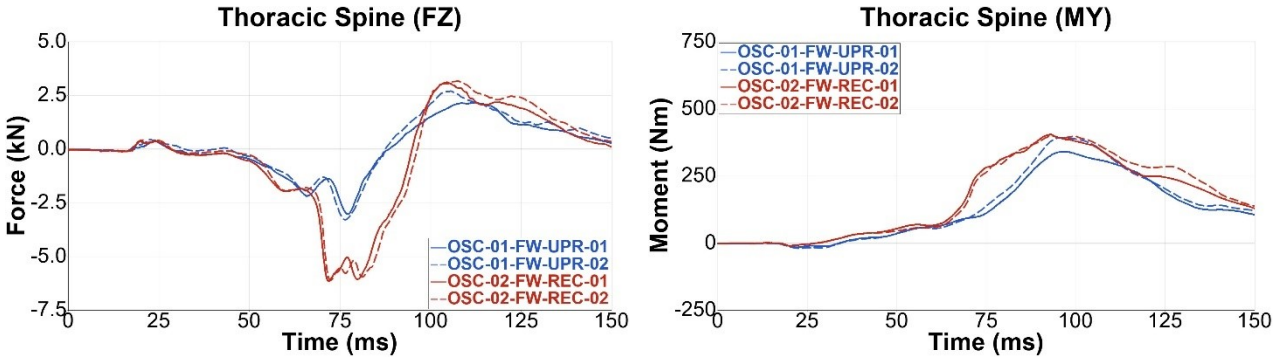

Figure 11 Lower thoracic spine (T12) accelerations & loadings for upright (blue) & reclined (red) seating position

Pelvis accelerations in the x-direction were about twice as high for the upright seating position, while z-accelerations were about twice as high in the reclined seating position (Figure 12). In addition, the pelvis rotated more than twice as much backwards in the reclined seating position. ASIS forces and moments in the upright seating position were symmetric with respect to peak loading and timing, whereas, in the reclined seating position CLT belt pull-through reduced the forces in the left ASIS (no CLT belt pull-through was observed in the upright seating position). Compared to the upright seating position, peak forces were not greater in the reclined seating position, however, peak load duration were longer which indicates greater energy input into the pelvis. In addition, both ASIS moments were positive resulting in an increased risk for submarining. Additional plots can be found in Appendix A1.1.1.

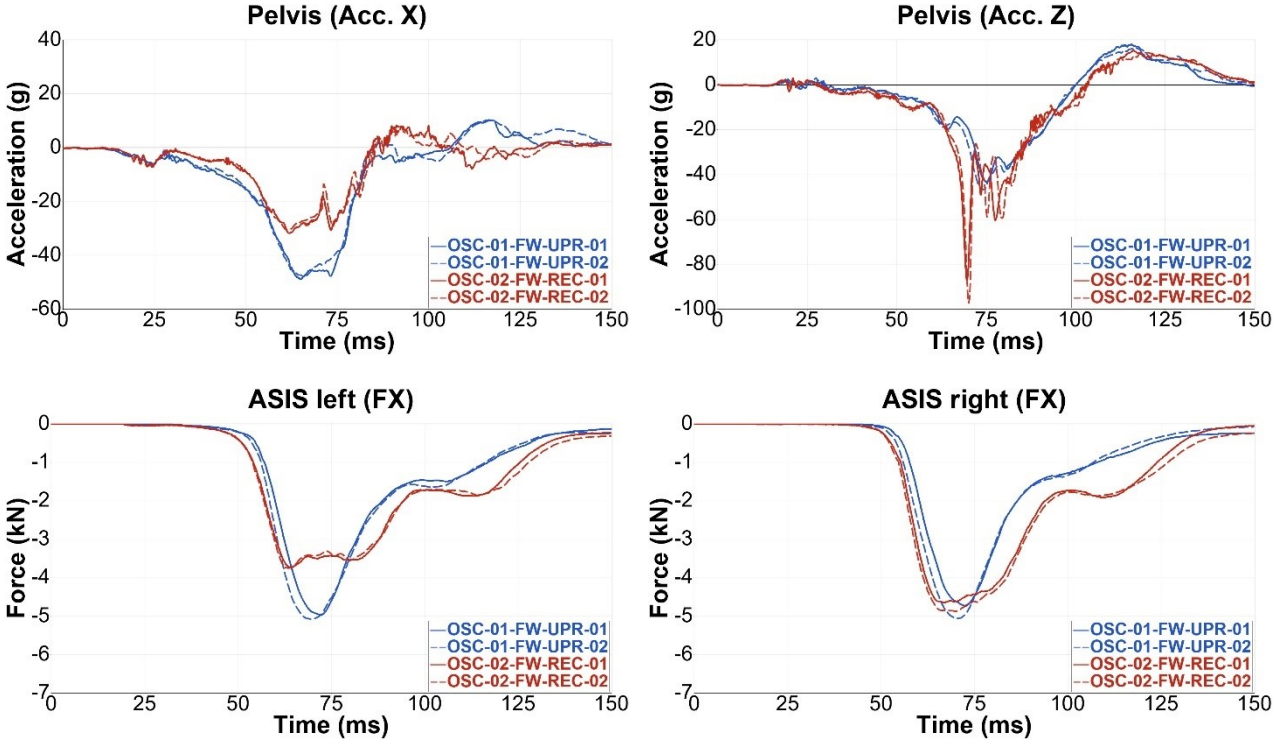

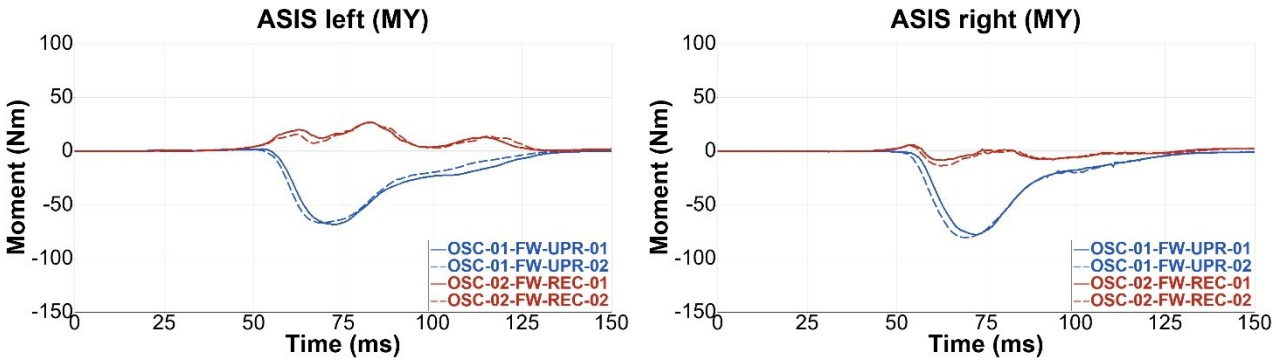

Figure 12 Pelvis accel., ASIS forces & moments - upright (blue) & reclined (red) seating position

3.1.3.3 SOTA Belt and SOTA DLPT Belt in Reclined Seating Position

The risk of submarining and compression loading to the lumbar spine increases in reclined seating positions. Protection principles, such as the SOTA DLPT belt developed in OSCCAR Deliverable D2.4, aimed at reducing these risks. To evaluate the effectiveness of the SOTA DLPT belt in reclined seating positions, the developed protection principle was compared with the SOTA belt.

Figure 13 shows the dummy kinematics of different restraint systems in the reclined seating position. Independent of the restraint system, the whole dummy moved (in its initial position) forwards into the belt and seat pan. As a result, the belt slid towards the neck and became trapped between the neck and spine box (shoulder belt entrapment).

Figure 13 Dummy kinematics reclined seating with SOTA (top) & SOTA DLPT belt (bottom)

With the SOTA DLPT belt the pelvis was restraint earlier resulting in less pelvis forward displacement and sooner forward rotation of the upper body. Compared to the SOTA belt, the upper body was more erected with the SOTA DLPT belt, however, in both cases the dummy never reached a fully vertical position.

Seat pan displacements were larger and occurred earlier in time with the SOTA DLPT belt while the anti-submarining ramp displacements were smaller (Figure 14). Both can be explained by the forward displacement of the dummy relative to the seat. With the SOTA belt the pelvis moved beyond the frontal edge of the seat pan resulting in a reduced loading of the seat pan while the anti-submarining ramp loading has increased. In contrast, due to pretensioning of the lap belt (SOTA DLPT belt) and the subsequent earlier pelvis-to-belt coupling the dummy remained on the seat pan. Belt forces at the upper diagonal belt (B3) were overall similar. For the lower diagonal belt (B4) and lap belt (B6) the pretensioning of the SOTA DLPT belt could be observed, however, the peak belt forces were almost identical. For the SOTA DLPT belt, pay-in at the shoulder retractor was smaller due to the previous / simultaneous pretensioning of the lap belt. Belt pay-out was comparable for both restraint systems when the differences in the belt pay-in are considered.

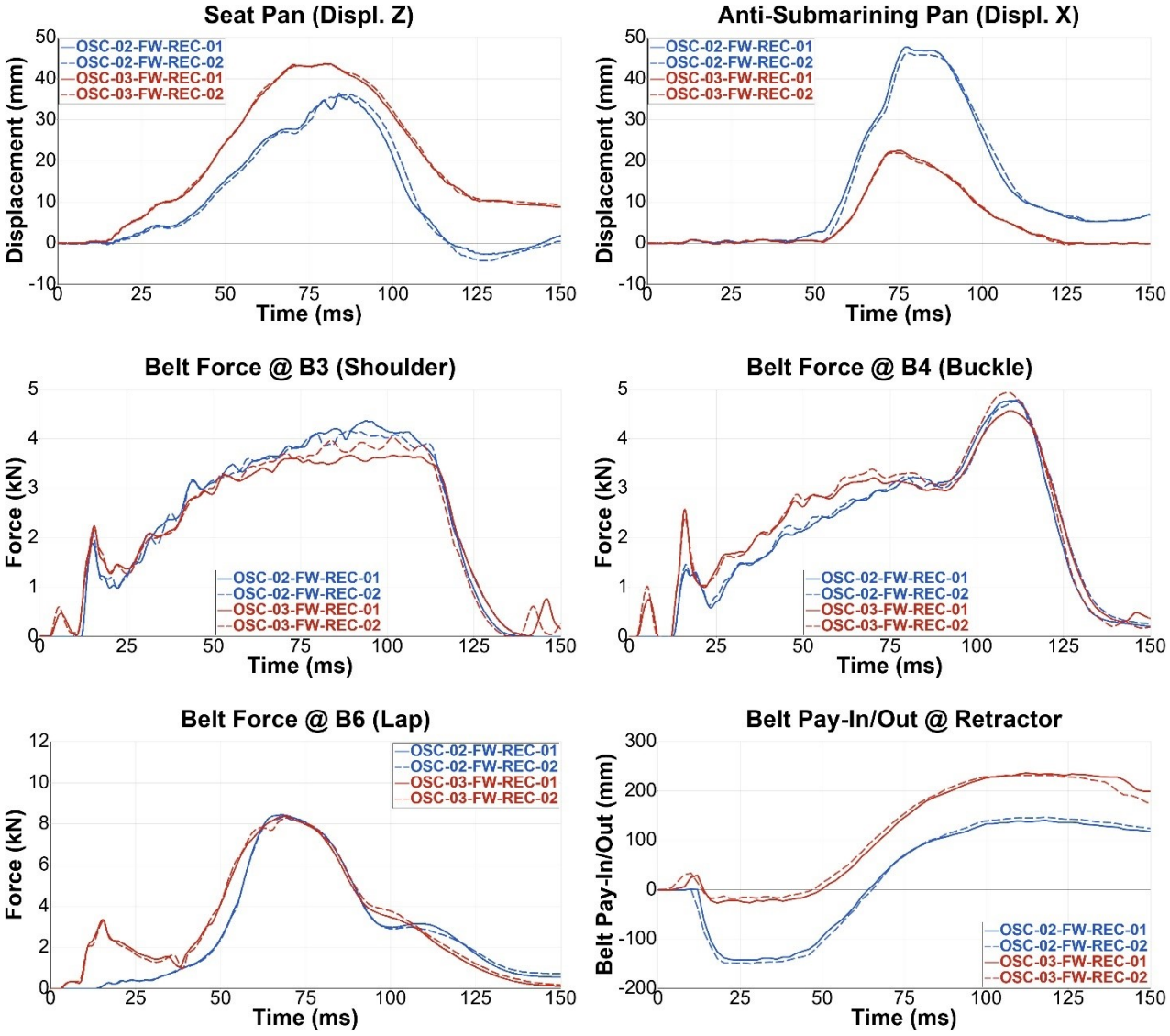

Figure 14 Seat displacements, belt forces & shoulder retractor belt pay-in/-out for SOTA (blue) & SOTA DLPT belt (red)

The earlier coupling of the dummy and belt due to lap belt pretensioning resulted in smaller lower thoracic spine accelerations and a reduced compression loading (Figure 15).

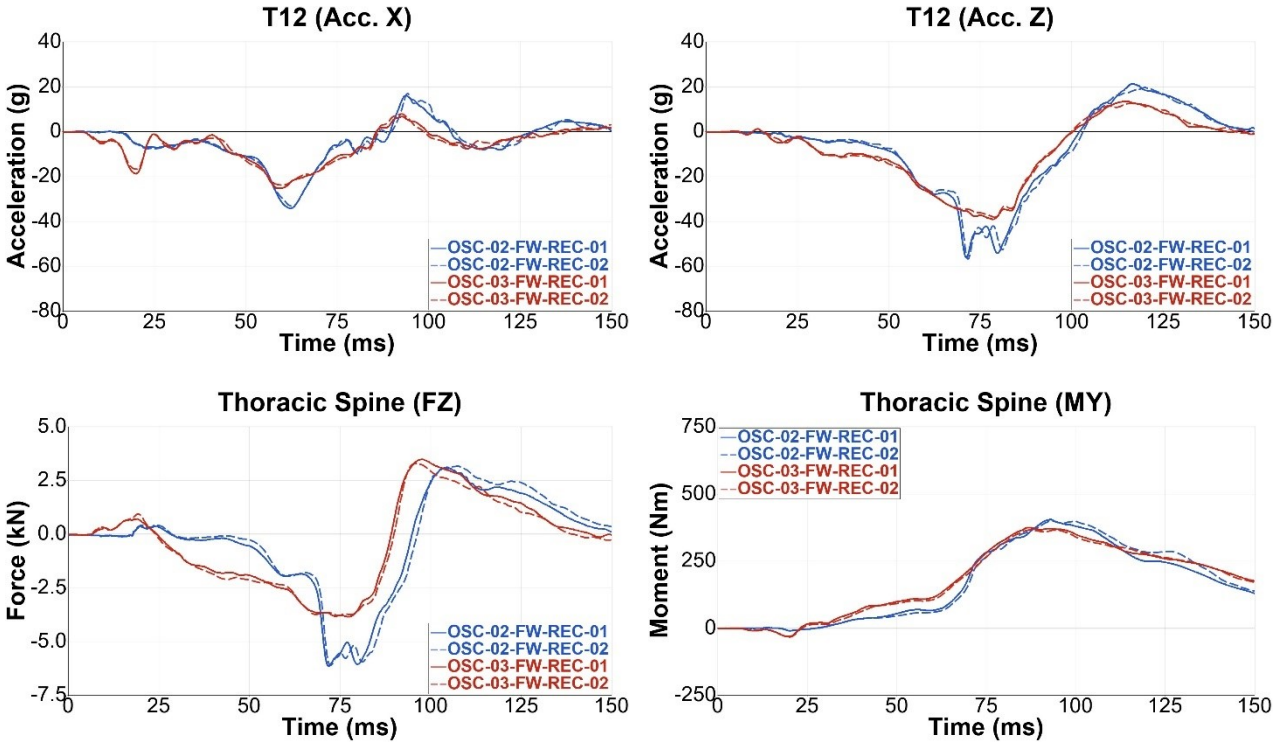

Figure 15 Lower thoracic spine(T12) accelerations & loadings for SOTA (blue) & SOTA DLPT belt (red)

Pelvis accelerations were affected by the pretensioning of the lap belt and the subsequent earlier pelvis-to-belt coupling (Figure 16). A sudden loading of the pelvis was consequently avoided and accelerations were generally lower with the SOTA DLPT belt. For both restraint systems the left and right ASIS forces were not symmetric with respect to peak loading and timing, which can be explained with the CLT belt pull-through. With the SOTA DLPT belt the left ASIS forces were higher, while ASIS moments were negative, thus significantly reducing the risk of submarining compared to the SOTA belt. Additional plots can be found in Appendix A1.1.2.

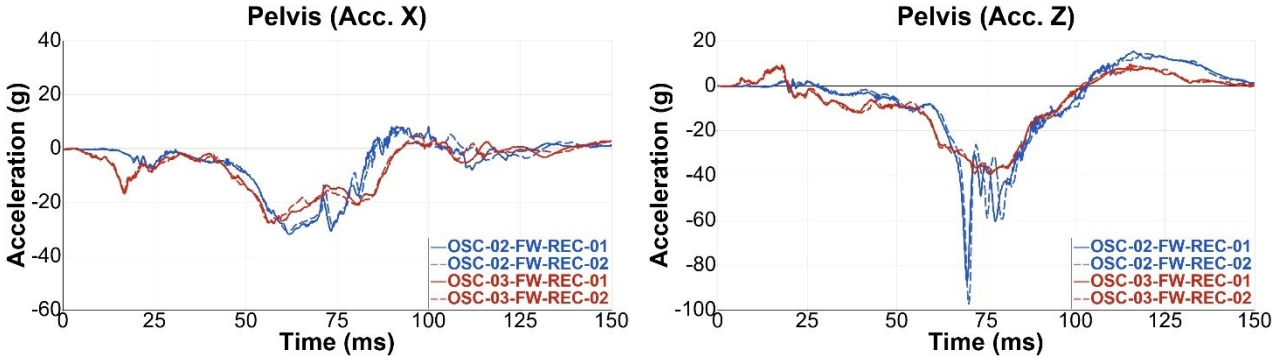

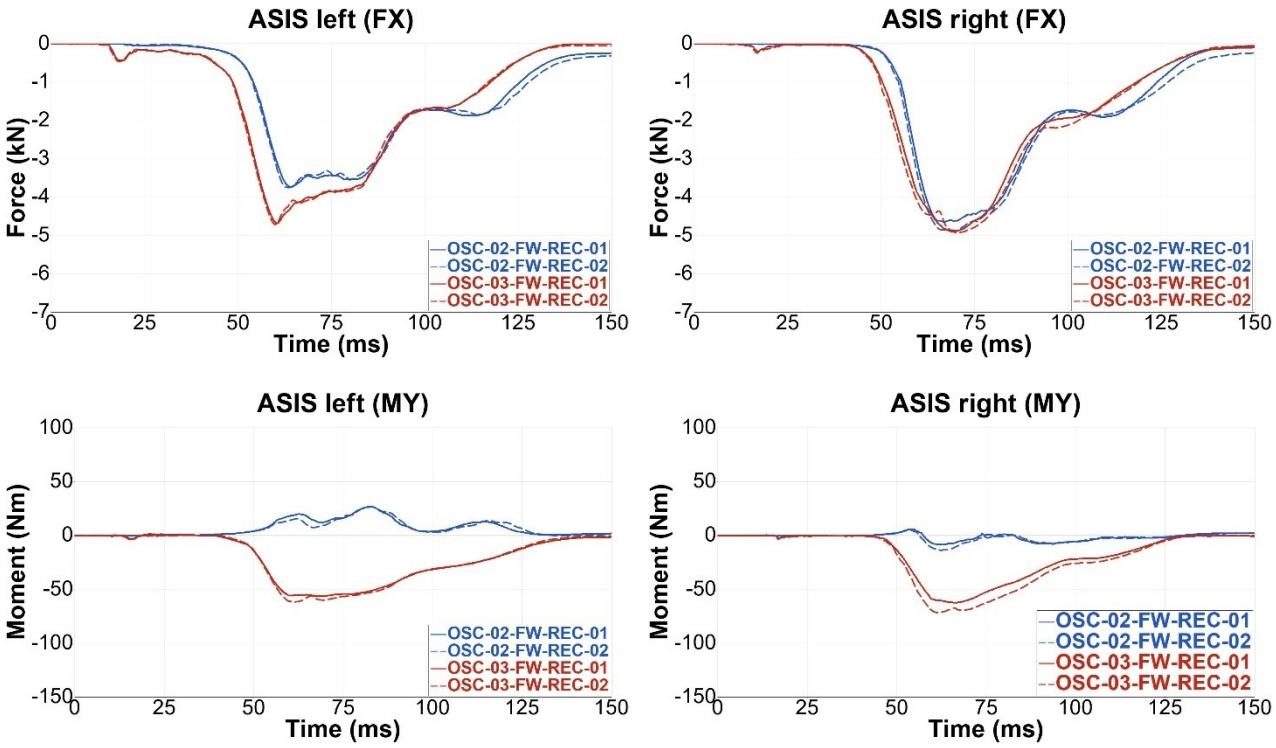

Figure 16 Pelvis accelerat. & ASIS forces & moments for SOTA (blue) & SOTA DLPT belt (red)

3.1.3.4 SOTA Belt and SOTA DLPT Belt in Oblique Pulses

In the previous chapters, the difference between upright and reclined seating positions as well as the suitability of the SOTA DLPT belt for reclined seating were discussed. In the first test series, the performance of the restraint systems under oblique pulses was also investigated. For the upright seating position, the SOTA belt was used (Table 2). Both oblique pulses were less severe than the full-frontal pulse, consequently loading to the dummy and environment (seat displacements and belt forces) as well as pelvis forward displacement were in general smaller and delayed. Y-accelerations and lower thoracic spine X-moments, however, changed due to the oblique impact. Neither submarining nor shoulder belt entrapment was observed in either load case.

Like for the upright seating position, loading to the dummy and environment was lower in the reclined seating position as a result of the less severe oblique pulse. As in the full-frontal load case, no submarining but shoulder belt entrapment was observed for both oblique load cases. Consequently, the performance of the SOTA DLPT remained given.

Plots of SCP1 and LTAP OD2 pulses in comparison to the full-frontal load cases can be found in Appendix A1.1.

3.1.3.5 First Test Series Summary and Limitations

Dummy kinematics and consequently the loads on the dummy changed with the reclined seating position. Compared to the upright seating position, the shoulder-to-belt interaction was delayed in the reclined seating position. As a result, the belt slipped towards the neck and shoulder belt entrapment was observed. Loading to the dummy in the reclined seating position was in the z-direction generally higher. The SOTA DLPT belt resulted in an earlier dummy-to-belt coupling, which generally led to earlier yet smaller accelerations and thoracic spine loadings when compared to the SOTA belt in the reclined seating position. Submarining was avoided in all load cases, whereby

the risk of submarining was significantly reduced when the pelvis was pretensioned. Performance of the SOTA DLPT belt was also demonstrated in additional frontal-oblique impacts.

Some limitations were identified in the first test series that should be addressed in future test series:

- The THOR dummy was used without its usual cotton trousers, resulting in a higher friction between the seat and the pelvis flesh. Thereby, the forward motion of the pelvis and the risk of submarining were reduced.
- The D-ring mount, especially in the upright seating position, was not completely rigid. During pre-tensioning of the shoulder retractor, the D-ring mounting bracket was bent downwards, which likely increased the belt pay-in by some millimetres.
- Comparisons for both oblique pulses as for the full-frontal configurations would have been interesting (SOTA DLPT belt and SOTA belt in the reclined seating position, upright versus reclined seating position with SOTA belt). However, corresponding tests with the SOTA belt in the reclined seating position were not foreseen for the oblique pulses, hence, not enough data to assess the results in this way was available.

3.1.4 Virtual Demonstrator

The virtual homologation demonstrator in WP4 requires validated environment simulation models for different numerical codes (LS-Dyna, VPS and Madymo). A virtual demonstrator was developed accordingly to the physical demonstrator from the first test series. Furthermore, the level of validation was quantified using the CORA-rating.

3.1.4.1 Model and Simulation Set-Ups

The virtual demonstrators in LS-Dyna, VPS and Madymo were modelled as closely as possible to the physical demonstrator described in Chapter 3.1.2. Thereby, measurements from the first test series were considered for adjusting the models, while positioning the ATD models or routing the belt. Some code-specific modifications to the seat and restraint system were necessary for VPS and Madymo. Results from the first test series were used to calibrate the models for each code separately.

For all seven test configurations from the first test series (Chapter 3.1.3.1), the corresponding simulation models were developed. The entire model and simulation set-up process, necessary adaptations and the calibration of the simulation models are described in Appendix A1.2.

3.1.4.2 Model Validation – SOTA belt in Upright Seating Position

Figure 17 shows the validated demonstrators in LS-Dyna, VPS and Madymo compared to the experiments in the upright seating position with SOTA belt. For LS-Dyna and VPS the forward rotation of the lower torso was comparable to the tests, while the rotation of the upper torso appeared to be higher. On the other hand, forward rotation of the torso was greater in Madymo. Compared to Madymo, the rotation around the z-axis as a result of the shoulder belt restraint was greater in LS-Dyna and VPS (50-70 ms). Furthermore, an increased pelvis upwards rotation could be observed for VPS and LS-Dyna. Unlike in the experiments and LS-Dyna and VPS, the shoes slightly slipped up the foot rest in Madymo.

Figure 17 Comparison of dummy kinematics for the upright seating position with SOTA belt

Seat pan displacements could be well predicted by LS-Dyna and VPS (Figure 18) while the displacements were underpredicted in Madymo which could be explained with the reduced pelvis forward displacement (Figure 20). In all codes the peak displacements occurred earlier in time than in the experiments. Displacements of the anti-submarining ramp were underpredicted in all codes.

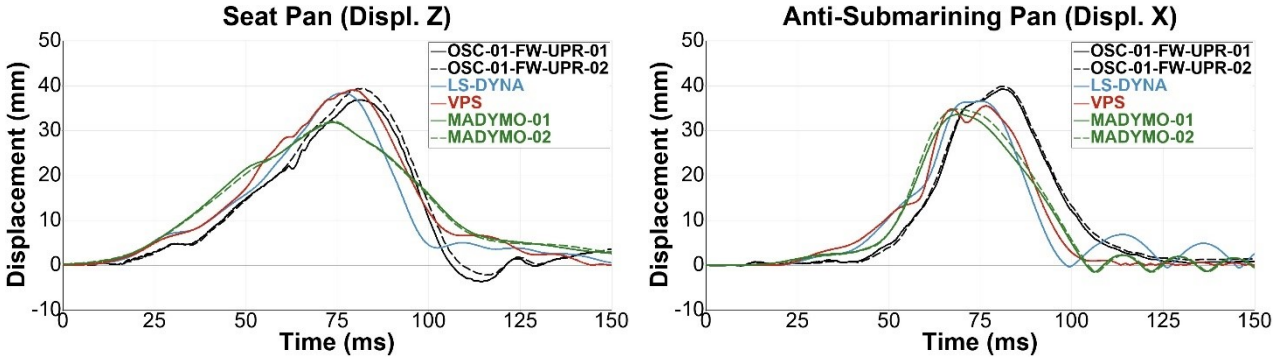

Figure 18 Seat pan and anti-submarining ramp displacements

Shoulder belt force (B3) was well predicted by LS-Dyna while the belt forces were overpredicted in VPS respectively underpredicted in Madymo (Figure 19). In all codes the B3 belt force dropped earlier in time. In LS-Dyna and VPS, belt forces at the lower diagonal belt (B4) could be well predicted to the peak loading at approx. 75 ms while the later constant force could not be reproduced. The B4 force in Madymo was underpredicted. Peak lap belt forces (B6) were generally overpredicted. Belt pay-ins were well replicated by Madymo, while there is some deviation for LS-Dyna and VPS which could be likely explained by the not completely rigid D-ring mount (see Chapter 3.1.3.5). In contrast, the belt pay-out could only be reproduced well by LS-Dyna.

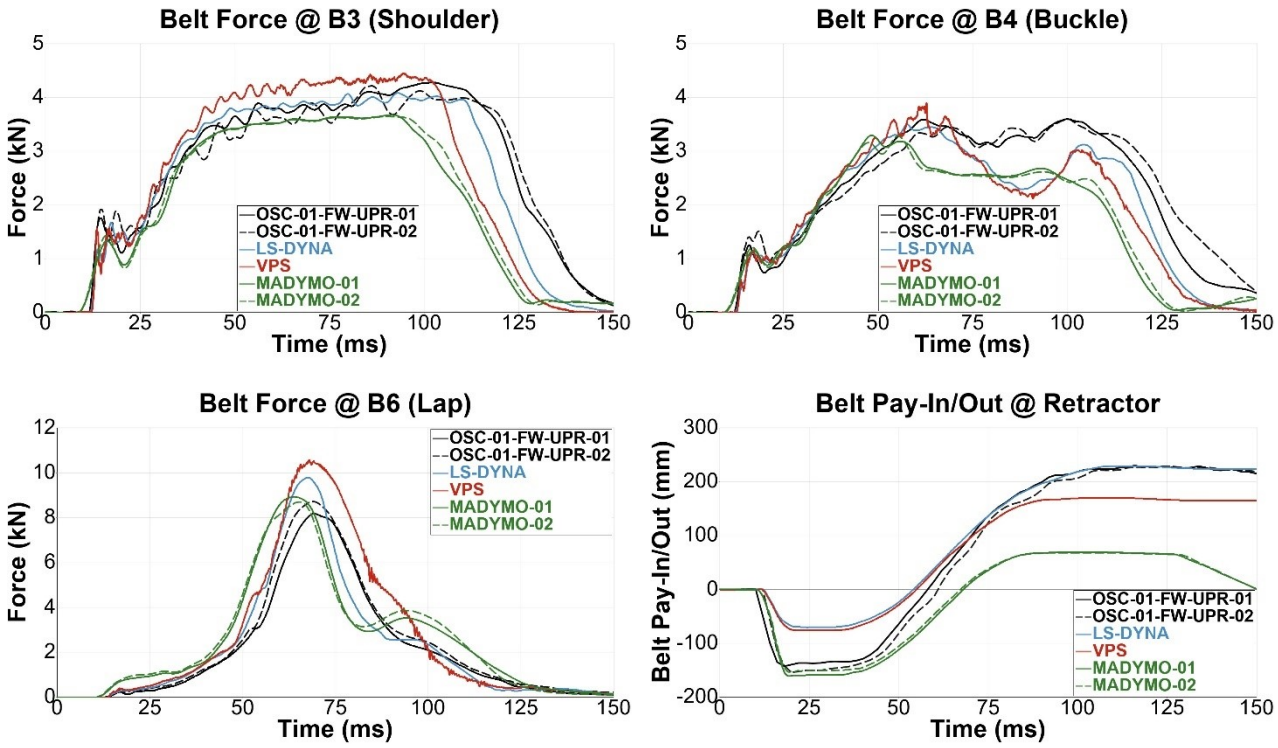

Figure 19 Seat belt forces and pay-in/out

In all codes, the pelvis x-acceleration was well predicted, although accelerations appeared to be slightly premature (Figure 20). Compared to the experiments, especially in LS-Dyna and VPS z-accelerations were overpredicted and signals were noisy. Pelvis peak forward displacements was best replicated in VPS while Madymo underpredicted the forward displacement by approx. 100 mm.

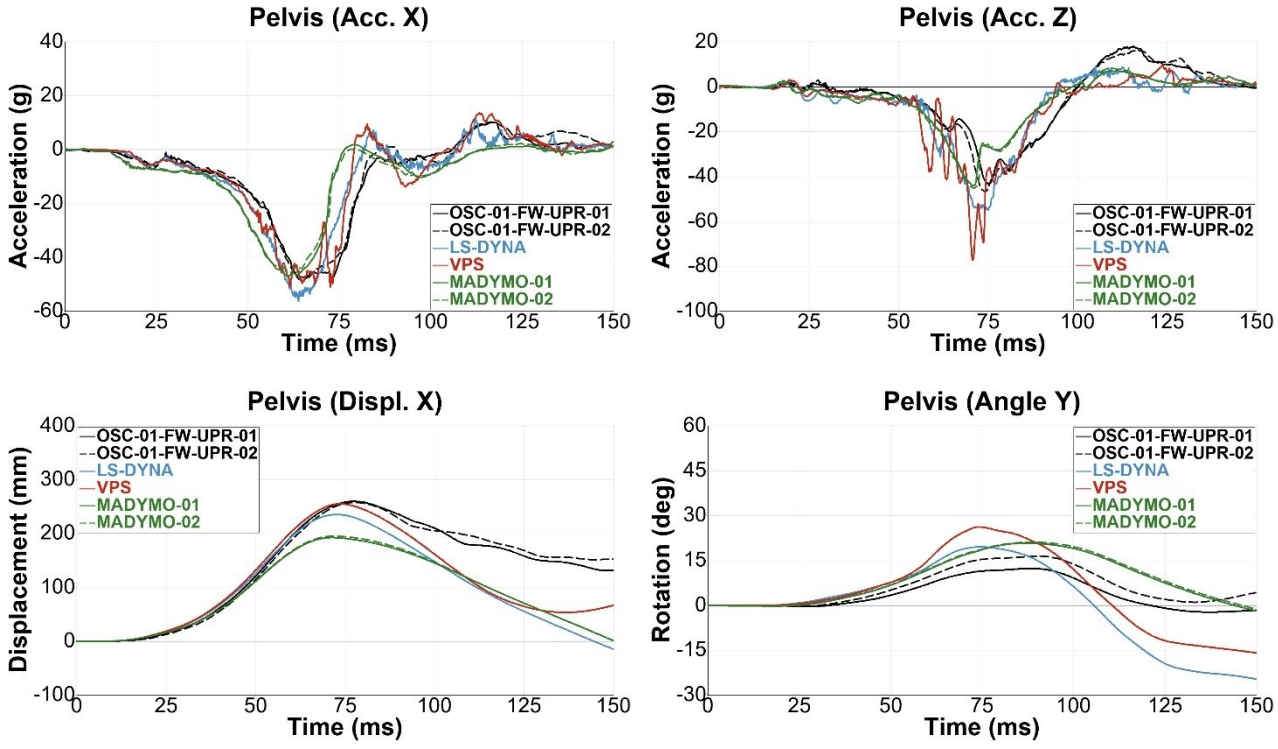

Figure 20 Pelvis accelerations, X-displacement and Y-angle

In all codes the peak displacement was sooner than in the experiment. As observed in the kinematics (Figure 17), pelvis rotation was overpredicted by LS-Dyna and VPS, furthermore, the pelvis rotated back into its initial position.

Compared to the sled tests, left and right ASIS forces were generally overpredicted while no submarining was observed (Figure 21). Left ASIS moments could not be modelled correctly in LS-Dyna due to the previously described poor pelvis-to-belt interaction. In Madymo, loading of both ASIS load cells (forces and moments) occurred earlier.

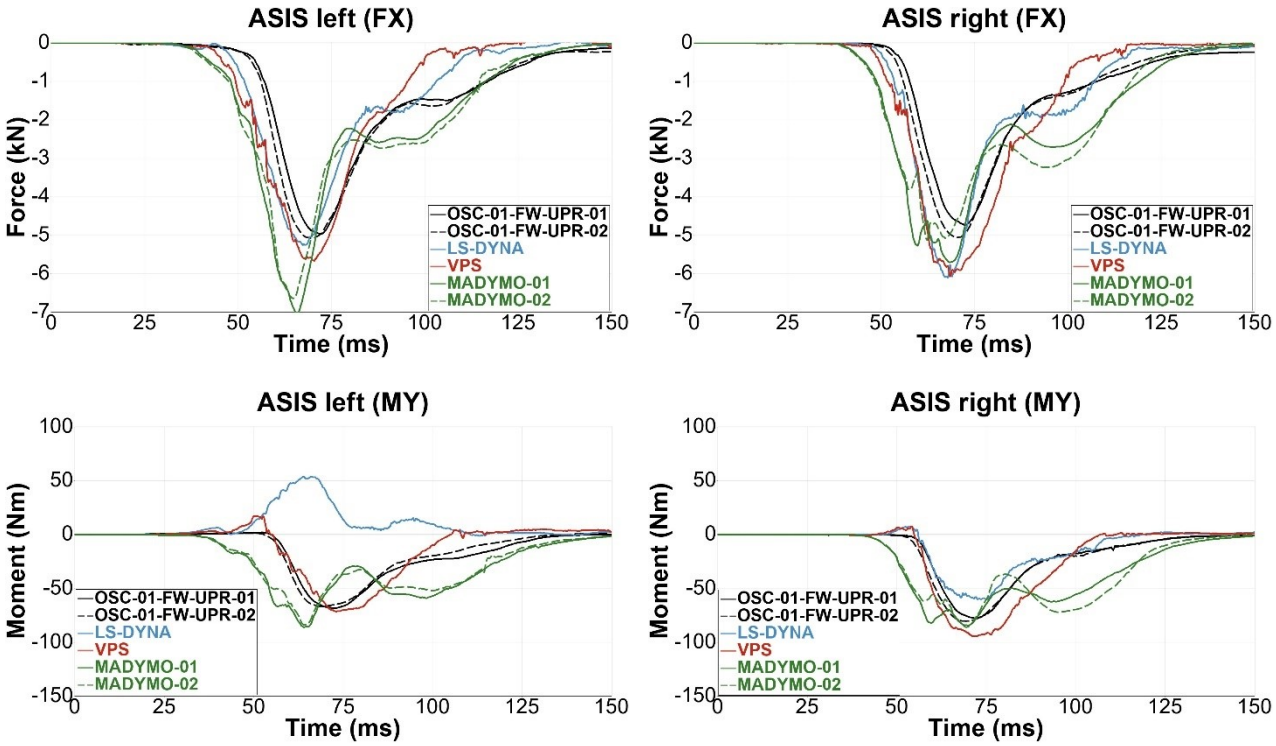

Figure 21 ASIS Fx and My

Although premature, lower thoracic spine (T12) x-accelerations were best predicted by Madymo, while larger oscillations in the signal were observed for LS-Dyna and VPS. Z-accelerations were overpredicted by LS-Dyna and VPS while the accelerations were underpredicted by Madymo. In all codes the peak accelerations were sooner than in the experiments. As observed in the kinematics (Figure 17), the increased forward rotation of the upper body results in greater y-moments for LS-Dyna and VPS. Lower thoracic spine forces could not be adequately replicated in all codes.

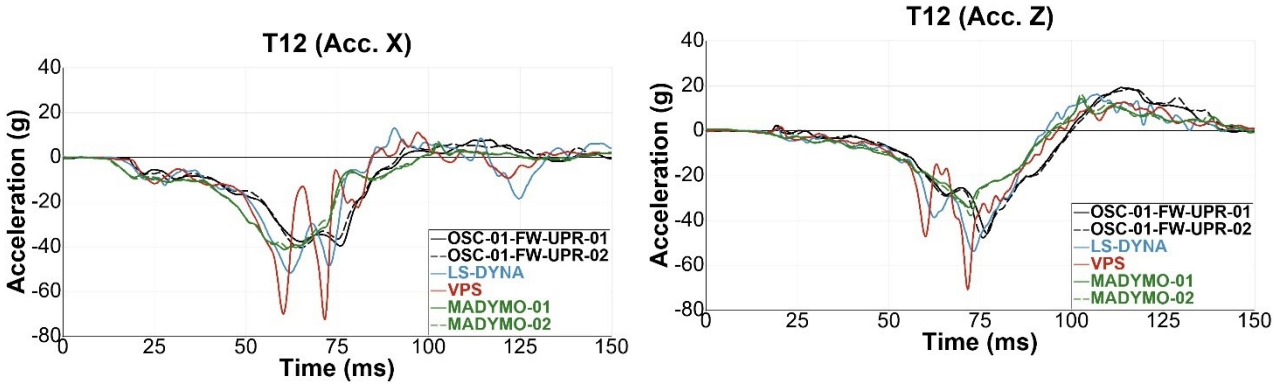

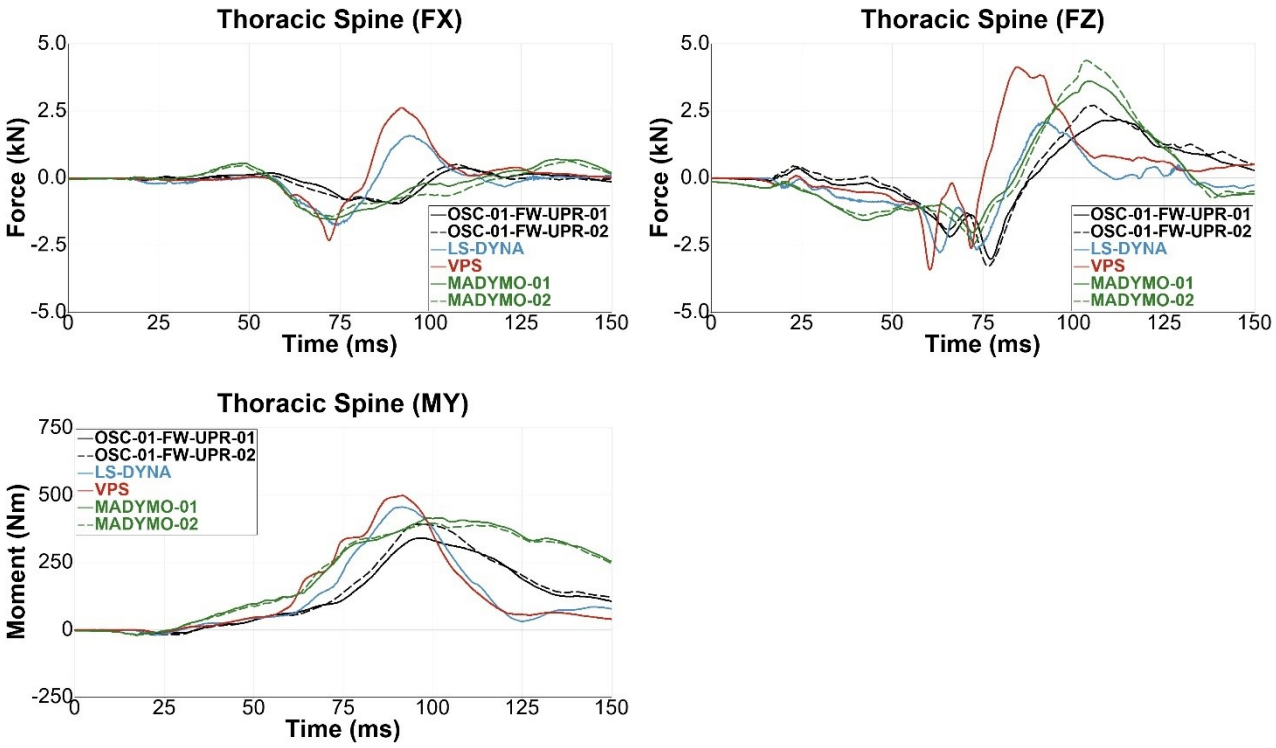

Figure 22 Lower thoracic spine accelerations & loadings

In all codes the forward displacement of the head was underpredicted (Figure 23; x-direction) while z-displacement was underpredicted by LS-Dyna and VPS and overpredicted by Madymo. Compared to experiments, peak displacements appeared earlier in the simulations. X-accelerations were well predicted by Madymo while z-acceleration were best replicated in LS-Dyna.

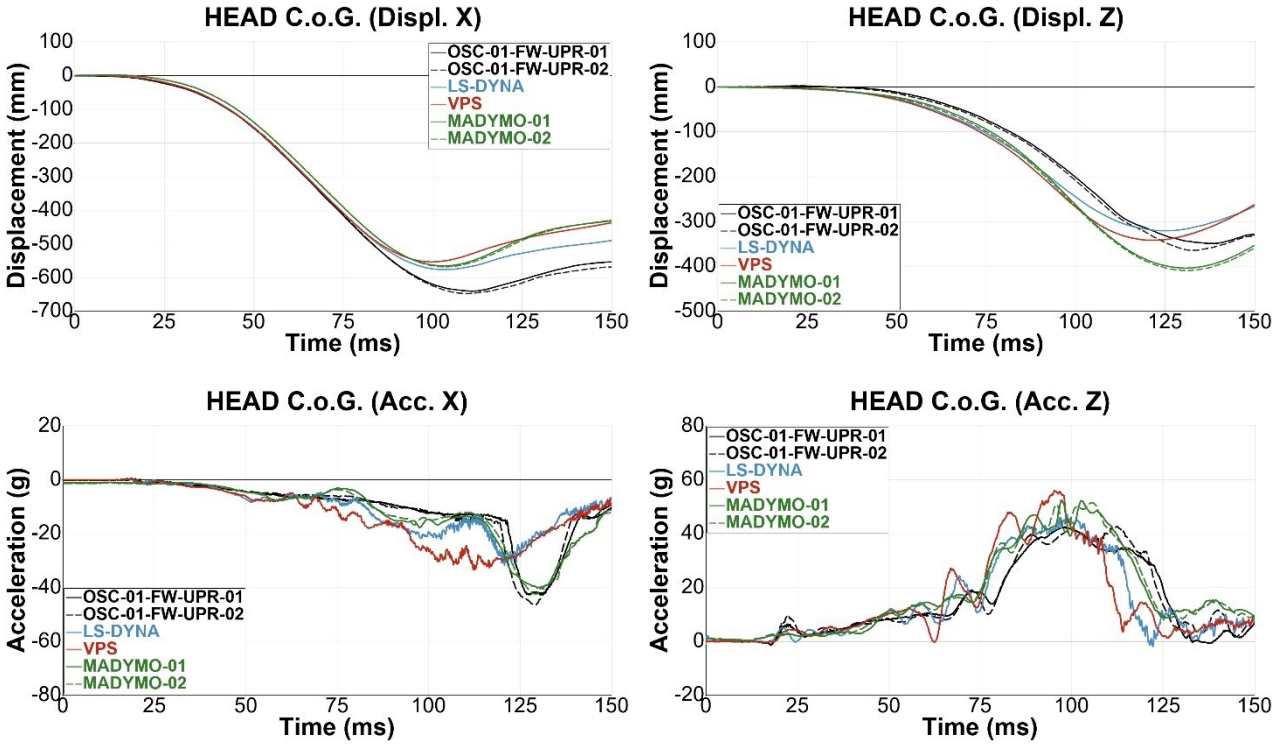

Figure 23 Head COG displacements and accelerations

Table 3 summarises the CORA ratings with the averaged (LS-Dyna and VPS) or individual (Madymo) test data as reference. Ratings are coloured in accordance to the sliding scale from ISO 18571 (excellent = green; good = white; fair = yellow; poor = red). The best correlation was observed for LS-Dyna. Thereby, especially the comparison to the environment (seat displacements, belt forces) was good, while lower thoracic spine forces, pelvis rotation and left iliac forces did not correlate well. The latter two could be explained by the belt-to-pelvis interaction and especially the missing bending stiffness of the belt, while differences in the lower thoracic spine forces were likely caused by the dummy modelling. For VPS and in particular Madymo, the correlation to the environment was worse, while the results for the dummy are generally comparable. Most noticeable here was the underpredicted belt pay-out which likely affected other results. As for LS-Dyna, lower thoracic spine forces did not correlate well in VPS and Madymo.

Channel	Virtual Demonstrator			
	LS-DYNA	VPS	MADYMO-01	MADYMO-02
Seat Pan (Displ. Z)	0.880	0.882	0.788	0.808
Anti-Submarining Ramp (Displ. X)	0.811	0.835	0.825	0.828
Upper Diag. Belt Force (B3)	0.909	0.806	0.769	0.777
Lower Diag. Belt Force (B4)	0.819	0.763	0.717	0.669
Lap-Belt outside Force (B6)	0.932	0.864	0.801	0.837
Belt Pay-In/-Out	0.822	0.675	0.376	0.449
Head COG (Acc. X)	0.774	0.692	0.914	0.947
Head COG (Acc. Z)	0.850	0.751	0.778	0.835
Head COG (Displ. X)	0.933	0.877	0.885	0.878
Head COG (Displ. Z)	0.932	0.904	0.866	0.883
T4 (Acc. X)	0.731	0.659	0.821	0.827
T4 (Acc. Z)	0.790	0.798	0.723	0.721
T12 (Acc. X)	0.738	0.684	0.815	0.822
T12 (Acc. Z)	0.818	0.799	0.782	0.778
T12 (Fo. X)	0.421	0.410	0.428	0.406
T12 (Fo. Z)	0.466	0.465	0.499	0.521
T12 (Mo. Y)	0.729	0.626	0.602	0.672
Pelvis (Acc. X)	0.899	0.902	0.758	0.744
Pelvis (Acc. Z)	0.741	0.715	0.711	0.737
Pelvis (Displ. X)	0.693	0.766	0.671	0.665
Pelvis (Ang. Y)	0.363	0.457	0.496	0.683
ASIS left (Fo. X)	0.877	0.817	0.756	0.788
ASIS right (Fo. X)	0.886	0.828	0.728	0.746
ASIS left (Mo. Y)	0.455	0.815	0.566	0.579
ASIS right (Mo. Y)	0.863	0.818	0.631	0.637
Environment	**0.862**	**0.804**	**0.713**	**0.728**
Dummy	**0.735**	**0.725**	**0.707**	**0.730**
Total	**0.765**	**0.744**	**0.708**	**0.729**

Table 3 Summary of CORA ratings for the upright seating position with SOTA belt

3.1.4.3 Model Validation – SOTA Belt in Reclined Seating Position

Figure 24 compares the validated demonstrators in the reclined seating position with SOTA belt. Thereby, a similar forward rotation of the torso and bending of the upper thorax could be observed for LS-Dyna. For VPS and MAYDMO, rotation of the upper thorax appeared to be greater. Compared to the experiments, the pelvis forward displacement was smaller in all codes, with VPS being closest to the tests. Furthermore, an increased upwards rotation of the pelvis could be observed for VPS.

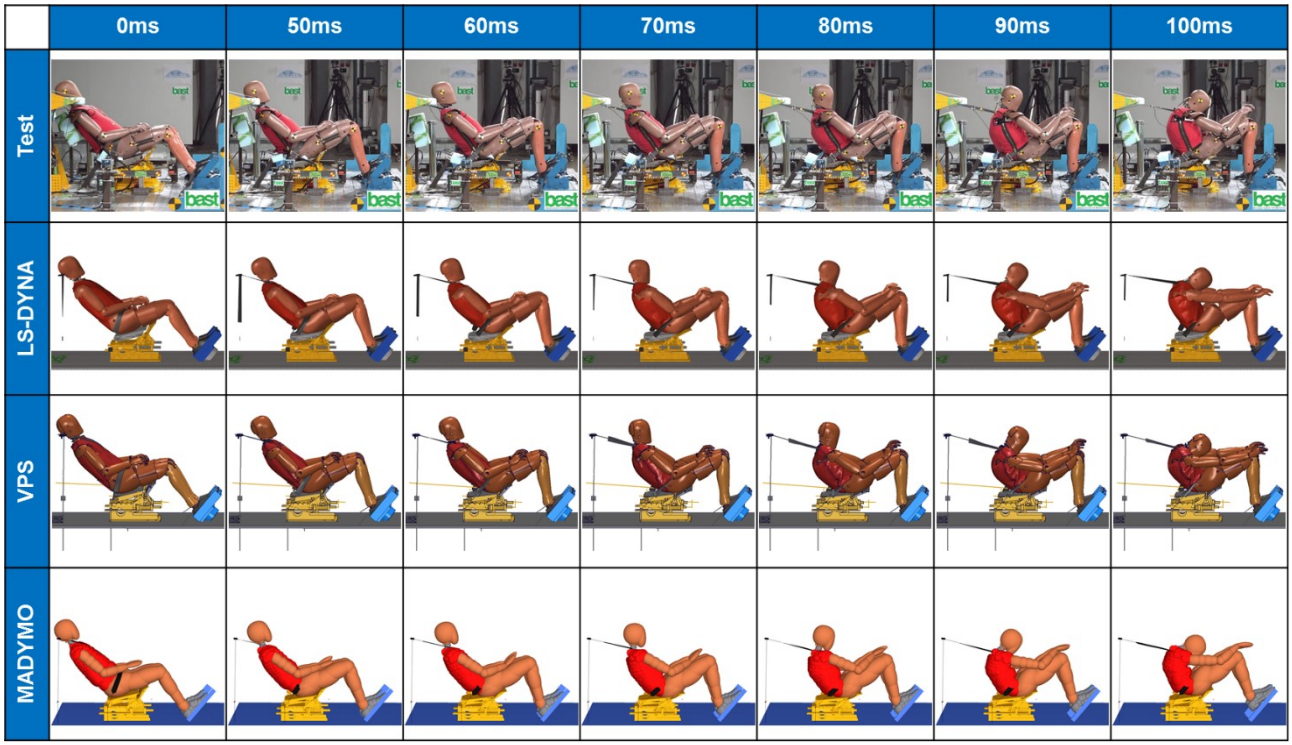

Figure 24 Comparison of dummy kinematics for the reclined seating position with SOTA belt

Seat pan displacements were underpredicted by LS-Dyna and VPS (Figure 25) while displacements in Madymo were overpredicted and premature. Displacements of the anti-submarining ramp were well replicated in LS-Dyna and VPS while Madymo underpredicted the displacements.

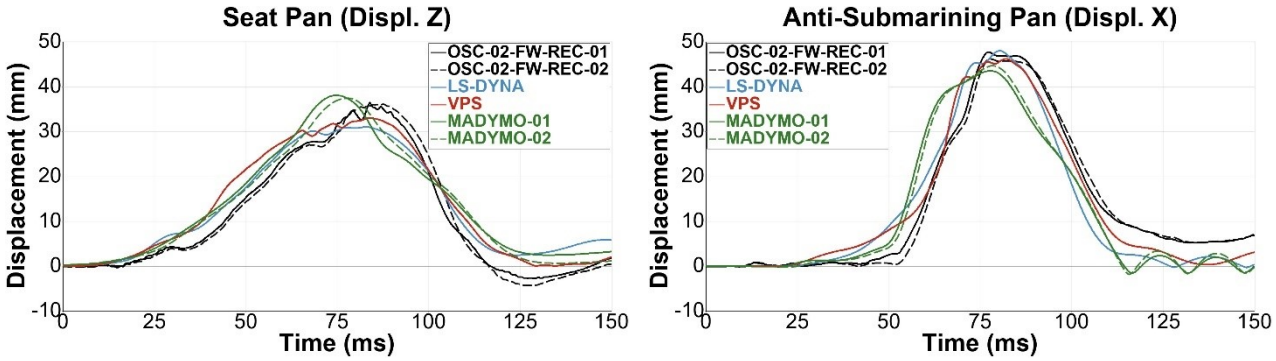

Figure 25 Seat pan and anti-submarining ramp displacements

The increasing shoulder belt force (B3) could only be simulated in VPS, while the belt forces remained at a constant level in LS-Dyna and Madymo (Figure 26). In contrast, the B3 belt forces in VPS and LS-Dyna drop too early. Belt forces at the diagonal belt near the buckle (B4) could be well

replicated in Madymo and LS-Dyna. Lap belt forces (B6) were well predicted by LS-Dyna and VPS, while the lap belt loading was overestimated in Madymo. Belt pay-in was well replicated for Madymo, while the belt pay-out could only be reproduced by LS-Dyna.

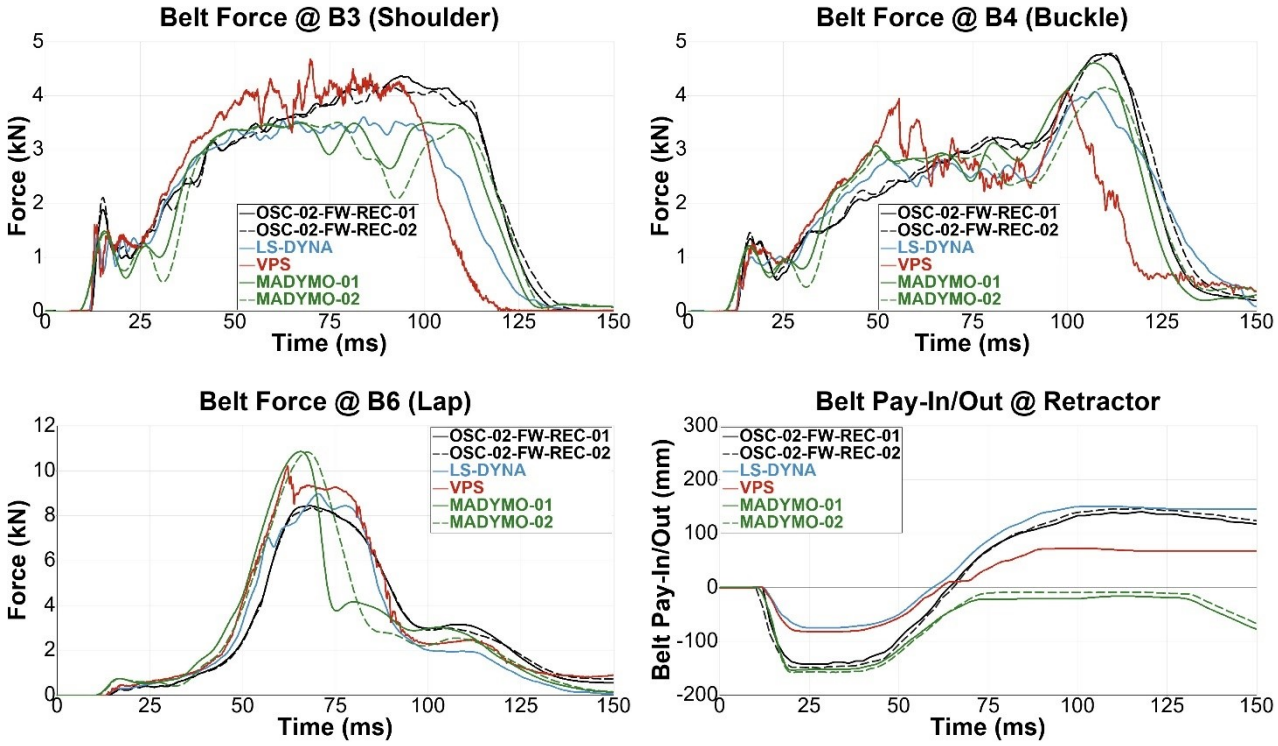

Figure 26 Seat belt forces and pay-in/out

Pelvis accelerations in LS-Dyna and VPS were quite noisy while acceleration in Madymo were overpredicted and premature. Consequently, pelvis accelerations could not be adequately replicated in all codes. No test data was available for the pelvis forward displacement due to technical limitations (Figure 27). However, from the kinematics (Figure 24), a greater forward displacement in the experiments could be assumed, whereby all codes underestimated the displacement. Rotation of the pelvis was well predicted by LS-Dyna and Madymo while VPS overpredicted the pelvis rotation.

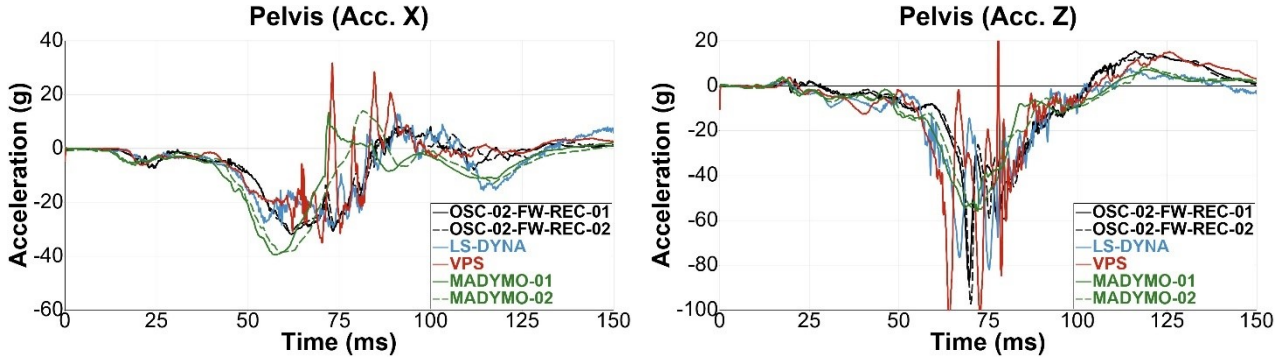

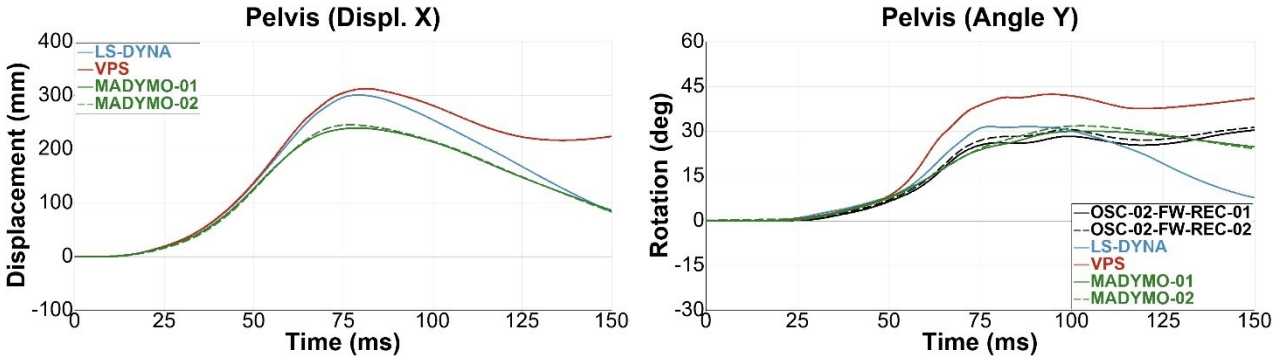

Figure 27 Pelvis accelerations, X-displacement and Y-angle

For LS-Dyna and VPS submarining was observed on the left ASIS (Figure 28) which could be explained by the previously described insufficient submarining behaviour of the FE models. No submarining was observed for Madymo. For the right ASIS no submarining was observed in all three codes while ASIS forces were generally overpredicted. ASIS moments could not be modelled correctly. Due to the previously described deviation between the three codes and the tests, the CORA rating was poor (except for the right ASIS).

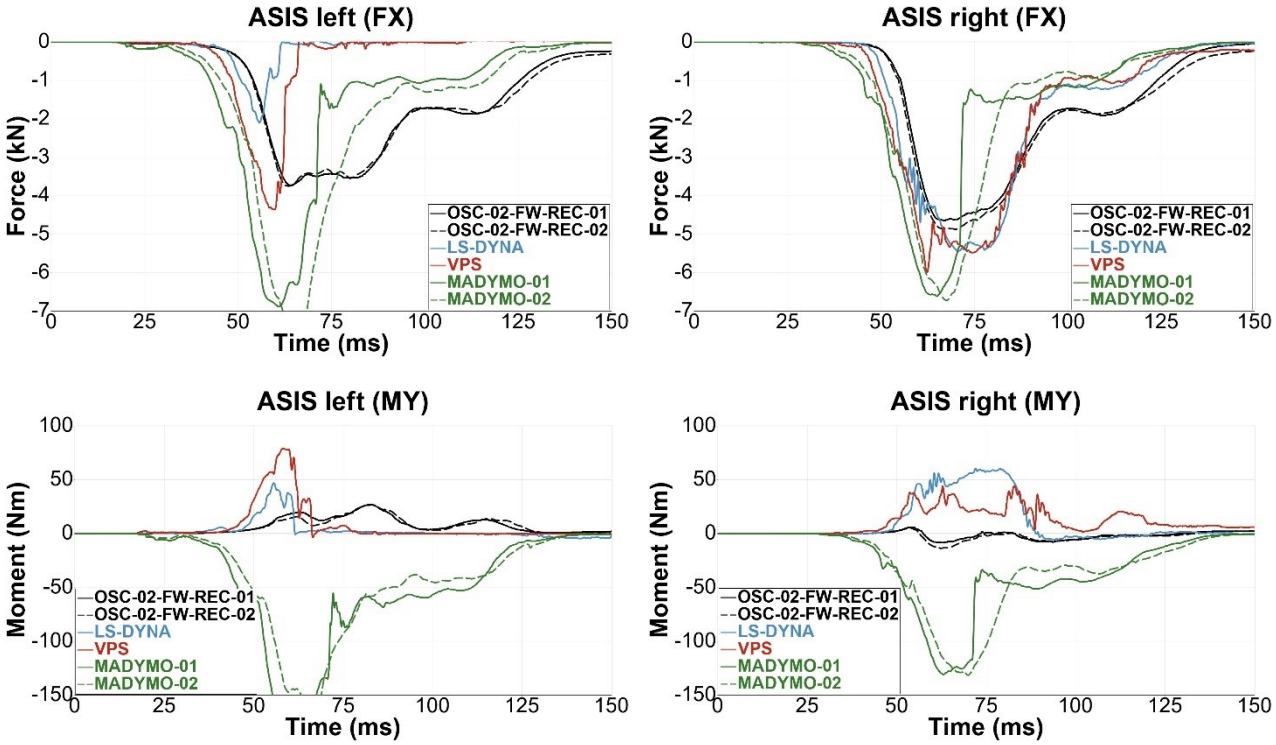

Figure 28 ASIS forces and moments

For LS-Dyna and VPS a lot of noise was observed in the lower thoracic spine (T12) accelerations (Figure 29). Regardless of the noise, the z-acceleration could be simulated well, while the x-accelerations could not be adequately replicated. As observed in the kinematics (Figure 24), the upper body bent more forwards in VPS and Madymo resulting in greater y-moments (Figure 29). Lower thoracic spine x-forces cannot be adequately replicated in all three codes, while z-forces were well predicted in Madymo.

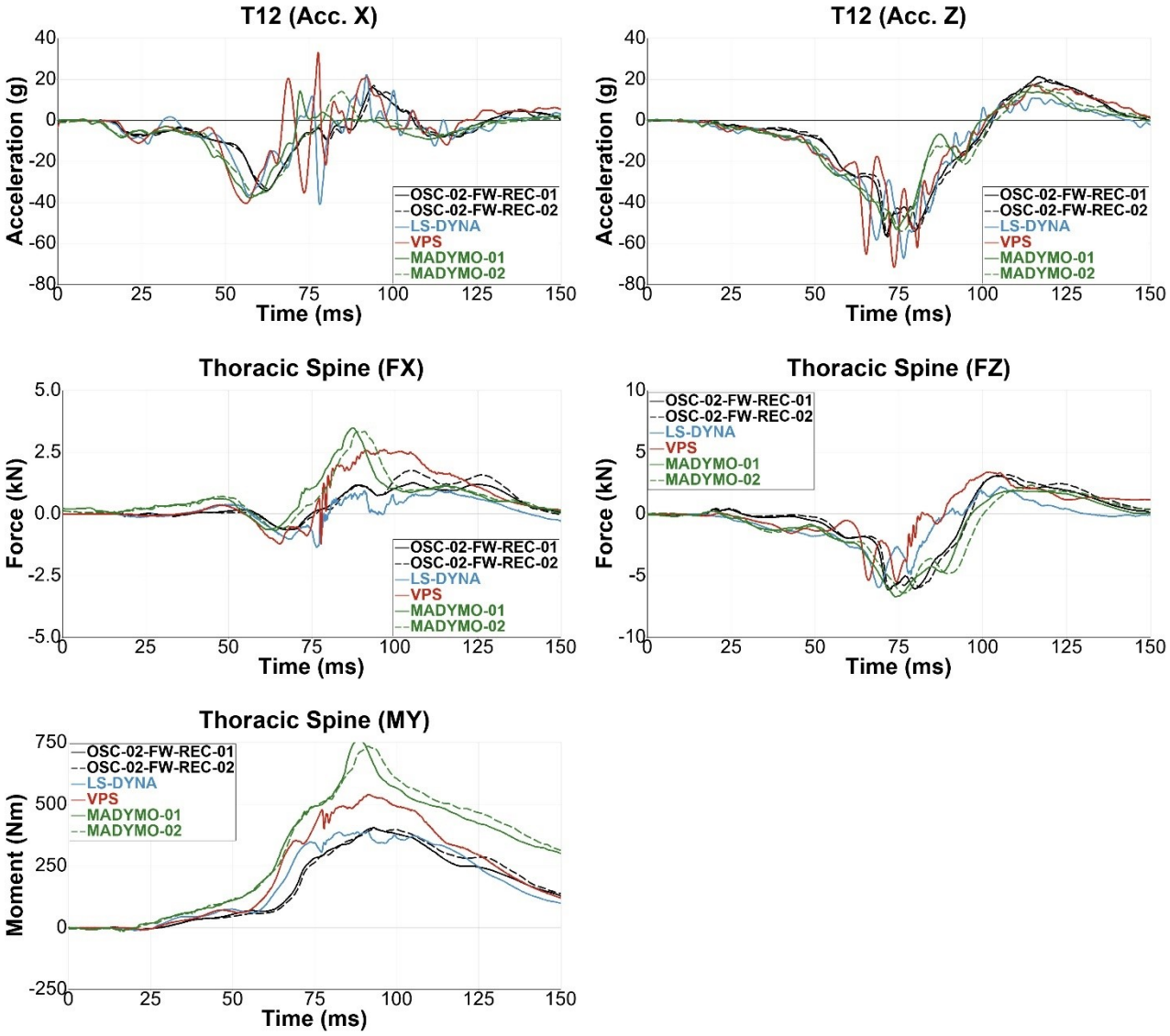

Figure 29 Lower thoracic spine (T12) accelerations & loadings

Head forward displacement (Figure 30; x-direction) was underpredicted by all codes while z-displacements were overpredicted in Madymo and VPS. Head accelerations were best replicated in Madymo, while especially in VPS the accelerations could not be predicted sufficiently.

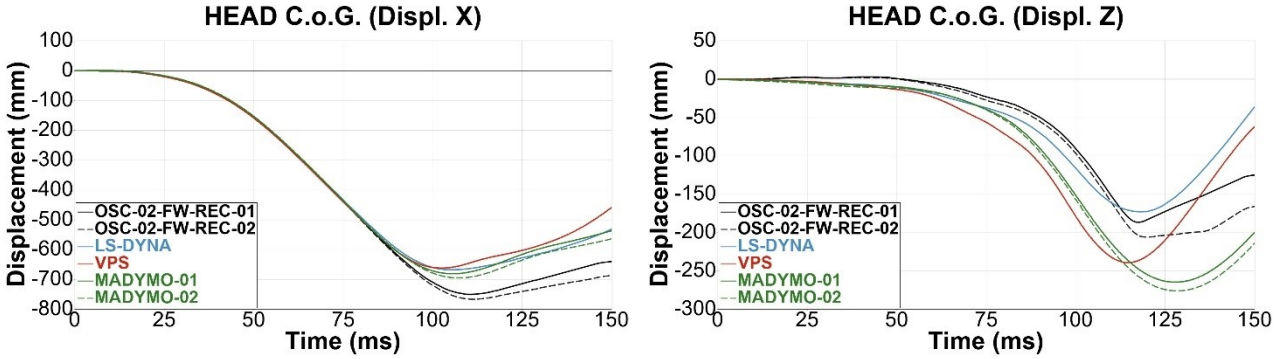

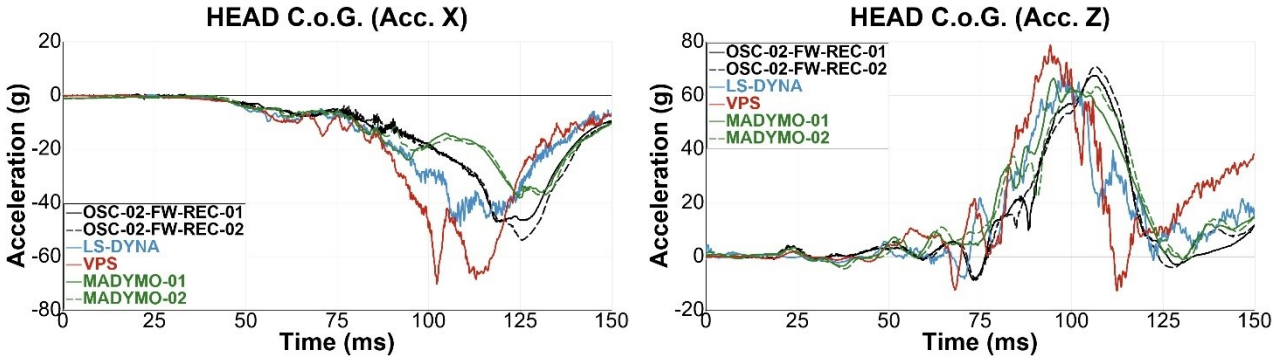

Figure 30 Head COG displacements and accelerations

Table 4 summarises the CORA ratings with the averaged (LS-Dyna and VPS) or individual (Madymo) test data as reference.

Channel	Virtual Demonstrator			
	LS-DYNA	VPS	MADYMO-01	MADYMO-02
Seat Pan (Displ. Z)	0.875	0.877	0.822	0.841
Anti-Submarin. Ramp (Displ. X)	0.872	0.924	0.825	0.823
Upper Diag. Belt Force (B3)	0.827	0.786	0.848	0.826
Lower Diag. Belt Force (B4)	0.902	0.750	0.931	0.895
Lap-Belt outside Force (B6)	0.920	0.893	0.805	0.835
Belt Pay-In/-Out	0.693	0.515	0.364	0.378
Head COG (Acc. X)	0.830	0.663	0.841	0.850
Head COG (Acc. Z)	0.777	0.615	0.873	0.890
Head COG (Displ. X)	0.921	0.890	0.928	0.921
Head COG (Displ. Z)	0.838	0.732	0.717	0.764
T4 (Acc. X)	0.771	0.631	0.660	0.701
T4 (Acc. Z)	0.827	0.845	0.823	0.857
T12 (Acc. X)	0.709	0.596	0.691	0.723
T12 (Acc. Z)	0.847	0.859	0.845	0.859
T12 (Fo. X)	0.552	0.613	0.463	0.502
T12 (Fo. Z)	0.575	0.612	0.819	0.763
T12 (Mo. Y)	0.906	0.771	0.576	0.572
Pelvis (Acc. X)	0.776	0.717	0.581	0.617
Pelvis (Acc. Z)	0.820	0.724	0.818	0.817
Pelvis (Displ. X)	*x*	*x*	*x*	*x*
Pelvis (Ang. Y)	0.794	0.648	0.956	0.959
ASIS left (Fo. X)	0.358	0.389	0.519	0.610
ASIS right (Fo. X)	0.868	0.818	0.639	0.694
ASIS left (Mo. Y)	0.476	0.431	0.267	0.278
ASIS right (Mo. Y)	0.409	0.275	0.272	0.318
Environment	**0.848**	**0.791**	**0.766**	**0.766**
Dummy	**0.725**	**0.657**	**0.683**	**0.705**
Total	**0.756**	**0.691**	**0.703**	**0.721**

Table 4 Summary of CORA ratings for the reclined seating position with SOTA belt

Ratings are coloured in accordance to the sliding scale from ISO 18571 (excellent = green; good = white; fair = yellow; poor = red). The best correlation was again observed for LS-Dyna. Thereby, especially the comparison to the environment (seat displacements, belt forces) was good, while the missing bending stiffness of the belt results in a poor pelvis-to-belt interaction (submarining). Similar to the upright seating position, belt pay-out was underpredicted in VPS and Madymo likely affecting other results. As for LS-Dyna, the pelvis-to-belt interaction was poor for the two other codes. In addition, the missing bending stiffness of the belt causes submarining in VPS.

3.1.4.4 Model Validation – SOTA DLPT Belt in Reclined Seating Position

Figure 31 compares the simulation results of the reclined seating position with SOTA DLPT belt to the experimental data. Thereby, the simulations models seemed to be more flexible, especially for VPS and Madymo where an increased forward rotation of the upper body was observed. Furthermore, an increased pelvis upwards rotation could be observed for VPS while LS-Dyna likely underpredicts the pelvis rotation. Unlike in the experiments and LS-Dyna and VPS, the shoes slipped up the foot rest in Madymo.

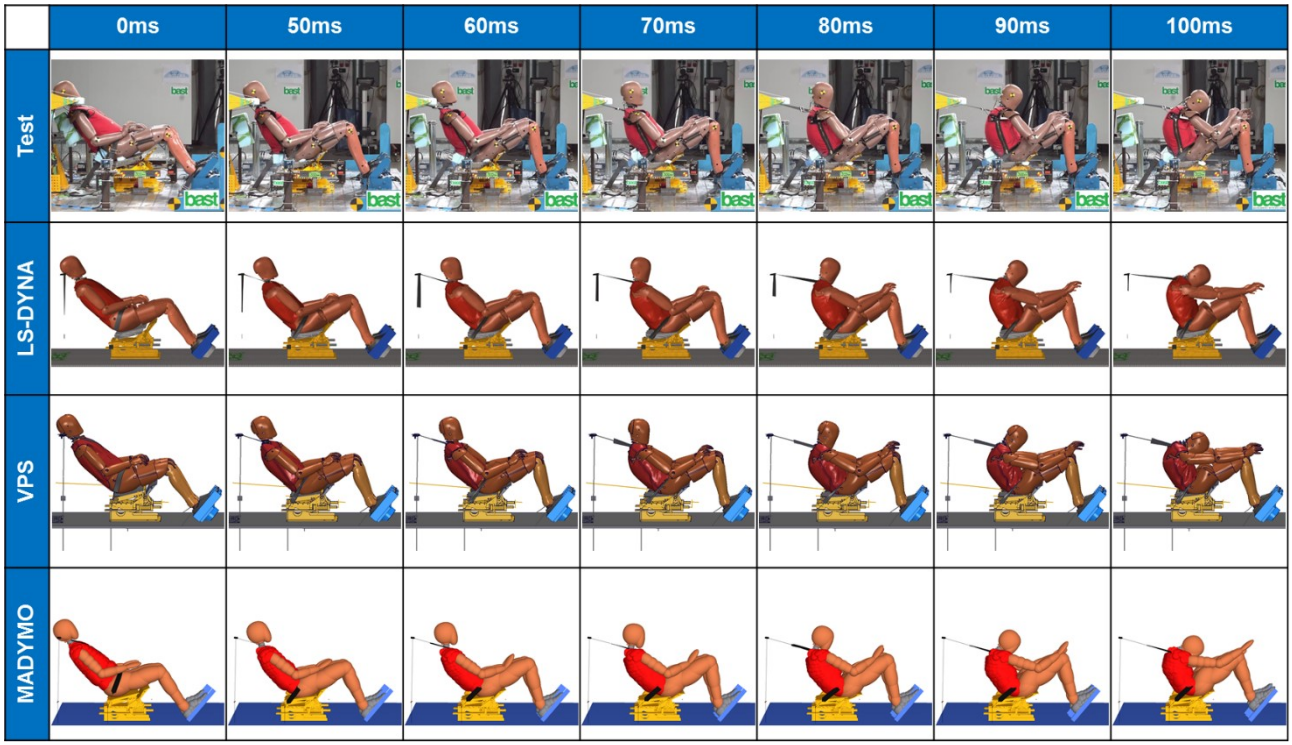

Figure 31 Comparison of dummy kinematics for reclined seating position with SOTA DLPT belt

Seat pan displacements were slightly underpredicted by all three codes while the rebound was modelled most accurately in VPS (Figure 32). Displacements of the anti-submarining ramp were overpredicted in Madymo while LS-Dyna and VPS underpredicted the anti-submarining ramp displacements.

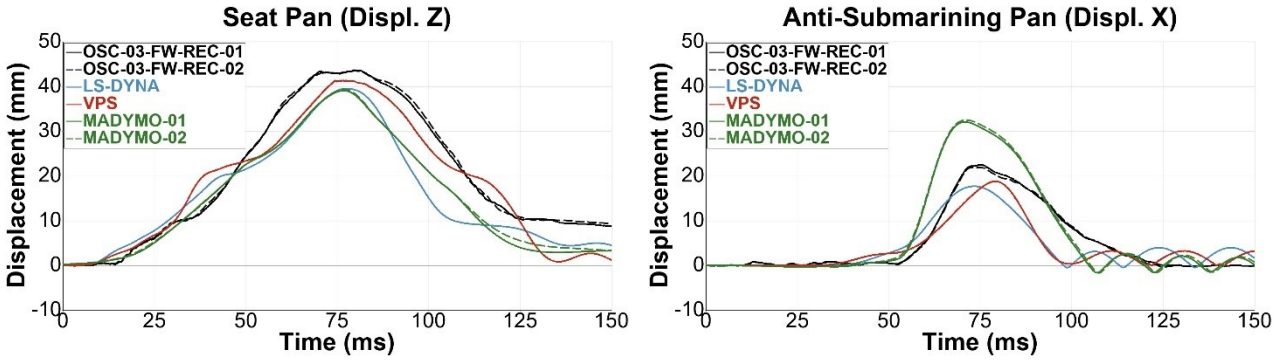

Figure 32 Seat pan & anti-submarining ramp displacements

Shoulder belt forces (B3) were well replicated in LS-Dyna and Madymo while in VPS the B3 belt force was overpredicted and loading reduced earlier (Figure 33). In all codes the experimental data from the B4 belt force (diagonal belt near buckle) could be well replicated until approx. 90 ms. The peak force at approx. 105 ms was only in LS-Dyna modelled correctly. Peak lap belt forces (B6) were generally overpredicted. Otherwise, a good correlation could be observed for LS-Dyna, while the lap belt loading appeared to be greater for VPS respectively smaller for Madymo. Belt pay-ins were well replicated for VPS and Madymo, while there was some deviation for LS-Dyna which could be likely explained by the not completely rigid D-ring mount (see Chapter 3.1.3.5). In contrast, the belt pay-out could only be reproduced well by LS-Dyna.

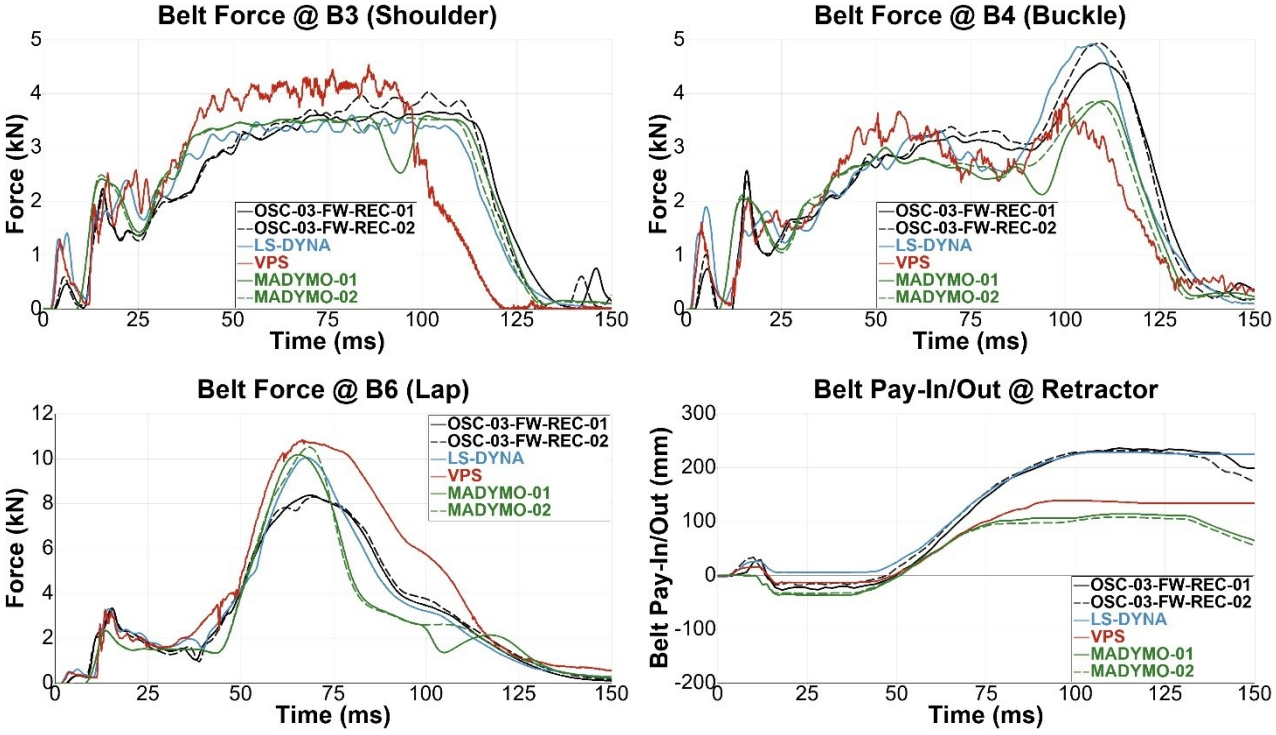

Figure 33 Seat belt forces & pay-in/out

In all codes the pelvis x-acceleration could only be reproduced insufficiently, while peak z-accelerations were generally overpredicted and slightly premature. Pelvis forward displacement was overpredicted by VPS while LS-Dyna and Madymo underpredicted the pelvis forward displacement. In all codes the peak displacement was sooner than in the experiment. As already observed in the comparison of the kinematics (Figure 31), pelvis rotation was overpredicted in VPS and underpredicted in LS-Dyna - in both cases the pelvis rotated more back into its initial position.

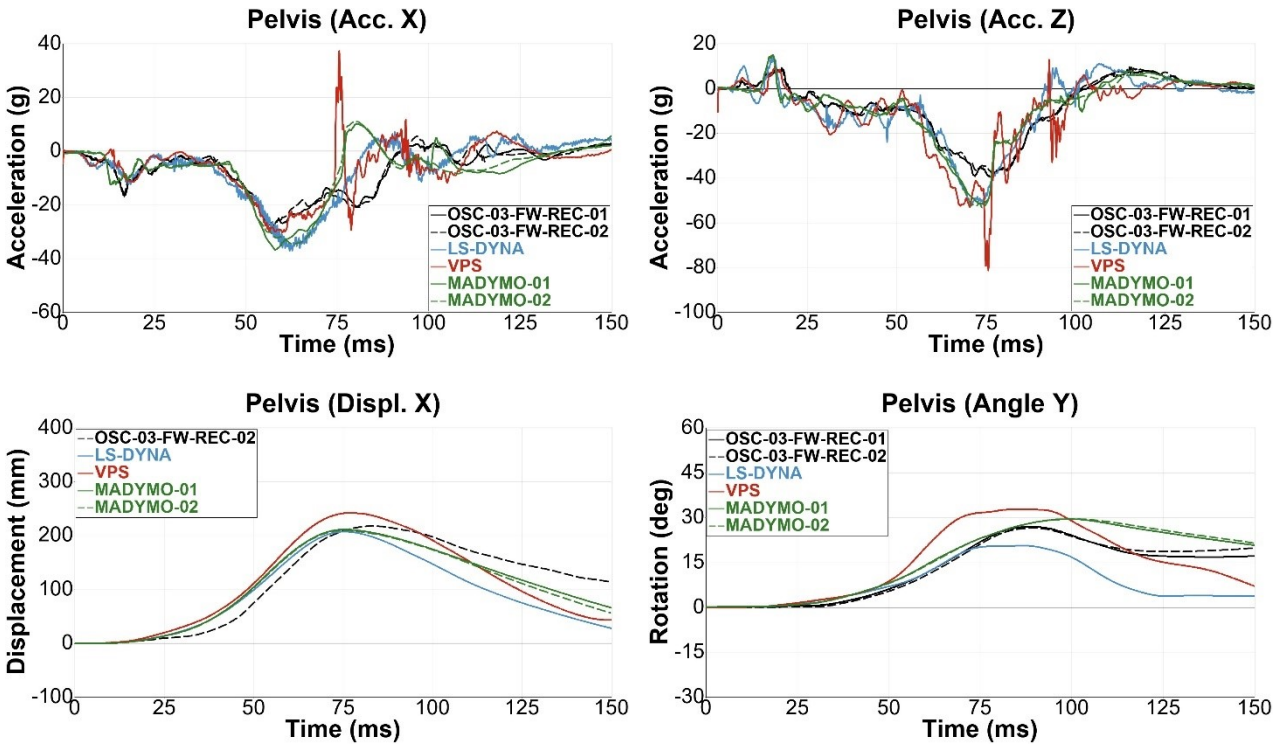

Figure 34 Pelvis accelerations, X-displacement & Y-angle

No submarining was observed in all three codes while left and right ASIS forces were slightly overpredicted (Figure 35). Left ASIS moments could not be modelled correctly in LS-Dyna and VPS due to the poor pelvis-to-belt interaction while Madymo overpredicted the left ASIS moments. On the right, ASIS moments of all three codes were comparable to the experimental data.

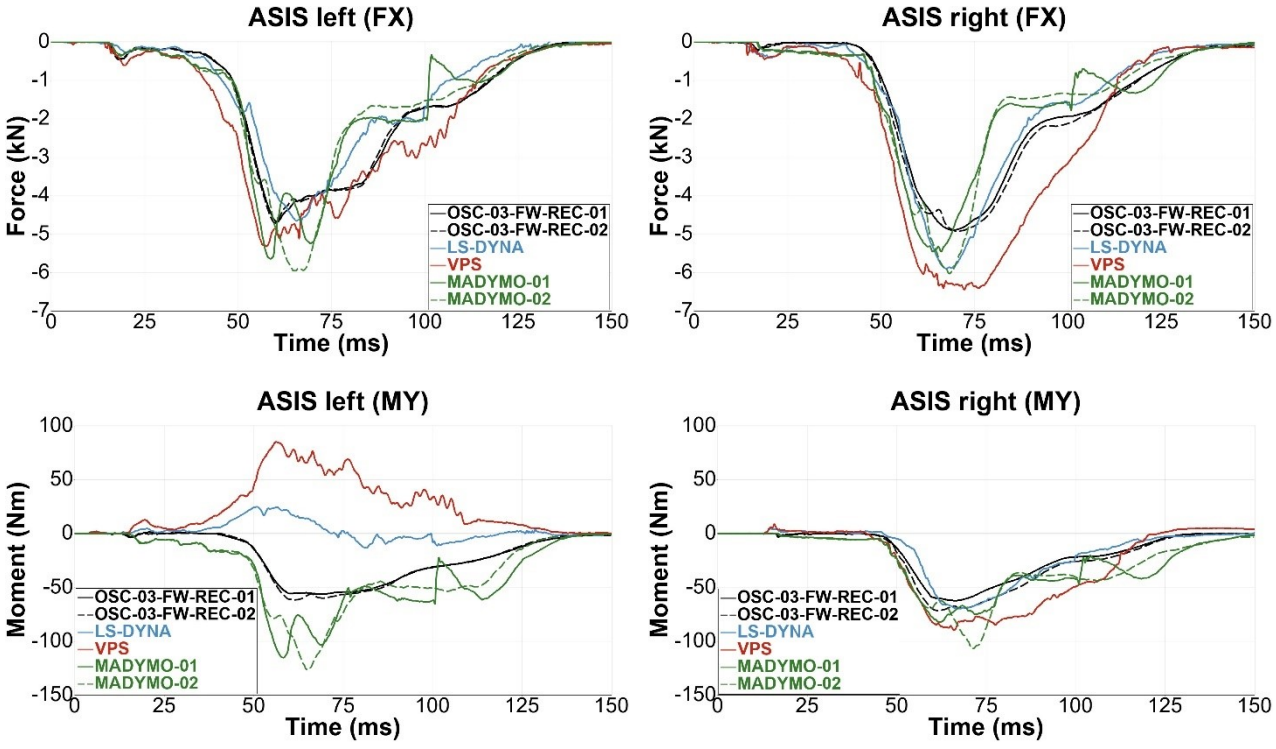

Figure 35 ASIS Fx & My with

For the lower thoracic spine (T12) accelerations some deviations could be observed, especially for the peak accelerations (Figure 36). As previously described, in VPS and Madymo the upper body bent more forwards (Figure 31) resulting in greater y-moments. Lower thoracic spine x-forces could not be adequately replicated in all three codes, while unloading in LS-Dyna was different for the z-forces.

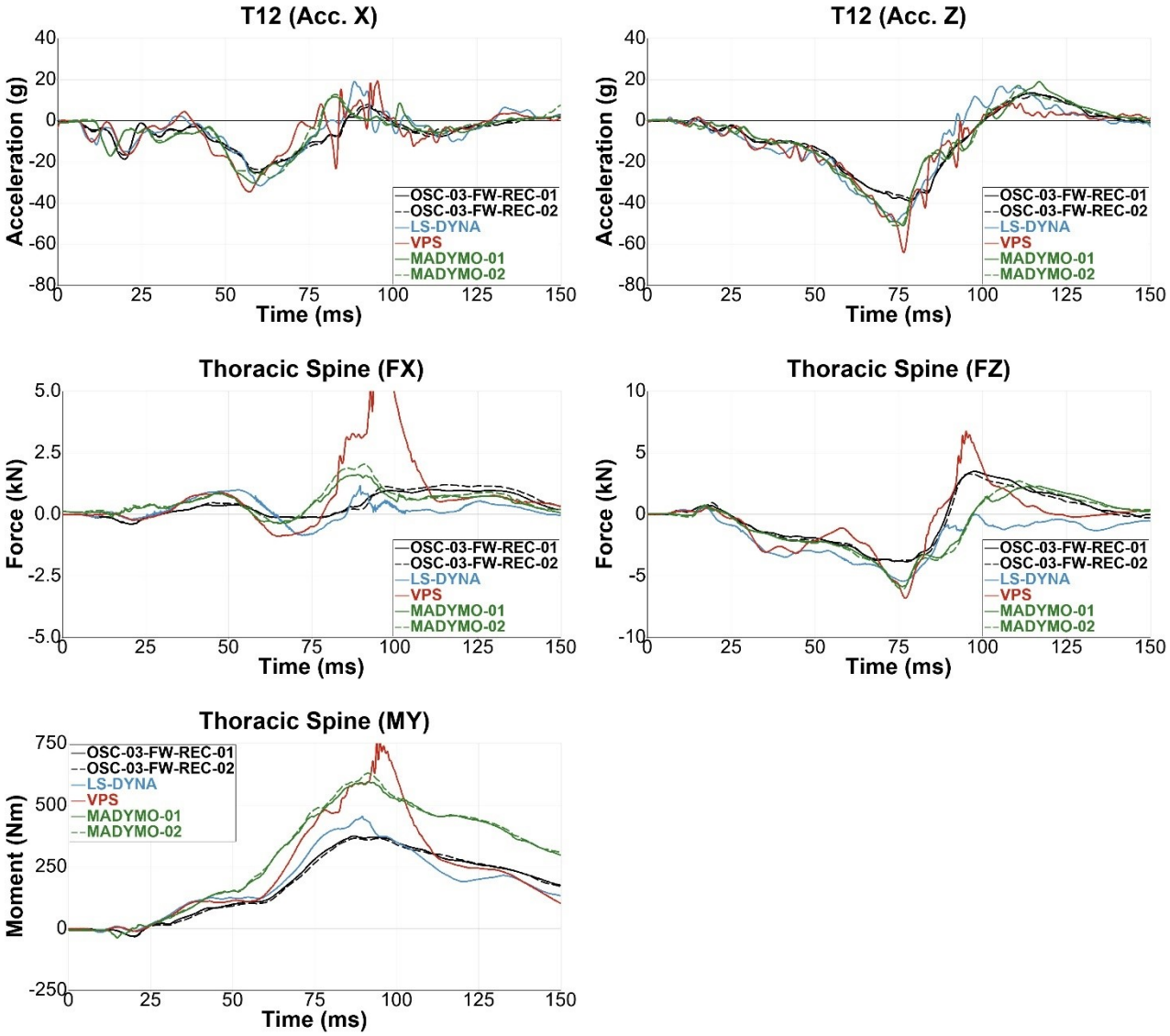

Figure 36 Lower thoracic spine (T12) accelerations & loadings

In all three codes the forward displacement of the head (Figure 37; x-direction) was underpredicted. Z-displacements of the head were overpredicted for Madymo and VPS while LS-Dyna tended to underpredict. Head accelerations were mainly caused by the inertia of the head, as there was no contact with other parts. Compared to experimental data, accelerations were well predicted by Madymo. Peak head accelerations in LS-Dyna and VPS occurred earlier with LS-Dyna underpredicting and VPS overpredicting the test data.

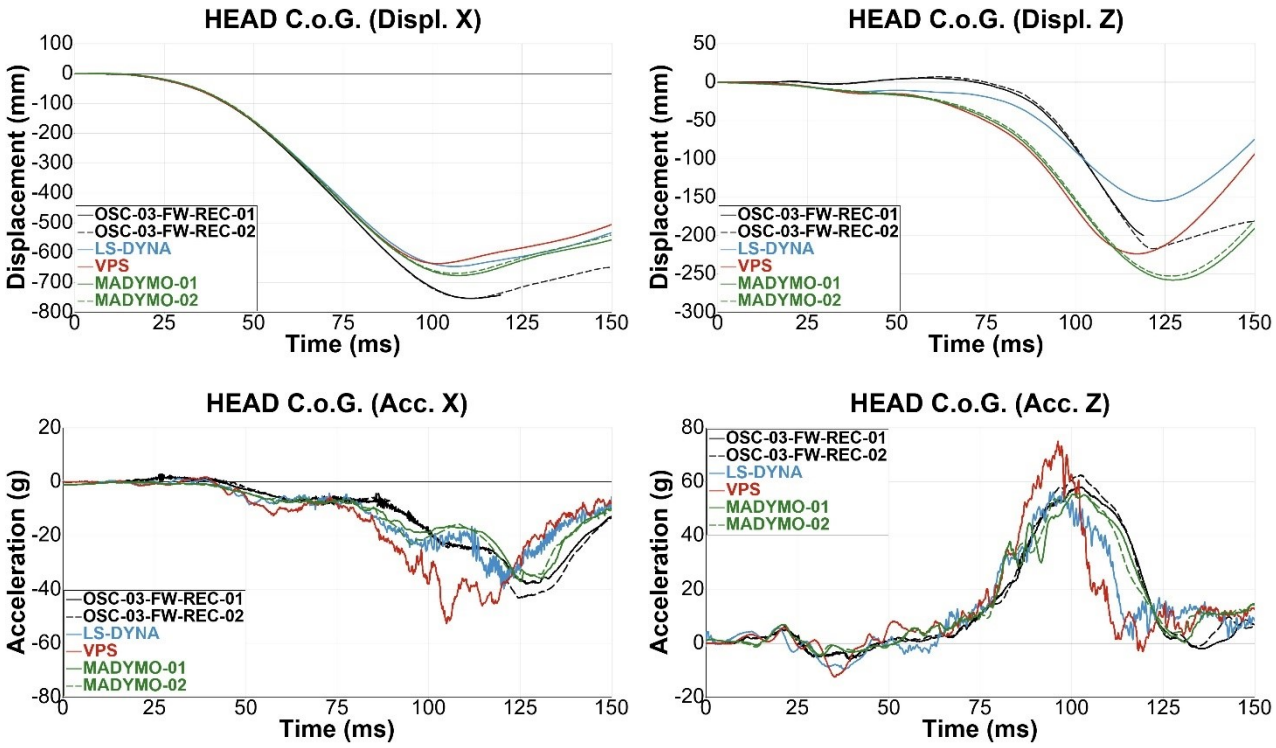

Figure 37 Head COG displacements & accelerations

For the homologation test case, correlation to the experiments was comparable for LS-Dyna and Madymo. The comparison to the environment (seat displacements, belt forces) was good for LS-Dyna, while results for the dummy were generally the best for Madymo. No submarining was observed in all codes while the missing bending stiffness of the belt affected the left iliac moments in LS-Dyna and VPS. In all codes, the lower thoracic spine x-forces did not correlate well. As noted previously, belt pay-out was underpredicted in VPS and Madymo likely affecting other results. Table 5 summarises the CORA ratings with the averaged (LS-Dyna and VPS) or individual (Madymo) test data as reference. Ratings are coloured in accordance to the sliding scale from ISO 18571 (excellent = green; good = white; fair = yellow; poor = red).

Channel	Virtual Demonstrator			
	LS-DYNA	VPS	MADYMO-01	MADYMO-02
Seat Pan (Displ. Z)	0.782	0.877	0.798	0.803
Anti-Submarining Ramp (Displ. X)	0.732	0.756	0.781	0.769
Upper Diag. Belt Force (B3)	0.889	0.702	0.898	0.907
Lower Diag. Belt Force (B4)	0.915	0.806	0.832	0.833
Lap-Belt outside Force (B6)	0.946	0.779	0.852	0.851
Belt Pay-In/-Out	0.960	0.687	0.622	0.593
Head COG (Acc. X)	0.809	0.643	0.898	0.849
Head COG (Acc. Z)	0.807	0.740	0.923	0.910
Head COG (Displ. X)	0.902	0.898	0.963	0.918
Head COG (Displ. Z)	0.794	0.667	0.683	0.751
T4 (Acc. X)	0.646	0.639	0.684	0.666
T4 (Acc. Z)	0.801	0.776	0.867	0.857

T12 (Acc. X)	0.717	0.646	0.729	0.712
T12 (Acc. Z)	0.811	0.820	0.873	0.872
T12 (Fo. X)	0.344	0.347	0.455	0.441
T12 (Fo. Z)	0.414	0.613	0.680	0.684
T12 (Mo. Y)	0.868	0.731	0.594	0.577
Pelvis (Acc. X)	0.657	0.673	0.620	0.601
Pelvis (Acc. Z)	0.774	0.693	0.827	0.794
Pelvis (Displ. X)	*x*	*x*	*x*	0.855
Pelvis (Ang. Y)	0.634	0.734	0.808	0.805
ASIS left (Fo. X)	0.882	0.867	0.869	0.863
ASIS right (Fo. X)	0.931	0.748	0.847	0.837
ASIS left (Mo. Y)	0.355	0.383	0.614	0.662
ASIS right (Mo. Y)	0.916	0.720	0.716	0.773
Environment	**0.871**	**0.768**	**0.797**	**0.793**
Dummy	**0.726**	**0.685**	**0.758**	**0.759**
Total	**0.762**	**0.706**	**0.768**	**0.767**

Table 5 Summary of CORA ratings for the reclined seating position with SOTA DLPT belt

3.1.4.5 Model Validation - Oblique Pulses

Differences between test data and simulation results were comparable between the oblique pulses and the full-frontal pulse. Thereby, problems already observed in the full-frontal load cases (e.g. reduced belt pay-out in Madymo, bad correlation of the left ASIS moments in LS-Dyna and VPS) were also noticed in the oblique load cases. However, for VPS prediction of belt pay-out improved.

Plots for the oblique pulses SCP1 and LTAP OD2 can be found in Appendix A1.2.6.

3.1.4.6 Virtual Demonstrator Summary and Limitations

For the virtual homologation demonstrator simulation models in different numerical codes (LS-Dyna, VPS and Madymo) were developed. In doing so, the physical demonstrator was replicated as closely as possible. For VPS and Madymo some code-specific modifications to the models were necessary. Using the CORA rating, the level of validation was assessed for the virtual homologation demonstrator. Thereby, the simulation models were considered to be sufficiently validated. The dummy version used and the missing bending stiffness of the belt resulted in insufficient submarining behaviour in LS-Dyna and VPS, especially in the reclined seating position with SOTA belt. Also, the iliac forces and moments were significantly influenced by this. Another limitation of the virtual demonstrator was the underestimation of belt pay-out in VPS and Madymo, which probably influenced any subsequent results. Necessary adjustments were not possible at the time, since all codes partly used encrypted models (e.g. dummies and restraint systems) whose properties could not be changed beyond some pre-defined, accessible parameters. Since updates addressing these limitations were unlikely to be released at the time, the simulation models were considered to be sufficiently validated for both seating positions and restraint systems.

3.1.5 Physical Demonstrator - Second Test Series Results

The primary objective for the second test series was to provide supplementary data to evaluate the validation methodology proposed by OSCCAR WP5, while considering improvements of the test

set-up resulting from limitations of the first test series. The proposed methodology required test data to calibrate the vehicle environment model as well as another consistent test set-up in another test loop to confirm the validation of the environment model. Furthermore, OSCCAR Deliverable D5.1 [8] identified three possible sources of scatter for validation of the vehicle environment (scatter in test execution, validation device and vehicle components). Therefore, another objective of the second test loop was to investigate the influence of scatter in the homologation demonstrator. Finally, the possibility to use a Hybrid III ATD as alternative validation device was investigated.

3.1.5.1 Test Matrix

For the second test series a revised mechanical design of the semi-rigid seat was used (see Chapter 3.1.2.1). Furthermore, limitations noted in the first test series (see Chapter 3.1.3.5) were corrected by equipping the dummy with cotton trousers and moving the belt tower between the upright and reclined seating position to limit the lever and thus minimising oscillation of the D-ring mounting bracket.

Using the THOR-50M ATD, two test configurations from the first test series were repeated to provide updated data for environment model calibration and scatter investigation. An additional configuration with a Hybrid III ATD in the reclined seating position was conducted. Eventually, three different configurations and a total of eight tests were performed in the second test series (Table 6). For scatter investigation one configuration was repeated four times in total, while the remaining configurations were repeated once.

#	Test No.	Pulse	Dummy	Position	Restraint System	Comment
1	OSC-01-FW-UPR-03	LAB 50 km/h	THOR-50M	Upright	SOTA belt	-
2	OSC-01-FW-UPR-04	LAB 50 km/h	THOR-50M	Upright	SOTA belt	Repetition
3	OSC-03-FW-REC-03	LAB 50 km/h	THOR-50M	Reclined	SOTA DLPT belt	-
4	OSC-03-FW-REC-04	LAB 50 km/h	THOR-50M	Reclined	SOTA DLPT belt	Repetition
5	OSC-03-FW-REC-05	LAB 50 km/h	THOR-50M	Reclined	SOTA DLPT belt	Repetition
6	OSC-03-FW-REC-06	LAB 50 km/h	THOR-50M	Reclined	SOTA DLPT belt	Repetition
7	OSC-10-FW-REC-01	LAB 50 km/h	Hybrid III	Reclined	SOTA DLPT belt	-
8	OSC-10-FW-REC-02	LAB 50 km/h	Hybrid III	Reclined	SOTA DLPT belt	Repetition

Table 6 Test matrix for the second test series

3.1.5.2 Comparison to the First Test Series

A comparison of the configurations “SOTA belt in upright seating position” and “SOTA DLPT belt in reclined seating position” was made between the second and the first test series, with the purpose to understand the influence of the test setup differences between the two test series.

SOTA belt in Upright Seating Position

Figure 38 shows seat pan and anti-submarining ramp displacements for the SOTA belt in the upright seating position, comparing the first (blue) and second (red) test series. The seat pan displacements were comparable between both test series until the damper used in the second test series prevented the rebound of the seat pan (starting at approx. 90 ms). The increased upwards rotation of the pelvis in the second test series results in a later contact with the anti-submarining ramp and hence less displacement compared to the first test series. As for the seat pan, the effect of the anti-rebound device (dampers) was clearly recognisable. Diagonal belt forces (B3 and B4) were similar, however, the earlier rebound of the dummy in the second test series resulted in an earlier decrease of these belt forces. Due to the reduced friction in the second test series the lap belt forces (B6) peaked earlier, while the peak loads were about equal. Belt pay-in of the shoulder retractor was overall comparable, while the belt pay-out was slightly larger in the second test series.

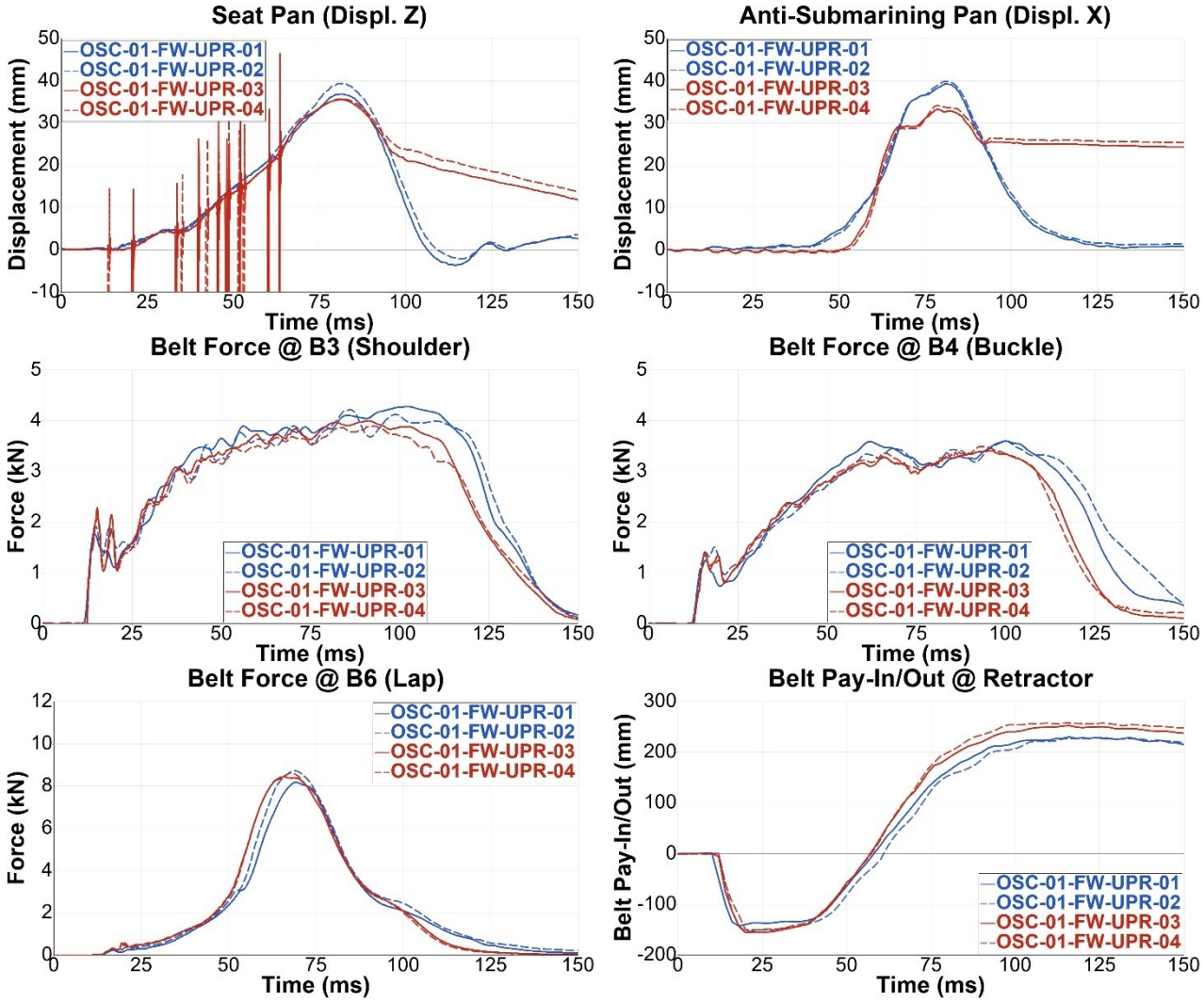

Figure 38 Seat displacements, belt forces & shoulder retractor belt pay-in/-out, comparing 1st (blue) & 2nd (red) test series

For the dummy, differences were mainly observed for the pelvis rotation and ASIS forces and moments. Thereby, the reduced friction in the second test series in combination with the prevented rebound of the seat pan resulted in an increased pelvis backward rotation (Figure 39), which influenced the acceleration in the x-direction (reduced) and z-direction (increased). Compared to the first test series, the ASIS forces increased and occurred earlier-in-time in the second test series. Both could be explained by the reduced friction between pelvis and seat. ASIS moments were reduced in the second test series, however, still uncritical with respect to submarining. In addition, the forward rotation of the upper thorax was greater in the second test series, resulting in an earlier loading of the lower thoracic spine (y-moment and x-force). Overall, the reduced friction shifted most dummy signals forward in time. Additional plots can be found in Appendix A1.3.1.1.

Note: ASIS moments are highly dependent of the belt position relative to the sensor. Thereby, differences of a few millimetres can have a huge influence.

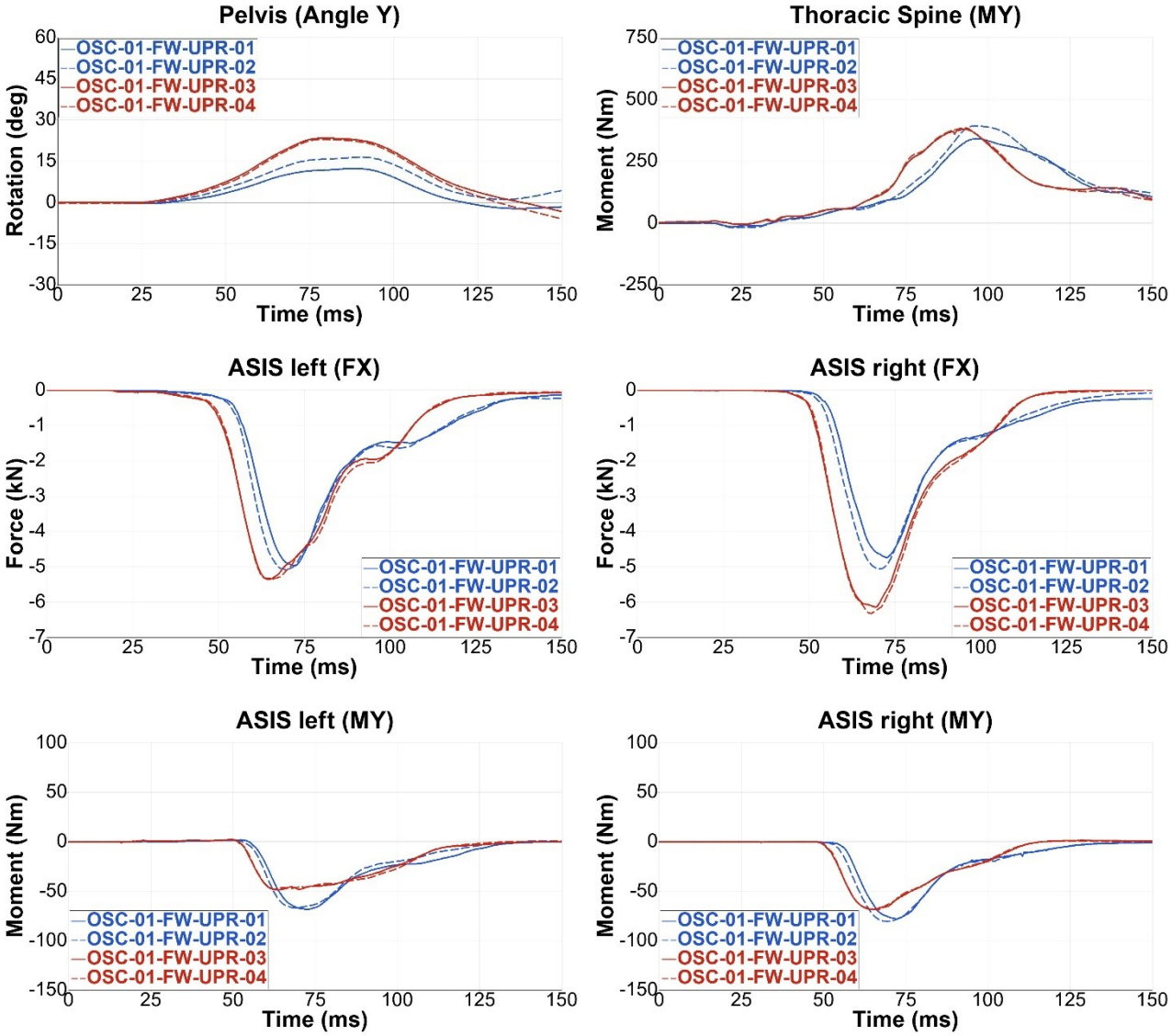

Figure 39 Lower thoracic spine moments, pelvis rotations & ASIS forces & moments, comparing 1st (blue) & 2nd (red) test series

SOTA DLPT belt in Reclined Seating Position

Figure 40 shows seat pan and anti-submarining ramp displacements for the SOTA DLPT belt in the reclined seating position, comparing the first (blue) and second (red) test series. Seat pan displacements were approx. 15 mm less in the second test series, due to a contact between the seat pan and anti-submarining ramp, by which the seat pan displacement was impeded by the anti-submarining ramp. The displacement of the anti-submarining ramp was also smaller for the second test series. For both seat displacements the influence of the dampers was recognisable. The reduced friction between pelvis and seat pan in the second test series allowed the dummy to move forward more quickly, resulting in earlier yet comparable peak lap belt forces (B6). The upper body was rotated into the shoulder belt by the already rebounding pelvis extending the loading of the upper diagonal belt (B3) while reducing the lower diagonal belt forces (B4). Belt pay-in/-out of the shoulder retractor was overall smaller for the second test series while some delay caused by the dummy kinematics could be seen for the peak belt pay-out. In both test series shoulder belt entrapment was observed.

Note: In the first test series a semi-rigid seat with a 20 mm shorter seat pan was used. This avoided contact between seat pan and anti-submarining ramp. In the second test series a seat with the original dimensions was used, which resulted in a contact between seat pan and anti-submarining ramp (see also Table 1).

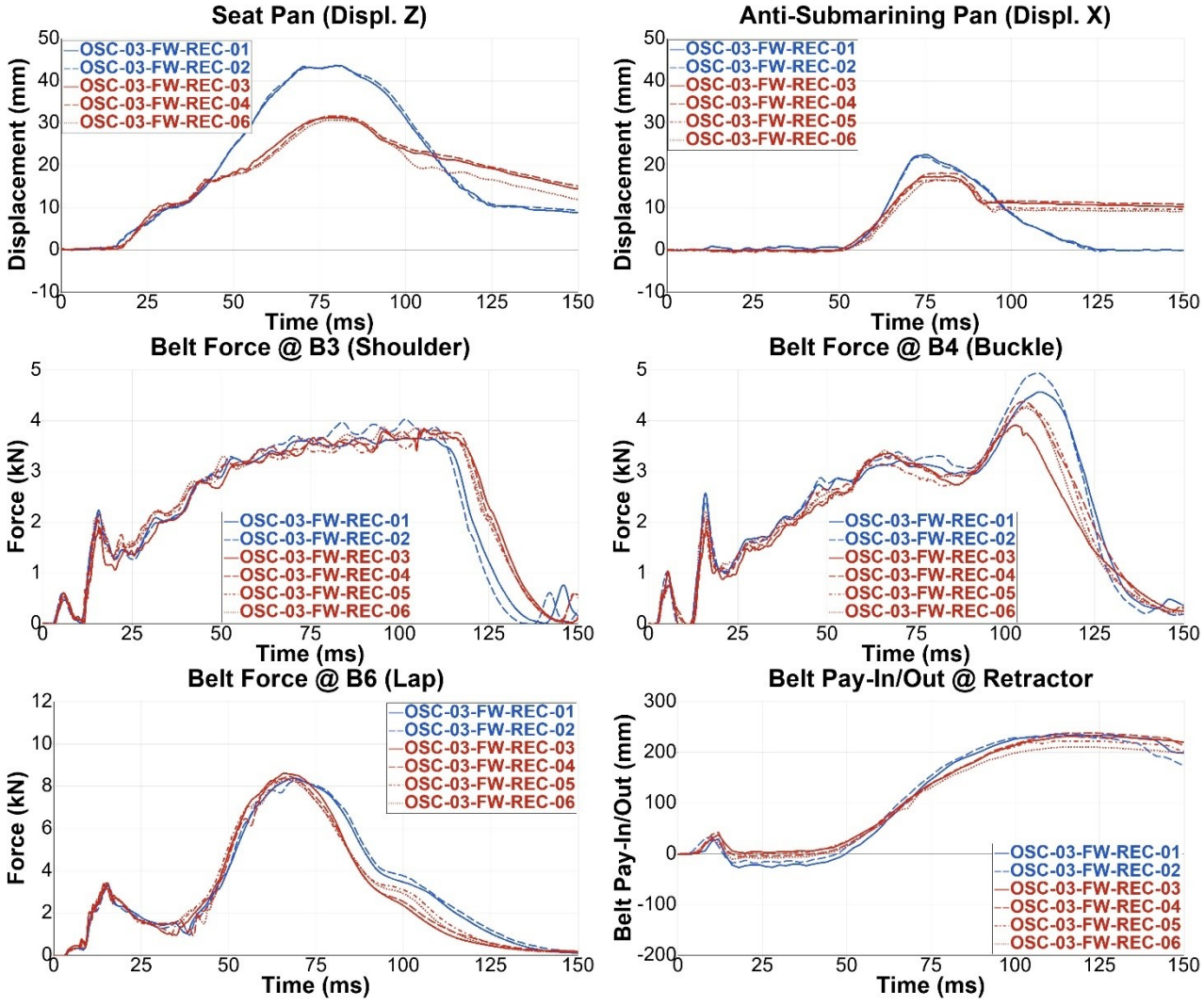

Figure 40 Seat displacements, belt forces & shoulder retractor belt pay-in/-out, comparing 1st (blue) & 2nd (red) test series

In the reclined seating position some differences for the pelvis rotation and lower thoracic spine loading were observed. Thereby, the reduced friction in combination with the impeded seat pan displacement resulted in less pelvis rotation for the second test series while the prevented rebound of the seat pan allowed the pelvis to rotate further back towards its initial position (Figure 41). Furthermore, the earlier rebound of the pelvis reduced the bending between the upper and lower torso resulting in reduced lower thoracic spine loadings (x-forces and y-moments). Differences in the seat pan displacements affected the lower thoracic spine z-forces. Thereby, the impeded seat displacement in the second test series increased the compression loading to the lower thoracic spine, while the reduced (positive) loading was a result of the blocked rebound of the seat pan. ASIS forces and moments and consequently the submarining risk were comparable between the first and second test series. Overall, the reduced friction shifted most dummy signals forward in time. Additional plots can be found in Appendix A1.3.1.2.

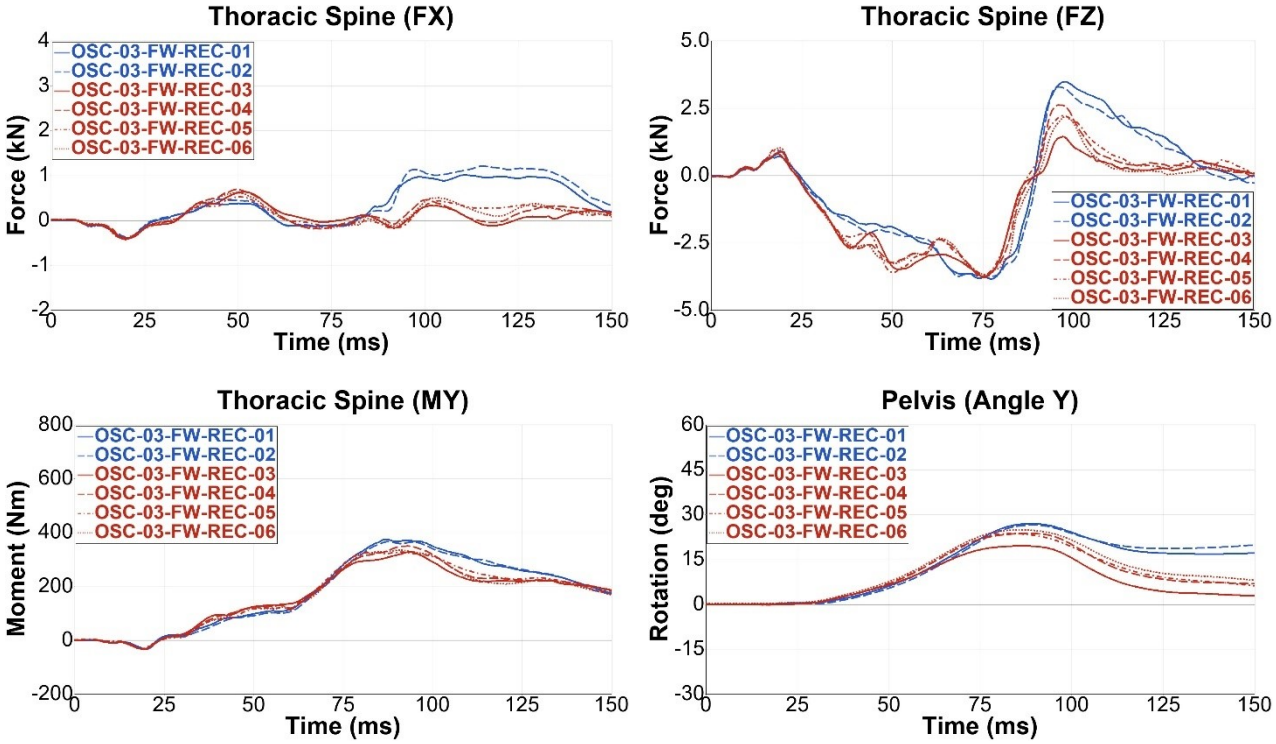

Figure 41 Lower thoracic spine loadings & pelvis rotations, comparing 1st (blue) & 2nd (red) test series

3.1.5.3 Test Repetability

Addressing the objective of test repeatability, the test result scatter was analysed for the four tests with SOTA DLPT belt in reclined seating position, comparing the test scatter of individual tests to each other and averaged data from all four tests.

Table 7 summarises the CORA ratings of each test with the averaged test data as reference. For calculating the averaged values, data from all four tests was used while obviously corrupted data was not considered. CORA-ratings are coloured in accordance to the sliding scale from ISO 18571 (excellent = green; good = white; fair = yellow; poor = red). Thereby, most channels achieved an excellent CORA-rating, while the remaining channels achieved at least a good CORA-rating. The poorest CORA-ratings were obtained for the lower thoracic spine loading in the x-direction (shear). With considerably smaller peak values compared to the z-force (compression), the relatively smaller deviations resulted in a stronger downgrading of the CORA rating. In the other CORA-ratings

classified as good, scatter in individual tests was the reason for some deductions. Noisy signals (oscillations) observed, for example, in the head and pelvis accelerations had a negligible influence on the CORA score.

Channel	Second Test Series			
	OSC-03-03	OSC-03-04	OSC-03-05	OSC-03-06
Seat Pan (Displ. Z)	0.995	0.993	x	0.979
Anti-Submarining Ramp (Displ. X)	0.992	0.977	0.992	0.973
Upper Diag. Belt Force (B3)	0.991	0.995	0.993	0.994
Lower Diag. Belt Force (B4)	0.971	0.988	0.994	0.996
Lap-Belt outside Force (B6)	0.995	0.994	0.996	0.997
Belt Pay-In/-Out	0.994	0.989	0.999	0.975
Head COG (Acc. X)	0.973	0.988	0.965	0.985
Head COG (Acc. Z)	0.993	0.983	0.982	0.993
T4 (Acc. X)	0.984	0.931	0.930	0.978
T4 (Acc. Z)	0.986	0.989	0.992	0.990
T12 (Acc. X)	x	0.978	0.983	0.993
T12 (Acc. Z)	x	0.995	0.996	0.995
T12 (Fo. X)	0.805	0.874	0.856	0.916
T12 (Fo. Z)	0.956	0.980	0.978	0.985
T12 (Mo. Y)	0.991	0.996	0.995	0.998
Pelvis (Acc. X)	0.970	0.982	0.973	0.981
Pelvis (Acc. Z)	0.986	0.987	0.992	0.989
Pelvis (Displ. X)	0.954	0.930	0.965	0.989
Pelvis (Ang. Y)	0.838	0.992	0.991	0.922
Iliac left (Fo. X)	0.985	0.999	0.983	0.976
Iliac right (Fo. X)	0.990	0.985	0.973	0.992
Iliac left (Mo. Y)	0.942	0.956	0.993	0.999
Iliac right (Mo. Y)	x	x	0.991	0.991

Table 7 CORA-rating for each test with averaged test data as reference

Table 8 compares the CORA-ratings from each test with another individual test as reference (OSC-03-03). In addition, the CORA rating of the reference data set compared to the average data is also shown in the table. In general, with some exceptions, the CORA rating and thus also the scatter was worse when compared to the individual test. By using averaged data to calculate the CORA rating, scatter of individual tests was mitigated. Nevertheless, individual results (usually single channels) had less scatter and hence a better CORA rating, as the averaged data was affected by outliers. As for the previous comparison, the worst CORA ratings were noted for the lower thoracic spine x-forces due to the relatively large scatter. Furthermore, significant differences were identified for the pelvis y-angle, with the first test showing strong variations from the other three tests. On the other hand, the CORA rating improved for some individual results (OSC-03-04: seat pan z-displacement and belt pay-in/-out).

A detailed analysis of the test scatter and results with the other three tests as reference can be found in Appendix A1.3.2.

Channel	Second Test Series			
	OSC-03-04	OSC-03-05	OSC-03-06	AVG
Seat Pan (Displ. Z)	0.998	x	0.956	0.995
Anti-Submarining Ramp (Displ. X)	0.985	0.976	0.926	0.992
Upper Diag. Belt Force (B3)	0.977	0.977	0.973	0.991
Lower Diag. Belt Force (B4)	0.943	0.953	0.963	0.971
Lap-Belt outside Force (B6)	0.987	0.984	0.984	0.995
Belt Pay-In/-Out	0.996	0.984	0.938	0.994
Head COG (Acc. X)	0.982	0.922	0.933	0.973
Head COG (Acc. Z)	0.971	0.958	0.976	0.993
T4 (Acc. X)	0.924	0.893	0.940	0.984
T4 (Acc. Z)	0.966	0.966	0.952	0.986
T12 (Fo. X)	0.778	0.622	0.671	0.805
T12 (Fo. Z)	0.911	0.917	0.925	0.956
T12 (Mo. Y)	0.982	0.973	0.986	0.991
Pelvis (Acc. X)	0.955	0.918	0.926	0.970
Pelvis (Acc. Z)	0.962	0.969	0.955	0.986
Pelvis (Displ. X)	0.869	0.934	0.913	0.954
Pelvis (Ang. Y)	0.810	0.803	0.735	0.838
Iliac left (Fo. X)	0.987	0.973	0.943	0.985
Iliac right (Fo. X)	0.977	0.952	0.971	0.990
Iliac left (Mo. Y)	0.874	0.915	0.936	0.942

Table 8 CORA rating for each test with the first test (OSC-03-03) as reference

3.1.5.4 Additional Input for Validation of the Virtual Demonstrators

The simulation models were calibrated and validated with the first test series. Despite some limitations, the models were considered to be sufficiently validated. For the second test series limitations from the first test series were corrected and another semi-rigid seat was used.

The comparability of the validated virtual demonstrators increased when compared to the second test series:

- By using the cotton trousers, the friction between dummy and pelvis was lower. As a consequence, the consistently observed time shift (see Chapter 3.1.4.2 to Chapter 3.1.4.4) between tests and simulations was significantly reduced.
- The impeded rebound of the seat pan in combination with the lower friction allowed the pelvis to rotate further back towards its initial position.
- Moving the belt tower in-between seating positions resulted in smaller oscillations of the D-ring mounting bracket, reducing the influence on the belt pay-in.

The influence of the impeded seat pan displacement in the reclined seating position would need to be further investigated.

Results of the virtual demonstrators compared to the first and second test series can be found in Appendix A1.3.3.

3.1.5.5 Second Test Series Summary and Limitations

In the second test series, eight tests were performed to investigate the test scatter and influence of limitations from the first test series. By using the cotton trousers, the friction between dummy and pelvis was lower. As a consequence, the dummy peak accelerations and forces shifted forward in time. Differences could be mainly observed in the seat compression due to the impeded seat pan displacement. The performance of both restraint systems did not change.

The test scatter of the four tests in the reclined seating position with SOTA DLPT belt was very low when compared to averaged data (CORA rating > 0.805). In general, CORA ratings and thus also the test scatter were worse when compared to the individual tests. With the additional test data, the comparability to the simulation models improved.

3.1.6 Overall Summary and Limitations

The used semi-rigid seat is stiffer in the vertical direction than most production seats likely resulting in an overestimation of the lower thoracic spine z-forces. Original dimensions of the seat could also result in a contact between the seat pan and the anti-submarining ramp, by which the seat pan displacement was impeded by the anti-submarining ramp. Furthermore, no side support to absorb lateral energy in oblique pulses was available.

The THOR dummy was developed for testing and evaluating systems restraining occupants in frontal vehicle crash scenarios in upright seating positions. Reclined seating positions, as tested here, were so far not considered in the development of the THOR dummy or any other dummy. Dummies suitable for reclined seating positions are currently under development. Therefore, the suitability of the dummy for reclined sitting positions as well as its biofidelity could not be definitively assessed. Further research on this is needed.

The submarining behaviour in the reclined seating position with SOTA belt could not be replicated in numerical simulations due to the used dummy model version (“hidden” ASIS load cells) and missing bending stiffness of the belt webbing simulation model. Thereby, these two problems seemed to negatively affect each other, further increasing the submarining problem. In addition, the belt pay-out was underestimated in VPS and Madymo, which likely influenced subsequent results.

3.1.7 Conclusion and Next Steps

The homologation demonstrator focused on a reclined seating position and the challenges for the restraint system and the test devices associated with such a configuration. With the purpose to provide input for WP4 and WP5, the test results were used to validate the numerical models, which were developed for three simulation codes (LS-Dyna, VPS and Madymo).

Dummy kinematics and consequently the loads on the dummy changed in the reclined seating position. Compared to the upright seating position, the whole dummy initially moved forward, and forward rotation of the upper body was delayed. Thereby, the diagonal belt slid on the torso towards the neck while accelerations and forces in z-direction generally increased. With both restraint systems submarining was avoided. The SOTA DLPT belt resulted in an earlier dummy-to-belt coupling, which generally led to earlier yet smaller accelerations and thoracic spine loadings. The risk of submarining was significantly reduced when the pelvis was pre-tensioned. Performance of the SOTA DLPT belt was also demonstrated in an oblique impact with two different pulses.

In the second test series, the impact of limitations found in the first test series and test scatter were investigated. By using the cotton trousers, the friction between dummy and pelvis was lower. As a consequence, the dummy’s peak accelerations and forces shifted forward in time. With the changes,

there was no change in the SOTA DLPT belt performance. The test scatter of the four tests in the reclined seating position with SOTA DLPT belt was very low when compared to averaged data (CORA rating > 0.805). In general, CORA ratings and thus also the test scatter were worse when compared to the individual tests.

Despite some limitations, especially with regard to submarining and belt pay-out, the simulation models were considered to be sufficiently validated for both seating positions and restraint systems. Necessary adjustments were not possible at the time, since all codes partly used encrypted models (e.g. dummies and restraint systems) whose properties could not be changed beyond some pre-defined, accessible parameters. The comparability of the validated virtual demonstrators increased when compared to the second test series.

Results from the second test series will be used to update the virtual demonstrator in LS-Dyna, which will also include updates that were previously not available. Within the simulation-study, the influence of the impeded seat pan displacement in the reclined seating position will be further investigated. Simulation results will be also used to discuss the validation procedure developed within WP5 [8]. Further discussion is needed on how to consider the test scatter in an objective rating method, as well as on the calculation method (averaged data vs. individual tests as reference), acceptance criteria for model validation and how to deal with missing / obviously corrupted data.

Another test series with different dummies (THOR-50M and THOR-AV-50M) was recently carried out. Results from these tests will be also used to analyse the validation procedure developed within WP5 [8]. Furthermore, WP5 [8] discussed the need for a validation device (VD) to validate a vehicle environment model for an HBM-based VT process. The results of the second test series (THOR and Hybrid III dummy) and the third test series (THOR-AV-50M) will be further analysed in that respect and reported within OSCCAR deliverables of WP5/WP6.

3.2 Protection Principle 2: Pre-Rotated Seat - Seat Inertia

This chapter summarises the setup and results of the physical as well as virtual demonstrators related to OSCCAR Protection Principle 2 (PP2). The tests and the corresponding simulations were conducted by ika and fka.

3.2.1 Motivation and Background

PP2 addresses an occupant who is sitting in a slightly rotated position (pointing away from the driving direction). If a crash is unavoidable, the seat is rotated into the crash direction during the pre-crash phase. The seat rotation is not caused by an actuator (as for Protection Principle 1) but due to the inertia of seat and occupant in the course of an active release of the seat. More information regarding the motivation and background of PP2 and the other protection principles within OSCCAR is given in Deliverable D2.4 [7].

In order to demonstrate the functionality of PP2, a physical demonstrator was built up and implemented on a test sled. In addition to the PP2 simulation studies documented in Deliverable D2.4 [7], further simulations were performed within the framework of a virtual demonstrator, which represented the defined test boundary conditions and allowed for further investigations.

3.2.2 Physical Demonstrator

Since PP2 addresses the pre-crash phase, the in-crash phase was not considered within the test series, i.e. the swivel seat was mounted on a test sled, which was decelerated by a defined braking pulse. By varying certain test parameters, the functionality of the protection principle could be demonstrated for different Test Cases.

3.2.2.1 Test Setup

Variable test parameters were the occupant anthropometries (dummy size), the seat rotation axis position and the placement of the feet. Fixed test parameters were the belt system, the initial seat rotation angle, the occupant position, the vehicle environment and the brake deceleration. In the following, the test setup is detailed.

Test Sled Setup

The test sled setup is illustrated in Figure 42. The trolley was equipped with a base plate and a vehicle carpet, which provides realistic friction behaviour. In the seat mounting area a bearing plate was added. Three on-board high-speed cameras were installed in front, side and top view position using a corresponding support frame. The cameras were synchronised with the brake system. An optical signal was given when the braking was triggered.

The test sled was guided and accelerated by means of a running rail. Braking was applied by a hydraulic braking system on all four wheels. The deformation elements at the front of the trolley were only for safety reasons, in case of brake failure. In order to measure the sled deceleration during braking, three axial acceleration sensors (A_x, A_y, A_z) were implemented in the centre of gravity of the trolley (nominal measuring range: +/-500 g, adjusted to +/-50 g).

Furthermore, a rotation rate sensor (nominal measuring range: +/-1500°/s, adjusted to +/-500°/s) was used to measure the angular velocity of the seat mounted on the trolley within the tests. With regard to the integrated belt system, a belt force sensor (nominal measuring range: 16 kN, adjusted to 5 kN) was integrated in the shoulder section to determine the seat belt force.

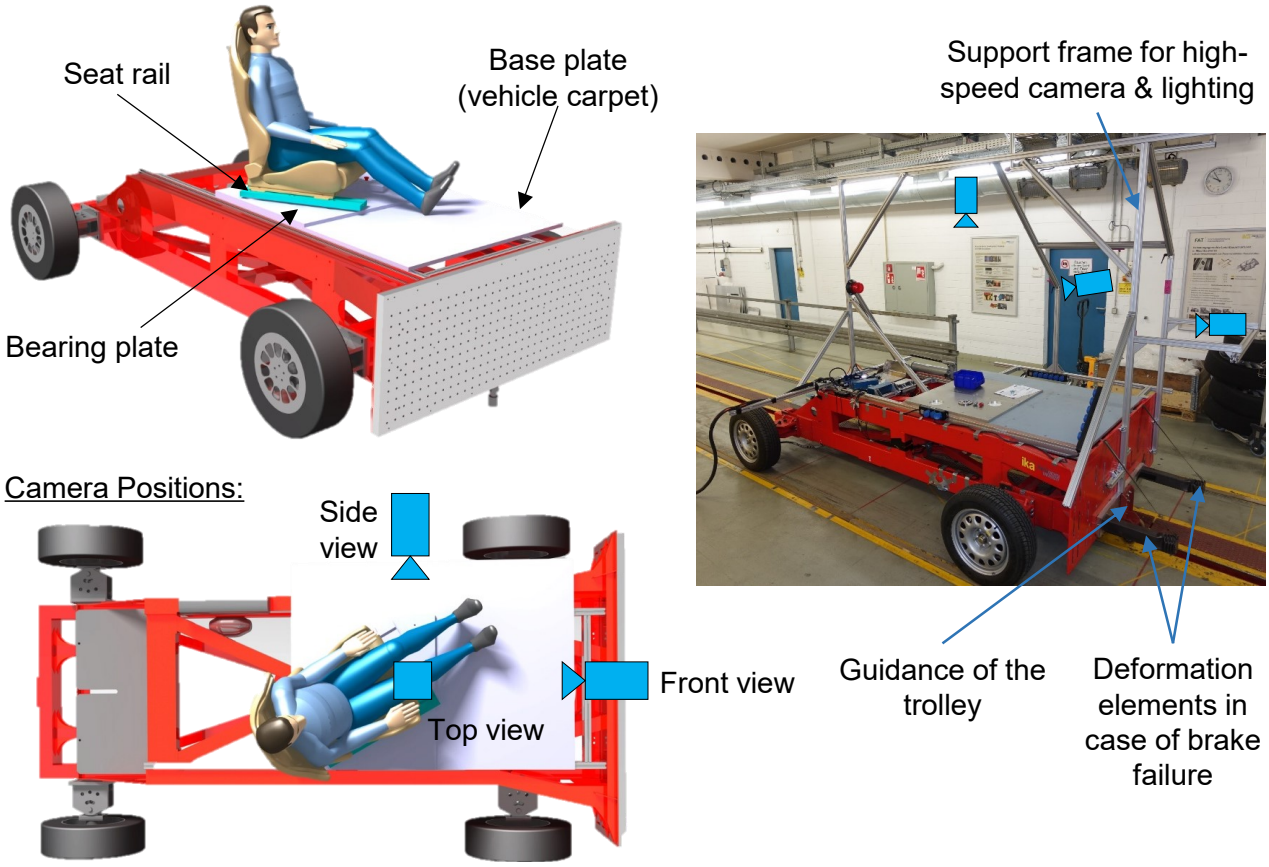

Figure 42 Test sled setup

Seat

Since the belt system had to move together with the seat, a seat with an integrated belt system was purchased. Therefore, a right front passenger seat out of a Ford B-Max (vehicle model: JK 2012-2017), a five-door van without b-pillar, was selected.

In order to simplify the test setup, a static belt pretensioning was implemented, i.e. the belt was pre-tensioned by 250 N prior to the test. The belt force was measurement during the entire test. Both the seat and the static belt pretensioning are shown in Figure 43.

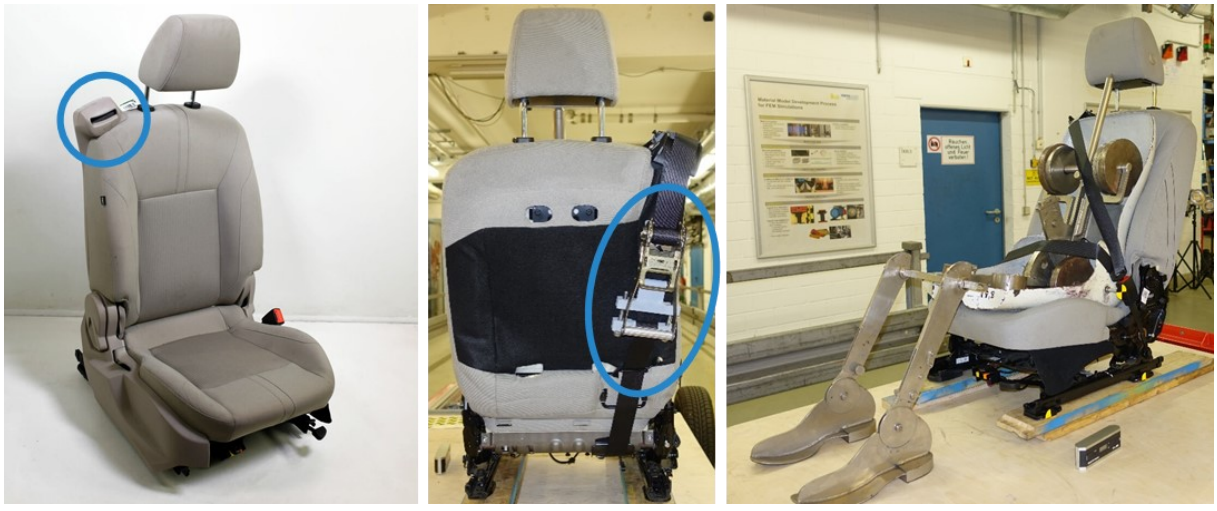

Figure 43 Seat with integrated belt system & static belt tensioner

Rotation Mechanism

The seat rotation was enabled by a mechanism specially designed for the PP2 test series and illustrated in Figure 44. Three different rotation axis positions could be set. Furthermore, the seat position was adjustable in longitudinal direction by sliding blocks. Both seat rails were equipped with ball bearings, so that they could move on the plate. This movement took place around the respective rotation axis and was realised by a cross roller bearing implemented at the rotation axis position. In this way, a rotation of the occupant from a 30° inward to a 0° rotated “standard” position was set.

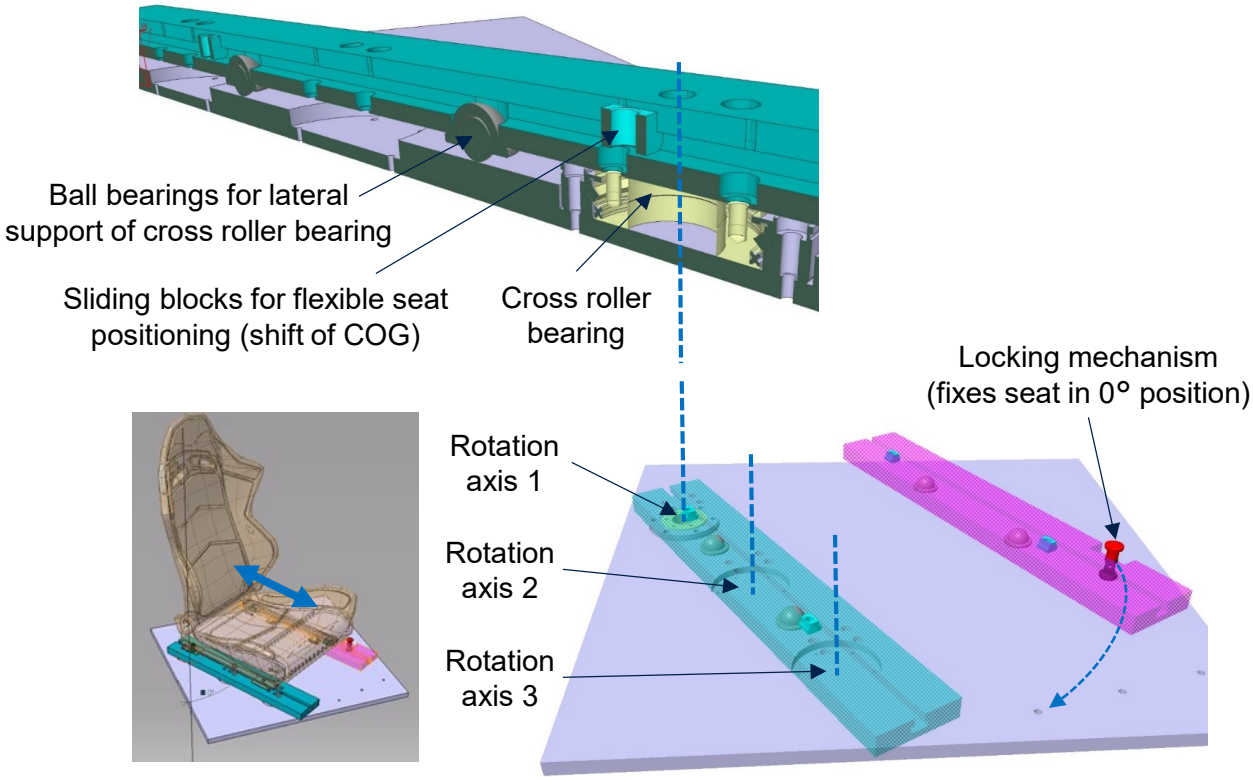

Figure 44 Seat rotation mechanism

A rotation of the seat prior to the braking of the test sled was prevented by a magnetic switch. When the seat reached the end stop at 0° position (passenger oriented in forward direction) during the braking phase, it was fixed by a spring-based locking mechanism. In order to better determine the seat rotation time, a contact switch was implemented at the end stop.

Seat Kinematics

Due to the design of the rotation mechanism, a wider range of possible rotation axis positions in longitudinal direction could be considered compared to the parameterisation defined for the corresponding PP2 simulation study in OSCCAR Deliverable D2.4 [7]. In order to address this larger span in longitudinal direction, the positions of rotation axis 1 and rotation axis 3 defined in the test series lay outside the parameter range considered in the simulation study in Deliverable D2.4 [7]. For the virtual demonstrator the rotation axis positions were adapted according to the test boundary conditions. More details on this as well as a comparison of the rotation axis positions are given in Chapter 3.2.3.1.

Based on the findings in Deliverable D2.4, rotation axis position 1 should be more effective than rotation position 3, i.e. the seat should rotate faster for rotation axis position 1. The rotation axis position also influences the overall package requirements for the seat rotation, e.g. the distance of the seat in 0° position to the interior trim, which turned out smaller for rotation axis position 1.

Footrest

The placement and rest of the feet have a decisive influence on the turning movement of the occupant. Two main configurations were defined for the PP2 test series (Figure 45). In configuration 1, the feet are up and the heels rest on the floor. Thus, during seat rotation, the heels are dragging on the floor. Parameters like friction coefficient and contact pressure are of importance here.

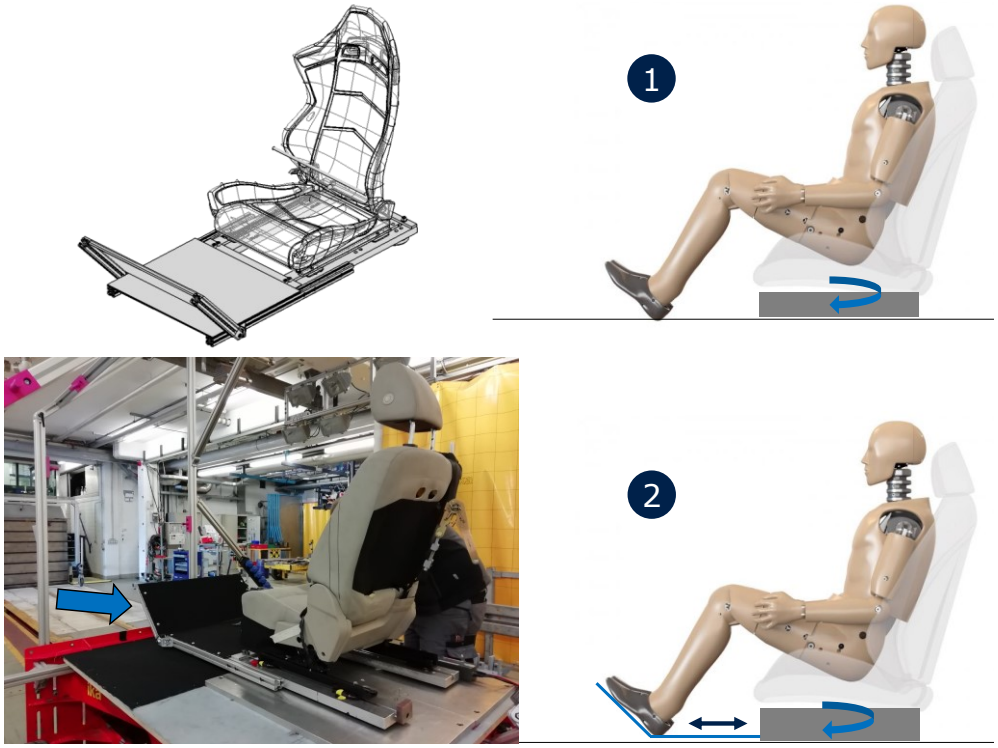

Figure 45 Footrest configurations

In order to decouple the feet from the floor, a footrest was designed which could be mounted to the seat (configuration 2). The footrest was adaptable to the different dummy sizes considered within the test series and enabled a comfortable sitting position.

Beside the two main configurations used for the basic tests, three additional tests with an unfavourable position of the feet were conducted. Here, the shoe soles were flat on the floor to increase the friction and hence the influence on the occupant rotation.

Dimensions & Masses

The positions of the different rotation axes, the H-point and the centre of gravity with and without footrest are given in Figure 46. All dimensions refer to a reference point located at the outermost rear point of the right seat rail (marked in green in Figure 46).

The position of the centre of gravity of the swivel seat depends on whether the footrest is mounted or not. Furthermore, it changes according to the footrest setting. In Figure 46 two orange dots indicate the centre of gravity position of the seat alone and the centre of gravity position with the footrest mounted and set to the 5th percentile female. The corresponding values for the 50th and 95th percentile male are provided by Figure 47. Due to the extension of the footrest with increasing dummy size (red coloured), the centre of gravity of the seat moves further forward (violet coloured). The positions of the different rotation axes (R1, R2, R3) and centres of gravity (without footrest, footrest setting for F5%, M50% & M95%) relative to the H-point coordinate system are given in Figure 218 within Chapter 2.1 of the Appendix.

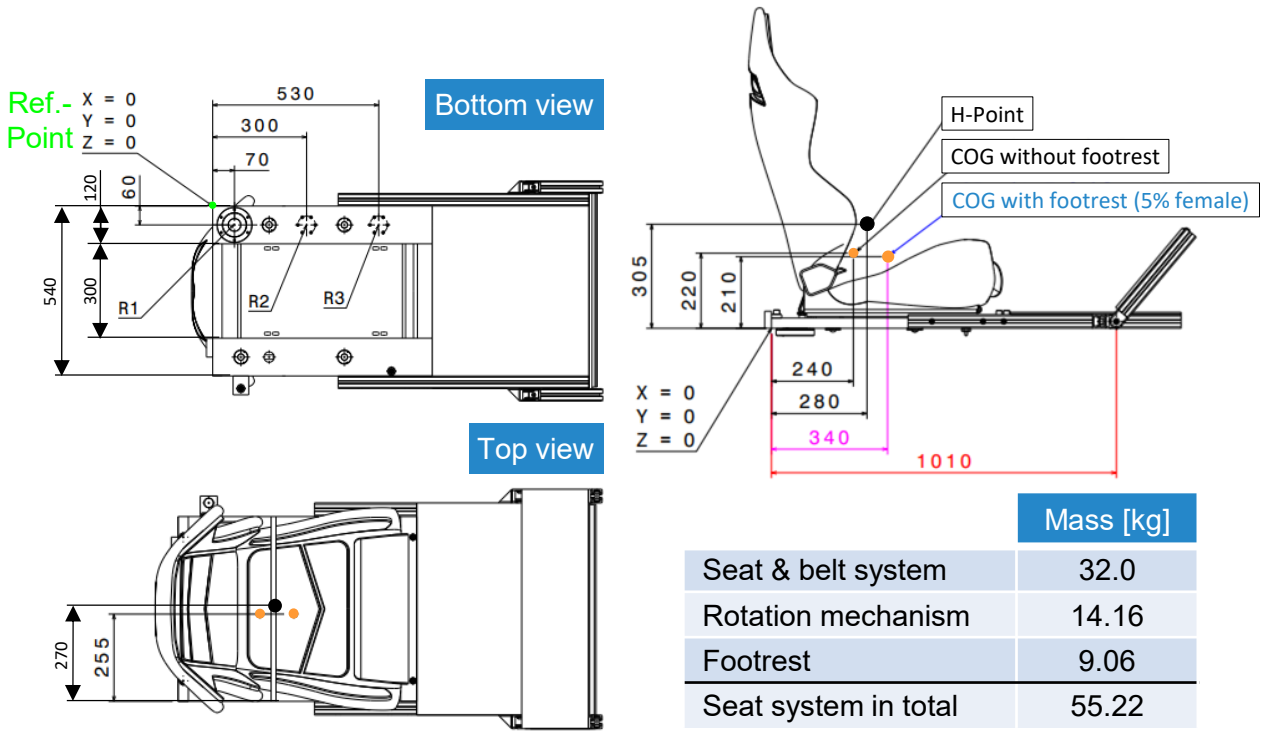

	Mass [kg]
Seat & belt system	32.0
Rotation mechanism	14.16
Footrest	9.06
Seat system in total	55.22

Figure 46 Swivel seat: Masses & dimensions (footrest setting for 5th percentile female)

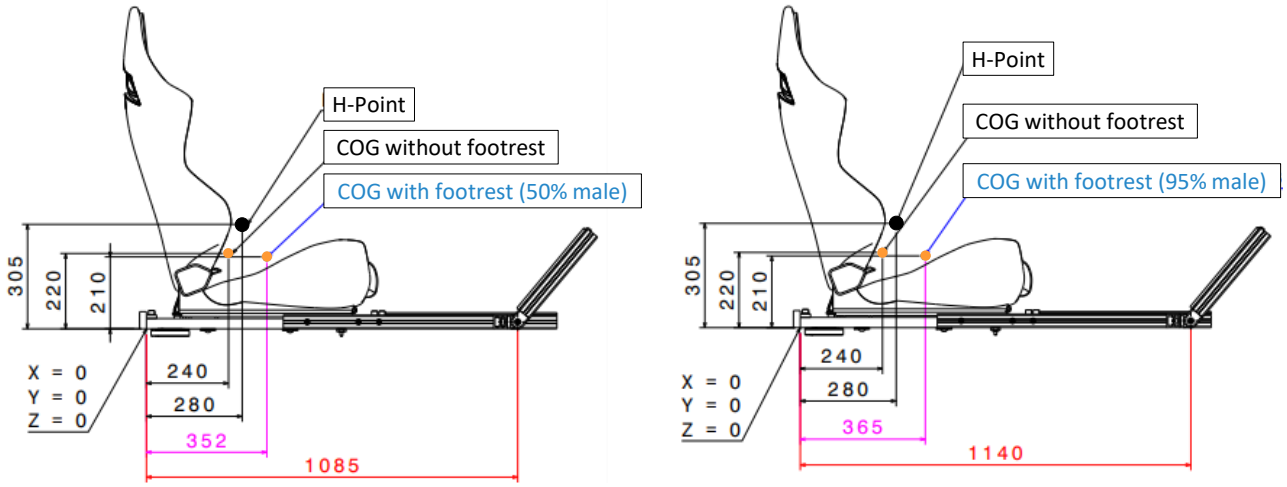

Figure 47 Swivel seat: Dimensions for footrest settings of 50th & 95th percentile male

The weight of the seat and the belt system including the static belt tensioner amounted to 32 kg. Adding the weight of the rotation mechanism (14.16 kg) as well as the footrest (9.06 kg), resulted in a total mass of the swivel seat of 55.22 kg. The total weight of the test setup, i.e. trolley, swivel seat and dummy, was kept constant at 1675 kg. This means that the additional mass due to increasing dummy sizes was compensated by the removal of weights in the test sled.

AEB Setup

The AEB pulse applied for the investigation of PP2 was modelled as generic curve, starting at a maximum time of 1 s before the crash (see Deliverable D2.4, Figure 51 [7]). The corresponding acceleration level ranges from 0.3 g to 0.8 g. The range of AEB levels represents different levels of brake force, from partial to full braking. Before the defined acceleration level is reached, a ramping function of 35 m/s³ is applied (according to the AEB definition in [11]).

On the basis of pre-tests, the brake ramp of 35 m/s³ according to the idealised OSCCAR AEB acceleration curve was set for the test sled (Figure 48). In general, the AEB ramping of the test sled setup can be adjusted in a corridor of 30 m/s³ to 400 m/s³, considering additional test runs.

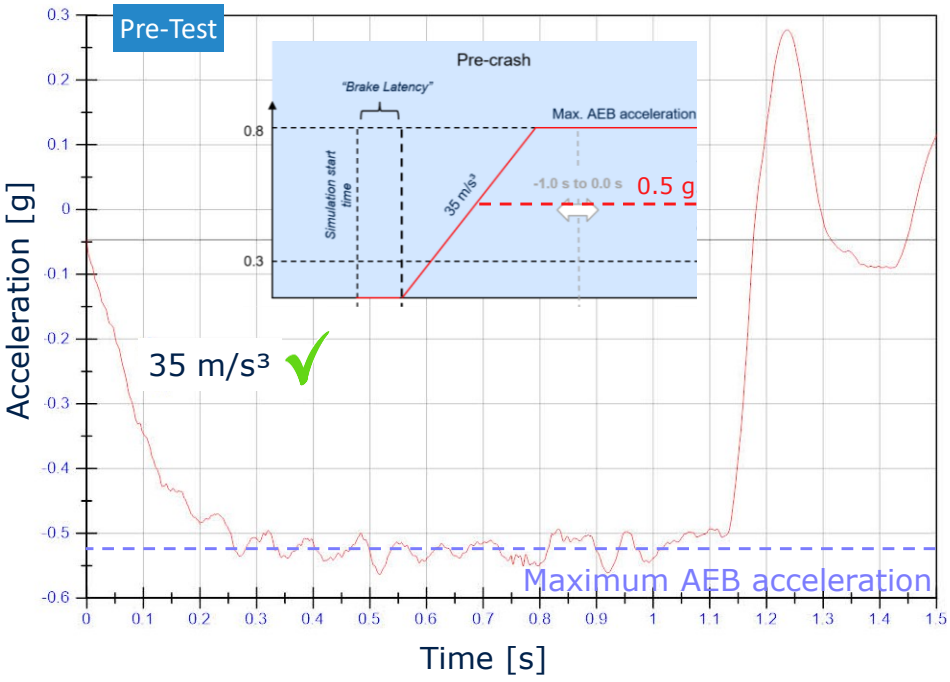

Figure 48 Implementation of idealised OSCCAR AEB acceleration curve / brake pulse

Compared to the generic curve, the target value for the maximum AEB acceleration had to be reduced from 0.8 g to 0.5 g for the PP2 test series (v_0 = 20 km/h), as illustrated in Figure 48. Within the pre-tests the brake pulse was most reproducible for a maximum value of 0.5 g since the tyres of the test sled were here in the range of maximum slip. For an increased value, i.e. up to 0.8 g, the tyres went into sliding friction, leading to strong oscillations in the signal. This was due to the strong pitching of the sled and thus the reduced axle load on the rear axle, which caused the tyres to lock. Because the trolley used for the PP2 test series did not have a spring-damper system (only springing through the tyres), it started bouncing for higher brake acceleration values. With regard to the functionality of PP2, the sled test series should demonstrate that the protection principle also works at a reduced maximum brake acceleration, thus confirming its robustness.

Dummies

Four occupant anthropometries were considered for the PP2 test series, covering a wide range of the European population. Different Hybrid III dummies were used in order to represent a 5th percentile female, a 50th and 95th percentile male as well as an obese male with a BMI of 35:

- Hybrid III 5th percentile female (49 kg)
- Hybrid III 50th percentile male (70.7 kg)
- Hybrid III 95th percentile male (101.3 kg)
- “Obese” Hybrid III 95th percentile male (124.1 kg, BMI 35)

The obese male was based on the Hybrid III 95th percentile male, which was equipped with an additional weight of 22.8 kg.

With regard to the sensors / channels considered for the dummies within the PP2 test series, the focus was on the upper body region, i.e. head, upper neck, chest and pelvis. Not every dummy is

equipped with all sensors. The simplest dummy is the Hybrid III 95th percentile male. Thus, it defines the selection of sensors to obtain comparable measurement results for each test. The sensors and channels considered for the PP2 test sled setup and the dummies are listed in Figure 219 within Chapter 2.2 of the Appendix.

Test Matrix

The testing boundary conditions described in this chapter, consisting of variable parameters (occupant anthropometries, rotation axis position, footrest) and fixed parameters (initial seat rotation angle, occupant position, braking characteristics, belt system), led to 24 basic configurations. The corresponding test matrix is shown in Figure 49.

Variable parameters	n	Description
Dummies	4	F5%, M50%, M95%, Obese
Rotation axis pos.	3	R1, R2, R3
Footrest config.	2	Heels on floor, Footrest
Number of tests	24	
	+3	+ Shoe soles on floor: Obese, R1 & R2 / M95%, R3
Total number	27	

Fixed parameters	Value
Initial seat rotation angle	30°
Occupant position	Upright
Average brake accel.	0.45 - 0.5 g
Brake gradient	35 m/s³
Shoulder belt PT force	250 N
Initial sled velocity	20 km/h

Figure 49 Test matrix

Due to three additional tests with an unfavourable footrest configuration (shoe soles flat on floor) of the obese and 95th percentile male with different rotation axis positions in each case, the total number of tests conducted amounts to 27.

3.2.2.2 Test Results - HIII 5th percentile female

Figure 50 shows the inertia-based seat rotation for the 5th percentile female, considering the rearmost rotation axis position (R1). Rotation axis position R1 usually evoked the fastest seat rotation and was therefore chosen for illustration in the current and the following chapters. The upper image sequence always refers to the test without footrest and the lower one to the test with footrest.

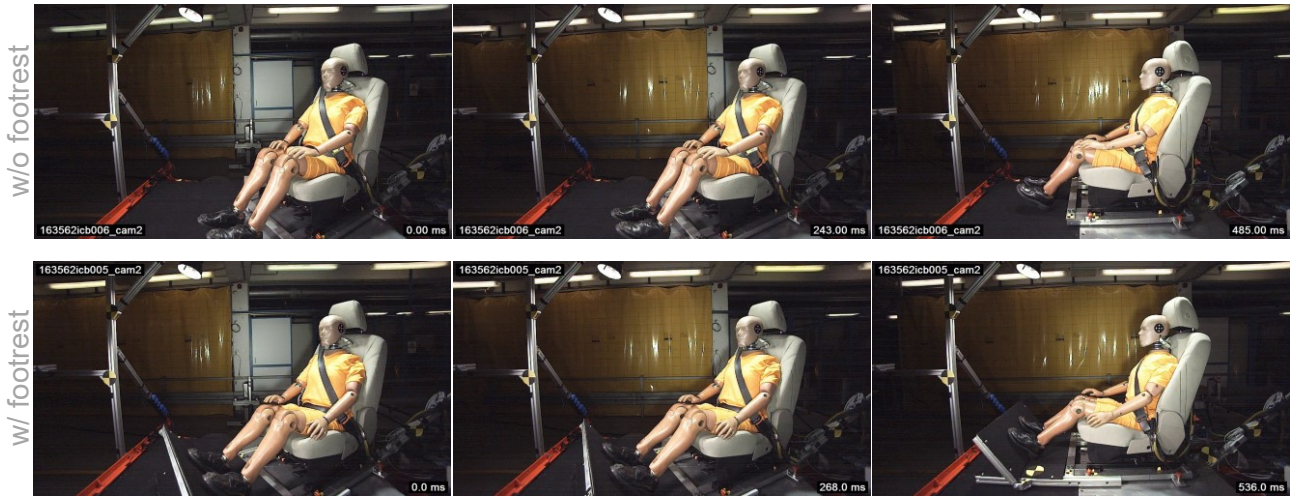

Figure 50 HIII 5th percentile female - rotation axis position R1 - without & with footrest

Measurement results are given for all rotation axis positions. Figure 51 illustrates the seat angular velocity (z). Each column represents a rotation axis position. Again the upper row refers to tests without footrest and the lower one to tests with footrest. This structure will be used for all PP2 measurement results in this chapter as well as in the Appendix. The rotation axis position R1 led to the fastest seat rotation (485 ms without footrest / 536 ms with footrest). The difference to R2 was quite small while R3 showed significantly longer seat rotation durations, close to 1 second. Differences between the tests without and with footrest occurred due to an interaction of the feet with the floor as well as a forward shift of the centre of gravity in case the footrest was implemented.

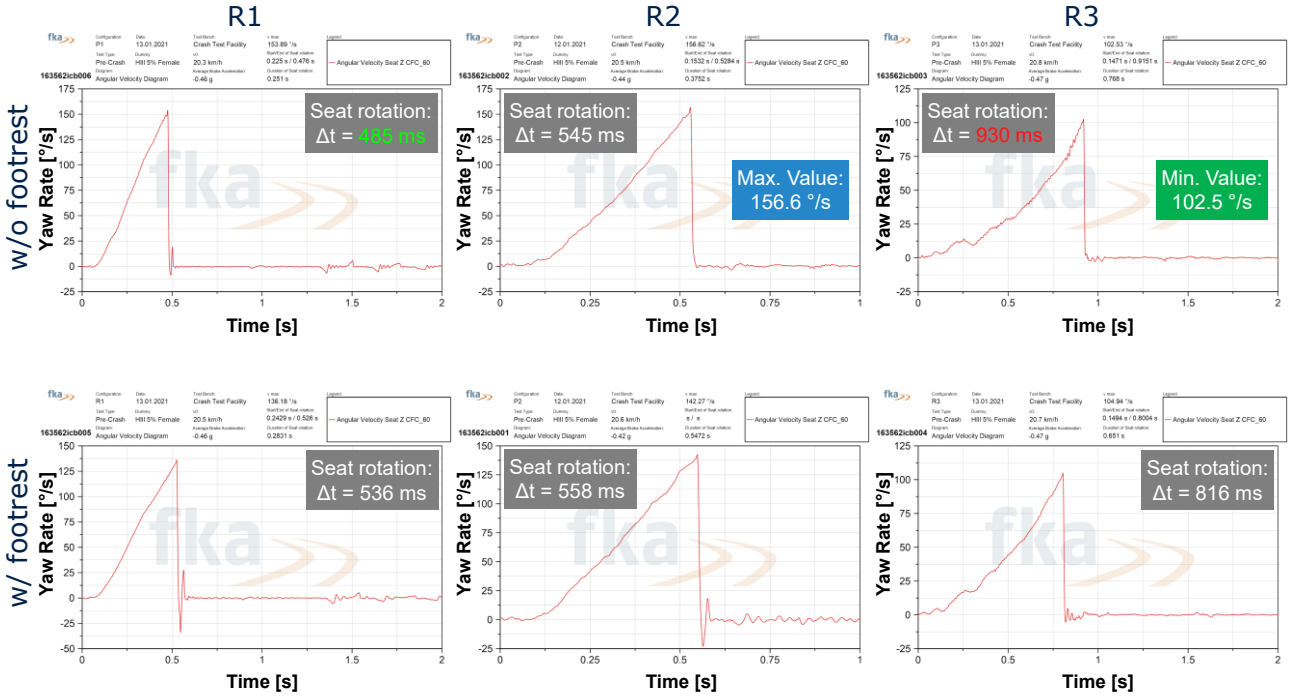

Figure 51 HIII 5th perc. female - seat angular velocity (z) - R1, R2, R3 - without & with footrest

The duration of the seat rotation given in the diagram headers is based on the data of the implemented contact switch, which, due to the spring travel, provides end and start times that are too inaccurate in relation to the short time span. Therefore, the rotation time was determined manually, starting at t_o (initiation of braking) and ending where the seat angular velocity had the first zero crossing after the peak value. These rotation durations are specified in the text boxes. Furthermore, the tests with the maximum and minimum values of the yaw rate are highlighted by a blue and green text box.

The dummy loadings, i.e. head acceleration, chest acceleration, pelvis acceleration, upper neck forces and moments, as well as the seat belt forces are listed in the Appendix. In case of the 5th percentile female, the results can be found in Chapter 2.3. In general, the dummy loadings of head, upper neck, chest and pelvis were very low, which was to be expected for a pre-crash situation with a braking deceleration of 0.45 to 0.5 g. All maximum values were far below the dummy injury thresholds. In Chapter 3.2.2.6 the results of the different dummies for rotation axis position R1 are compared and finally discussed.

3.2.2.3 Test Results - HIII 50th percentile male

The seat rotation of the HIII 50th percentile male without and with footrest is illustrated for rotation axis position R1 in Figure 52.

Figure 52 HIII 50th percentile male - rotation axis position R1 - without & with footrest

For the 50th percentile male rotation axis position R2 evoked the fastest seat rotation, although the difference to R1 was marginal (Figure 53). Here it must be mentioned that the average brake acceleration achieved in the R1 test without footrest (-0.43 g) was lower than in the corresponding R2 test (-0.47 g). The seat rotation time for R3 was again considerably longer.

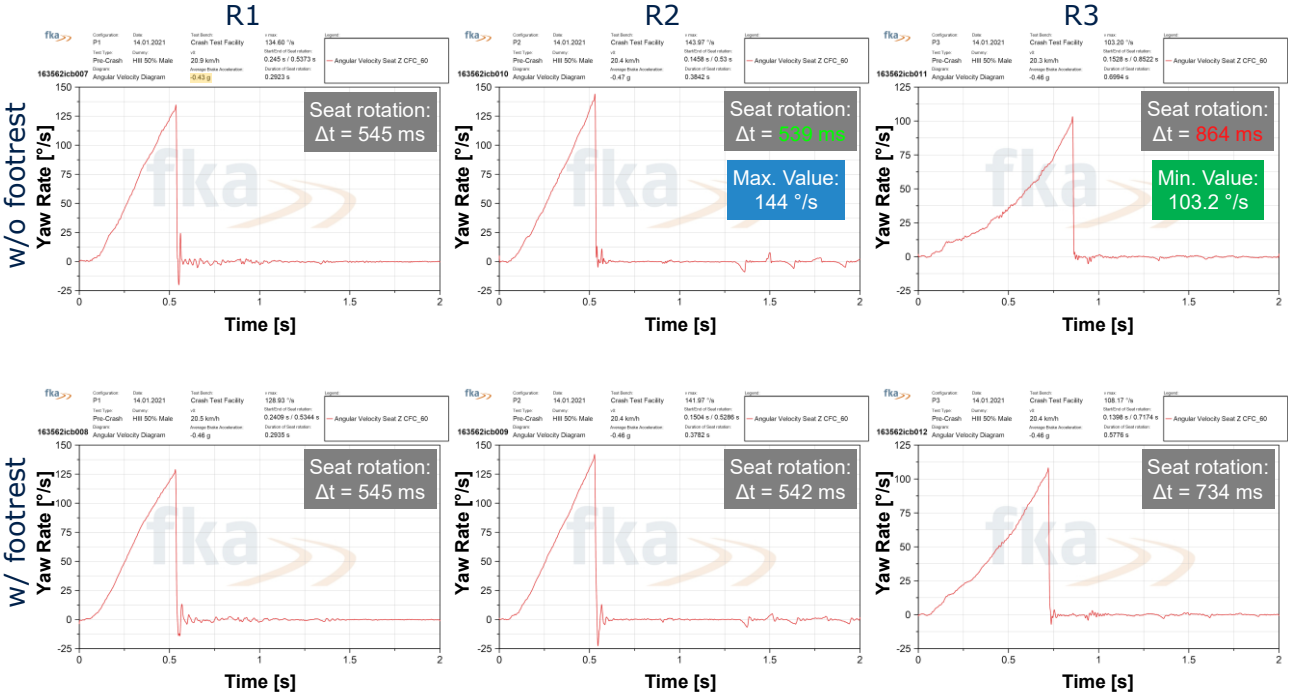

Figure 53 HIII 50th perc. male - seat angular velocity (z) - R1, R2, R3 - without & with footrest

The dummy loadings and the seat belt forces for the HIII 50th percentile male are given in Chapter 2.4 of the Appendix.

3.2.2.4 Test Results - HIII 95th percentile male

Figure 54 shows the seat rotation of the HIII 95th percentile male without and with footrest for rotation axis position R1.

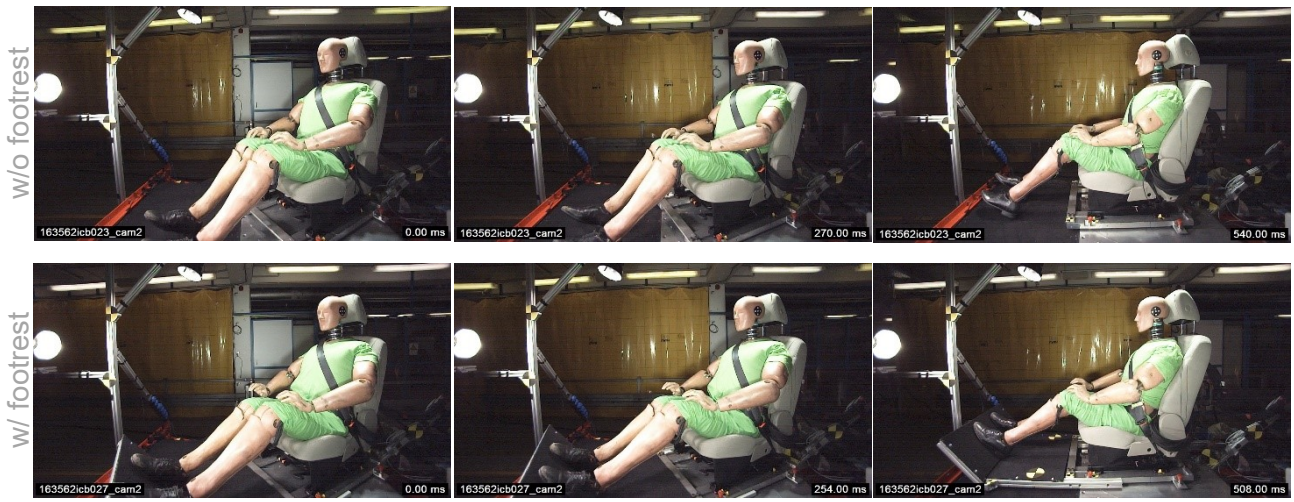

Figure 54 HIII 95th percentile male - rotation axis position R1 - without & with footrest

The rotation axis position R1 led to the fastest seat rotation of the 95th percentile male (Figure 55). Unlike the two previous dummies (F50% & M50%), the 95th percentile male showed clearly faster rotations in the tests with an implemented footrest.

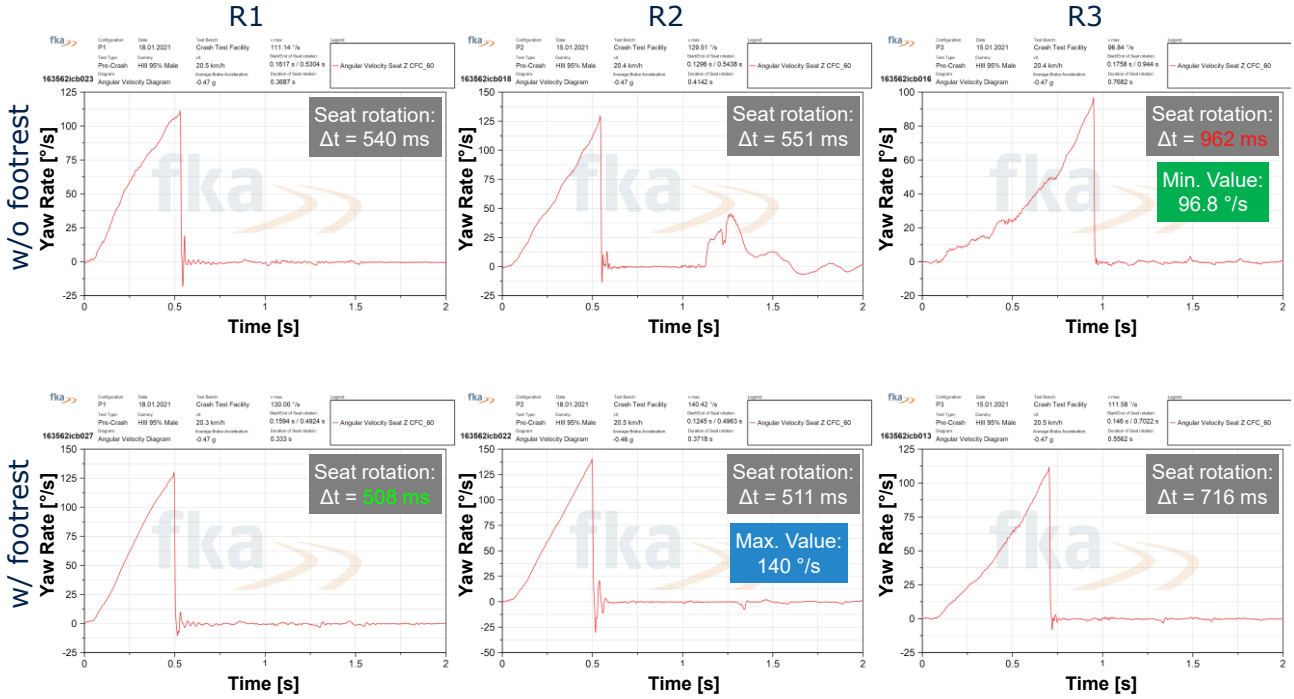

Figure 55 HIII 95th perc. male - seat angular velocity (z) - R1, R2, R3 - without & with footrest

For the additional test with the HIII 95th percentile male in most unfavourable configuration (R3, shoe soles flat on floor) the seat rotation did not work (see limitations in Chapter 3.2.2.6). The corresponding data and the M95% dummy loadings can be found in Chapter 2.5 of the Appendix.

3.2.2.5 Test Results - Obese ATD BMI 35 male

Figure 56 illustrates the R1 seat rotation of the Obese ATD BMI 35 male without and with implementation of a footrest.

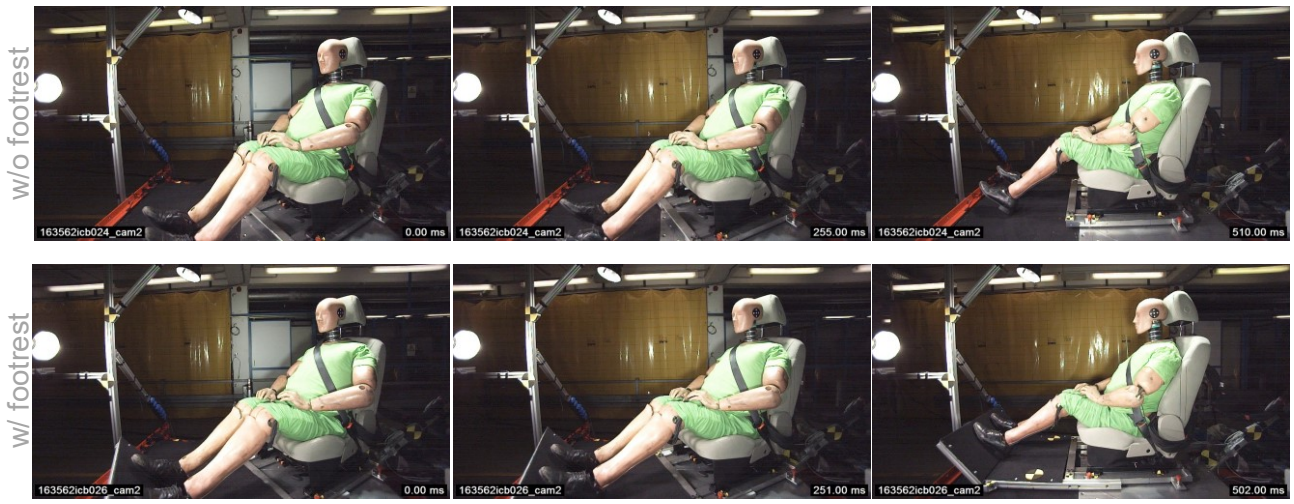

Figure 56 Obese ATD BMI 35 male - rotation axis position R1 - without & with footrest

Figure 57 shows the seat angular velocity (z). The obese BMI 35 male reached slightly shorter durations than the 95th percentile male. Again, the tests with an implemented footrest showed faster rotations but not as significant as for the 95th percentile male. Furthermore, the difference between rotation axis positions R1 and R2 was marginal.

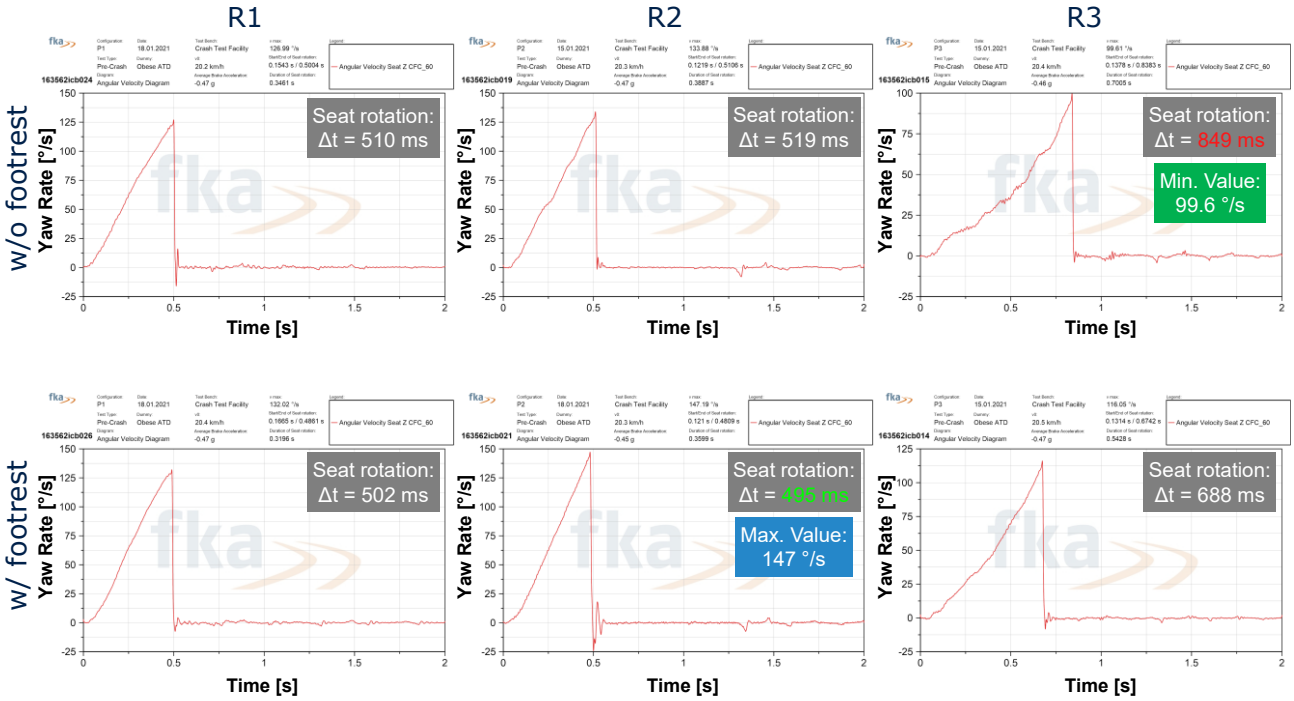

Figure 57 Obese BMI 35 male - seat angular velocity (z) - R1, R2, R3 - without & with footrest

Regarding the obese BMI 35 male two additional tests with the configuration “Shoe soles flat on floor” were conducted for rotation axis positions R1 (Figure 58) and R2. Both showed longer rotation durations compared to the corresponding tests in Figure 57, i.e. 538 ms for R1 and 567 ms for R2, which were still in the range of half a second and thus demonstrating the robustness of the protection principle. The corresponding data as well as the dummy loadings for all obese BMI 35 male tests can be found in Chapter 2.6 of the Appendix.

Figure 58 Obese ATD BMI 35 male - rotation axis position R1 - shoe soles flat on floor

3.2.2.6 Summary and Limitations

For all 24 basic configurations, a complete seat rotation could be achieved within a total time of 1 second (starting point: t_0, initiation of braking) for a maximum brake acceleration of only 0.5 g. The rearmost rotation axis position (R1) evoked the fastest seat rotation but the difference to R2 was quite small, especially for the male dummies. Figure 59 compares the R1 results in terms of the influence of the dummy size (left) and the feet rest configuration (right) on the seat rotation. For all tests the seat rotation durations lay in the range of half a second.

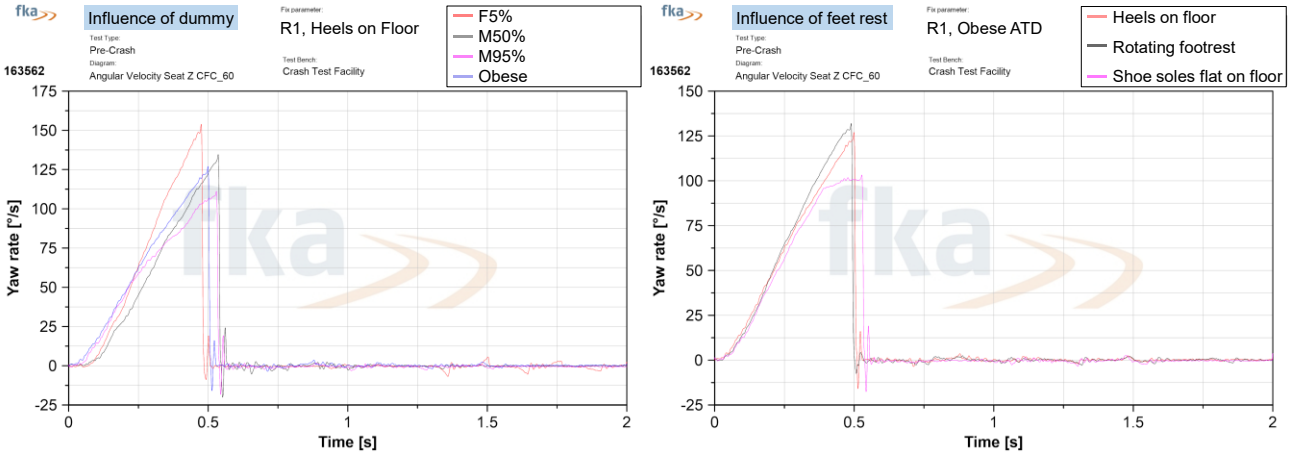

Figure 59 Seat Angular Velocity (z) - rotation axis position R1

The fastest R1 seat rotation was achieved by the 5th percentile female (485 ms), the longest by the 50th percentile male (545 ms) and the 95th percentile male (540 ms), all without footrest and with heels on floor. The obese BMI 35 male reached slightly lower durations than the 95th percentile male (510 ms, without footrest, heels on floor).

The implementation of a footrest showed an inverse relationship. It led to an increased rotation duration for the 5th percentile female (536 ms) and a reduced rotation duration for the 95th percentile male (508 ms), while for the 50th percentile male no change was observed. Since the dummy heels slide relatively unhindered (see limitations), the main influence parameter here was probably the forward shift of the centre of gravity due to the implementation of the footrest.

The configuration “Shoe soles flat on floor” showed the longest rotation durations. For the obese BMI 35 male the duration slightly increases from 510 ms (heels on floor) to 538 ms, while due the implementation of a footrest a duration of 502 ms was achieved. Only for the most unfavourable configuration (R3, 95th percentile male, shoe soles flat on floor) the seat rotation did not work.

In general, the dummy loadings of head, upper neck, chest & pelvis were very low, which was to be expected for a pre-crash situation with a braking deceleration of 0.45 to 0.5 g. All maximum values were far below the dummy thresholds. For a more detailed assessment a comparison to pre-crash volunteer test data would be reasonable. In the following figures, the head accelerations (Figure 60),

the chest accelerations (Figure 61), the pelvis accelerations (Figure 62) and the seat belt forces (Figure 63) are compared for rotation axis position R1 depending on the dummy size (left) as well as the feet rest configuration (right). The peak values occurred at the time of the hard stop of the seat, i.e. no damper or any other optimisation was taken into account, as would be the case in a series application.

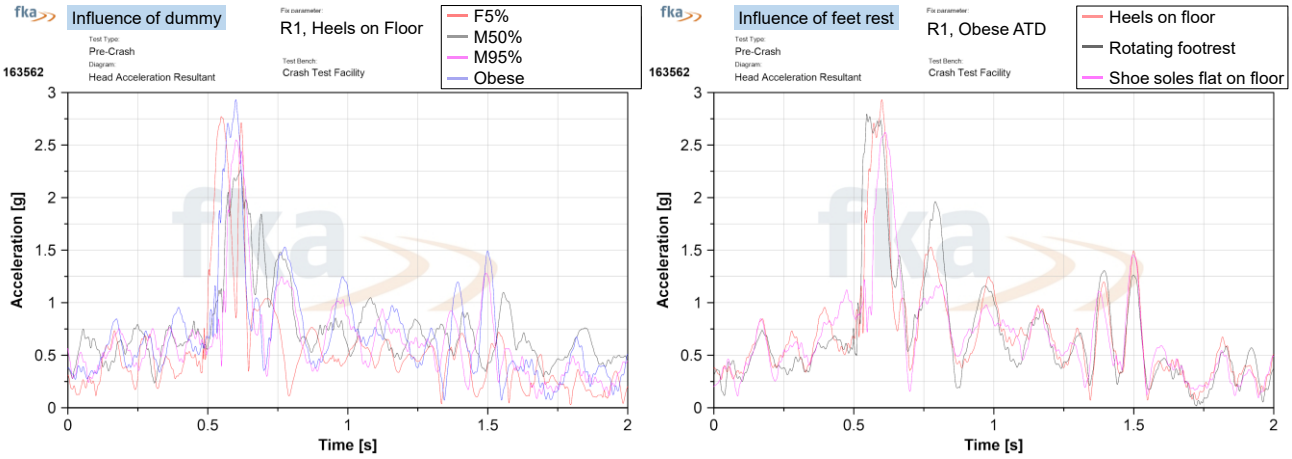

Figure 60 Head acceleration (res.) - rotation axis position R1

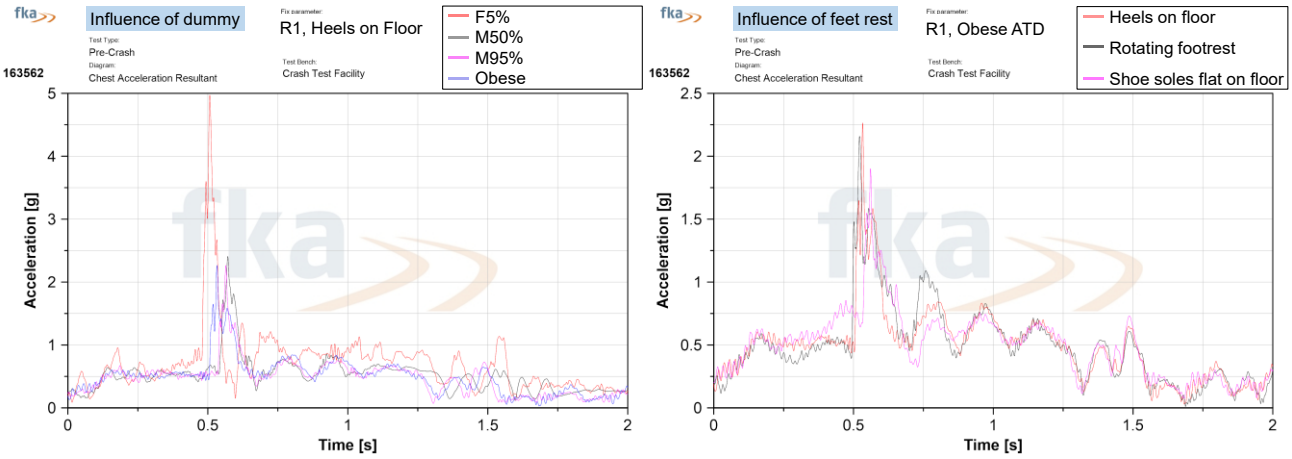

Figure 61 Chest acceleration (res.) - rotation axis position R1

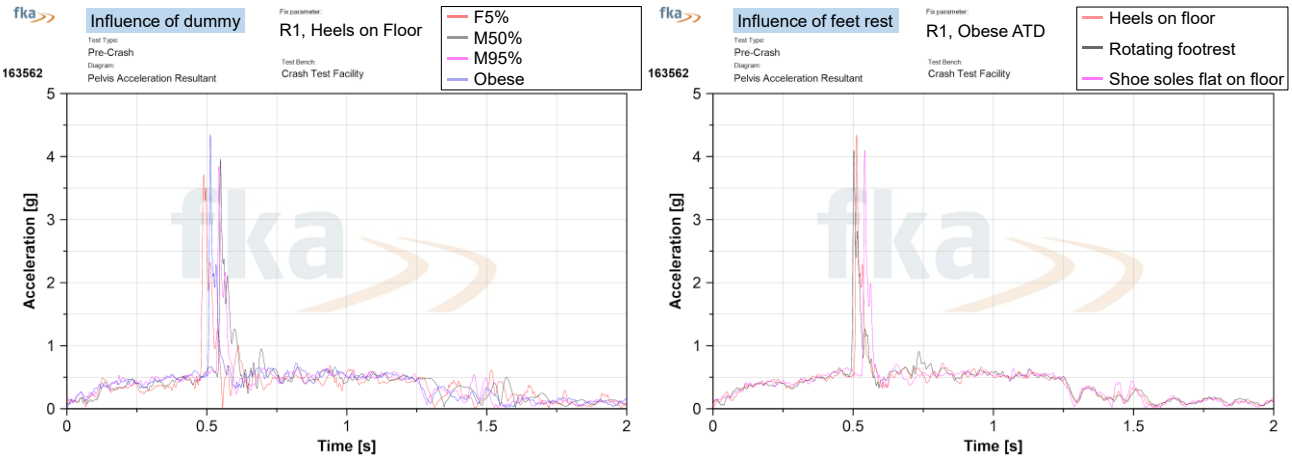

Figure 62 Pelvis acceleration (res.) - rotation axis position R1

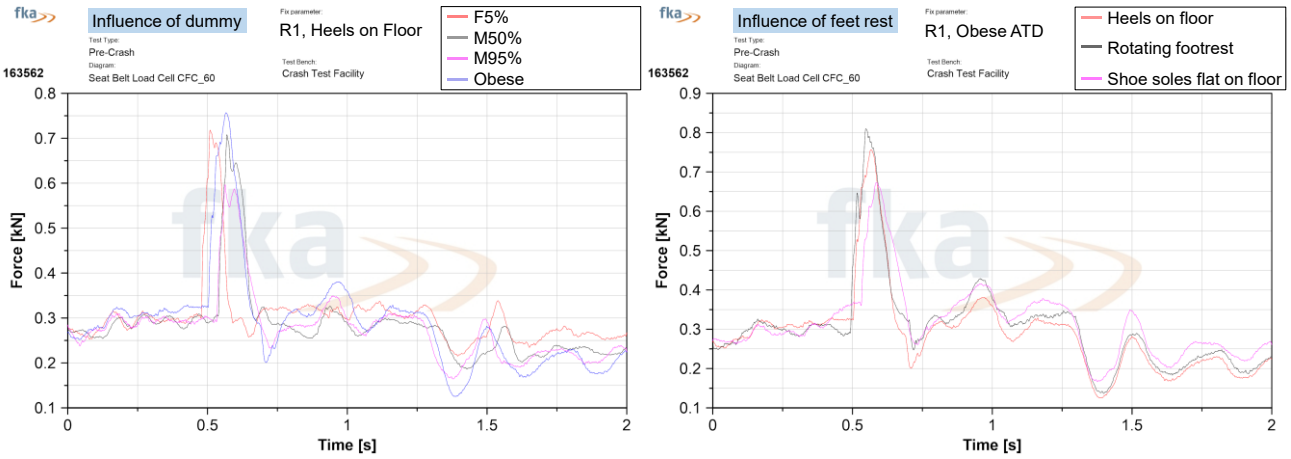

Figure 63 Seat belt force - rotation axis position R1

Limitations

The HIII dummy was neither designed to conduct seat rotations nor to address the associated low loadings in the pre-crash phase. Its knee joints are so stiff around the y-axis that hardly any weight of the heels or feet is exerted on the floor. This minimised the friction between the shoes and the floor. So the dummy shoes slid with little resistance during the seat rotation. Furthermore, compared to humans, the leg and ankle joints are stiff around the x-axis, i.e. twisting of legs is more difficult. This is especially relevant for the configuration with increased friction between feet and floor (shoe soles flat on floor). Some general investigations showed significant differences in this regard. This means that the legs tend to twist rather than pulling the shoes along. Without a rotatable footrest, an unfavourable leg posture after the rotation of the seat can be expected. To investigate this further, it would be necessary to carry out appropriate volunteer tests.

3.2.3 Virtual Demonstrator

In relation to the previously presented physical demonstrator tests, additional virtual simulations were conducted to calibrate the PP2 virtual demonstrator initially presented in Deliverable D2.4 [7]. The virtual demonstration is shown exemplarily for a 50th percentile male occupant for three different rotation axis positions without footrest.

3.2.3.1 Environment and Restraint System Models

The virtual tests were simulated using the generic Madymo interior model described in OSCCAR Deliverable D2.1 [14], representing a driver and front passenger compartment of a passenger car. The model was adapted for the simulation studies on PP2 (see Deliverable D2.4 [7]) and is in this context used for the virtual demonstration of the physical tests described in Chapter 3.3.2. Based on the physical demonstrator several general adaptions were done to the model.

The generic interior model, as it is shown in Figure 64, consists of an interior trim (grey), a rotatable seat in a 30° inwards rotated initial position (yellow), an airbag (blue), as well as a seat-integrated three-point belt system (black). The model was simulated in Simcenter Madymo R2020.1 using a quality (Q) facet Hybrid III (HIII) 50th percentile dummy model (70.7 kg) and a Simcenter Madymo AHM v3.1 50th percentile occupant model (75.3 kg). The AHM settings were defined as in the PP2 simulation studies documented in Deliverable D2.4 [7]. To enable a free motion of the occupant and the seat within all tested rotation axis positions, all contacts between occupant and interior trim were deactivated apart from the contact between the floor and the occupant. The contact friction between

the occupant and the floor and between the occupant and the seat were parametrised as preparation for the model validation. To simulate the same mass distribution as it was measured in the physical tests, the seat mass was adjusted to 46.16 kg (without footrest) and the centre of gravity was shifted relative to the seats H-Point according to the measured position in the physical setup (see Figure 47). No additional seat characteristics were aligned between physical and virtual demonstrators.

As only the pre-crash phase was physically and virtually demonstrated, the airbag and the (in-crash) belt pretensioner were deactivated. To represent the pretensioned belt of the physical setup, as it can be seen in Figure 64 the virtual motorised seat belt (MSB) tensioned the belt at the retractor at -1.25 s with a target force of 250 N within the virtual model. The peak force is reached at about -1.2 s simulation time, avoiding a jerk motion of occupant and seat at the release of the seat and the initiation of the AEB pulse at -1 s simulation time. The timing of the different actions is illustrated at the bottom of Figure 64.

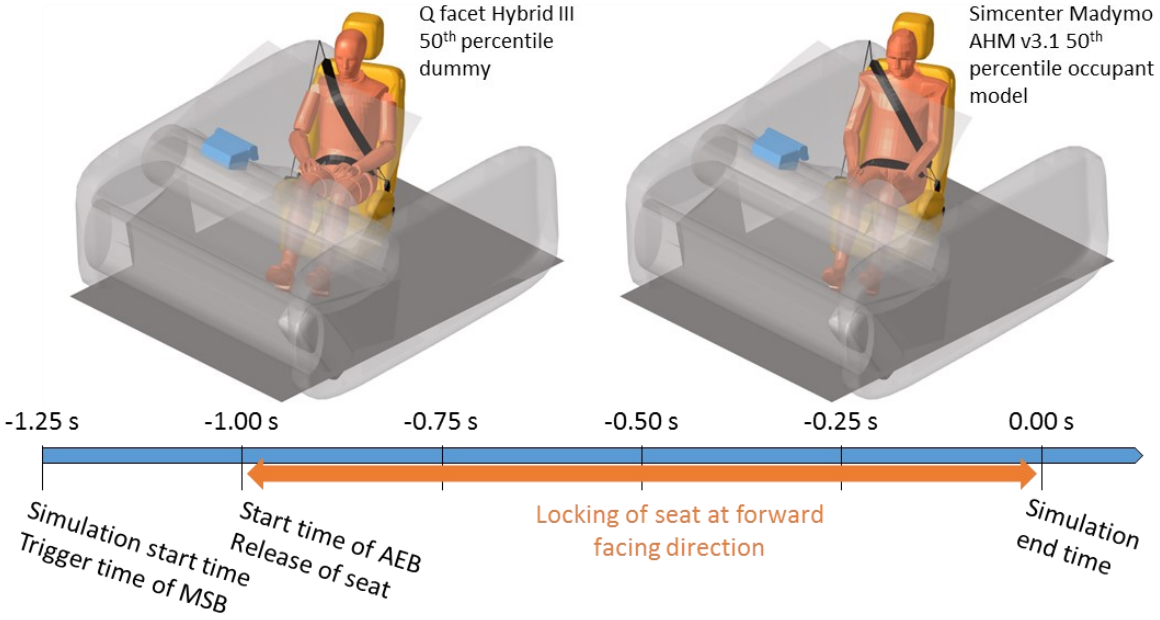

Figure 64 Simulation environment and timing

Additional to the general model adaptions the following specifications in Table 9 apply to the three different simulation setups for the rotation axis positions R1, R2, and R3. The x, y and z translational acceleration components of the AEB pulses, measured in the physical tests and applied to the virtual demonstrator, are shown in Figure 65. A CFC 10 filter according to SAE was applied to the measured pulses before they were used to simulate the brake pulse in the virtual model. Within the timeframe between -1.25 s and -1 s the acceleration was kept constant at 0 g to ensure the pretensioning of the three-point belt acting before the initiation of the seat rotation.

	R1	R2	R3
Rot. axis coordinates	Appendix Figure 218	Appendix Figure 218	Appendix Figure 218
Initial velocity	20.9 km/h	20.4 km/h	20.3 km/h
Acceleration pulse	Figure 65 blue curve	Figure 65 red curve	Figure 65 green curve

Table 9 Setup specific simulation settings derived from physical testing

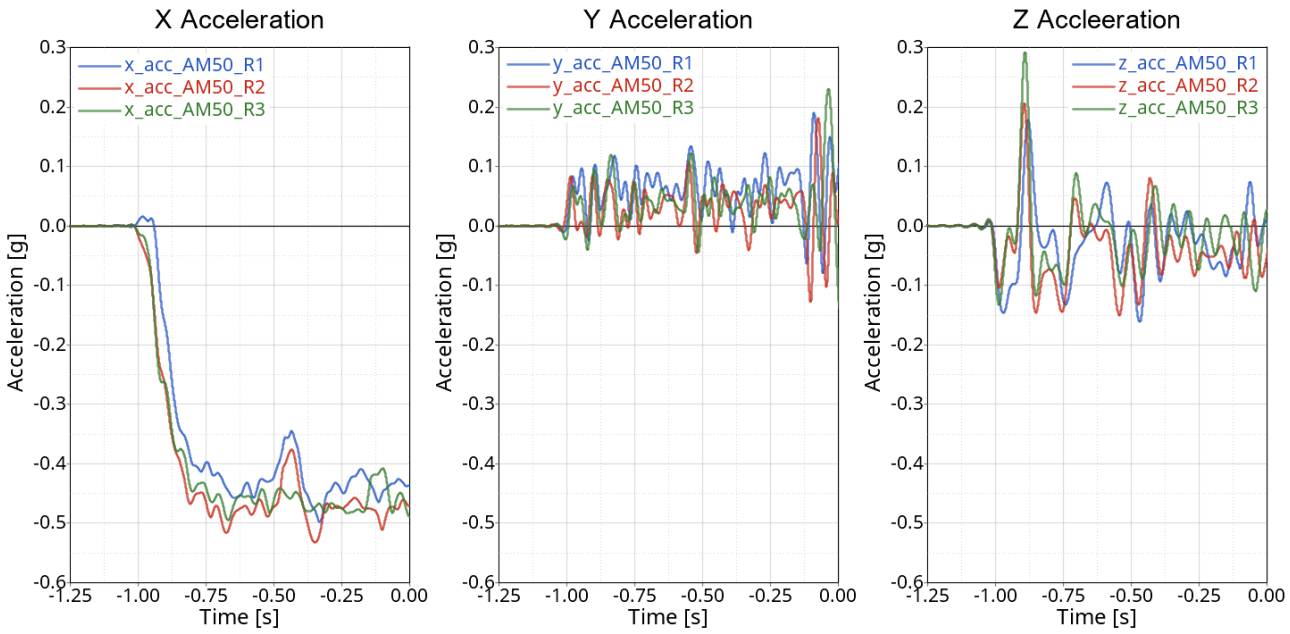

Figure 65 Acceleration pulses for rotation axis positions R1, R2 and R3 from physical testing

3.2.3.2 Calibration

Within this section the virtual demonstrator (hereinafter referred to as SIMULATION) calibration in terms of adjustment of simulation model settings based on the physical test results (herein after referred to as TEST) is presented. The calibration focus was on the general rotation behaviour of the seat in interaction with the occupant. It has to be mentioned that the applied seat model within the simulations differed in several characteristics from the hardware seat. A validation on material property and geometrical level was not intended. The seat, which was used in the physical demonstrator (see Chapter 3.2.2.1) represented a vehicle specific production seat and therefore differed from the generic seat model, which was intentionally used for the PP2 studies to assess the protection principle on a broader level. The difference in geometry can clearly be seen when comparing the physical seat and the simulation model illustrated in Figure 66. Due to this difference a precise alignment of the occupant position between tests and simulations was not possible. However, the occupant was qualitatively positioned in a comparable position.

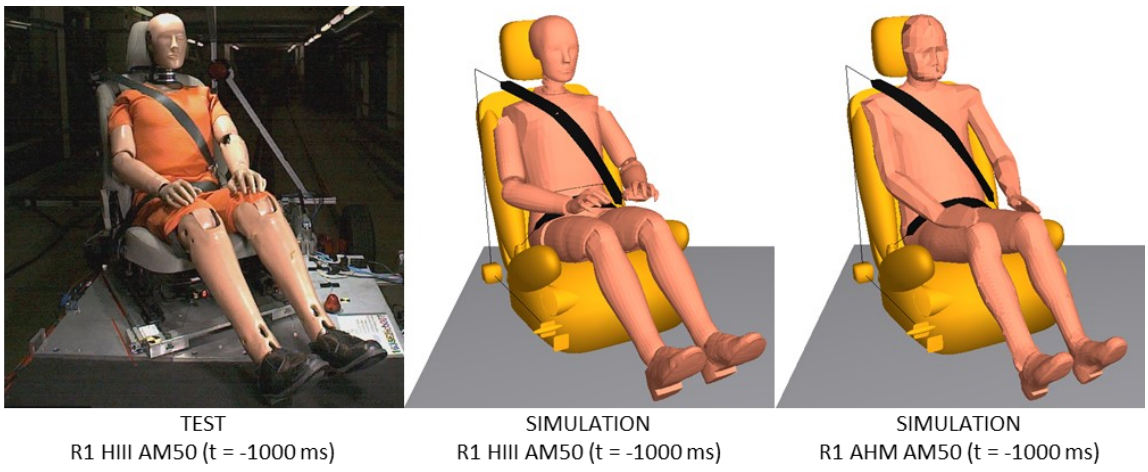

Figure 66 Initial occupant position of physical and virtual demonstrators (HIII & AHM) for R1

Without measurement of the friction between the floor and the dummy in the tests and because in some cases barely no contact force existed between the occupant and the floor due to the stiff dummy leg joints, a parametric study was conducted on the friction coefficient ranging its value from 0.01 to 0.5. The friction settings were adjusted depending on the investigated rotation axis positions (R1, R2, R3) and the dummy positioning to better match the test results (one test for each configuration). To validate the general rotation behaviour of the model, two parameters were investigated: the required rotation time to rotate seat and occupant from 30° to 0° (Figure 67 and Table 10) and the maximum rotation velocity (Figure 68 and Table 11).

The calibration curves for the two investigated parameters are shown in the following Figure 67 and Figure 68 for R1, R2 and R3. For R1 and R2 the contact friction coefficient occupant-floor was increased to 0.5 and the occupant-seat contact coefficient was set to 0.3 (default). For R3 the contact friction coefficient occupant-floor was set to 0.3 (default) and for occupant-seat to 0.17. The settings were chosen based on the results of the HIII AM50 dummy simulations. The AHM response curves are also shown as reference with identically chosen friction coefficient settings and were close to the HIII response for R1 but slightly deviated for R2 and R3.

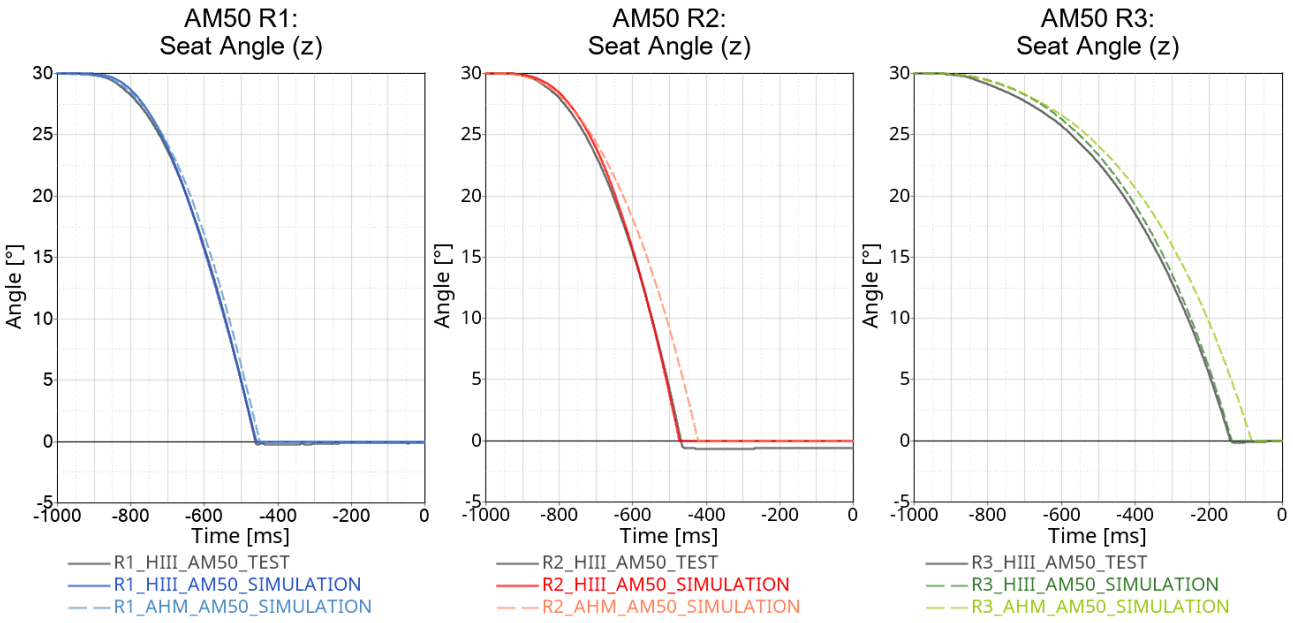

Figure 67 Response of seat rotation angle per time for R1, R2 and R3 for the AM50 occupant

Time for seat rotation from 30° to 0°			
Rotation axis pos.	R1	R2	R3
HIII AM50 (TEST)	**545 ms**	**539 ms**	**864 ms**
HIII AM50 (SIMULATION)	541 ms *(-0.73 %)*	527 ms *(-2.23 %)*	862 ms *(-0.23 %)*
AHM AM50 (SIMULATION)	551 ms *(+1.1 %)*	578 ms *(+7.24 %)*	916 ms *(+6.02 %)*

Table 10 Time for seat rotation (deviation to physical demonstrator in brackets)

For R2 the maximum deviation between virtual and physical demonstrator was equal to -2.23% when comparing the required rotation duration to rotate the seat from 30° to 0° using the HIII dummy (time

difference of 12 ms). Higher deviations were measured for the AHM, which can be explained by the overall differences in modelling and behaviour of human body models and ATD models, e.g. the occupant model geometry and the muscle activity. The highest deviation between AHM simulation and HIII physical test amounted to +7.24% (time difference of 39 ms) for R2. In general the AHM model needed more time to fulfil the rotation.

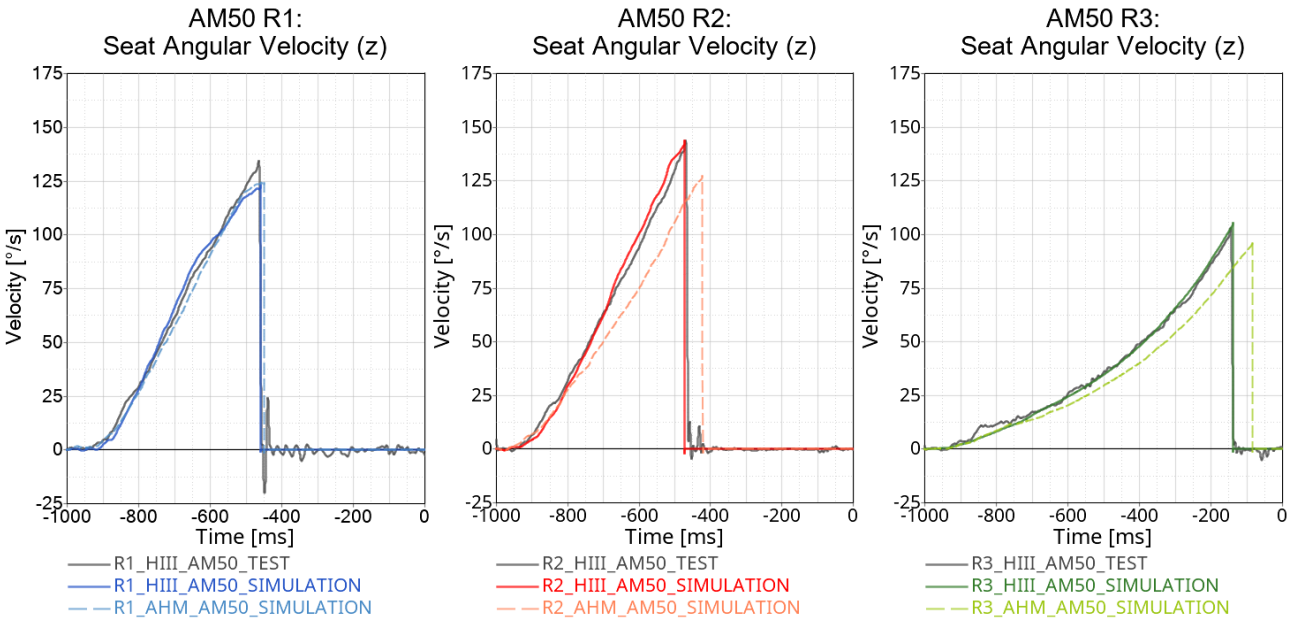

Figure 68 Response of seat angular velocity (z) per time for R1, R2 & R3 for AM50 occupant

Max. seat angular rotation velocity (z)			
Rotation axis pos.	R1	R2	R3
HIII AM50 (TEST)	**134.6 °/s**	**144.0 °/s**	**103.2 °/s**
HIII AM50 (SIMULATION)	123.7 °/s *(-8.1 %)*	144.1 °/s *(+0.07 %)*	105.7 °/s *(+2.42 %)*
AHM AM50 (SIMULATION)	124.5 °/s *(-7.5 %)*	127.8 °/s *(-11.25 %)*	97.2 °/s *(-5.81 %)*

Table 11 Time for seat rotation (deviation from physical demonstrator in brackets)

For the HIII dummy the maximum angular velocity of the seat showed the highest difference between virtual and physical demonstrator in case of rotation position R1. This deviation was -8.1% (rotation velocity difference of 10.9 °/s). The AHM simulations showed higher deviations to the physical demonstrator for R2 and R3 while R1 was close to the deviation of the HIII dummy simulation model with respect to the tests. The highest deviation of the AHM simulations was measured for R2 with -11.25% difference compared to the tests (rotation velocity difference of 16.2 °/s). As can be seen in the previous section, the longer rotation duration of the AHM was also reflected in the lower rotation velocities compared to the physical demonstrator.

In general the virtual HIII dummy demonstrator showed a good correlation to the physical HIII dummy demonstrator in terms of rotation duration and maximum angular velocity. The virtual AHM demonstrator showed larger deviations, which could be due to the model differences (e.g. mass) and the consideration of muscle activity.

3.2.3.3 Simulation Results - Occupant Kinematics

Within this section, the rotational movement is compared for the 50th percentile male occupant between the HIII physical dummy, the HIII dummy simulation model and the AHM. The results are given with respect to the physical tests, considering all three simulated rotation axis positions R1, R2 and R3.

The image sequences are shown in a frontal view which was aligned as much as possible between virtual and physical demonstrator. Differences due to the view perspective cannot be fully prevented. The results are shown in the following by Table 12, Table 13 and Table 14.

R1			
Time	TEST (HIII)	SIMULATION (HIII)	SIMULATION (AHM)
-1000 ms	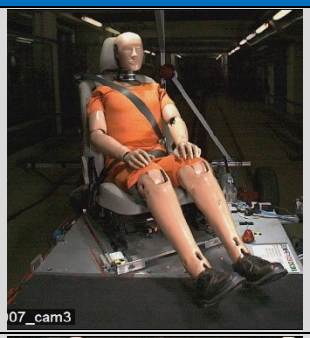	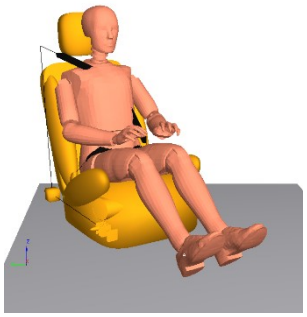	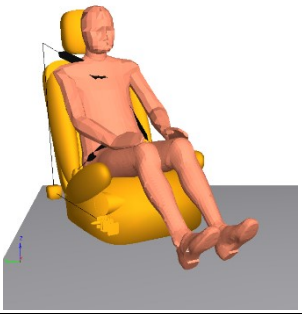
-750 ms		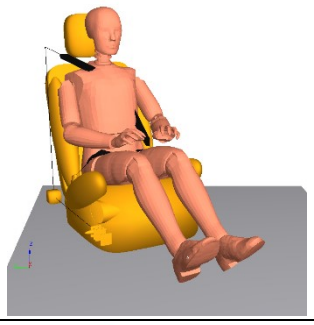	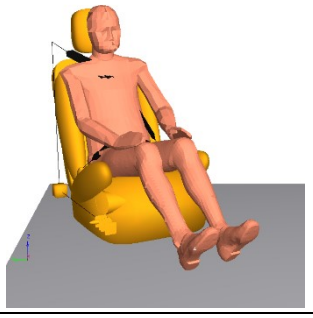
-500 ms	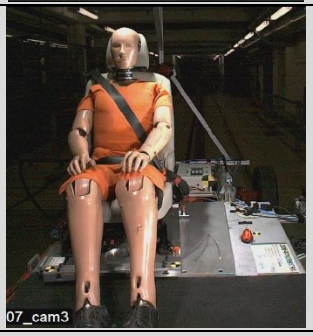	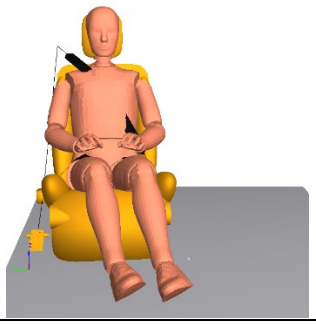	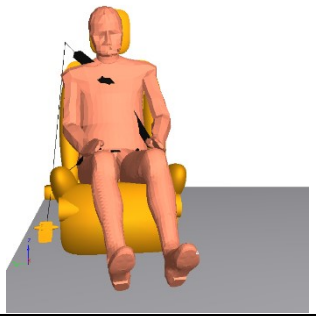
Seat rotation time	-455 ms 	-459 ms 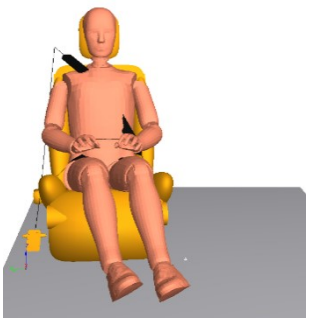	-449 ms 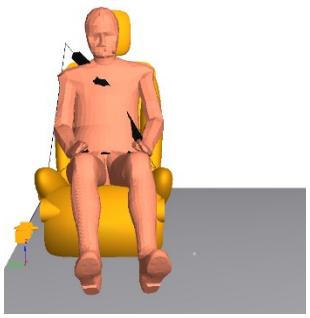

-250 ms		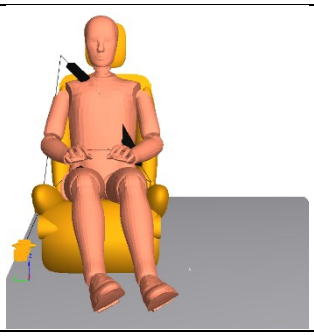	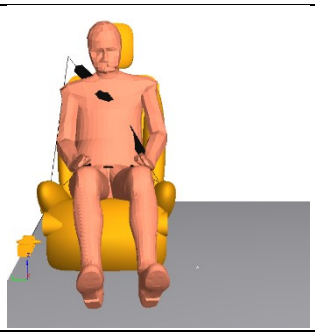

Table 12 Visual comparison of physical and virtual demonstrator for R1 in front view

R2			
Time	TEST (HIII)	SIMULATION (HIII)	SIMULATION (AHM)
-1000 ms		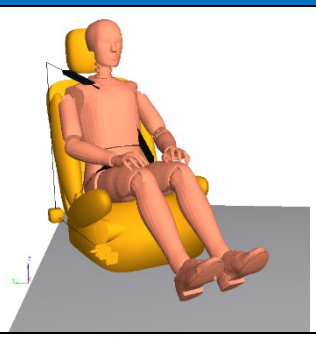	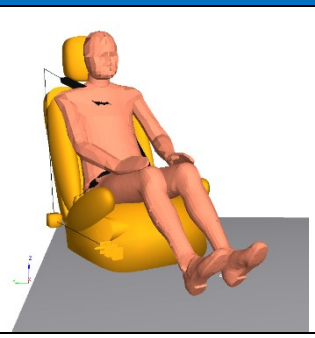
-750 ms		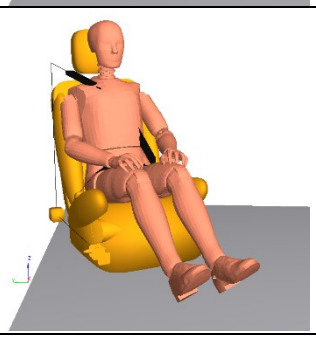	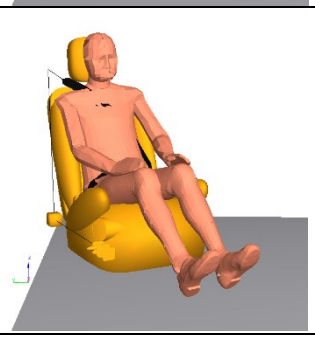
-500 ms		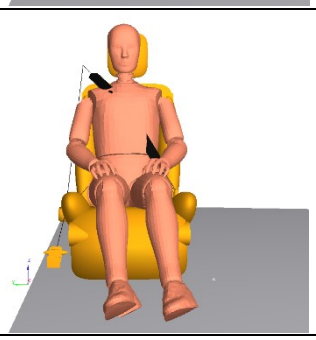	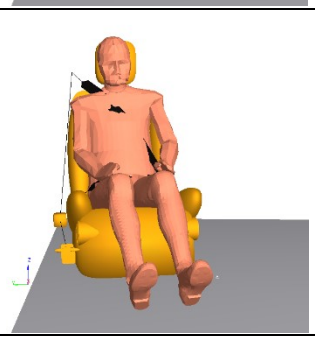

Seat rotation time	-461 ms	-473 ms	-422 ms
		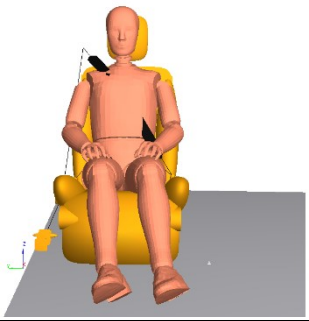	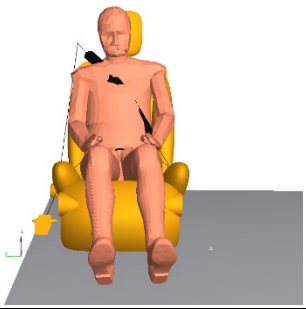
-250 ms		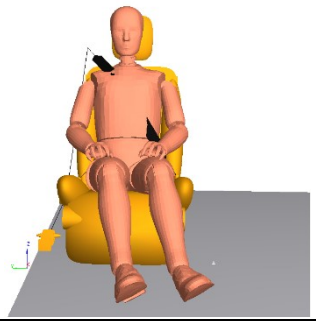	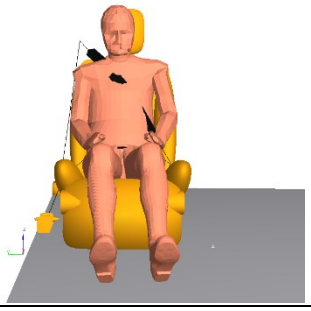

Table 13 Visual comparison of physical and virtual demonstrator for R2 in front view

R3			
Time	TEST (HIII)	SIMULATION (HIII)	SIMULATION (AHM)
-1000 ms	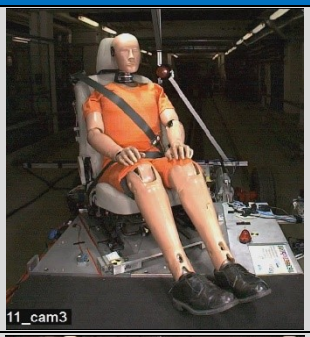	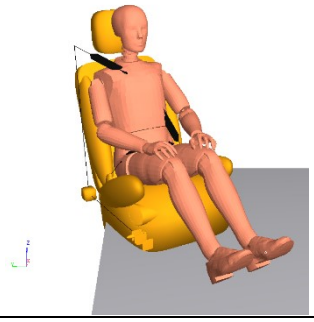	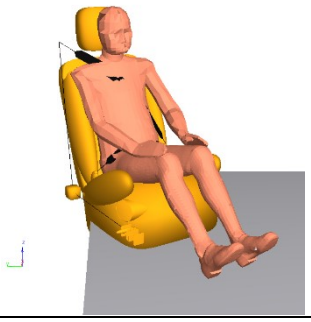
-750 ms	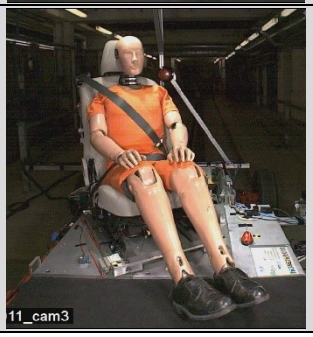	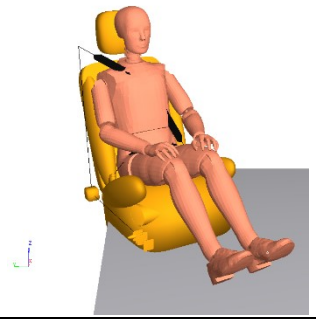	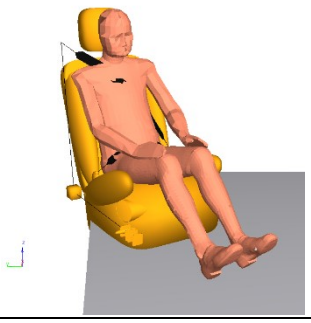

-500 ms		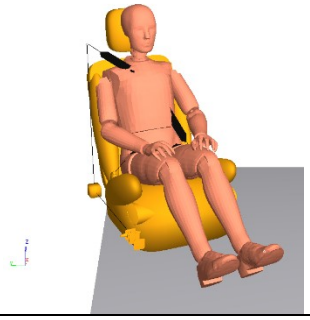	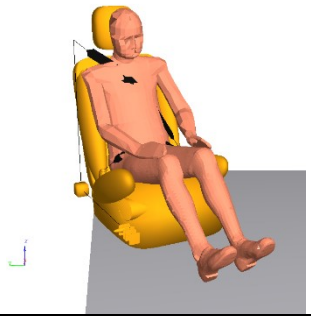
-250 ms		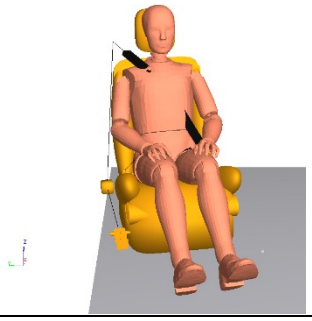	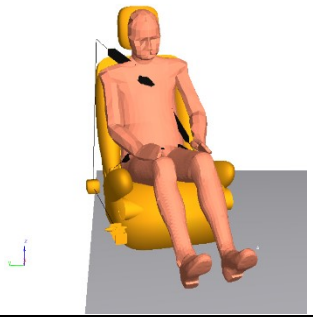
Seat rotation time	-136 ms 	-138 ms 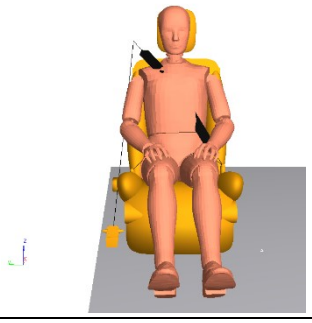	-84 ms 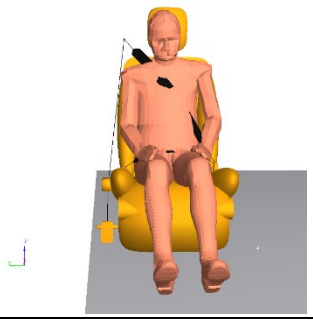

Table 14 Visual comparison of physical and virtual demonstrator for R3 in front view

In Table 12, it can be observed, that for R1 the final occupant position differs between the physical and the virtual demonstrators. The highest deviation can be seen for the lower extremities. Also differences between the lower extremity movement between AHM and HIII dummy can be observed. Also the head movement between AHM and HIII dummy is different, which can be explained by the active muscles of the AHM. A clarification whether the difference in lower extremity position is based only on the friction setting or also on other parameters cannot be elaborated in this context due to the limitations described with regard to the physical demonstrator (see Chapter 3.3.2.8).

The smaller deviations described above between virtual and physical demonstrator for R1 (Table 12) can also be seen for R2 and R3 (Table 13 and Table 14). In general, the occupant followed the seat rotation in all cases in a comparable way. A difference for the lower extremity motion has to be acknowledged.

3.2.3.4 Simulation Results - Occupant Accelerations

In this section a comparison of the resultant accelerations for head, chest and pelvis of the 50th percentile male occupant is given with regard to the physical demonstrator (grey curves) and the virtual demonstrators (coloured curves). Within Figure 69, Figure 70 and Figure 71 the resultant acceleration curves are shown for the three rotation axis positions R1, R2 and R3.

From all body region accelerations (Figure 69 to Figure 71) it appeared, that the accelerations at the time of the final seat position (0°) were much higher in the tests than in the simulations. Differences with regard to the seat rotation stop between experiment and simulation could be the reason for these deviations. First of all, the rotation stop of the seat within the simulation was defined on the rotation axis itself, whereas in the tests the rotation stop is further forward on the seat rail. Moreover, the rotation stop was not modelled via a contact definition but via constraining the rotational degree of freedom of the seat rotation joint when a seat angle of 0° was reached. Overall, the accelerations measured for head, chest and pelvis were on a very low level (accelerations of virtual demonstrators < 2 g; accelerations of physical demonstrator < 4 g). For the different rotation axis positions, no clear trend could be observed apart from the difference in rotation time until the forward facing seat position was reached.

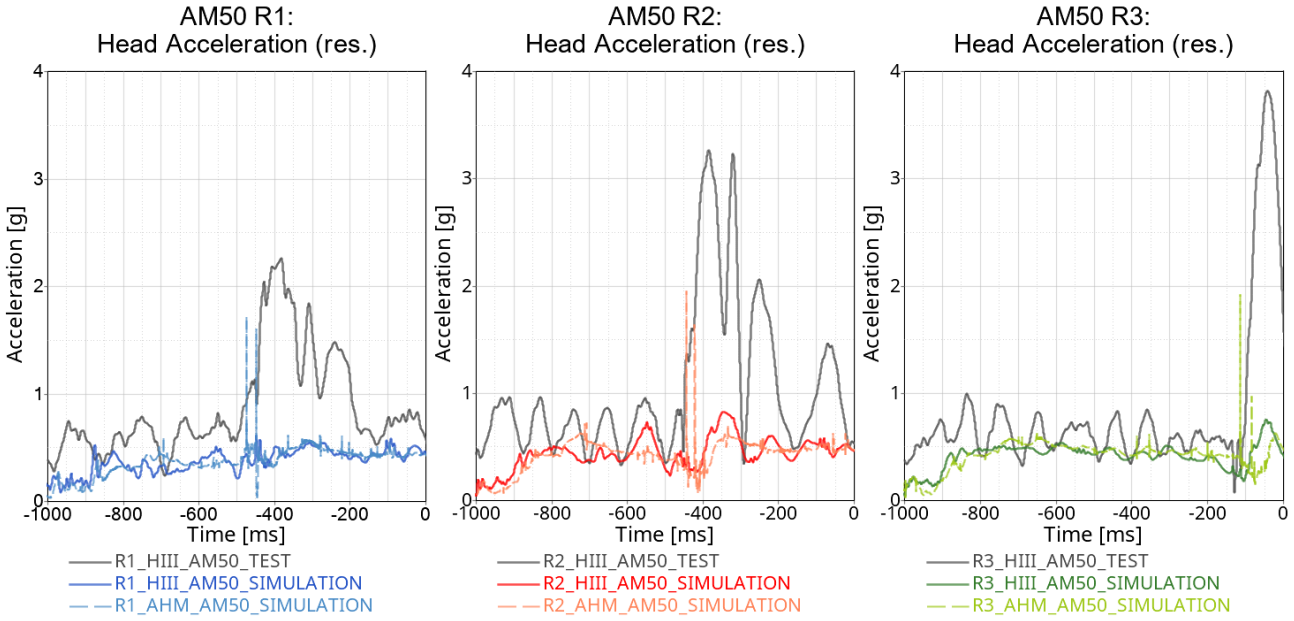

Figure 69 Resultant head acceleration

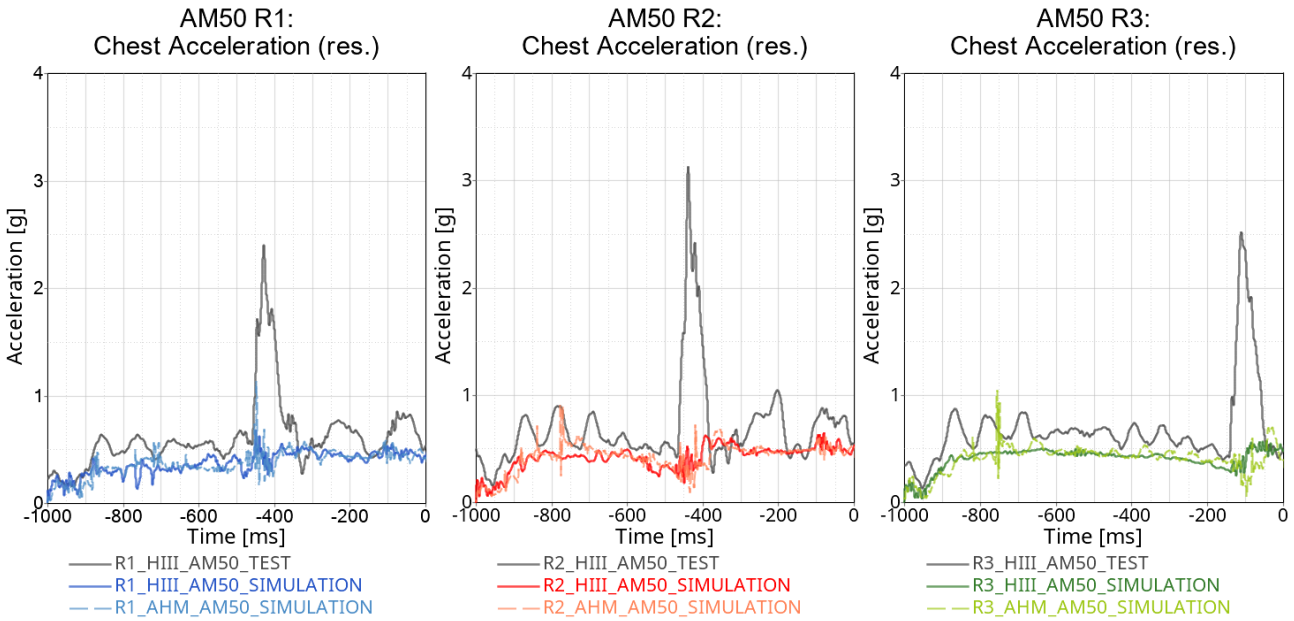

Figure 70 Resultant chest acceleration

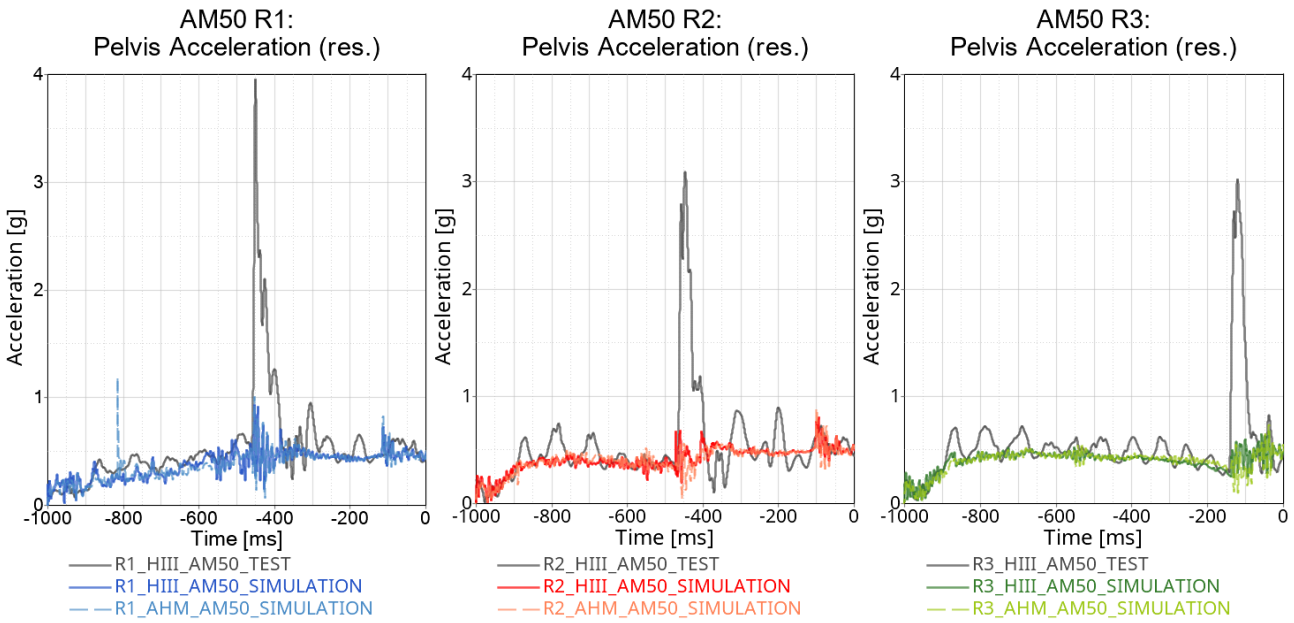

Figure 71 Resultant pelvis acceleration

During the rotation process (30° > seat angle > 0°), the accelerations for head, chest and pelvis for R1, R2 and R3 were on a comparable level. In this timeframe, the measured acceleration values from the HIII dummy model and AHM matched well the ones obtained in the tests. However, in the timeframe of the rotation stop, high deviations of the body accelerations between physical and virtual demonstrator were observed.

3.2.3.5 Summary and Limitations

Overall, the simulations showed comparable results to the physical demonstrator in terms of rotation duration, maximum rotation velocity and occupant upper body kinematics. In simulations and tests the measured accelerations were on a low level (< 4 g) and the required rotation time was for all rotation axis positions within the defined time boundary of 1 s. All simulated rotation axis positions successfully rotated the 50th percentile occupant to the forward facing seating position.

The lower extremities and the measured body accelerations for head, chest and pelvis showed some deviations between physical and virtual demonstrator, especially in the timeframe of the rotation stop. For the lower extremities especially the leg orientation and ankle joint behaviour varied between tests and simulations as well as between the HIII dummy model and the AHM. In comparison to the tests, the simulations showed generally less rotation of the lower extremities for all cases. The upper body position was only marginally affected by this. The body accelerations were on a comparable level during the seat rotation. At the time when the final seat angle was reached, the body accelerations in the tests showed a peak, which was not measured to that extend in the simulations. This might be due to differences with regard to the mechanical stop and locking of the rotation in the physical demonstrator. In the simulations, a sensor switch was applied for the locking mechanism, which locked the rotational degrees of freedoms of the seat rotation joint, whereas in the tests a hard stop for the seat rotation was implemented further forward on the seat rail.

As the physical tests only provided one test per setup, no conclusion on the scatter of the physical tests could be drawn. Thus, the calibration of the rotation behaviour of the simulation models was based on only one physical test each. Furthermore, the limitations of the physical tests have to be taken into account as well (see Chapter 3.2.2.6). The HIII hardware dummy as well as the HIII dummy simulation model were not designed for the load case investigated. The dummy was not

validated for rotational movement of an occupant nor for low acceleration levels (< 1 g) and acted more as a ballast mass than as an injury assessment tool in the tests. In addition, different seat models and thus also slightly different initial seating positions of the occupant were considered for the physical and the virtual demonstrator. The only parameters that could be adapted for the seat simulation model were the centre of gravity and the mass. The position of the dummy feet and the low contact conditions between the dummy feet and the floor could not be accurately reproduced from the tests. Furthermore, no information on the brake pitching of the sled was measured and therefore not considered in the respective pulses of the simulation model.

Despite the numerous limitations, the physical and the virtual demonstrators showed the overall functionality of PP2 for a large variety of rotation axis positions and demonstrated that a fast seat rotation, caused only by brake deceleration, is possible.

3.2.4 Conclusion and Next Steps

The conducted test series considering four different dummy models, three rotation axis positions and different feet configurations demonstrated the functionality of PP2 in general. All tested configurations rotated the seat and occupant from a 30° inward to a 0° rotated “standard” position. The rotation allowed a repositioning of the occupant to a forward-facing seating position within a total time of less than 1 s (starting point: t_0, initiation of braking). This rotation to the “standard” seat position could be achieved for a maximum brake deceleration of only 0.5 g. For the fastest rotation axis, found to be at the rearmost and very outwards position of the seat base, rotation durations in the range of 0.5 s were achieved. Only for the most unfavourable configuration (rotation axis position at the furthest forward position, 95th percentile male, shoe soles flat on floor) the seat rotation did not work. Besides the physical tests, corresponding simulations for the 50th percentile male occupant models HIII and AHM were conducted within the framework of a virtual demonstrator.

When rotating the seat, the occupant body followed the seat in slightly different ways, depending on the body region. This was shown in the simulation studies of PP2 in Deliverable D2.4 [7]. Especially the lower extremities showed less rotation compared to the other body parts, leading to rotated feet positions, pointing away from the driving direction at the end of the seat rotation. This effect was observed especially in the simulations and not in the tests. For most of the tests, the legs were in line with the upper body. The amount of feet rotation varied between the setups and could not be fully aligned between physical and virtual demonstrator, as the friction conditions between floor and feet also depended on the leg and ankle joint stiffness of the dummy. Some general investigations revealed that human legs tend to twist rather than pulling the shoes along. Without a rotatable footrest, an unfavourable leg posture after the rotation of the seat can be expected. To investigate this further, it would be necessary to carry out appropriate volunteer tests, since the applied occupant models are not validated for the investigated rotational load case. The AHM showed a comparable rotation behaviour of the feet as the HIII model but the reaction of a real human in the investigated use case remains uncertain, as sudden reactions or an occupant trying to resist the rotation might affect the functionality of the principle.

The investigated protection principle did not provide any additional restraint to the occupant, and aimed only at repositioning the occupant into a standard seating direction. The interaction with a restraint system after rotation and during the subsequent in-crash phase was not investigated, neither with the physical demonstrator nor with the virtual demonstrator. The PP2 studies showed a possible way to enable rotated seats in future interiors. The principle needs to be combined with state of the art restraint systems (e.g. airbags) and also consider environmental information (e.g. the initial seat rotation angle) to provide an efficient overall protection function. It has to be seen in the context of an integrated restraint concept, including information on crash detection as well as monitoring of the occupant and the interior.

3.3 Protection Principle 6: Far-Side Load Case

As expressed in OSCCAR Deliverable D2.4 [7], the results of the accident analysis conducted in WP1 (OSCCAR Deliverable D1.1 [2]) supported the investigation of a protection principle addressing the safety of occupants of AD vehicles in a far-side load case. The findings were transferred into the design and development of Protection Principle 6 (PP6), which consists of a double lap belt pre-tensioning (SOTA DLPT belt) system combined with seat side supports for occupant restraint. An inboard belt configuration both with and without seat side supports was also investigated.

Chapter 3.3 describes the test series performed at CTAG-IDIADA to evaluate the effectiveness of PP6 in a sled test environment (physical demonstrator) as well as the corresponding virtual demonstrator.

3.3.1 Motivation and Background

Side collisions where an AD vehicle is being hit by an opponent car will represent around 20% of collisions at intersections in urban or rural areas in future mixed traffic (OSCCAR Deliverable D1.1 [2]). Thus, considering the future L4/L5 AD vehicle concepts and their new interiors that should allow more flexibility in terms of seat position, occupant tasks (working, reading or resting), it was found crucial to investigate the protection of occupants in a far-side load case. More specifically, one of the challenges would be to restraint an occupant's pelvis and thorax without a vehicle centre console. In future cars, the centre console is expected to disappear, offering the possibility to the occupants to rotate their seats into a '*living room*' configuration for example.

To do so, a previous study by Petit et al., 2019 [9] was taken as a reference. This study conducted series of far-side sled testing activities comparing the performance of the WorldSID dummy with Post Mortem Human Subjects (PMHS). The generic environment of [9] was used for the evaluation of OSCCAR PP6 (Figure 72). In consequence, the OSCCAR tests could also provide data to assess the WorldSID dummy biofidelity in a far-side load case since two of the tests represented the test configuration of [9].

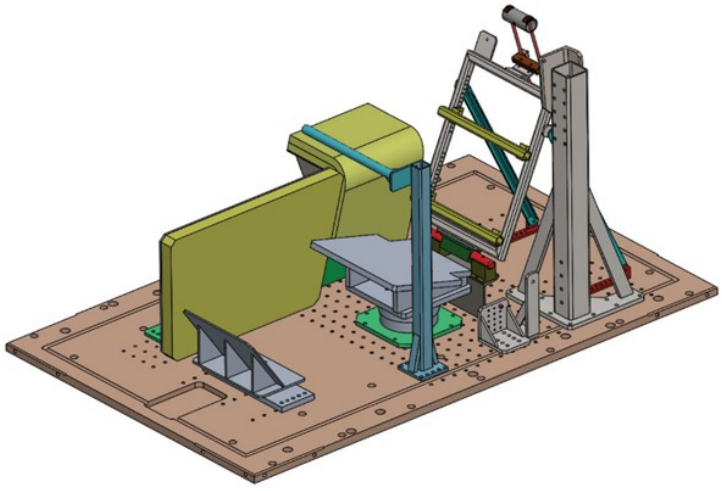

Figure 72 Testing rig from [9] used in the PP6 physical sled tests

Additionally, the PP6 investigation allowed to compare the response of the THUMS HBM with the WorldSID hardware dummy as well as numerical dummy model in order to highlight the differences in their kinematics, interaction with the belt and other components of the environment. This is important to understand the injury risk assessment by the two human surrogates [7].

3.3.2 Physical Demonstrator

The test set-up of [9] was borrowed for the PP6 sled test series performed at CTAG-IDIADA. The complete environment and the equipment involved in the tests are described in the following.

3.3.2.1 Environment

The test set-up consisted of separated components assembled in a common rigid frame as shown in Figure 73. The components respective positions were adjustable thanks to the several holes available on the rigid frame. Similarly, the seatbelt anchorage points could be adjusted on the brackets along the longitudinal and vertical axes thanks to the holes performed every 25 mm and 20 mm respectively (3 longitudinally and 5 vertically).

Apart from the rigid frame the hardware included a rigid inclined seat pan, a rigid frame with two horizontal bars as seatback, a rigid footrest and four independent structures to attach the belt anchorage points (D-ring, inside buckle and outside anchor attachment points). The first two tests were performed under exactly the same conditions as in [9] using the pelvis and the leg centre consoles and a static pretension to confirm that the rig and sensor performance were similar to [9]. However, for the tests performed at CTAG-IDIADA, the crossbar and the headrest mounted on the seatback frame were removed as can be seen in Figure 73.

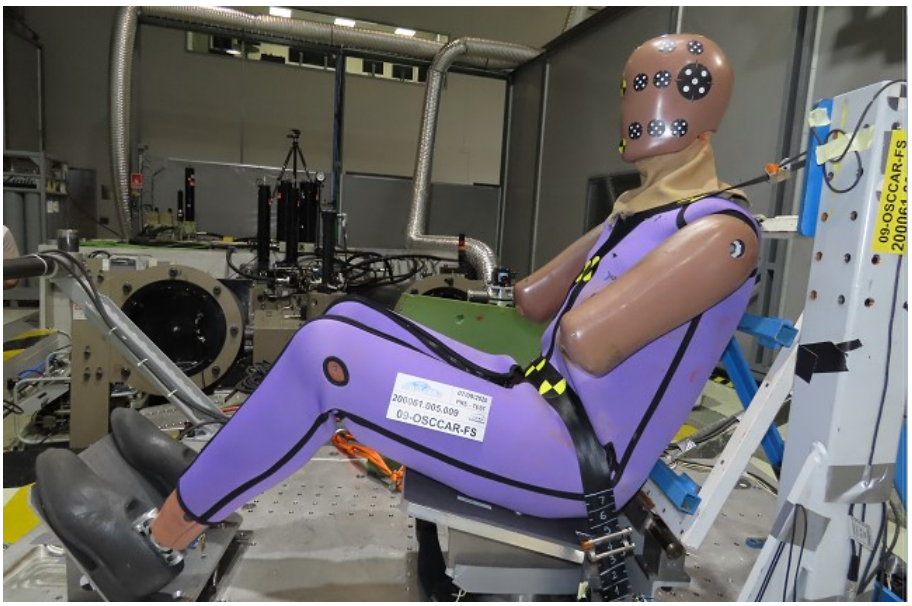

Figure 73 PP6 test set-up in CTAG-IDIADA facilities (09-OSCCAR-FS)

The components of the testing rig changed during the test series to represent the different required testing conditions. Thus, the environment was adapted to different seatbelt configurations (D-ring on B-pillar position, seat-mounted driver left-handed side position and seat-mounted front passenger right-handed side position), with the presence of the centre console first and then with the assembly / disassembly of the seat side supports on the rigid frame to achieve the three main setups to be tested. Those three configurations are illustrated in Appendix 3.2, which represent the environments used for tests 01, 03, 06-OSCCAR-FS of the series and their corresponding repetitions and variations (see Table 17).

In alignment with the latest Euro NCAP far-side test protocol [10], the test setup was mounted with its centreline at 75º ±3º towards the direction of travel of the sled. Figure 74 shows the relative position of the test rig with respect to the sled facilities in CTAG-IDIADA.

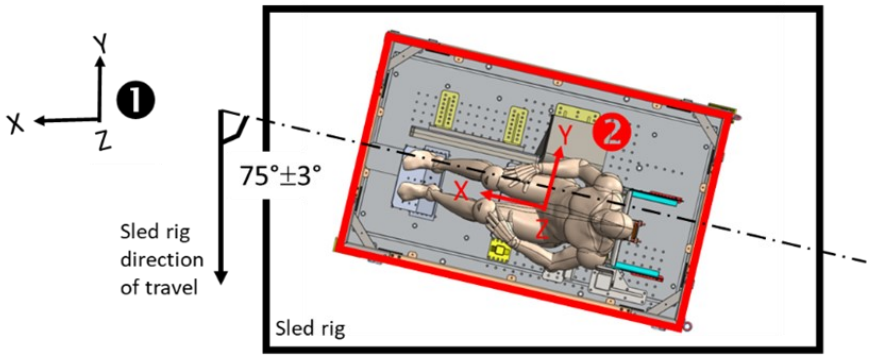

Figure 74 Test set-up orientation on CTAG-IDIADA Hy-Ge reverse acceleration sled

Seat pan and backrest

The seat was designed to be of an aluminum plate mounted on a 6-axes load cell to measure the contact forces between the dummy and the seat. The seat pan was angled by 15º with respect to the horizontal plane and was trimmed in the rear to avoid interaction with the lap belt path, as can be seen in Figure 75.

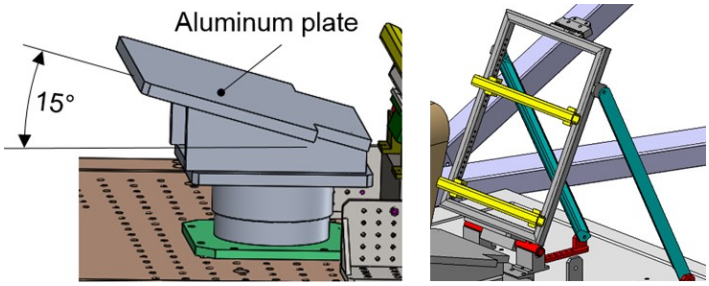

Figure 75 Rigid seat pan mounted on the 6-axes load cell and seat backrest

The backrest consisted of two horizontal tubes with square cross-section whose position could be adjusted along a metal frame. The angle of the frame was also adjustable. In order to replicate the test conditions of [9], the frame was adjusted to 24° ±1º with respect to the vertical. The horizontal tubes were adjusted on the frame such that the dummy chest tilt sensor recorded 0° ±1º and the targets placed on the dummy back were visible.

Footrest

The footrest contained an aluminum rigid plane inclined by 125º with respect to the base plate that was mounted onto a 3-axes load cell to measure the contact forces between the dummy feet and the footrest.

Centre console

The initial test set-up from [9] included two consoles: one for the interaction with the pelvis and one for the legs. The pelvis console was instrumented with two load cells, which allowed to derive the contact forces between the dummy and the console. Both rigid structures were covered by Ethafoam TM 180 from Sealed Air (https://www.sealedair.com/products/protective-packaging/fabricated-foams-packaging) according the following specifications:

- Two layers of 25 mm thickness shaped around the pelvis console and glued together by neoprene glue and attached to the console rigid frame by double face tape,
- One layer of 50 mm thickness attached to the leg console using double face tape

In order to obtain repeatable test conditions, the foam layers were changed after each test.

3.3.2.2 Protection Principle 6

SOTA DLPT belt

The *state-of-the-art* double lap belt pretension belt (SOTA DLPT belt) used for PP6 (Figure 76) was provided by Autoliv and was also used within the OSCCAR PP3 studies. It consisted of a 3-point seatbelt that included 2 pretensioners in the lap belt. The shoulder retractor included a 3.5 kN load limiter and a 2 kN pretensioner. The SOTA DLPT belt was mounted in all the tests from 03-OSCCAR-FS to 10-OSCCAR-FS, either used in driver left-handed side position or in front passenger right-handed side position. The triggering times in all cases were 8 ms for both the shoulder retractor and outer lap belt (non-buckle side) pretensioners and 1 ms for the buckle pretensioner.

Figure 76 Autoliv 3-point seatbelt with double lap pretensioner

Seat side supports

The seat side supports were designed to reproduce the shape and restraint conditions of a racing seat usually used in motorsports vehicles to minimise the lateral motion of the occupant. The supports consisted of two metal plates of following dimensions:

- Torso support: 155 x 171 mm
- Pelvis support: 400 x 255 mm

Both plates were covered with a 50 mm layer of Ethafoam TM 180 from SEALED AIR and mounted on a side structure attached to the sled rigid frame (Figure 77). The side structure was covered with a rubber sheet to avoid any WorldSID contact with sharp edges.

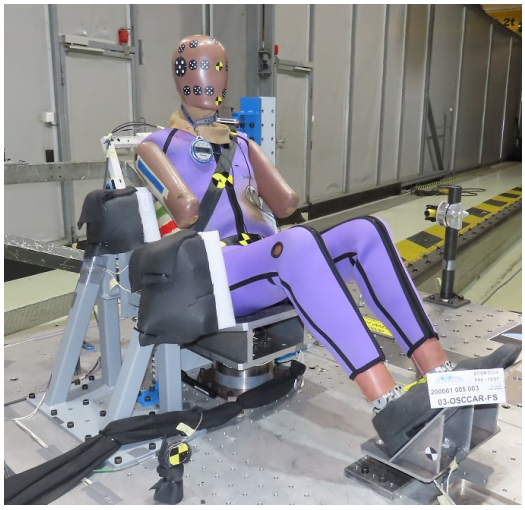

Figure 77 PP6 seat side supports (03-OSCCAR-FS)

3.3.2.3 WorldSID Dummy

The WorldSID version and settings were prepared according to the latest Euro NCAP Far-side test protocol [10]. The dummy was equipped with the half arm assembly on both sides and was clothed in a sleeveless suit, which was a modified version of the sleeved suit with sleeves removed. Given the number of previous tests performed, the WorldSID was fully calibrated in the CTAG-IDIADA certification laboratory at the beginning of the test series.

3.3.2.4 Instrumentation and Data Processing

The full list of sensors mounted in the test campaign can be found in Appendix 3.3. Except for the seat side supports, the load transfers between the dummy and the environment (seat, footrest, centre console and seatbelt) were measured. To calculate the contact forces between the dummy and the environment (seat, pelvis console and footrest), a test without the dummy was performed. As an example, the contact force between the dummy and the seat was calculated as shown in Figure 78.

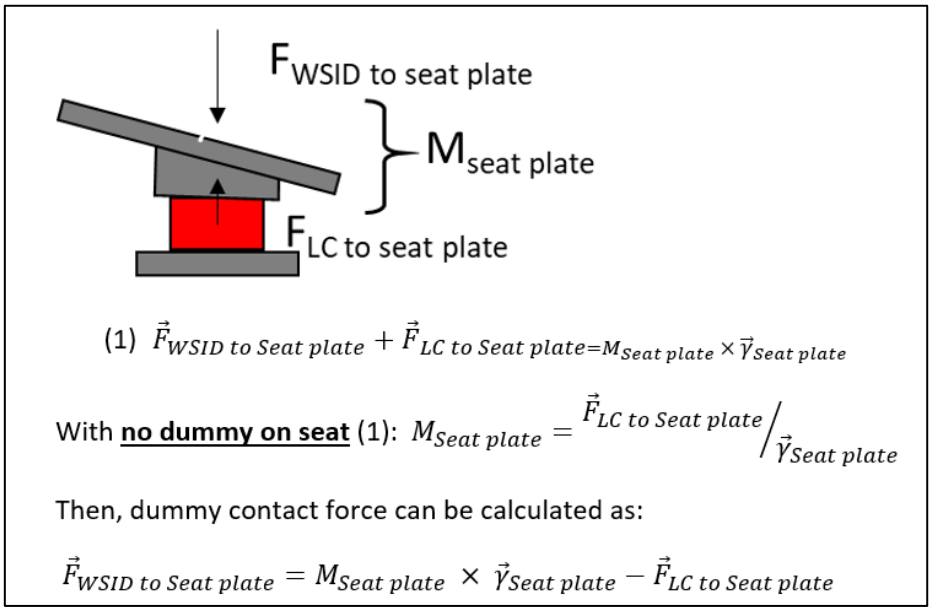

Figure 78 Computation of the contact forces between WorldSID and the seat

The WorldSID used an in-dummy acquisition system and was instrumented on the right side to measure rib deflections due to the contact with the centre console or the seat side supports. The WorldSID head 3D linear accelerations and 3D angular velocities were used to compute the head COG excursion. These results were compared with the analysis of the video tracking (Figure 255 of Appendix 3.6). All test channels were acquired with a 20 kHz sampling rate.

3.3.2.5 Cameras and Landmarks

Camera setting

Six high-speed cameras recorded the impact scene (5 on-board and 1 static from above) at a sampling rate of 2000 frames per second. Figure 79 shows the relative position of the cameras for the test series:

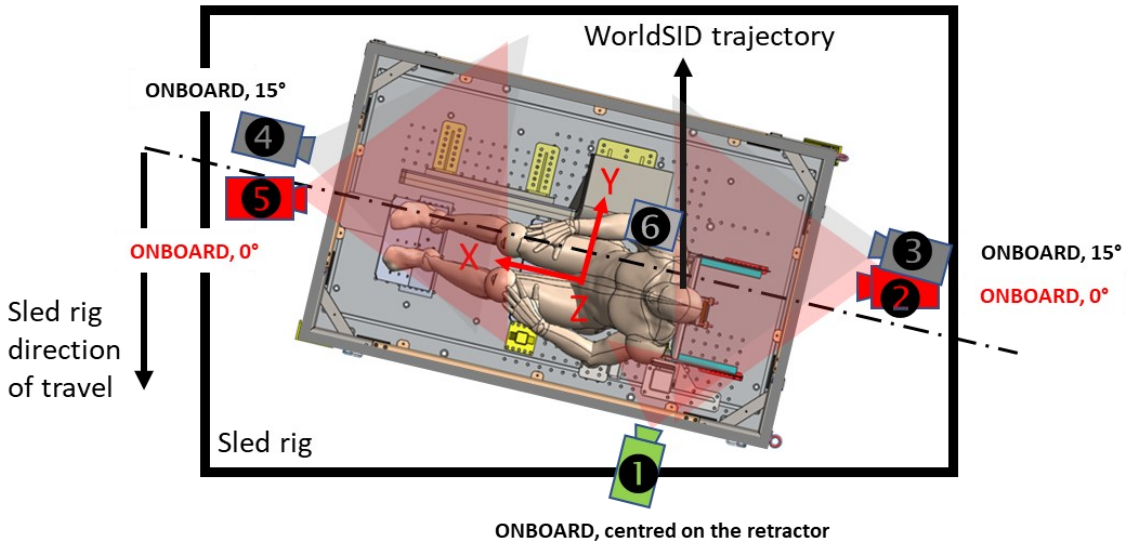

Figure 79 Camera positioning relative to the sled setup

The position of camera n°1 in Figure 79 was modified between tests with outboard and inboard seatbelt configurations to provide further information by recording the belt pay-in/out at the shoulder retractor (B1) for the driver left-handed side belt configuration. Thus, for the front seat passenger right-handed side belt configuration (or called in following chapters “inboard belt”) the camera n°1 position was not changed and recorded in this case the motion of the buckle. Figure 80 shows the position of camera n°1 in test 05-OSCCAR-FS and a screenshot of the movie at 10 ms before time zero. When the buckle was mounted on the seat side support side (for example in test 03-OSCCAR-FS), another camera was included in the test setup to enhance the analysis of the test results. For this test configuration, seven cameras were used in total. Camera n°7 was positioned to capture the pretension as shown in Figure 80.

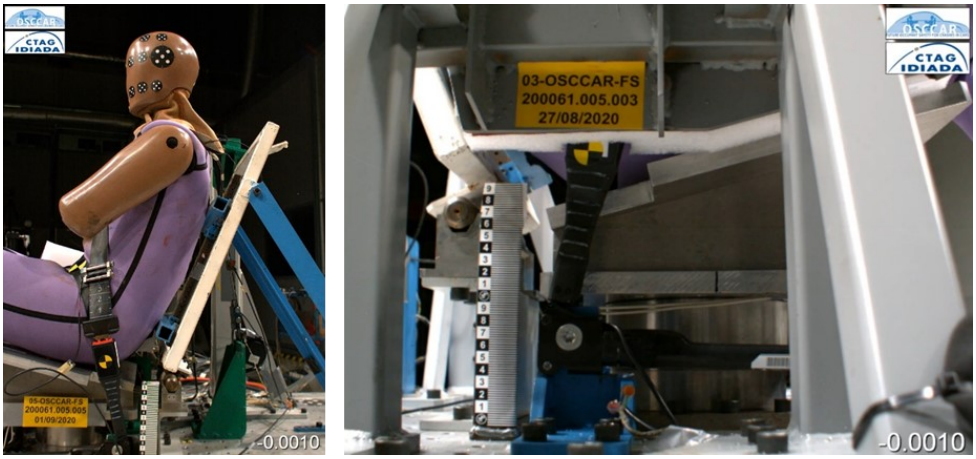

Figure 80 View of cameras n°1 (left) & n°7 (right) in tests 05-OSCCAR-FS & 03-OSCCAR-FS

Series of targets were placed both on the dummy and on the setup to support the analysis of the dummy excursion during the test. For this, two markers in the front and three markers in the rear of the dummy head were placed. On each side of the head mould, one target was positioned at the external head Centre Of Gravity (COG). Furthermore, five targets were placed in the dummy back (over the suit) at each rib level. The targets placed on the dummy head and back as well as on the seatbelt can be seen in Figure 81.

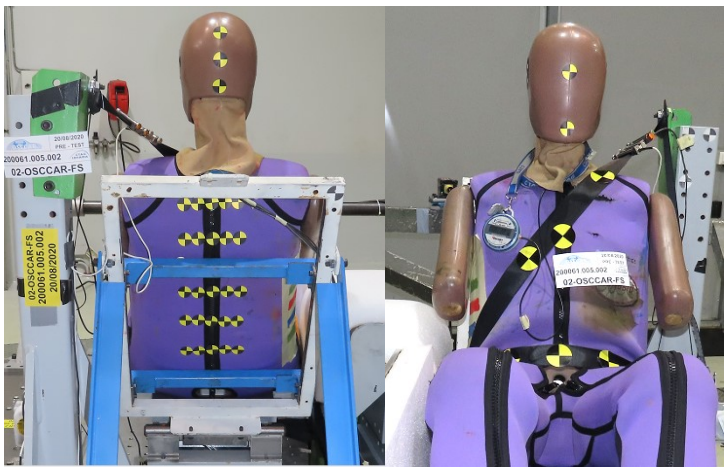

Figure 81 WorldSID back and seatbelt targets

For the video analysis, a specific procedure was applied using the TEMA software from IMAGESYSTEMS (https://www.imagesystems.se/tema/) to process the WorldSID head excursion during the tests. Using the images from two high-speed cameras (cameras n°4 and n°5) and several small MXT targets placed around the dummy head (Figure 82), it was possible to calculate the exact position of the WorldSID head every ms. Furthermore, since the dummy head had been previously 3D scanned (Figure 83), the most external point of the head could also be calculated at each ms. It was therefore possible to verify whether the dummy head crossed the lines defined in the Euro NCAP testing protocol. However, the complete video analysis could only be performed from tests 03-OSCCAR-FS to 10-OSCCAR-FS in which additional targets were placed on the dummy head (Figure 82).

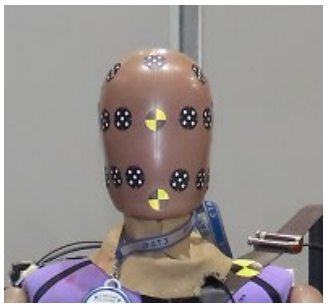

Figure 82 MXT targets for the 3D analysis of head excursion

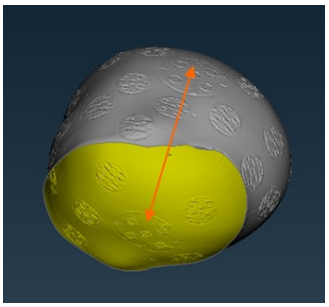

Figure 83 3D scan of the WSID used for the COG calculation

3.3.2.6 Test Matrix

A total of 10 sled tests were performed to study the effect of PP6 in the far-side sled test series. Five different test configurations with one repetition each assessed the performance of PP6. The first two tests were executed to validate the environment used in Petit et al., 2019 study [9], including a B-pillar mounted 3-point belt with a 200 N static pretention and a centre console.

Then, the SOTA DLPT belt was tested in combination with the seat side supports and reversing its position to outboard position. Finally, the seat side supports were removed and the SOTA DLPT belt was evaluated as the only protection principle for the far-side load case both in outboard and inboard position. Table 15 summarises the test matrix of the series and the times to fire (TTF) of the different pretensioners: 8 ms for the shoulder retractor pretensioner, 8 ms for the outer lap belt pretensioner and 1 ms for the buckle pretensioner.

OSCCAR Far-side tests @ CTAG-IDIADA					
OSCCAR test number	**Seat**	**Belt**	**TTF**	**Anchorages**	**Side support**
01-OSCCAR-FS	CEESAR rigid seat	3-pt No PT/200 N static load	None	CEESAR (B-Pillar)	Pelvis+Legs console
02-OSCCAR-FS	CEESAR rigid seat	3-pt No PT/200 N static load	None	CEESAR (B-Pillar)	Pelvis+Legs console
03-OSCCAR-FS	CEESAR rigid seat	SOTA DLPT belt	8ms for shoulder and outer lap belt and 1ms for buckle	Belt in seat	Side seat supports
04-OSCCAR-FS	CEESAR rigid seat	SOTA DLPT belt	8ms for shoulder and outer lap belt and 1ms for buckle	Belt in seat	Side seat supports
05-OSCCAR-FS	CEESAR rigid seat	SOTA DLPT belt	8ms for shoulder and outer lap belt and 1ms for buckle	Belt in seat - INBOARD	Side seat supports
06-OSCCAR-FS	CEESAR rigid seat	SOTA DLPT belt	8ms for shoulder and outer lap belt and 1ms for buckle	Belt in seat - INBOARD	Side seat supports
07-OSCCAR-FS	CEESAR rigid seat	SOTA DLPT belt	8ms for shoulder and outer lap belt and 1ms for buckle	Belt in seat - INBOARD	NO
08-OSCCAR-FS	CEESAR rigid seat	SOTA DLPT belt	8ms for shoulder and outer lap belt and 1ms for buckle	Belt in seat - INBOARD	NO
09-OSCCAR-FS	CEESAR rigid seat	SOTA DLPT belt	8ms for shoulder and outer lap belt and 1ms for buckle	Belt in seat	NO
10-OSCCAR-FS	CEESAR rigid seat	SOTA DLPT belt	8ms for shoulder and outer lap belt and 1ms for buckle	Belt in seat	NO

Table 15 OSCCAR PP6 far-side series test matrix

3.3.2.7 Test Results

Pulses

The test pulse was the same as the one of [9] and intended to reproduce a vehicle pulse in a side collision. Some variability between the tests was observed, as it can be seen in Figure 84, resulting in a velocity peak ranging between 7.5 m/s and 8.2 m/s. This variability is a common phenomenon when performing test series in the HYGE reverse sled and was judged acceptable for this test series. In addition to the sled acceleration, an accelerometer sensor was placed on the non-struck side B-pillar of the test set-up, following the Euro NCAP protocol, and in order to measure the test set-up accelerations along its local coordinate system.

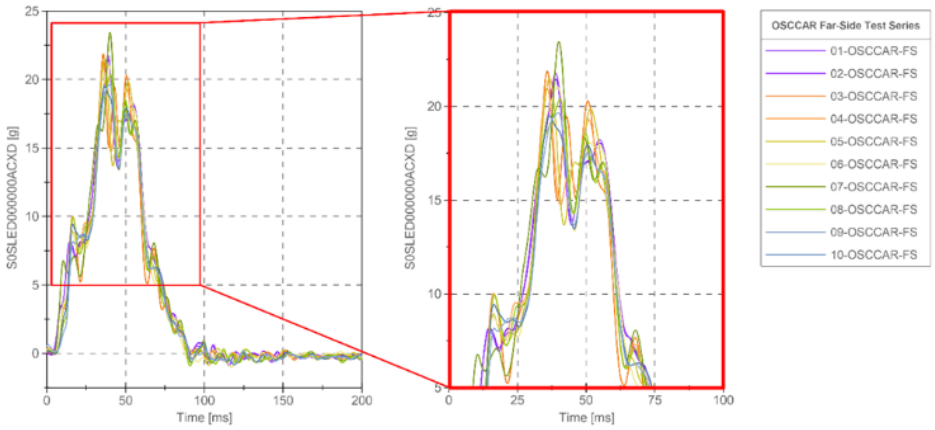

Figure 84 Acceleration for the sled test pulse in the test series

B3 and B6 seatbelt forces

In general, a good correlation between test pairs can be observed for both B3 (Figure 85) and B6 (Figure 86) forces. Major differences in B3 and B6 performance are seen in tests 07-OSCCAR-FS and 08-OSCCAR-FS (no centre console and no seat side support, seatbelt in inboard position). This could be explained by the pulse variability and the strong dependence on the seatbelt system for the restraint of the dummy in that configuration. The B6 signal in test 08-OSCCAR-FS was disturbed due to the contact of the sensor with the dummy.

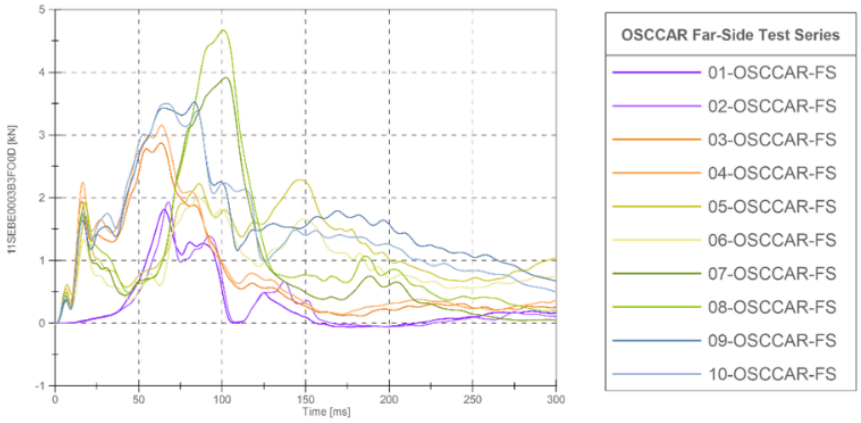

Figure 85 Performance of B3 within the PP6 test series

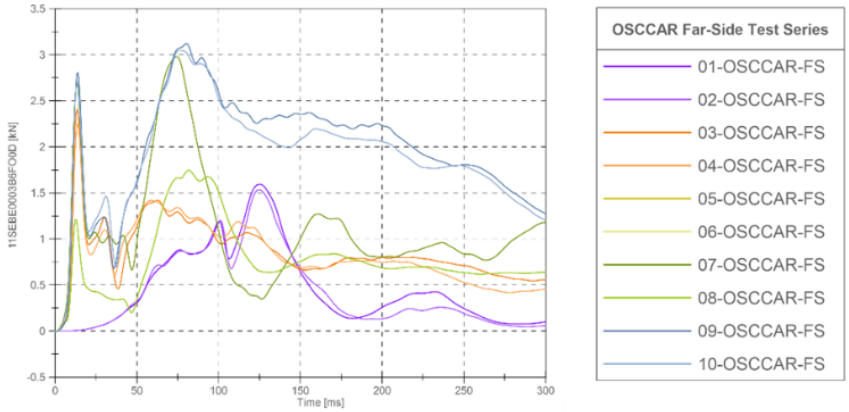

Figure 86 Performance of B6 within the PP6 test series

WorldSID channels

Considering the WSID performance in terms of kinematics, again a good correlation between tests and their repetitions is observable in a general overview of the results.

Tests 01-OSCCAR-FS and 02-OSCCAR-FS had a delayed head linear acceleration peak and the highest head angular velocity was observed for this initial configuration (Figure 87). This behaviour was related to the dummy impacting with the centre console. From Figure 88 it can be observed that the pelvis acceleration peak due to the centre console interaction appeared at around 60 ms (red circle). The removal of the centre console and the seat side supports brought a completely different kinematics for the lower extremities with respect to previous tests.

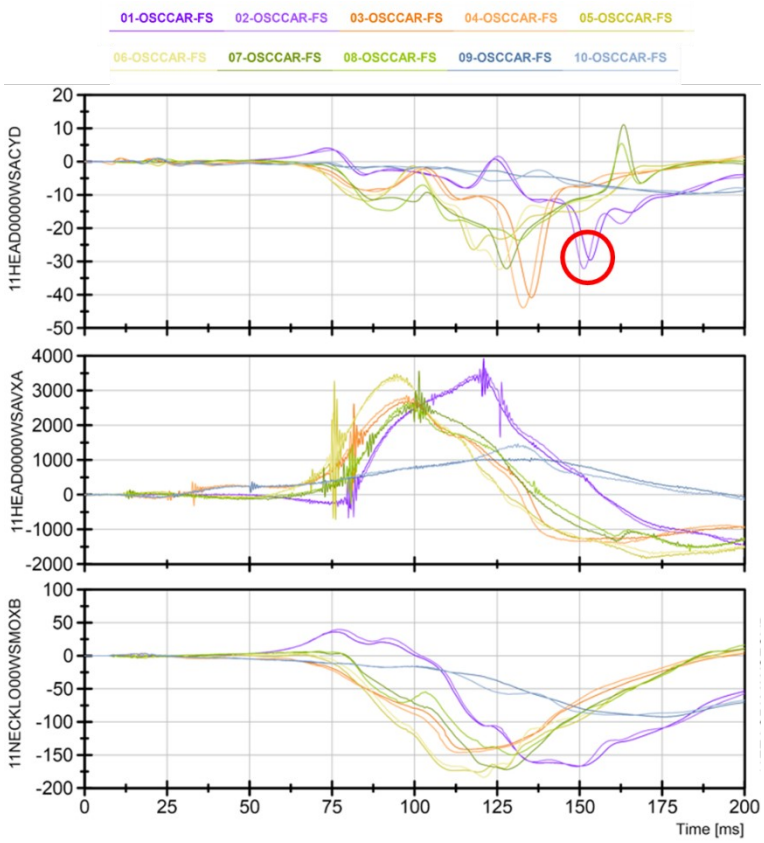

Figure 87 Dummy head linear y-acceleration, head angular x-velocity and lower neck Mx

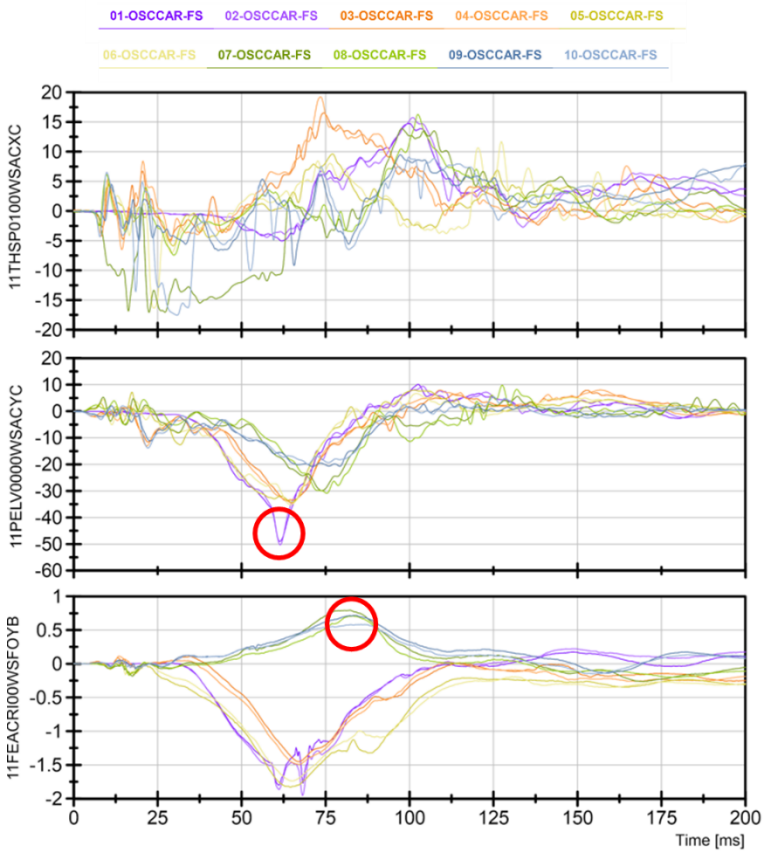

Figure 88 Dummy spine and pelvis linear x-acceleration and femur Fy

The setup in tests 07-OSCCAR-FS and 09-OSCCAR-FS (without any side support) reduced the loadings (Fy) on the femurs (Figure 88) since the legs were able to move freely during the whole test. It should be highlighted that this leg kinematics may lead to interaction with any other element or occupant within the vehicle interior. The differences in leg response with and without the seat side supports can be observed in Figure 89, comparing the femur kinematics between tests 03-OSCCAR-FS (with seat side supports) and 09-OSCCAR-FS (without seat side supports) at 200 ms.

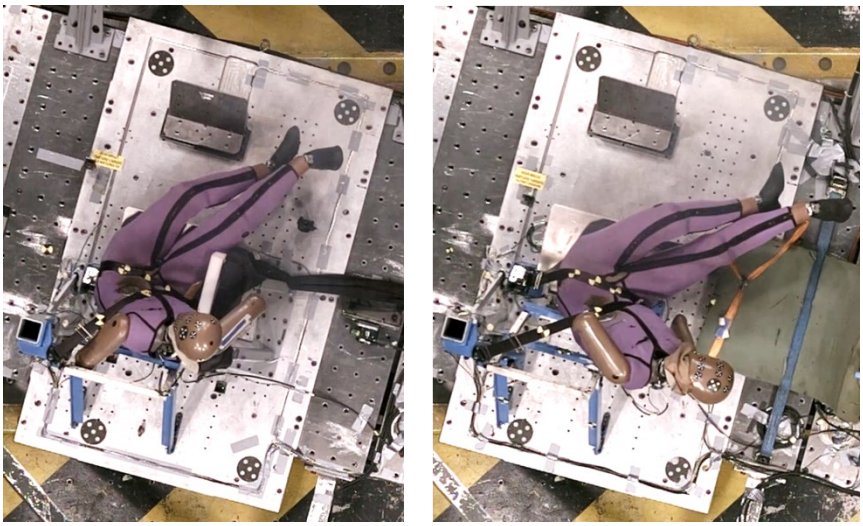

Figure 89 Top view of tests 03 (left) and 09 (right) showing WSID kinematics at 200 ms

The main differences in the WorldSID leg kinematics can be observed in Figure 90, where the odd tests of the series are shown at 75 ms. The presence of the console and the seat side supports affected not only the lower extremity kinematics but also the kinematics of the upper body.

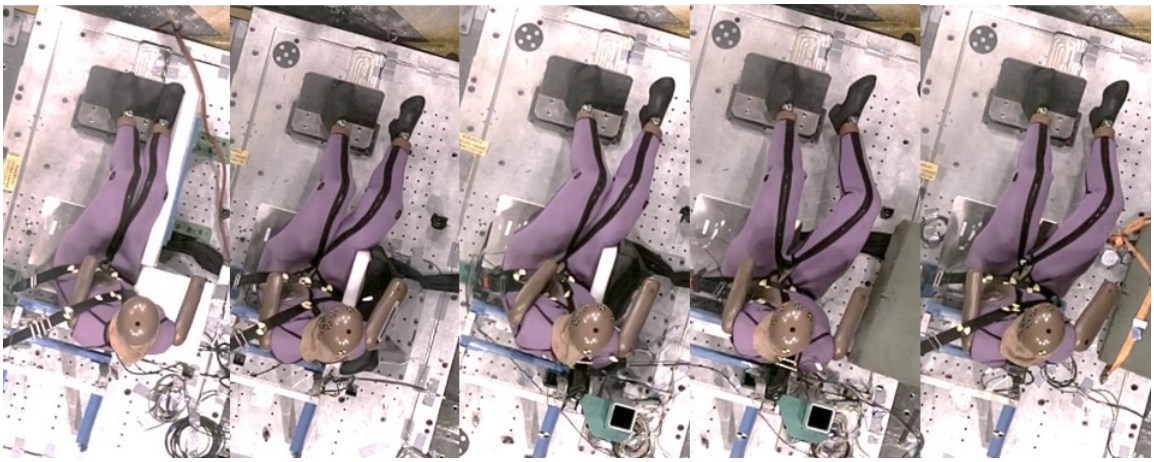

Figure 90 Left to right: Tests 01- 03- 05- 07- and 09-OSCCAR-FS at 75 ms

Head excursion

The excursion of the head in the far-side load case evaluates the risk of the occupant to interact with other passengers and/or elements of the vehicle including the door panel of the struck side. In the OSCCAR test series, the WorldSID head excursion was measured using video tracking analysis. To do so, the latest Euro NCAP protocol was taken as a reference to define the green, yellow, and orange lines determining the excursion level achieved with each of the PP6 configurations (Figure 91).

Since the generic environment used for the sled tests was based on a single seat setup, the definition of the head excursion lines considered an average centre console width of 210 mm (corresponding to an SUV segment). Thus, the orange line was defined by mirroring the distance from the mid centre console line to the dummy H-point. This orange line corresponds to the sagittal plane of a theoretical passenger seat. The yellow and green lines were defined from the orange line by adding 125 mm and 250 mm towards the centre console centre line. The red line was not defined since it should be based on the struck side intrusion line of the vehicle obtained from the Euro NCAP side impact test.

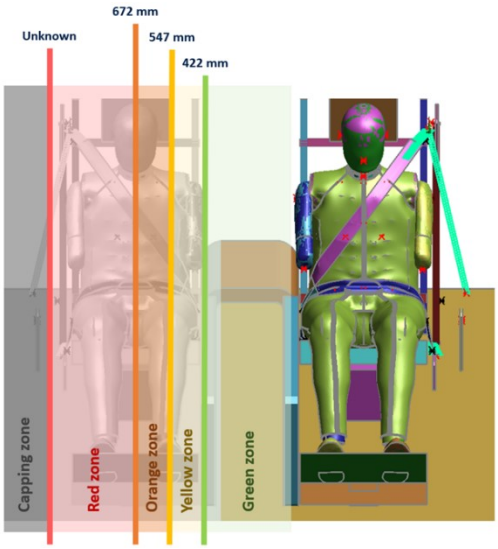

Figure 91 Diagram showing the position of the head excursion lines

Tests from 03-OSCCAR-FS to 06-OSCCAR-FS had the lowest head excursions due to the restraint of the upper body regions of the dummy by the seat side supports. As can be seen in Figure 92 all tests stayed in the yellow zone defined earlier. Among those, the inboard position of the DLPT seatbelt (tests 03-OSCCAR-FS and 04-OSCCAR-FS) provided additional reduction on the head displacement, achieving the lowest excursion of the head.

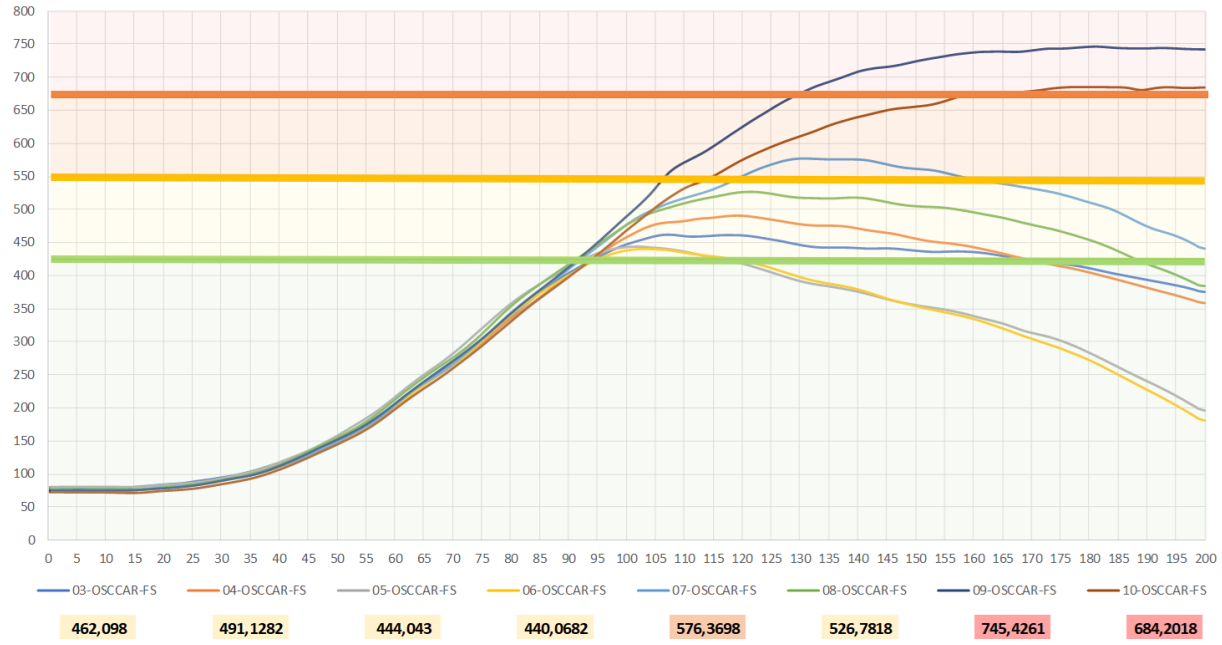

Figure 92 Maximum Y position of the WorldSID head respect to the seat

The head excursion increased when the side supports were removed, shifting from the yellow zone to the orange one when the DLPT belt system was mounted in inboard position (test 07-OSCCAR-FS) and even reaching the red zone for the belt in standard position (tests 09-OSCCAR-FS and 10-OSCCAR-FS).

The seatbelt routing had a direct influence on the dummy upper body kinematics, regardless of whether the seat side supports were present or not. Isolating the DLPT belt system in tests from 07-OSCCAR-FS to 10-OSCCAR-FS allowed to identify the effect of the seatbelt mounting position on the head excursion, as shown in Figure 93.

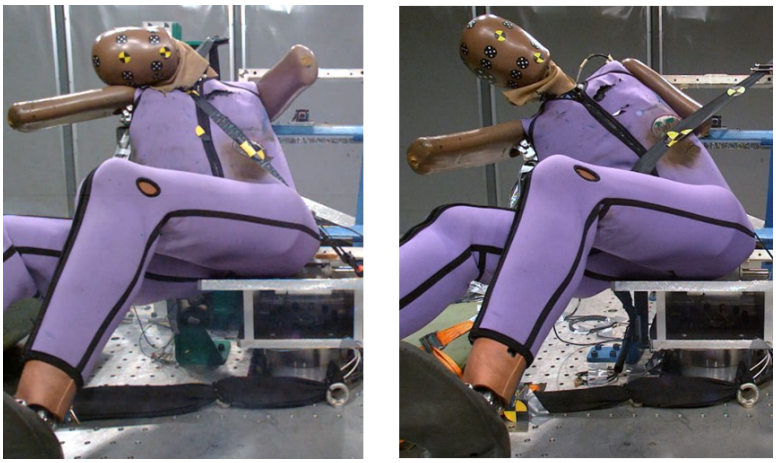

Figure 93 Image tests 07-OSCCAR-FS (left) and 09-OSCCAR-FS (right) at 130 ms

WorldSID Biomechanics

In Figure 94 and Figure 95 main WorldSID measurements from head, neck, thoracic and abdominal ribs and lumbar spine are presented. For the performance evaluation of the PP6 variations, the injury criteria limits defined in the Euro NCAP protocol were used as a reference.

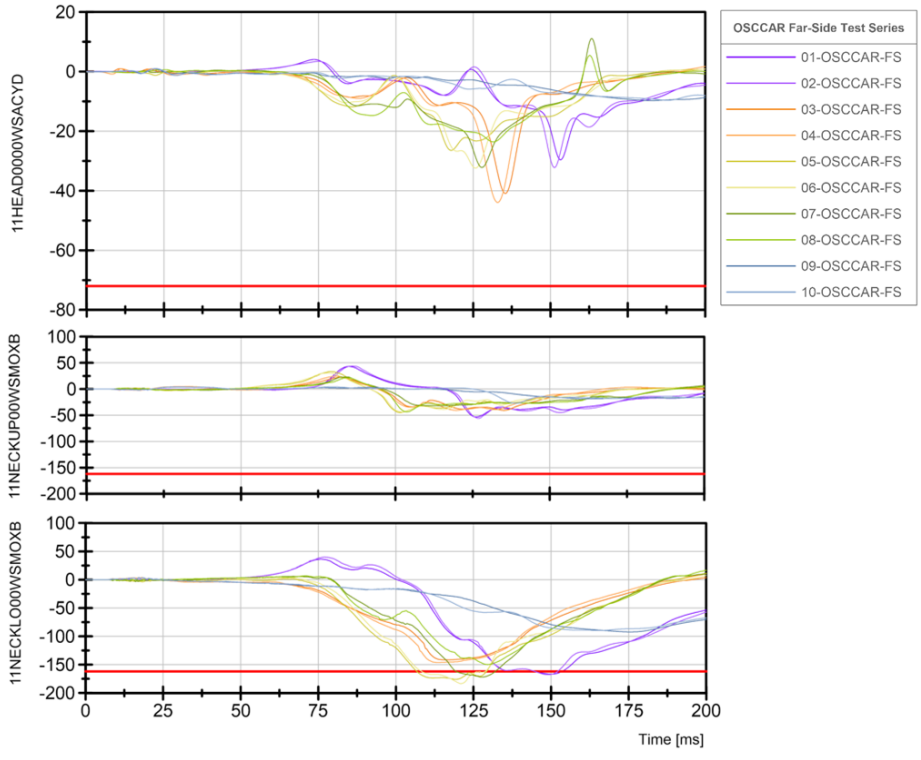

Figure 94 Dummy head linear y-acceleration, upper and lower neck Mx

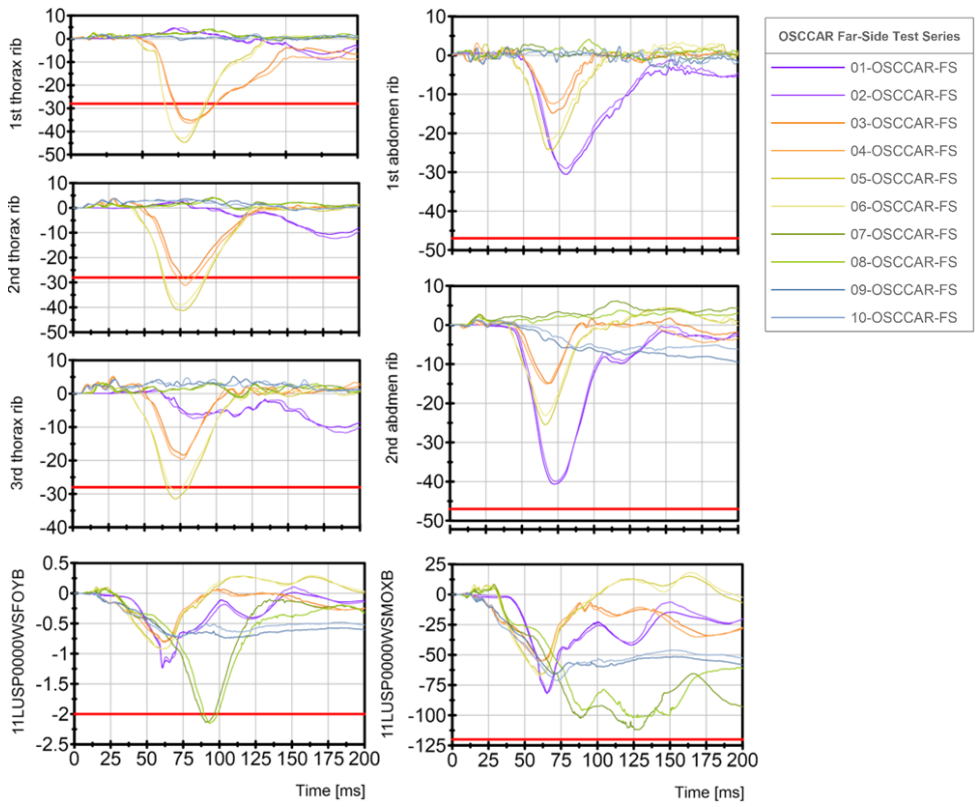

Figure 95 Dummy thoracic and abdomen ribs deflections and lumbar spine Fy and Mx

When looking at the lower neck moment Mx most of the tests were close and even reaching the Euro NCAP limit, except in tests 09-OSCCAR-FS and 10-OSCCAR-FS, in which no side support and in-board belt were used. On the other hand, the 1st and 2nd thoracic rib deflections were above the Euro NCAP limits when the seat side supports were installed (tests from 03-OSCCAR-FS to 06-OSCCAR-FS) whilst the 3rd thoracic rib deflection reached the limits when the seatbelt was in inboard position and with the seat side supports configuration. Higher abdominal rib displacements were observed for the first two tests of the series, with the presence of the centre console and the standard seatbelt configuration, but none of them exceeded the limits. Finally, lumbar spine Fy values were above the Euro NCAP limit at around 90 ms in the tests with no side support and the DLPT seatbelt in the inboard position.

Given the good repeatability between each of the pairs, the odd tests (01-OSCCAR-FS to 09-OSCCAR-FS) were selected to plot specific WorldSID responses. Furthermore, in Table 16 the five test pairs with the different setup configurations are summarised again to ease the WorldSID response analysis with respect to the test configuration.

01-02	03-04	05-06	07-08	09-10
3-point belt, No PT	SOTA DLPT belt	SOTA DLPT belt	SOTA DLPT belt	SOTA DLPT belt
B-pillar mounted	Belt in seat	Belt in seat - Inboard	Belt in seat - Inboard	Belt in seat
Centre console	Seat side supports	Seat side supports	None	None

Table 16 Summary of the different test setup configurations

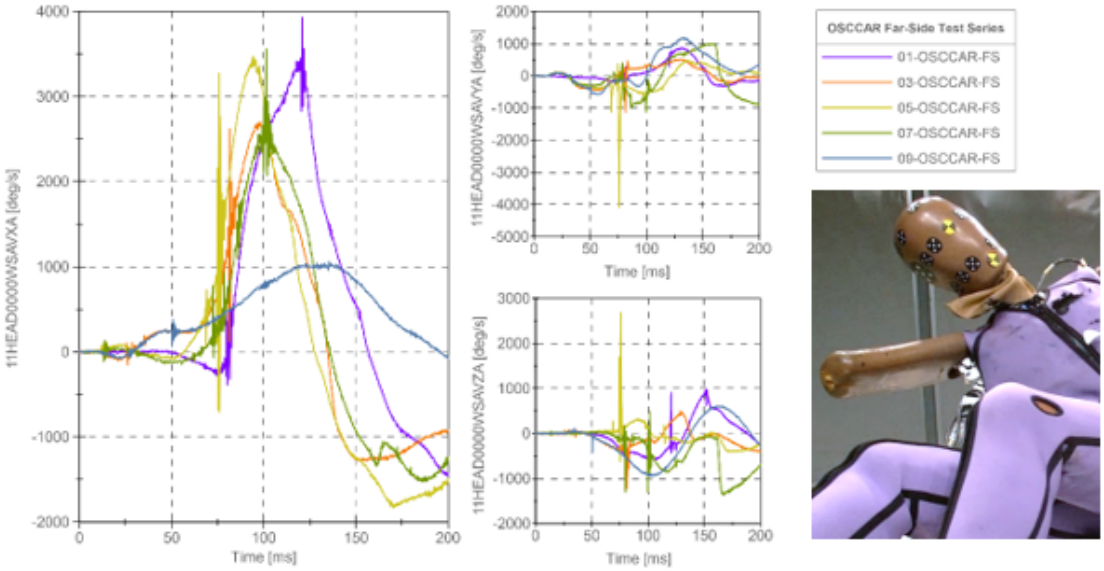

Figure 96 Head angular velocity and image of 09-OSCCAR-FS at 125 ms

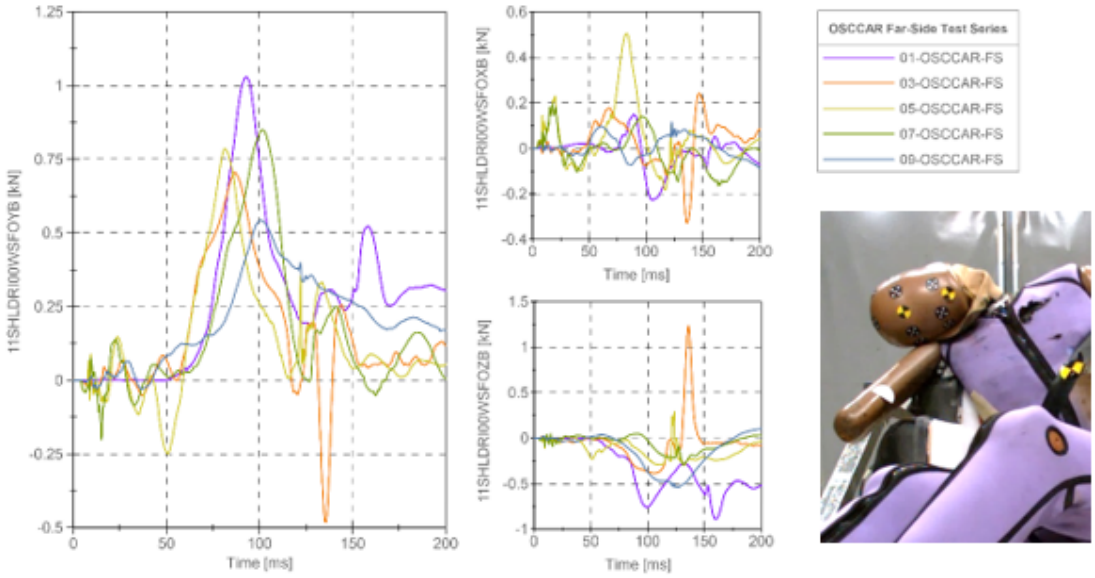

Figure 97 Shoulder right forces and image of 03-OSCCAR-FS at 130 ms

The head angular velocity (Figure 96) reached 3000 deg/s for most of the tests, especially when the seatbelt was located in the inboard position. In the configuration with only the DLPT belt system in the standard position, the head rotated much less (test 09-OSCCAR-FS) and the whole body of the WorldSID achieved higher displacements in the Y axis and the neck rotation was reduced (from movie analysis). The main dummy restraint in this configuration was provided by the lap belt which increased the load in the lumbar spine and did not hold the dummy sufficiently to prevent an interaction with internal vehicle components or a possible side occupant.

Shoulder right forces (Figure 97) were similar in all the tests despite the fact that there was a small offset in tests without side support (07-OSCCAR-FS and 09-OSCCAR-FS). However, in test 03-OSCCAR-FS the WorldSID armpit was blocked by the seat side support at around 130 ms producing a hard contact of the head against the shoulder as in can be seen on the trace of head linear y-acceleration (Figure 94) and the shoulder force response (Figure 97).

A time offset on T12 accelerations was observed with the removal of the side supports. The peak acceleration in Y moved from 60 ms with seat side supports (03 and 05-OSCCAR-FS) to around 100 ms with no seat side supports (07 and 09-OSCCAR-FS). Still, the inboard position of the DLPT belt system (09-OSCCAR-FS) had a similar impact on the T12 acceleration given that the WorldSID was fully restrained by the seatbelt at neck and pelvis.

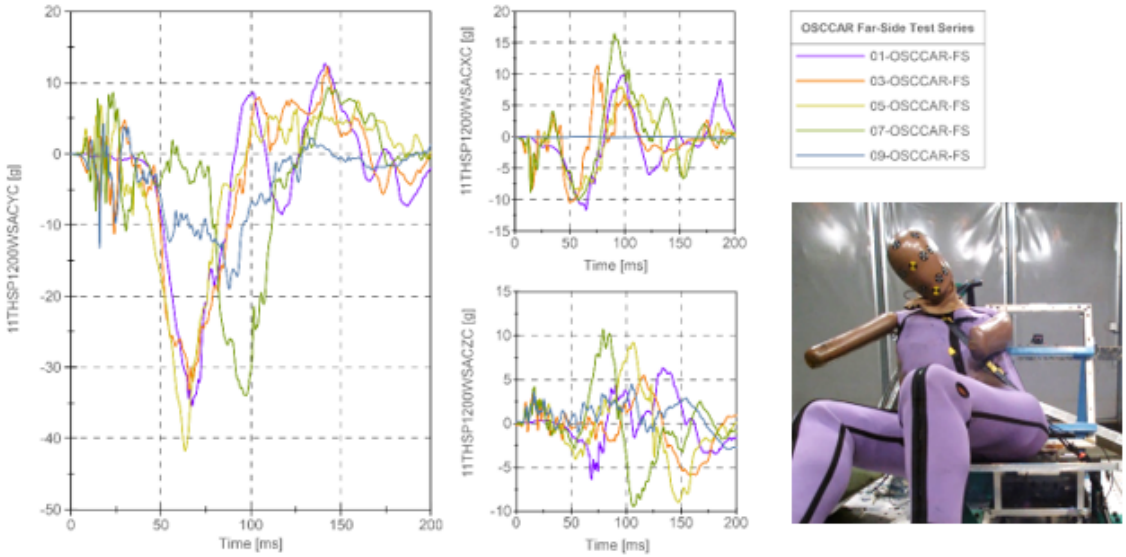

Figure 98 T12 acceleration and image from 07-OSCCAR-FS at 100 ms

The lumbar spine lateral flexion is shown in Figure 99, where it can be seen that the WorldSID was stopped at a similar time (60 ms) by the centre console and by the seat side supports. The seat side supports allowed to achieve the lowest lumbar spine Mx peak of all tests.

With no side supports, the SOTA DLPT belt in standard position reached a peak of 60 Nm at 75 ms and stabilised above 50 Nm. Finally, the test without side supports and the SOTA DLPT belt in inboard position showed the highest Mx since the seatbelt is the only restraint system preventing the WorldSID to move away from the seat.

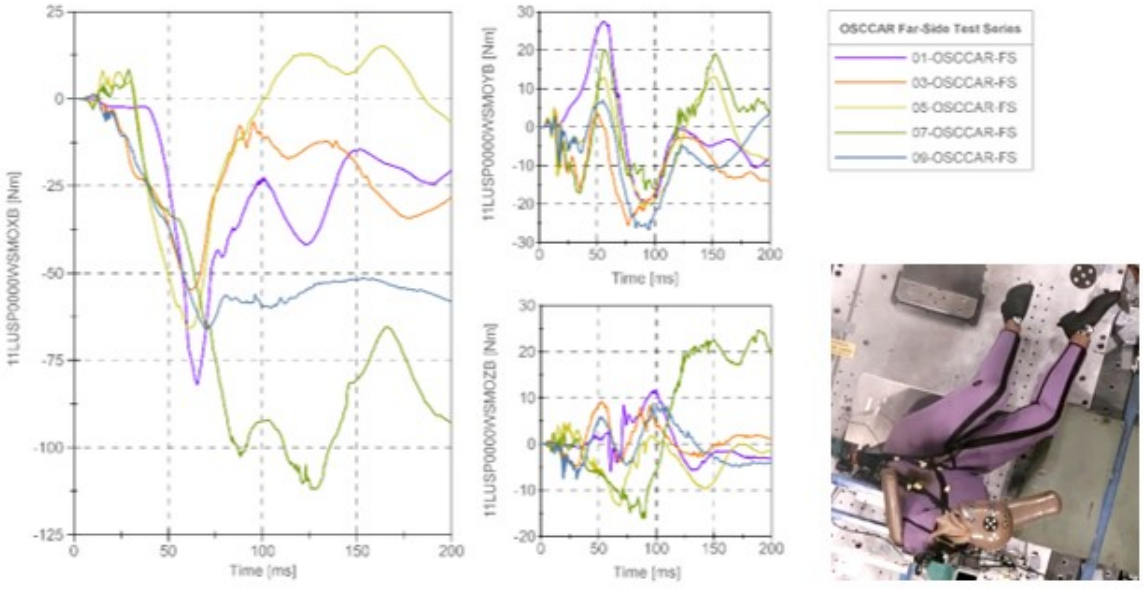

Figure 99 Lumbar spine lateral flexion and image from 07-OSCCAR-FS at 125 ms

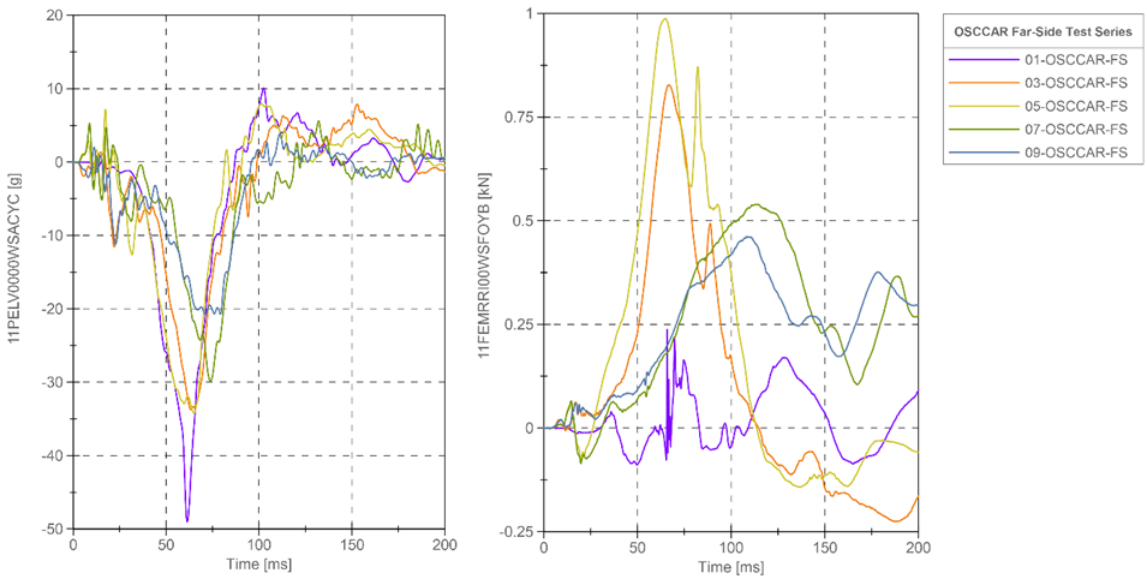

Figure 100 Pelvis acceleration and femur right forces in Y axis

Figure 100 shows the WorldSID pelvis and femur loads. The highest value of the pelvis acceleration was observed for the configuration with the centre console while the lowest value was achieved for test 09-OSCCAR-FS when there was more free movement of the body and the pelvis interacted less with the SOTA DLPT belt. The femur forces in Y axis were the highest with the seat side supports and the lowest with the centre console and the belt only configurations. With the centre console, the leg motion was controlled, preventing shearing forces in the femur. In the seatbelt only cases, the leg inertia created shearing forces in the femur but to a lesser extent than when the upper femur motion was additionally prevented by the seat side supports.

3.3.2.8 Summary and Limitations

A total of 10 sled tests were executed to study the performance of Protection Principle 6 in a far-side load case; combining a SOTA belt with a double lap belt pre-tensioning, a standard and an inverted belt position and seat side supports. Furthermore, the standard 3-point seatbelt was evaluated together with a centre console to validate the environment according to a previous study by [9].

The combination of double lap belt pre-tensioning and seat side supports was the best compromise to control occupant kinematics while mitigating injury assessment values. The standard position of the SOTA DLPT seatbelt in this configuration brought additional protection for the WorldSID, reducing the value of its lower neck lateral flexion, its chest compression, and its head excursion. Further padding or some flexibility in the seat side supports may decrease the thoracic rib deflections. The neck bending and the overall head excursion might further be decreased by the integration of additional countermeasures to restrain the head such as a seat-mounted airbag.

The introduction of seat-mounted airbags instead of seat side supports may also be a solution to better distribute the loadings on the chest region and prevent the dummy to have hard contacts with other occupants or interior components of the vehicle. Another countermeasure to be further investigated could be a 5-point seat belt (as used in motorsport vehicles), which may help to better restraint the WorldSID body, especially if there is no side support.

3.3.3 Virtual Demonstrator

The original virtual demonstrator was validated under LS-Dyna. The Finite Element Model (FEM) was initially developed within the collaborative project between LAB, CEESAR and Toyota which presented their research findings in [9]. The SOTA DLPT belt model provided by Autoliv, which was also used for the homologation demonstrator, was added to the model. The LS-Dyna FEM was provided to Siemens to develop a corresponding Madymo model.

3.3.3.1 Environment and Restraint System Models

The test environment was a generic one representing the main features of a medium sized passenger car. Therefore, the FEM was quite simple and consisted mainly of rigid parts (seat, footrest, centre console or seat side supports). The standard 3-point belt model was provided by Toyota and the SOTA DLPT belt FEM was the same as the one used for the homologation demonstrator.

LS-Dyna Model

The FEM (Figure 101) was created from the CAD model developed to build the physical set-up. As already described in Deliverable D2.4 [7], the original FEM environment consisted of a rigid inclined seat pan, a rigid seatback, a footrest, two rigid centre consoles and a standard 3-point belt model. All components were rigidly constrained to the sled base including the seatbelt anchorage points.

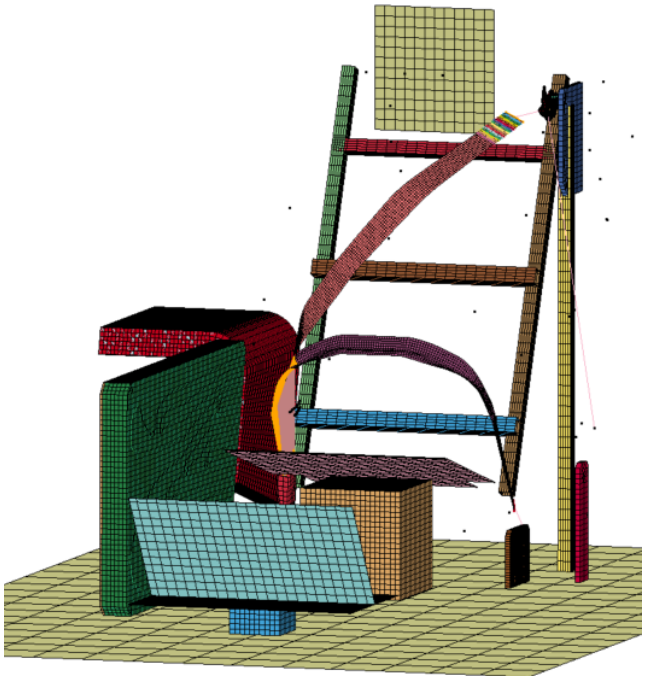

Figure 101 Far-side test set-up FEM

The centre consoles were covered by 50 mm thick sheets of Ethafoam modelled as *MAT_LOW_DENSITY_FOAM under LS-Dyna and using the experimental quasi-static stress-strain curve as loading curve of the material card (Figure 102).

The SOTA DLPT belt was modelled using the encrypted FEM provided by Autoliv for the homologation demonstrator. The seat side supports were also modelled as rigid and covered by the same 50 mm thick Ethafoam layers with the same material card as for the pelvis and leg centre consoles.

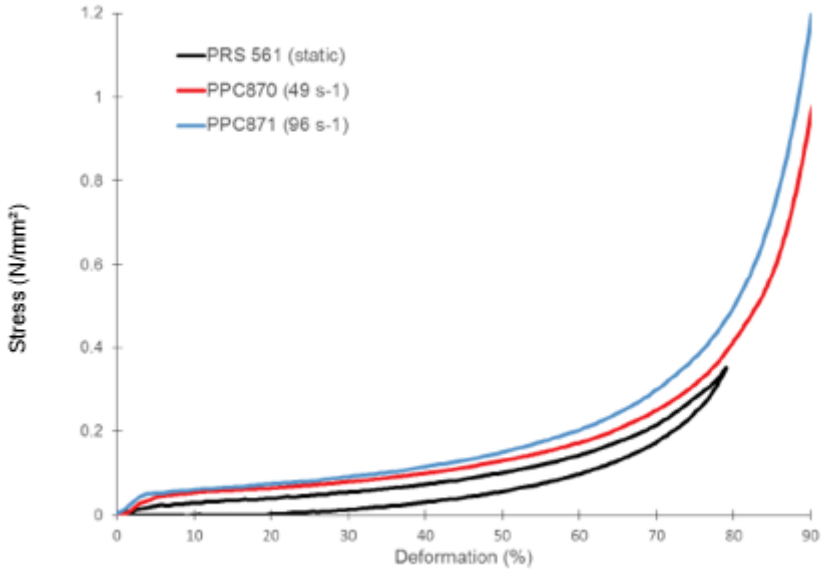

Figure 102 Ethafoam TM 180 quasi-static and dynamic stress-strain responses

The WordSID FEM developed internally at Toyota Motor Corporation (TMC) was used. The model components (head, neck, shoulder, thorax, abdomen and pelvis) were validated according to the ISO 15830 test procedure. Additional validation was performed for the neck and lumbar spine of the dummy model, as the response of these components has a significant influence on the dummy excursion. The WorldSID FEM head excursion was validated in sled tests of [9] and results were presented in Figures 147 and 148 of Deliverable D2.4 [7].

The contact forces between the environment (seat pan, footrest, centre consoles) and the WorldSID dummy were extracted from the model. The seatbelt forces were extracted using *DATABASE_CROSS_SECTION_SET.

The velocity curves along the x and y axis measured during the tests were applied to the FEM base plate using *BOUNDARY_PRESCRIBED_MOTION_RIGID along the x and y axis of the model (Figure 103).

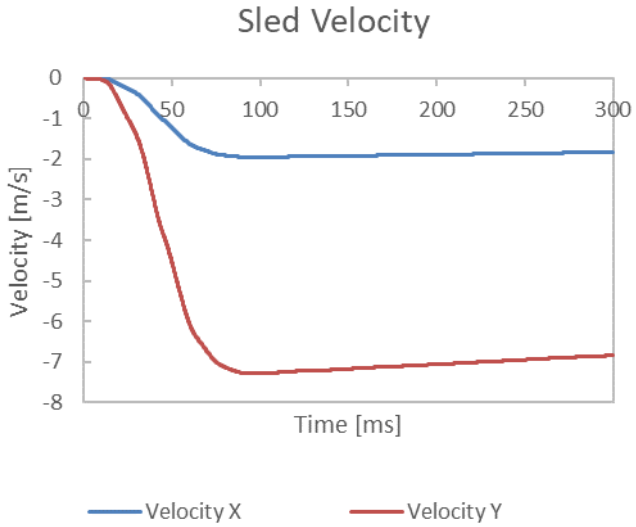

Figure 103 Velocity curves applied to the FEM base plate

Simcenter Madymo Model

The Madymo model (see Figure 104) was created using Simcenter Madymo v2020.2, based on the geometry of the LS-Dyna model supplied by Toyota. The seat pan, footrest and floor were modelled using rigid multibody planes and the seatback straps using ellipsoids to ensure contact stability.

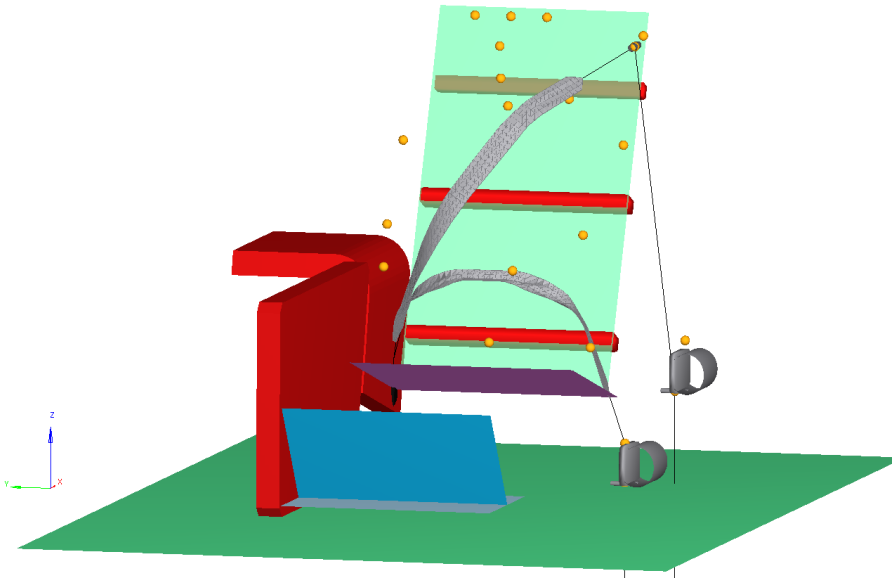

Figure 104 Far-side test set-up in Madymo

The FE surface mesh of the console was imported from the LS-Dyna model and the quadrilateral shell elements were defined as rigid, with the compliance and damping of the foam material captured in a multibody contact characteristic definition. The experimentally-derived curves shown in Figure 102 were used to define the stress-based load characteristics, with an assumed thickness of 60 mm (for numerical stability, with a stiffness function representing 50 mm foam thickness) and a damping coefficient of 100.0. The same methodology and characteristics were used for the side supports.

The SOTA DLPT belt was modelled using an encrypted Madymo model of the system, provided by Autoliv for the homologation demonstrator.

The Madymo WorldSID model supplied in the 2020.2 distribution (version 4.1) was used. This is a multibody representation of the ATD with a facet (rigid elements supported on rigid bodies) surface description. Due to the nature of far-side loading and the local shoulder mesh, contact issues between the belt edges and the internal faces of the shoulder assembly were encountered, and additional multibody ellipsoid surfaces were defined in the shoulder gaps to smooth the interaction. This had no practical effect on the belt interaction besides to remove numerical instabilities.

Output was requested for the kinematics, the belt forces, the contact forces and the model energy.

3.3.3.2 Calibration

Due to the simplified test environment (mainly rigid components) and the fact that the SOTA DLPT belt was encrypted, small model adjustments had to be done after aligning the seatbelt anchorage point locations in the FEM with the tests.

LS-Dyna Model

The test set-up and the seatbelt anchorage points in the FEM were defined based on the CAD model used to build the test set-up and therefore matched the tests perfectly.

The WordSID FEM was positioned once and this positioning was kept for all simulations. The WorldSID FEM main landmarks were aligned as close as possible to the dummy landmarks measured in the tests (Figure 105).

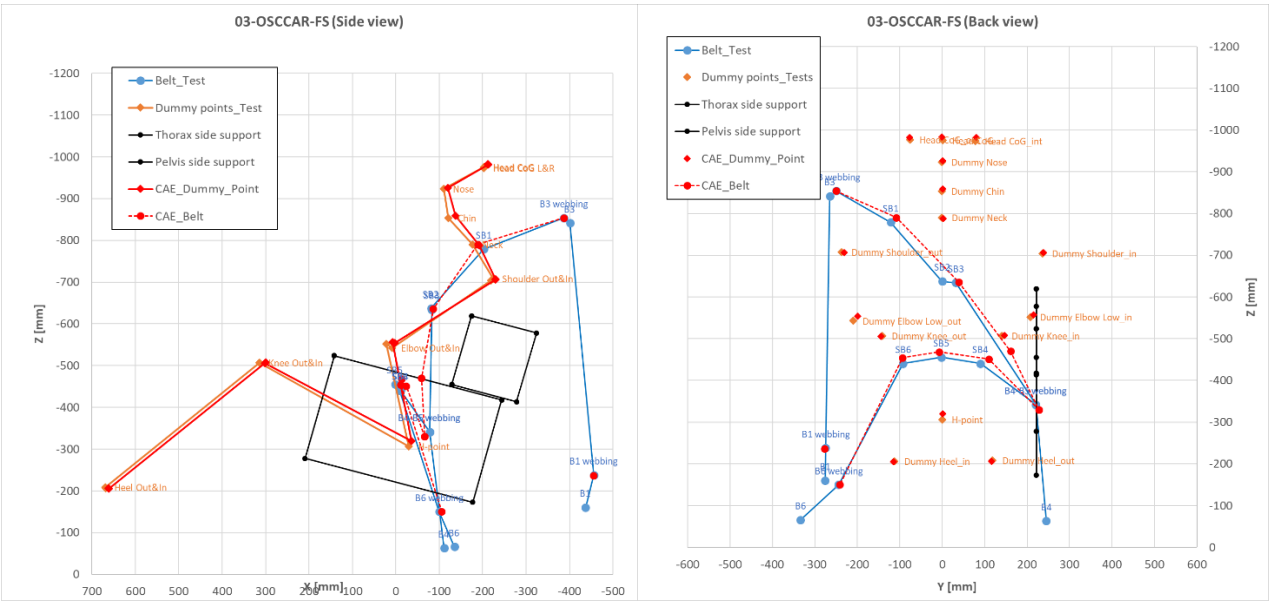

Figure 105 Test and FEM main landmark overlay (side and rear view)

The following friction values were defined for the different contacts:

- Dummy-to-seat contact: μ=0.4
- Dummy-to-seatbelt contact: μ=0.3
- Dummy-to-seat side supports: μ=0.4

Madymo Model

The Madymo model followed the same geometry as the CAD/LS-Dyna model to match the test setup. The model position for all tests was the same. As the repeatability of the positioning between all tests was good, the values for 02-OSCCAR-FS were chosen and the dummy model positioned to match the hardware landmarks. The loading pulse used was taken from the second repeat of each test.

Due to issues with Madymo's contact algorithm in modelling the belt-dummy interactions, additional surfaces were added to the WorldSID dummy to smooth the geometry inside the shoulder. This prevent nodes becoming trapped in the complex mesh of this region.

The following friction values were used:

- Dummy-to-seat contact: μ=0.4
- Dummy-to-seatbelt contact: μ=0.3
- Dummy-to-seat side supports: μ=0.6

3.3.3.3 Results

Model Results

Four simulations each were performed with the LS-Dyna and the Madymo model, representing the respective test configurations of the physical demonstrator. The associated test and simulation IDs are shown in Table 17.

Simulation ID	Test ID	Belt	Anchorages	Other
WS3_2	03-OSCCAR-FS	SOTA DLPT belt	Belt in seat	Seat side supports
	04-OSCCAR-FS			
WS5_2	05-OSCCAR-FS	SOTA DLPT belt	Belt in seat Inboard	Seat side supports
	06-OSCCAR-FS			
WS4_2	07-OSCCAR-FS	SOTA DLPT belt	Belt in seat Inboard	None
	08-OSCCAR-FS			
WS2_2	09-OSCCAR-FS	SOTA DLPT belt	Belt in seat	None
	10-OSCCAR-FS			

Table 17 PP6 simulation matrix

Seatbelt forces, neck, lumbar spine and pelvis loads as well as rib deflections were compared between the models and the tests where relevant, i.e. in the case of interactions with the environment. The LS-Dyna results are presented in detail in Appendix 3.9. It has to be noted that the shoulder belt force at B4 could not be measured in the tests with the seat side supports (WS3_2 and WS5_2) due to the little space between the seat and the side supports.

Belt forces, WorldSID model kinematics and head excursion are presented in Table 18, Table 19 and Figure 108 respectively.

Generally, the shoulder belt slipped off the dummy's shoulder at about the same time in the LS-Dyna simulations and in the tests, except in simulation WS3_2 (SOTA DLPT belt with side supports). In the latter case, a slightly later and less pronounced belt slip-off was observed in the LS-Dyna simulation compared to the test. The reason for this was unclear, but could be related to slight variations between dummy hardware and model, such as differences in shoulder geometry and/or dummy jacket.

The inner shoulder belt force (B4) and the outer lap force (B6) were higher in the LS-Dyna simulations than in the tests. A similar trend was observed in the Madymo simulations.

The Madymo belt forces showed generally good agreement with the test data once the contact issues around the shoulder had been addressed.

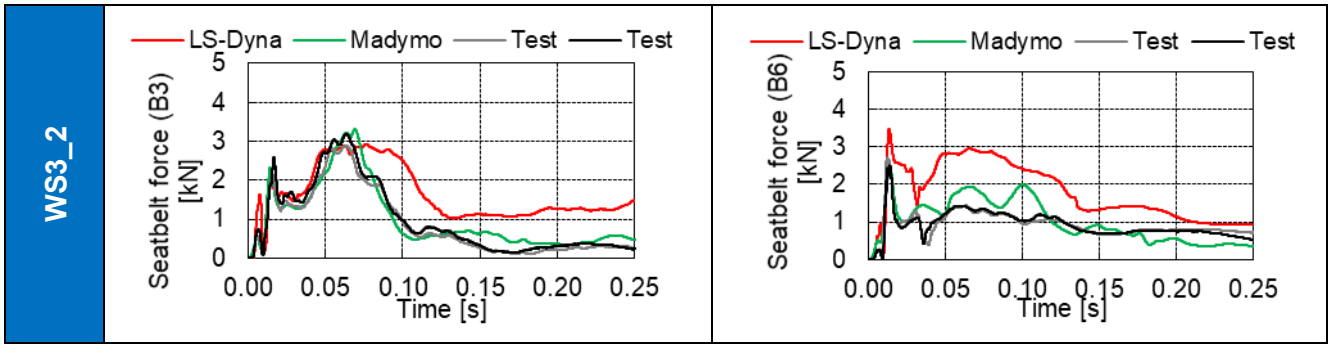

WS5_2	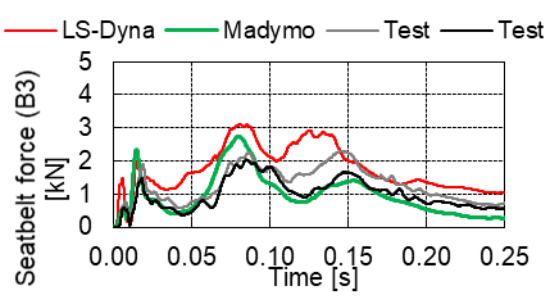	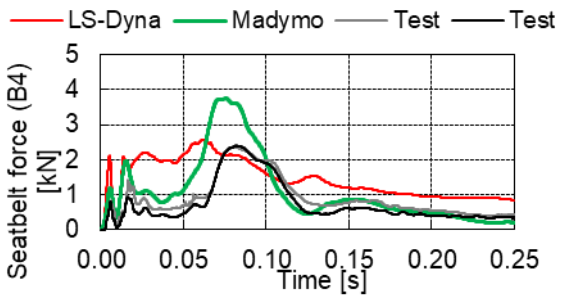
WS4_2	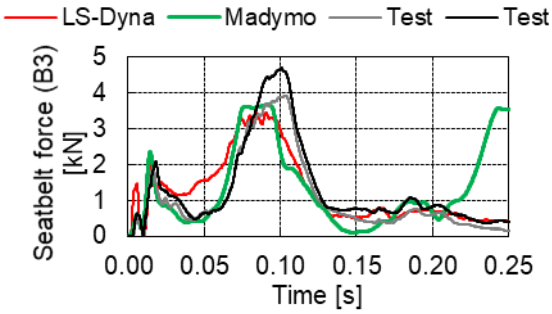	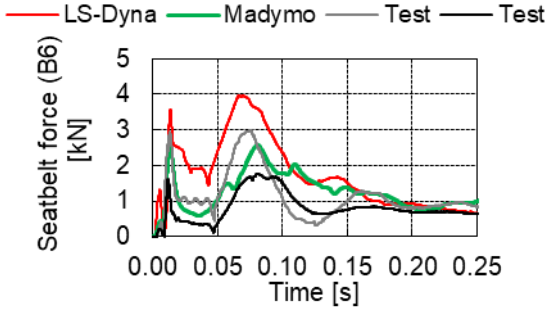
	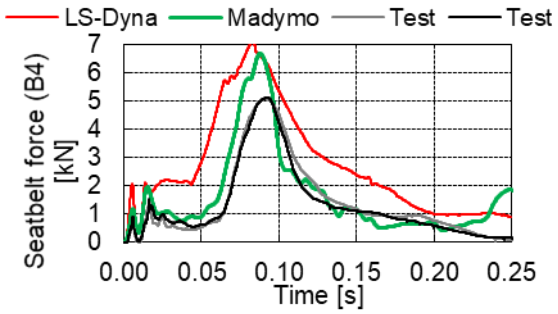	
WS2_2	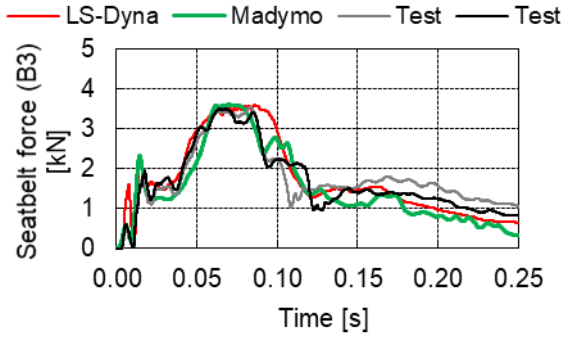	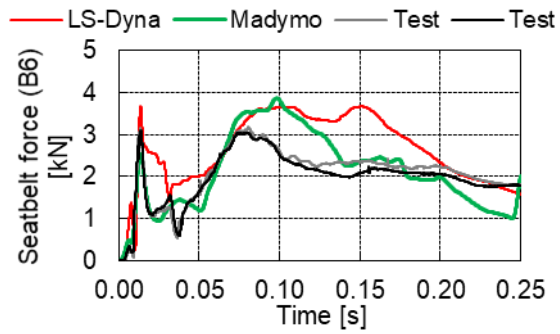
	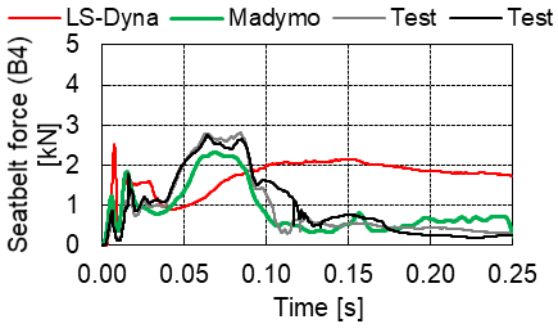	

Table 18 Seatbelt forces in simulations (red: LS-Dyna, green: Madymo) and tests

	0 ms	50 ms	100 ms	150 ms
03-OSCCAR-FS		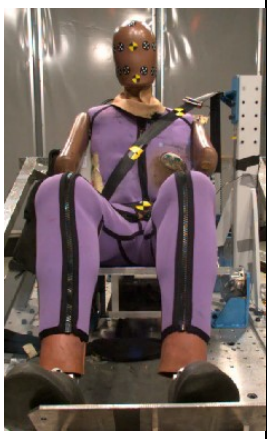		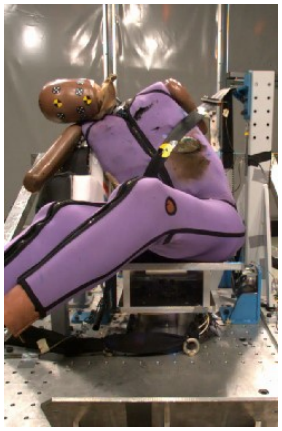
WS3_2 (LS-Dyna)	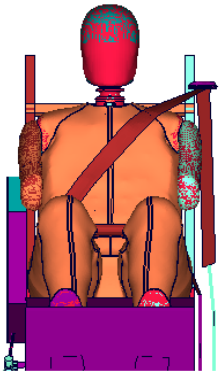	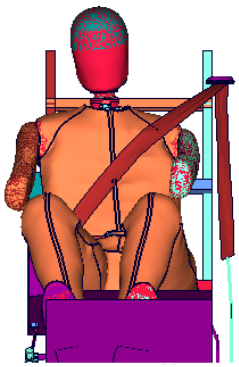	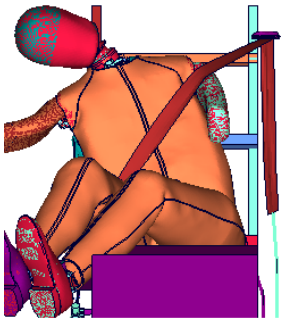	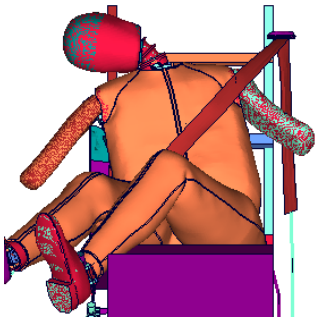
WS3 (Madymo)	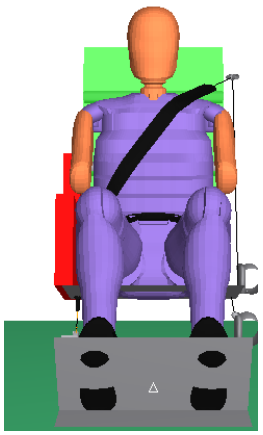	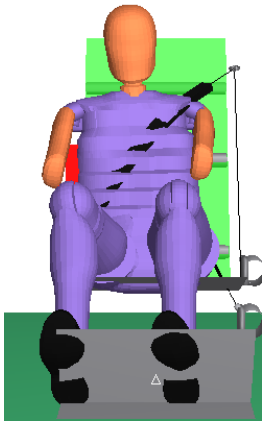	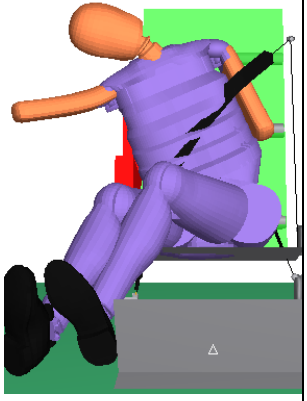	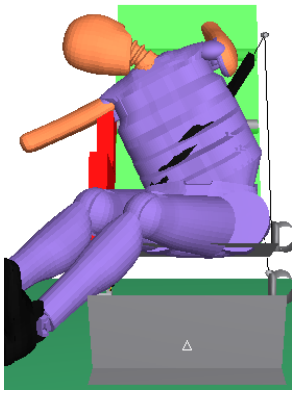
05-OSCCAR-FS			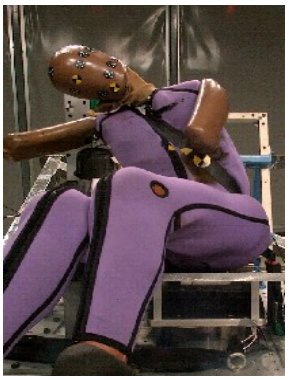	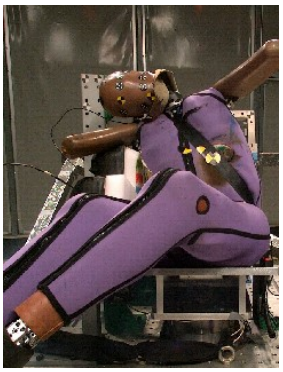

WS5_2 (LS-Dyna)	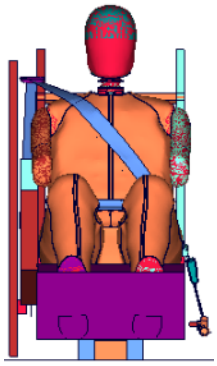	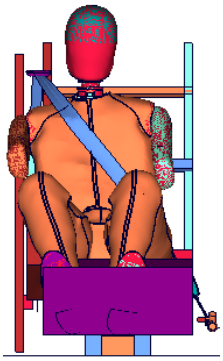	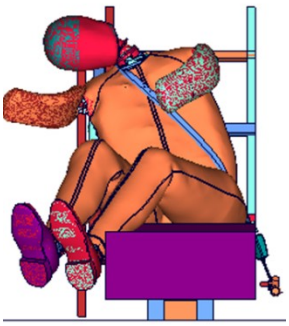	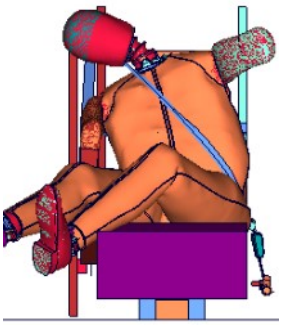
WS5 (Madymo)	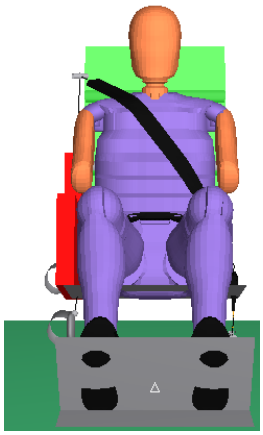	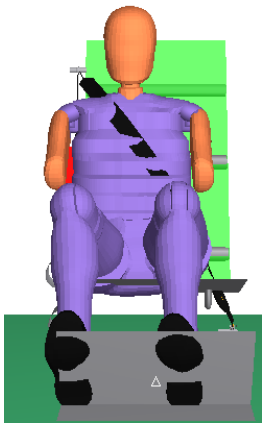		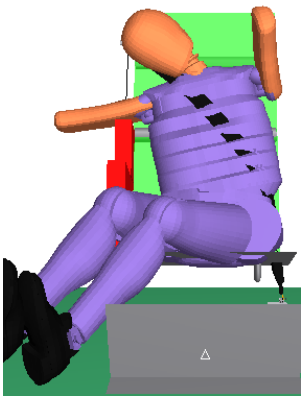
07-OSCCAR-FS		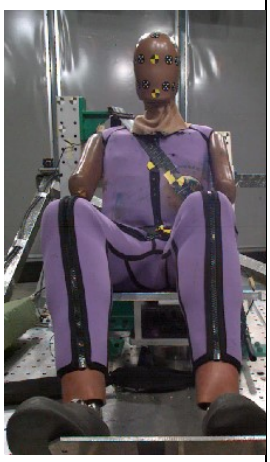		
WS4_2 (LS-Dyna)	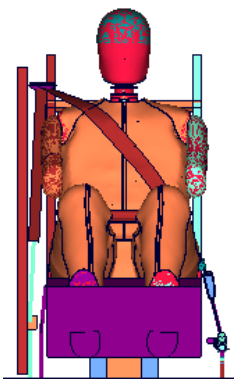	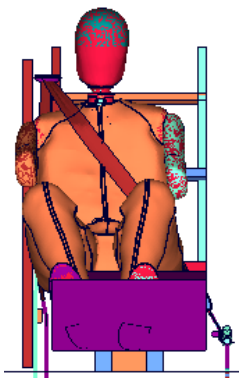	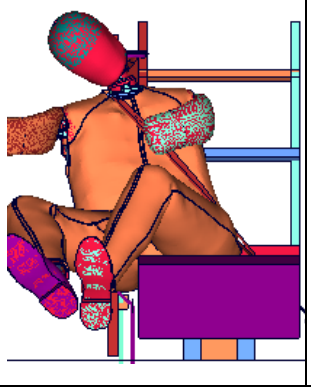	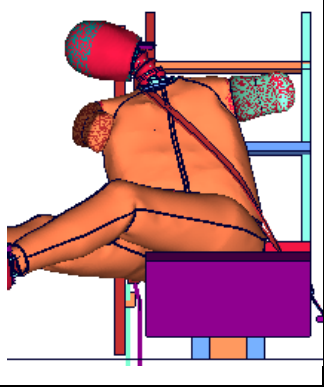

WS4 (Madymo)	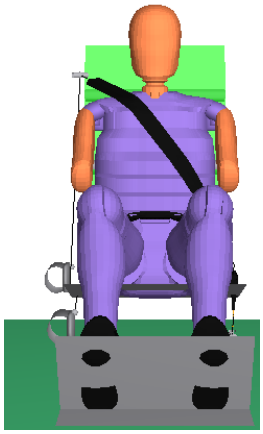	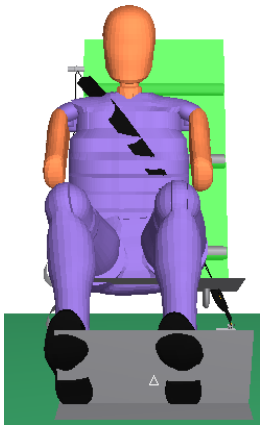	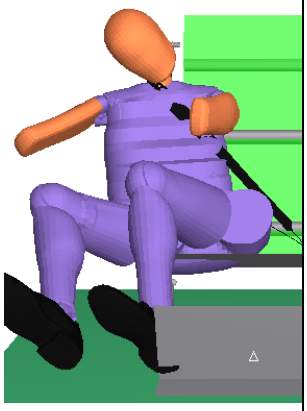	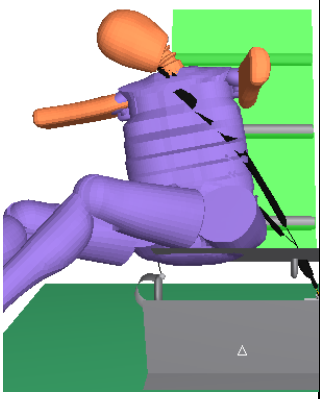
09-OSCCAR-FS			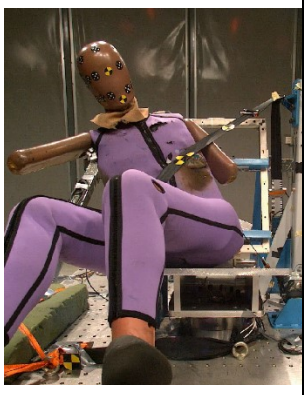	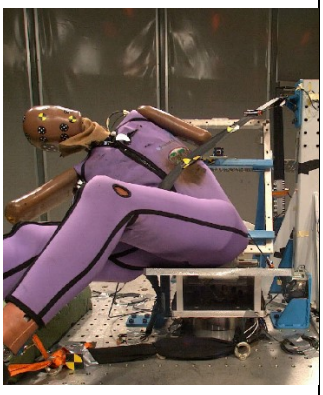
WS2_2 (LS-Dyna)	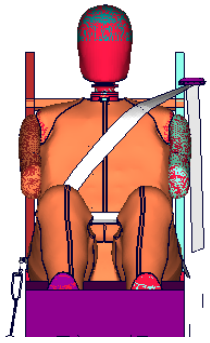	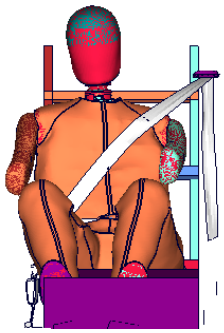	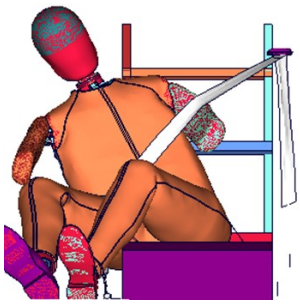	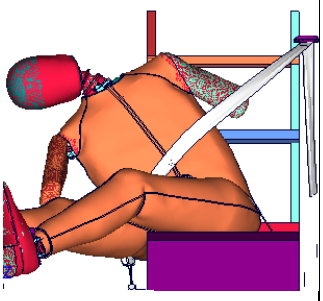
WS2 (Madymo)	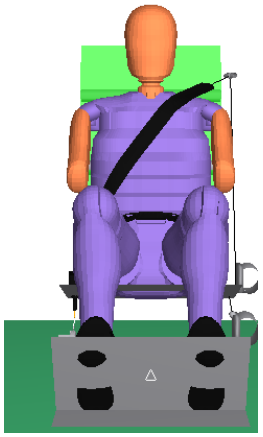	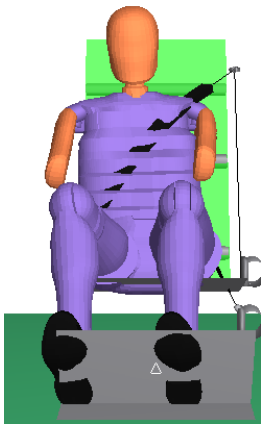	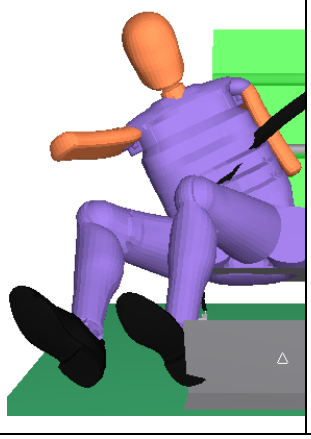	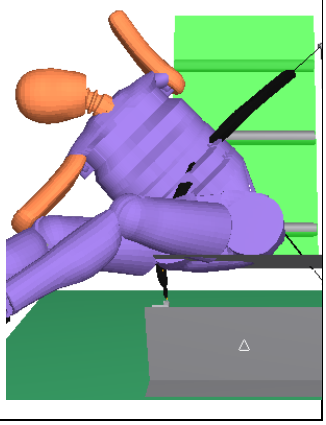

Table 19 WorldSID kinematics and belt interaction in simulations and tests

From the LS-Dyna simulation movies it was visible that the pretensioners in the lap belt applied a higher pretension in the simulation than in the tests, preventing the pelvis to move upwards (Figure 106, Figure 107). Additionally, it has to be noted that the SOTA DLPT belt model was validated for a frontal impact but not for a far-side load case.

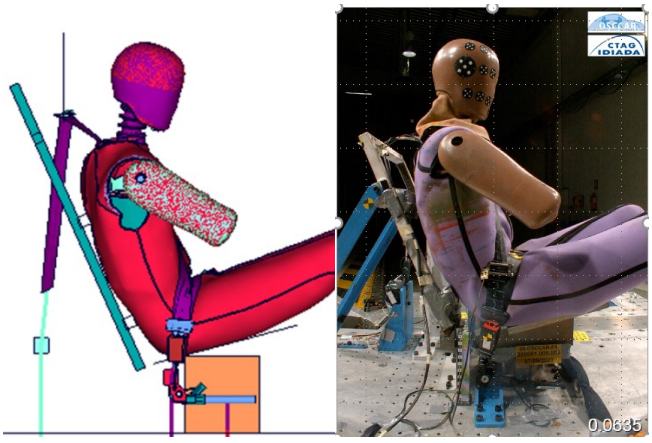

Figure 106 LS-Dyna simulation WS2_2 and 09-OSCCAR-FS test at 64 ms

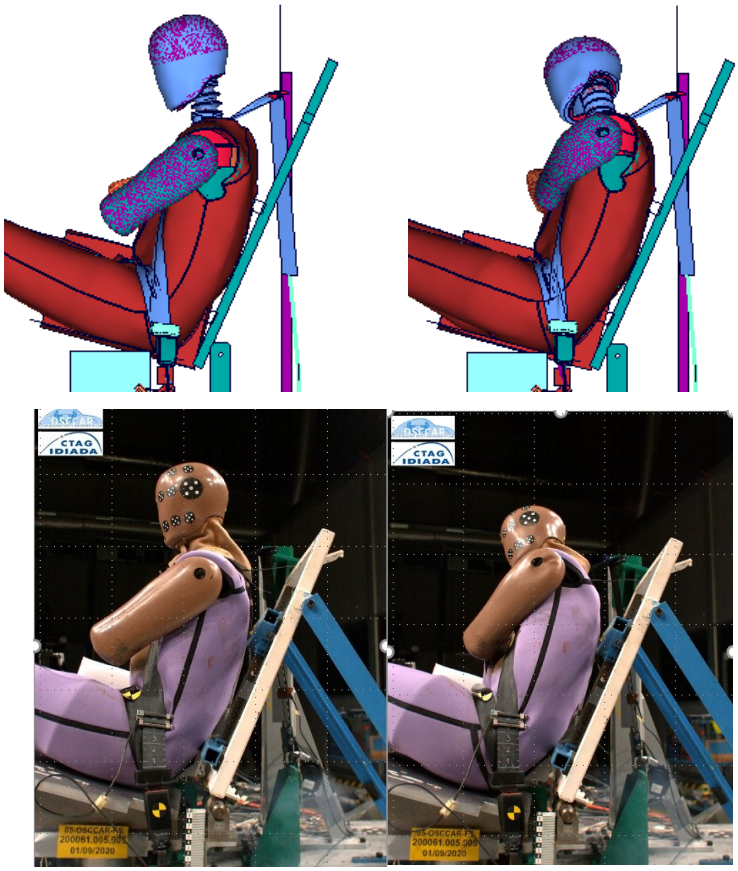

Figure 107 LS-Dyna simulation WS5_2 and 07-OSCCAR-FS test at 63 and 85 ms

In the Madymo simulations, the interaction between the side panels and the thorax was found to be sensitive to the precise point of contact and, while optimised for lateral loading, was too stiff under the vertical component of thorax bending. It could be seen that the model did not “fold” over the supports as the hardware and FE dummies did.

The difference in pelvis restraint may explain some of the variations in head COG excursion seen in Figure 108 between the LS-Dyna simulations and the tests. However, these variations were small along the y-axis (maximum value of 30 mm) and of similar magnitude than discrepancies measured between repeated tests.

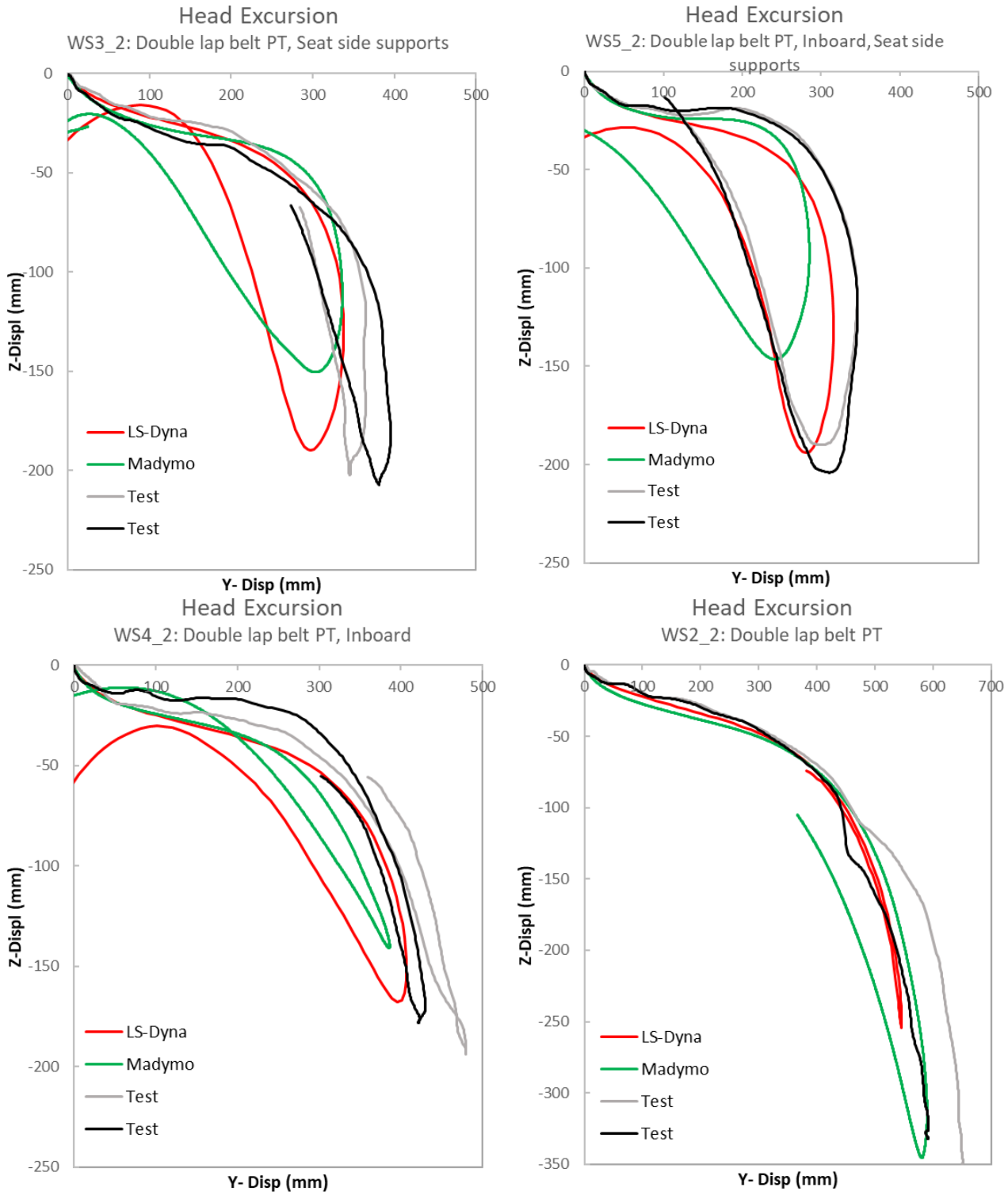

Figure 108 WorldSID model head COG excursion (red: LS-Dyna, green: Madymo) & test data

The highest difference was found in simulation WS2_2 when the dummy was only restrained by the SOTA DLPT belt. In this configuration, the head excursion along the y-axis was in good agreement

with the tests but less excursion was measured along the z-axis (around 100 mm less in simulation) possibly due to less pelvis upwards motion. The difference in pelvis restraint had less effect in WS4_2 due to the inboard belt which restrained the dummy through the shoulder belt.

The Madymo results show that for the analyses with belts good agreement could be obtained with experimental head excursion results. As described above, the dummy model ribs appear to be too stiff in out-of-plane loading, meaning that the dummy does not fold over the side supports but rotates and is pushed away with a more whole-body motion. This limits the x and z displacements of the head and changes the kinematic response, as can be seen most clearly in the rebound phase of the curves. As a consequence the correlation of head kinematics in Madymo simulations was better where the restraint was provided solely by the belt.

The dummy injury assessment values from the simulations are shown in Appendix 3.9 and Appendix 3.10 for LS-Dyna and Madymo respectively. Lower and upper neck forces and moments, lumbar spine force and moment, pelvis forces (pubic and sacro-iliac Fy) and chest/abdomen rib deflections matched well the test results. The simulation results were in good agreement with those of the tests.

3.3.3.4 Summary and Limitations

PP6 and its testing environment were replicated under LS-Dyna and Madymo. The SOTA DLPT belt simulation model was taken from the homologation demonstrator and it has to be noted that the SOTA DLPT belt was not validated previously for a far-side loading. In the LS-Dyna model, it was observed that the pelvis retention by the lap belt was higher, giving small pelvis motion in the simulation. Although the lap belt forces were not reproduced perfectly by the LS-Dyna model, the dummy head excursions reproduced fairly the ones obtained in the tests, especially along the y-axis. The dummy injury assessment values from the LS-Dyna simulations were generally in good agreement with those of the tests. Due to the SOTA DLPT belt model encryption it was not possible to further improve the model validation. However, further checks could first be done to compare lap belt pretension at both ends in tests and simulations, as well as belt slippage through the Crash Locking Tongue (CLT). Indeed, the CLT activation in the tests depends on the force difference between the shoulder belt and the lap belt, whereas in the simulations, the CLT was activated at 1 ms. Additionally, WorldSID dummy jacket and shoulder pad conditions of the tests may have played a role in the shoulder belt interaction with the dummy chest. These are sensitive parameters difficult to reproduce in simulations.

Where side supports were used in the Madymo models, the accuracy of the validation was limited by modelling choices in the multibody architecture of the WorldSID model, which was designed and validated with nearside impacts in mind. Similar design choices led to numerical contact issues in cases where the WorldSID was loaded such that the shoulder was driven out of the belt – this arose as the far side load case is as yet untested with the model, and was solved with the addition of simplified contact surfaces in and around the shoulder joint. This Madymo model reproduced the kinematics and belt loading response of the environment well in the test setups without side supports and showed a good level of validation of the environment in these cases.

3.3.4 Conclusion and Next Steps

Protection Principle 6 consisted of the SOTA DLPT belt as baseline combined with seat side supports. Configurations with an inboard seatbelt routing were also tested. In total 10 sled tests were performed with a WorldSID dummy to evaluate the effect of the different countermeasures compared to a B-pillar mounted seatbelt with a centre console as in [9]. The objective was to assess the occupant protection in an AD car interior configuration submitted to a far side load case. PP6 aimed

at restraining the occupant through seat mounted restraints to allow freedom in seat positions (e.g. rotated seats).

The combination of the double lap belt pre-tensioning and seat side supports was the best compromise to control occupant kinematics while mitigating injury assessment values among the evaluated protection principles. However, further padding or some flexibility should be included in the seat side supports to decrease thoracic rib deflections. The neck bending and the head excursion might also be decreased by the integration of further countermeasures to support the head during the crash, such as a seat-mounted airbag.

Generic models of the environment were created under LS-Dyna and Madymo that could be used in future research and related Virtual Testing activities. Overall, the finite element model replicated well the dummy head excursion and the dummy measurements. The simulation of the interaction between the shoulder belt and the dummy was sensitive and belt slippage over the dummy shoulder was later than in test in one of the configurations. Therefore, the comparison between WorldSID and HBM simulations regarding belt interaction should be considered with caution especially if WorldSID finite element model interaction with the seatbelt has not been validated through tests. A similar challenge as for the homologation demonstrator study was therefore highlighted for the PP6 virtual demonstrator regarding dummy and belt interaction.

For the multibody model, care must be taken when comparing ATD and HBM simulations in the side support load cases. The Madymo AHM is validated for lateral thoracic loading, but with impactors only, and it can be seen that far-side loading into a large plate gives a different kinematic load to the occupant. However, the multibody structure of the AHM is more robust and less specialised than that of the WorldSID model.

Further investigation would be necessary to check the validation of the SOTA DLPT belt model under a far-side load case, especially considering the belt slippage across the CLT, the belt pretension of the lap belt anchorages and the belt pay-in/out at the shoulder retractor.

Considering future vehicle interiors and the ‘living room’ use case, it would be of interest to check that occupant-to-occupant interaction could be limited with PP6 under various crash configurations.

4 DISSEMINATION, EXPLOITATION AND STANDARDISATION

4.1 Homologation Demonstrator

Dissemination:

Schießler, M., Ott, J., Eggers, A. (2020) User Experience with THOR-Dummy in Reclined Seating Positions. *European CAE Thor Users Meeting*, 2020, Web Meeting.

Schießler, M., Ott, J., Eggers, A., Peldschus, S. (2021) How to consider test scatter for model validation in a Virtual Testing procedure. *automotive CAE Grand Challenge*, 2021, Hanau, Germany.

Schießler, M., Ott, J., Eggers, A. (2021) Comparison of THOR-Dummies in Reclined Seating Positions - Experiences from the OSCCAR project. *European Crash Meeting by Humanetics*, 2021.

Exploitation:

Results and experiences from this task will be used by BASt in future discussions with German regulators, type approval authorities and technical services on the possibility for type-approval of future seating positions. To demonstrate the procedures and concepts related to vehicle environment validation [8] results from the second test series will be used. Further discussion on how to handle test scatter are planned. Conclusions will be shared with the Euro NCAP VTC WG, for example. In addition, BASt's participation in national and international working groups for regulation and standardization ensures the further exploitation of the results.

Project transfer:

Experiences and limitations from the second test series will be considered in the ENOP project and internal projects (BASt plans to conduct additional tests series with dummies of different stature like the female 5th percentile dummy). An updated version of the virtual homologation demonstrator will be shared with the THUMS User Committee (TUC) with the aim to use it for the validation of HBMs.

4.2 Protection Principle 2

Dissemination:

fka Mobility Podcast:

Episode 28: “The project OSCCAR - Future Occupant Safety for Crashes in Cars”

https://www.fka.de/en/coming-up/world-of-research/podcast.html

The podcast is in German.

Exploitation:

A knowledge transfer to education within the Master degree courses “Automotive Engineering M.Sc.” and “Fahrzeugtechnik und Transport M.Sc.” at RWTH Aachen University was done in terms of the research studies. This was accompanied by raising awareness for the topics of occupant safety and future restraint strategies.

Project transfer:

Transfer of simulation results and findings to EU Horizon 2020 project SAFE-UP (Grand Agreement No. 861570)

4.3 Protection Principle 6

Dissemination:

Toyota and IDIADA plan to submit a paper on WorldSID test results and simulation performed with the dummy model and THUMS HBM.

Exploitation:

The tests performed at CTAG-IDIADA repeating the test configuration of [9], have been shared with Euro NCAP VTC WG working on WorldSID FEM validation catalogue.

The virtual demonstrator has been shared with THUMS User Committee with the aim to use it for the validation of HBMs in far-side.

5 SUMMARY AND OUTLOOK

This report describes the work of OSCCAR Task 2.4 and can be divided into three parts. The first part deals with the homologation demonstrator test series and the validation of corresponding simulation models for different simulation codes. The homologation demonstrator evaluated a reclined seating position and the challenges for the restraint system and the testing devices associated with such a configuration, especially with regard to the restraint of the occupant's pelvis. The focus was on the provision of a robust test setup and complete test results for the validation of the associated virtual demonstrator. The second and third part of the report illustrate the demonstration of the functionality and effectiveness of two selected protection principles (PP2 and PP6) out of Task 2.3 by physical as well as virtual demonstrators.

The **homologation demonstrator** consisted of a generic seat pan in combination with a 48° reclined backrest, thus representing a reclined seating position. The assembly was mounted on a sled and subjected to one frontal and two frontal-oblique pulses. A THOR ATD 50th percentile was used to simulate the occupant. The homologation demonstrator was equipped with a 3-point belt system including a pretensioner in the shoulder retractor, a crash locking tongue and a double lap belt pretensioner, called “SOTA DLPT”. The SOTA DLPT belt is designed to properly restrain the occupant’s pelvis in order to prevent submarining in a reclined seating position and was compared to a state-of-the-art belt system (SOTA belt). Two test series were performed (loop 1 & loop 2, 19 tests in total). The first test series evaluated the effectiveness of the SOTA DLPT belt for an upright and a reclined seatback. The second test series investigated the robustness of the first test series by adjusting some of the test parameters and evaluated test scatter by repeating four tests under exactly the same conditions. In both the tests with and without SOTA DLPT belt, no submarining was observed in the reclined position. However, the THOR ASIS measurements revealed that the tests in the reclined position were close to submarining and that the SOTA DLPT belt helped to prevent submarining (negative values of the ASIS My).

A virtual homologation demonstrator was developed and validated for LS-Dyna, VPS and Madymo. The respective simulation models are used in OSCCAR WP4 to investigate various aspects with regard to Virtual Testing with HBMs. More specifically, the validation of the environment and the prediction of submarining were of first importance for the considered demonstrator test cases (full-frontal and frontal-oblique load cases with regard to a reclined seating position). Despite some limitations, the simulation models were considered to be sufficiently validated for both seating positions and restraint systems (necessary updates were not available at the time). The validation of the environment was assessed using the CORA rating. Overall, it achieved a “fair” rating (value between 0.71 and 0.77) according to ISO scale. However, the belt pay-in/out was in general slightly underpredicted and the CORA ratings for the lumbar spine forces and moments as well as for the ASIS were bad. This was identified as being partly related to the THOR FEM and the belt FEM models and will require further work in the future.

Next steps for the homologation demonstrator were highlighted such as checking the effect of the revised seat pan used in loop 2 by simulation, further work on the validation score calculation method (average data vs. individual test) and validation acceptance criteria as well as further model improvements concerning belt and dummy interaction to overcome limitations due to encrypted models.

Protection Principle 2 addressed an occupant who is sitting in a slightly rotated position (pointing away from the driving direction). If a crash is unavoidable, the seat is rotated into the crash direction during the pre-crash phase. The seat rotation is not caused by an actuator but due to the inertia of seat and occupant in the course of an emergency braking prior to the crash with a simultaneous

release of the seat. The conducted test series considering four different dummy models (5th percentile female, 50th & 95th percentile male as well as an obese male dummy), three rotation axis positions and different feet configurations demonstrated the functionality of PP2 in general. The rotation allowed a repositioning of the occupant from a 30° inward to a 0° rotated “standard” position within a total time of less than 1 s (starting point: t_0, initiation of braking). This rotation to the “standard” seat position could be achieved for a maximum brake deceleration of only 0.5 g. For the fastest rotation axis, found to be at the rearmost and very outwards position of the seat base, rotation durations in the range of 0.5 s were achieved. Besides the physical tests, corresponding simulations for the 50th percentile male occupant models HIII and AHM were conducted within the framework of a virtual demonstrator.

In order to further investigate the biomechanical behaviour of the lower extremities in cases without a rotatable footrest, it would be necessary to carry out appropriate volunteer tests, since the applied occupant models are not validated for the investigated rotational load case. The PP2 studies showed a possible way to enable rotated seats in future interiors. In a next step, the principle needs to be combined with state of the art restraint systems (e.g. airbags) and also consider environmental information (e.g. the initial seat rotation angle) to provide an efficient overall protection function. It has to be seen in the context of an integrated restraint concept, including information on crash detection as well as monitoring of occupants and interior.

Protection Principle 6 investigated a far-side load case, representing a future crash scenario for vehicles with flexible interiors without the presence of a centre console. The physical demonstrator was based on the SOTA DLPT belt and included seat side supports as well as inboard belt routing. It was evaluated in ten far-side sled tests using the WorldSID ATD. The combination of the SOTA DLPT belt and the seat side supports helped to limit the WorldSID head excursion while staying below best performance injury assessment values, except for the upper and middle chest rib deflections. The inboard SOTA DLPT belt with seat side supports helped to reduce the WorldSID head excursion compared to the outboard SOTA DLPT belt but increased the lower neck Mx value above the best performance injury limits. Further padding or some flexibility of the seat side supports may decrease the thoracic rib deflections. Additionally, the neck bending may be further controlled by a seat-mounted airbag.

Generic simulation models of the PP6 environment were created under LS-Dyna and Madymo. A good agreement with the test data was found for the dummy kinematics and measurements. Nevertheless, a further check of the SOTA DLPT belt model response in the far-side load case would be required as the SOTA DLPT was not validated for this load case. The interaction of the shoulder belt with the WorldSID chest and its engagement with the dummy shoulder was a sensitive parameter that could also be affected by variations between hardware and simulation model, such as the shoulder geometry or the dummy jacket.

Next steps could be further comparisons of the WorldSID ATD versus the HBMs responses and potentially future tests/simulations that may evaluate the occupant-to-occupant interaction in a ‘living room’ use case under different far-side crash conditions.

6 REFERENCES

[1] Jakobsson L., Fornells A., Köhler A. L., Mayer C. (2018) Test Case Matrix and selecting Demonstrator Test Cases; Deliverable D2.1, OSCCAR Project, Grant Agreement No. 768947.

[2] Dobberstein J., Lich T., Schmidt D. (2018) Accident data analysis – remaining accidents and crash configurations of automated vehicles in mixed traffic; Deliverable 1.1, OSCCAR Project; Grant Agreement No 768947.

[3] Dobberstein J., Ostling M., Höschele P., Schmidt D., Bálint A. (2021) Final results on detailed crash configurations from collisions expected to remain for automated vehicles; Deliverable D1.3; OSCCAR Project, Grant Agreement No. 768947.

[4] Schaub S., Becker J., D'Addetta G. A., Mayer C. (2018) Selection of Viable Advanced Passenger Protection Principles for Further Investigation, OSCCAR EU project, GA 768947.

[5] Uriot, J., Potier, P., Baudrit, P., Trosseille, X., Petit, P., Richard, O., Compigne, S., Masuda, M., Douard, R. (2015) Reference PMHS Sled Tests to Assess Submarining. Stapp Car Crash Journal. Vol 59.

[6] Siemens PLM Software, THOR 50th percentile Dummy, in *Simcenter Madymo Model Manual Version 7.8*, 2019, pp. 119-142.

[7] Hamacher M., Becker J., D'Addetta G. A. (2018) Final virtual design of advanced passenger protection principles, Deliverable 2.4, OSCCAR Project; Grant Agreement No 768947.

[8] Eggers A., Ott J., Peldschus S., Dussinger S. (2021) Standardised procedure for validating a vehicle environment for VT, Deliverable 5.1, OSCCAR Project, Grant Agreement No 768947.

[9] Petit P., Trosseille X., Uriot J. (2019) Far side impact injury threshold recommendations based on 6 paired WorldSID / Post Mortem Human Subjects tests, Stapp Car Crash Journal, Vol. 63, 19S-23, November 2019.

[10] Euro NCAP (2019) FAR SIDE Occupant Test & Assessment Procedure, Version 2.0, June 2019.

[11] Jin X.; Hou H.; Shen M.; Wu H.; King H.Y. (2018) Occupant Kinematics and Biomechanics with Rotatable Seat in Autonomous Vehicle Collision: A Preliminary Concept and Strategy. In *Proceedings of the IRCOBI Conference*.

[12] Mroz, K., Östling, M., Richardsson, R., Kerrigan, J., Forman, J., & Pipkorn, B. (2020). Effect of Seat and Seat Belt Characteristics on the Lumbar Spine and Pelvis Loading of the SAFER Human Body Model in Reclined Postures. In *Proceedings of the IRCOBI Conference*.

[13] Dahlgren, M., Vishwanatha, A., Soni, A., Engstrand, K., Forsberg, J., & Yeh, I. Belt Modelling in LS-Dyna®.

[14] Becker J. , Sprenger M., Schaub S. (2019) Interior Models for Occupant Protection Simulations in OSCCAR, Deliverable 2.2, OSCCAR Project; Grant Agreement No. 768947.

[15] Richardson, R., Donlon, J.P., Jayathirtha, M., Forman, J., Shaw, G., Gepner, B., Kerrigan J., Ostling, M., Mroz, K. and Pipkorn, B. (2020) Kinematic and Injury Response of Reclined PMHS in Frontal Impacts. Stapp Car Crash Journal, Vol. 64 (November 2020).

[16] Euro NCAP Technical Bulletin TB 026 – THOR Specification and Certification (Version 1.1). October 2020.

[17] Humanetics Innovative Solutions, Inc. Pre-simulation Positioning - Release Version 1.6.1. November 2018.

[18] Eggers A., Ott J., Pipkorn B., Bråse D., Mroz K., Lopez Valdes F., Hynd D., Peldschus S. (2017) A new generic frontal occupant sled test set-up developed within the EU-project SENIORS. *25th ESV conference*, Detroit, USA. 2017.

[19] Shaw G., Parent D., Purtsezov S., Lessley D., Crandall J., Kent R., Guillemot H., Ridella S., Takhounts E., Martin P. (2009) Impact response of restrained PMHS in frontal sled tests: skeletal deformation patterns under seat belt loading (No. 2009-22-0001). *SAE Technical Paper*, 2009.

[20] Perez-Rapela D., Forman J. L., Acosta S. M. et al. (2017) Comparison of WorldSID to PMHS shoulder-to-belt interaction in far-side impact configurations. www.researchgate.net/publication (link), Preprint – October 2017.

A. APPENDIX

1 HOMOLOGATION DEMONSTRATOR

1.1 Physical Demonstrator – First Test Series Results

1.1.1 Comparison of Reclined and Upright Seating Positions

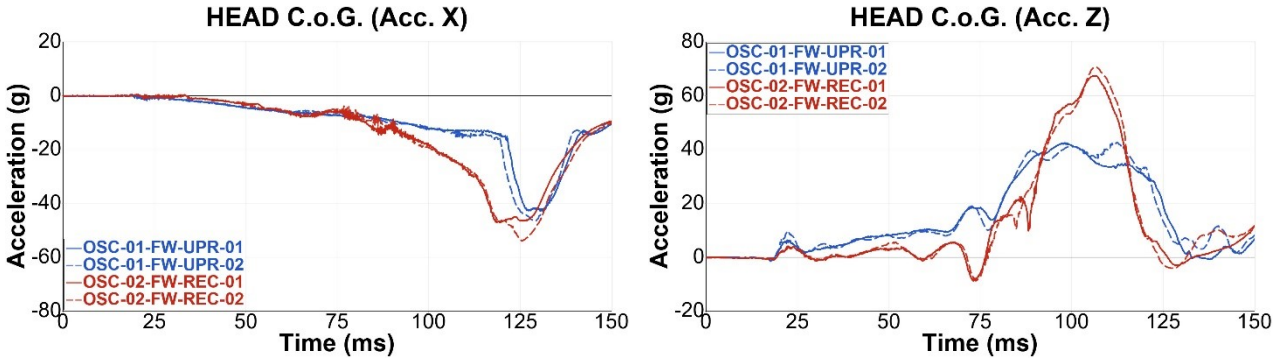

Figure 109 Head COG accelerations

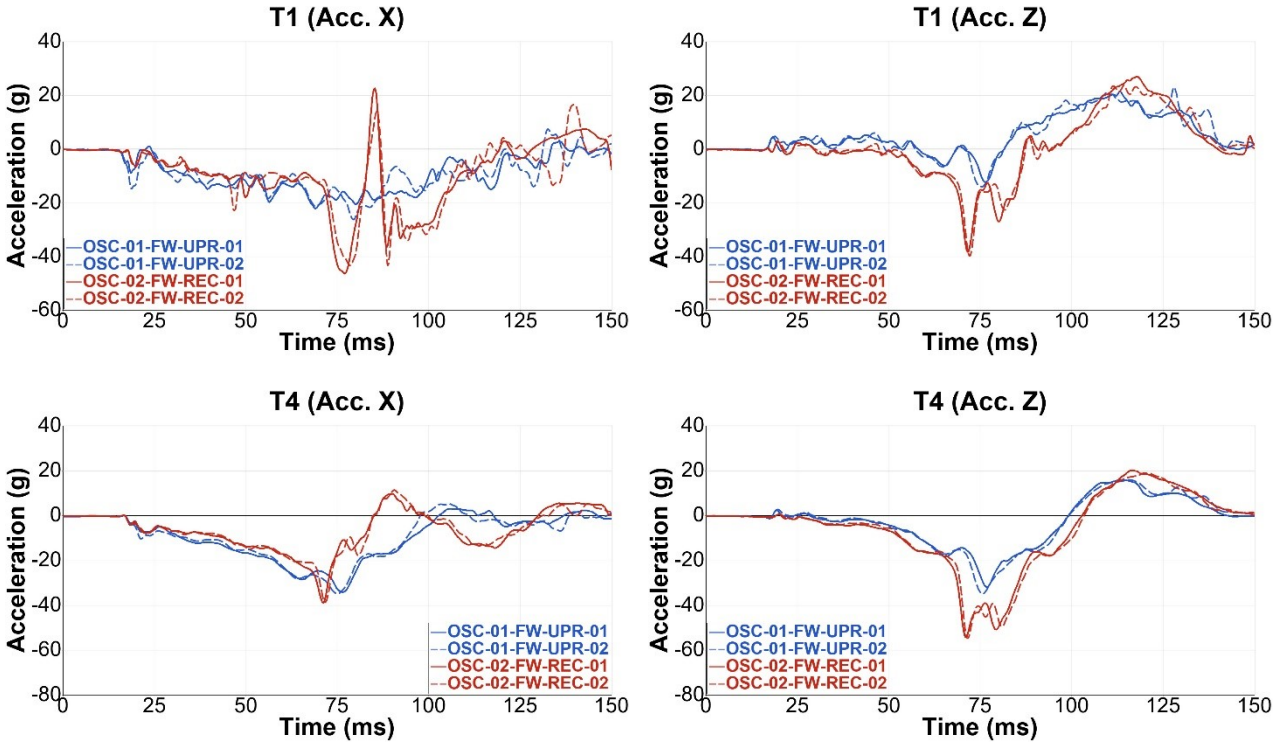

Figure 110 Thoracic spine accelerations (T1 & T4)

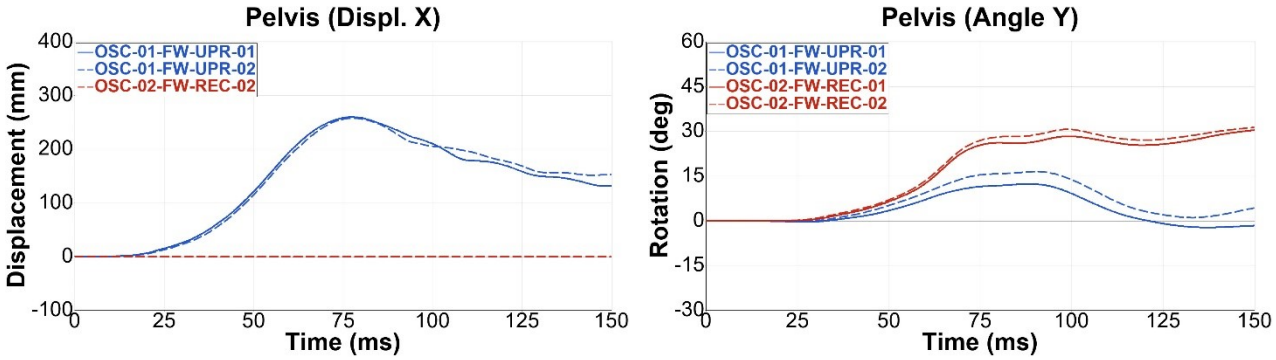

Figure 111 Pelvis X-displacement and Y-angle

1.1.2 SOTA Belt and SOTA DLPT Belt in Reclined Seating Position

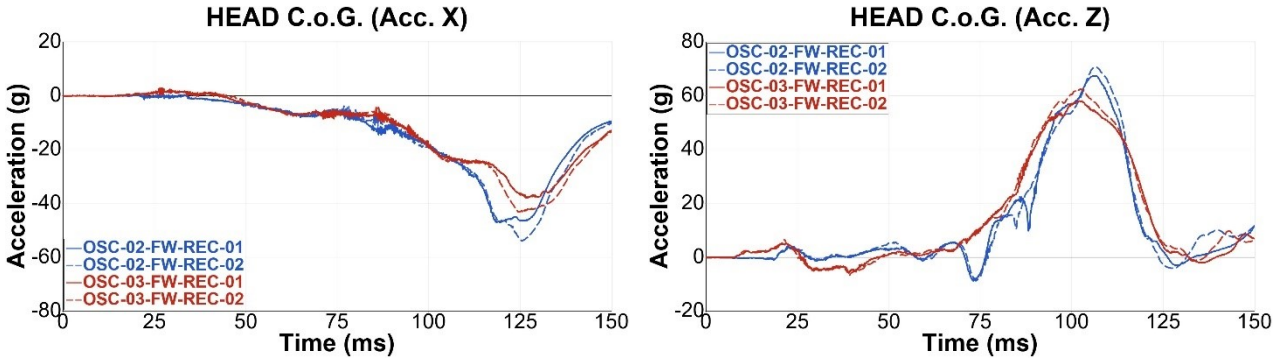

Figure 112 Head COG accelerations

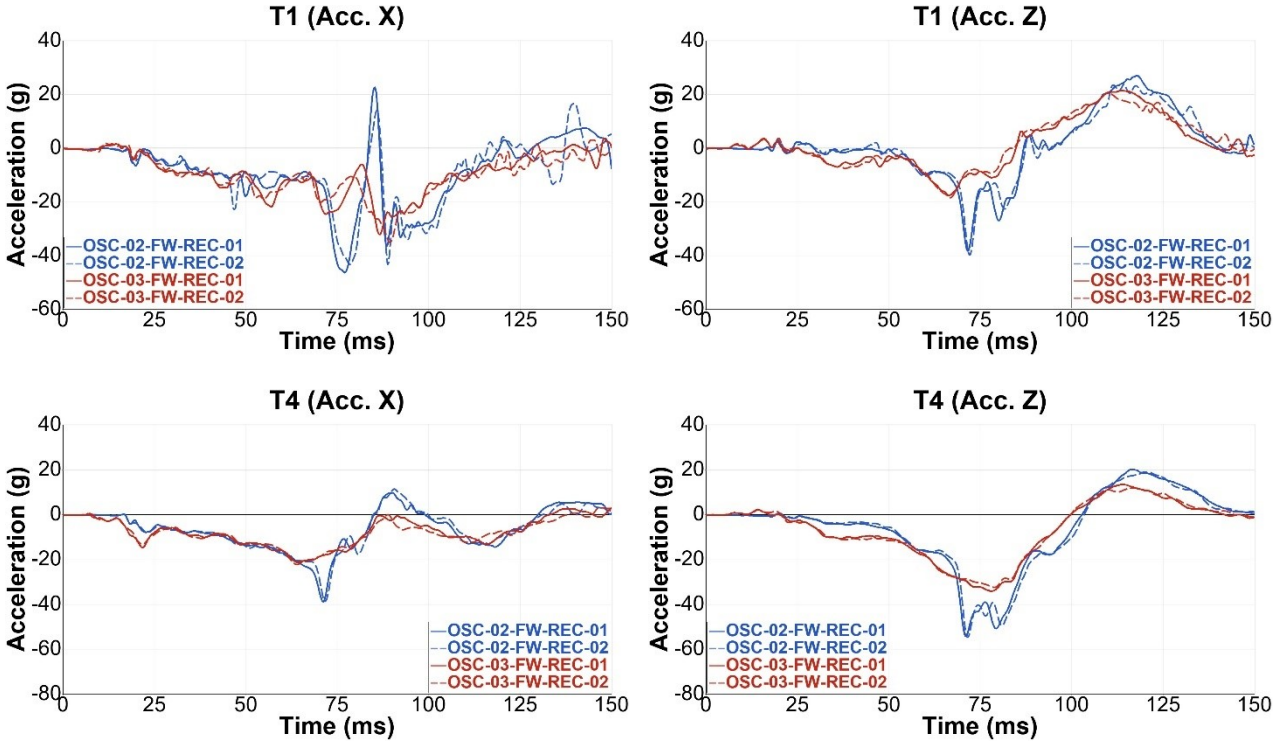

Figure 113 Thoracic spine accelerations (T1 & T4)

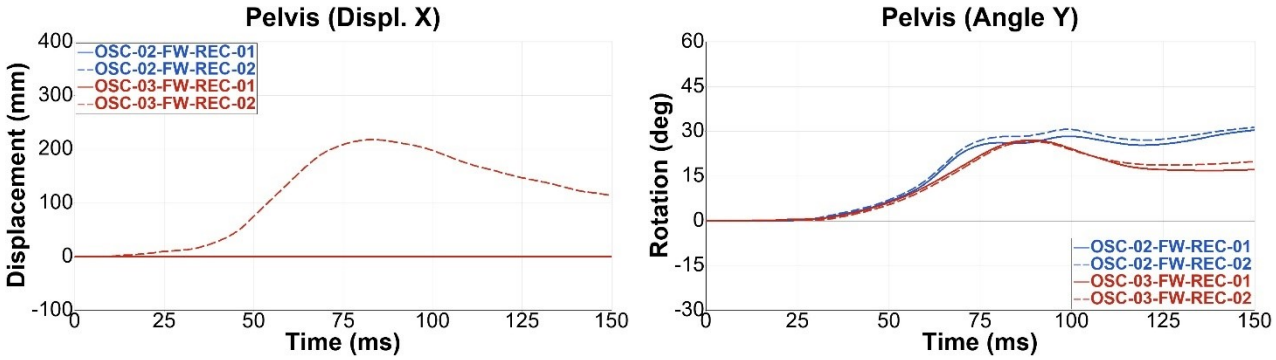

Figure 114 Pelvis X-displacement and Y-angle

1.1.3 SCP1 – Upright Seating Position with SOTA Belt (OSC-05-OB-UPR)

Results from the oblique tests are compared in the following to the corresponding tests in the full-frontal configuration.

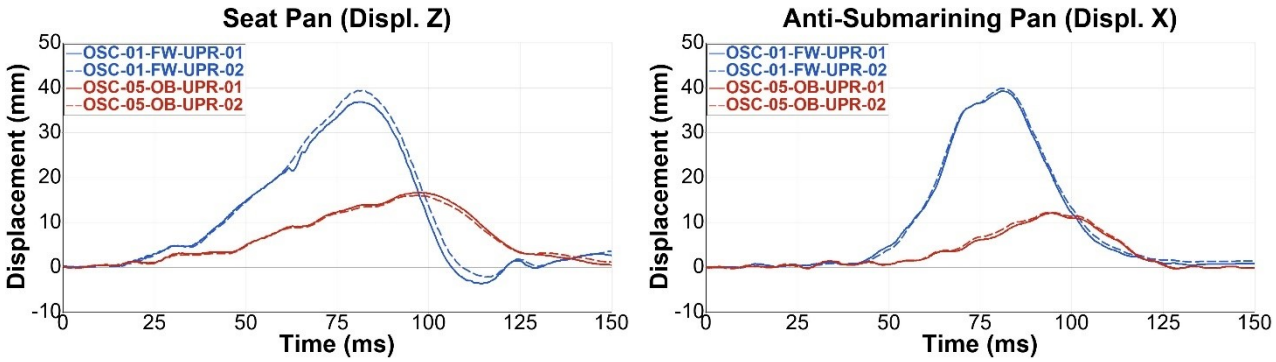

Figure 115 Seat pan and anti-submarining ramp displacements

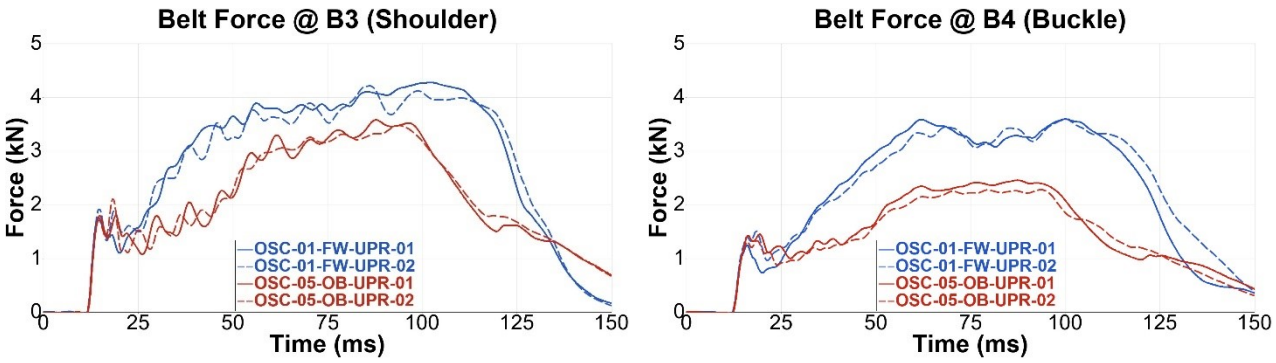

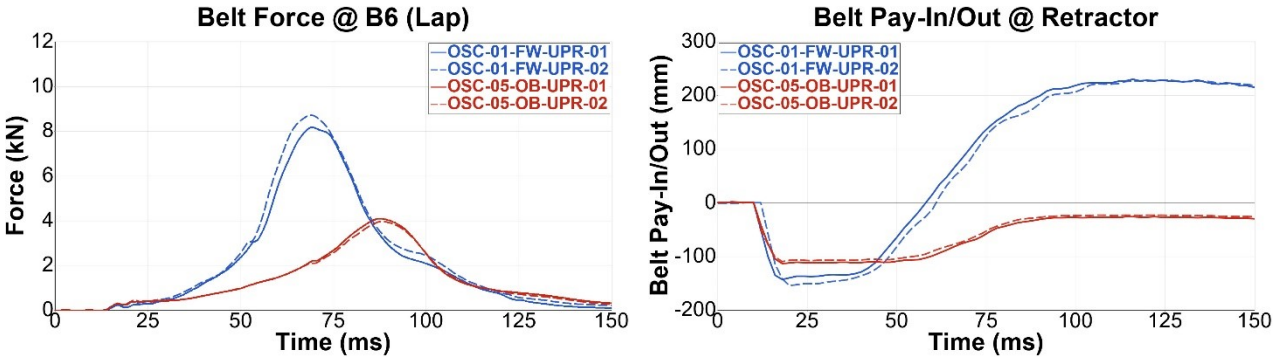

Figure 116 Seat belt forces and shoulder retractor belt pay-in/-out

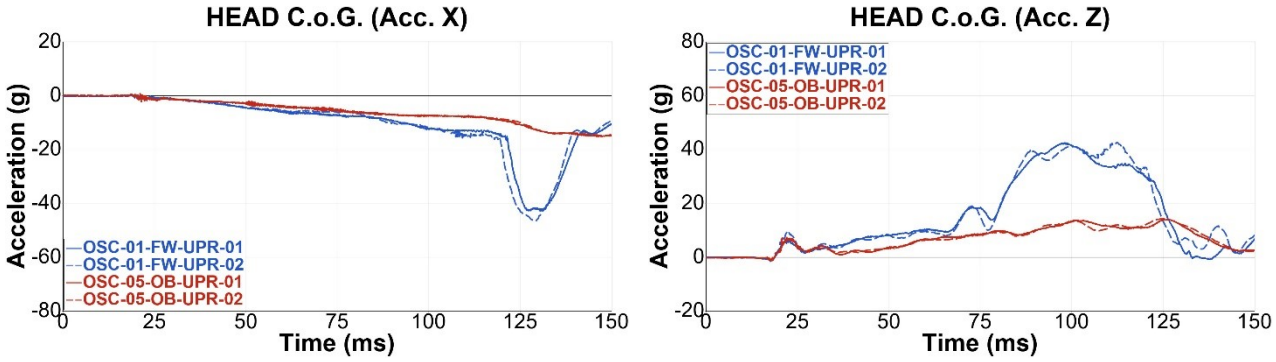

Figure 117 Head COG accelerations

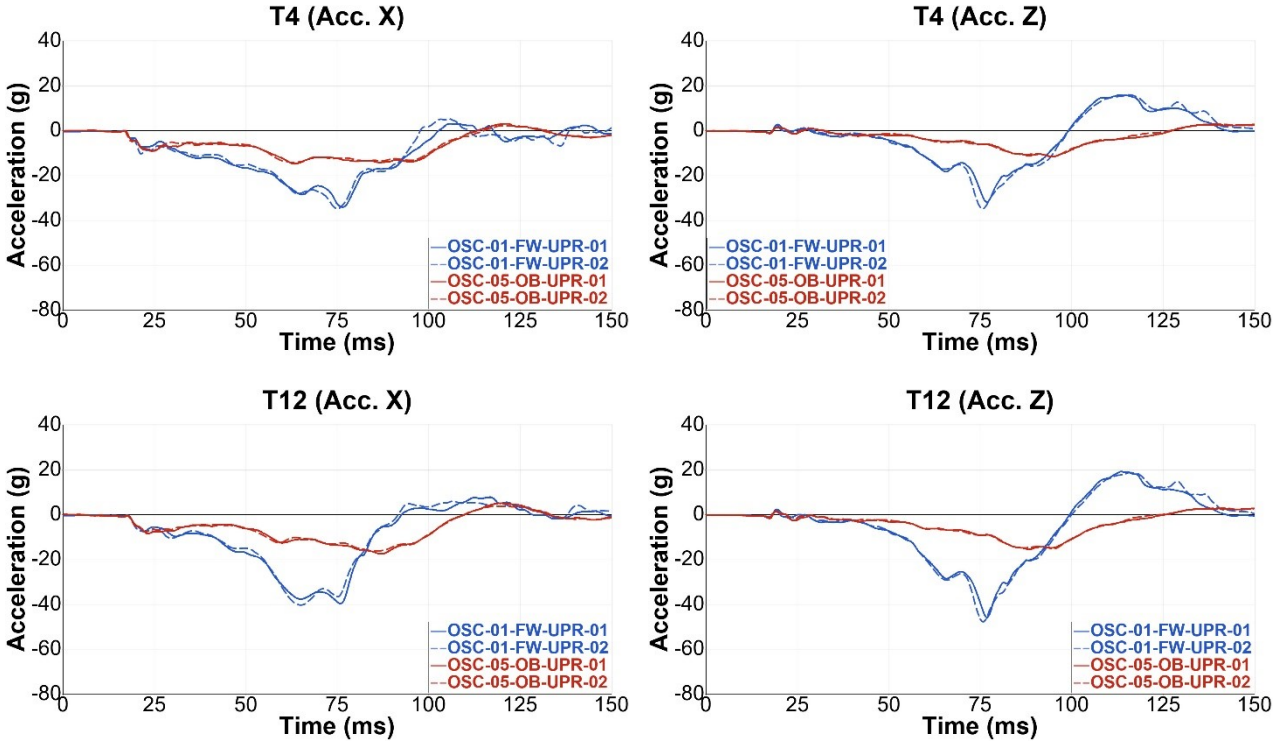

Figure 118 T4 and T12 accelerations

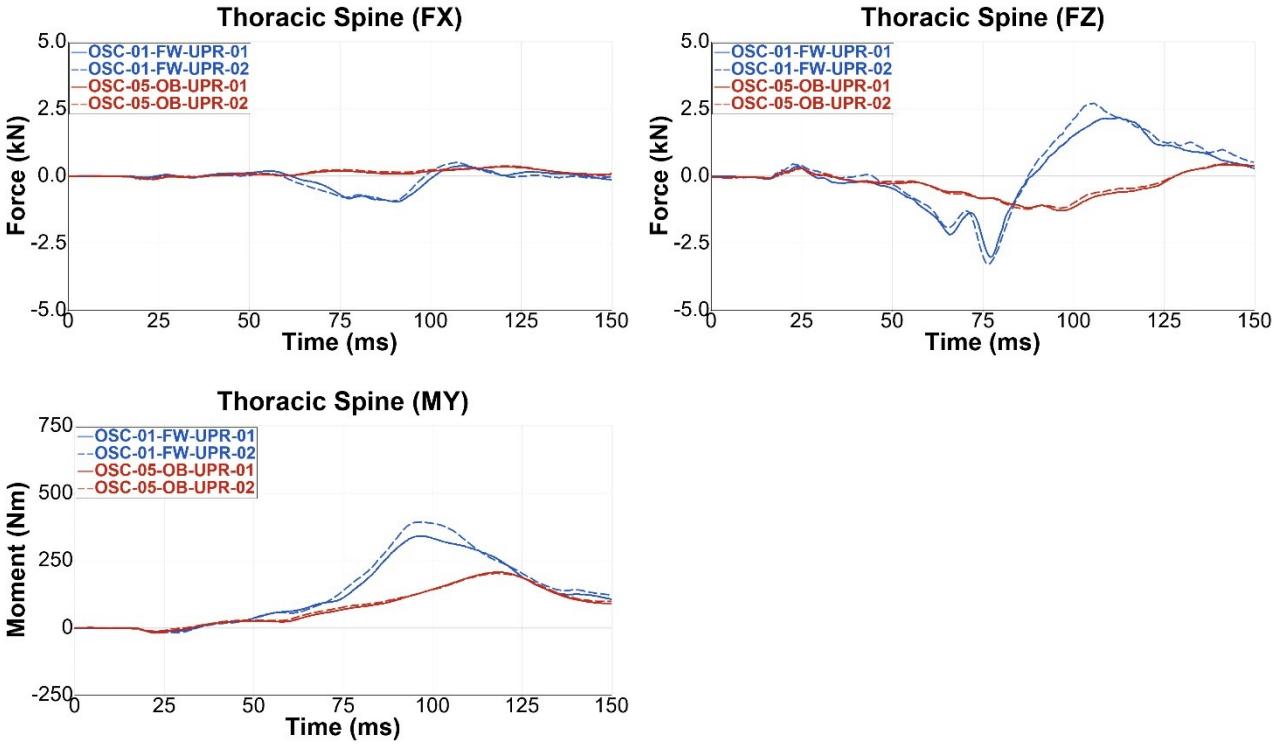

Figure 119 Lower thoracic spine forces and moments

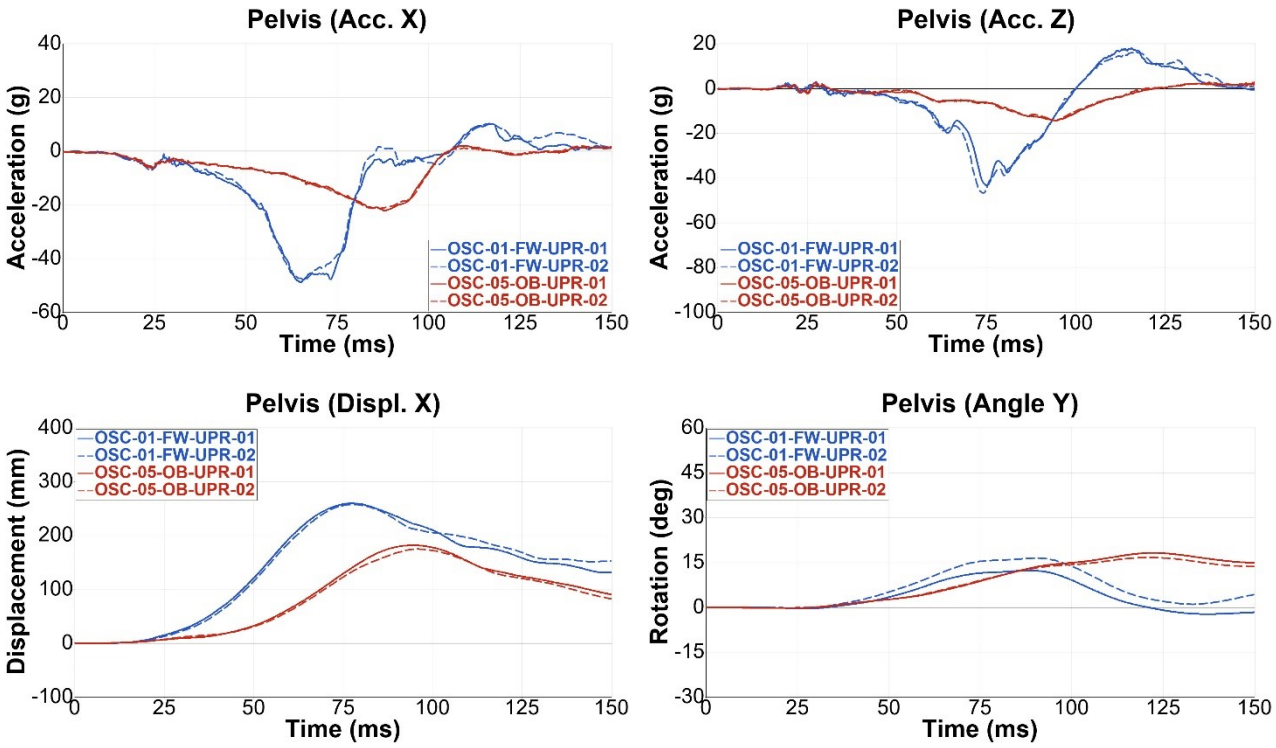

Figure 120 Pelvis accelerations, X-displacement and Y-angle

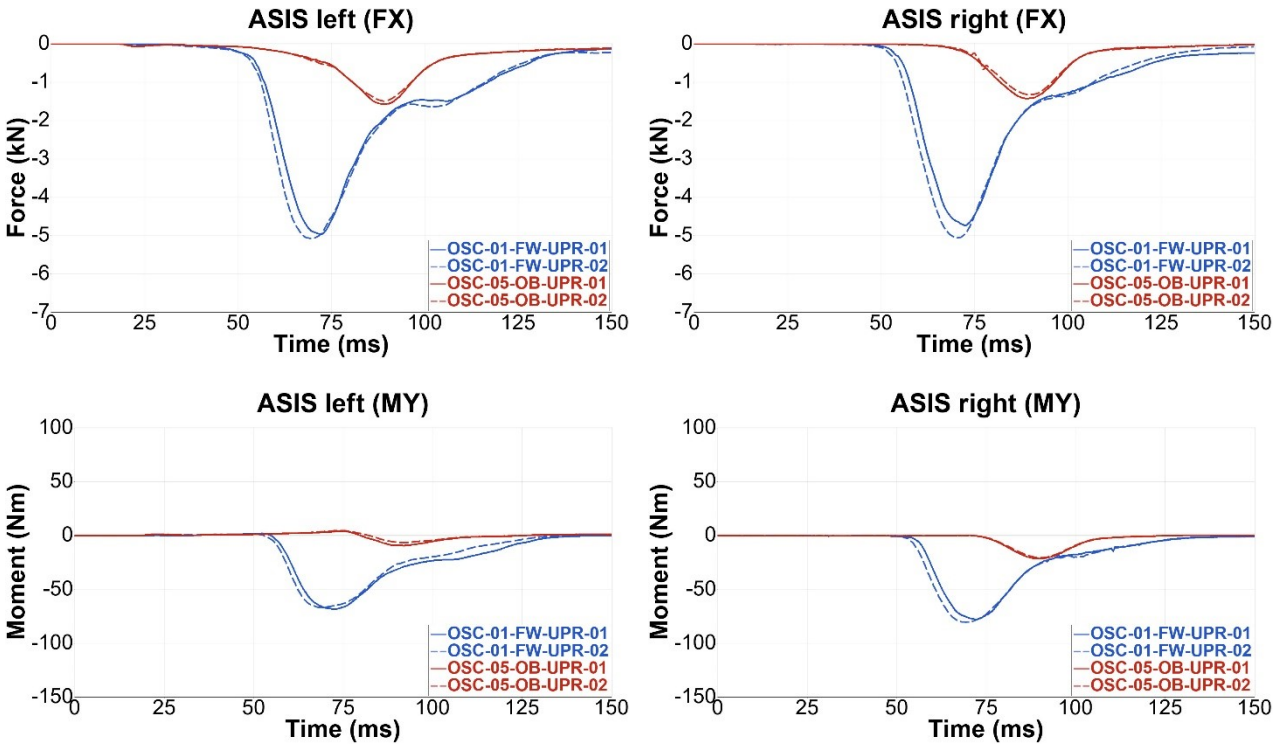

Figure 121 ASIS X-forces and Y-moments

1.1.4 SCP1 – Reclined Seating Position with SOTA DLPT Belt (OSC-06-OB-REC)

Results from the oblique tests are compared in the following to the corresponding tests in the full-frontal configuration.

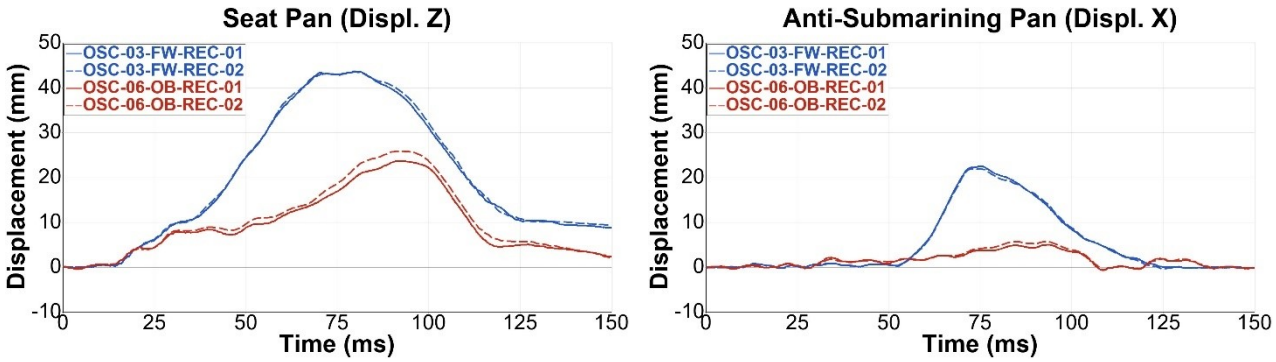

Figure 122 Seat pan and anti-submarining ramp displacements

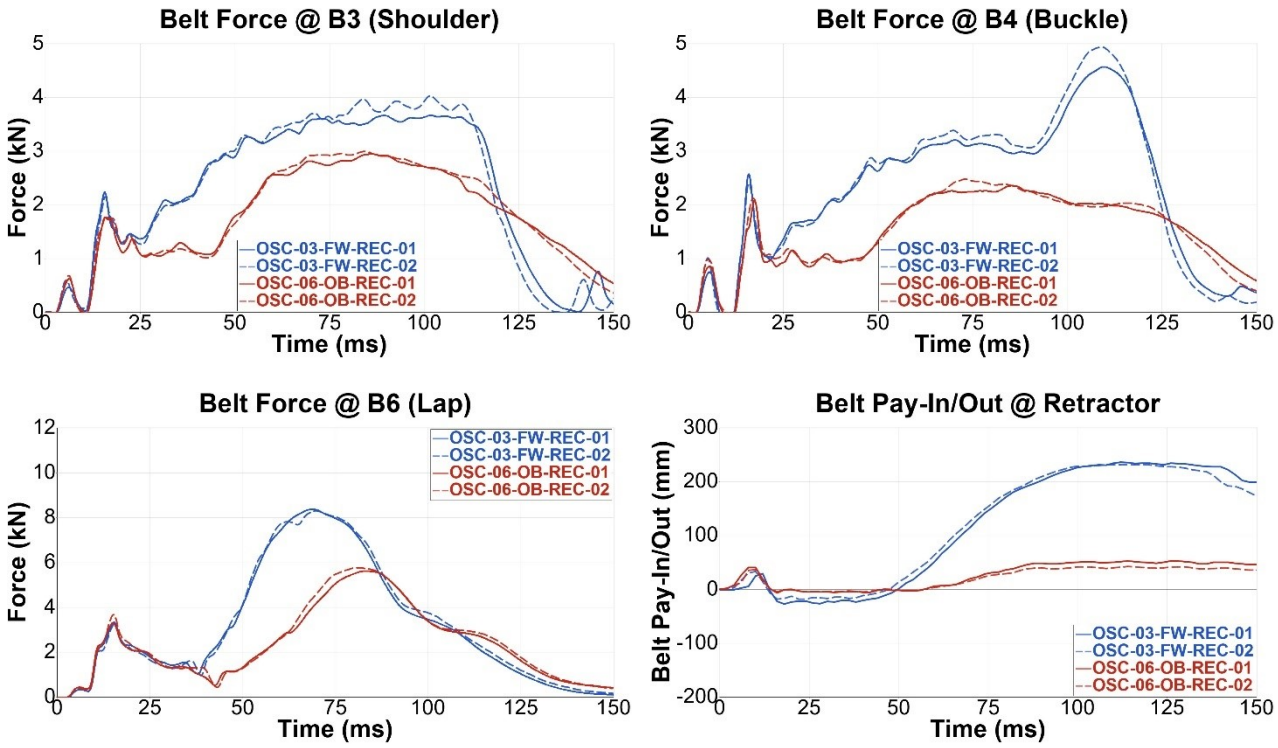

Figure 123 Seat belt forces and shoulder retractor belt pay-in/-out

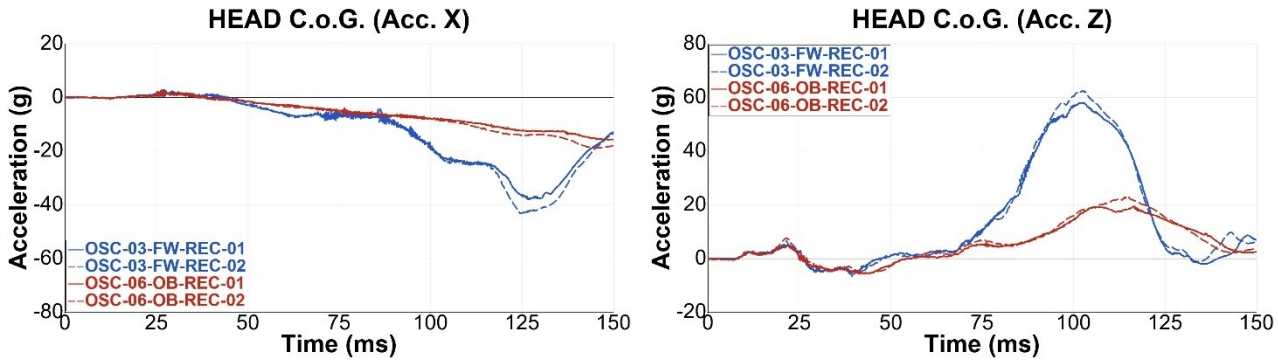

Figure 124 Head COG accelerations

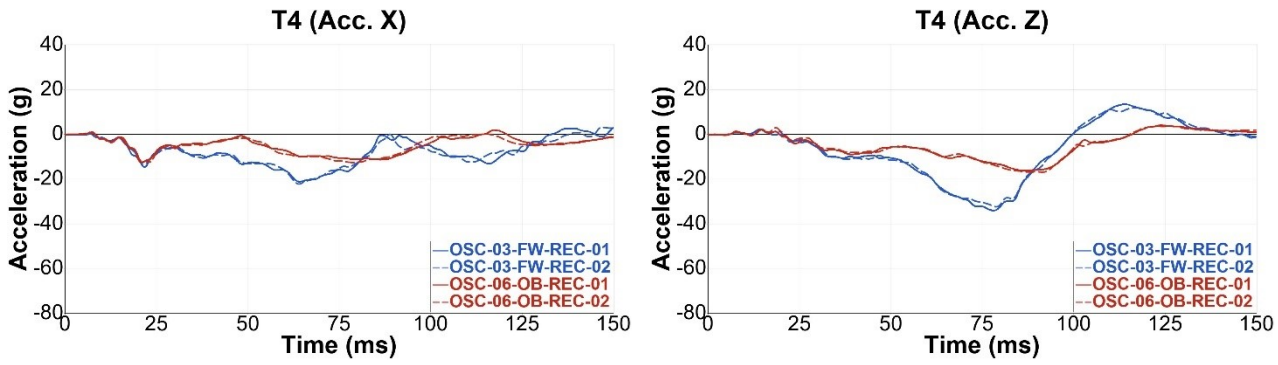

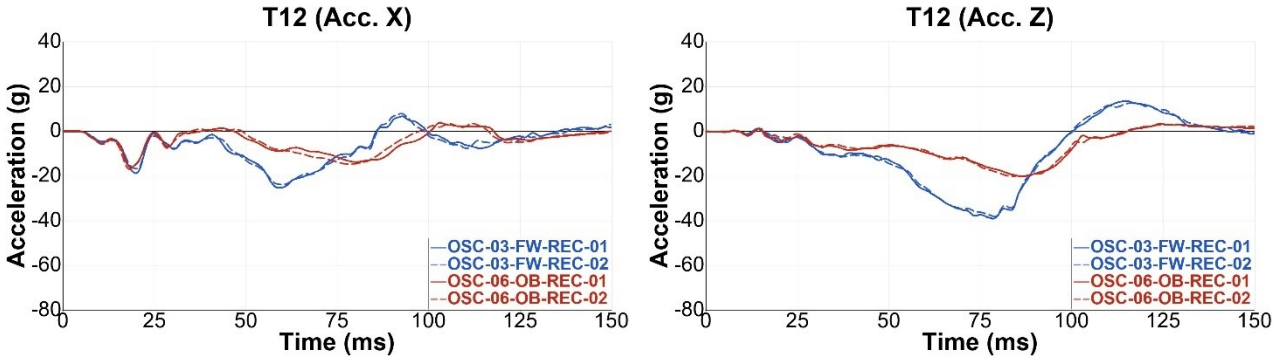

Figure 125 T4 and T12 accelerations

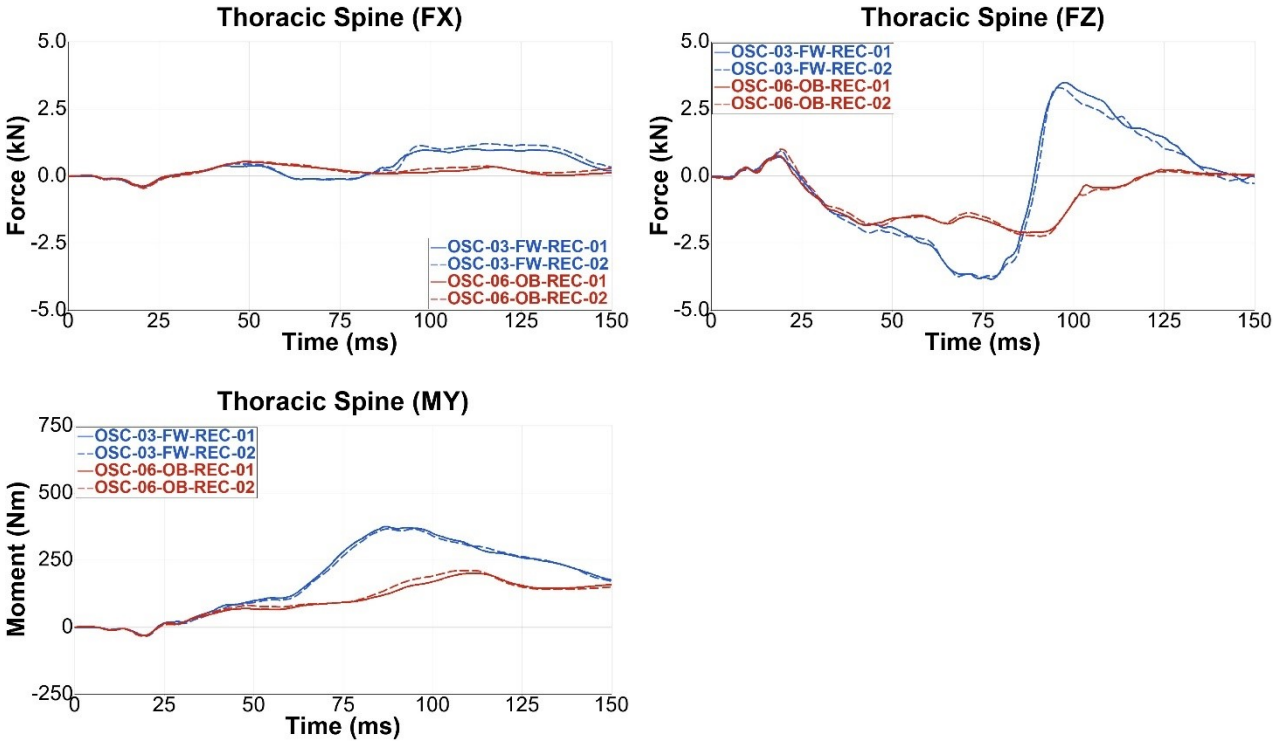

Figure 126 Lower thoracic spine forces and moments

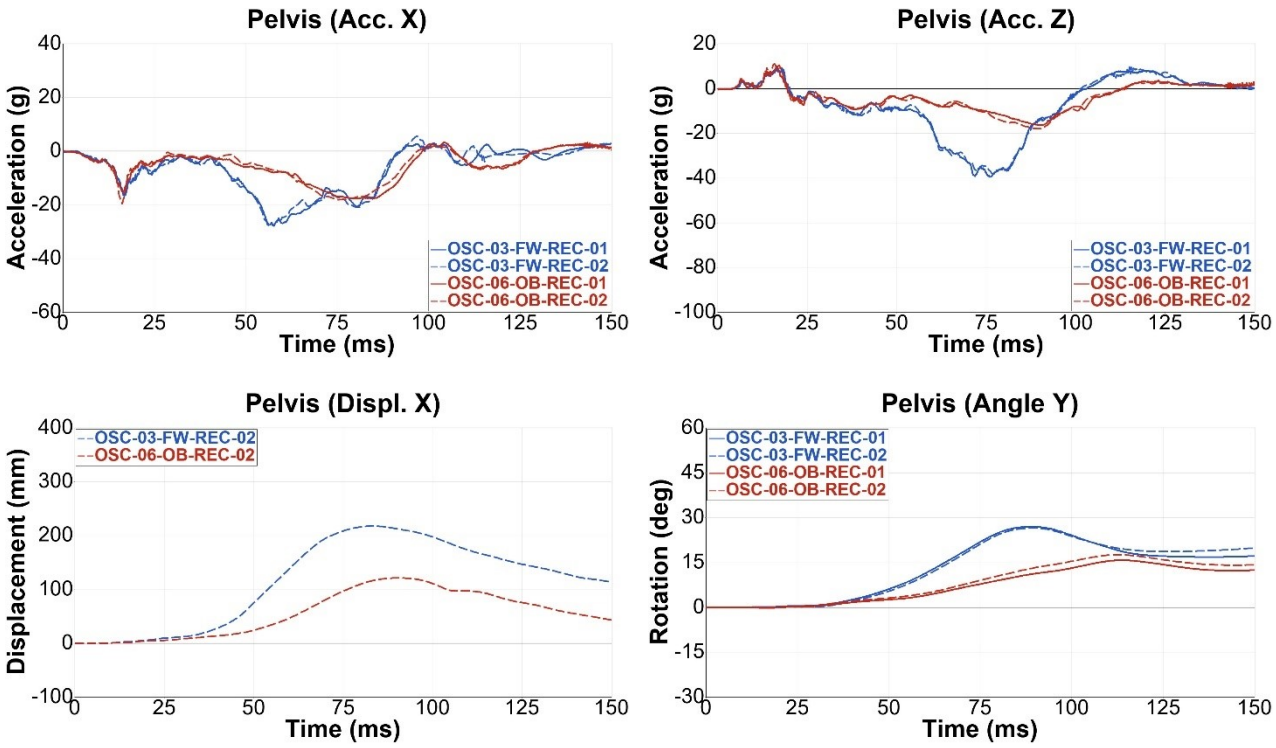

Figure 127 Pelvis accelerations, X-displacement and Y-angle

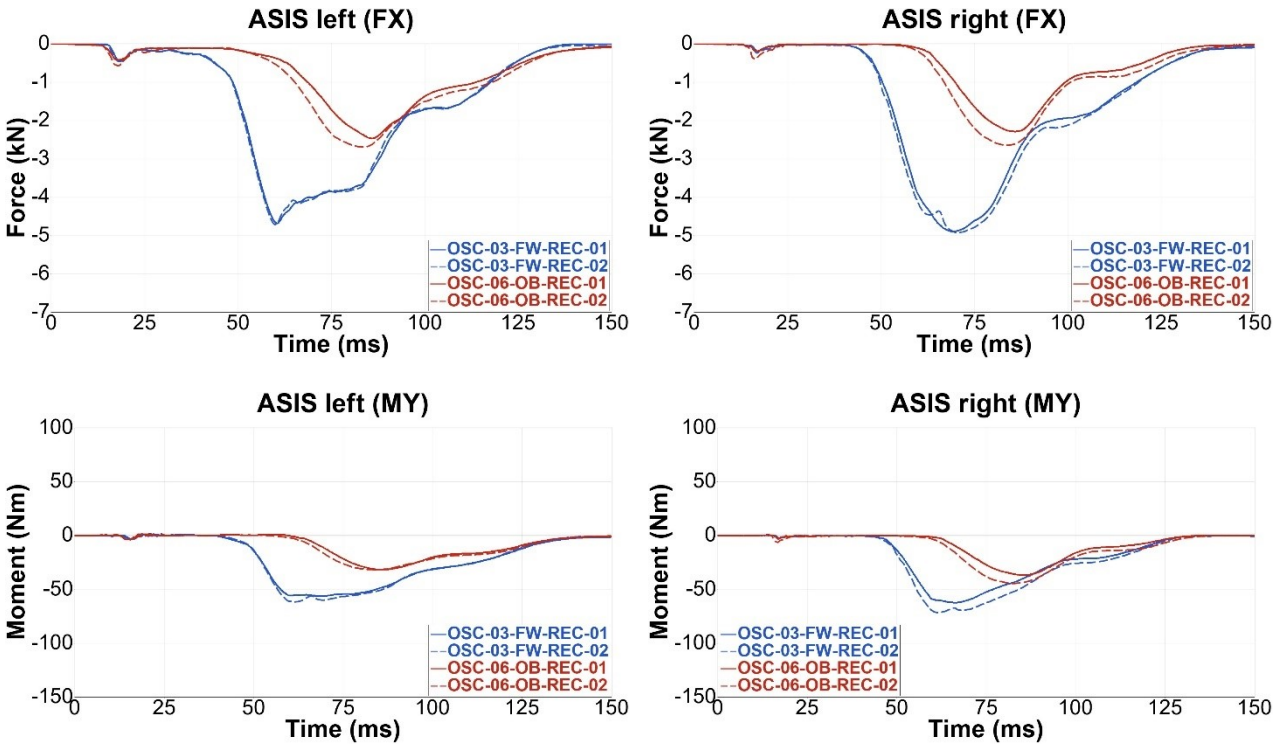

Figure 128 ASIS X-forces and Y-moments

1.1.5 LTAP OD2 – Upright Seating Position with SOTA Belt (OSC-08-OB-UPR)

Results from the oblique tests are compared in the following to the corresponding tests in the full-frontal configuration.

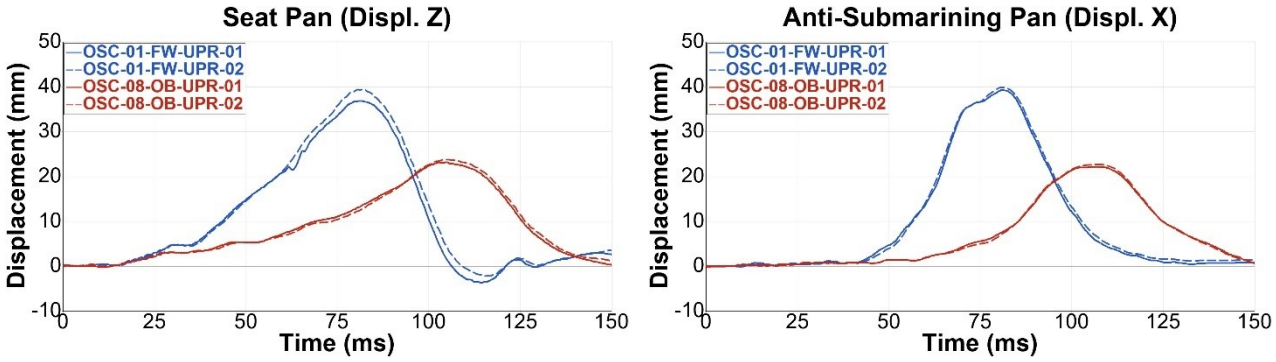

Figure 129 Seat pan and anti-submarining ramp displacements

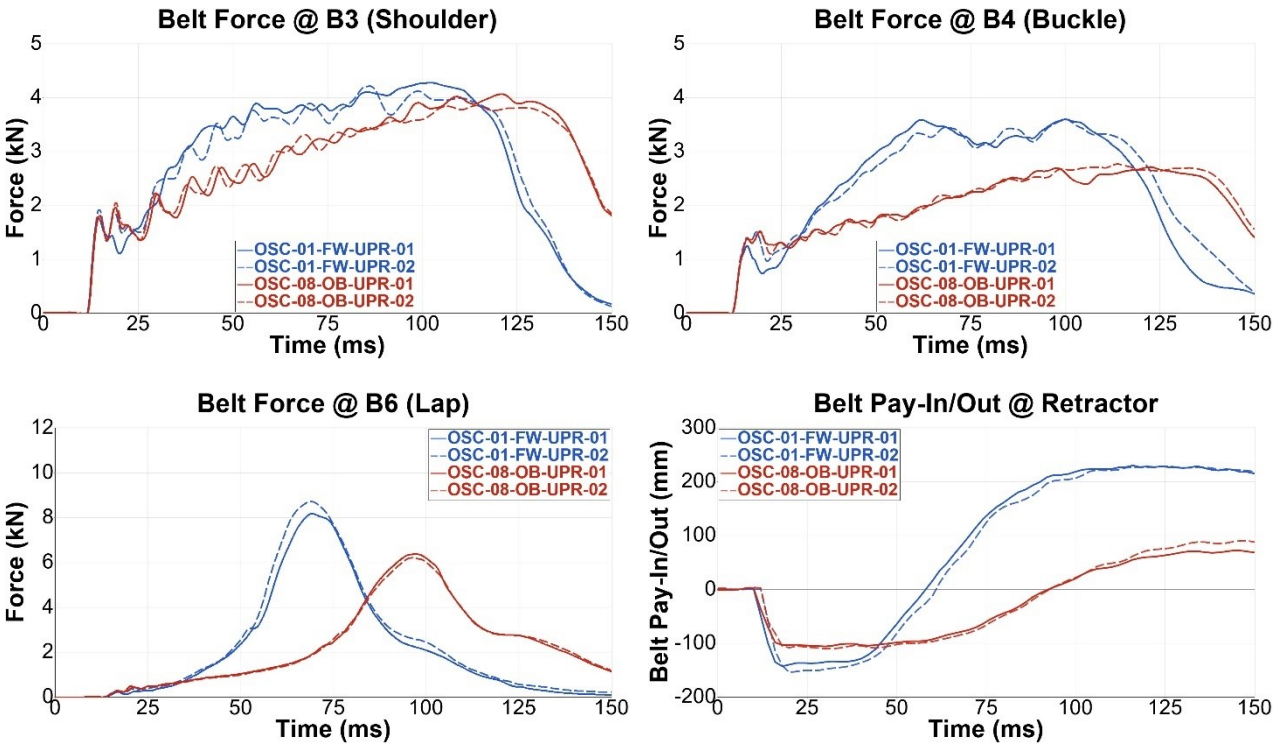

Figure 130 Seat belt forces and shoulder retractor belt pay-in/-out

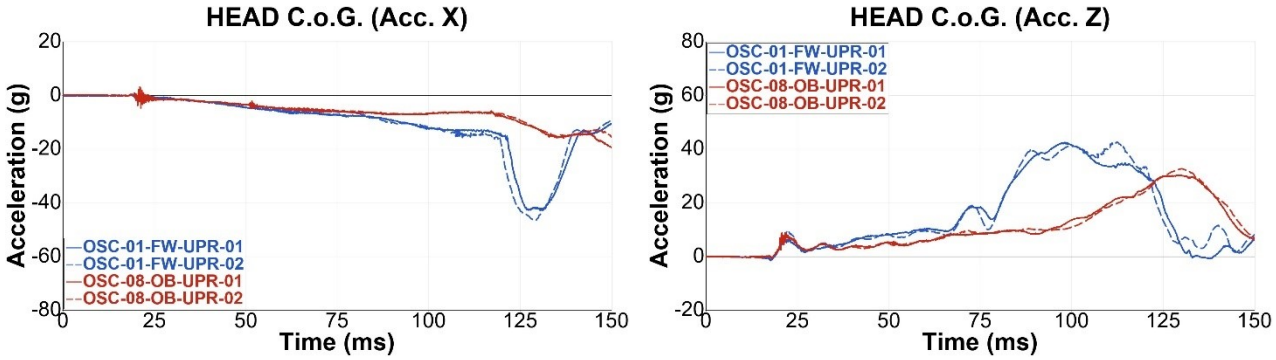

Figure 131 Head COG accelerations

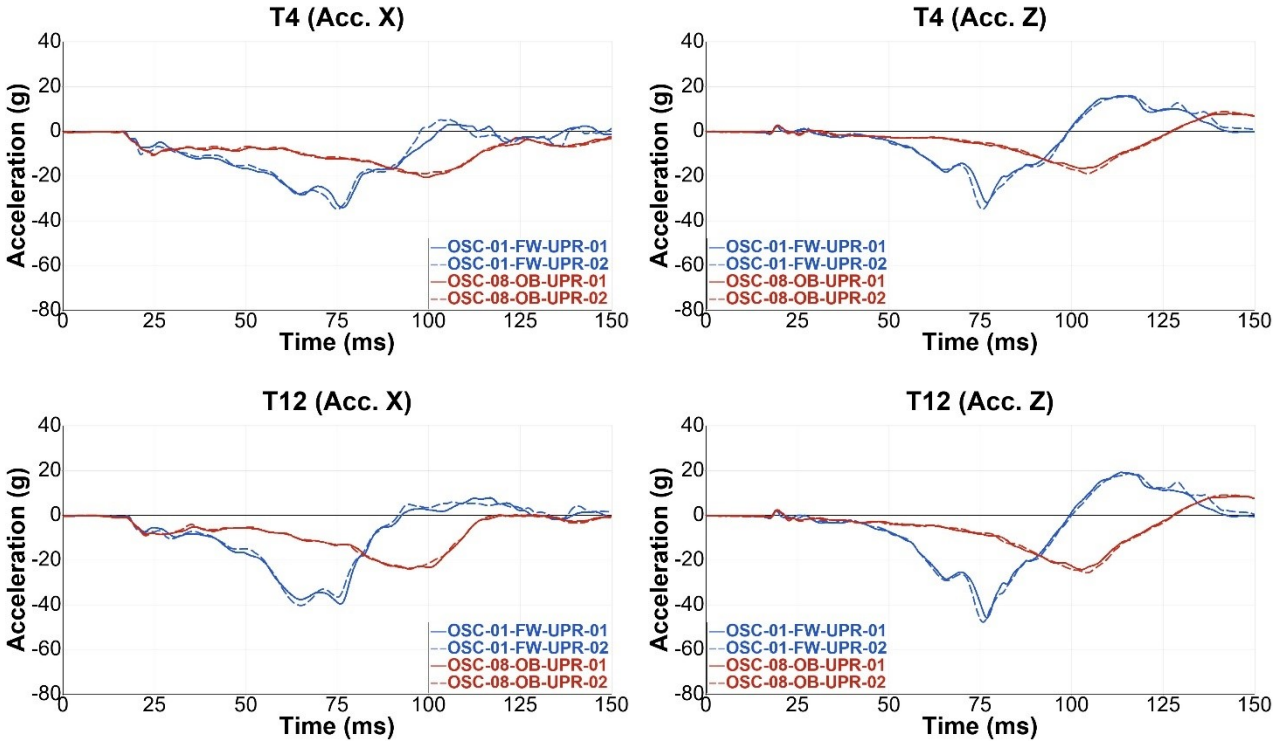

Figure 132 T4 and T12 accelerations

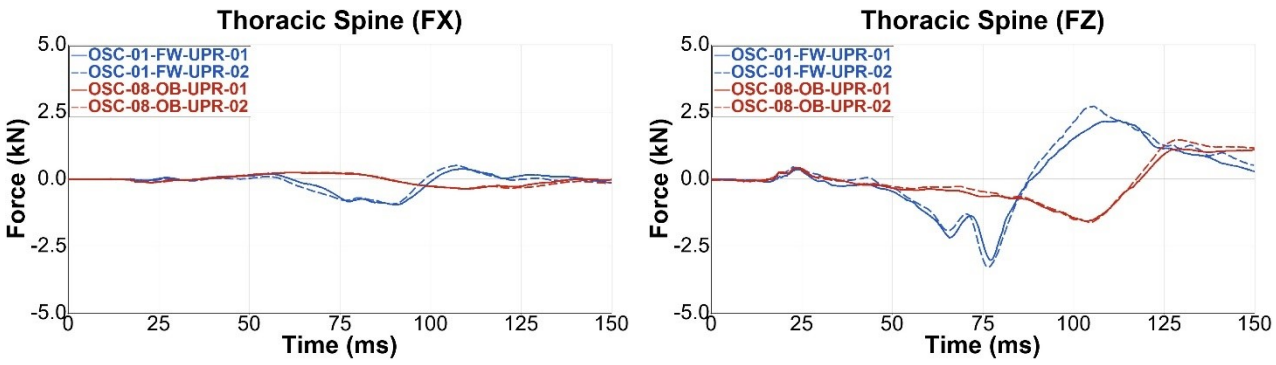

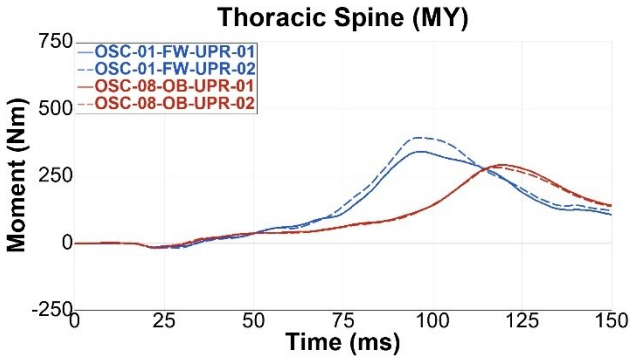

Figure 133 Lower thoracic spine forces and moments

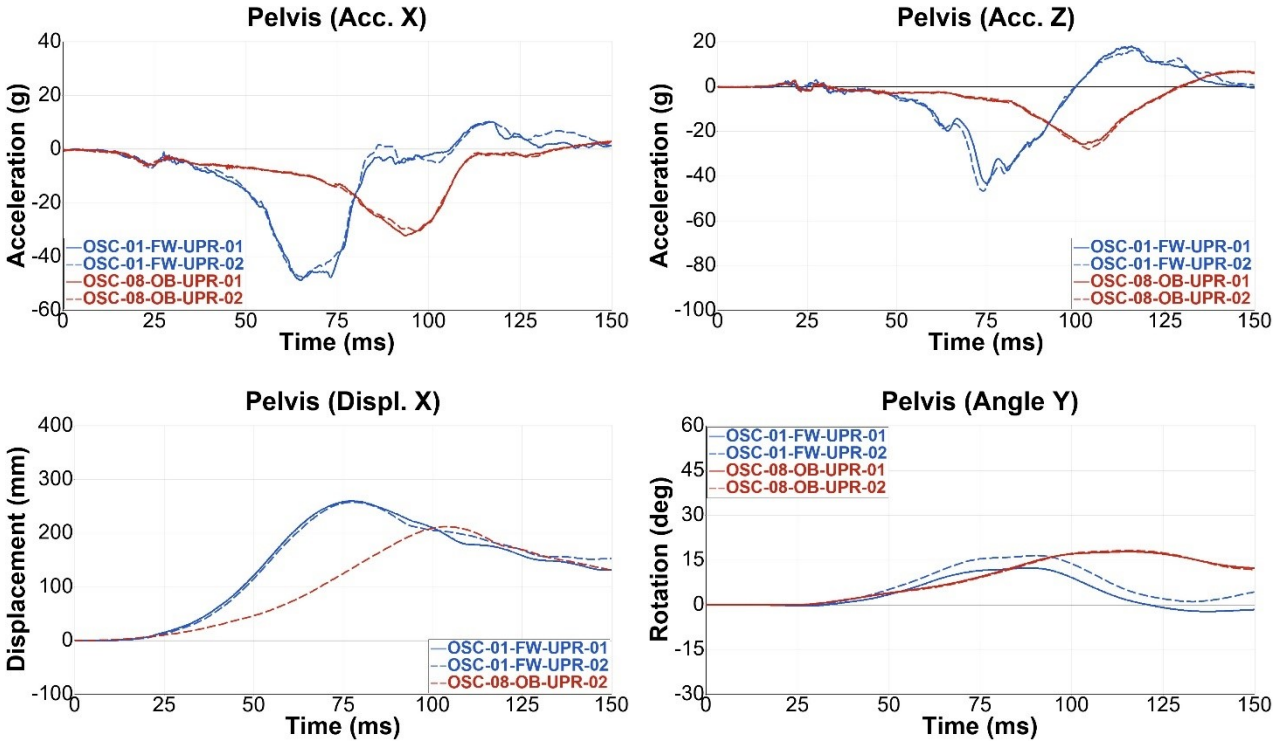

Figure 134 Pelvis accelerations, X-displacement and Y-angle

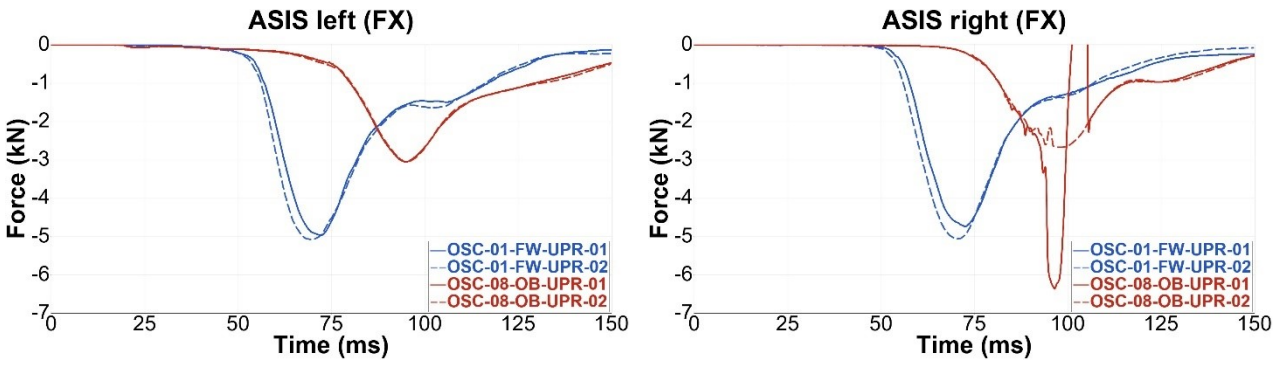

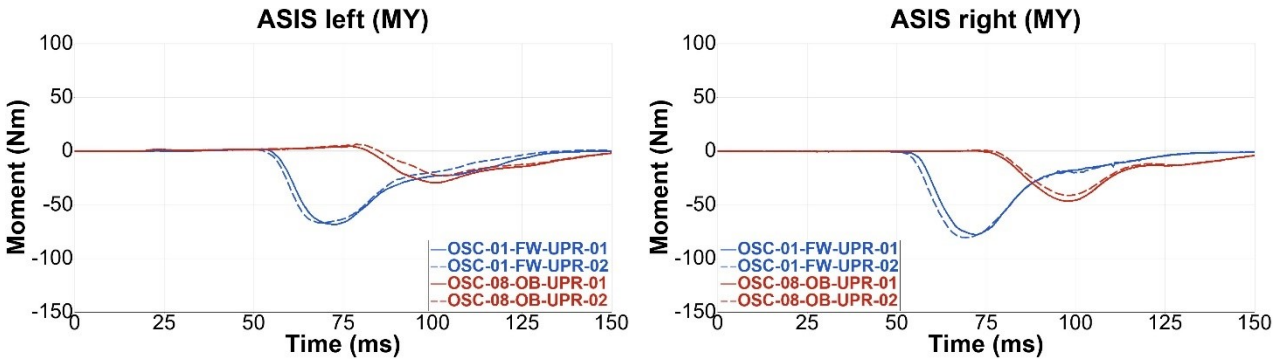

Figure 135 ASIS X-forces and Y-moments

1.1.6 LTAP OD2 – Reclined Seating Position with SOTA DLPT Belt (OSC-09-OB-REC)

Results from the oblique tests are compared in the following to the corresponding tests in the full-frontal configuration.

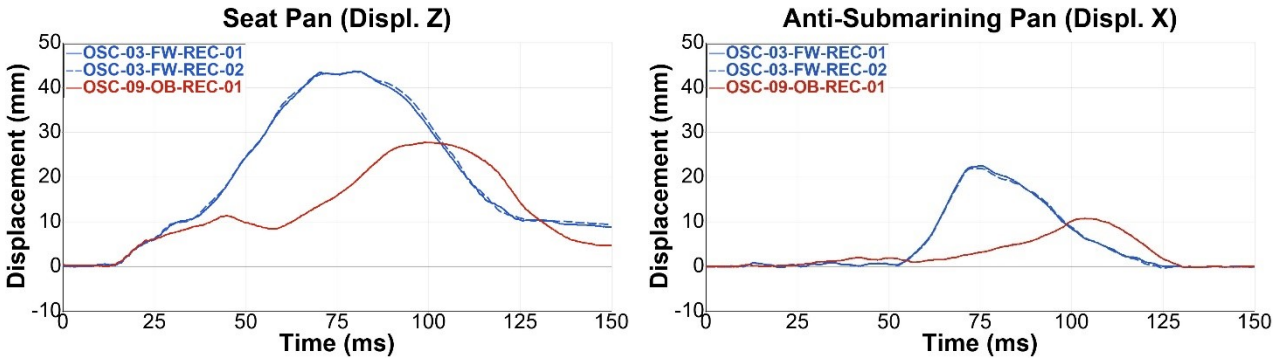

Figure 136 Seat pan and anti-submarining ramp displacements

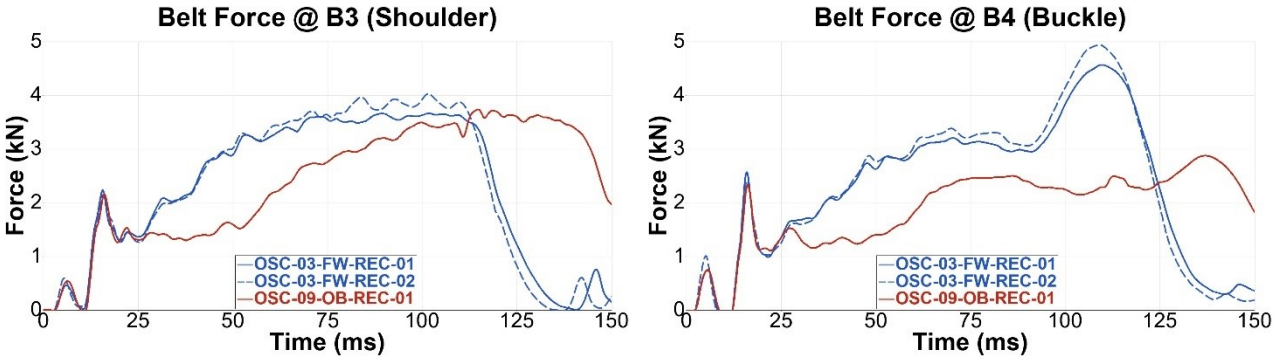

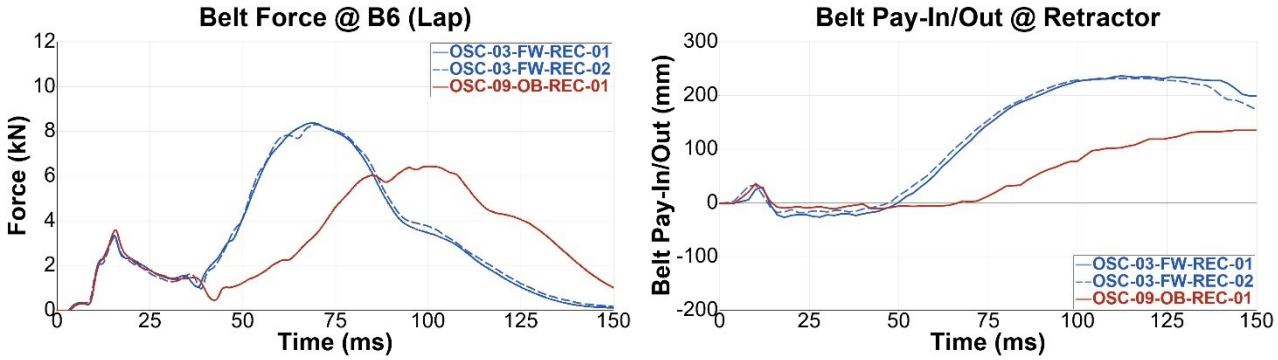

Figure 137 Seat belt forces and shoulder retractor belt pay-in/-out

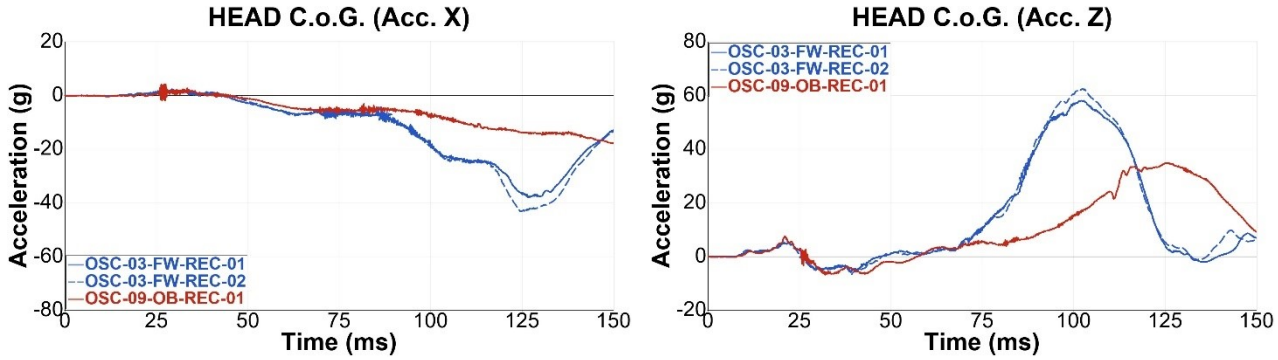

Figure 138 Head COG accelerations

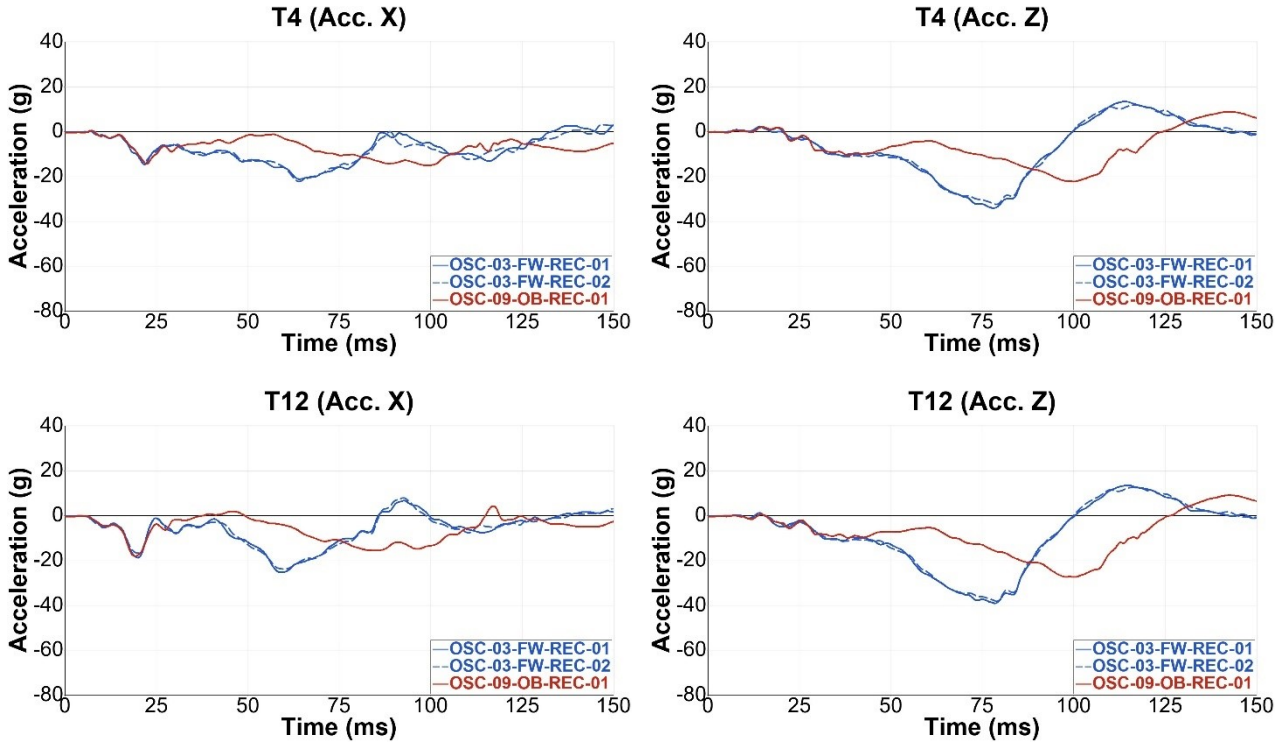

Figure 139 T4 and T12 accelerations

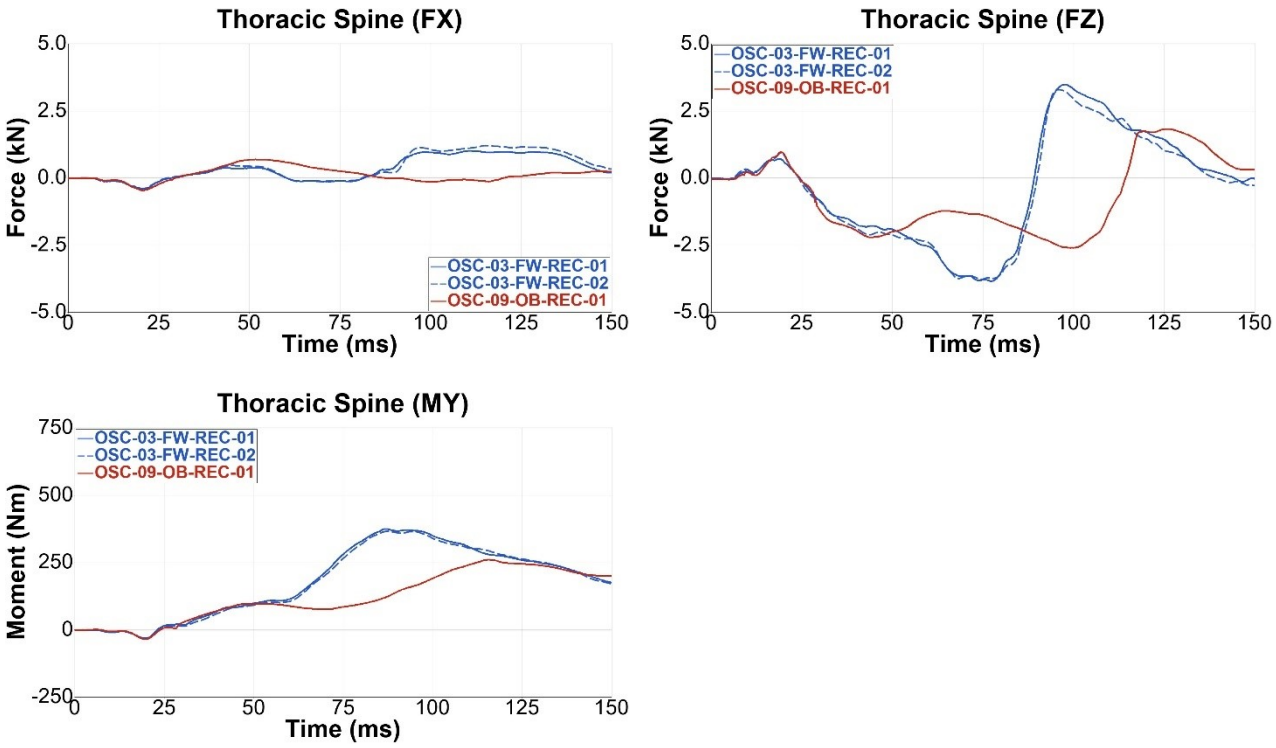

Figure 140 Lower thoracic spine forces and moments

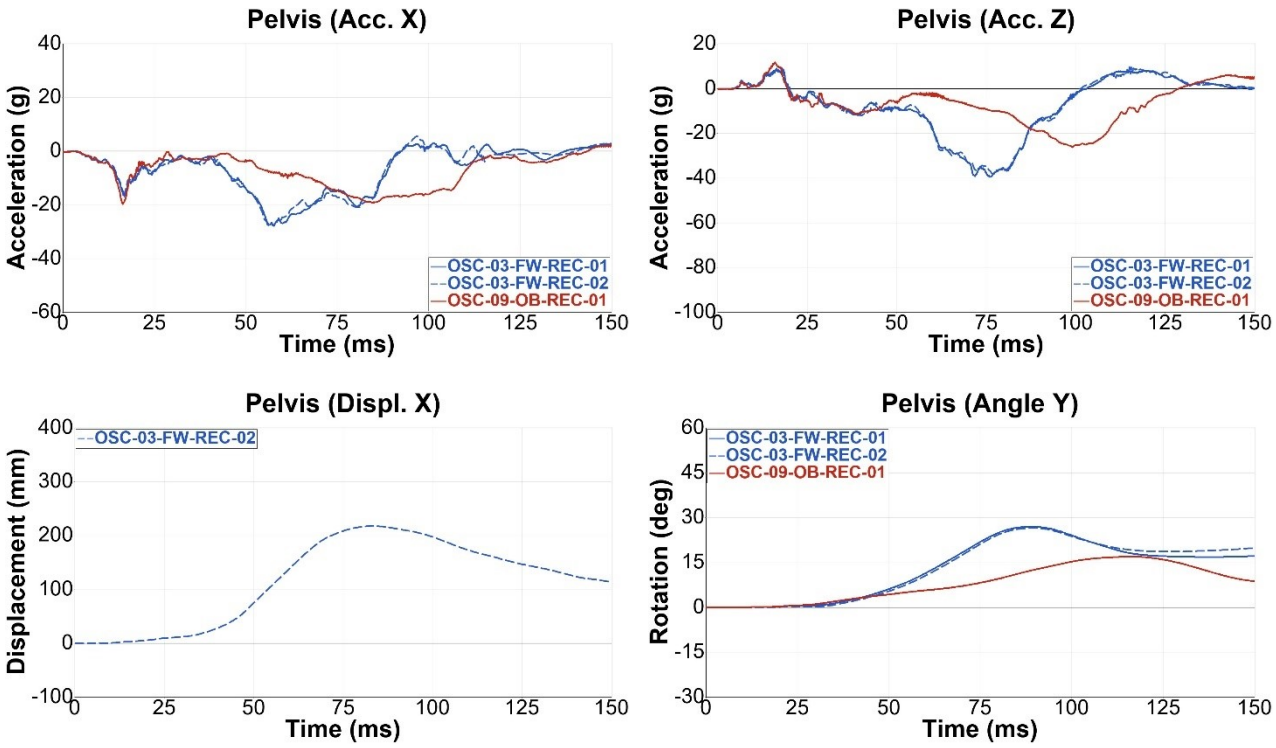

Figure 141 Pelvis accelerations, X-displacement and Y-angle

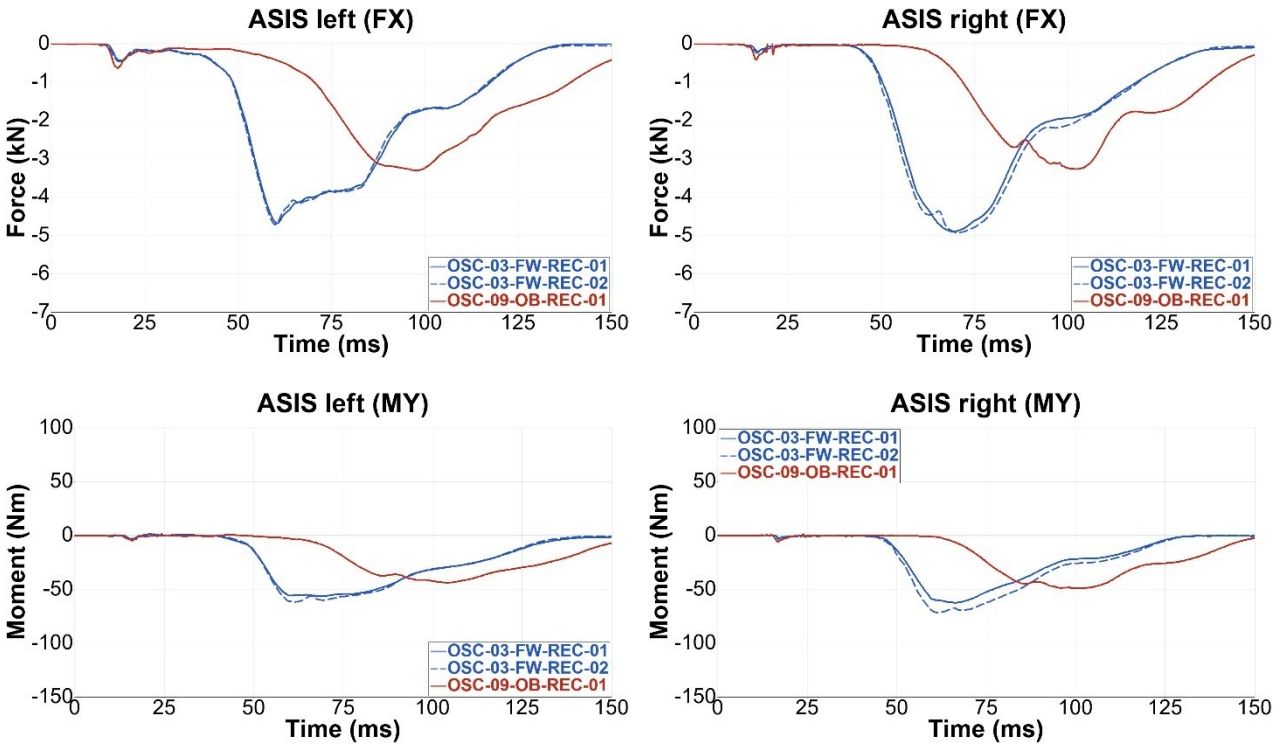

Figure 142 ASIS X-forces and Y-moments

1.2 Set-Up and Calibration of the Virtual Demonstrator

1.2.1 Environment Models

The simulation models of the virtual demonstrator were modelled as closely as possible to the experimental setup described in Chapter 3.1.2. Most parts used in the virtual demonstrator were beforehand validated against data from component and / or full-scale tests (e.g. dummy, semi-rigid seat and belt components / restraint system).

In the following, the main (environment) components of the simulation model are described, as well as necessary changes to these models.

LS-Dyna Model

The LS-Dyna Finite Element (FE) model of the semi-rigid seat was provided by Autoliv and is an enhancement of the original model, which was initially developed within the Sub-BIO project, a private consortium consisting of GIE PSA-Renault, PDB, TME, Faurecia S.A and CEESAR. The Sub-BIO project was held between December 1st, 2012 and October 30th, 2014. Major results of this project on PMHS testing were made available in Uriot et al. (2015) paper [5]. Additional validation of the seat was reported in [12]. A good correlation between the FE-model and the hardware seat was observed. The seat pan and anti-submarining ramp angles were adjusted to the averaged measurements of the first test series (see also Chapter A1.2.3), except that, no further modifications were made to the seat model.

An encrypted FE model of the seat belt system was also provided by Autoliv. Retractors, pretensioners and belt webbing properties of the seat belt system model have been validated separately during the modelling process and are frequently reviewed - the entire seat belt system has been validated by Autoliv using sled tests with the semi-rigid seat. The anchor points of the seat

belt system were modelled as a rigid constraint to the sled and are identical to these measured in the first test series.

A FE model of the foot rest was available from the SENIORS project [18]. The additional belt on the legs was not modelled for LS-Dyna model.

The completed LS-Dyna FE model was the basis for translation into the other codes.

VPS Model

The LAB seat setup for VPS includes the sled platform, seat, footrest and belt system. Most components were provided by BAST in LS Dyna format, whereas the belt system with pyrotechnical pretensioner was provided by Autoliv in both LS-Dyna and VPS format in the form of mostly encrypted input files. The belt systems for LS-Dyna and VPS differed noticeably in global position, relative location of anchor points as well as belt routing (Figure 143). In addition the pyrotechnical pretensioner for VPS has been delivered in two versions (original and updated) due to correlation issues to LS Dyna in conversion tests.

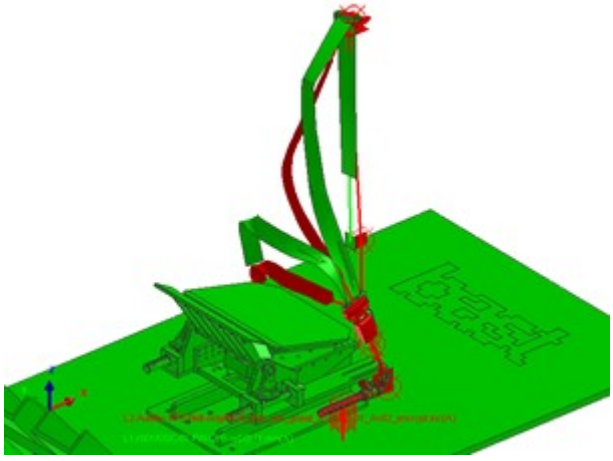

Figure 143 Encrypted Autoliv belt systems (LS-Dyna green / VPS red) with different geometry

The differences in geometry have been eliminated for the VPS belt system by adopting newly converted 2D elements from the Dyna input, local remeshing and local transformations.

The 2D belt material for VPS was revalidated and updated based on tension tests with VPS/LS-Dyna as shown in Figure 144. Due to encryption of the inputs patch tests have been performed instead of single element tests. The resulting belt forces correlate well between VPS and LS-Dyna (Figure 145).

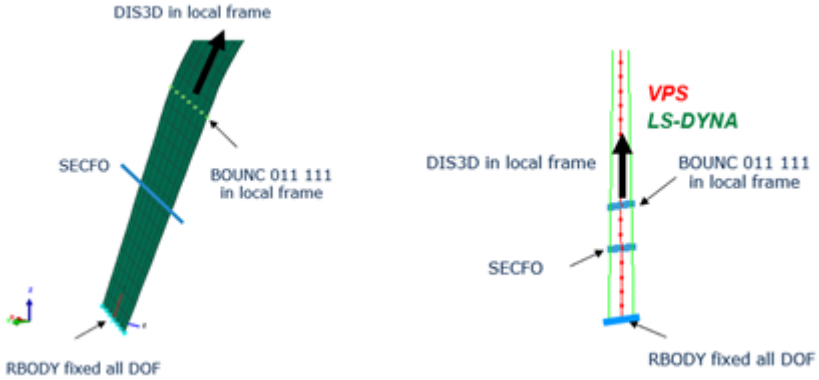

Figure 144 Belt patch test setup 2D VPS vs. 2D LS-Dyna (left) & 1D VPS vs. 2D LS-Dyna

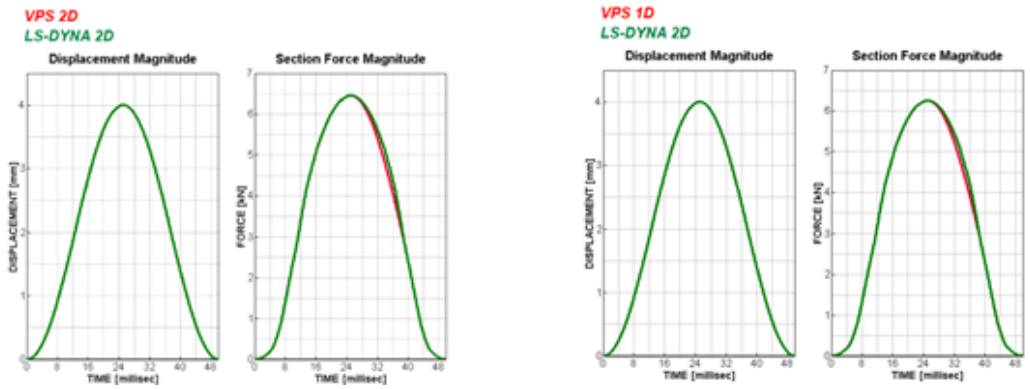

Figure 145 Results belt patch elongation and force 2D/1D VPS versus 2D LS-Dyna (left/right)

The remaining setup was converted from scratch from LS-Dyna to VPS. Mass and inertia for rigid bodies have been defined respective LS-Dyna model, the same applies for time history output entities. From the 1D elements the rack and pinion joint in LS-Dyna has been replaced with a combination of a revolute joint and an additional contact between the rack and the pinion part. A slight repositioning of the rack and adaption of contact surfaces was required to have correct contact behaviour between both parts (Figure 146).

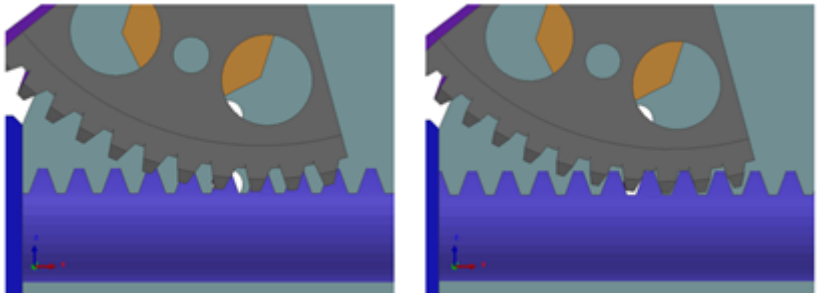

Figure 146 Rack & pinion parts from VPS model before (left) & after (right) geometric update

The dynamic response of the seat has been validated by applying substitute forces (smoothly ramped up to 5 kN) on both sub-pan and seat-pan (Figure 147 and Figure 148).

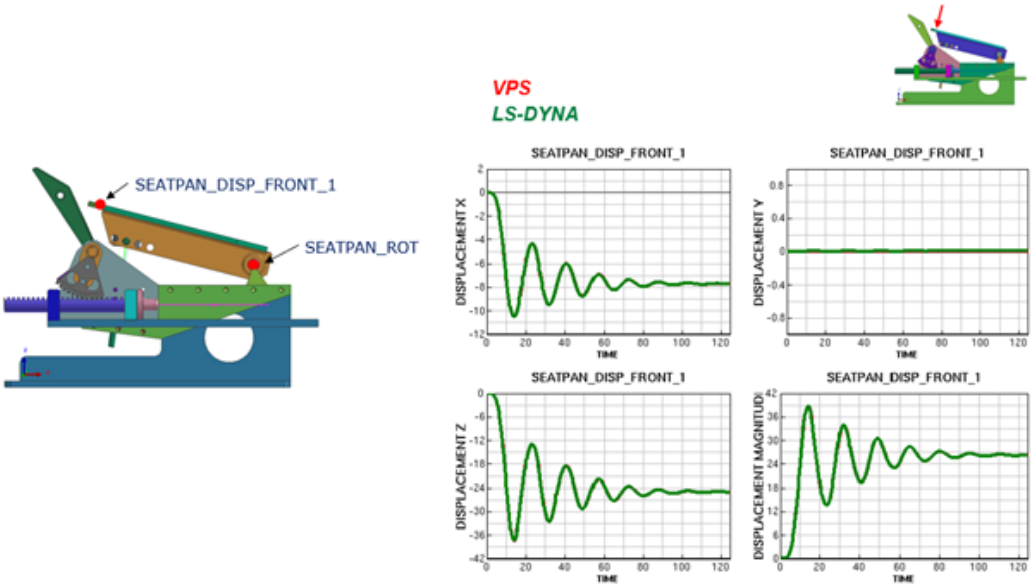

Figure 147 Evaluation scheme & results for seat pan with substitute loading (LS-Dyna & VPS)

Figure 147 is illustrating the seat-pan substitute load case and the good correlation achieved between LS-Dyna and VPS. The correlation for the sub-pan load case is comparably good and is shown in Figure 148.

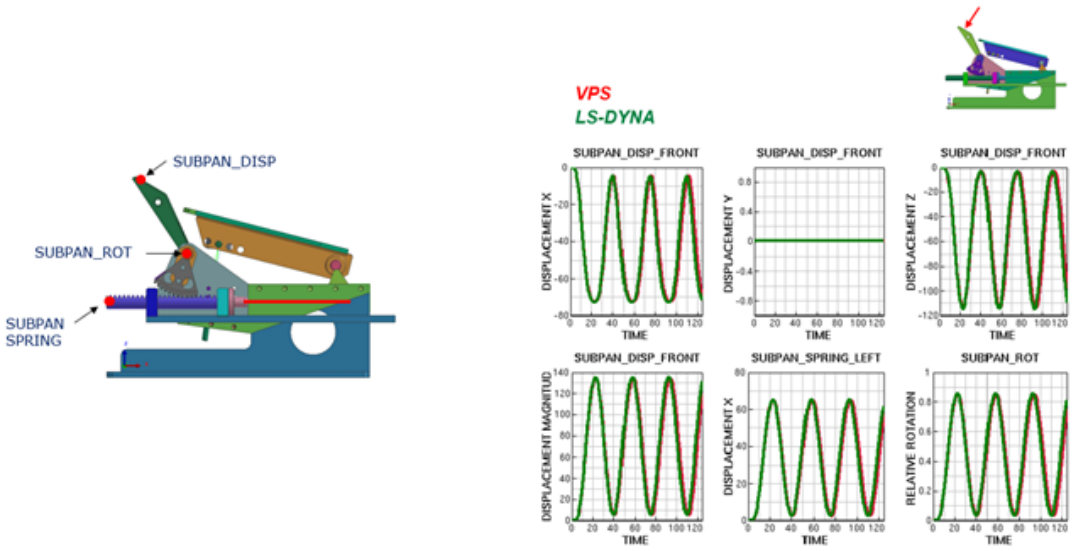

Figure 148 Evaluation scheme & results for sub pan with substitute loading (LS-Dyna & VPS)

Madymo Model

In this section, the Madymo Virtual Demonstrator model is described. The LAB seat model was translated from a FE-model provided by Autoliv, to Madymo Version 7.8 as shown in Figure 149 and its characteristics were tuned to match the design parameters.

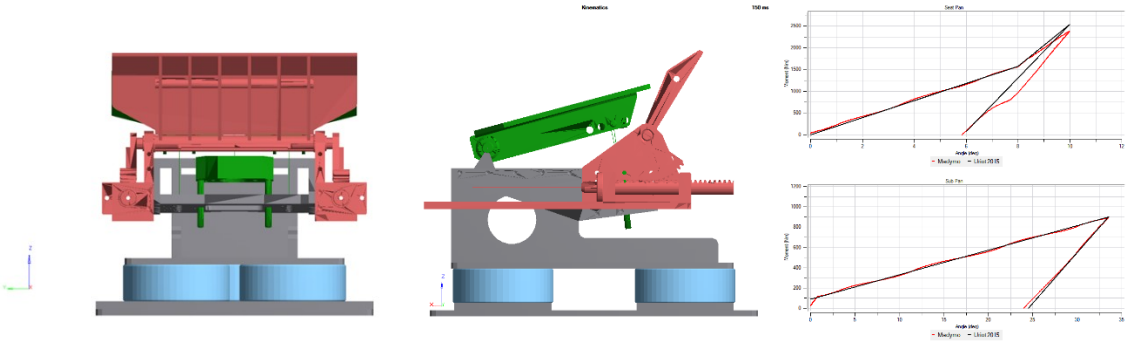

Figure 149 Madymo LAB seat model

A representation of an adjustable back support and a feet rest were added to the LAB seat sled model.

The Demonstrator model was equipped with an experimental 3-point belt system, provided by Autoliv as an encrypted model. This belt system contained 3 belt pretensioners at the buckle, the retractor and the anchor location. The system was set-up and could be triggered by means of Defines. The sled model including the LAB seat model was positioned for each individual test set-up using the data from the recorded seat settings and FARO 3D-measurements provided by BASt, as shown in Figure 150.

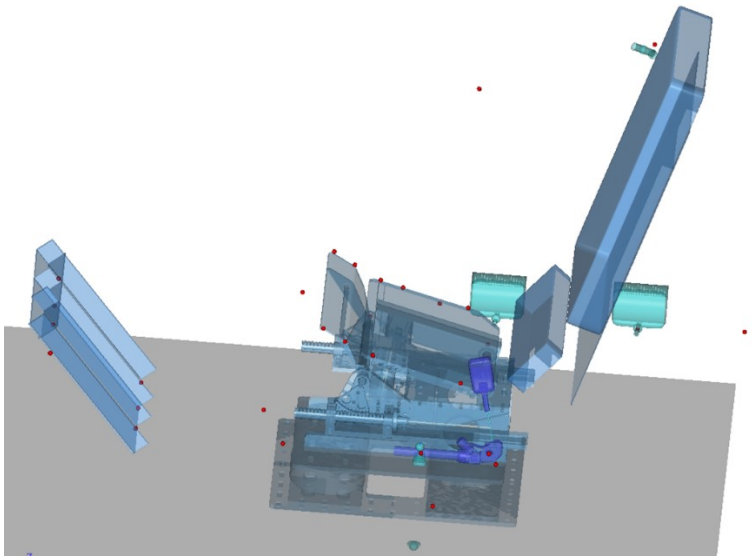

• : FARO data points

Figure 150 Madymo sled model with FARO reference points

1.2.2 THOR Dummy Models

All simulations to calibrate the virtual demonstrator were performed in the second half of 2019. Thereby, at the time available FE-models from Humanetics (version 1.6.1.) were used for LS-Dyna and VPS. As shown by [12], these FE-models (and earlier versions) cannot replicate the submarining behaviour sufficiently.

Note: In the meantime, Humanetics has released improved FE-models representing the THOR-50M dummy (version 1.8.1) with various improvements to the pelvis and abdominal region, which should have a positive influence on submarining behaviour.

LS-Dyna THOR Model

For this study the latest available FE-model of the THOR-50M from Humanetics (version 1.6.1; SBL-B equipped with Hybrid III legs) was used. For the dummy a detailed validation report with tests on component and whole dummy level is available.

VPS THOR Model

Humanetics THOR EuroNCAP dummy model version 1.6.1 has been used. This was the latest available version at the time when the study began.

Madymo THOR Model

For the Madymo demonstrator models, the Madymo 50th percentile THOR-M ellipsoid EuroNCAP model with Hybrid III 50th lower legs, version 3.1 was used in Simcenter Madymo Release Version 7.8. This model was created conform the NHTSA drawing package from August 2016, updated to build level B. More detailed information regarding this ATD can be found in the Simcenter Madymo Model Manual [6].

1.2.3 THOR Model Initial Positioning and Belt Routing

Dummy positioning and belt routing used an averaged position for LS-Dyna and VPS virtual demonstrators whereas dummy positioning and belt routing used the position of each test for Madymo demonstrator.

LS-Dyna

The averaged seating position for the virtual demonstrator was calculated from the following tests:

- OSC-05-OB-UPR (2 tests) and OSC-08-OB-UPR (2 tests) for the upright seating position
- OSC-03-FW-REC (2 tests), OSC-06-OB-REC (2 tests) and OSC-09-OB-REC (1 test) for the reclined seating position

Due to some irregularities with the position of the legs (not centred), the tests OSC-01-FW-UPR (2 tests) and OSC-02-FW-REC (2 tests) were excluded from the calculation of the averaged seating position.

The dummy position was adjusted in accordance to the pre-simulation manual for LS-Dyna [17]. For positioning the dummy, the following measurements were specially considered:

- Head (XYZ-coordinates and Y-angle)
- Shoulder (XZ-coordinates)
- Thorax / Spine Box (XZ-coordinates and Y-angle)
- Pelvis / H-Point (XYZ-coordinates and Y-angle)
- Knee (XZ-coordinates and Y-distance)
- IR-TRACCs (XYZ-coordinates)

For both seating positions no major differences between the averaged position and the simulation model were observed. Figure 151 and Figure 152 are showing the positioned dummy in LS-Dyna and VPS.

The belt was fitted to the dummy using the pre-processor PRIMER, thereby an averaged belt path was used. No major differences between the averaged belt path and the simulation model were observed.

VPS

The VPS dummy model has been positioned utilizing the dedicated pre-simulation input as part of the delivery package from Humanetics.

In the first step the overall position and orientation of the dummy together with the articulation of the limbs have been achieved with respect to the average target position from experiments.

For comparability between codes the outer ends of the IRTRACC fixations have been simulated in a second step to match the position of the LS-Dyna model.

Due to differences in the outer shape of the dummy jacket between LS-Dyna and VPS the belt routing has been adapted in an additional simulation step to achieve a close fit to the VPS dummy model.

All previous steps have been performed independently for both the upright and the reclined seating positions. Figure 151 and Figure 152 are illustrating the comparison of the seated dummies for LS-Dyna and VPS.

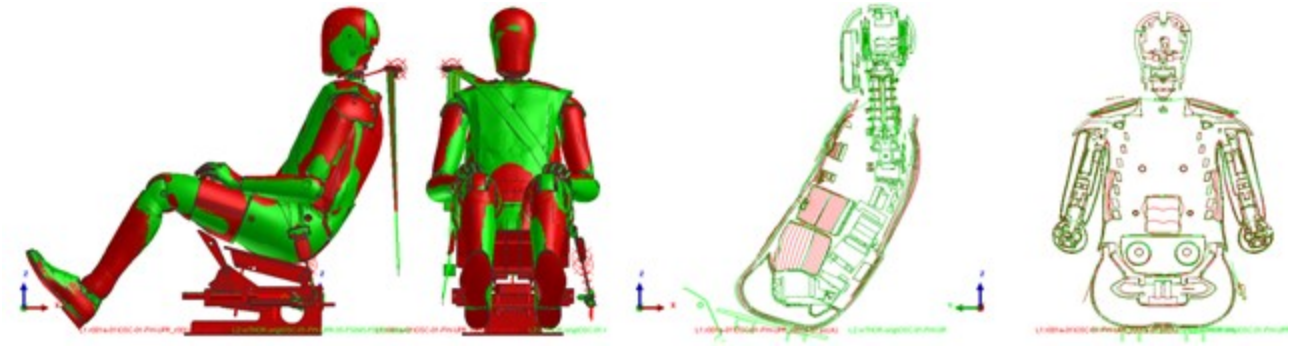

Figure 151 Comparison seated dummy models - upright position - LS-Dyna green & VPS red

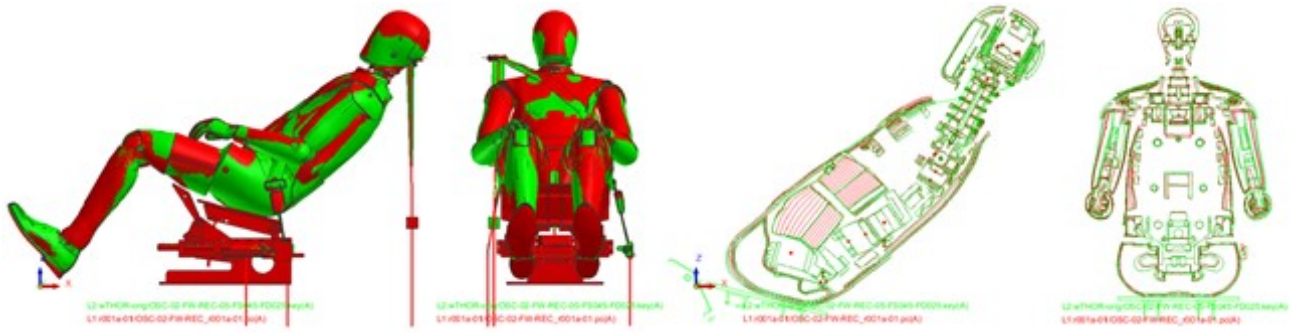

Figure 152 Comparison seated dummy models - reclined position - LS-Dyna green & VPS red

Madymo

The THOR model in these test set-ups was positioned on the LAB semi-rigid seat model using the measured internal sensor readings from the THOR dummy and the pre-test FARO measurements of the actual tests (Figure 153). With the use of a series of formulas and 'Defines' in the Madymo input deck, the recorded dummy position sensor data was calculated automatically to the respective joint degree of freedom settings of the Madymo model. The remaining joint settings were then defined using the reference of the FARO 3D-meausurements taken before each test by BASt.

- : FARO data points

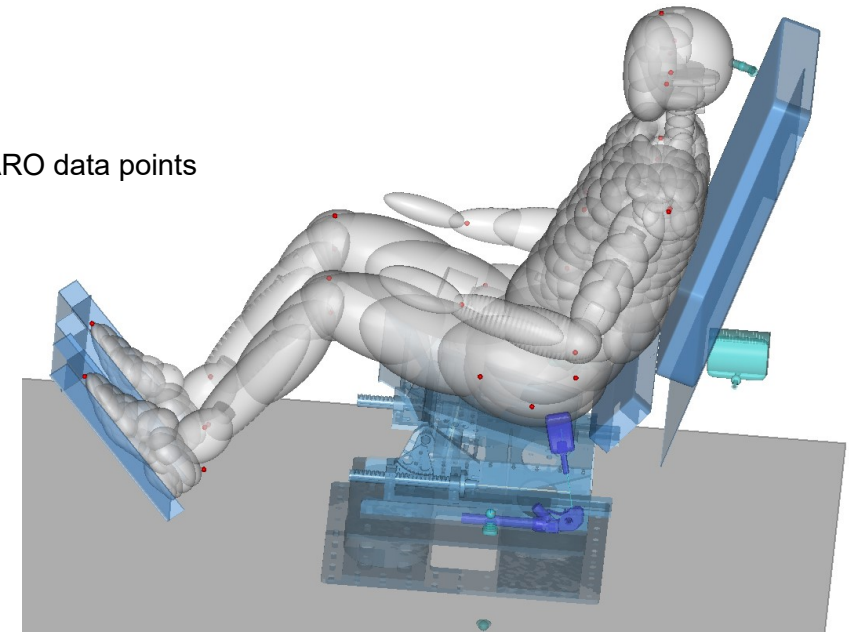

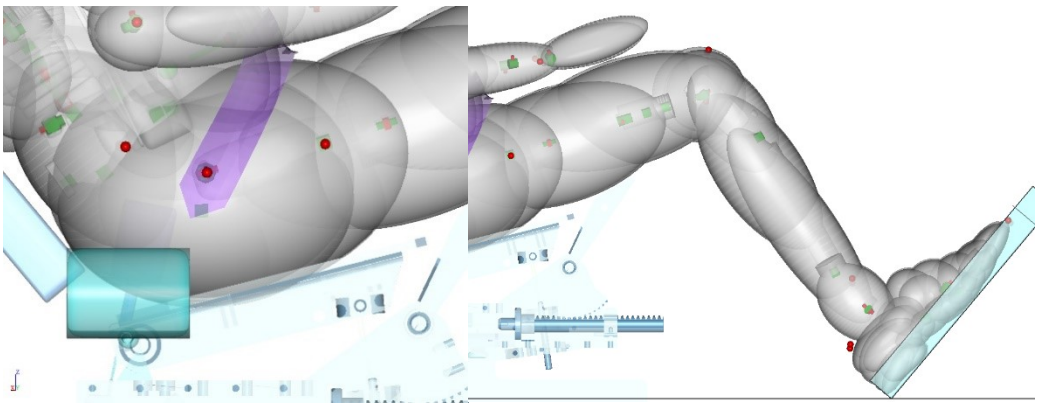

Figure 153 THOR positioning, using FARO reference points

The THOR model was positioned so that the corresponding points on the hip, shoulders, head, elbow, wrist, knees and ankles matched as close as possible the FARO data points. This positioning procedure was performed for each individual test of the test matrix.

Subsequently, the seat belt was fitted on the THOR dummy model, using the Madymo belt fitting utility. With the help of up to three adjustment points the belt was routed as close as possible to the measured FARO reference points, as shown in Figure 154 here below.

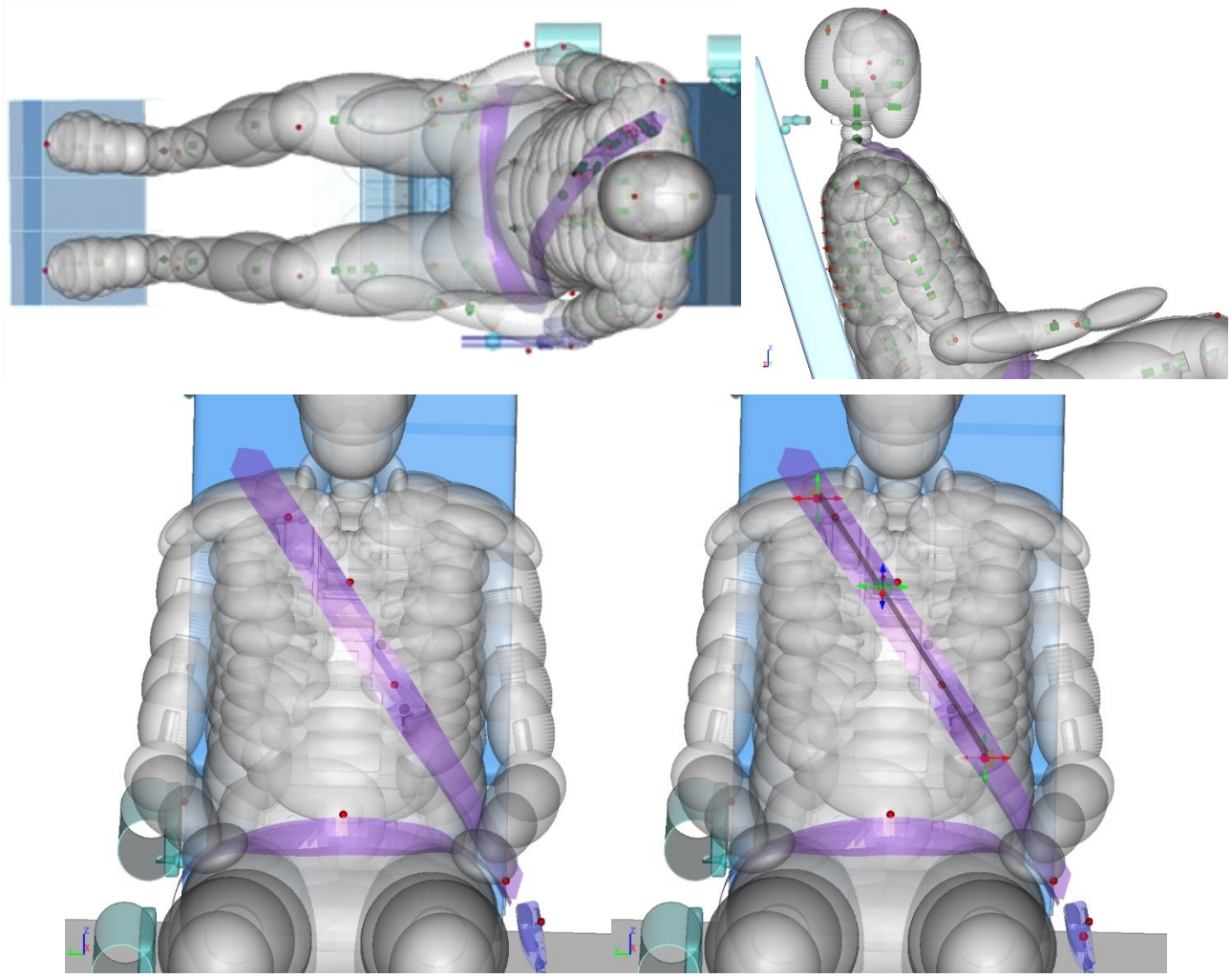

Figure 154 Belt routing with FARO reference points

1.2.4 Model Outputs

The modelling techniques used for replicating the sensors of the experiments are gathered in the Table 20.

Measurement	Test sensor	LS-Dyna	VPS	Madymo
Seat pan disp. Z	String Potentiometer	Discrete spring element (DEFORC) between seat pan and sled base	Time history element THELE between seat pan and sled base, rel. displ. magnitude	Z-Displacement of SeatPan_bod body, relative to Seat Base
Anti-submarining disp. X	String Potentiometer	Discrete spring element (DEFORC) between anti-submarining ramp and sled base	Time history element THELE between sub pan rack and sled base, rel. displ. magnitude	X-Position (joint DOF-1) of SubPanRack_jnt translational joint
Seat belt force B3	Belt sensor	Cross section force (SECFORC) at test sensor location	Cross section force magnitude at test sensor location	MB belt segment resultant force at D-ring to clavicle
Seat belt force B4	Belt sensor	Cross section force (SECFORC) at test sensor location	Cross section force SECFO magnitude at test sensor location	MB belt segment resultant force at lower rib to buckle
Seat belt force B6	Belt sensor	Cross section force (SECFORC) at test sensor location	Cross section force SECFO magnitude at test sensor location	MB belt segment resultant force at abdomen to lap pretractor
Seat belt pay-in/out	Video analysis	Length of slipped belt element from seat belt output (SBTOUT)	Retractor slipring SLIPR length of slipped belt	Displacement of retractor body (Encrypted Autoliv model)
THOR pelvis disp.	Potentiometer betw. pelvis back and seat back	Discrete spring element (DEFORC) between pelvis and seat back	Time history element THELE betw. pelvis back and seat back, rel. displ. magnitude	X-Displacement of Pelvis_bod body, relative to sled
THOR pelvis angle	Dummy Measurements	Angular displacement from pelvis angular rate sensor (NODOUT)	Local coordinate system output THLOC pelvis, integrated angular velocity around local y	Angular (theta) displacement of Pelvis_bod body

Table 20 Test and simulation output methods

The unfiltered data was extracted using a template for Hyperview. The data was processed with the ISOVerter in accordance to ISO 13499.

1.2.5 Model Calibration

In the following, the efforts to calibrate the models with the first test series are described.

LS-Dyna Model

The LS-Dyna model was calibrated using the first three load cases (upright with SOTA belt, reclined with SOTA belt and reclined with SOTA DLPT belt). Thereby, all tuneable parameters were adjusted to the settings (e.g. retractor trigger time) or averaged measurements (e.g. webbing left on shoulder retractor) from the first test series. Friction remained as the last unknown parameter and was used for tuning the model:

- Torso to belt $\mu_S = \mu_D = 0.40$
- Pelvis to belt $\mu_S = \mu_D = 0.50$
- Pelvis to seat pan $\mu_S = 0.40$ and $\mu_D = 0.25$
- Pelvis to anti-submarining ramp $\mu_S = 0.45$ and $\mu_D = 0.30$

Most adequate friction parameters were identified in a simulation study. As noted in Chapter 3.1.4.3, dummy modelling and missing bending stiffness of the belt model result in an insufficient submarining behaviour for the used THOR FE-model. In consequence, replicating the submarining behaviour in the reclined seating position with SOTA belt (OSC-02-FW-REC) correctly was the most challenging aspect of the calibration process.

*Note: Due to the above discussed issues, the submarining behaviour could not be reproduced successfully in the reclined seating position with SOTA belt. Friction parameters were tuned to best match other measurements like accelerations. Ignoring the second load case (*OSC-02-FW-REC*) while calibrating the FE model would likely result in slightly reduced friction parameters.*

VPS Model

Due to different static and dynamic friction values in the LS-Dyna input for the contact interfaces pelvis to seat pan as well as pelvis to anti-submarining ramp a friction variation in VPS has been performed at an early stage over all load cases. The friction coefficients 0.25, 0.325, 0.40 have been tested for the contact to seat pan, for the contact to anti-submarining ramp the coefficients 0.30, 0.375, 0.45 have been tested. The best correlation to experiments was achieved when choosing coefficients 0.25 for the seat pan contact and 0.30 for the anti-submarining pan contact, which corresponds to the dynamic friction values from the LS-Dyna input.

Regarding validation of the belt system, the belt model was still missing a representative modelling of the CLT to mimic variable friction coefficients over time.

The slipring option in the latest VPS version does not support a variable friction over time. Therefore, a substitute modelling had to be defined and validated.

As reference for the validation of the substitute CLT model served simulation runs with a standard slipring and constant low or high friction coefficients over time (0.13 and 0.4). The CLT substitute model was correlated in the non-activated state against the constant low friction behaviour. For validation of the high friction the CLT substitute model was activated at the beginning of the simulation. An additional simulation was performed with the substitute model CLT being activated at 40 ms to confirm robustness, stability and plausibility. Figure 155 illustrates the component loading test for the CLT substitute model. For validation the belt slip length over time as well as the belt section forces on both sides of the slipring are evaluated. Figure 156 to Figure 158 present the results for the different cases. In all cases results are plausible. Furthermore a good correlation to the reference simulations has been achieved.

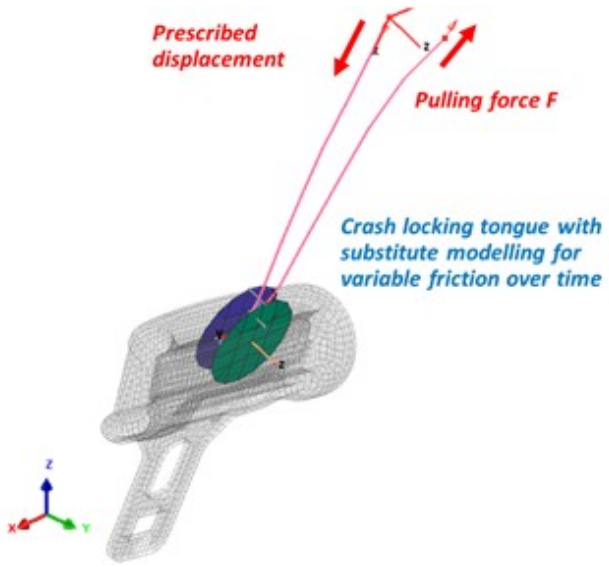

Figure 155 Component test crash locking tongue & substitute model for variable friction

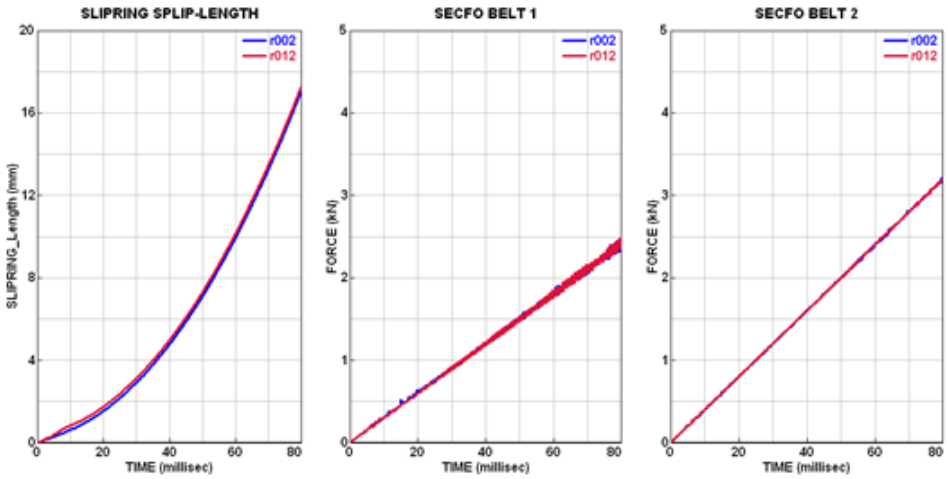

Figure 156 Resulting belt slip length & forces for constant low friction, reference simulation / substitute model (blue / red)

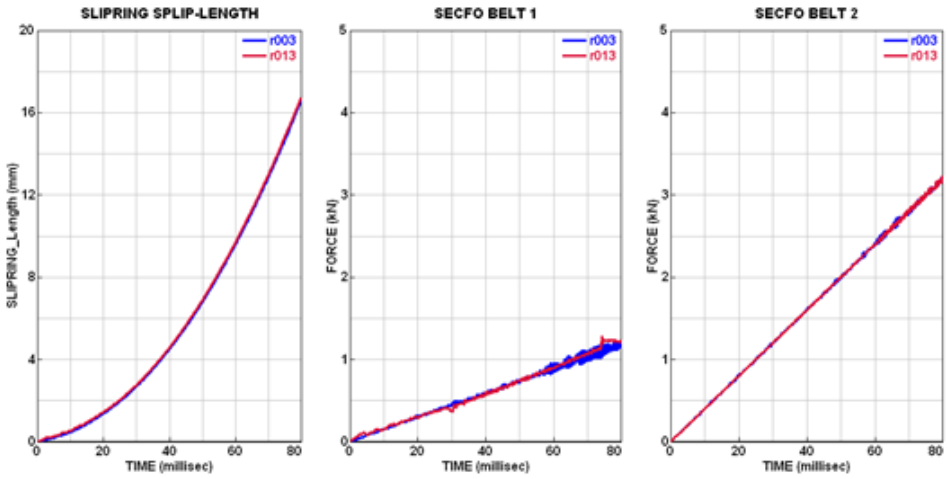

Figure 157 Resulting belt slip length & forces for constant high friction, reference simulation / substitute model (blue / red)

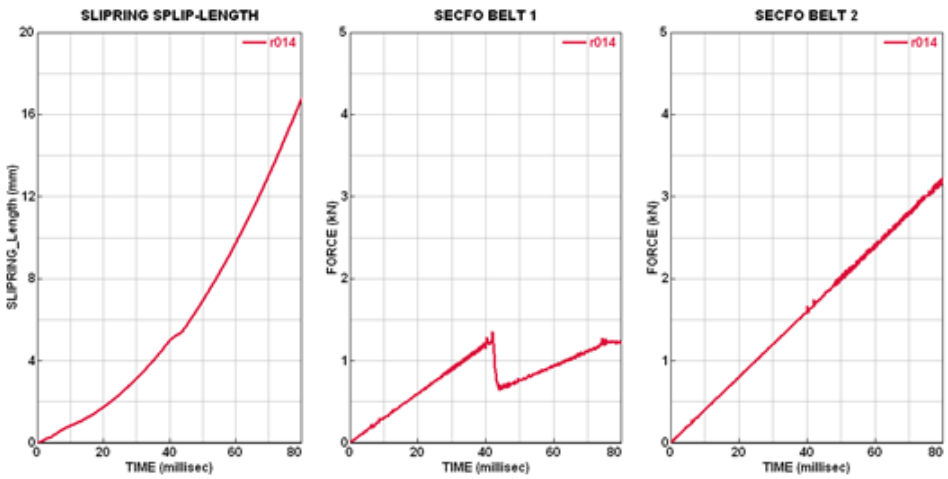

Figure 158 Results belt slip length & forces for switch from low to high friction at 40 ms, substitute model (red)

For further validation of the belt and seat model against results from LS-Dyna various tests have been performed with a rigidified outer surface of the dummy. Figure 159 is showing a setup and results for a test with rigid dummy surface and belt, the shoulder retractor is activated at 9 ms.

It can be observed that the belt displacements between LS-Dyna and VPS are comparable, the maximum deviation is around 5 mm. The belt forces are still showing noticeable differences, especially for section B5 (Figure 159 and Figure 160).

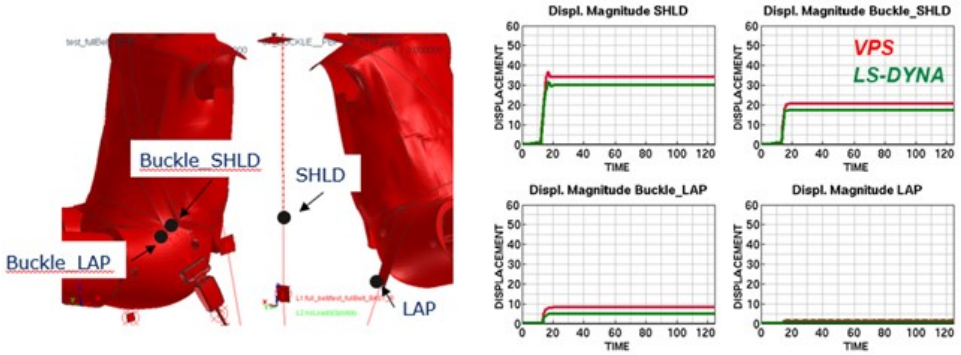

Figure 159 Belt against rigid dummy surface, shoulder retractor activated at 9 ms, displ. results

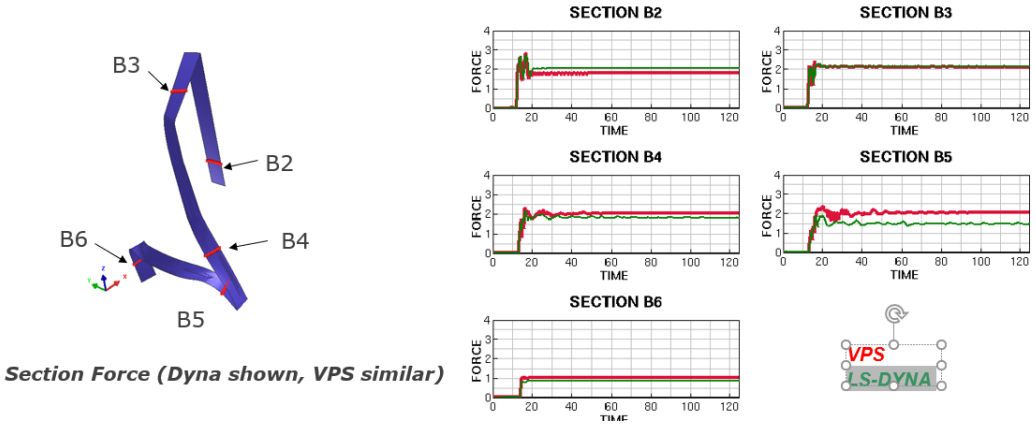

Figure 160 Belt against rigid dummy surface, shoulder retractor activated at 9 ms, force results

Madymo Model

The simulation model was set-up following the recommended modelling guidelines as outlined in the Simcenter Madymo Model Manual [1]. The LAB seat model was validated as outlined in section 3.1.4.1. The already validated restraint system model was used as supplied by Autoliv.

Almost all parameters eligible for tuning the test set-ups were pre-defined by measurements. Only a few unknown parameters remained, that were used for fine tuning the model:

- Belt slack in the various belt segments: Added 20 mm extra length to the D-ring-to-shoulder segment and 20 mm to the Lap_pretractor-to-lap segment.
- Friction in the D-ring and the buckle: Both initially set to 0.2, the buckle friction increased to 0.4 after the CLT lock timer was activated.
- Orthogonal friction coefficients between the seat belts and the dummy:

  Set to 0.2 in length direction of the belt and to 0.6 in cross direction, for all belt contacts.
- Friction coefficient between the dummy and the LAB seat: Set to 0.3.

The model was tuned to correlate the first test set-up (OSCCAR-01-FW-UPR-01) and it's repeat test, the same settings were then used in all other test set-ups, without test-specific tuning.

While tuning the model, it was observed that the THOR dummy model showed somewhat excessive motion of the upper legs, resulting in a too high pelvis rotation. An additional rotational restraint was added to the hip joints. An update to the changed restraint is expected to be incorporated in an upcoming THOR model release.

1.2.6 Model Validation Comparison (Oblique Pulses)

1.2.6.1 SCP1 – Upright Seating Position with SOTA Belt

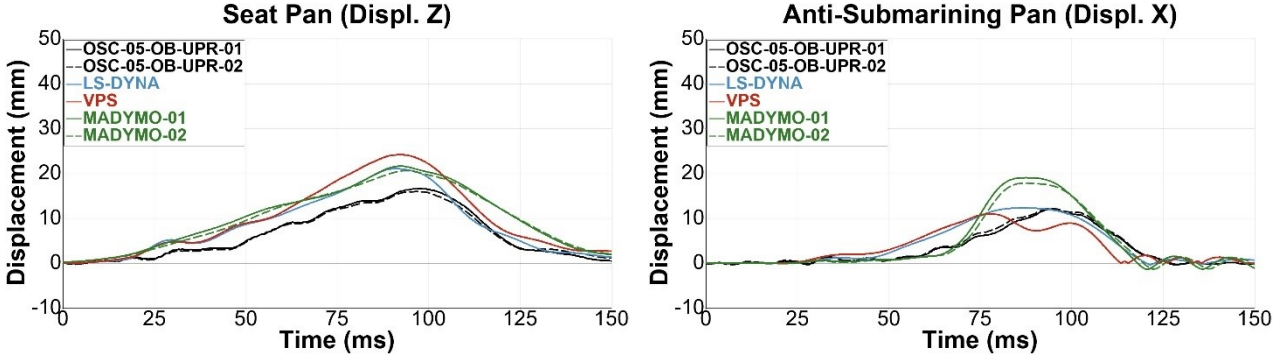

Figure 161 Seat pan & anti-submarining ramp displacements

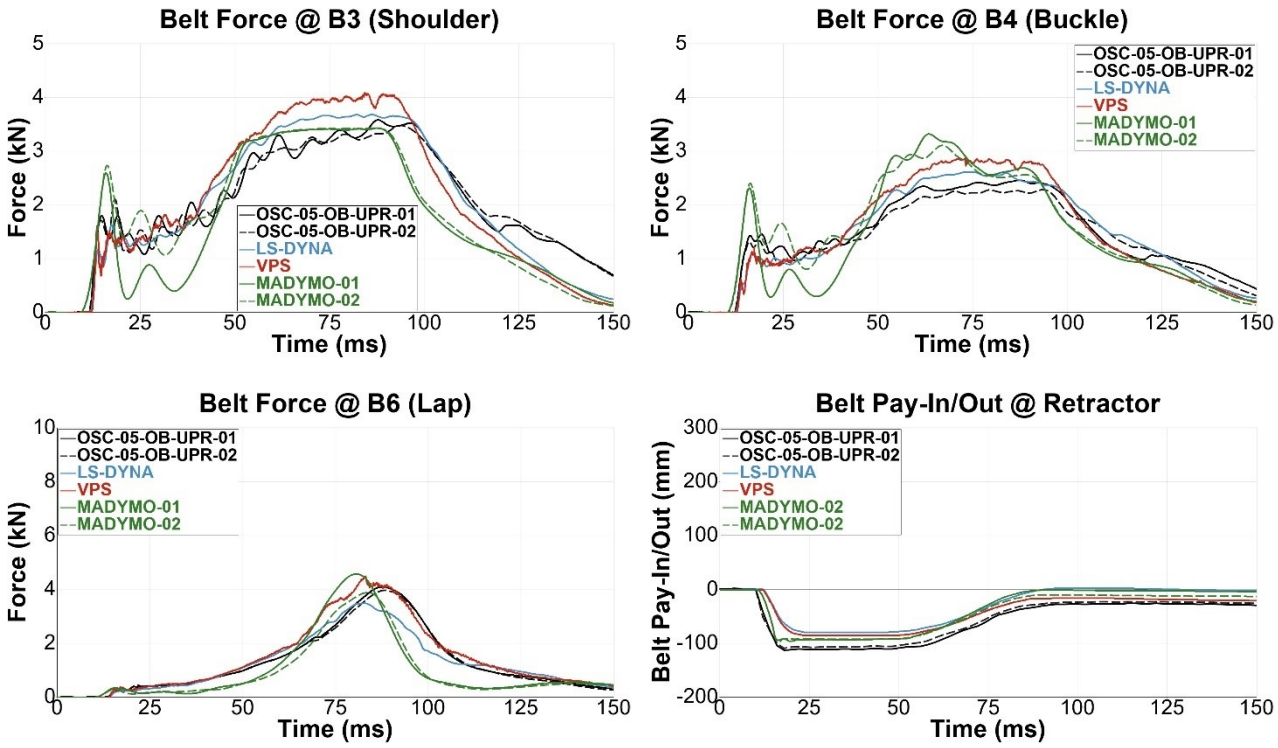

Figure 162 Seat belt forces & shoulder retractor belt pay-in/-out

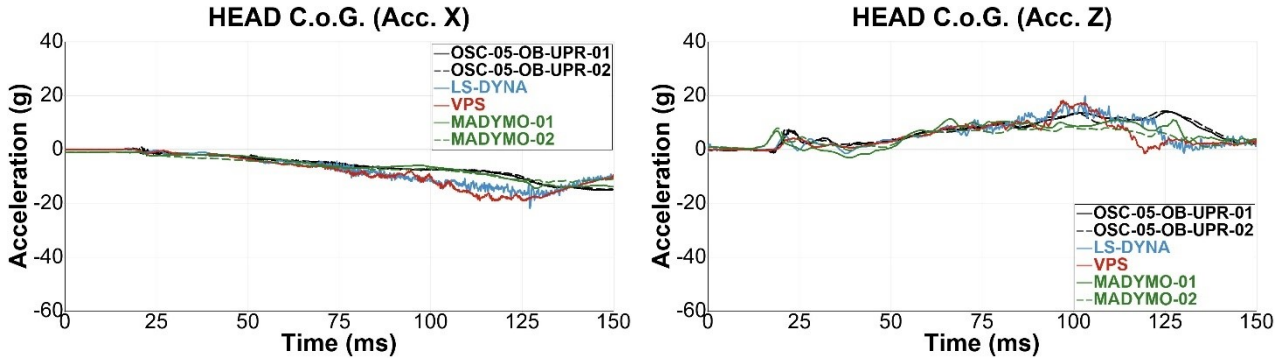

Figure 163 Head COG accelerations

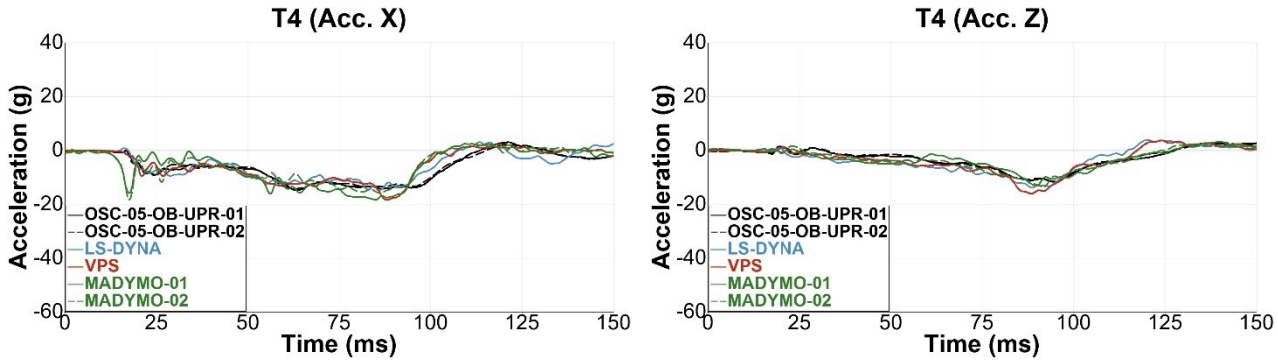

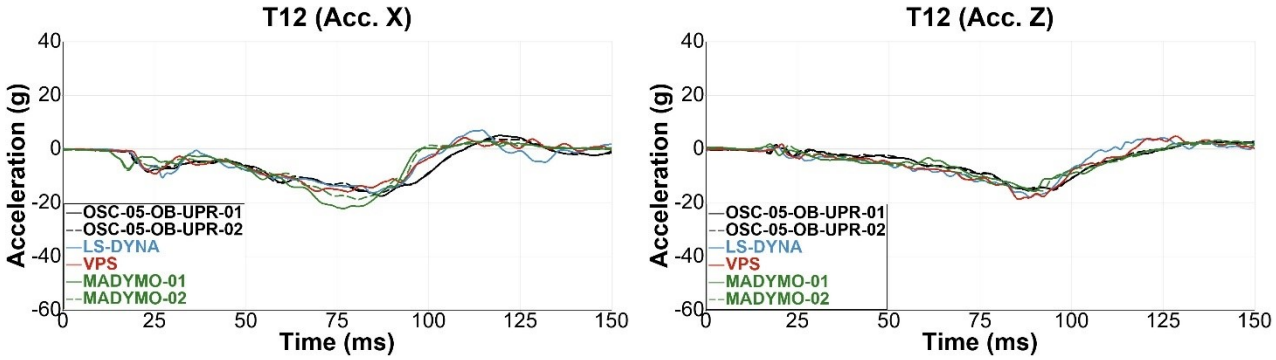

Figure 164 T4 and T12 accelerations

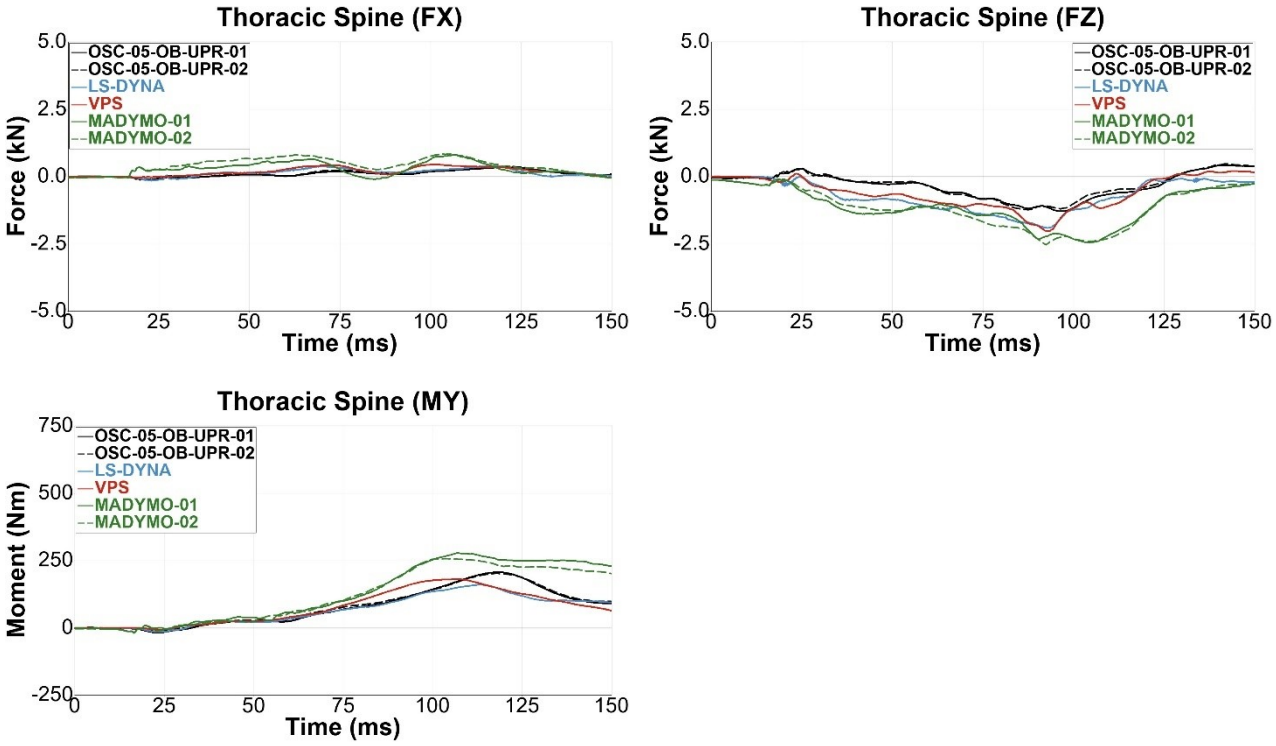

Figure 165 Lower thoracic spine forces and moments

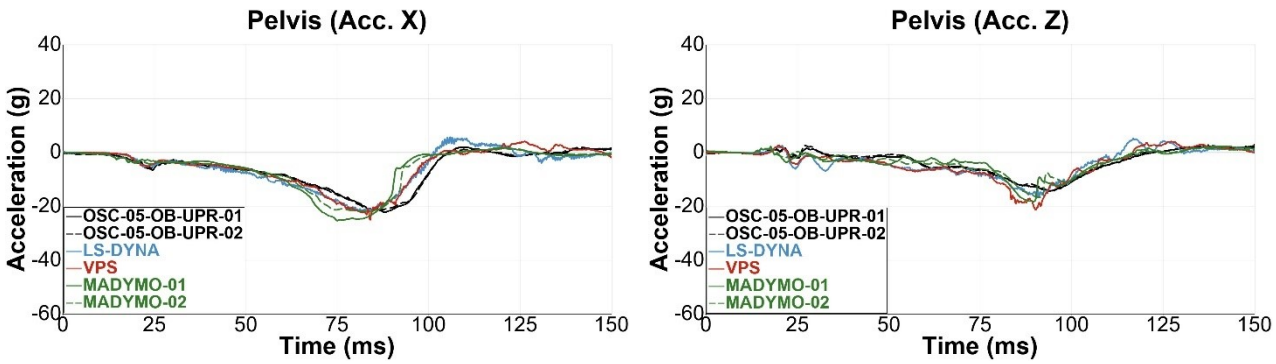

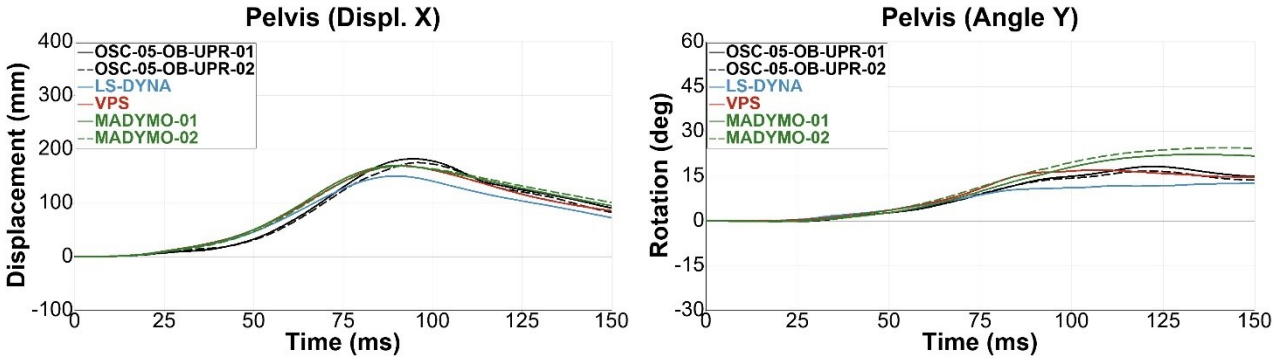

Figure 166 Pelvis accelerations, X-displacement and Y-angle

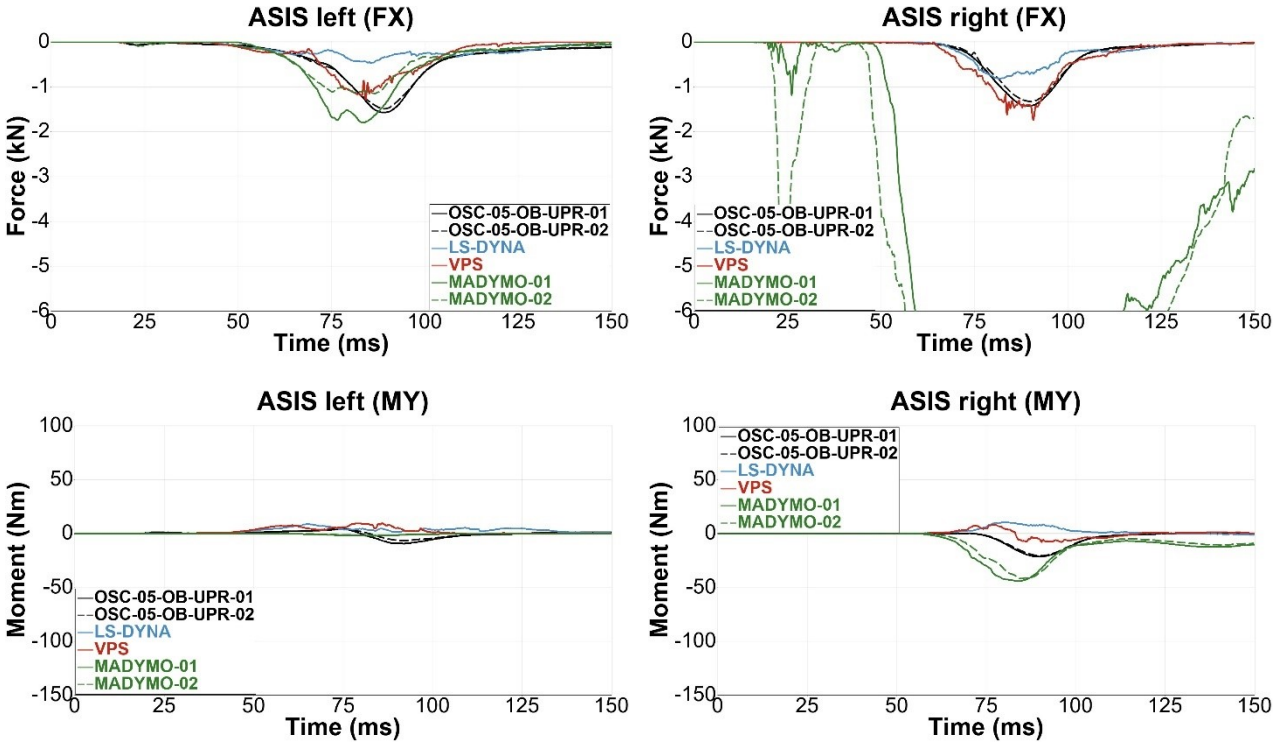

Figure 167 ASIS X-forces and Y-moments

Table 21 summarises the CORA ratings with the averaged (LS-Dyna and VPS) or individual (Madymo) test data as reference. Ratings are coloured in accordance to the sliding scale from ISO 18571 (excellent = green; good = white; fair = yellow; poor = red).

Channel	Virtual Demonstrator			
	LS-DYNA	VPS	MADYMO-01	MADYMO-02
Seat Pan (Displ. Z)	0.776	0.679	0.629	0.631
Anti-Submarining Ramp (Displ. X)	0.808	0.708	0.750	0.783
Upper Diag. Belt Force (B3)	0.892	0.792	0.754	0.793
Lower Diag. Belt Force (B4)	0.916	0.832	0.744	0.752
Lap-Belt outside Force (B6)	0.925	0.935	0.756	0.769

Belt Pay-In/-Out	0.565	0.776	0.647	0.798
Head COG (Acc. X)	0.754	0.713	0.956	0.894
Head COG (Acc. Z)	0.754	0.685	0.701	0.656
T4 (Acc. X)	0.772	0.804	0.677	0.751
T4 (Acc. Z)	0.676	0.764	0.833	0.837
T12 (Acc. X)	0.793	0.811	0.709	0.789
T12 (Acc. Z)	0.743	0.826	0.883	0.879
T12 (Fo. X)	0.656	0.601	0.309	0.339
T12 (Fo. Z)	0.474	0.581	0.320	0.316
T12 (Mo. Y)	0.882	0.857	0.653	0.693
Pelvis (Acc. X)	0.870	0.902	0.780	0.875
Pelvis (Acc. Z)	0.753	0.768	0.830	0.865
Pelvis (Displ. X)	0.889	0.961	0.958	0.946
Pelvis (Ang. Y)	0.809	0.930	0.830	0.710
ASIS left (Fo. X)	0.684	0.827	0.807	0.829
ASIS right (Fo. X)	0.822	0.910	0.393	0.342
ASIS left (Mo. Y)	0.416	0.477	0.428	0.378
ASIS right (Mo. Y)	0.534	0.571	0.511	0.574
Environment	**0.814**	**0.787**	**0.713**	**0.754**
Dummy	**0.722**	**0.764**	**0.681**	**0.687**
Total	**0.746**	**0.770**	**0.689**	**0.704**

Table 21 CORA ratings for upright seating position with SCP1 pulse and SOTA belt

1.2.6.2 SCP1 – Reclined Seating Position with SOTA DLPT Belt

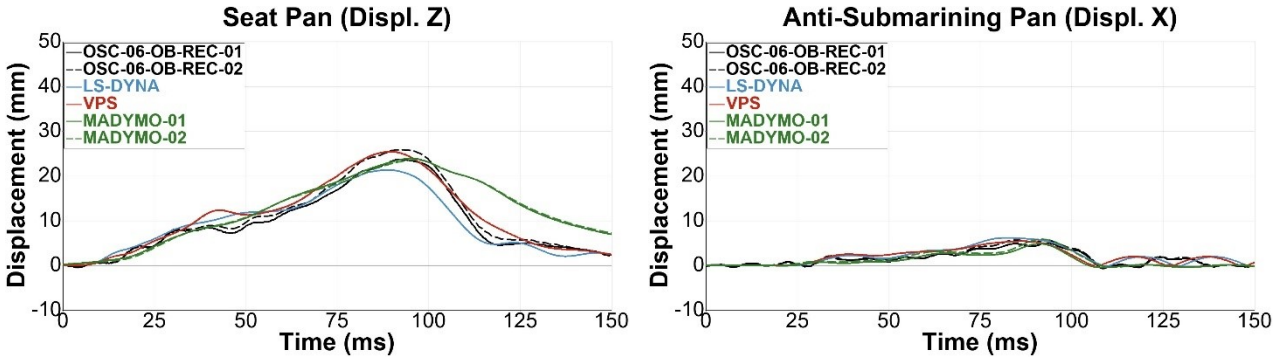

Figure 168 Seat pan & anti-submarining ramp displacements

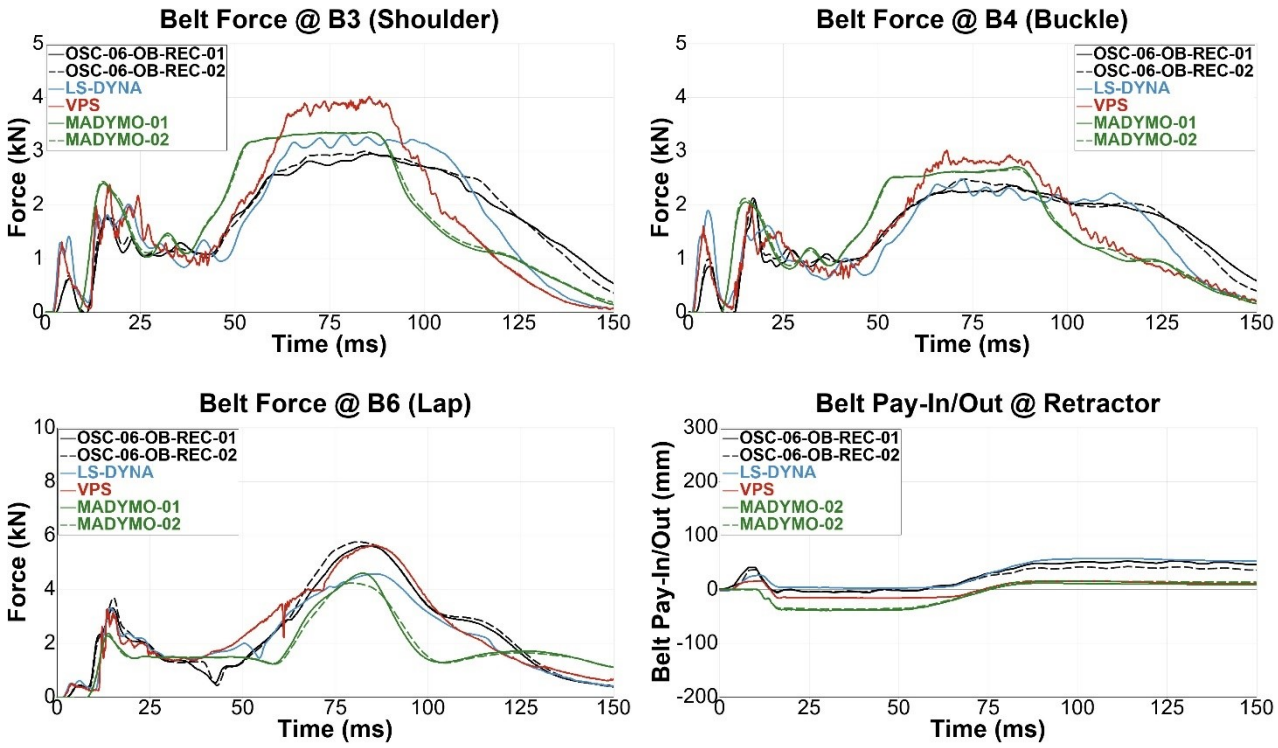

Figure 169 Seat belt forces & shoulder retractor belt pay-in/-out

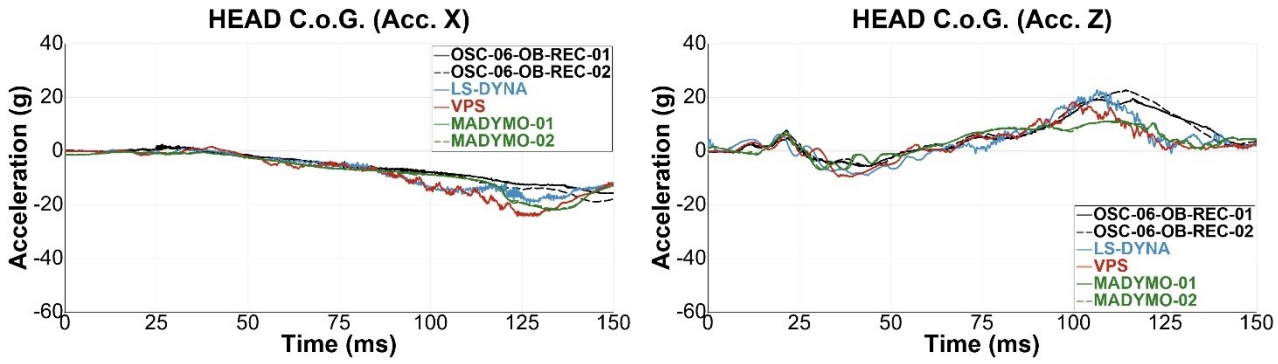

Figure 170 Head COG accelerations

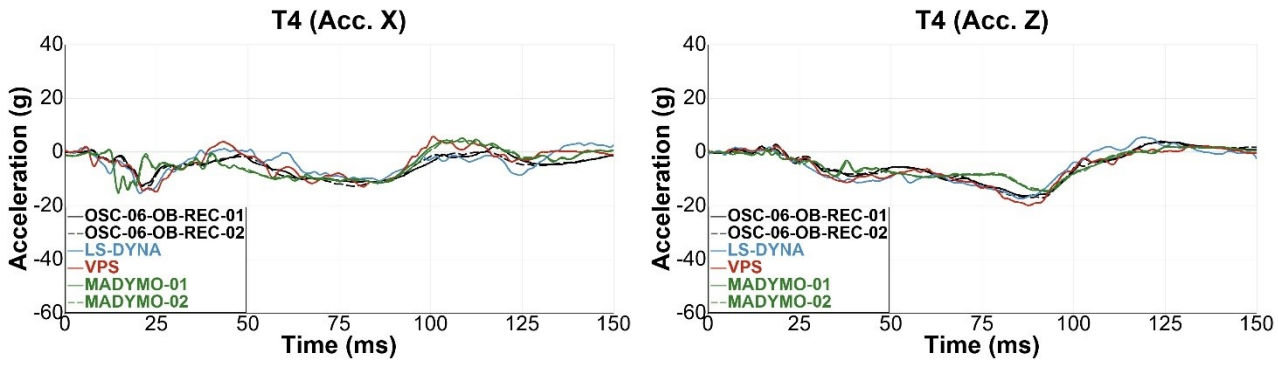

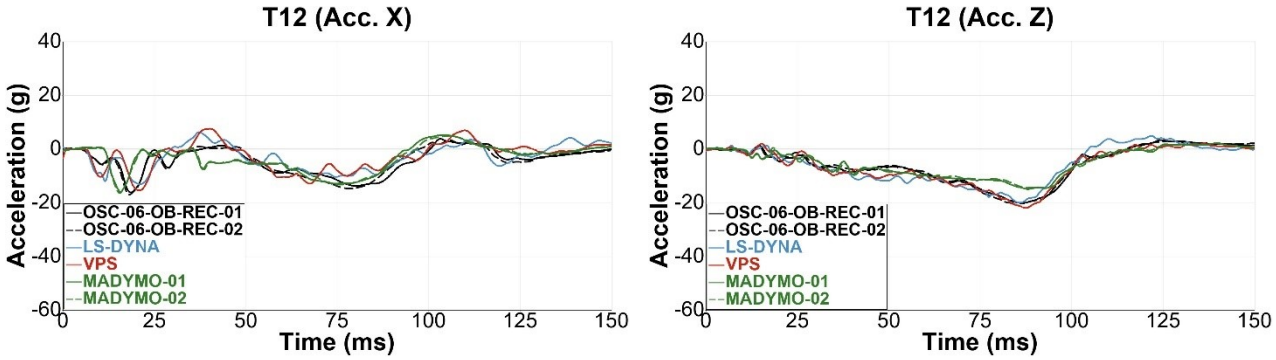

Figure 171 T4 and T12 accelerations

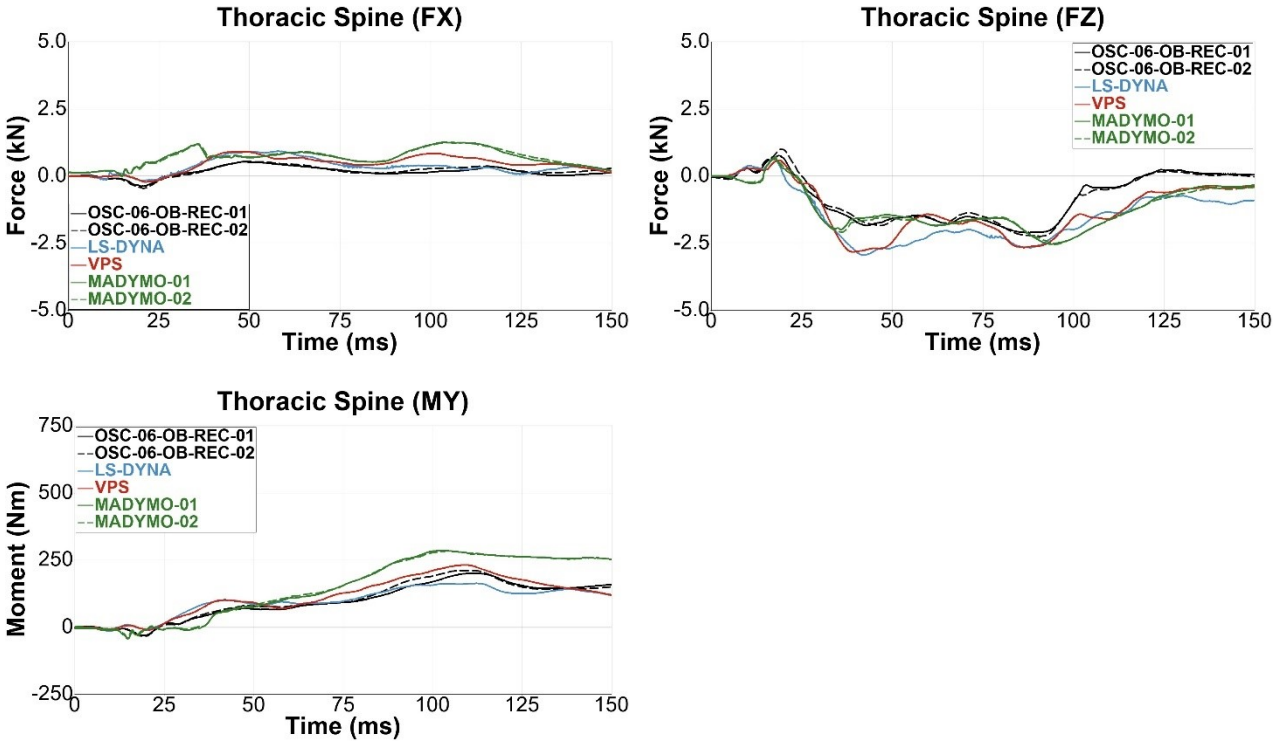

Figure 172 Lower thoracic spine forces and moments

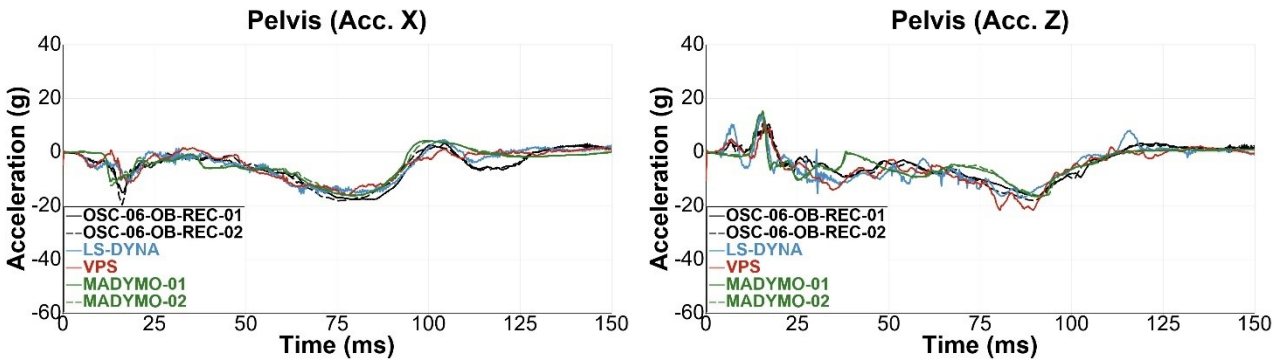

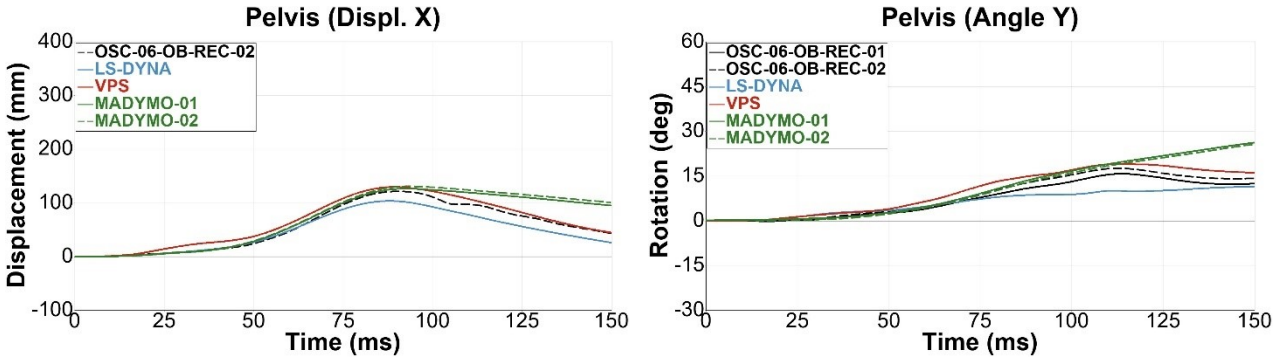

Figure 173 Pelvis accelerations, X-displacement and Y-angle

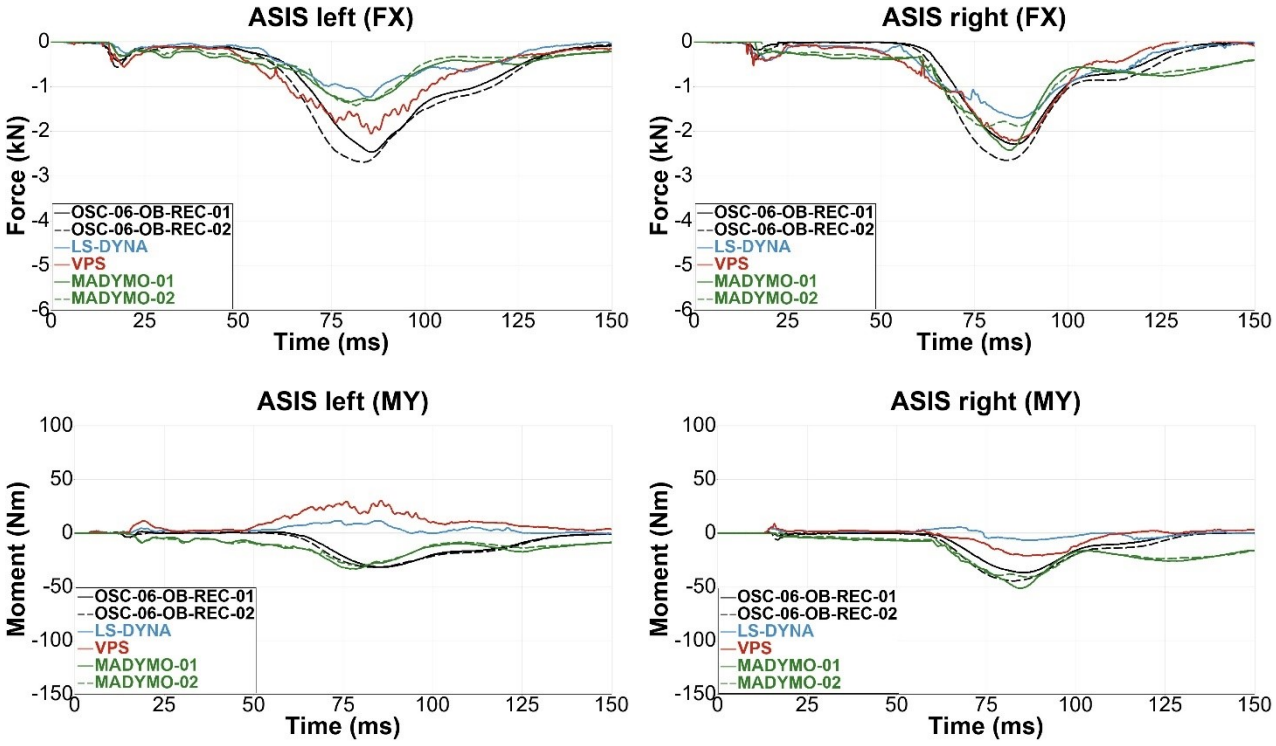

Figure 174 ASIS X-forces and Y-moments

Table 22 summarises the CORA ratings with the averaged (LS-Dyna and VPS) or individual (Madymo) test data as reference. Ratings are coloured in accordance to the sliding scale from ISO 18571 (excellent = green; good = white; fair = yellow; poor = red).

Channel	Virtual Demonstrator			
	LS-DYNA	VPS	MADYMO-01	MADYMO-02
Seat Pan (Displ. Z)	0.907	0.941	0.768	0.805
Anti-Submarining Ramp (Displ. X)	0.738	0.719	0.726	0.796
Upper Diag. Belt Force (B3)	0.817	0.672	0.663	0.694
Lower Diag. Belt Force (B4)	0.849	0.740	0.651	0.707

Lap-Belt outside Force (B6)	0.886	0.924	0.712	0.692
Belt Pay-In/-Out	0.741	0.281	0.198	0.231
Head COG (Acc. X)	0.805	0.724	0.796	0.850
Head COG (Acc. Z)	0.712	0.673	0.639	0.652
T4 (Acc. X)	0.602	0.674	0.661	0.666
T4 (Acc. Z)	0.813	0.882	0.819	0.805
T12 (Acc. X)	0.643	0.642	0.696	0.715
T12 (Acc. Z)	0.850	0.933	0.844	0.830
T12 (Fo. X)	0.490	0.404	0.222	0.249
T12 (Fo. Z)	0.497	0.621	0.623	0.614
T12 (Mo. Y)	0.866	0.859	0.611	0.625
Pelvis (Acc. X)	0.800	0.746	0.748	0.760
Pelvis (Acc. Z)	0.742	0.777	0.731	0.719
Pelvis (Displ. X)	*x*	*x*	*x*	0.793
Pelvis (Ang. Y)	0.756	0.799	0.731	0.832
ASIS left (Fo. X)	0.733	0.819	0.719	0.684
ASIS right (Fo. X)	0.838	0.859	0.775	0.785
ASIS left (Mo. Y)	0.381	0.403	0.572	0.617
ASIS right (Mo. Y)	0.462	0.644	0.547	0.726
Environment	**0.823**	**0.713**	**0.620**	**0.654**
Dummy	**0.687**	**0.716**	**0.671**	**0.701**
Total	**0.724**	**0.715**	**0.657**	**0.689**

Table 22 CORA ratings for reclined seating position with SCP1 pulse and SOTA DLPT belt

1.2.6.3 LTAP OD2 – Upright Seating Position with SOTA Belt

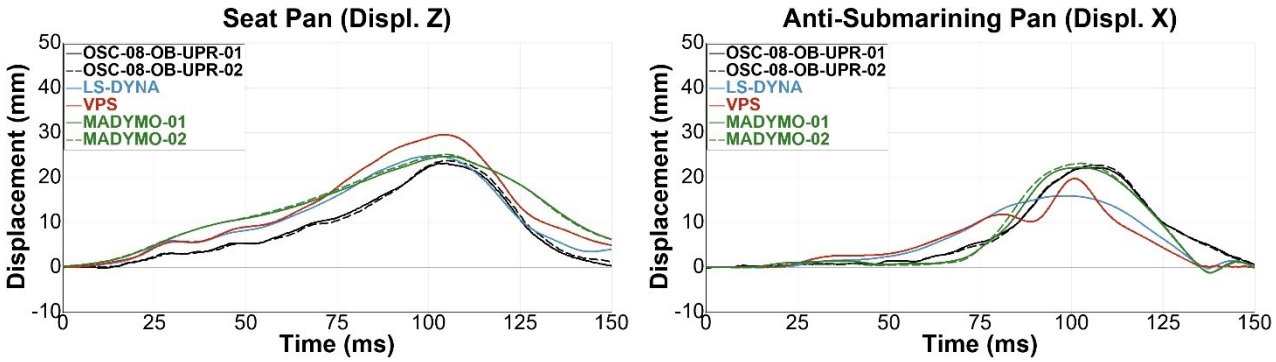

Figure 175 Seat pan & anti-submarining ramp displacements

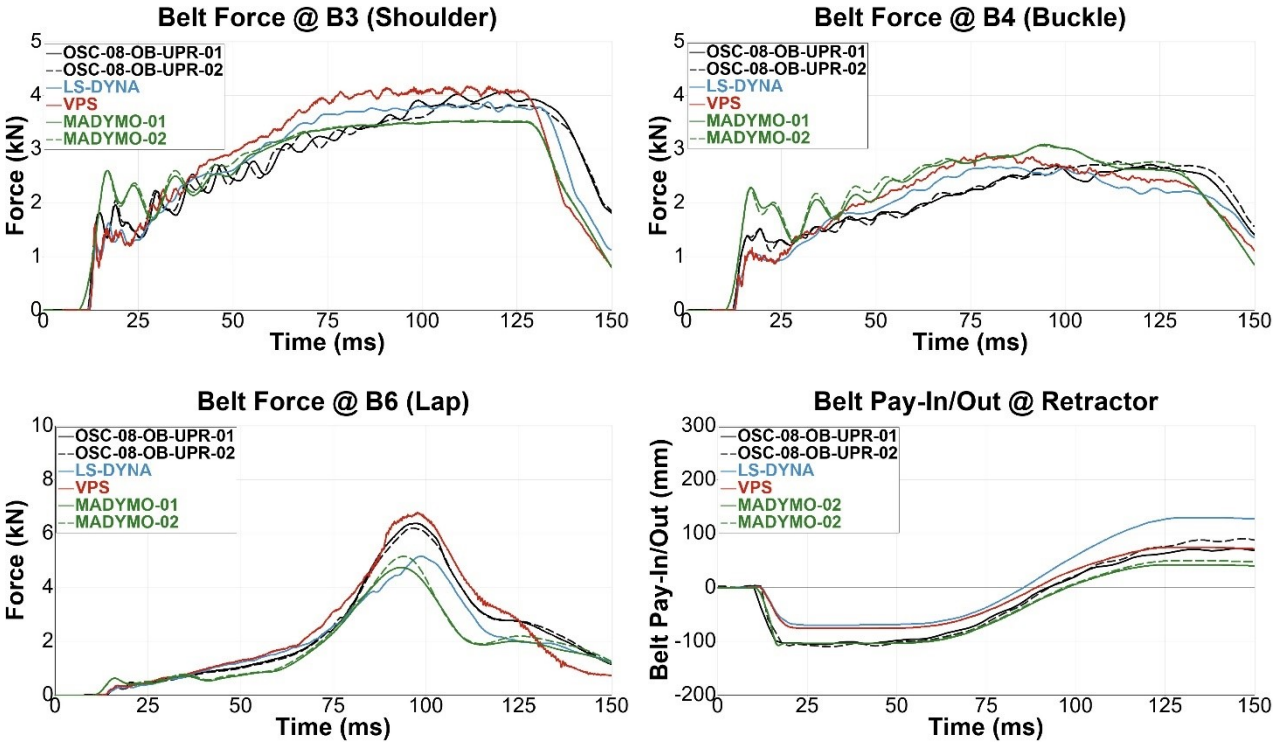

Figure 176 Seat belt forces & shoulder retractor belt pay-in/-out

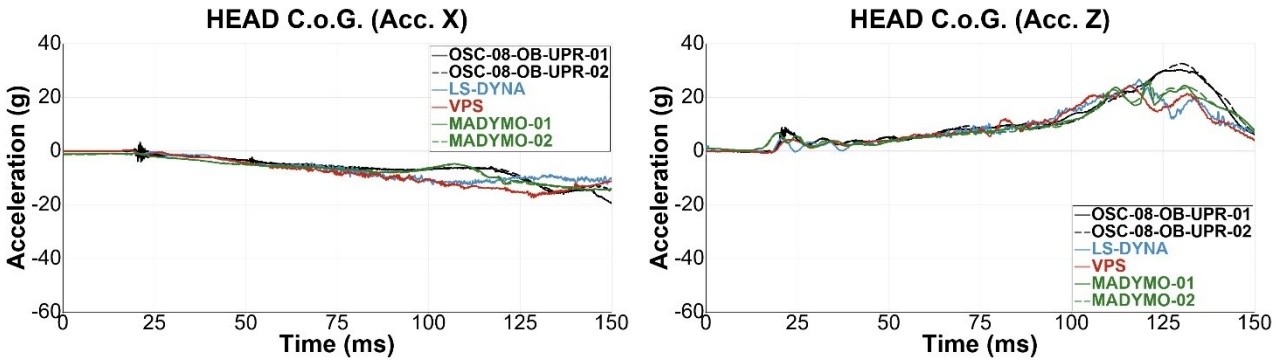

Figure 177 Head COG accelerations

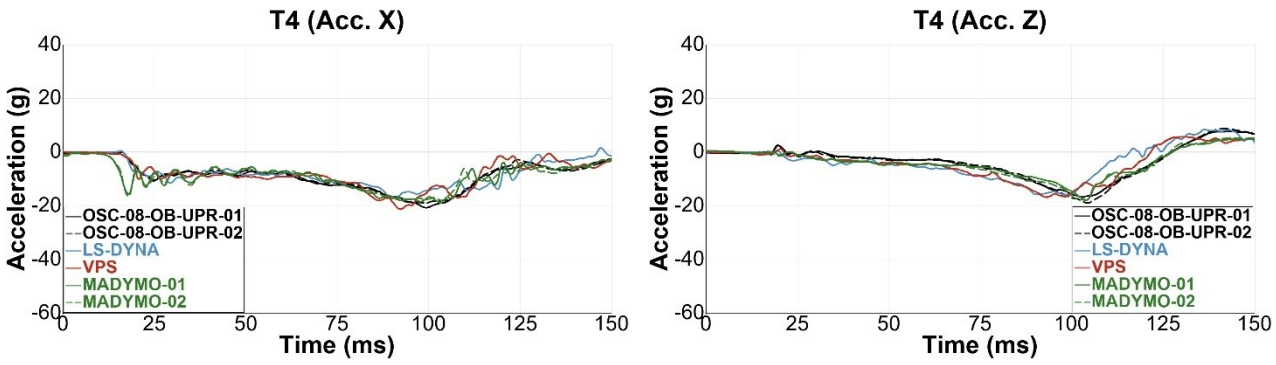

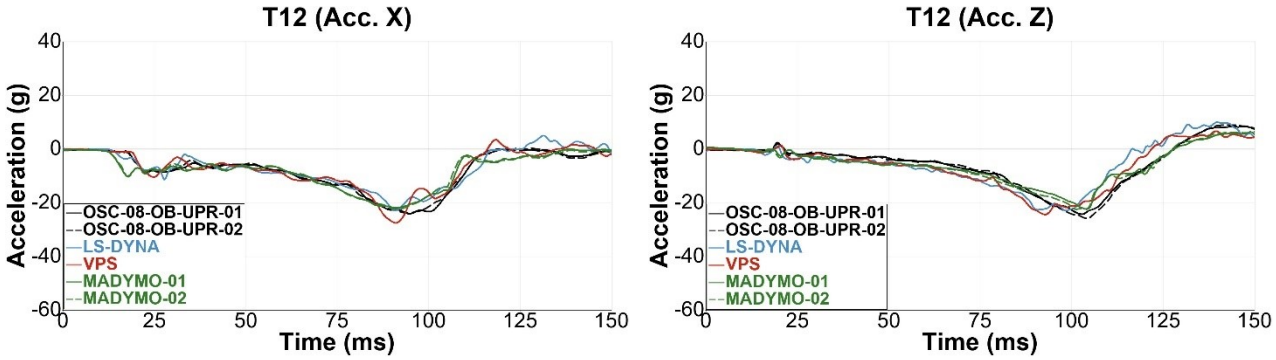

Figure 178 T4 and T12 accelerations

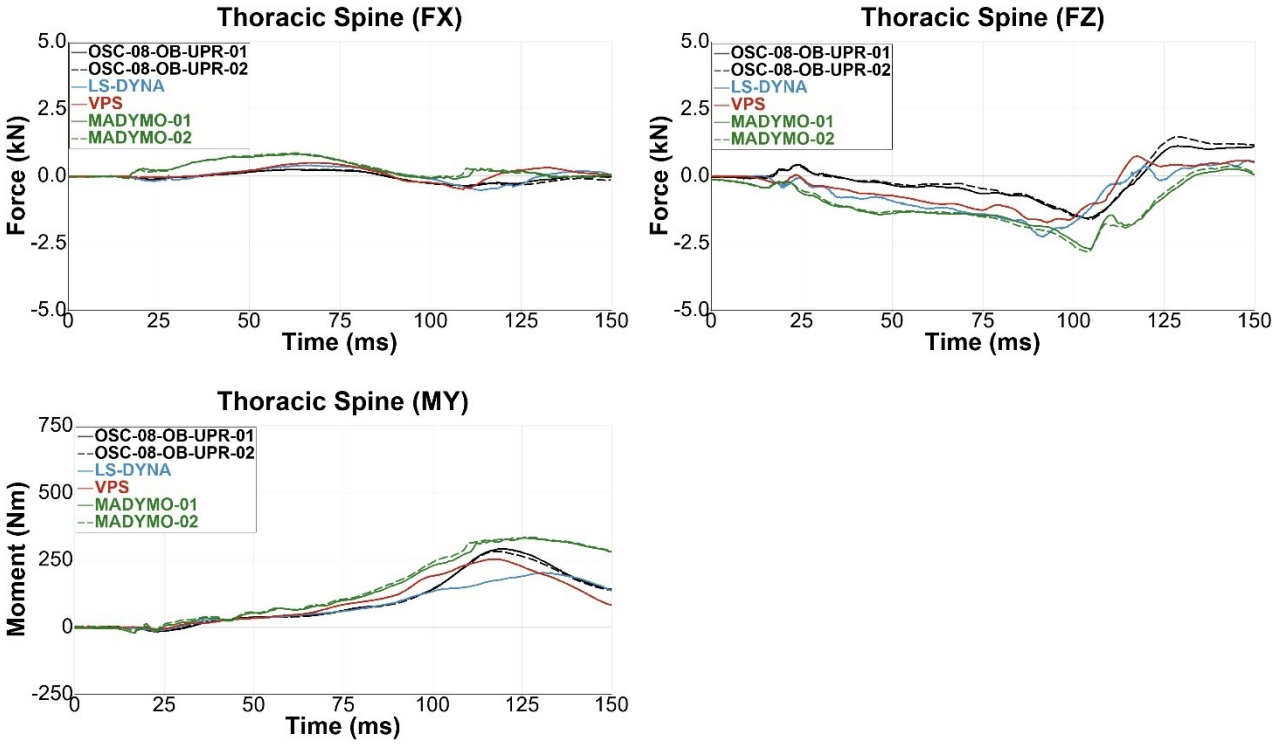

Figure 179 Lower thoracic spine forces and moments

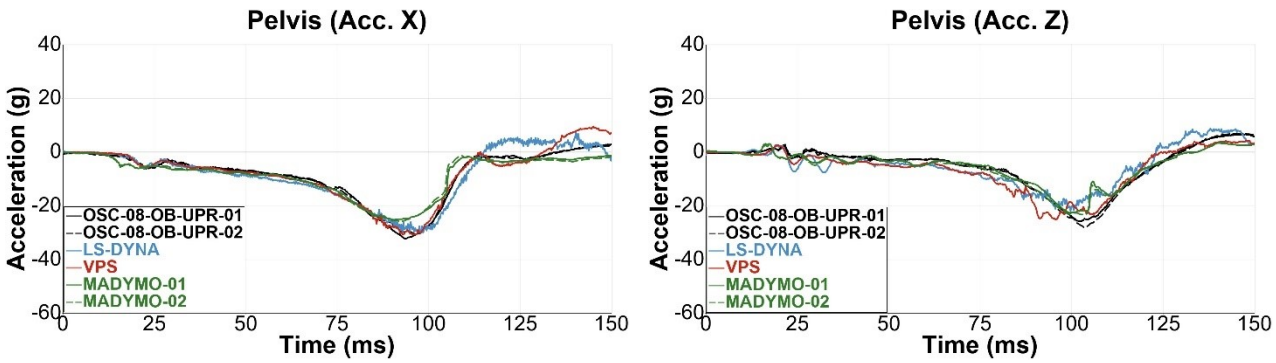

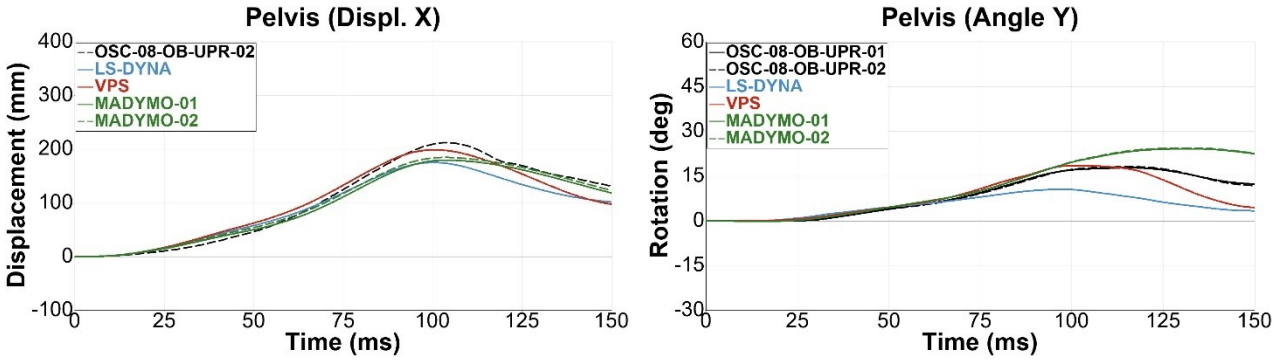

Figure 180 Pelvis accelerations, X-displacement and Y-angle

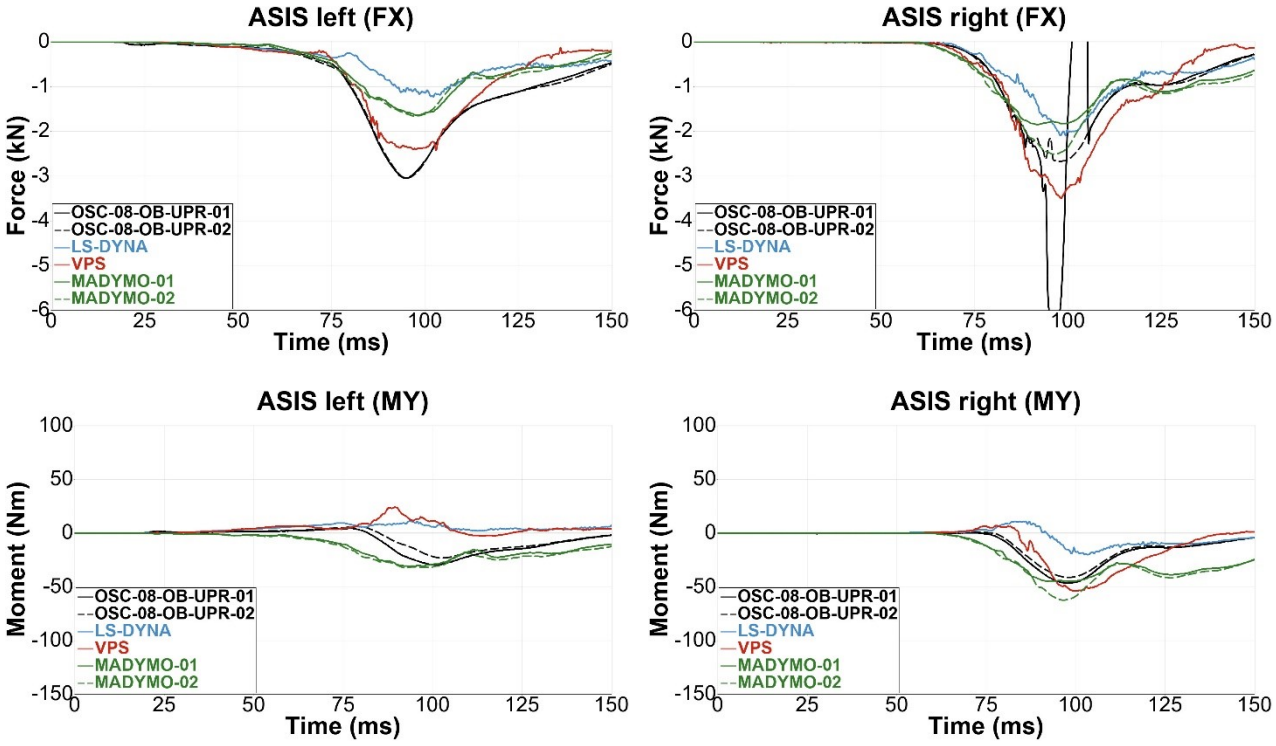

Figure 181 ASIS X-forces and Y-moments

Table 23 summarises the CORA ratings with the averaged (LS-Dyna and VPS) or individual (Madymo) test data as reference. Ratings are coloured in accordance to the sliding scale from ISO 18571 (excellent = green; good = white; fair = yellow; poor = red).

Channel	Virtual Demonstrator			
	LS-DYNA	VPS	MADYMO-01	MADYMO-02
Seat Pan (Displ. Z)	0.832	0.704	0.664	0.667
Anti-Submarining Ramp (Displ. X)	0.746	0.693	0.931	0.917
Upper Diag. Belt Force (B3)	0.941	0.844	0.870	0.892
Lower Diag. Belt Force (B4)	0.887	0.854	0.791	0.767

Lap-Belt outside Force (B6)	0.904	0.941	0.842	0.869
Belt Pay-In/-Out	0.477	0.747	0.825	0.820
Head COG (Acc. X)	0.765	0.744	0.925	0.888
Head COG (Acc. Z)	0.823	0.811	0.879	0.884
T4 (Acc. X)	0.835	0.872	0.898	0.894
T4 (Acc. Z)	0.711	0.788	0.856	0.869
T12 (Acc. X)	0.877	0.898	0.888	0.884
T12 (Acc. Z)	0.803	0.856	0.882	0.887
T12 (Fo. X)	0.505	0.446	0.252	0.218
T12 (Fo. Z)	0.362	0.449	0.252	0.243
T12 (Mo. Y)	0.858	0.899	0.757	0.704
Pelvis (Acc. X)	0.902	0.944	0.900	0.905
Pelvis (Acc. Z)	0.805	0.862	0.879	0.883
Pelvis (Displ. X)	*x*	*x*	*x*	0.961
Pelvis (Ang. Y)	0.638	0.865	0.785	0.779
ASIS left (Fo. X)	0.718	0.864	0.789	0.795
ASIS right (Fo. X)	0.754	0.808	0.676	0.933
ASIS left (Mo. Y)	0.401	0.433	0.631	0.448
ASIS right (Mo. Y)	0.570	0.743	0.667	0.599
Environment	**0.798**	**0.797**	**0.821**	**0.822**
Dummy	**0.708**	**0.768**	**0.745**	**0.751**
Total	**0.732**	**0.776**	**0.765**	**0.770**

Table 23 CORA ratings for upright seating position with LTAP OD2 pulse and SOTA belt

1.2.6.4 LTAP OD2 – Reclined Seating Position with SOTA DLPT Belt

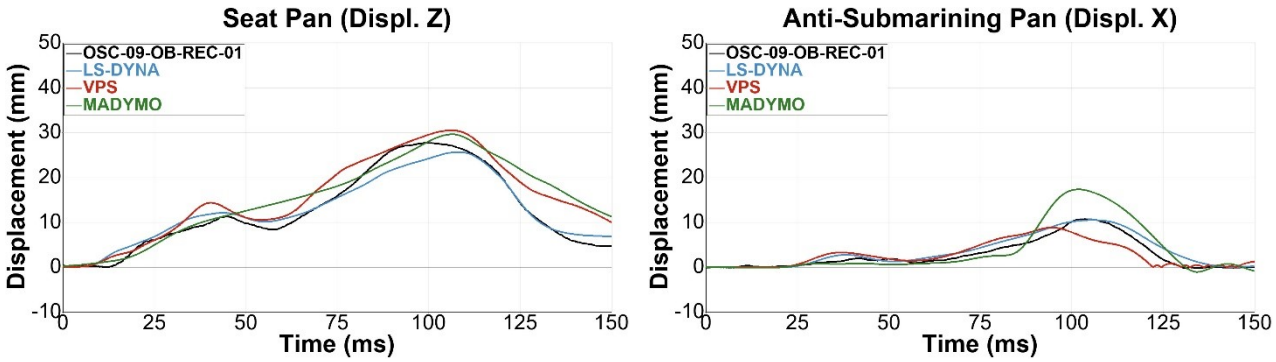

Figure 182 Seat pan & anti-submarining ramp displacements

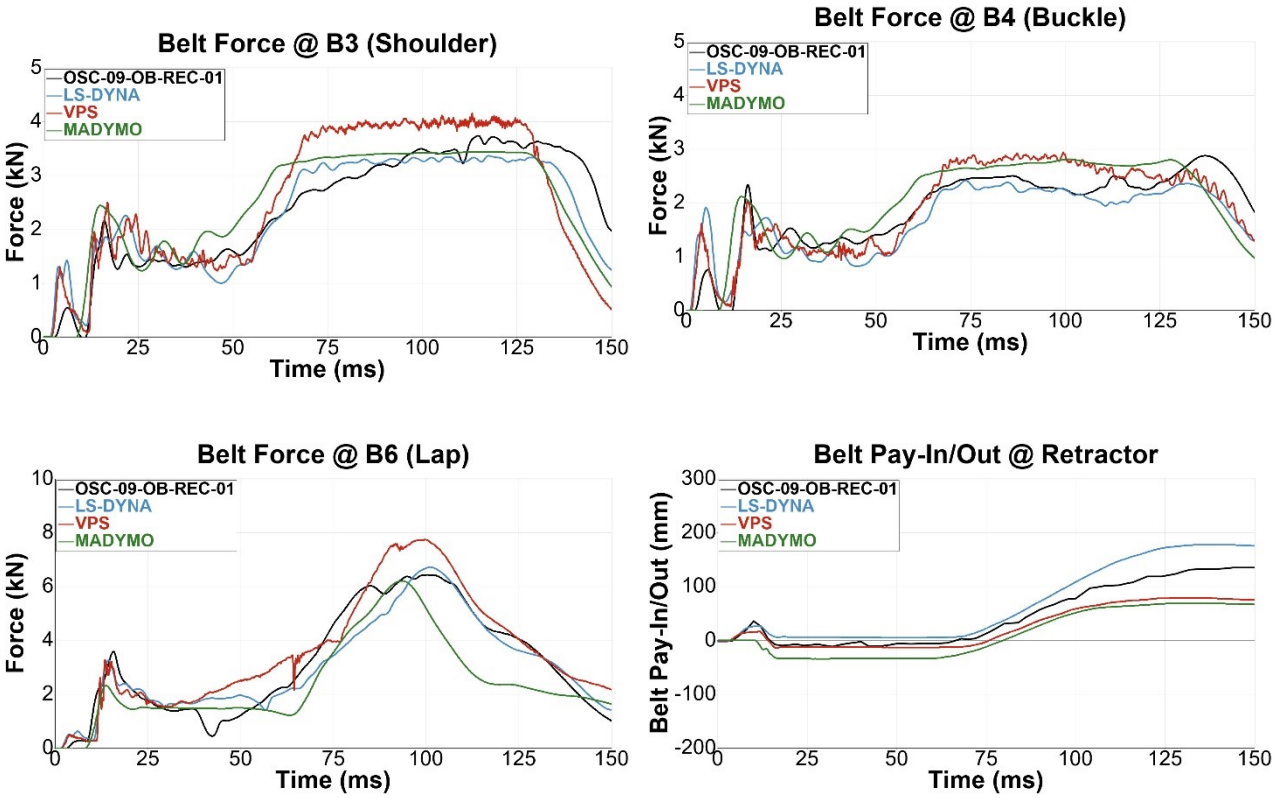

Figure 183 Seat belt forces & shoulder retractor belt pay-in/-out

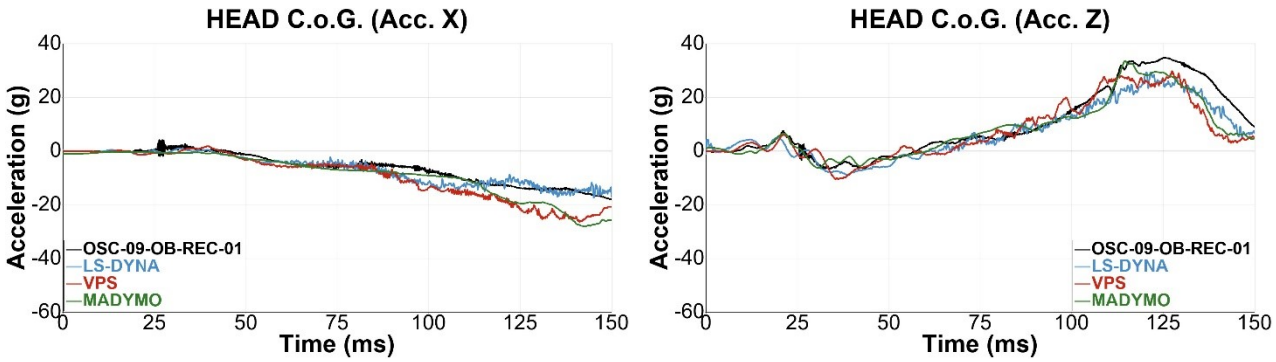

Figure 184 Head COG accelerations

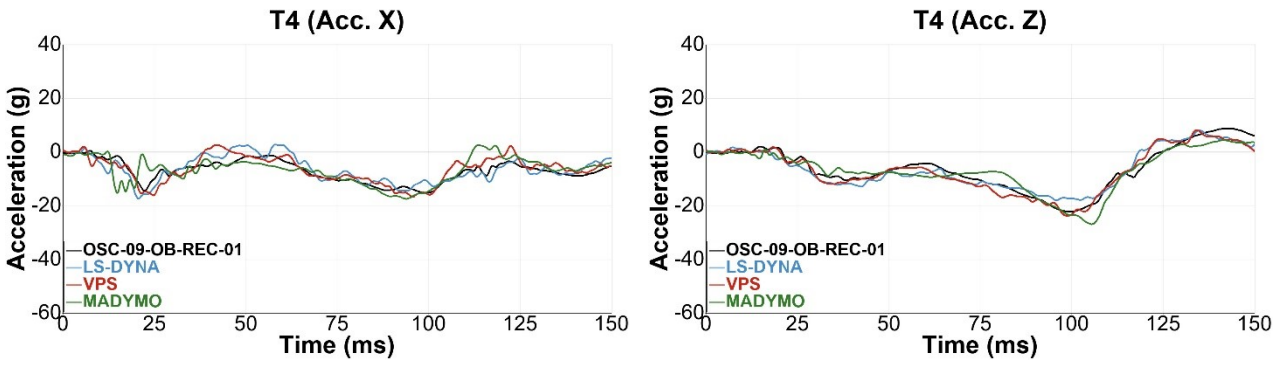

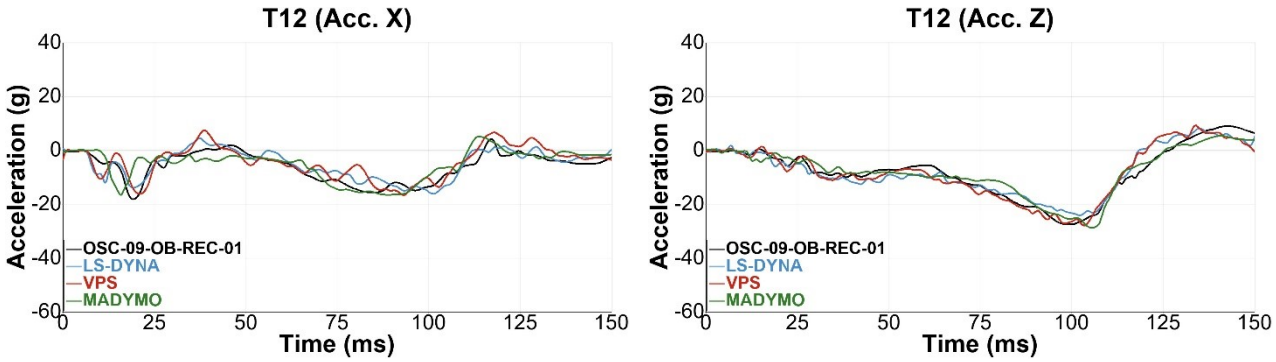

Figure 185 T4 and T12 accelerations

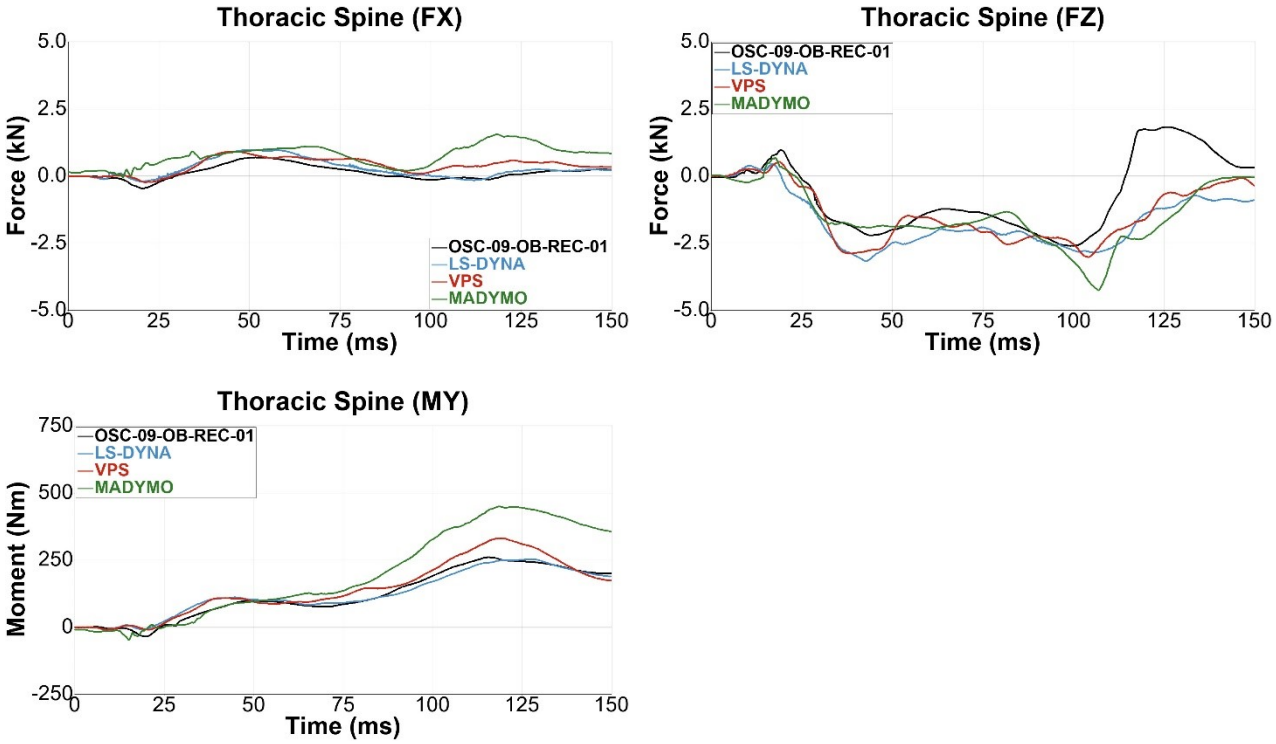

Figure 186 Lower thoracic spine forces and moments

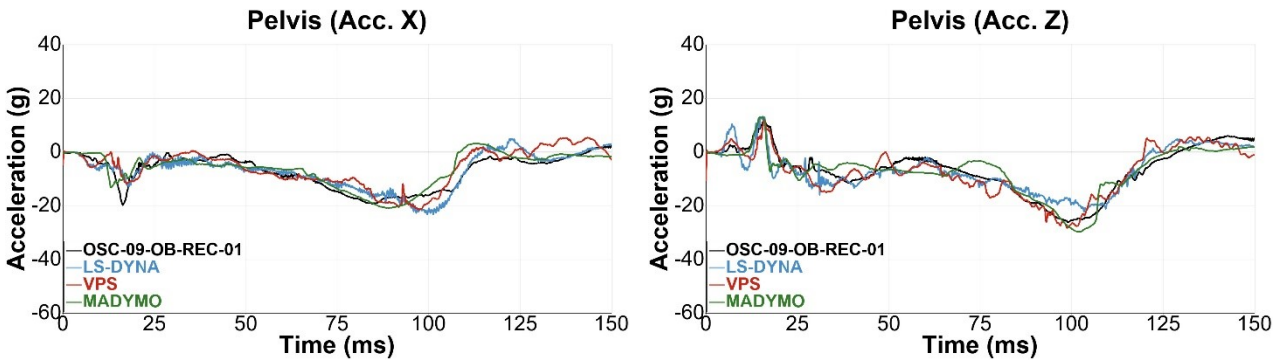

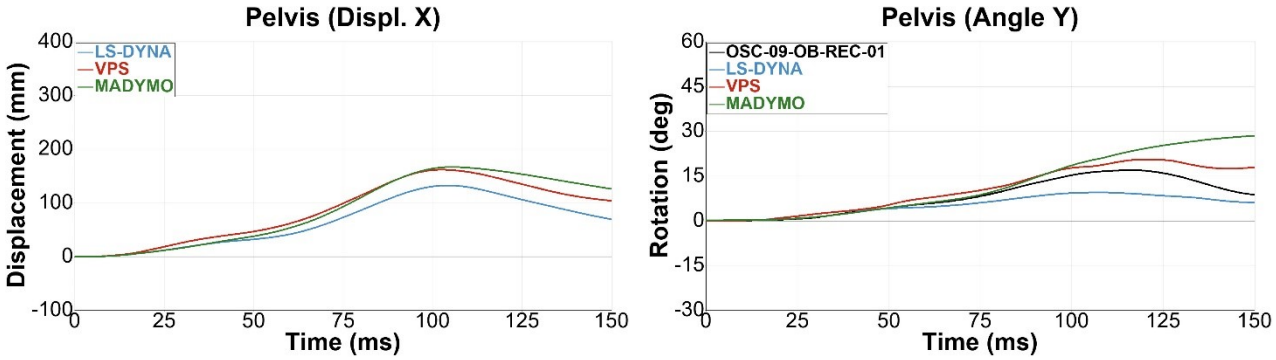

Figure 187 Pelvis accelerations, X-displacement and Y-angle

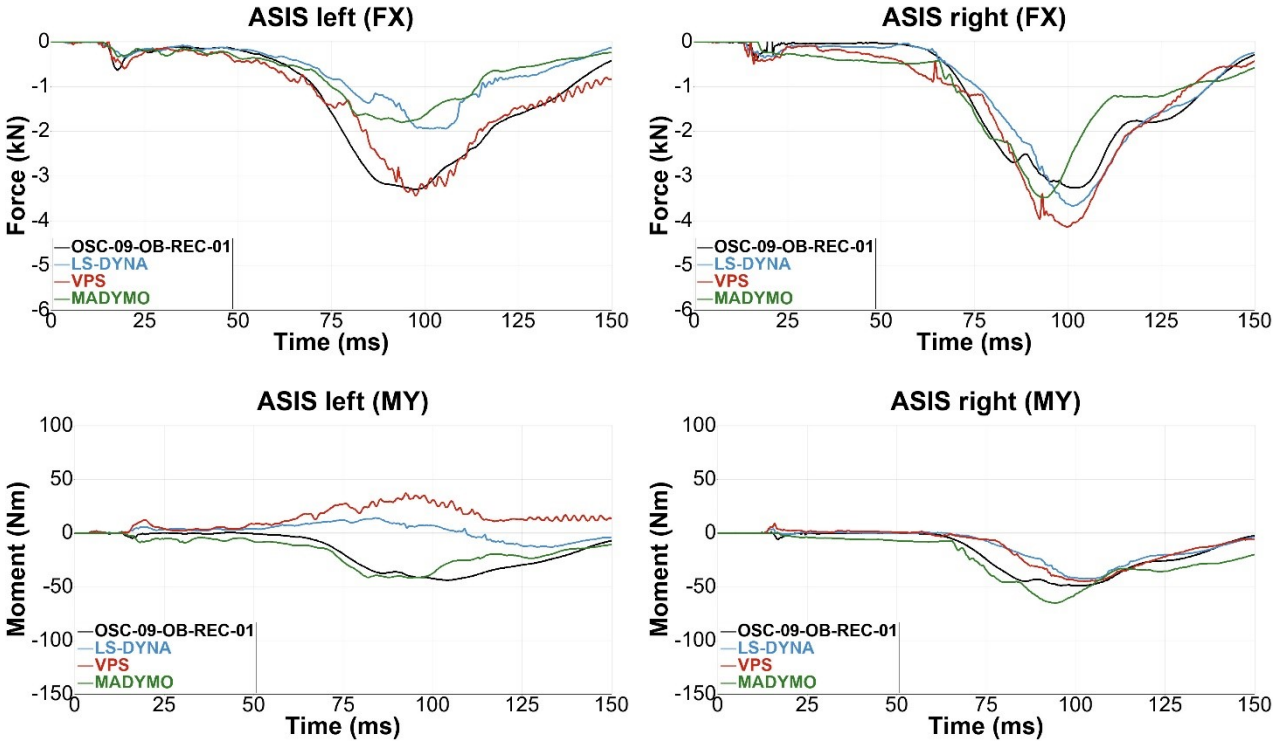

Figure 188 ASIS X-forces and Y-moments

Table 24 summarises the CORA ratings with the averaged (LS-Dyna and VPS) or individual (Madymo) test data as reference. Ratings are coloured in accordance to the sliding scale from ISO 18571 (excellent = green; good = white; fair = yellow; poor = red).

Channel	Virtual Demonstrator		
	LS-DYNA	VPS	MADYMO
Seat Pan (Displ. Z)	0.943	0.837	0.816
Anti-Submarining Ramp (Displ. X)	0.867	0.770	0.739
Upper Diag. Belt Force (B3)	0.896	0.768	0.835
Lower Diag. Belt Force (B4)	0.837	0.854	0.799

Lap-Belt outside Force (B6)	0.909	0.856	0.763
Belt Pay-In/-Out	0.743	0.740	0.504
Head COG (Acc. X)	0.866	0.707	0.774
Head COG (Acc. Z)	0.819	0.785	0.842
T4 (Acc. X)	0.767	0.783	0.747
T4 (Acc. Z)	0.844	0.902	0.825
T12 (Acc. X)	0.777	0.691	0.740
T12 (Acc. Z)	0.877	0.904	0.886
T12 (Fo. X)	0.614	0.407	0.182
T12 (Fo. Z)	0.445	0.535	0.529
T12 (Mo. Y)	0.952	0.856	0.645
Pelvis (Acc. X)	0.807	0.727	0.794
Pelvis (Acc. Z)	0.806	0.817	0.807
Pelvis (Displ. X)	*x*	*x*	*x*
Pelvis (Ang. Y)	0.700	0.792	0.719
ASIS left (Fo. X)	0.689	0.933	0.684
ASIS right (Fo. X)	0.925	0.858	0.824
ASIS left (Mo. Y)	0.341	0.339	0.757
ASIS right (Mo. Y)	0.781	0.814	0.753
Environment	**0.866**	**0.804**	**0.743**
Dummy	**0.751**	**0.741**	**0.719**
Total	**0.782**	**0.758**	**0.726**

Table 24 CORA ratings for relined seating position with LTAP OD2 pulse and SOTA DLPT belt

1.3 Physical Demonstrator - Second Test Series Results

1.3.1 Additional Tests – Comparison to the First Test Series

1.3.1.1 SOTA belt in Upright Seating Position

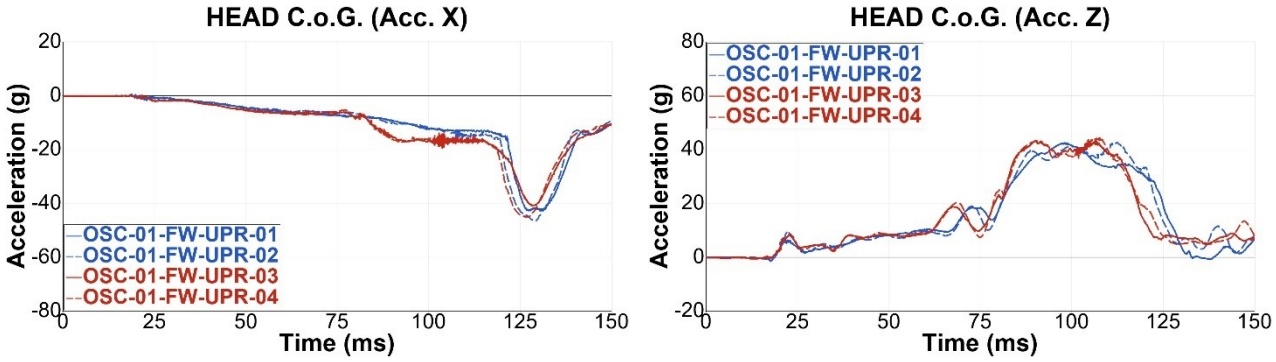

Figure 189 Head COG accelerations, comparing 1st (blue) & 2nd (red) test series

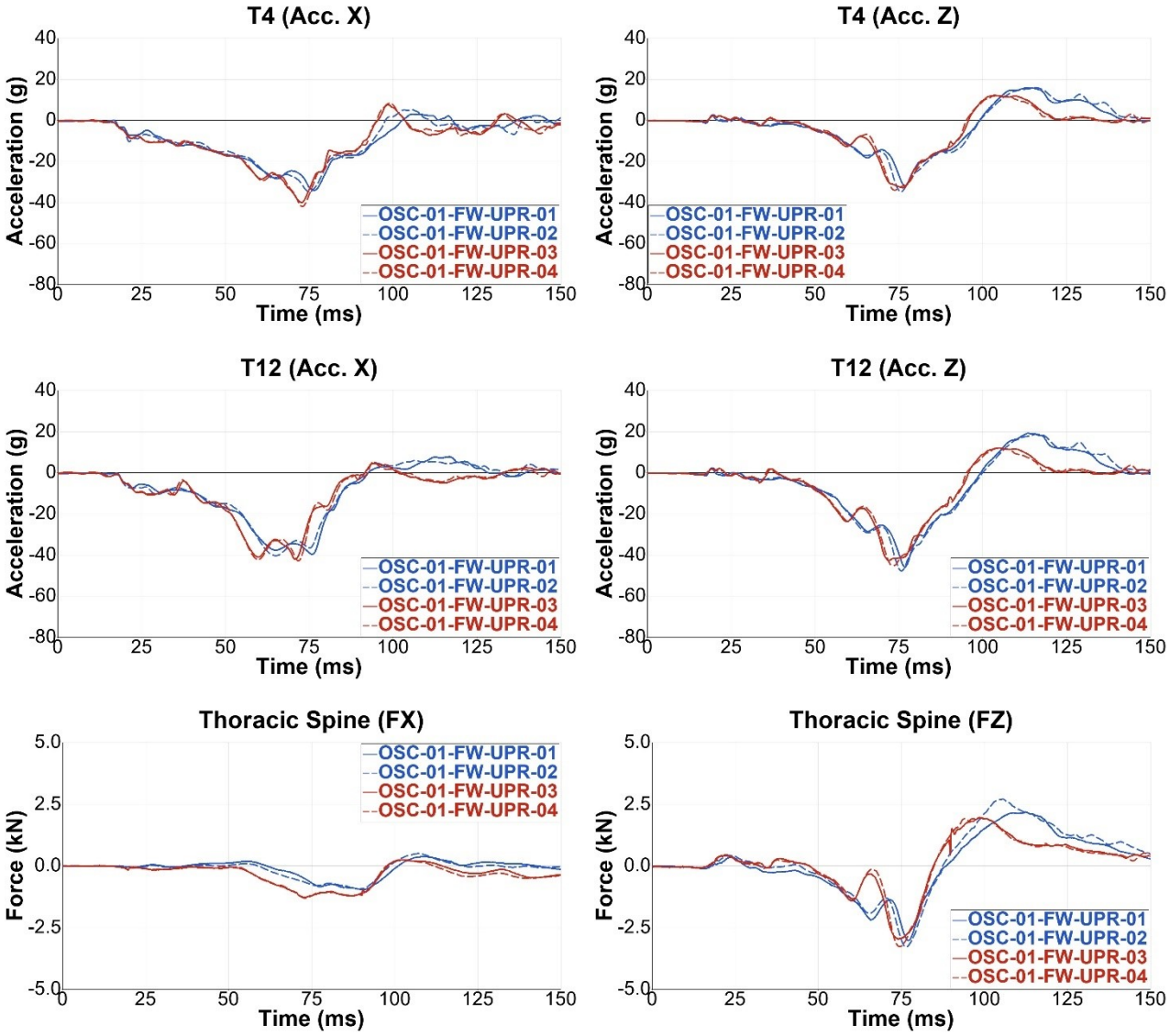

Figure 190 Thoracic spine accelerations (T4 & T12) and loadings (T12), comparing 1st (blue) & 2nd (red) test series

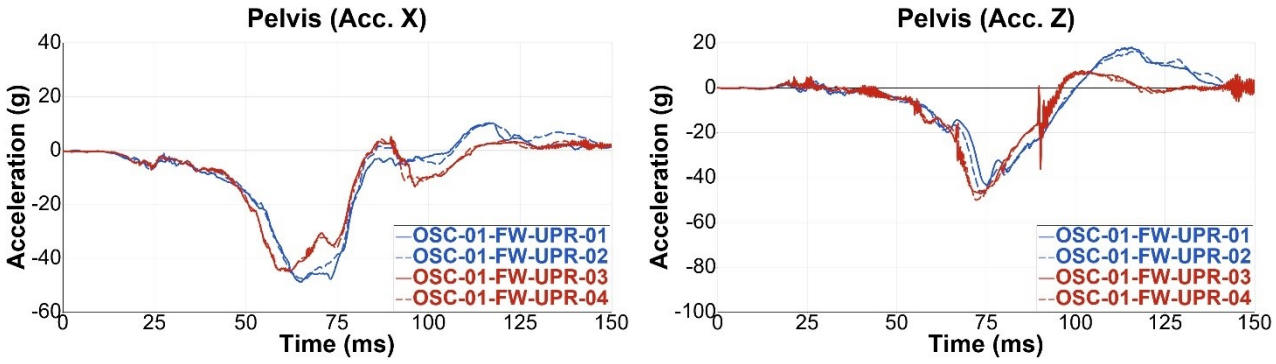

Figure 191 Pelvis accelerations, comparing 1st (blue) & 2nd (red) test series

1.3.1.2 SOTA DLPT belt in Reclined Seating Position

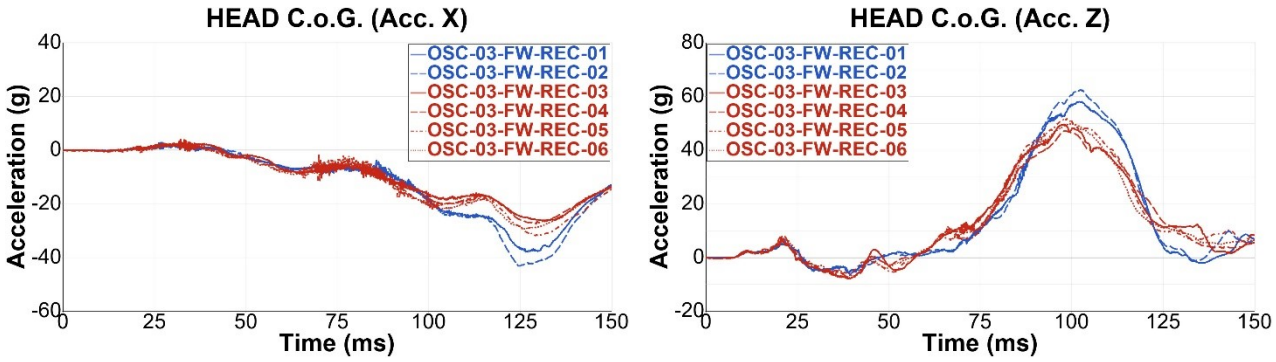

Figure 192 Head COG accelerations, comparing 1st (blue) & 2nd (red) test series

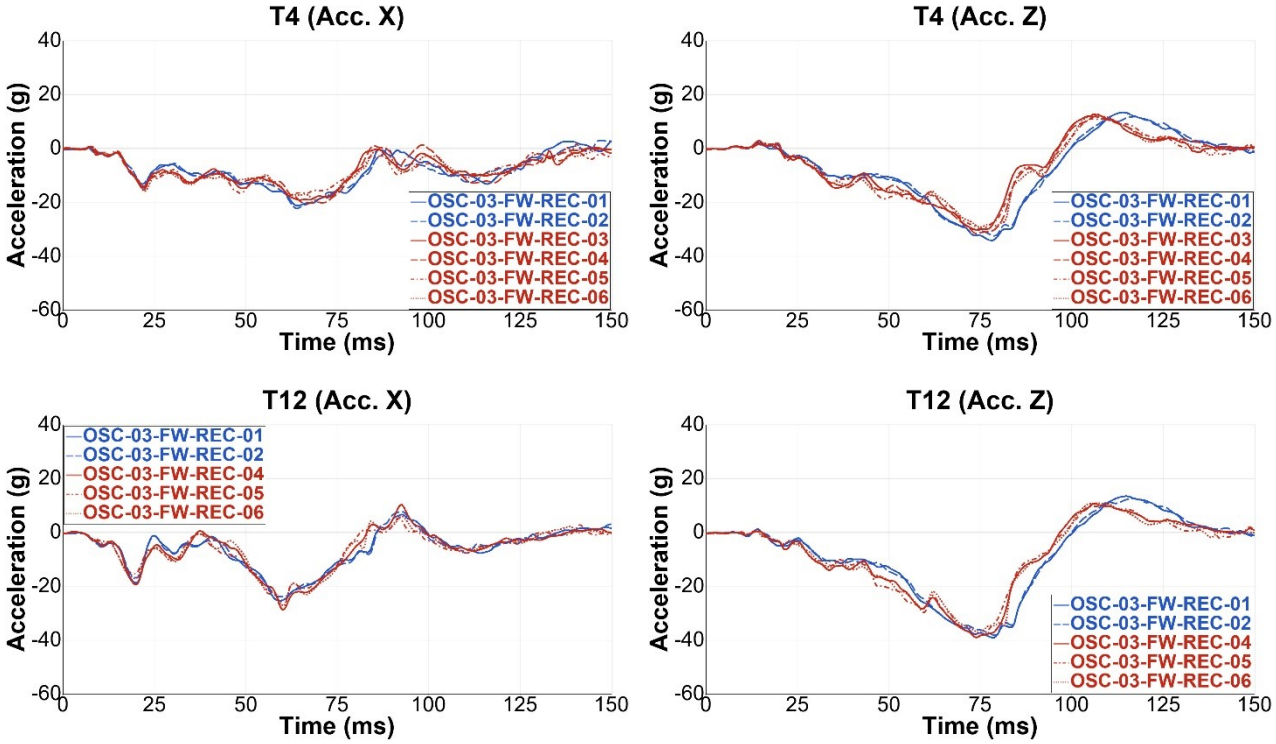

Figure 193 Thoracic spine accelerations (T4 & T12), comparing 1st (blue) & 2nd (red) test series

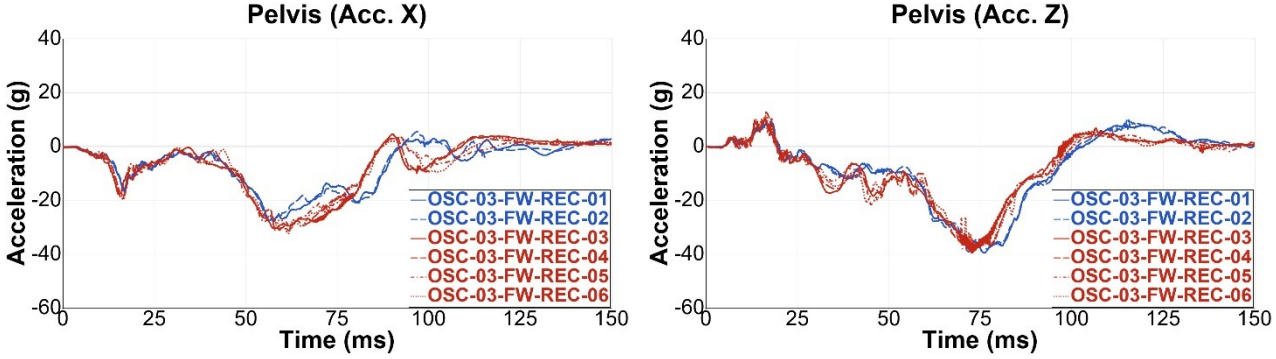

Figure 194 Pelvis accelerations, comparing 1st (blue) & 2nd (red) test series

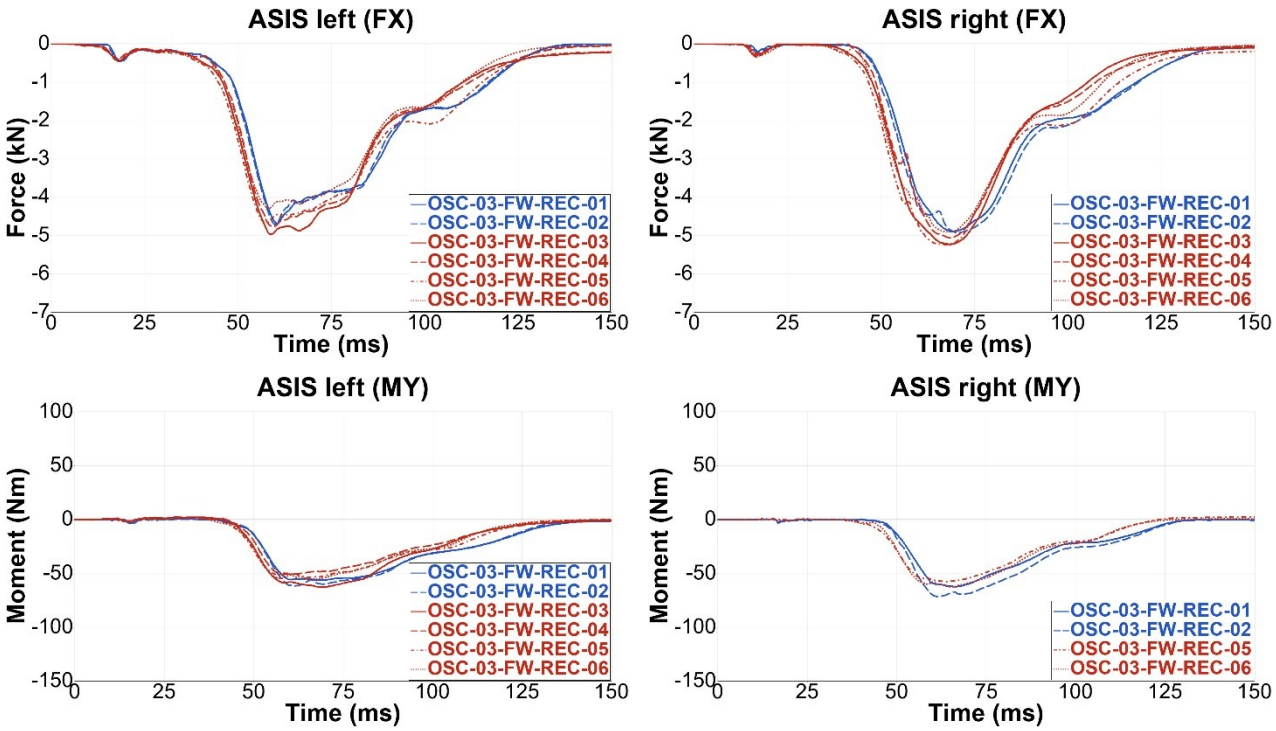

Figure 195 ASIS forces and moments, comparing 1st (blue) & 2nd (red) test series

1.3.2 Test Repeatability

First, the test scatter of individual tests is compared to averaged test data. Therefore, data from all four tests was used to calculate average values for each channel, obviously corrupted data was not considered. The averaged data was used as reference when calculating a CORA rating for each test and channel. Thereby, each graph shows the data from the four tests (red), the averaged data (black) as well as the inner (blue) and outer (grey) corridor from the CORA method.

CORA ratings for the seat pan and anti-submarining ramp displacements were almost perfect (CORA > 0.99) for two tests each. In the other tests the dampers slowing down the rebound responded differently, which affected the size (correlation rating) and corridor rating, resulting in slightly worse CORA rating (Figure 195Figure 196).

Note: For seat pan displacement data from test OSC-03-05 was not considered due to sensor error.

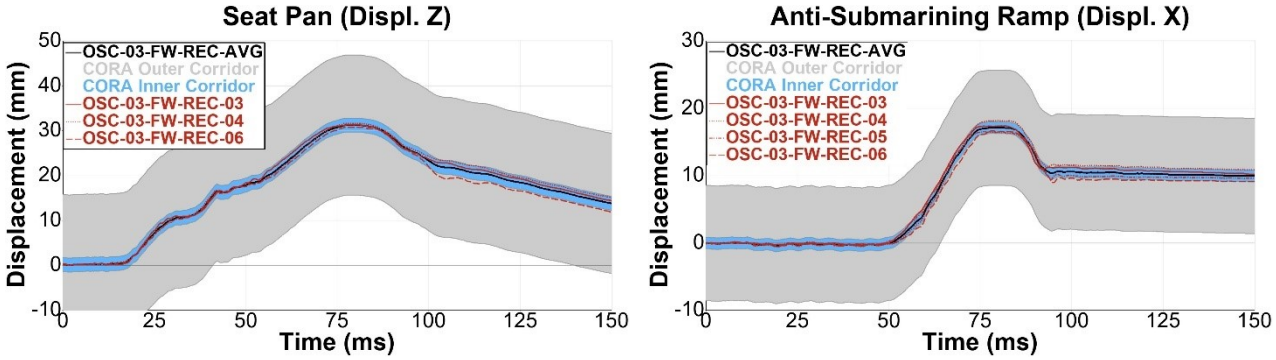

OSC-03-03	0.995	**OSC-03-04**	0.993
OSC-03-05	N/A	**OSC-03-06**	0.979

OSC-03-03	0.992	**OSC-03-04**	0.977
OSC-03-05	0.992	**OSC-03-06**	0.973

Figure 196 Seat pan & anti-submarining ramp displacements with corresponding CORA scores

In all four tests the scatter of the shoulder (B3) and lap (B6) belt forces was very low, accordingly CORA ratings were almost perfect (CORA > 0.99). Compared to the average data, the belt loading at B4 was reduced in the first test (peak force smaller and earlier) due to an incorrect position of the belt force sensor after pretensioning, affecting the size and corridor rating. This was not observed in the other three tests resulting in a better CORA rating. For three out of four tests the CORA ratings for the belt pay-in/-out were almost perfect, while a reduced belt pay-out in the last test ($\Delta_{max} \approx$ 15 mm) affected the size and corridor rating and consequently led to a slightly worse CORA rating (Figure 197).

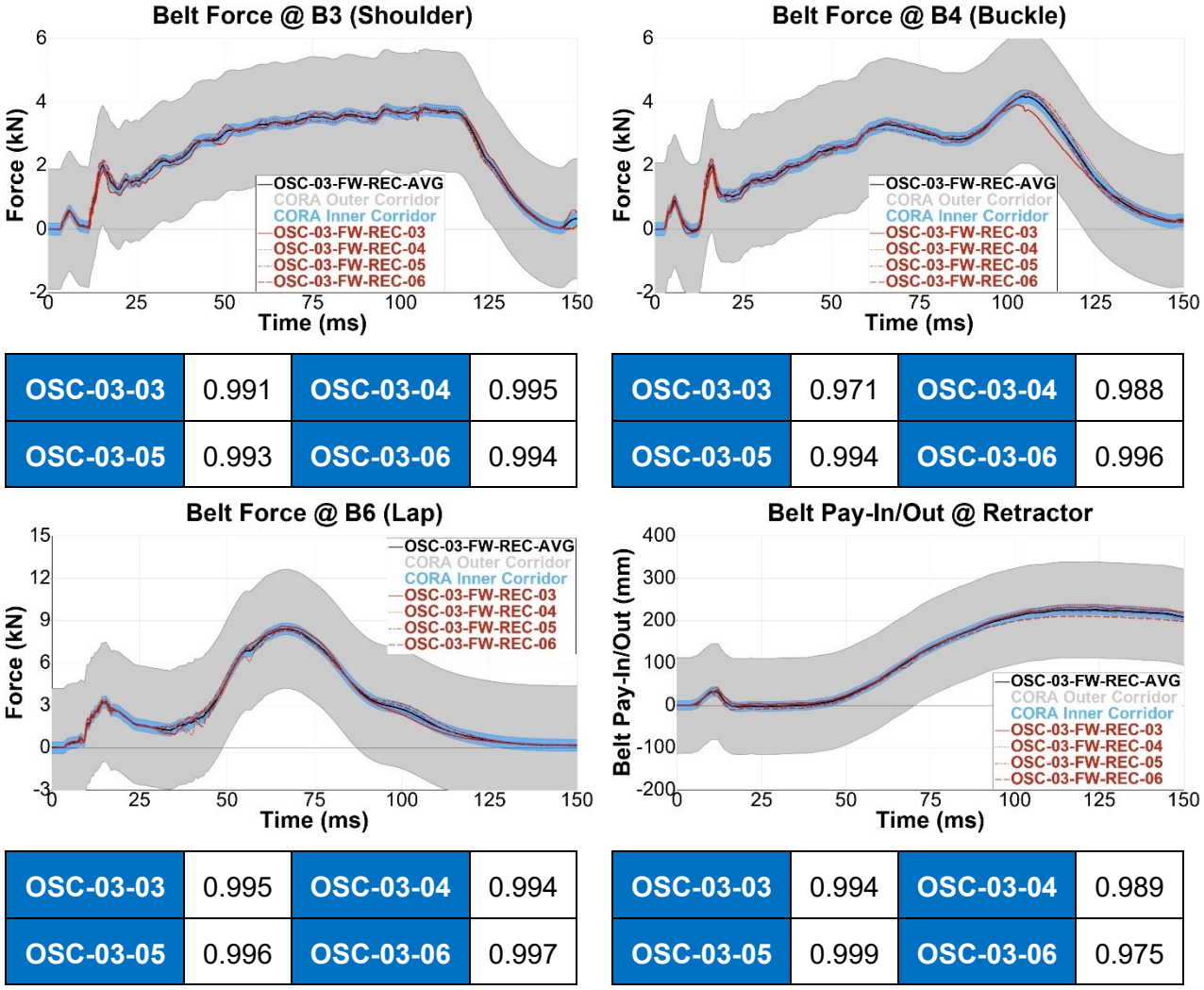

OSC-03-03	0.991	OSC-03-04	0.995
OSC-03-05	0.993	OSC-03-06	0.994

OSC-03-03	0.971	OSC-03-04	0.988
OSC-03-05	0.994	OSC-03-06	0.996

OSC-03-03	0.995	OSC-03-04	0.994
OSC-03-05	0.996	OSC-03-06	0.997

OSC-03-03	0.994	OSC-03-04	0.989
OSC-03-05	0.999	OSC-03-06	0.975

Figure 197 Seat belt forces & pay-in/out with corresponding CORA scores

Head COG accelerations in the z-direction (Figure 198) only differ in the peak value by approx. 2 g (no timely delay), resulting in some reductions for the size rating. For the x-accelerations deviations can be observed in the peak values ($\Delta_{max} \approx$ 3 g; timely delayed), affecting the size and corridor rating and consequently leading to a slightly worse CORA rating. Observed oscillations (noisy signal), especially for the x-acceleration, have a negligible influence on the CORA rating.

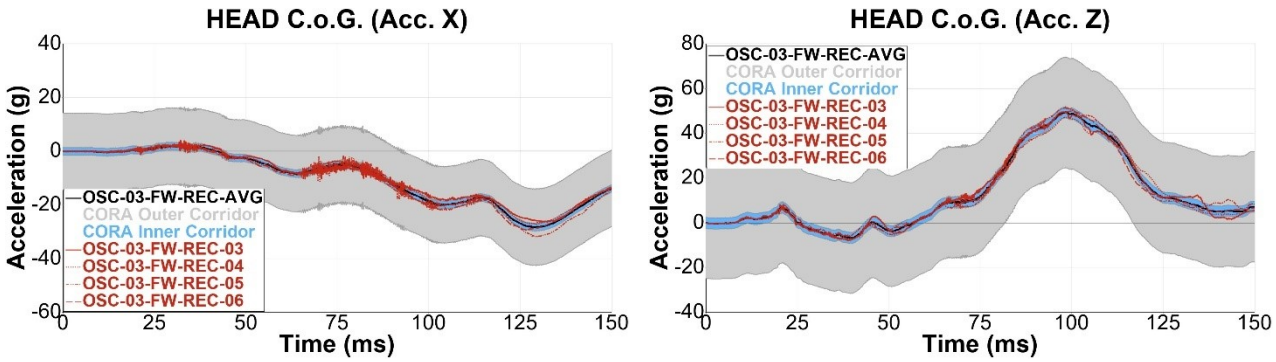

OSC-03-03	0.973	OSC-03-04	0.988
OSC-03-05	0.965	OSC-03-06	0.985

OSC-03-03	0.993	OSC-03-04	0.983
OSC-03-05	0.982	OSC-03-06	0.993

Figure 198 Head COG accelerations with corresponding CORA scores

Some scatter in T4 accelerations in the x-direction (Figure 199; differing curve shapes) was observed mostly influencing the corridor method (rating ≈ 0.9). For the z-acceleration the test scatter was small, accordingly CORA ratings were good.

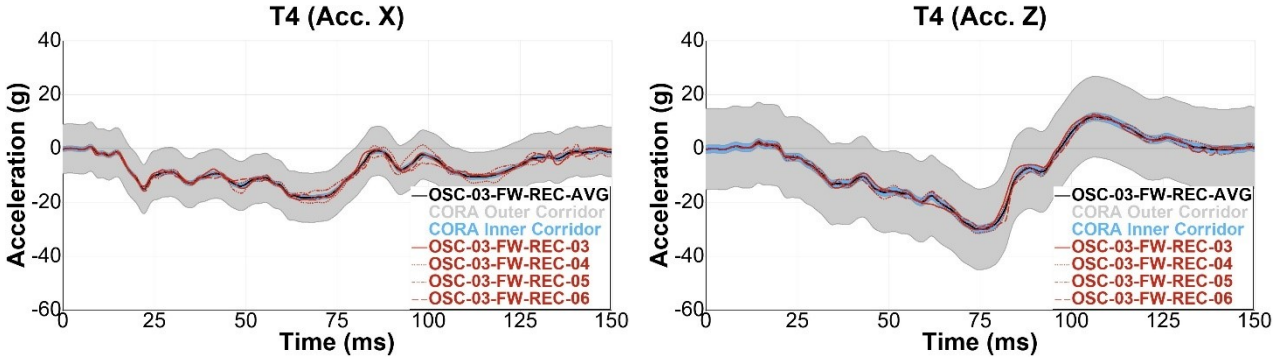

OSC-03-03	0.984	OSC-03-04	0.931
OSC-03-05	0.930	OSC-03-06	0.978

OSC-03-03	0.986	OSC-03-04	0.989
OSC-03-05	0.992	OSC-03-06	0.990

Figure 199 T4 accelerations with corresponding CORA scores

The CORA rating for the T12 x-acceleration (Figure 200) is influenced by differences of approx. 2 g in the (positive) peak values, resulting in deductions for the size and corridor rating and consequently leading to a slightly worse CORA rating. For the z-acceleration the test scatter was minimal, accordingly CORA ratings were almost perfect (CORA > 0.99).

Note: T12 accelerations from one test (OSC-03-03) were not considered due to a cable rupture during the test.

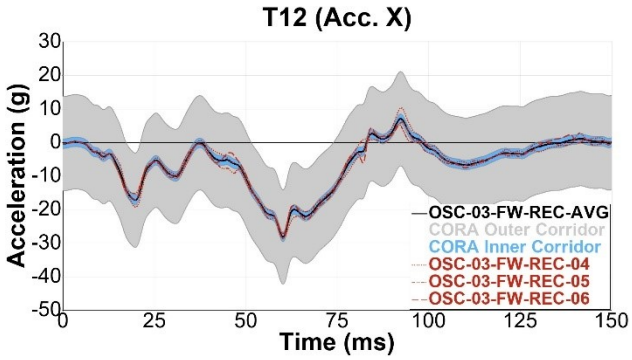

OSC-03-03	N/A	OSC-03-04	0.978
OSC-03-05	0.983	OSC-03-06	0.993

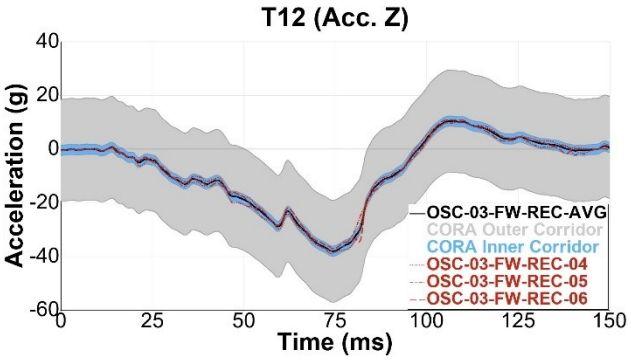

OSC-03-03	N/A	OSC-03-04	0.995
OSC-03-05	0.996	OSC-03-06	0.995

Figure 200 T12 accelerations with corresponding CORA scores

For the lower thoracic spine, maximum differences of about 250 N in the x-forces result in a significant reduction of the CORA rating (Figure 201). Z-forces differ by approx. 500 N in the (positive) peak loading, resulting in deductions for the corridor rating and cross correlation function and consequently leading to a slightly worse CORA rating. Notably, the smaller deviations in the x-forces (approx. 250 N) result in a stronger downgrading of the CORA rating than the differences in the z-forces (approx. 500 N). Test scatter of the y-moment was minimal; accordingly, CORA ratings were almost perfect (CORA > 0.99).

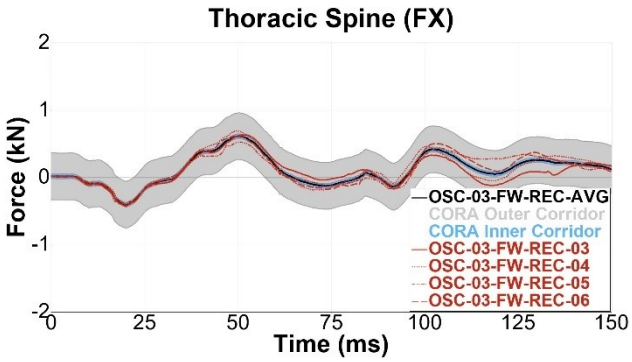

OSC-03-03	0.805	OSC-03-04	0.874
OSC-03-05	0.856	OSC-03-06	0.916

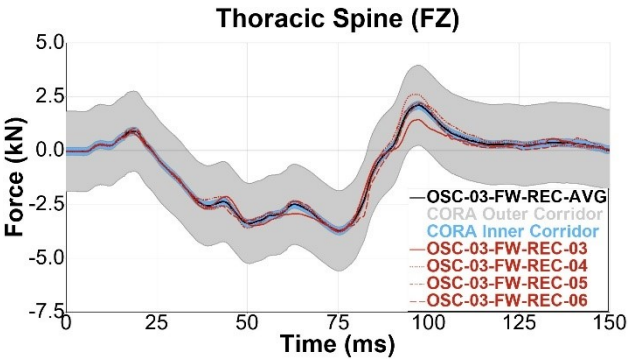

OSC-03-03	0.956	OSC-03-04	0.980
OSC-03-05	0.978	OSC-03-06	0.985

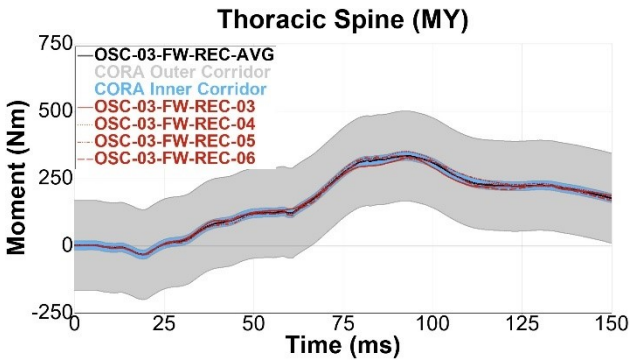

OSC-03-03	0.991	OSC-03-04	0.996
OSC-03-05	0.995	OSC-03-06	0.998

Figure 201 Lower thoracic spine forces & moments with corresponding CORA scores

Pelvis x-accelerations are influenced by some scatter at approx. 90 ms (beginning of rebound) affecting the CORA rating (Figure 202). On the other hand, oscillations (noisy signal) in the z-accelerations have a negligible effect on the CORA rating. More severe scatter can be observed for the pelvis forward displacement and y-angle, consequently the CORA rating for both channels is not that good.

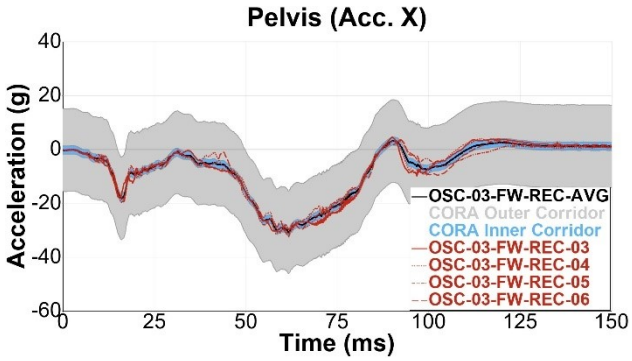

OSC-03-03	0.970	OSC-03-04	0.982
OSC-03-05	0.973	OSC-03-06	0.981

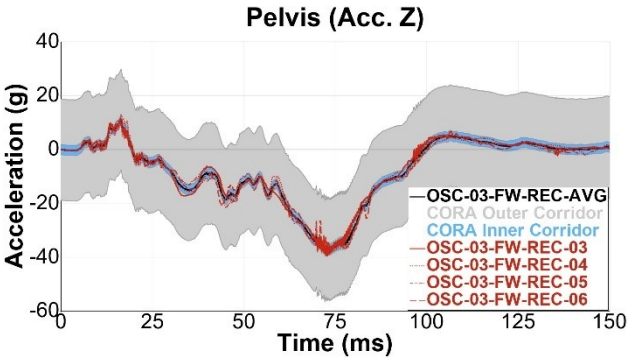

OSC-03-03	0.986	OSC-03-04	0.987
OSC-03-05	0.992	OSC-03-06	0.989

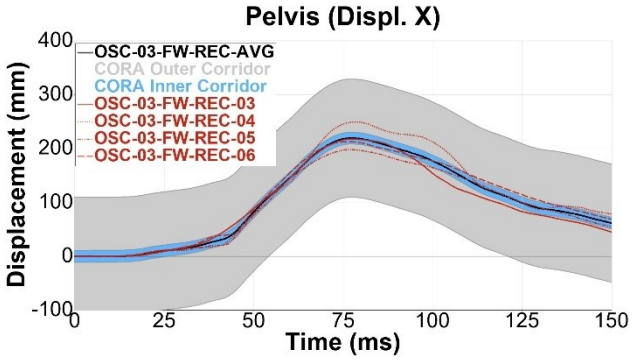

OSC-03-03	0.954	OSC-03-04	0.930
OSC-03-05	0.965	OSC-03-06	0.989

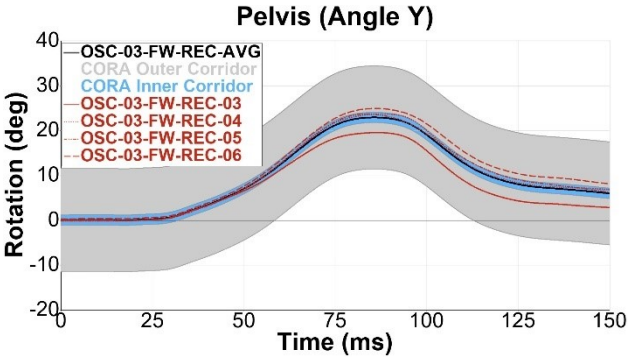

OSC-03-03	0.838	OSC-03-04	0.992
OSC-03-05	0.991	OSC-03-06	0.922

Figure 202 Pelvis accelerations, X-displacement & Y-angle with corresponding CORA scores

For the ASIS forces and moments (Figure 203) deviations between individual and averaged test data are recognisable, which are also reflected in the CORA rating. Thereby, scatter of the left ASIS force is caused by differences in the CLT belt pull-through. Furthermore, variances in the ASIS-to-belt position are responsible for the deviations in the left ASIS moments.

Note: Right ASIS moments from the first two tests (OSC-03-03 & OSC-03-04) were not considered due to a sensor problem.

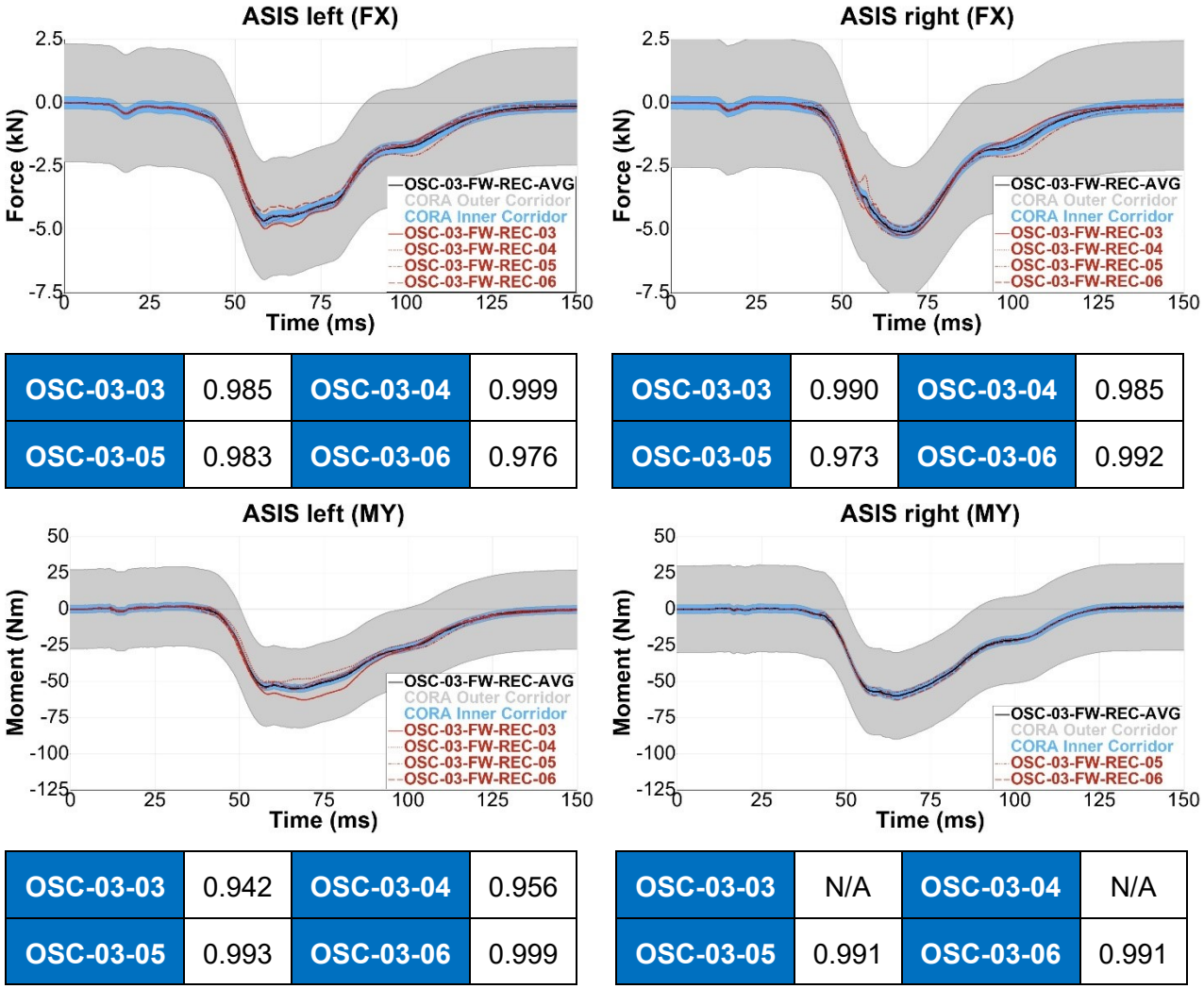

OSC-03-03	0.985	OSC-03-04	0.999
OSC-03-05	0.983	OSC-03-06	0.976

OSC-03-03	0.990	OSC-03-04	0.985
OSC-03-05	0.973	OSC-03-06	0.992

OSC-03-03	0.942	OSC-03-04	0.956
OSC-03-05	0.993	OSC-03-06	0.999

OSC-03-03	N/A	OSC-03-04	N/A
OSC-03-05	0.991	OSC-03-06	0.991

Figure 203 ASIS forces (X) & moment (Y) with corresponding CORA scores

Table 25 to Table 27 summarise the CORA ratings with individual tests as reference.

	Channel	OSC-03-03	OSC-03-04	OSC-03-05	OSC-03-06	AVG
OSC-03-04	Seat Pan (Displ. Z)	0.998	-	x	0.943	0.993
	Anti-Submarining Ramp (Displ. X)	0.984	-	0.934	0.904	0.977
	Upper Diag. Belt Force (B3)	0.977	-	0.985	0.993	0.995
	Lower Diag. Belt Force (B4)	0.937	-	0.987	0.981	0.988
	Lap-Belt outside Force (B6)	0.987	-	0.980	0.992	0.994
	Belt Pay-In/-Out	0.996	-	0.972	0.917	0.989
	Head COG (Acc. X)	0.981	-	0.938	0.963	0.988
	Head COG (Acc. Z)	0.973	-	0.943	0.965	0.983
	T4 (Acc. X)	0.919	-	0.807	0.908	0.931
	T4 (Acc. Z)	0.964	-	0.961	0.971	0.989
	T12 (Acc. X)	x	-	0.931	0.953	0.978
	T12 (Acc. Z)	x	-	0.983	0.984	0.995
	T12 (Fo. X)	0.765	-	0.657	0.830	0.874
	T12 (Fo. Z)	0.910	-	0.960	0.963	0.980

	T12 (Mo. Y)	0.980	-	0.996	0.993	0.996
	Pelvis (Acc. X)	0.953	-	0.925	0.952	0.982
	Pelvis (Acc. Z)	0.963	-	0.964	0.972	0.987
	Pelvis (Displ. X)	0.852	-	0.862	0.914	0.930
	Pelvis (Ang. Y)	0.777	-	0.999	0.960	0.992
	Iliac left (Fo. X)	0.987	-	0.970	0.968	0.999
	Iliac right (Fo. X)	0.978	-	0.939	0.988	0.985
	Iliac left (Mo. Y)	0.892	-	0.946	0.952	0.956
	Iliac right (Mo. Y)	x	-	x	x	-

Table 25 CORA rating for each test with the second test (OSC-03-04) as reference

	Channel	OSC-03-03	OSC-03-04	OSC-03-05	OSC-03-06	AVG
OSC-03-05	Seat Pan (Displ. Z)	x	x	-	x	-
	Anti-Submarining Ramp (Displ. X)	0.978	0.943	-	0.978	0.992
	Upper Diag. Belt Force (B3)	0.979	0.986	-	0.983	0.993
	Lower Diag. Belt Force (B4)	0.949	0.988	-	0.990	0.994
	Lap-Belt outside Force (B6)	0.985	0.981	-	0.989	0.996
	Belt Pay-In/-Out	0.984	0.975	-	0.977	0.999
	Head COG (Acc. X)	0.905	0.928	-	0.964	0.965
	Head COG (Acc. Z)	0.955	0.936	-	0.975	0.982
	T4 (Acc. X)	0.902	0.827	-	0.912	0.930
	T4 (Acc. Z)	0.967	0.964	-	0.973	0.992
	T12 (Acc. X)	x	0.931	-	0.961	0.983
	T12 (Acc. Z)	x	0.983	-	0.983	0.996
	T12 (Fo. X)	0.651	0.703	-	0.870	0.856
	T12 (Fo. Z)	0.919	0.962	-	0.931	0.978
	T12 (Mo. Y)	0.973	0.997	-	0.988	0.995
	Pelvis (Acc. X)	0.918	0.927	-	0.961	0.973
	Pelvis (Acc. Z)	0.970	0.964	-	0.971	0.992
	Pelvis (Displ. X)	0.943	0.885	-	0.959	0.965
	Pelvis (Ang. Y)	0.770	0.999	-	0.966	0.991
	Iliac left (Fo. X)	0.976	0.971	-	0.937	0.983
	Iliac right (Fo. X)	0.952	0.937	-	0.961	0.973
	Iliac left (Mo. Y)	0.927	0.943	-	0.993	0.993
	Iliac right (Mo. Y)	x	x	-	0.974	0.991

Table 26 CORA rating for each test with the third test (OSC-03-05) as reference

	Channel	OSC-03-03	OSC-03-04	OSC-03-05	OSC-03-06	AVG
OSC-03-06	Seat Pan (Displ. Z)	0.957	0.945	x	-	0.979
	Anti-Submarining Ramp (Displ. X)	0.931	0.913	0.978	-	0.973
	Upper Diag. Belt Force (B3)	0.973	0.993	0.982	-	0.994
	Lower Diag. Belt Force (B4)	0.960	0.982	0.990	-	0.996

	Lap-Belt outside Force (B6)	0.985	0.992	0.989	-	0.997
	Belt Pay-In/-Out	0.947	0.928	0.980	-	0.975
	Head COG (Acc. X)	0.924	0.960	0.968	-	0.985
	Head COG (Acc. Z)	0.976	0.963	0.976	-	0.993
	T4 (Acc. X)	0.940	0.914	0.903	-	0.978
	T4 (Acc. Z)	0.954	0.974	0.974	-	0.990
	T12 (Acc. X)	x	0.956	0.963	-	0.993
	T12 (Acc. Z)	x	0.985	0.984	-	0.995
	T12 (Fo. X)	0.675	0.846	0.849	-	0.916
	T12 (Fo. Z)	0.926	0.965	0.931	-	0.985
	T12 (Mo. Y)	0.986	0.993	0.988	-	0.998
	Pelvis (Acc. X)	0.921	0.950	0.958	-	0.981
	Pelvis (Acc. Z)	0.957	0.972	0.971	-	0.989
	Pelvis (Displ. X)	0.915	0.928	0.952	-	0.989
	Pelvis (Ang. Y)	0.689	0.957	0.963	-	0.922
	Iliac left (Fo. X)	0.949	0.971	0.944	-	0.976
	Iliac right (Fo. X)	0.973	0.989	0.964	-	0.992
	Iliac left (Mo. Y)	0.943	0.947	0.992	-	0.999
	Iliac right (Mo. Y)	x	x	0.972	-	0.991

Table 27 CORA rating for each test with the last test (OSC-03-06) as reference

1.3.3 Validated Virtual Demonstrators versus Second Test Series

1.3.3.1 Upright Seating Position with SOTA Belt (OSC-01-FW-UPR)

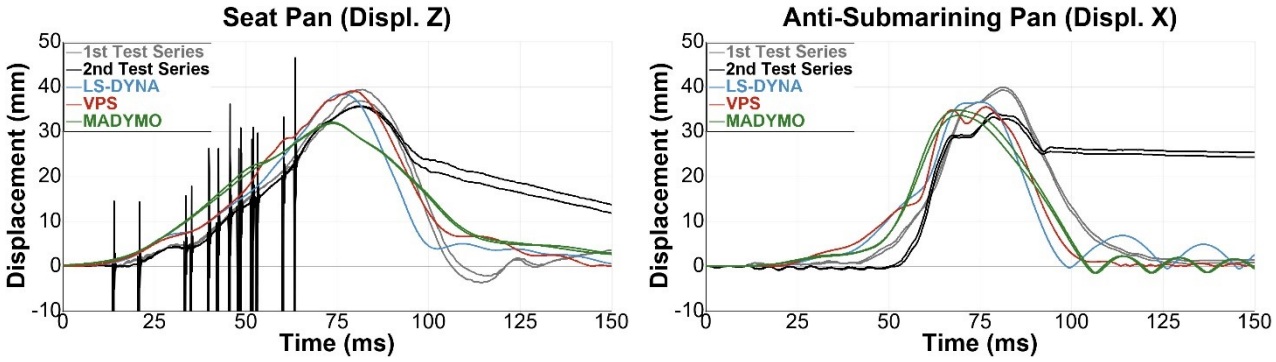

Figure 204 Seat pan and anti-submarining ramp displacements

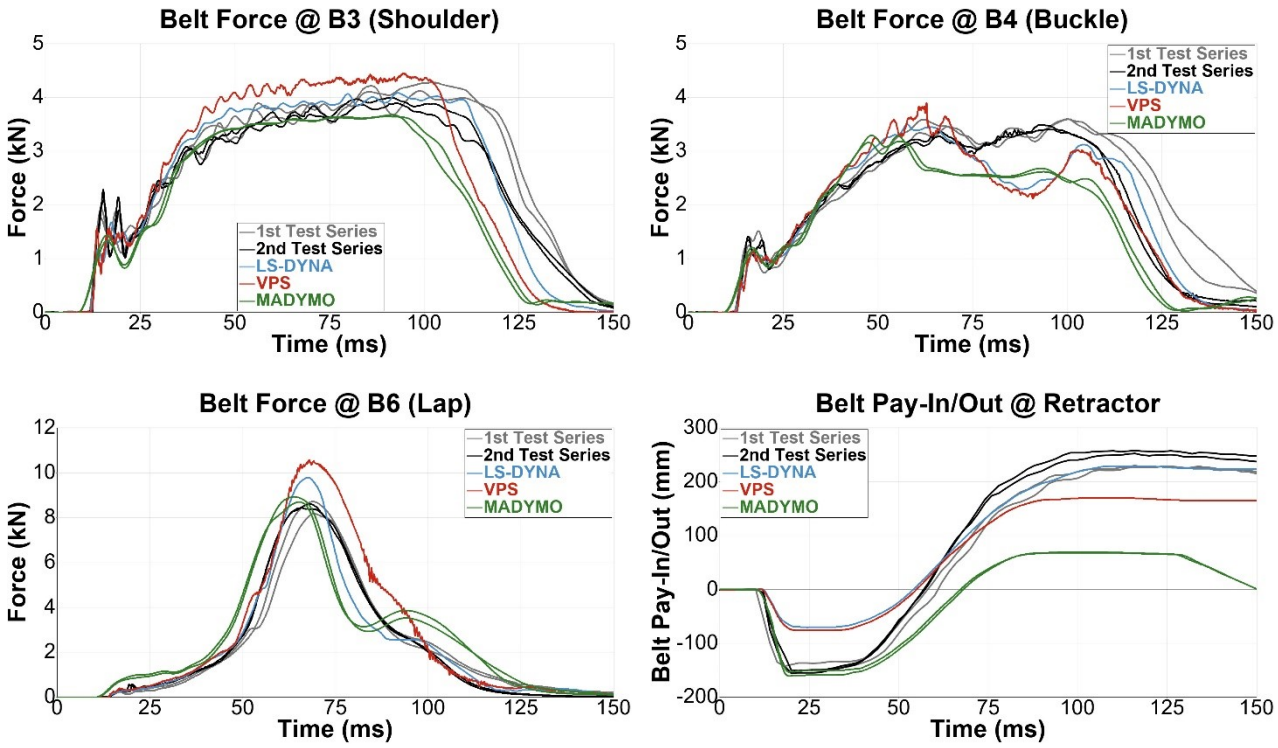

Figure 205 Seat belt forces and shoulder retractor belt pay-in/-out

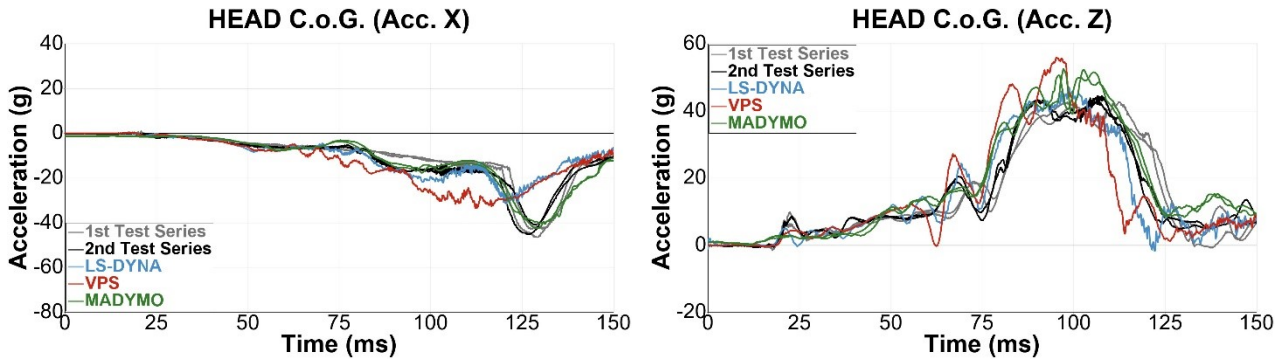

Figure 206 Head COG accelerations

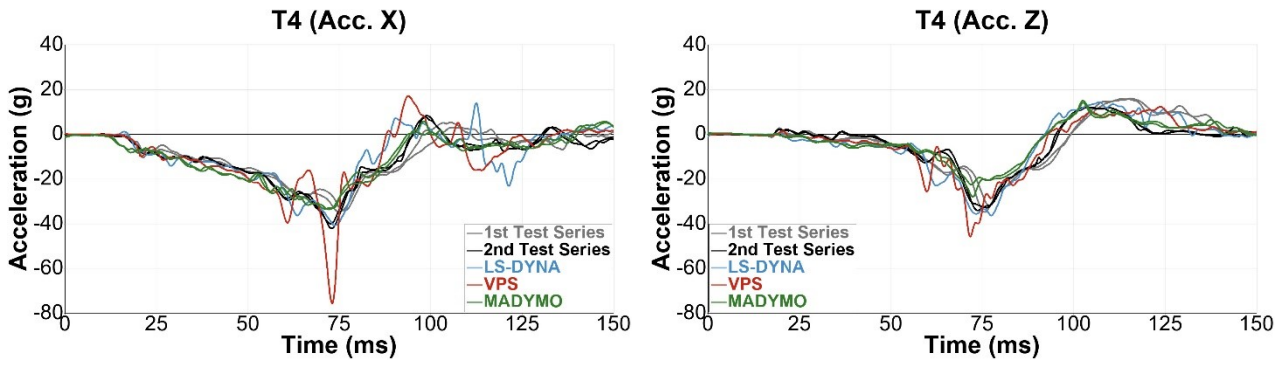

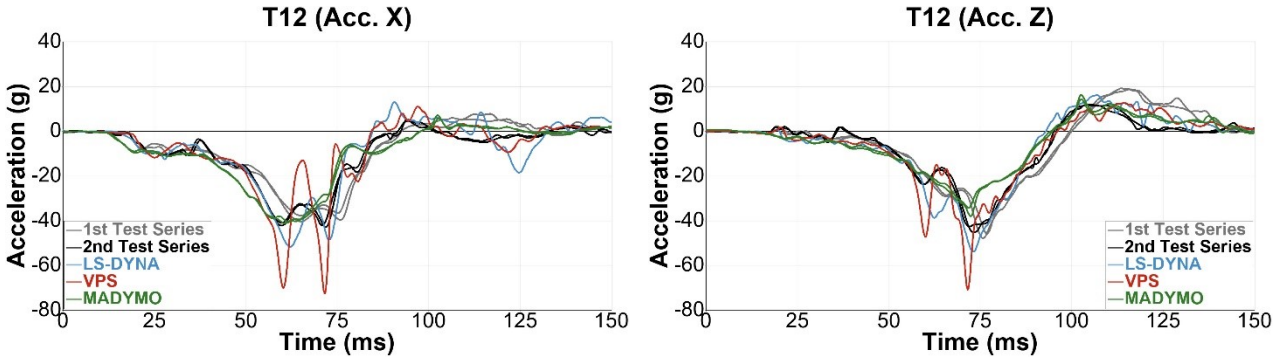

Figure 207 T4 and T12 accelerations

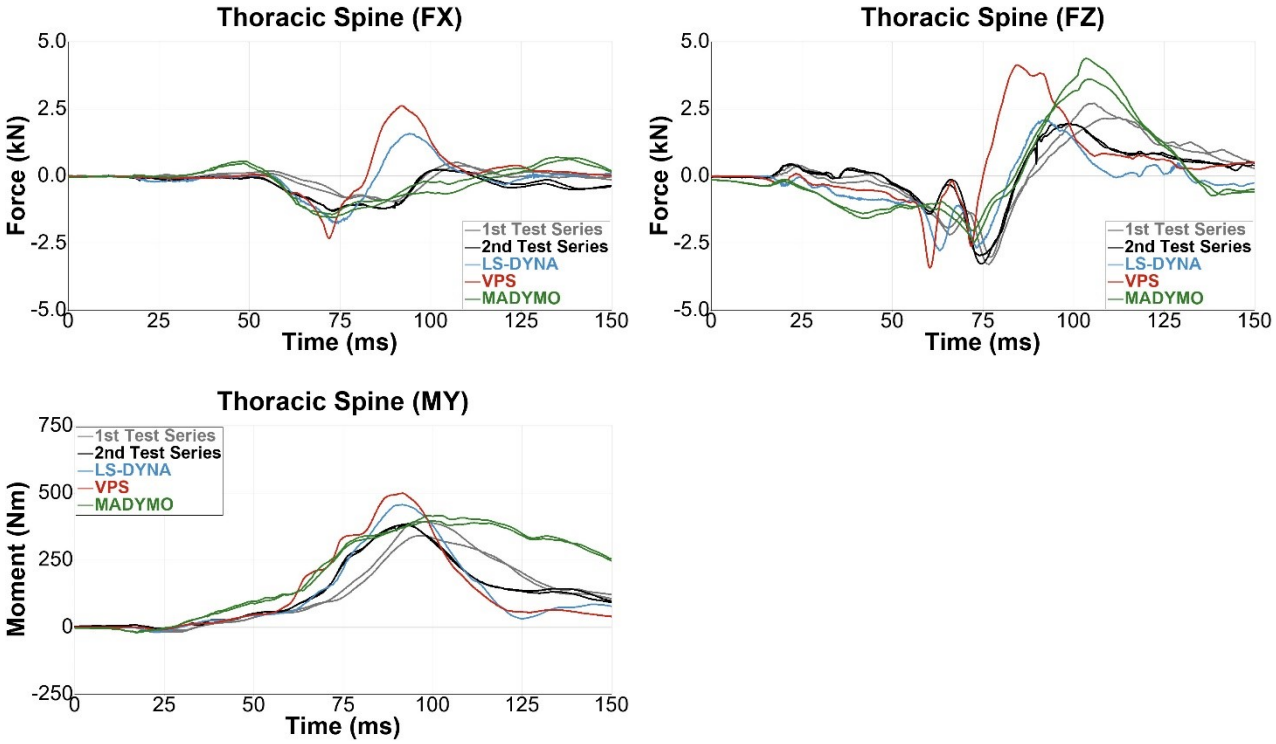

Figure 208 Lower thoracic spine forces and moments

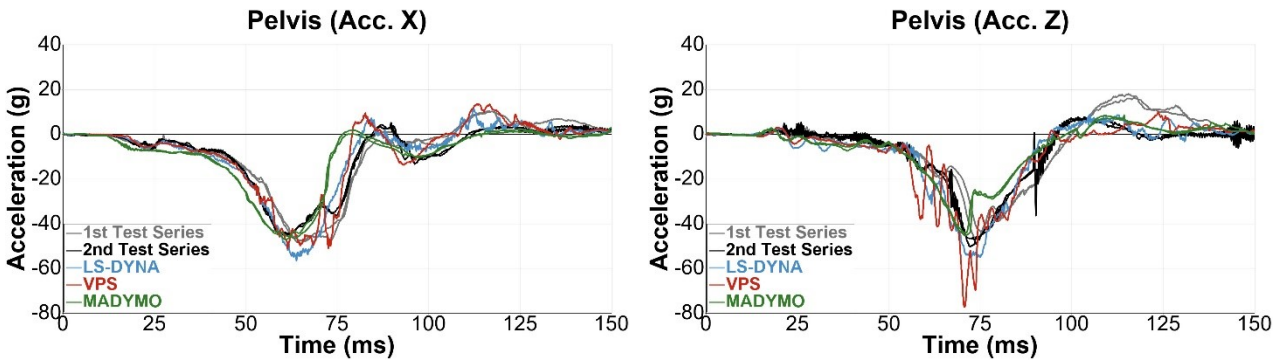

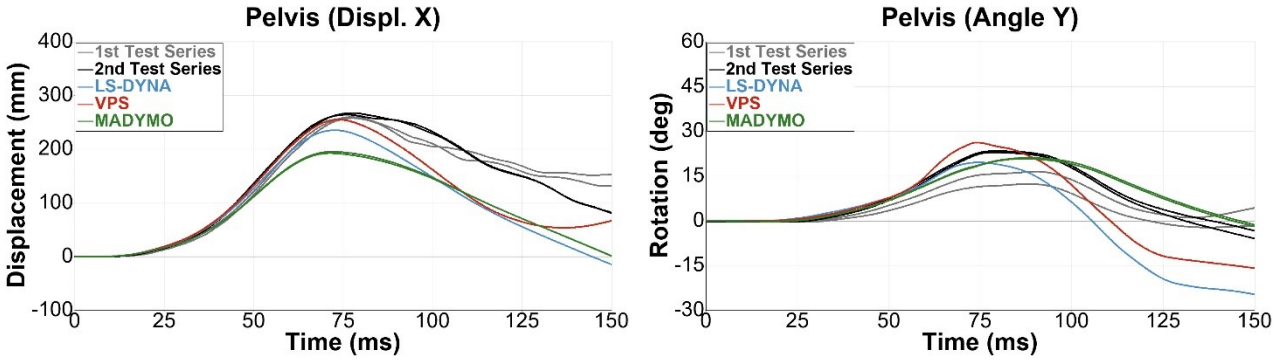

Figure 209 Pelvis accelerations, X-displacement and Y-angle

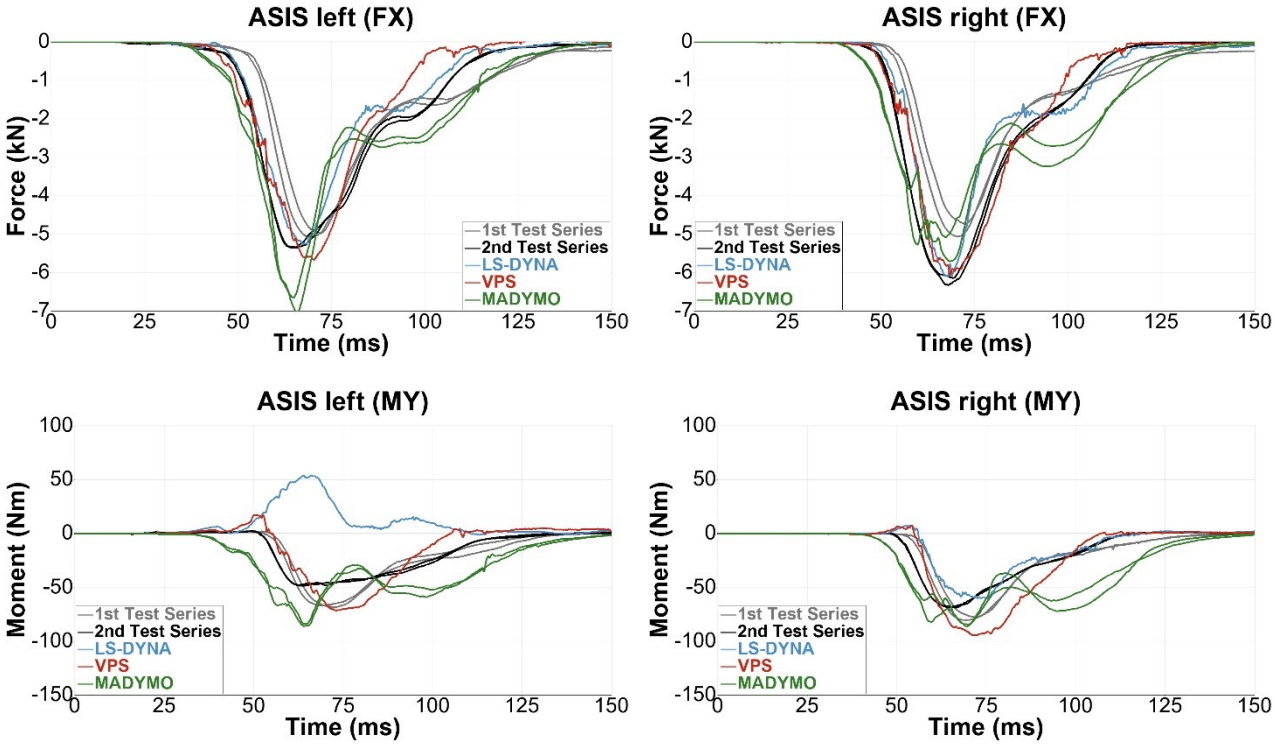

Figure 210 ASIS X-forces and Y-moments

1.3.3.2 Reclined Seating Position with SOTA DLPT Belt (OSC-03-FW-REC)

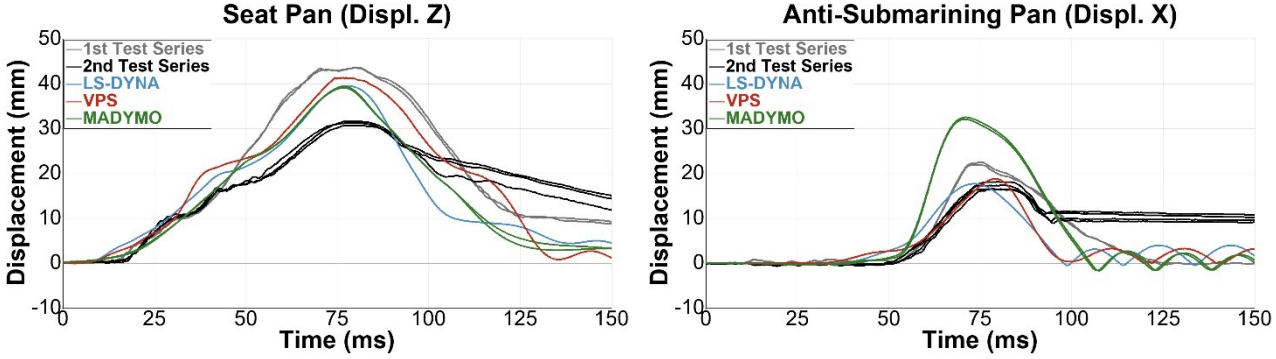

Figure 211 Seat pan and anti-submarining ramp displacements

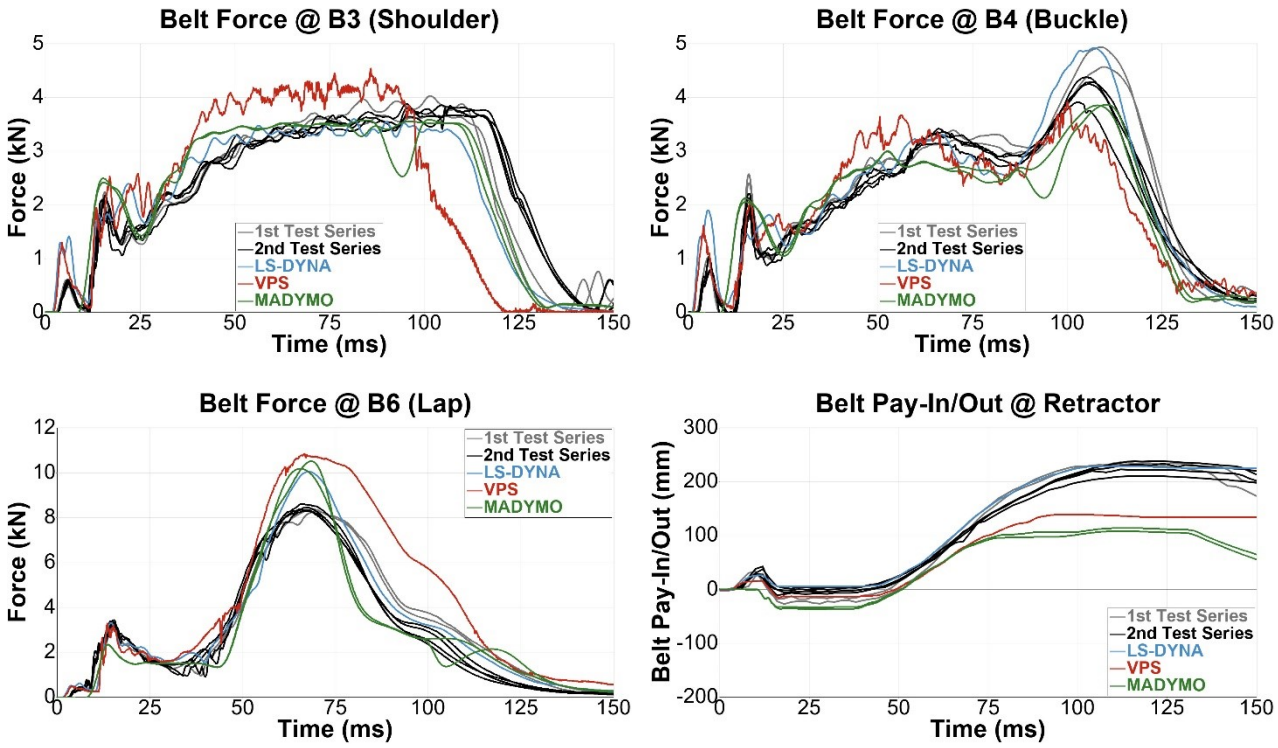

Figure 212 Seat belt forces and shoulder retractor belt pay-in/-out

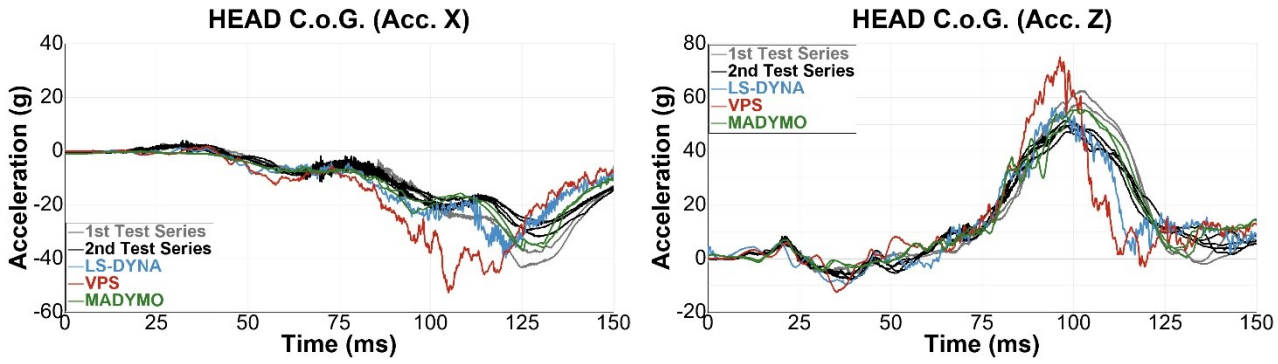

Figure 213 Head COG accelerations

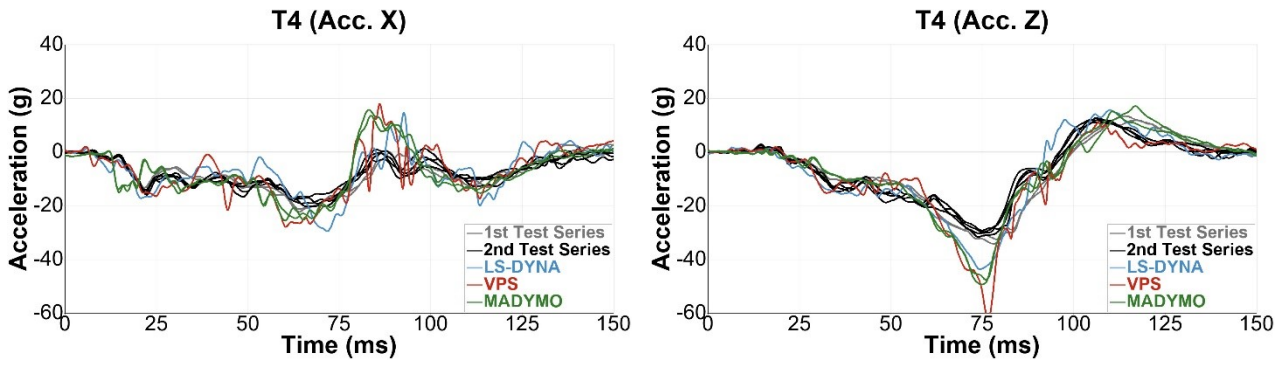

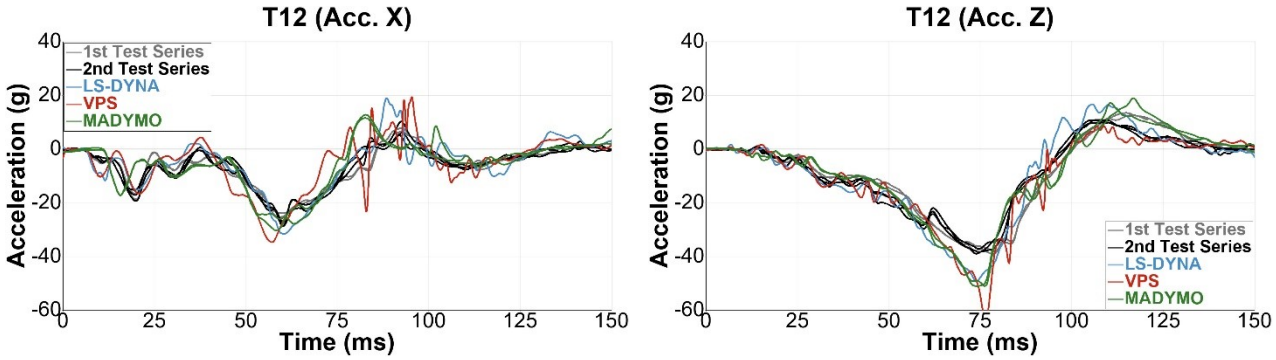

Figure 214 T4 and T12 accelerations

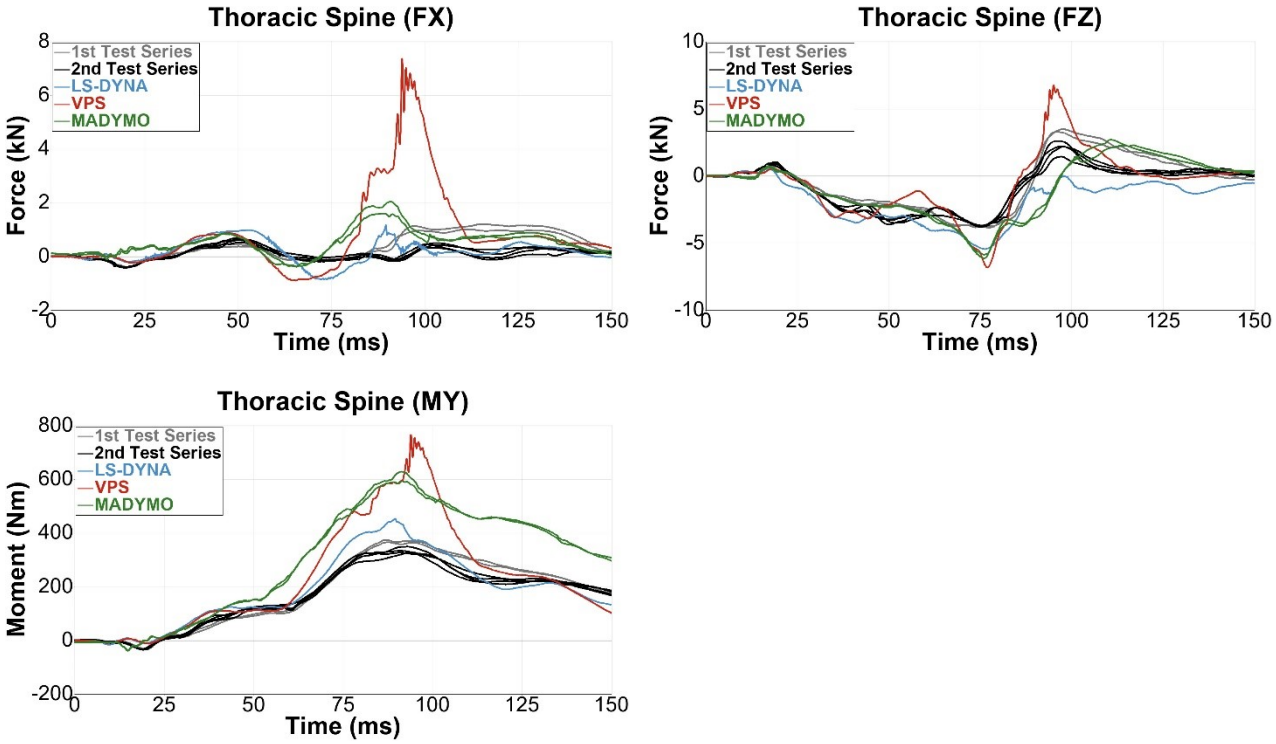

Figure 215 Lower thoracic spine forces and moments

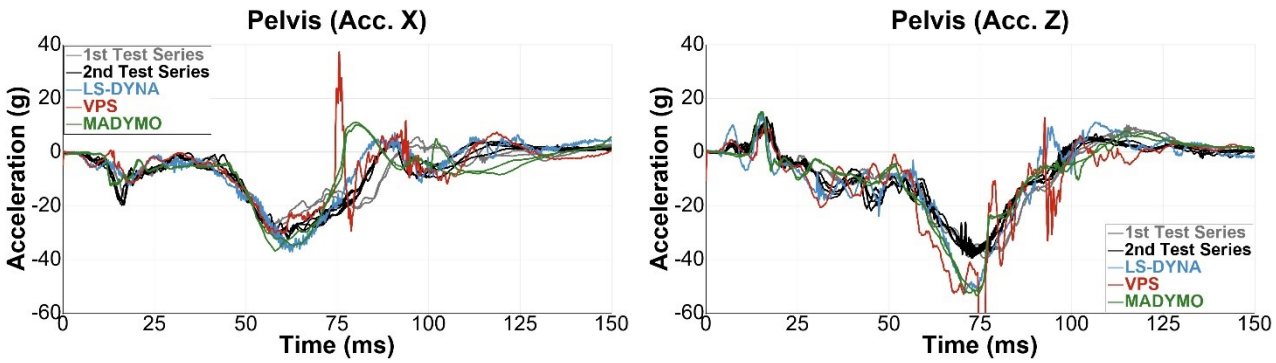

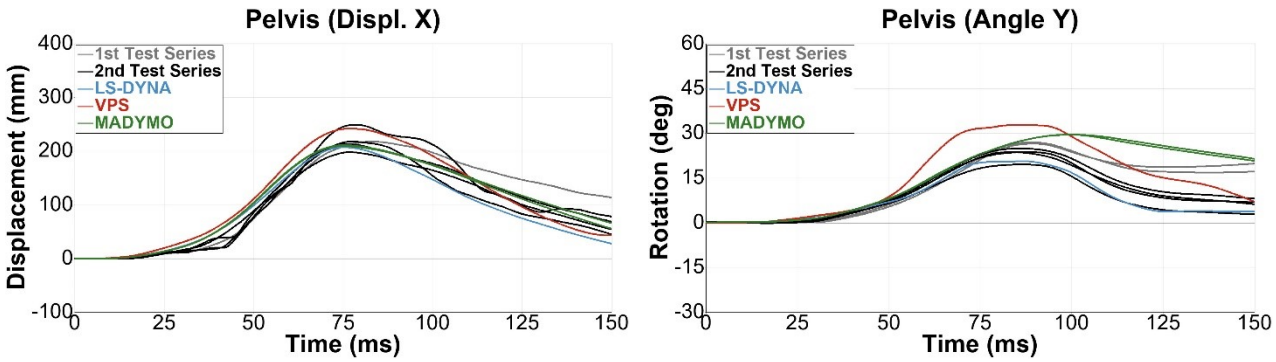

Figure 216 Pelvis accelerations, X-displacement and Y-angle

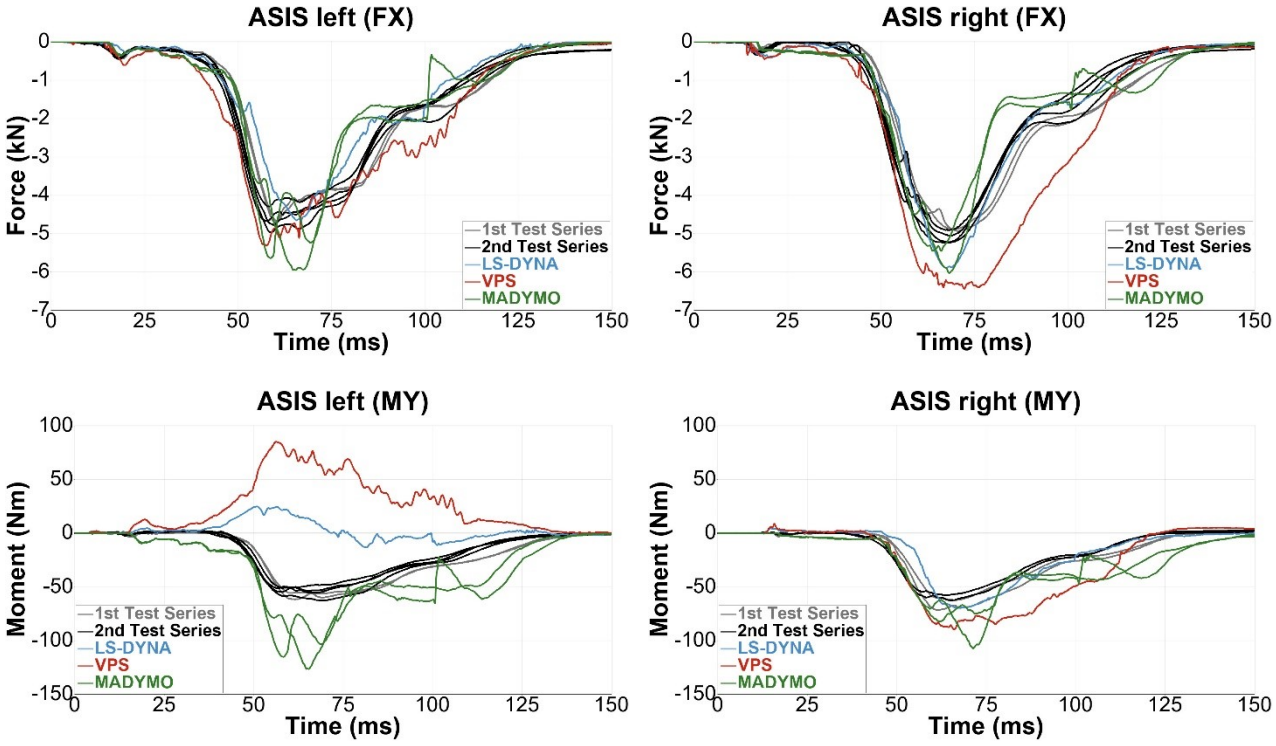

Figure 217 ASIS X-forces and Y-moments

2 PROTECTION PRINCIPLE 2: PRE-ROTATED SEAT - SEAT INERTIA

2.1 Dimensions of Swivel Seat

Positions relative to PP2 H-point coordinate system			
	x [mm]	y [mm]	z [mm]
H-Point	0	0	0
R1	210	210	-305
R2	-20	210	-305
R3	-250	210	-305
COG without footrest	40	15	-85
COG with footrest (F5%)	-60	15	-95
COG with footrest (M50%)	-72	15	-95
COG with footrest (M95%)	85	15	-95

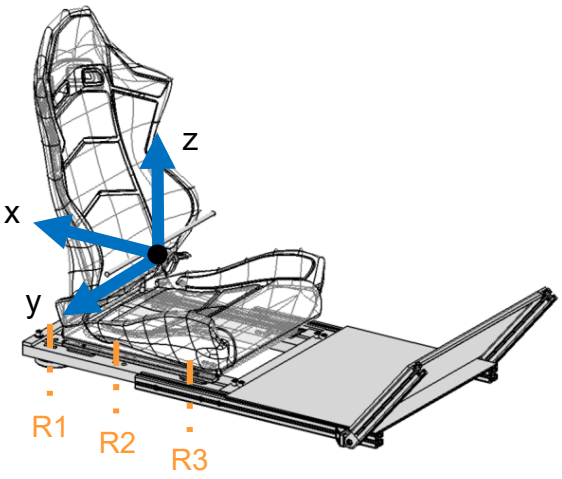

Figure 218 Dimensions of swivel seat relative to H-point

2.2 Sensors / Channels

Location	Parameter	Number of Channels
Sled CoG	Accelerations: A_x, A_y, A_z	3
Passenger Seatbelt Shoulder Section	Force: F_diagonal	1
Seat rotation axis	Angular Velocity	1
Head	Accelerations: A_x, A_y, A_z	3
Neck Upper	Forces: F_x, F_y, F_z	3
Neck Upper	Moments: M_x, M_y, M_z	3
Chest	Accelerations: A_x, A_y, A_z	3
Pelvis	Accelerations: A_x, A_y, A_z	3
		20

Figure 219 Sensors / channels considered for PP2 test series

2.3 Dummy Loadings - HIII 5th percentile female

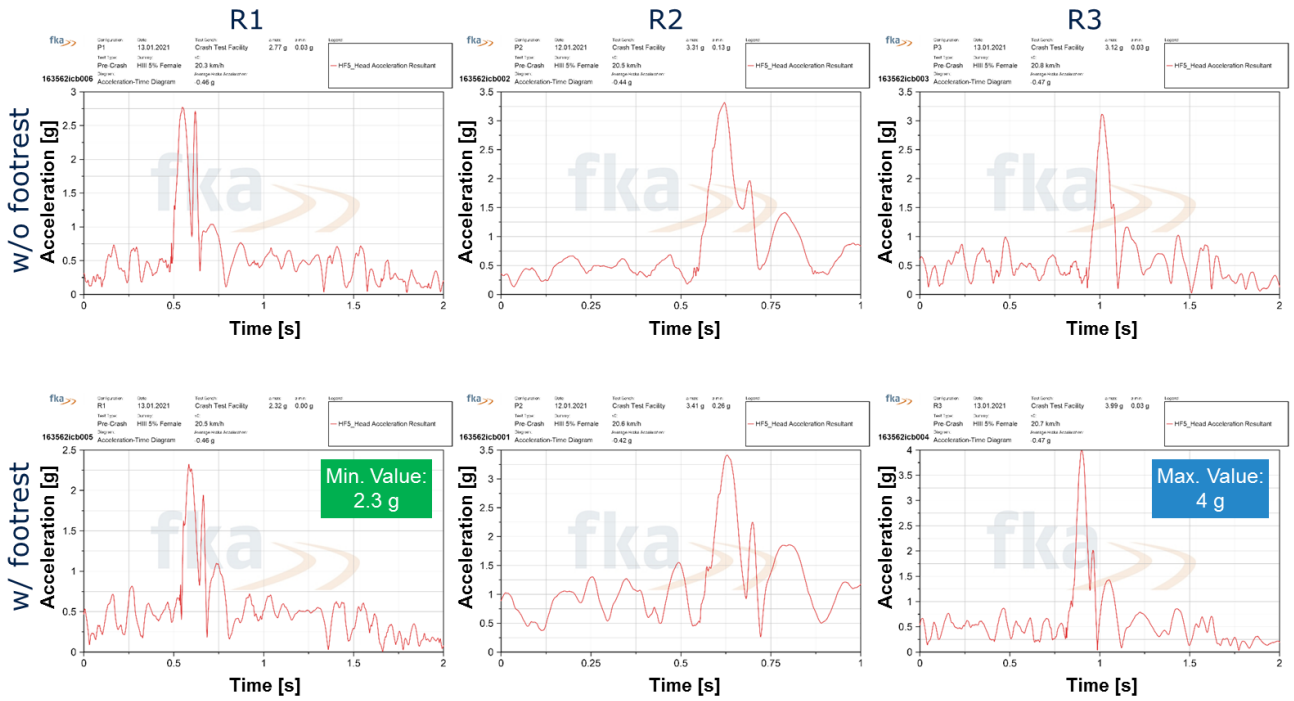

Figure 220 HIII 5th perc. female - head acceleration (res.) - R1, R2, R3 - without & with footrest

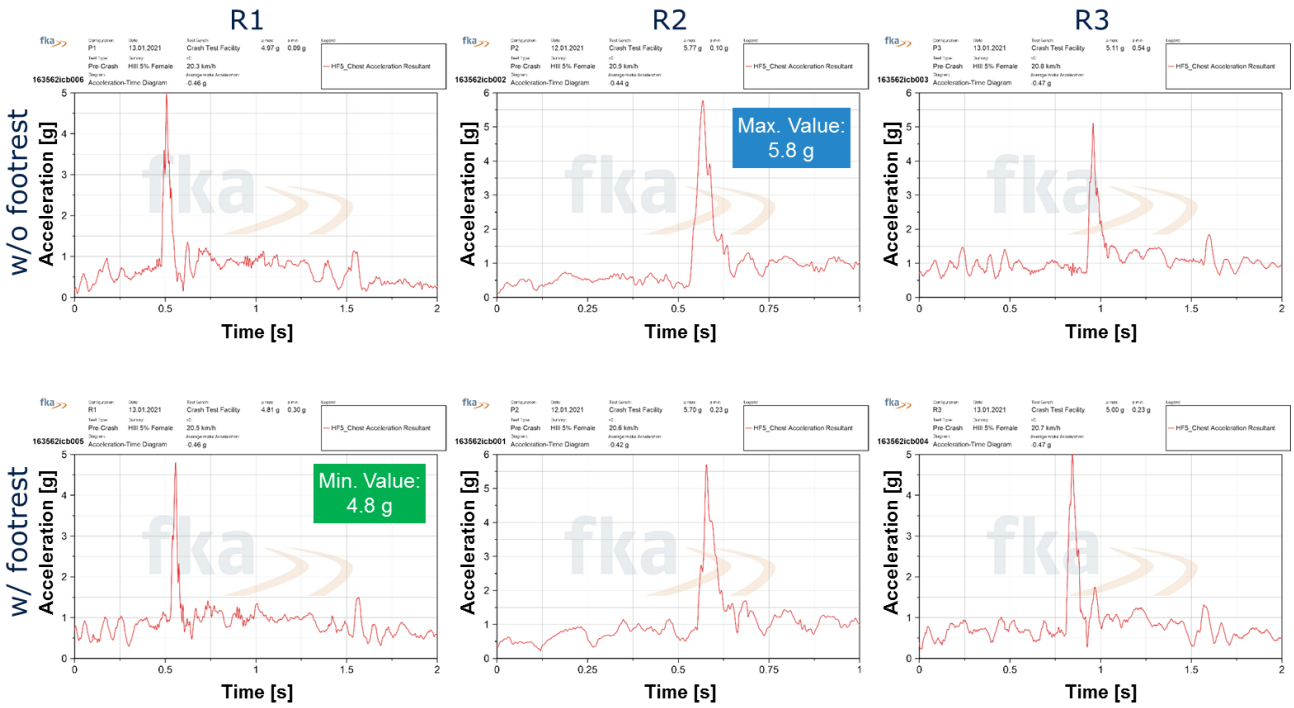

Figure 221 HIII 5th perc. female - chest acceleration (res.) - R1, R2, R3 - without & with footrest

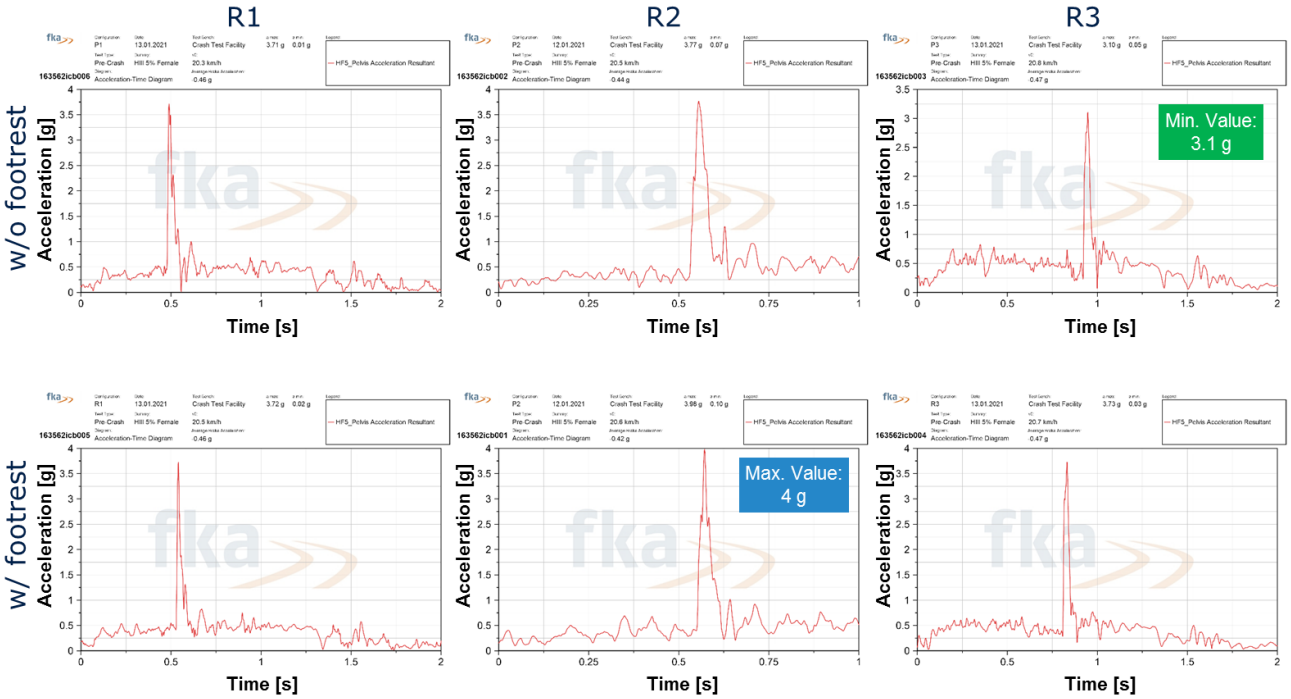

Figure 222 HIII 5th perc. female - pelvis acceleration (res.) - R1, R2, R3 - without & with footrest

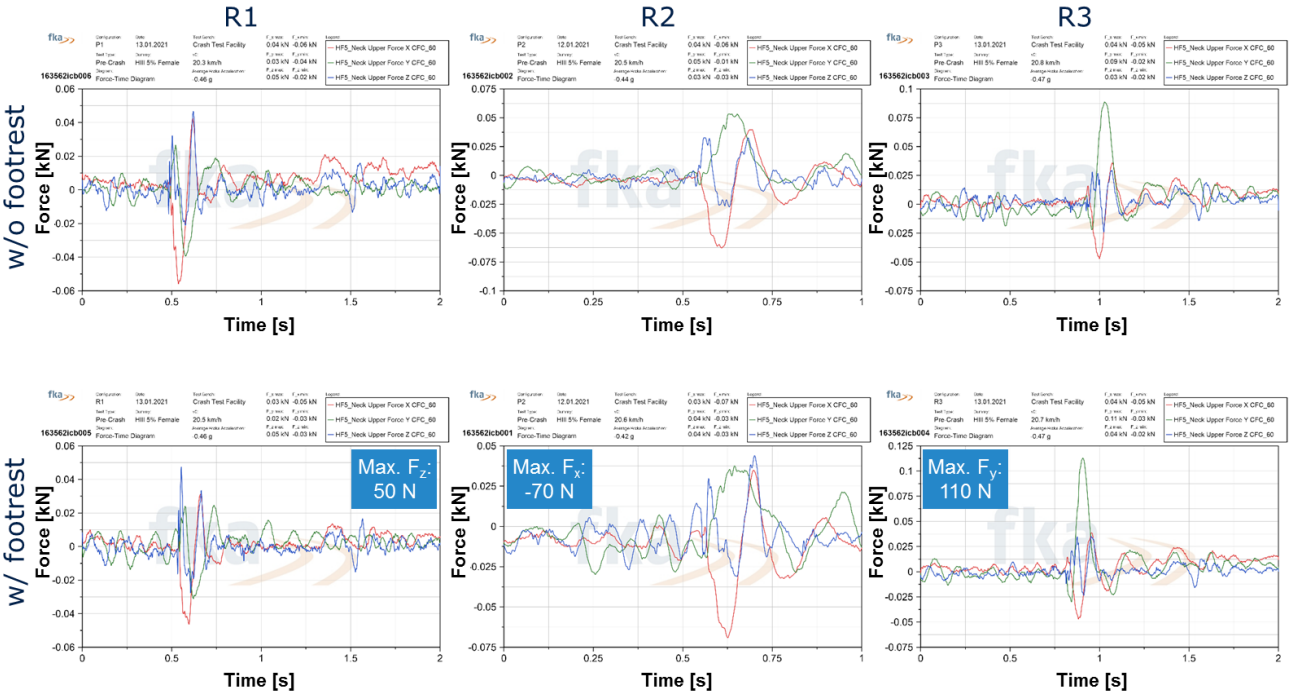

Figure 223 HIII 5th perc. female - upper neck force (x, y, z) - R1, R2, R3 - without & with footr.

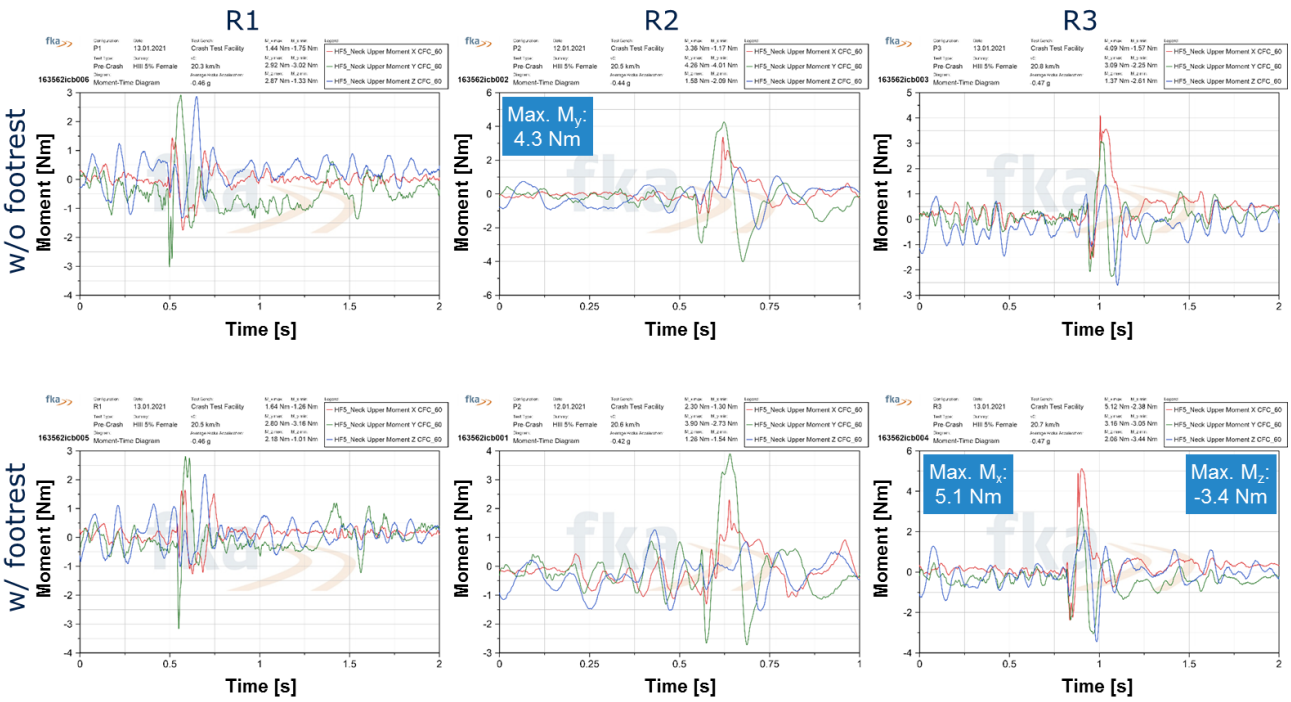

Figure 224 HIII 5th perc. female - upper neck mom. (x, y, z) - R1, R2, R3 - without & with footr.

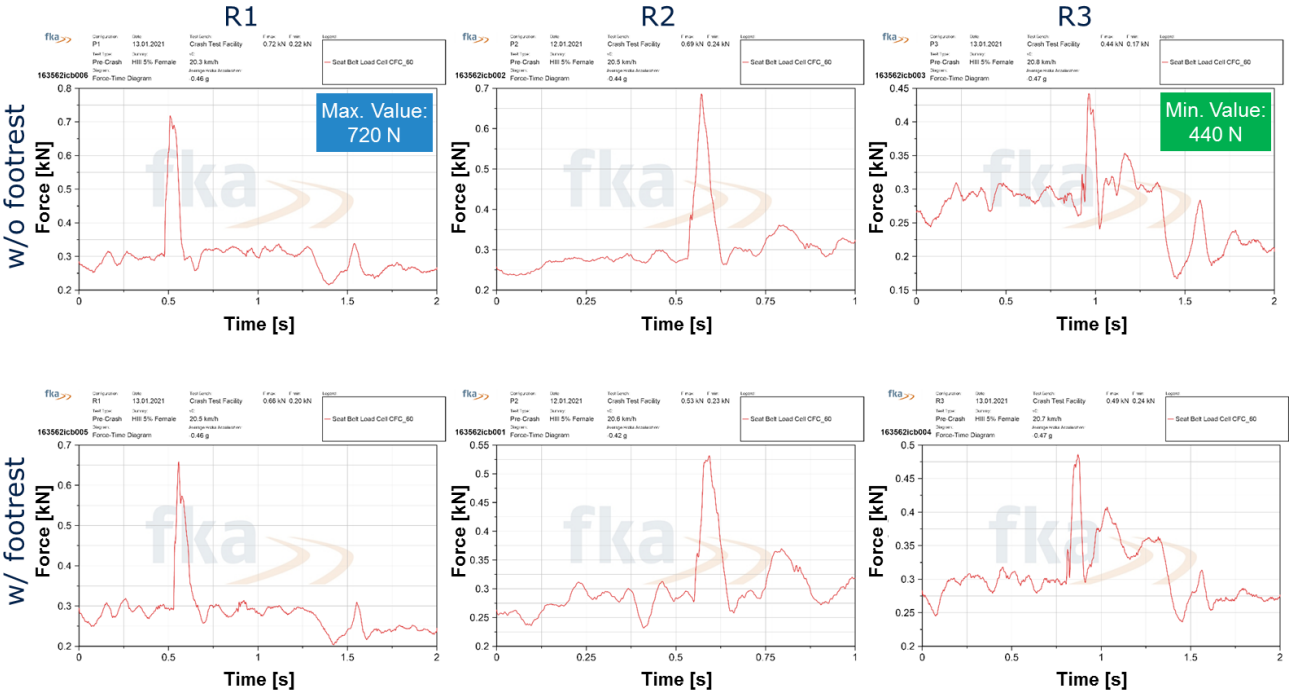

Figure 225 HIII 5th perc. female - seat belt force - R1, R2, R3 - without & with footrest

2.4 Dummy Loadings - HIII 50th percentile male

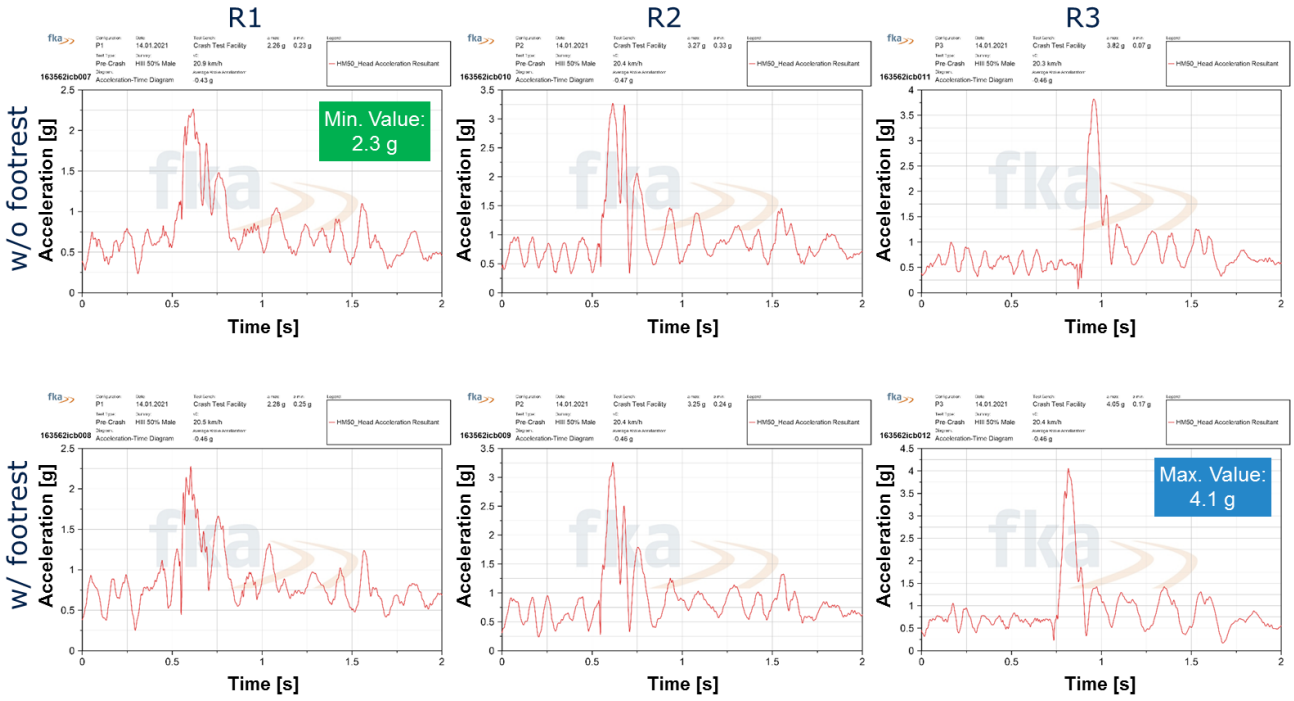

Figure 226 HIII 50th perc. male - head acceleration (res.) - R1, R2, R3 - without & with footrest

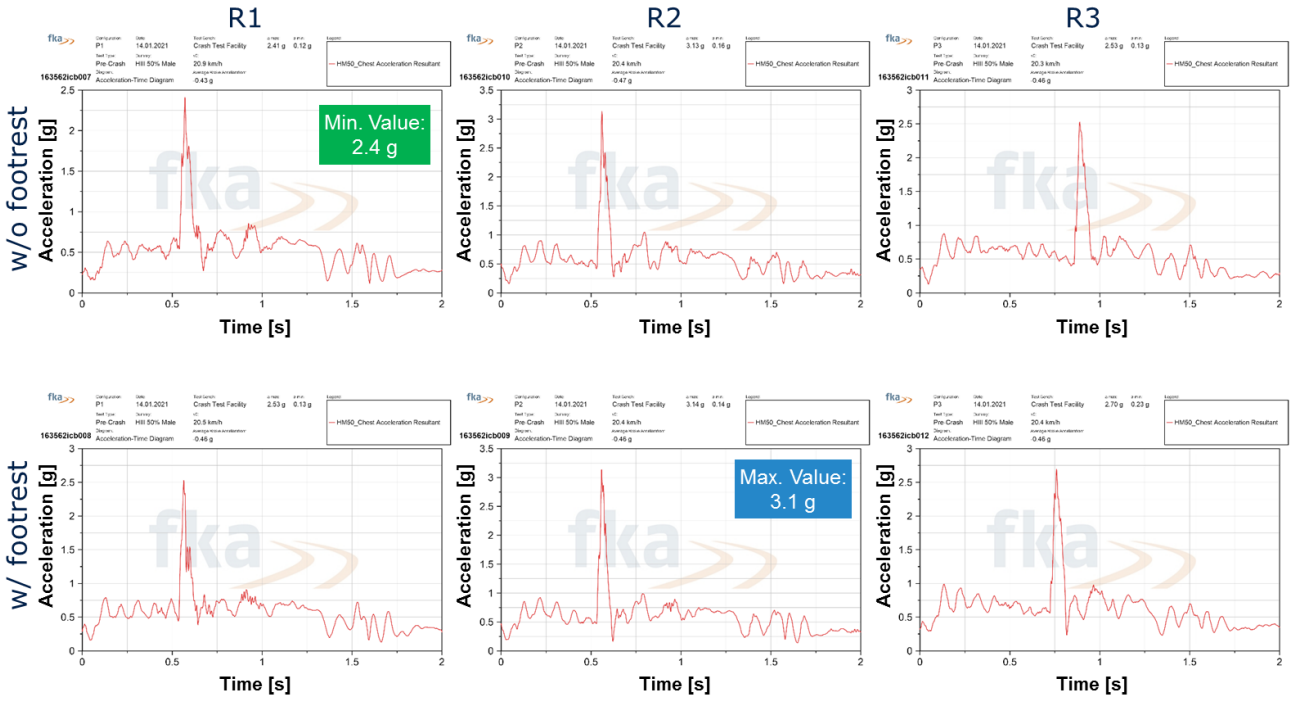

Figure 227 HIII 50th perc. male - chest acceleration (res.) - R1, R2, R3 - without & with footrest

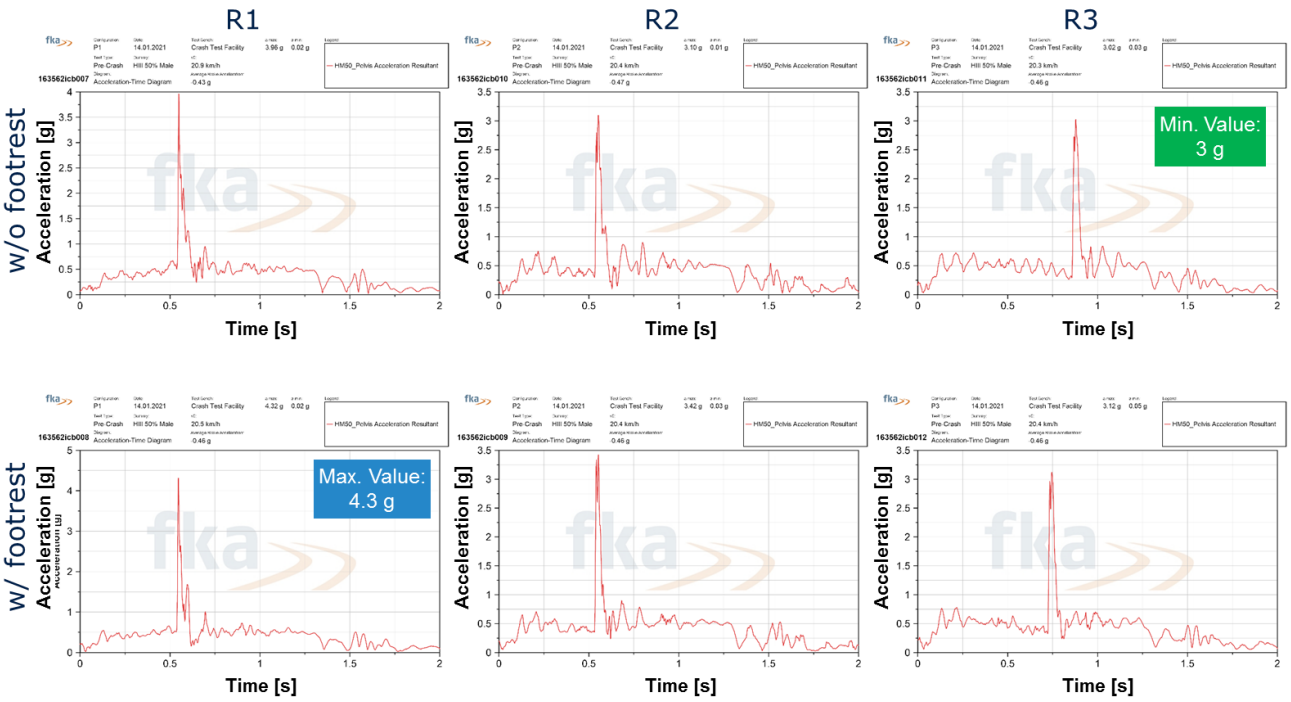

Figure 228 HIII 50th perc. male - pelvis acceleration (res.) - R1, R2, R3 – without & with footrest

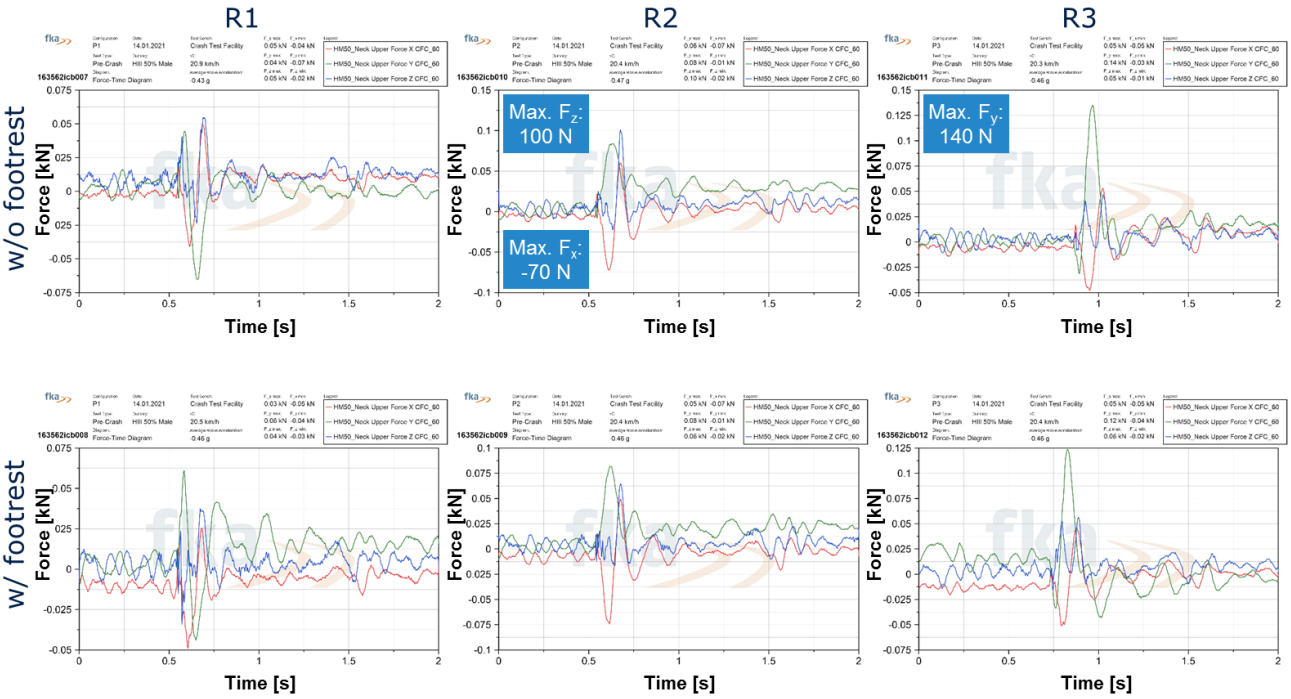

Figure 229 HIII 50th perc. male - upper neck force (x, y, z) - R1, R2, R3 - without & with footrest

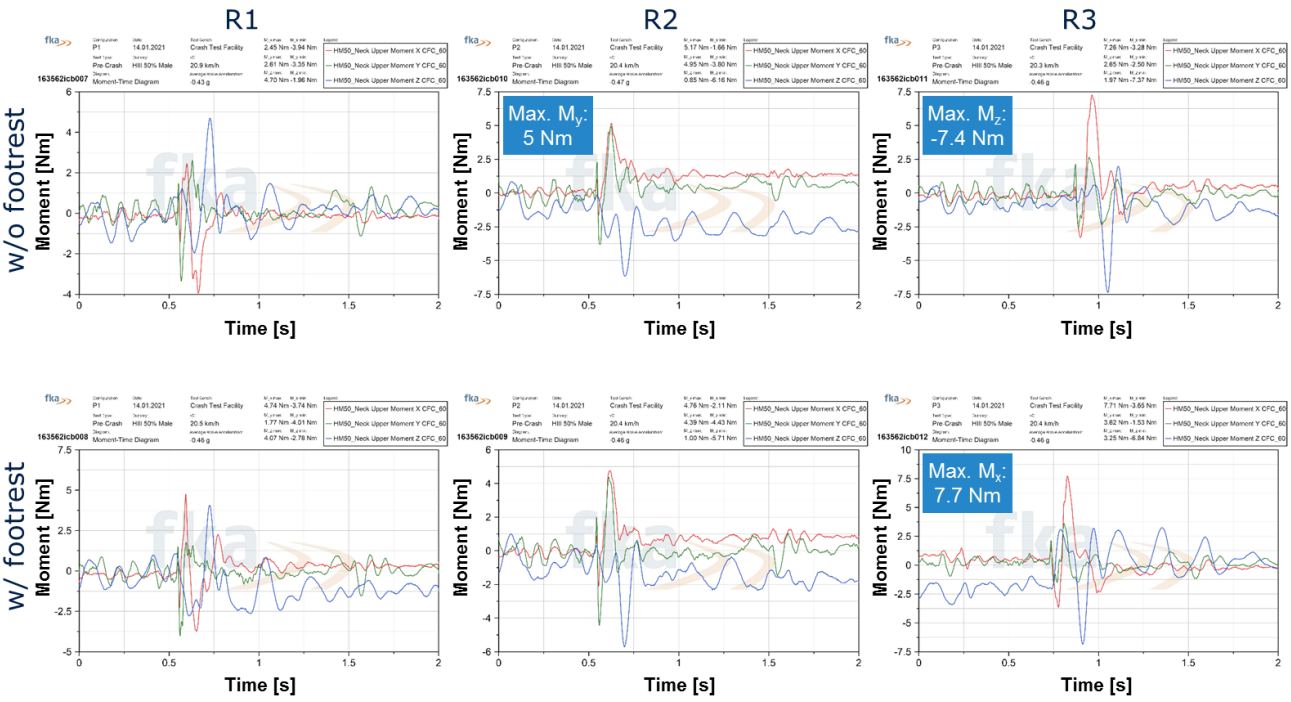

Figure 230 HIII 50th perc. male - upper neck mom. (x, y, z) - R1, R2, R3 - without & with footr.

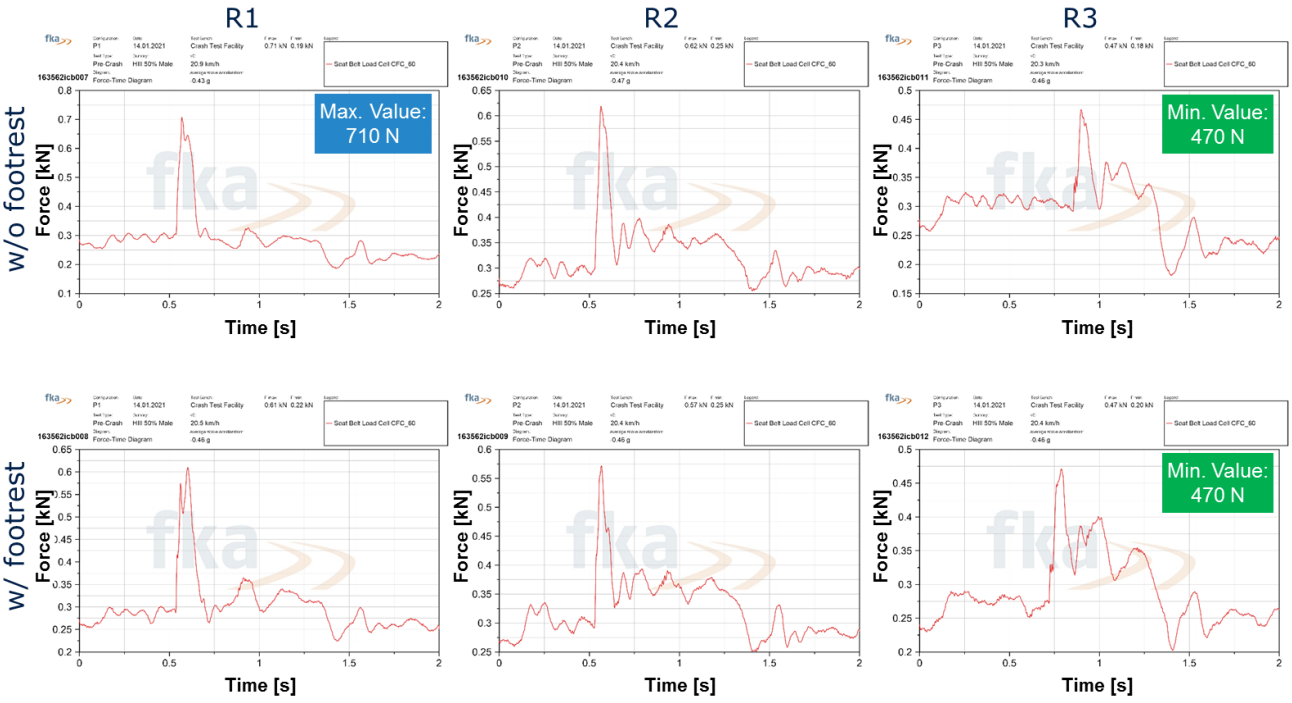

Figure 231 HIII 50th perc. male - seat belt force - R1, R2, R3 - without & with footrest

2.5 Dummy Loadings - HIII 95th percentile male

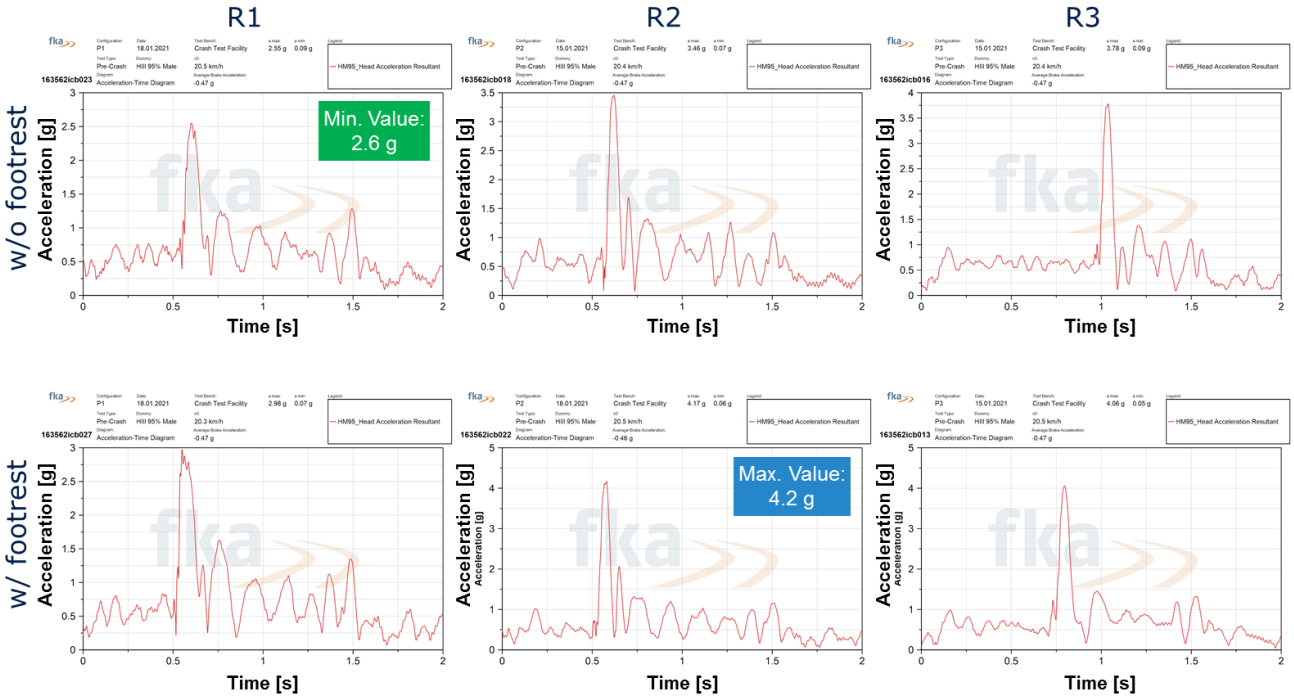

Figure 232 HIII 95th perc. male - head acceleration (res.) - R1, R2, R3 - without & with footrest

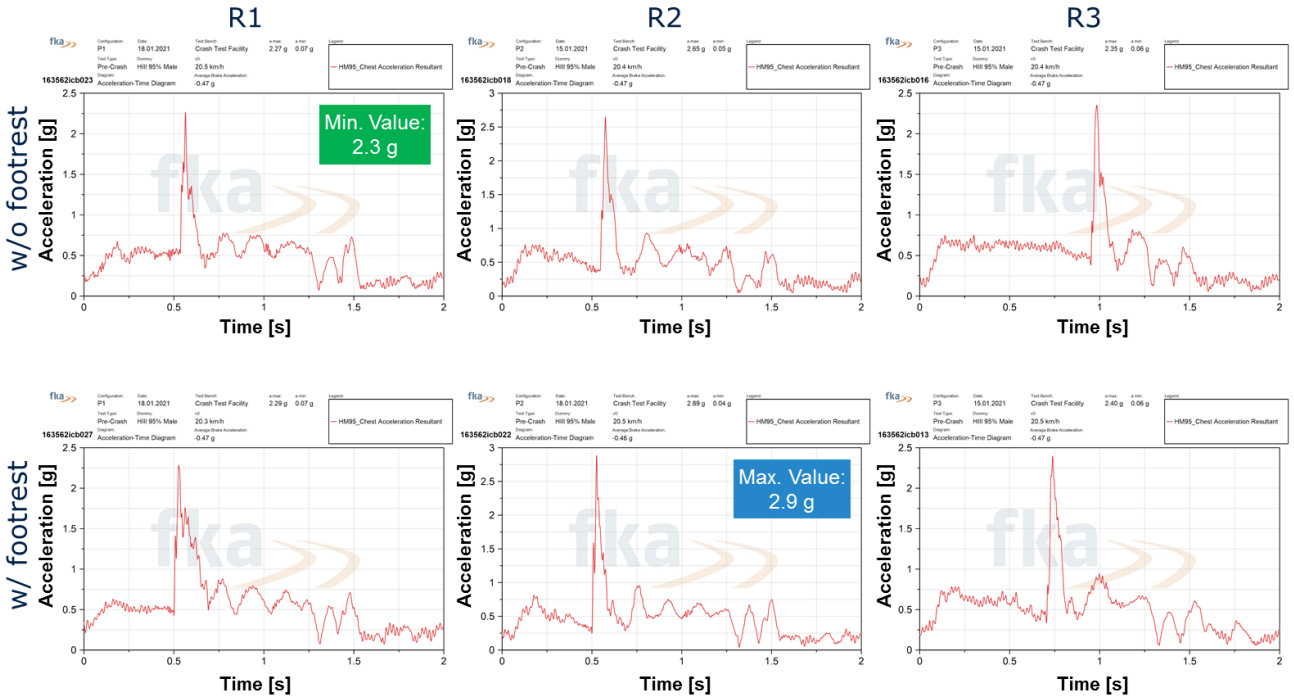

Figure 233 HIII 95th perc. male - chest acceleration (res.) - R1, R2, R3 - without & with footrest

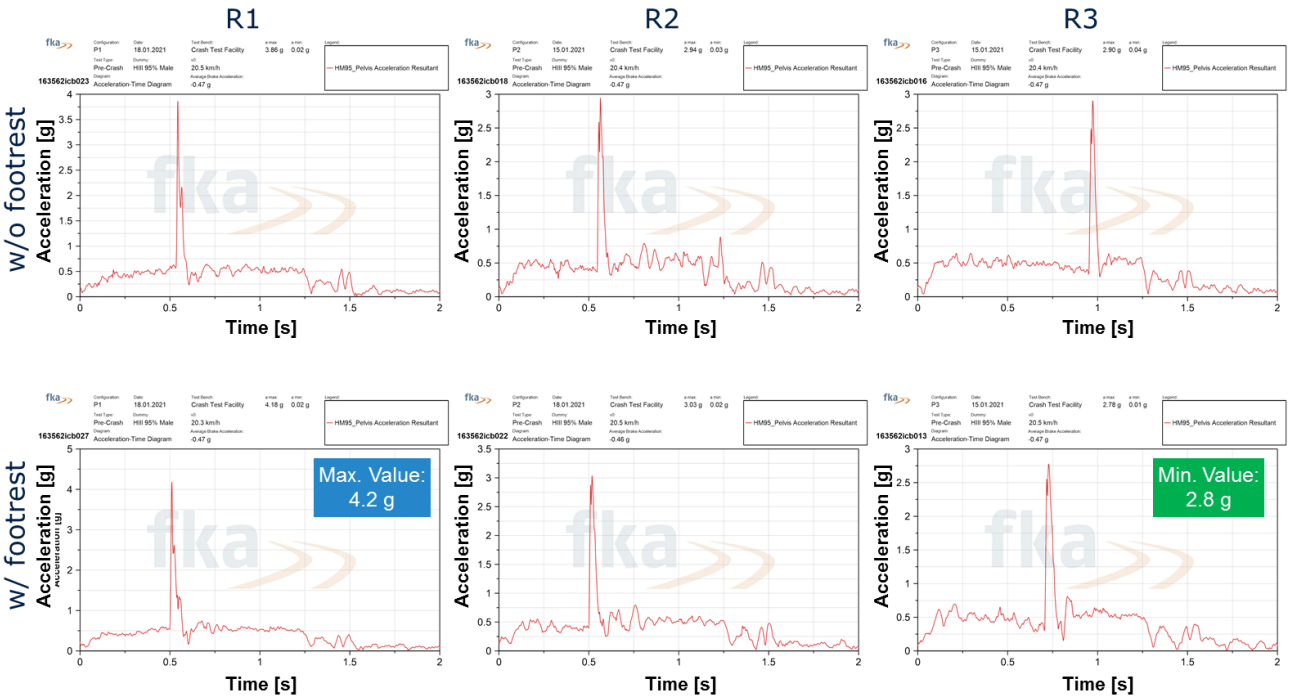

Figure 234 HIII 95th perc. male - pelvis acceleration (res.) - R1, R2, R3 - without & with footrest

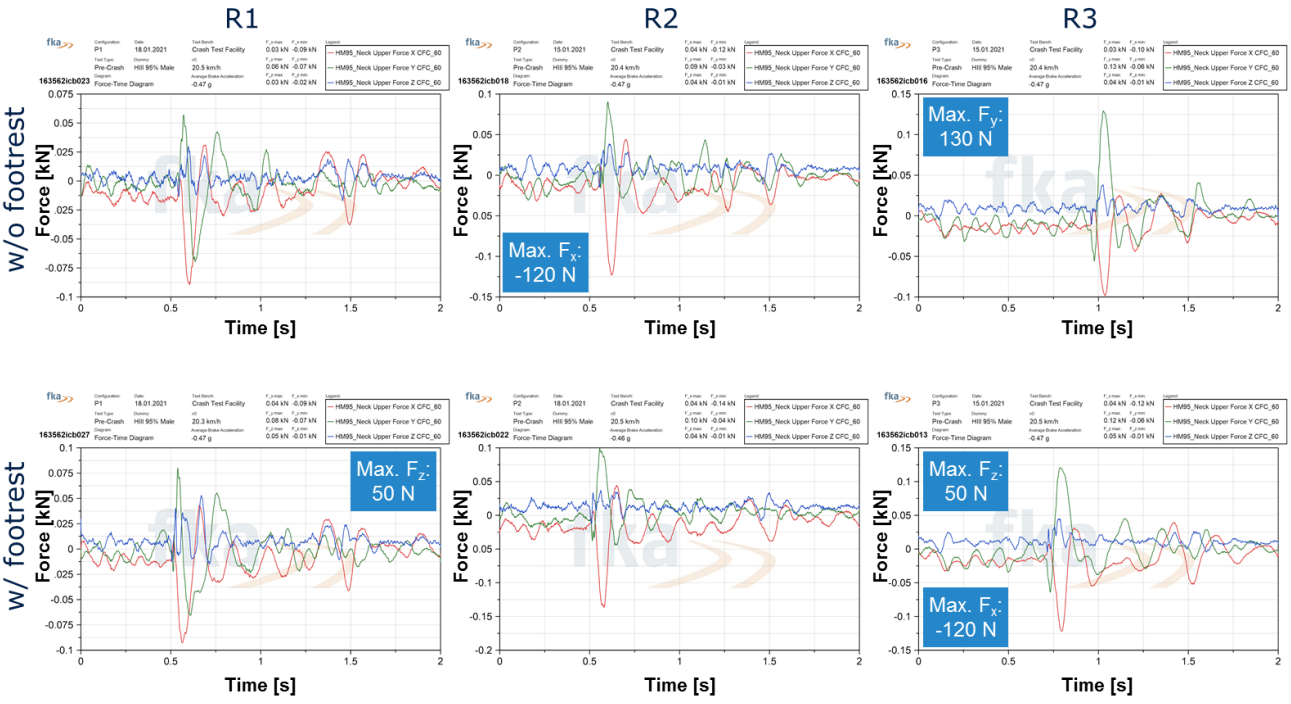

Figure 235 HIII 95th perc. male - upper neck force (x, y, z) - R1, R2, R3 - without & with footrest

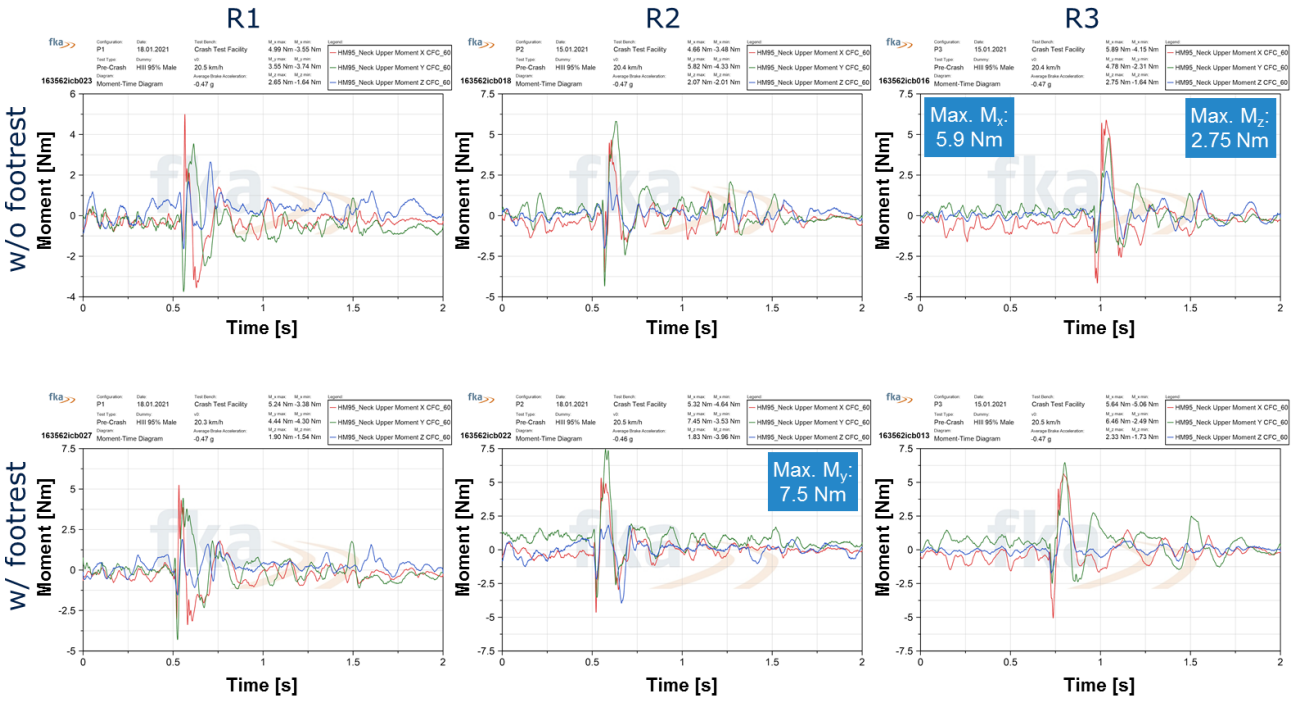

Figure 236 HIII 95th perc. male - upper neck mom. (x, y, z) - R1, R2, R3 - without & with footr.

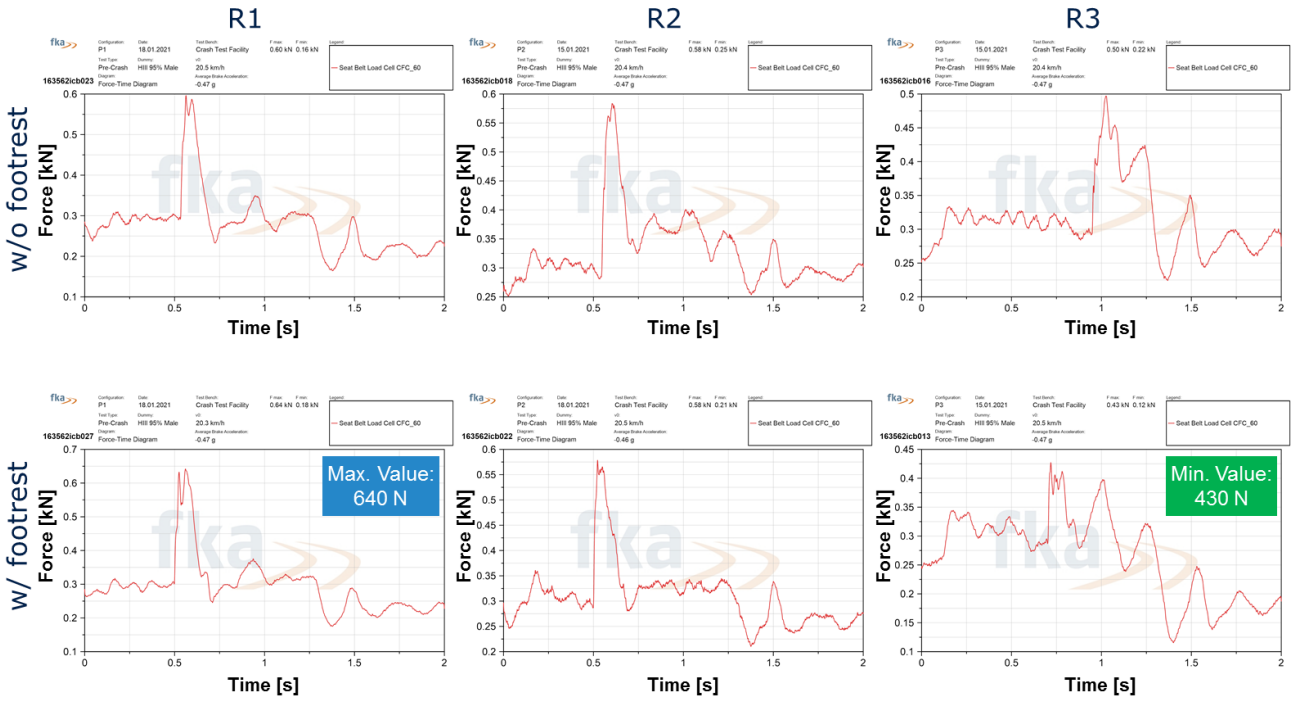

Figure 237 HIII 95th perc. male - seat belt force - R1, R2, R3 - without & with footrest

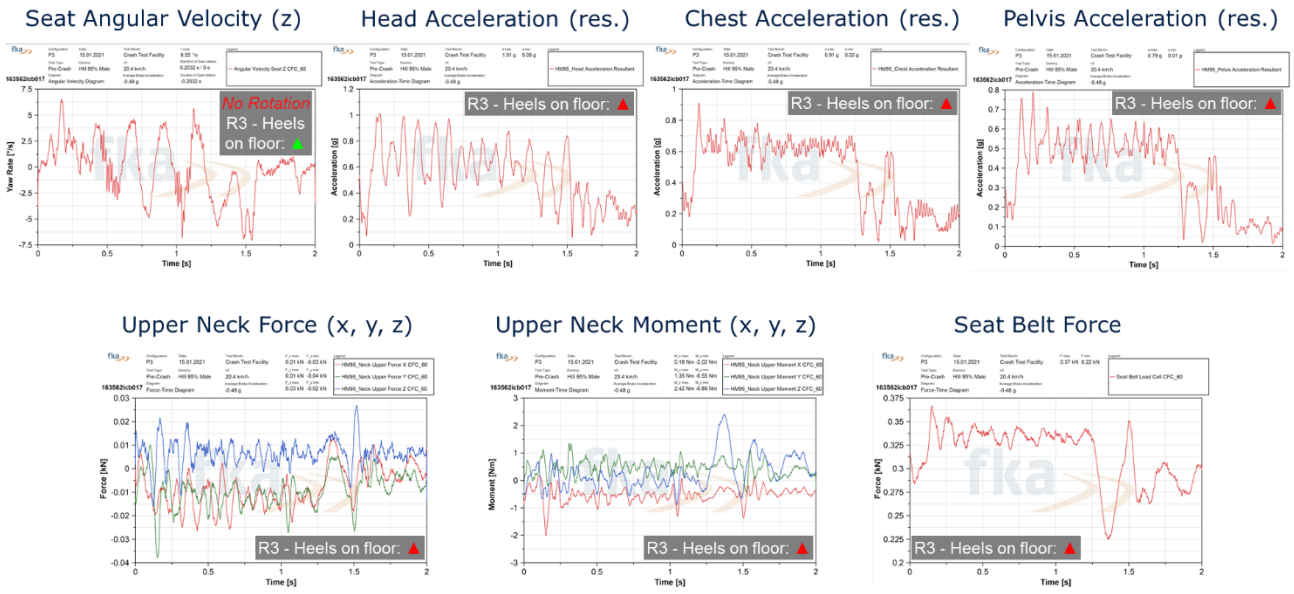

Figure 238 HIII 95th perc. male - shoe soles on floor (R3)

2.6 Dummy Loadings - Obese ATD BMI 35 male

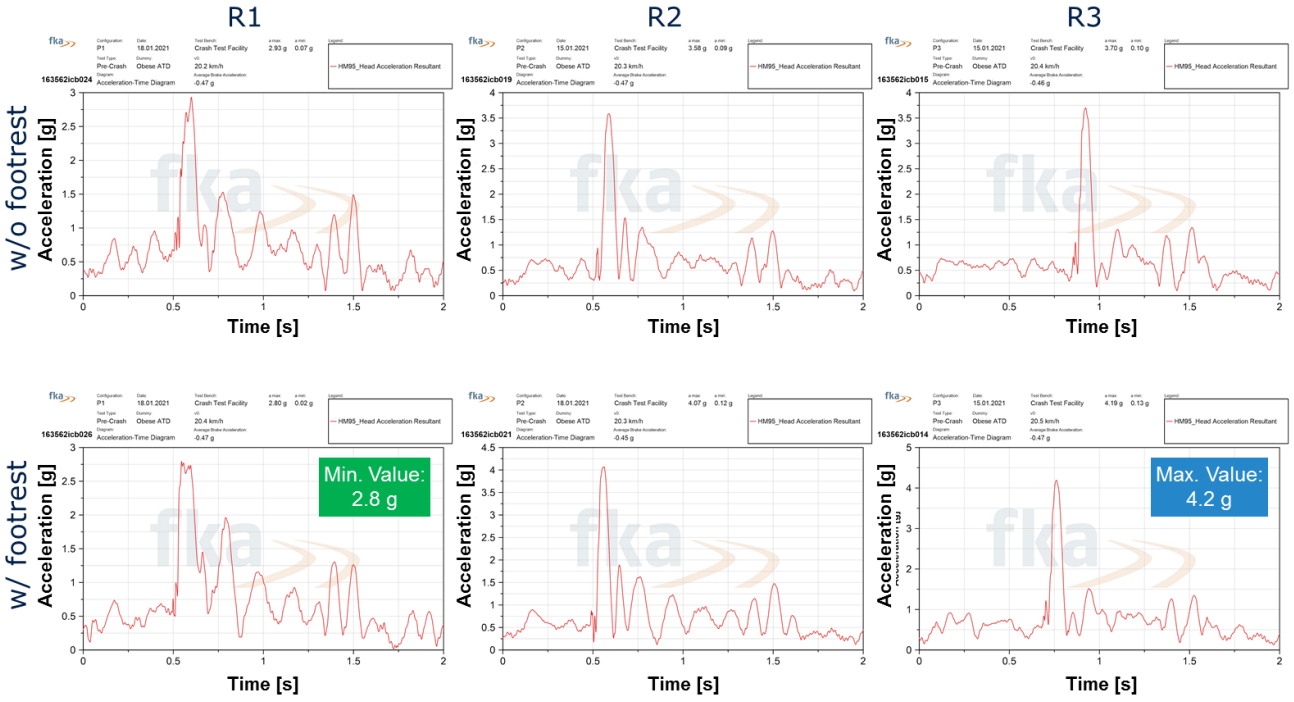

Figure 239 Obese BMI 35 male - head acceleration (res.) - R1, R2, R3 - without & with footrest

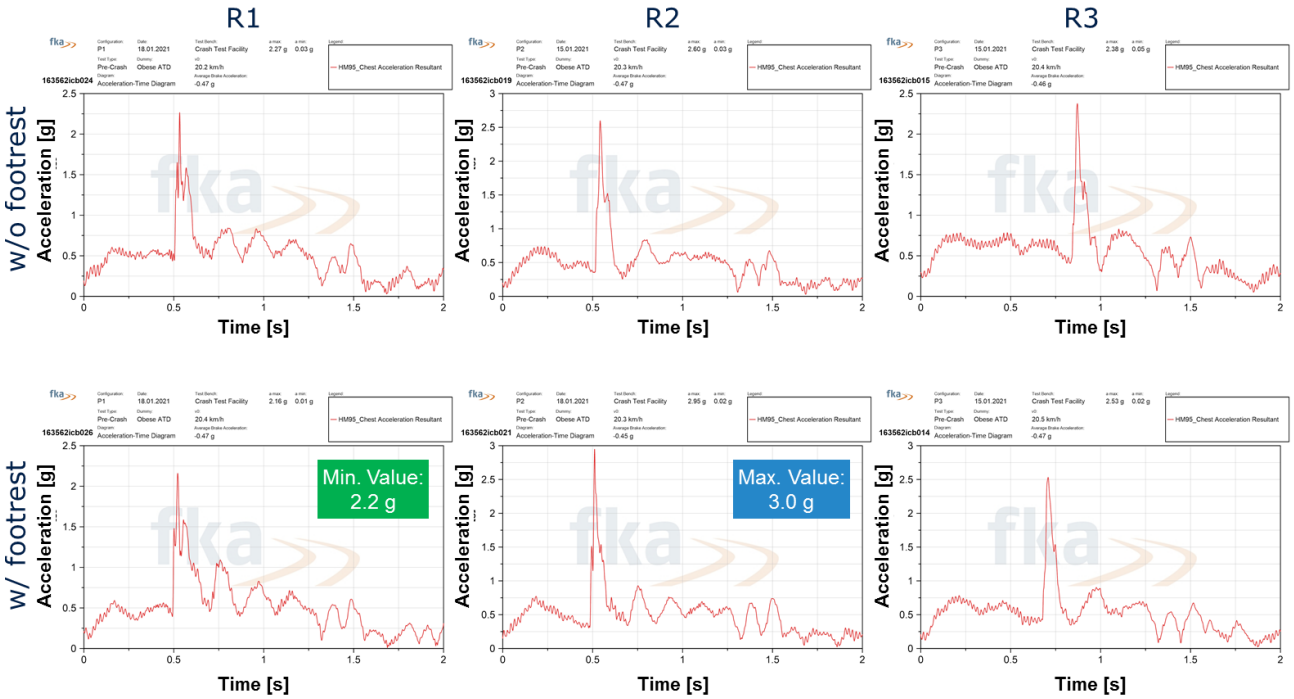

Figure 240 Obese BMI 35 male - chest acceleration (res.) - R1, R2, R3 - without & with footrest

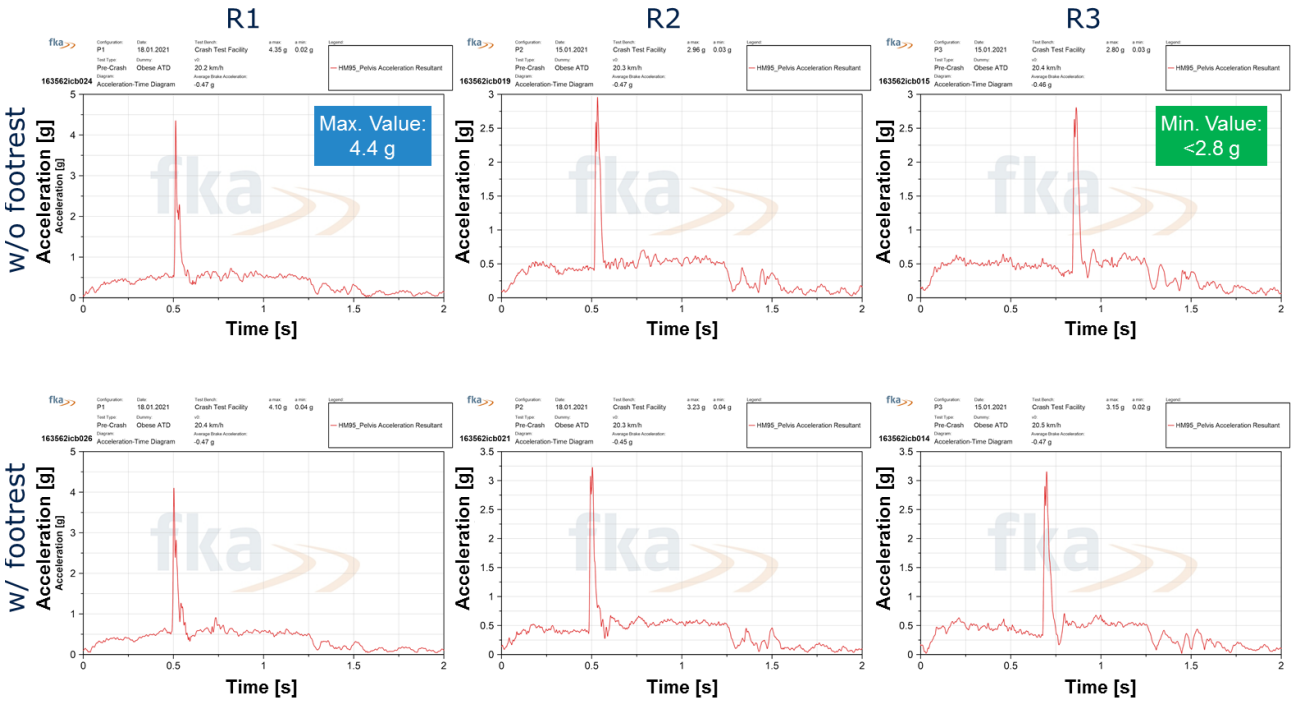

Figure 241 Obese BMI 35 male - pelvis acceleration (res.) - R1, R2, R3 - without & with footrest

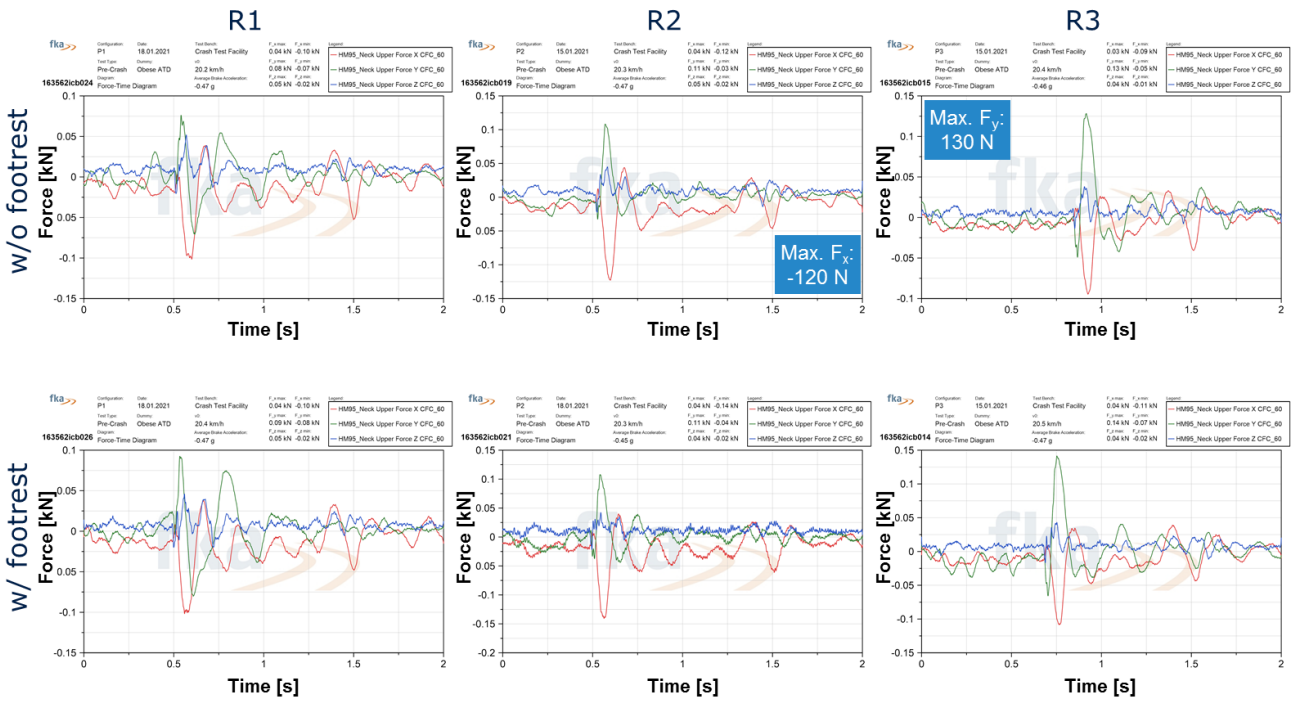

Figure 242 Obese BMI 35 male - upper neck force (x, y, z) - R1, R2, R3 - without & with footr.

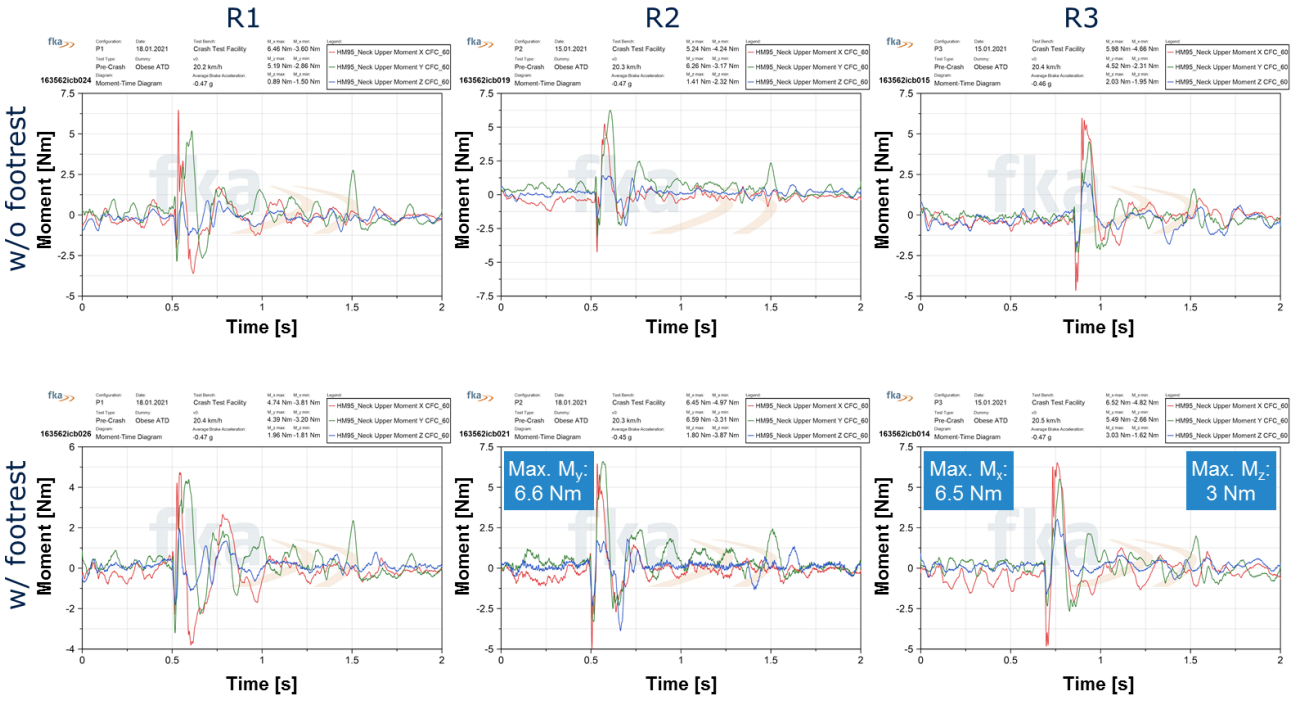

Figure 243 Obese BMI 35 male - upper neck mom. (x, y, z) - R1, R2, R3 - without & with footr.

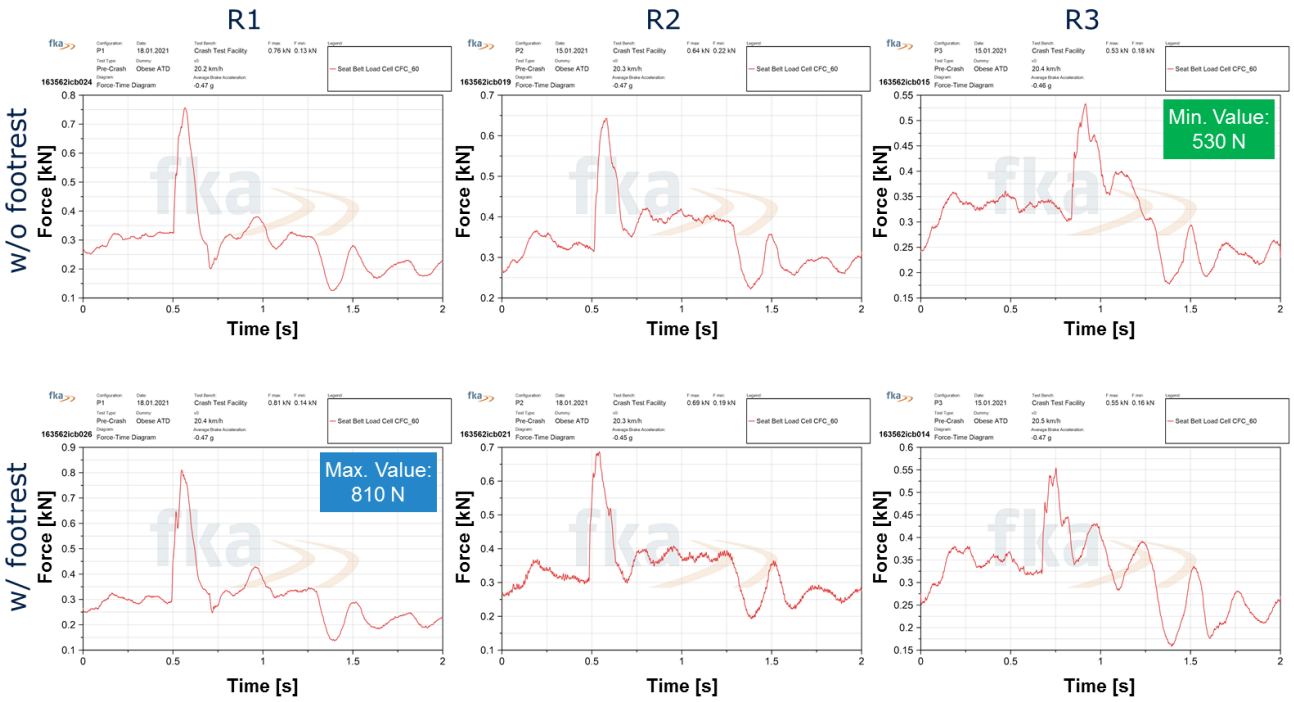

Figure 244 Obese BMI 35 male - seat belt force - R1, R2, R3 - without & with footrest

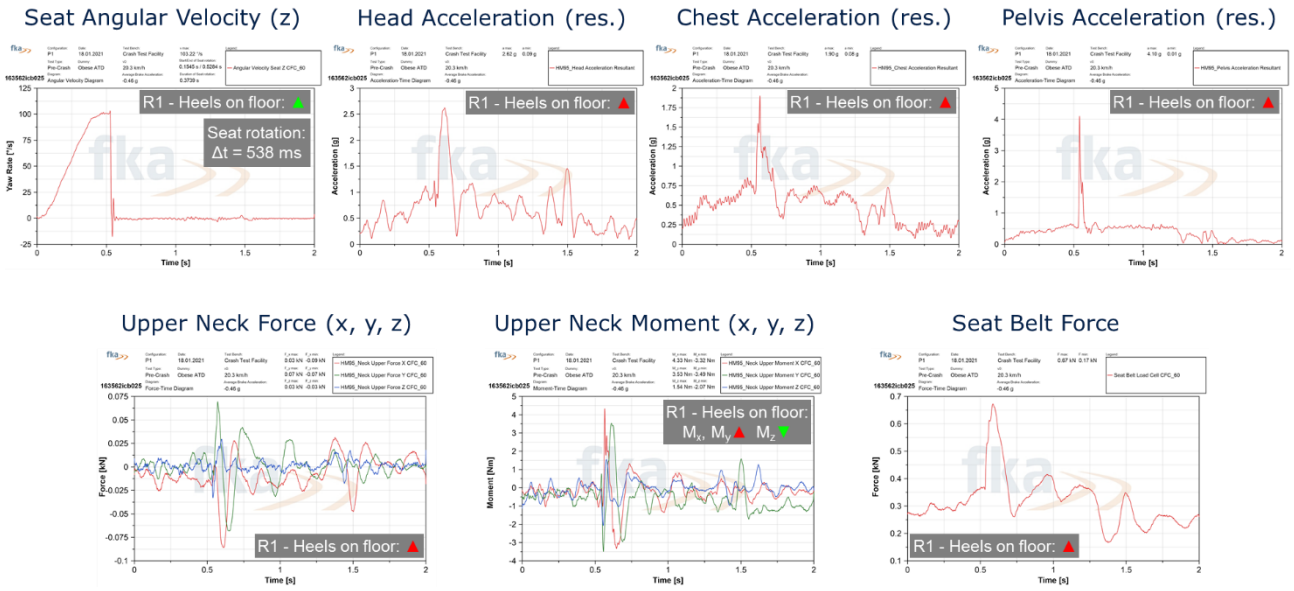

Figure 245 Obese BMI 35 male - shoe soles on floor (R1)

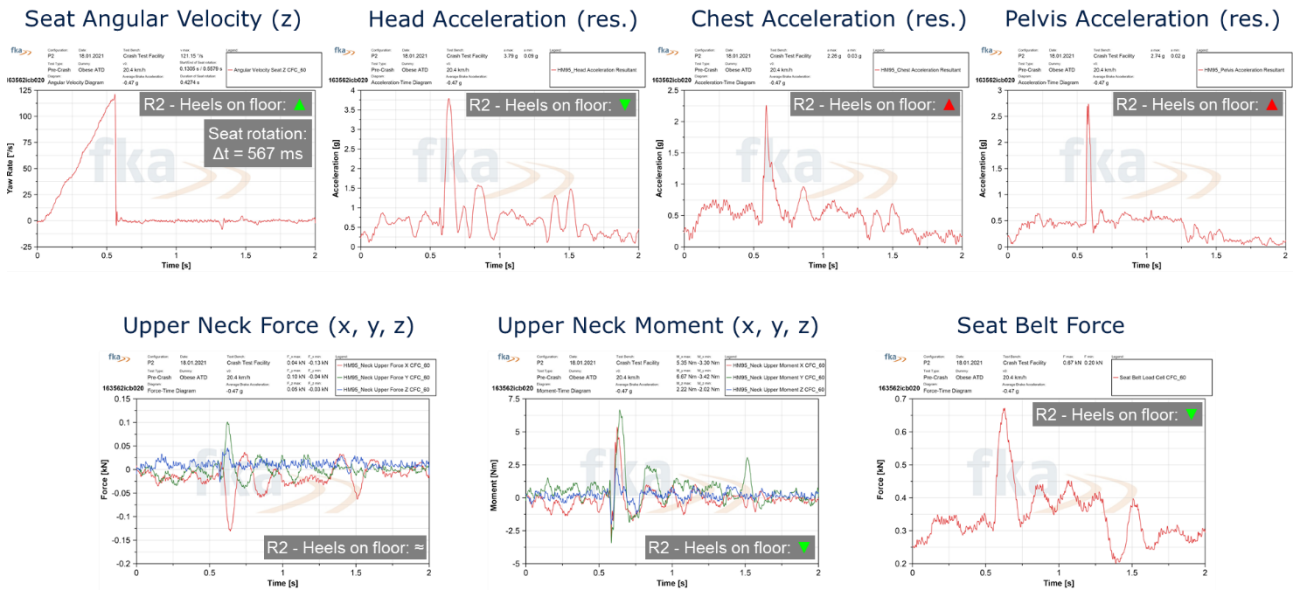

Figure 246 Obese BMI 35 male - shoe soles on floor (R2)

3 PROTECTION PRINCIPLE 6: FAR-SIDE LOAD CASE

3.1 Toyota 3-Point Seatbelt

A Toyota 3-point belt was used in tests 01-OSCCAR-FS and 02-OSCCAR-FS. In all tests, the slack of this seatbelt is removed after dummy positioning by the mean of a rope that exerts a vertical pull in the shoulder belt. The pull force is equal to **200 N** and is generated by an electric actuator connected to a load cell on the shoulder. The pretension is activated a few minutes before the tests and it is kept during it. In order to limit the force received by the actuator, mechanical fusible is used to connect it to the belt.

To develop the concept of the mechanical fusible, several options were assessed. A nylon cable tie turns up the best element to develop this function because of the repeatability of the results and the simplicity of its mounting. The thickness and the number of cable ties in order to achieve the correct level of force, was chosen performing several tests. The best results were obtained with one cable tie with 3 mm thickness.

Figure 247 Toyota 3-point seatbelt

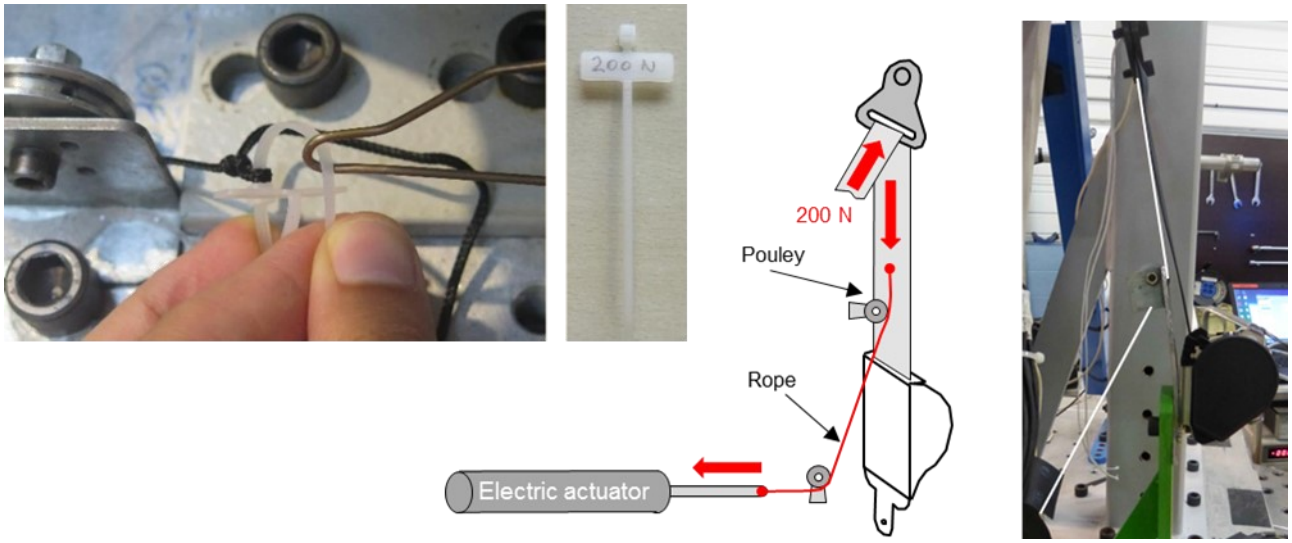

Figure 248 Connection of the electric actuator to the seatbelt

3.2 Test Set-Ups

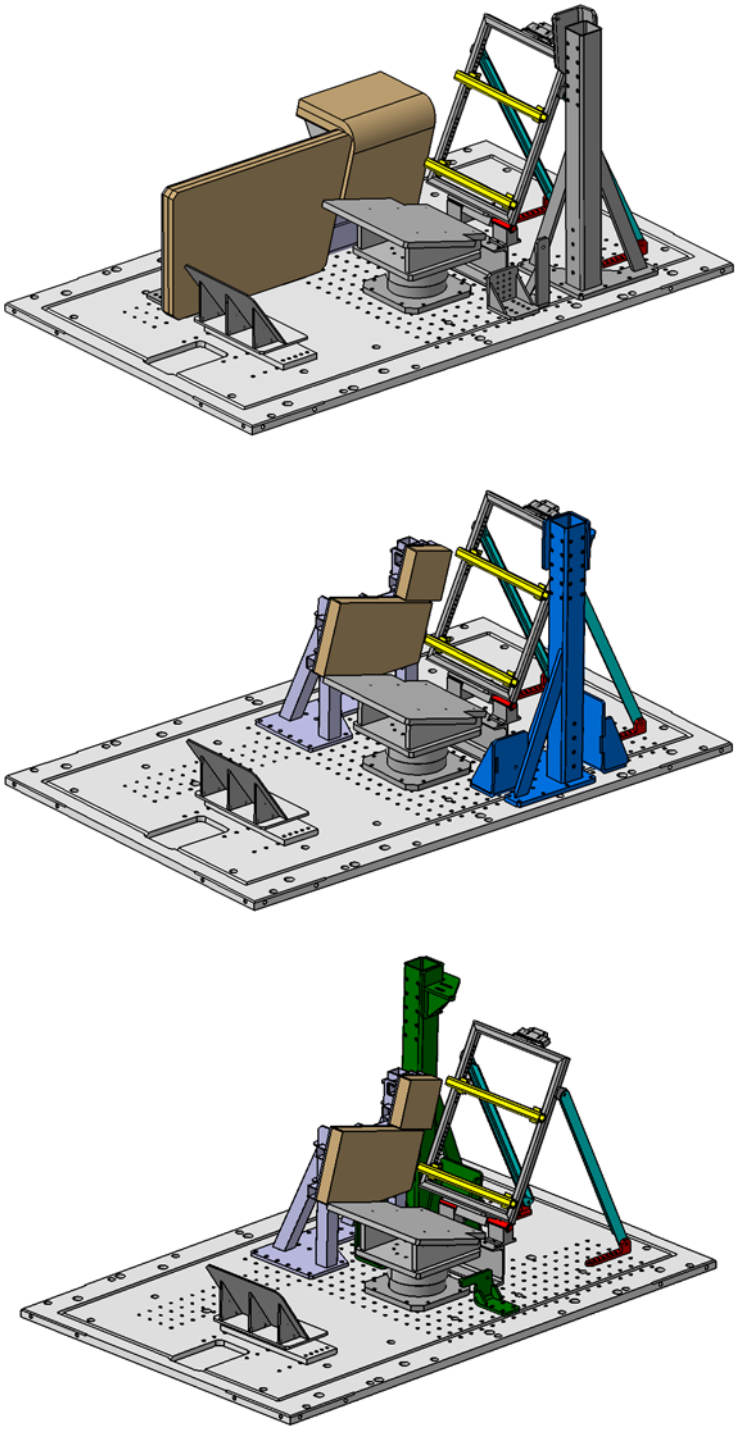

Figure 249 Testing rig configuration for the three main different setups

3.3 Camera Structure Development

Since cameras n°4 and n°5 were used for the post-crash video analysis, it was necessary to reduce the vibrations on the mounting structure. For this reason, a specific mounting frame was modelled and simulated with a pulse 1.5 times higher than the one used in the tests (Figure 250). After

achieving a maximum displacement peak less than 1.5 mm (oscillations in the optimised design are about 55 % of the peak value in the original mounting) the final design of the frame was built and installed on the testing rig.

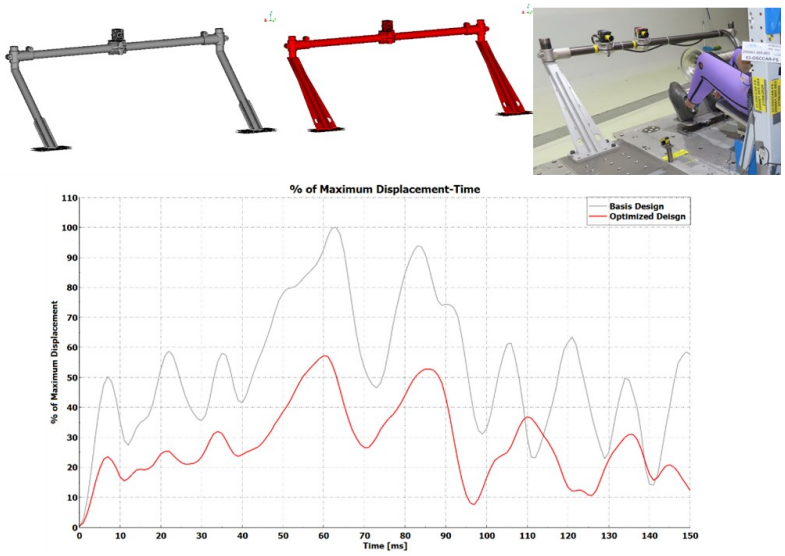

Figure 250 Noise vibration comparison between the two designs and final structure setup

3.4 Side Support Simulations

FEM of the side structure and supports was developed to confirm these components could sustain 1.5 times the test pulse without plastic deformations. Figure 251 shows that a maximum Von Misses stresses of 150 MPa was achieved well below the 355 MPa plastic stresses for steel S355 used to build the components.

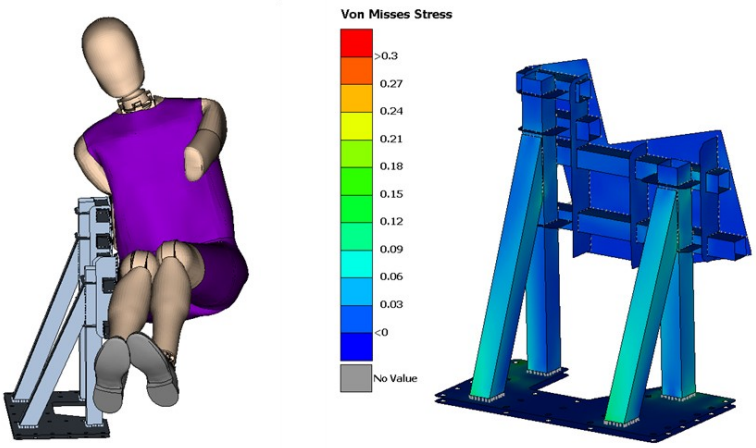

Figure 251 Max Von Mises Stresses (GPa) on the side structure and seat side supports

3.5 Instrumentation

Location	Type	Direction			CFC	Coordinate System (see Figure 74)
		X	Y	Z		
SLED	Acceleration	☑			60	Sled rig (pulse)
TEST SET_UP BASE (LEFT)	Acceleration	☑	☑		60	Test set-up
SEAT UPPER PLATE	Acceleration	☑	☑		60	Test set-up
PELVIS CONSOLE	Acceleration	☑	☑		60	Test set-up
FOOTREST	Acceleration	☑	☑		60	Test set-up
SEAT	Force	☑	☑	☑	60	Test set-up
	Moment	☑	☑		60	
PELVIS CONSOLE (1)	Force	☑	☑	☑	60	Test set-up
FOOTREST	Force	☑	☑	☑	60	Test set-up
	Moment	☑			60	

Table 28 Test rig instrumentation

Location	Type	Direction			CFC
		X	Y	Z	
SHOULDER BELT OUTER	Force	☑			60
SHOULDER BELT INNER	Force	☑			60
LAP BELT OUTER	Force	☑			60
BUCKLE FIXATION	Force	☑			60
RETRACTOR BELT PAY-IN/OUT	Displacement	☑			180
BUCKLE RETRACTION (only with SOTA DLPT belt)	Displacement	☑			180
OUTER LAP BELT RETRACTION (only with SOTA DLPT belt	Displacement	☑			180

Table 29 Seatbelt instrumentation

Body region	Type	X	Y	Z	CFC
HEAD	Acceleration	☑	☑	☑	1000
	Angular velocity	☑	☑	☑	180
UPPER NECK	Force	☑	☑	☑	1000
	Moment	☑	☑	☑	600
LOWER NECK	Force	☑	☑	☑	1000
	Moment	☑	☑	☑	600
SHOULDER (RIGHT)	Force	☑	☑	☑	600
	Acceleration	☑	☑	☑	180
SHOULDER S-TRACC (RIGHT)	Displacement		☑		180
	Rotation			☑	180
THORAX 1 (UPPER RIGHT)	Acceleration	☑	☑	☑	1000
THORAX 1 (UPPER RIGHT)) IR-TRACC	Displacement		☑		180
	Rotation			☑	180
THORAX 2 (MID RIGHT)	Acceleration	☑	☑	☑	1000
THORAX 2 (MID RIGHT) IR_TRACC	Displacement		☑		180
	Rotation			☑	180
THORAX 3 (MID RIGHT)	Acceleration	☑	☑	☑	1000
THORAX 3 (MID RIGHT) IR_TRACC	Displacement		☑		180
	Rotation			☑	180
ABDOMEN 1 (UPPER RIGHT)	Acceleration	☑	☑	☑	1000
ABDOMEN 1 (UPPER RIGHT) IR_TRACC	Displacement		☑		180
	Rotation			☑	180
ABDOMEN 2 (MID RIGHT)	Acceleration	☑	☑	☑	1000
ABDOMEN 2 (MID RIGHT) IR_TRACC	Displacement		☑		180
	Rotation			☑	180

T1 / UPPER SPINE	Acceleration	☑	☑	☑	180
T4 / UPPER SPINE	Acceleration	☑	☑	☑	180
T12 / UPPER SPINE	Acceleration	☑	☑	☑	180
THORAX / SPINE BOX	Angular velocity	☑		☑	180
LUMBAR SPINE	Force	☑	☑	☑	1000
	Moment	☑	☑	☑	1000
PELVIS	Acceleration	☑	☑	☑	1000
	Angular velocity	☑			180
PUBIS SYMPHYSIS	Force		☑		600
ILIAC WING (RIGHT)	Force	☑	☑	☑	600
	Moment	☑	☑	☑	600
FEMUR ACETABULUM / NECK (RIGHT)	Force	☑	☑	☑	600
FEMUR (RIGHT)	Force	☑	☑	☑	600
	Moment	☑	☑	☑	600

Table 30 WorldSID channels

3.6 Dummy Paintings

Following the Euro NCAP far-side assessment protocol, the dummy had masking tapes placed on the areas to be painted using specific colours for the body regions as detailed in Table 31. The tapes were covered with the coloured paints close to the time of the test to ensure that the paint was wet on impact. Post impact pictures of environment showed WorldSID body region interaction with the environment as in Figure 252, for example.

Body region	Color
Shoulder Arm	Blue
2nd Thorax Rib	Green
3rd Thorax Rib	Red
1st Abdomen Rib	Green
2nd Abdomen Rib	Blue
Pelvis	Orange

Table 31 Dummy paintings

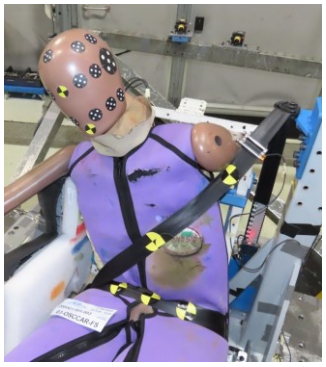

Figure 252 Post-test picture showing WorldSID interaction with the seat side support

3.7 Positioning

Within all the test campaign, a good repeatability of the initial WSID dummy positioning was obtained. Figure 253 shows the overlay of the head COG, neck, shoulder joint, H-point, knee and heel points of the WorldSID across the different tests. The measurements were performed with a FARO arm and the summary of all the points measured can be found in the Appendix 3.6.

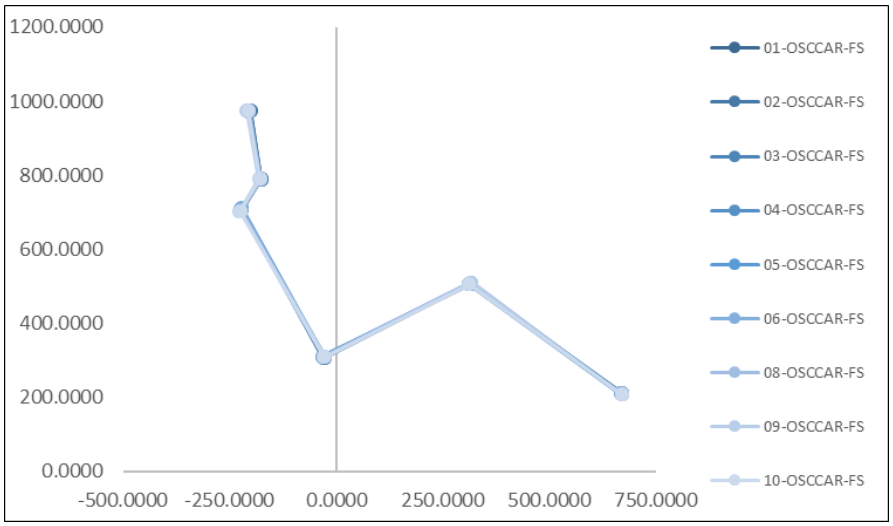

Figure 253 WorldSID positioning in the far-side test series

3.8 Test Results

	Dummy Head COG		Dummy Neck		Dummy Shoulder		Dummy H-Point		Dummy Knee		Dummy Heel	
	x	z	x	z	x	z	x	z	x	z	x	z
01-OSCCAR-FS	-200.51	975.36	-175.89	790.05	-221.23	708.02	-32.74	310.91	312.22	505.55	669.80	211.56
02-OSCCAR-FS	-202.77	974.47	-176.59	789.33	-222.73	709.53	-26.26	307.01	313.88	506.53	667.51	210.30
03-OSCCAR-FS	-203.17	974.94	-176.92	790.23	-224.57	707.87	-29.73	306.50	314.21	506.74	671.14	210.41
04-OSCCAR-FS	-205.13	975.85	-178.68	792.13	-224.21	706.57	-30.54	309.77	312.44	504.80	670.09	207.79
05-OSCCAR-FS	-207.31	975.76	-179.28	791.52	-221.77	711.02	-28.91	310.55	317.14	509.85	667.67	210.53
06-OSCCAR-FS	-205.75	973.03	-177.15	788.41	-221.60	707.32	-31.90	310.13	310.80	506.68	668.11	210.29
07-OSCCAR-FS	-205.56	972.06	-178.06	788.31	-223.27	700.83	-28.08	308.27	313.56	505.93	671.11	207.89
08-OSCCAR-FS	-205.37	974.49	-178.29	789.86	-223.57	704.99	-28.56	308.89	313.62	507.02	670.42	210.16
09-OSCCAR-FS	-210.17	973.90	-181.00	789.97	-226.76	702.41	-26.33	310.78	317.90	509.98	670.18	206.55
10-OSCCAR-FS	-206.61	973.90	-179.23	789.60	-225.83	702.76	-28.81	309.34	312.26	504.96	671.13	207.08

Table 32 WorldSID initial positioning

Figure 254 Left to right: Tests 02-OSCCAR-FS, 04-OSCCAR-FS & 06-OSCCAR-FS at 100ms

	01-OSCCAR-FS	02-OSCCAR-FS	03-OSCCAR-FS	04-OSCCAR-FS	05-OSCCAR-FS	06-OSCCAR-FS	07-OSCCAR-FS	08-OSCCAR-FS	09-OSCCAR-FS	10-OSCCAR-FS
Slip-out time (ms)	73.00	75.00	63.00	62.00	N/A	N/A	N/A	N/A	66.00	67.00
Loss category	Partial loss	Partial loss	Total loss	Total loss	No loss	No loss	No loss	No loss	Total loss	Total loss
Configuration	Outboard	Outboard	Outboard	Outboard	Inboard	Inboard	Inboard	Inboard	Outboard	Outboard

Table 33 Belt / shoulder interaction (slip out timing according to [20])

			01-OSCCAR	02-OSCCAR	03-OSCCAR	04-OSCCAR	05-OSCCAR	06-OSCCAR	07-OSCCAR	08-OSCCAR	09-OSCCAR	10-OSCCAR
HEAD	Excursion zone		Yellow (*)	Yellow (*)	Yellow	Yellow	Yellow	Yellow	Orange	Yellow	Red	Red
	HIC_{15}		102.11	109.25	65.50	84.57	133.02	128.29	72.73	65.72	13.85	14.31
	Resultant Acc.(g)		36.13	38.27	39.40	42.69	39.27	38.78	35.57	30.98	15.73	16.92
NECK	Tension Fz (kN)	Upper Neck	1.44	1.53	1.06	1.14	1.53	1.52	1.02	0.88	0.59	0.65
		Lower Neck	1.61	1.71	0.96	1.01	1.47	1.57	1.09	1.19	0.63	0.66
	Lateral Flexion (Nm)	MxOC	54.46	56.08	47.80	49.24	48.73	50.72	46.87	50.70	24.88	28.92
		Mx (base neck)	166.72	167.69	141.58	146.29	175.91	183.61	171.99	149.75	92.23	89.78
	Extension (Nm)	MyOC	-29.74	-29.68	-12.63	-12.78	-10.47	-12.77	-28.04	-26.00	-26.60	-23.51
		My (base neck)	-32.23	-30.61	-21.86	-14.30	-8.73	-5.79	-30.74	-46.53	-62.34	-55.62
CHEST & ABDOMEN	Chest lateral compr.(mm)	Top	6.59	8.96	35.20	36.33	44.69	42.81	1.72	1.64	2.70	2.69
		Middle	10.63	12.31	28.61	31.15	41.27	39.06	2.81	3.00	0.87	1.12
		Bottom	10.12	11.70	18.38	19.57	31.47	28.93	1.13	1.24	0.00	0.00
	Abd lateral compress (mm)	Top	30.55	29.03	14.81	12.41	24.47	21.61	1.17	1.44	4.28	3.01
		Bottom	40.60	39.89	14.84	15.04	25.46	23.07	0.00	0.00	10.07	6.79
PELVIS	Pubic Symphysis force (kN)		1.23	1.22	0.83	0.85	1.07	1.02	0.22	0.72	0.20	0.24
	Lumbar Fy (kN)		1.24	1.21	0.81	0.79	0.92	0.92	2.14	2.15	0.74	0.72
	Lumbar Fz (kN)		3.02	3.08	1.78	1.74	1.49	1.40	1.30	1.25	1.92	1.62
	Lumbar Mx (Nm)		81.88	81.15	54.90	54.95	65.74	66.90	112.02	101.95	66.12	71.25
Overall Far Side Assessment			**11.780**	**11.735**	**10.691**	**10.485**	**8.318**	**8.302**	**5.651**	**8.000**	**6.000**	**6.000**

Table 34 WorldSID biomechanics assessment according to the Euro NCAP protocol

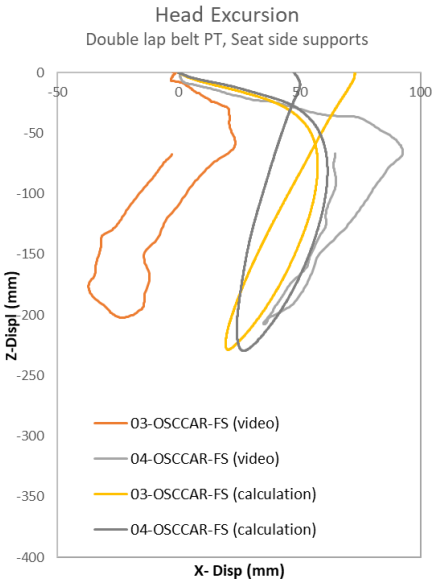
Head Excursion
Double lap belt PT, Seat side supports
Z-Displ (mm)
X- Disp (mm)
03-OSCCAR-FS (video)
04-OSCCAR-FS (video)
03-OSCCAR-FS (calculation)
04-OSCCAR-FS (calculation)

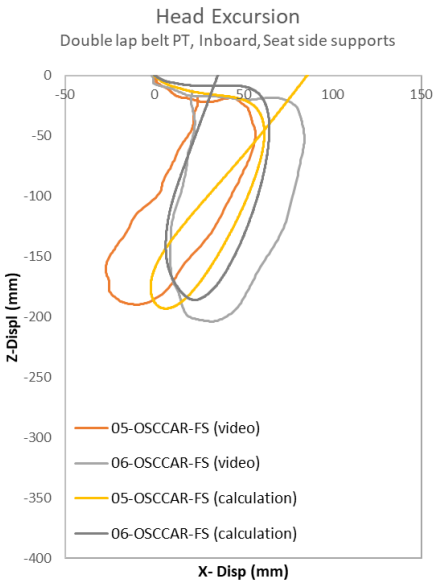
Head Excursion
Double lap belt PT, Inboard, Seat side supports
Z-Displ (mm)
X- Disp (mm)
05-OSCCAR-FS (video)
06-OSCCAR-FS (video)
05-OSCCAR-FS (calculation)
06-OSCCAR-FS (calculation)

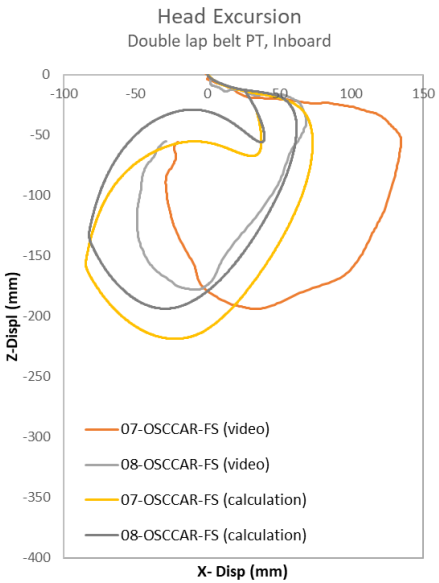
Head Excursion
Double lap belt PT, Inboard
Z-Displ (mm)
X- Disp (mm)
07-OSCCAR-FS (video)
08-OSCCAR-FS (video)
07-OSCCAR-FS (calculation)
08-OSCCAR-FS (calculation)

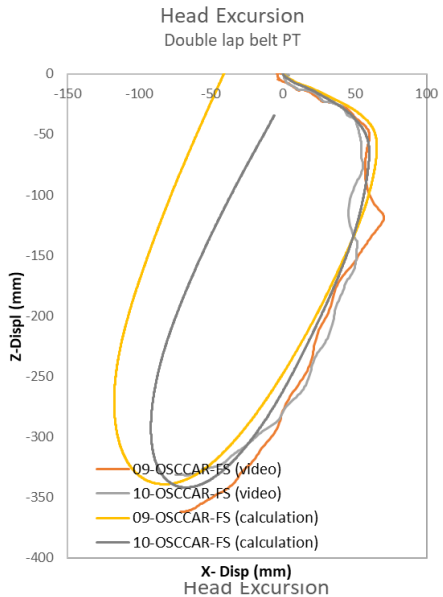
Head Excursion
Double lap belt PT
Z-Displ (mm)
X- Disp (mm)
09-OSCCAR-FS (video)
10-OSCCAR-FS (video)
09-OSCCAR-FS (calculation)
10-OSCCAR-FS (calculation)

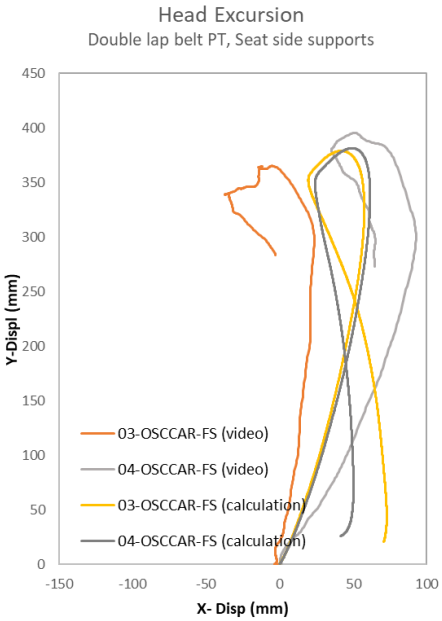
Head Excursion
Double lap belt PT, Seat side supports
Y-Displ (mm)
X- Disp (mm)
03-OSCCAR-FS (video)
04-OSCCAR-FS (video)
03-OSCCAR-FS (calculation)
04-OSCCAR-FS (calculation)

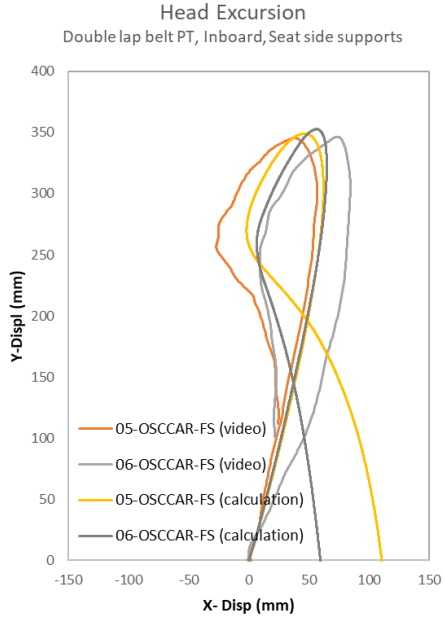
Head Excursion
Double lap belt PT, Inboard, Seat side supports
Y-Displ (mm)
X- Disp (mm)
05-OSCCAR-FS (video)
06-OSCCAR-FS (video)
05-OSCCAR-FS (calculation)
06-OSCCAR-FS (calculation)

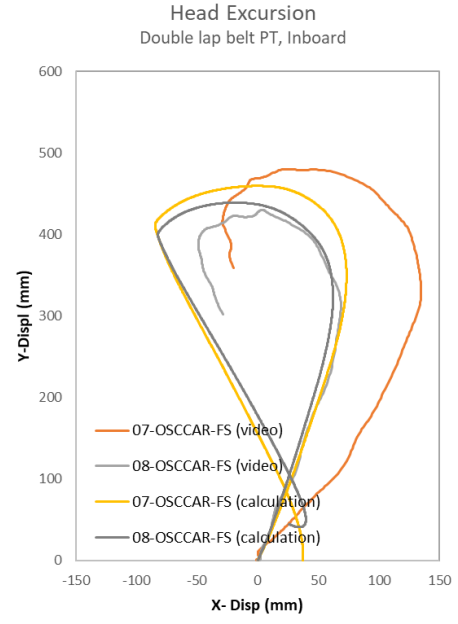
Head Excursion
Double lap belt PT, Inboard
Y-Displ (mm)
X- Disp (mm)
07-OSCCAR-FS (video)
08-OSCCAR-FS (video)
07-OSCCAR-FS (calculation)
08-OSCCAR-FS (calculation)

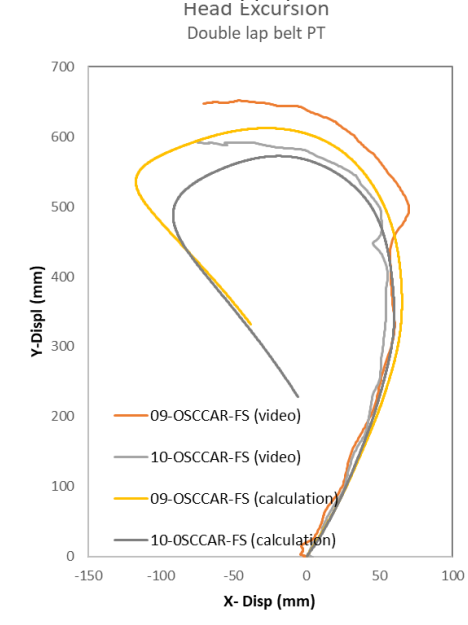
Head Excursion
Double lap belt PT
Y-Displ (mm)
X- Disp (mm)
09-OSCCAR-FS (video)
10-OSCCAR-FS (video)
09-OSCCAR-FS (calculation)
10-OSCCAR-FS (calculation)

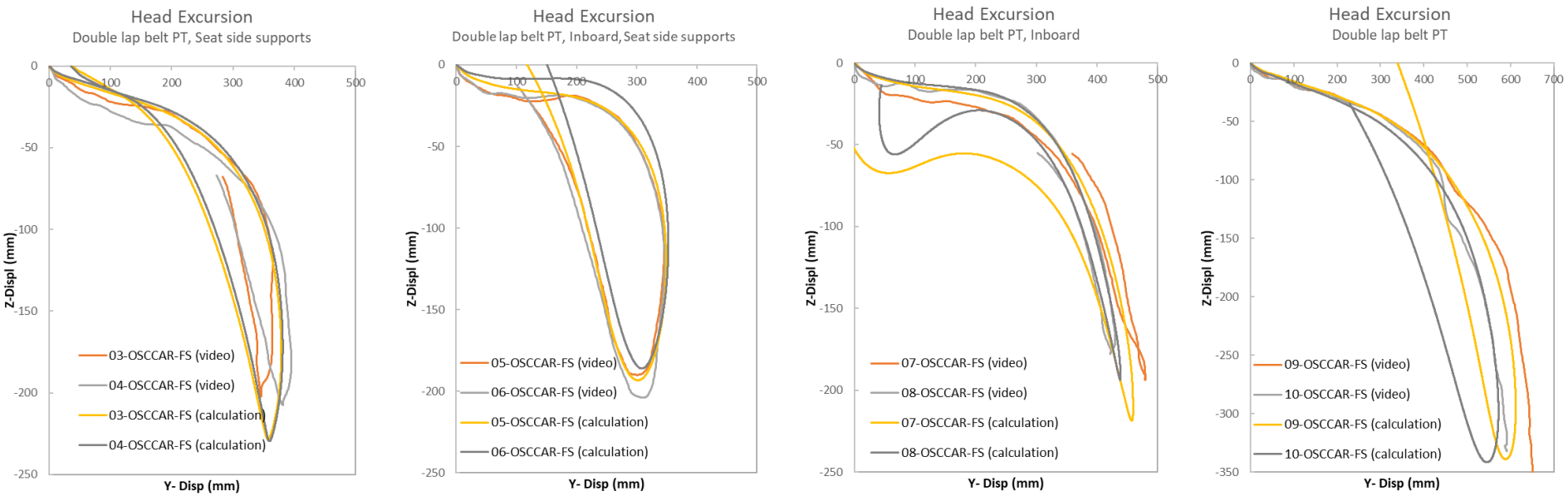

Figure 255 World SID head COG excursion - Comparison between video analysis & calculation

3.9 LS-Dyna Simulation Results

3.9.1 WS3_2 Simulation and Test Comparison

WS3_2 simulation used the SOTA DLPT belt and the seat side supports.

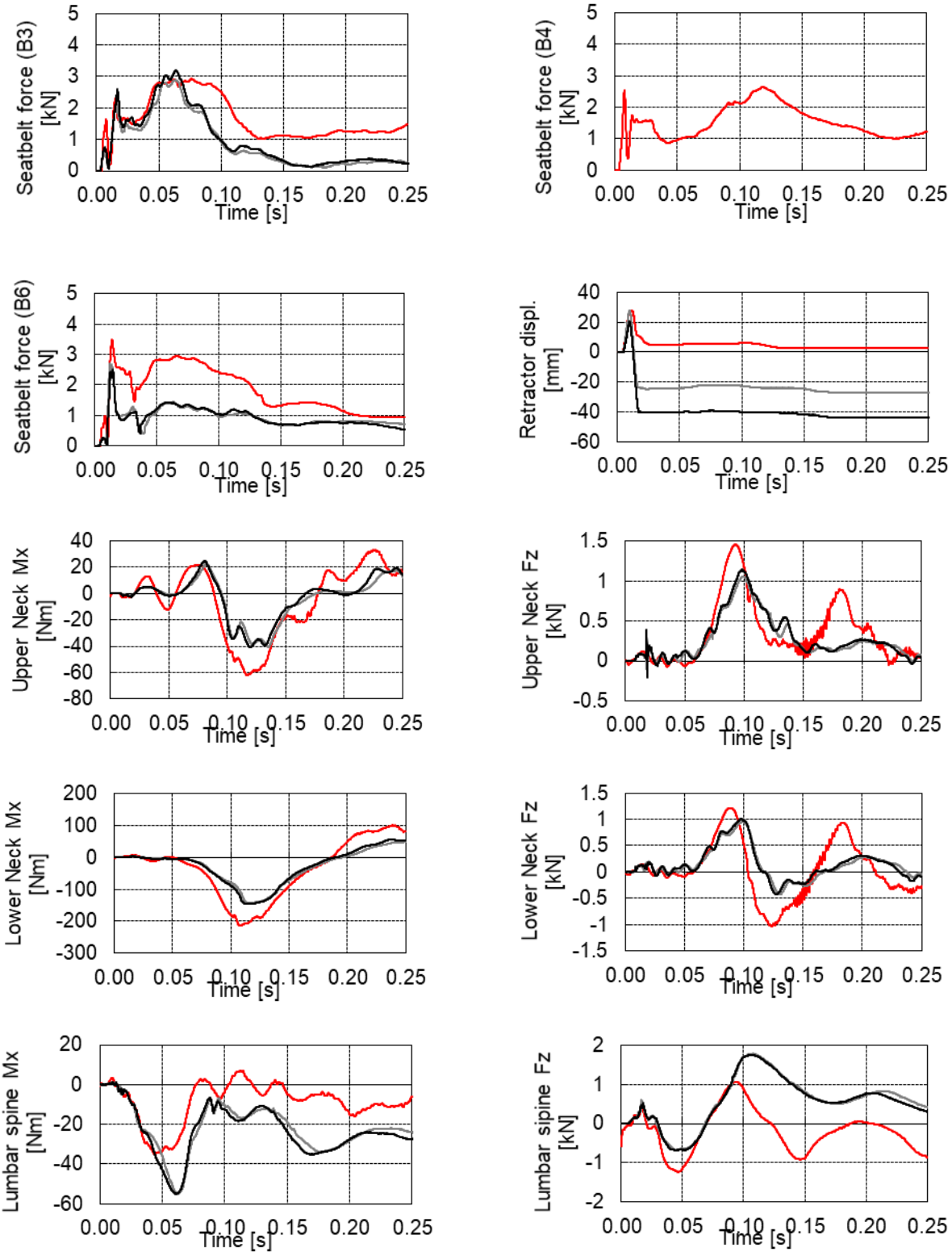

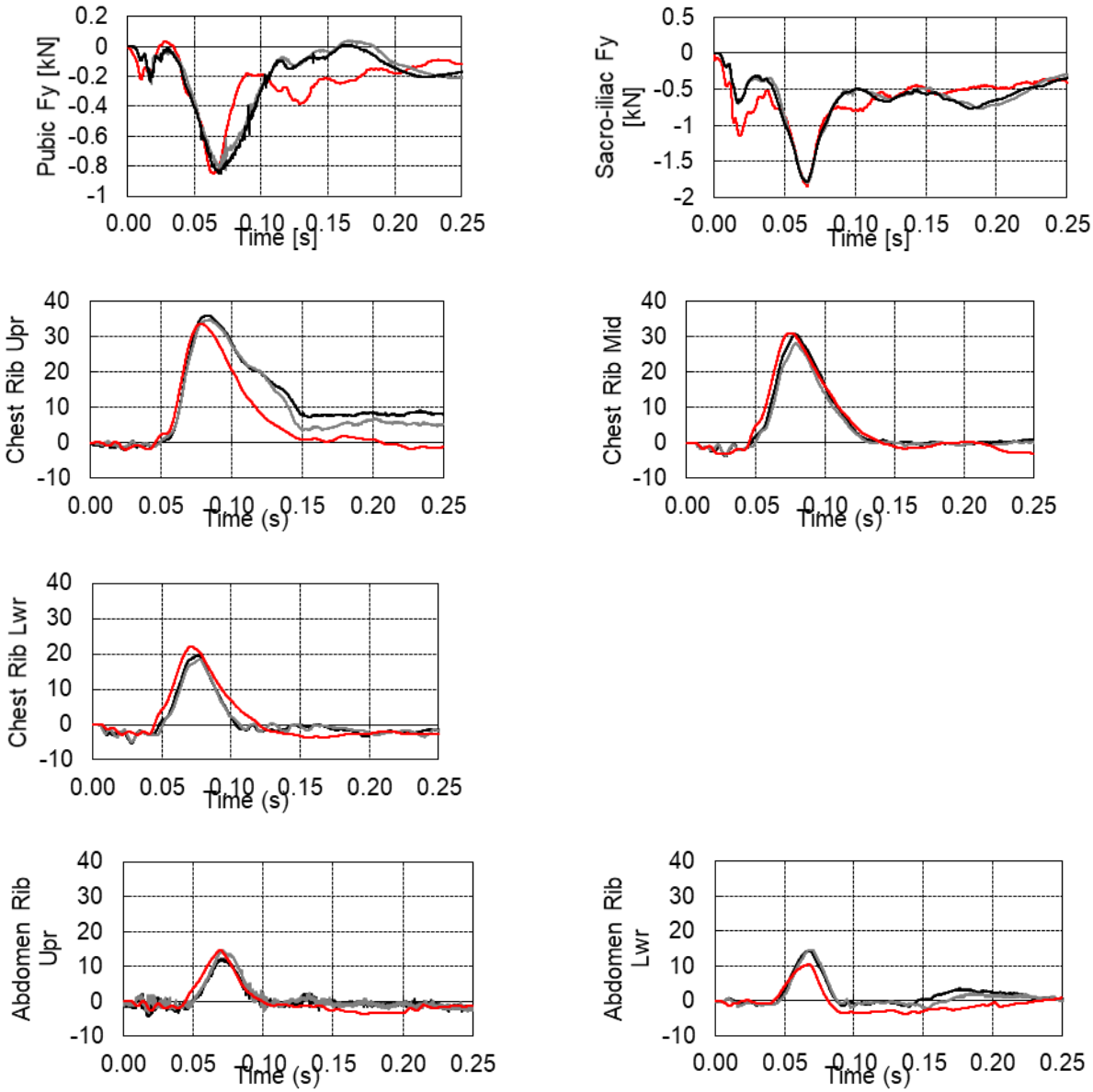

Figure 256 WS3_2 simulation (in red) compared with test data (in grey & black)

3.9.2 WS5_2 Simulation and Test Comparison

WS5_2 simulation used the SOTA DLPT belt mounted inboard and the seat side supports.

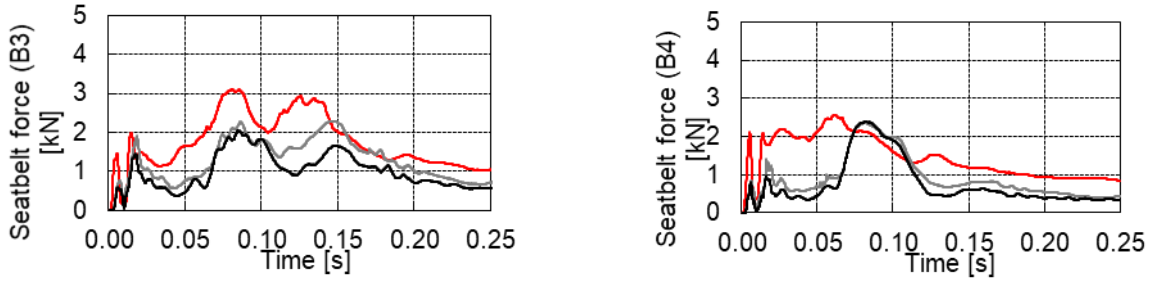

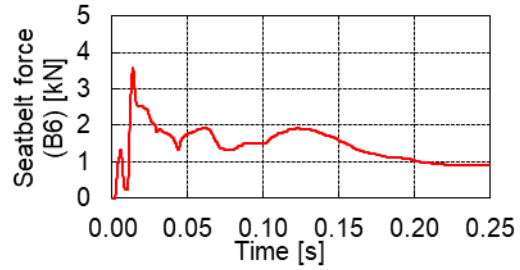
Seatbelt force (B6) [kN]
Time [s]

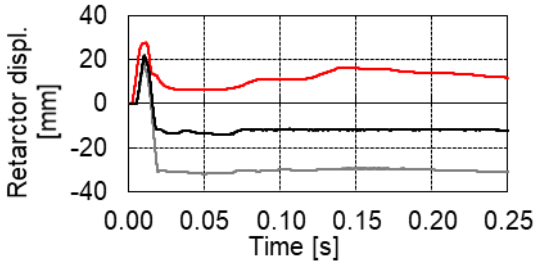
Retarctor displ. [mm]
Time [s]

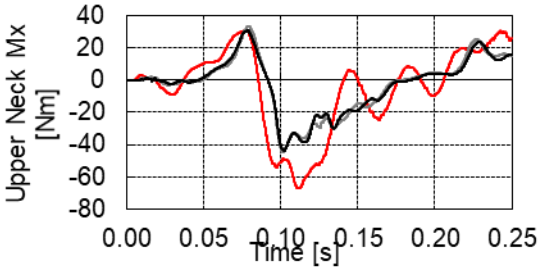
Upper Neck Mx [Nm]
Time [s]

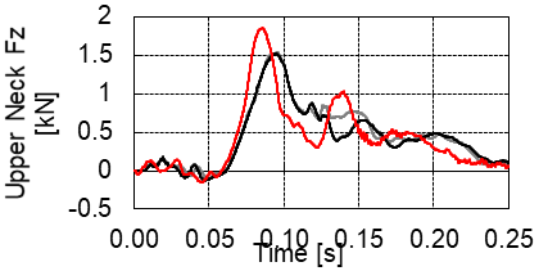
Upper Neck Fz [kN]
Time [s]

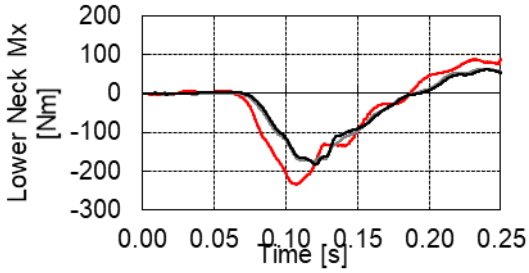
Lower Neck Mx [Nm]
Time [s]

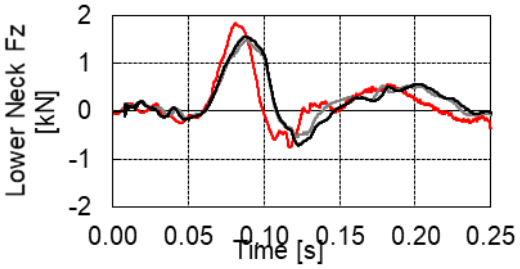
Lower Neck Fz [kN]
Time [s]

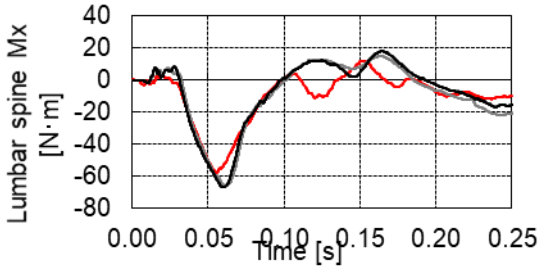
Lumbar spine Mx [N·m]
Time [s]

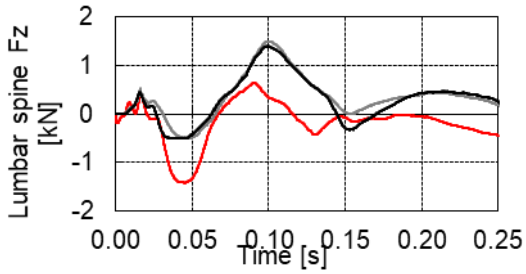
Lumbar spine Fz [kN]
Time [s]

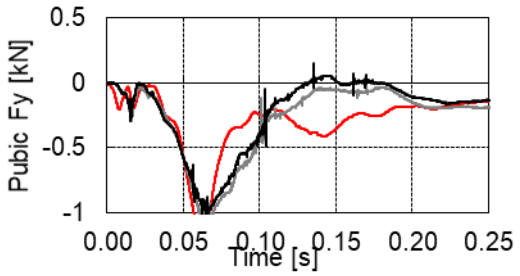
Pubic Fy [kN]
Time [s]

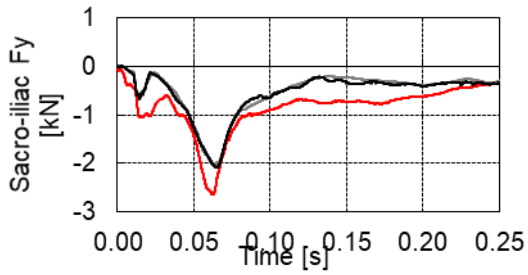
Sacro-iliac Fy [kN]
Time [s]

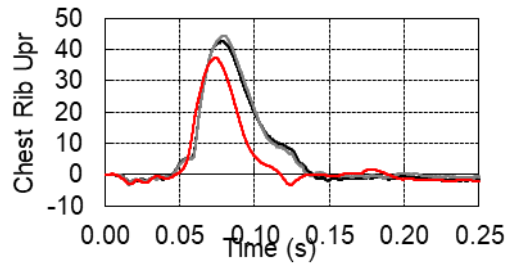
Chest Rib Upr
Time (s)

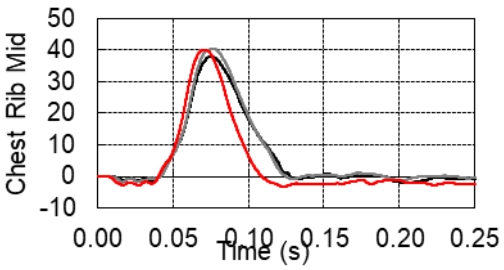
Chest Rib Mid
Time (s)

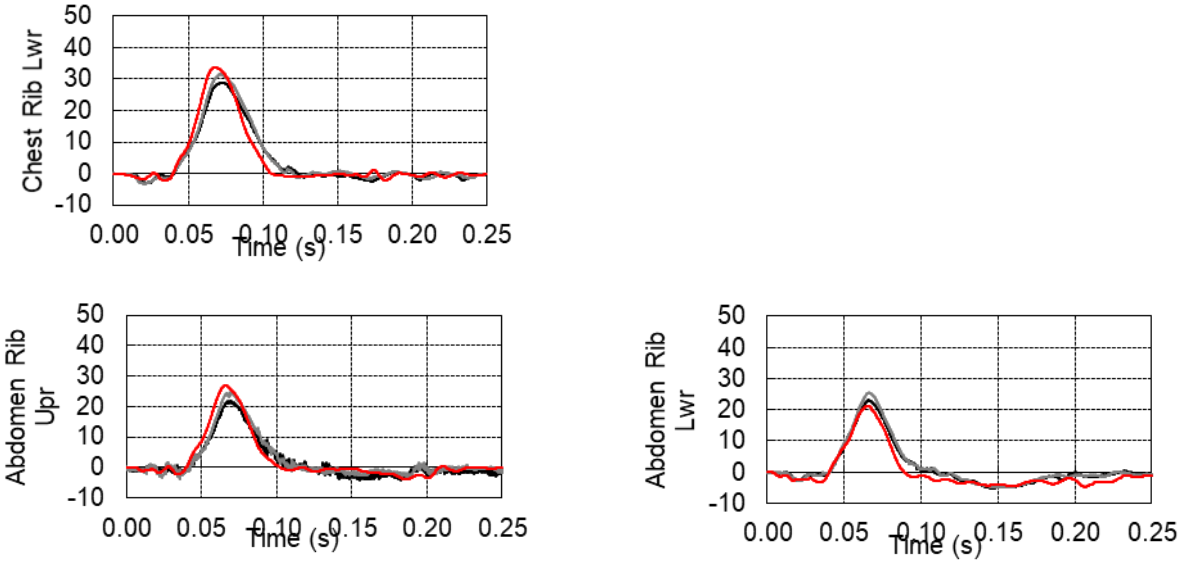

Figure 257 WS5_2 simulation (in red) compared with test data (in grey & black)

3.9.3 WS4_2 Simulation and Test Comparison

WS4_2 simulation used the SOTA DLPT belt mounted inboard.

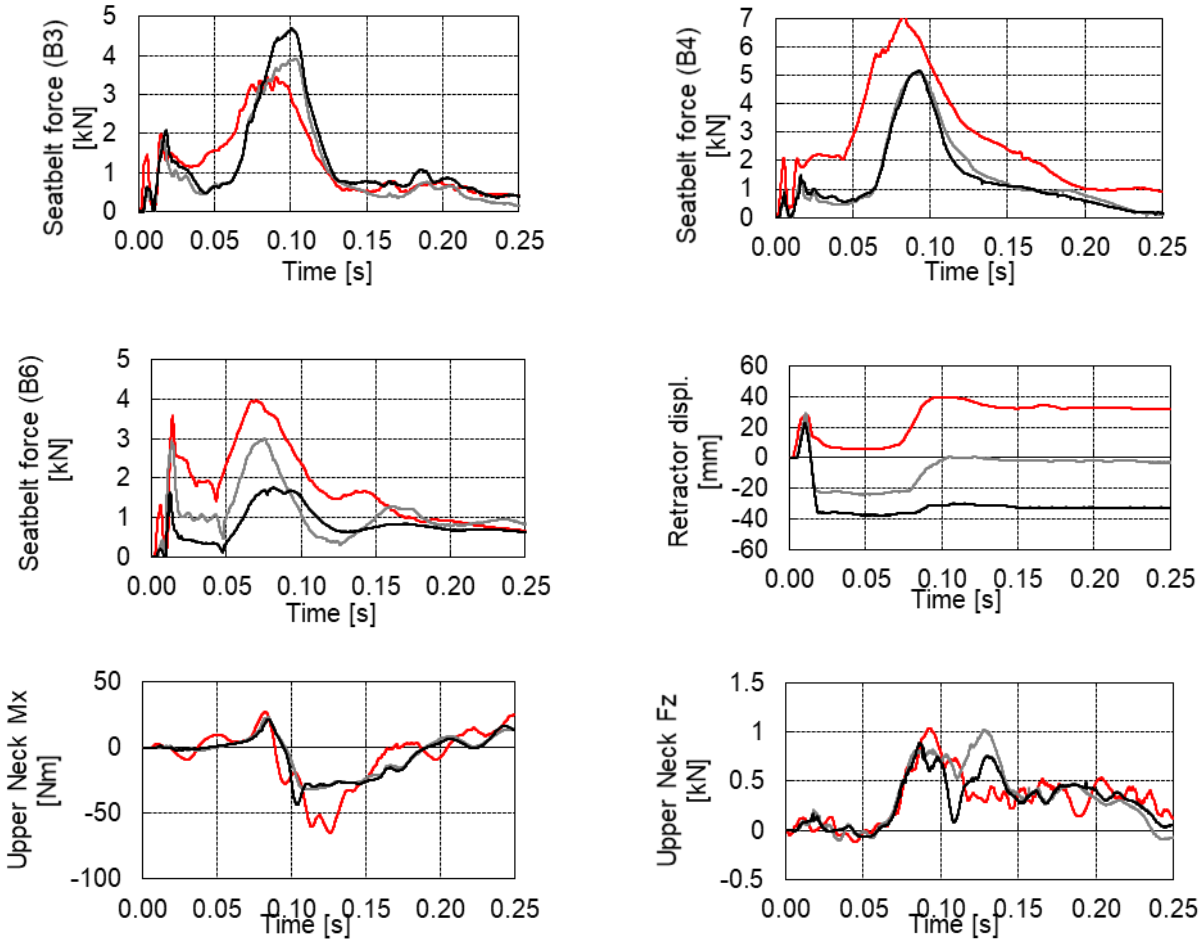

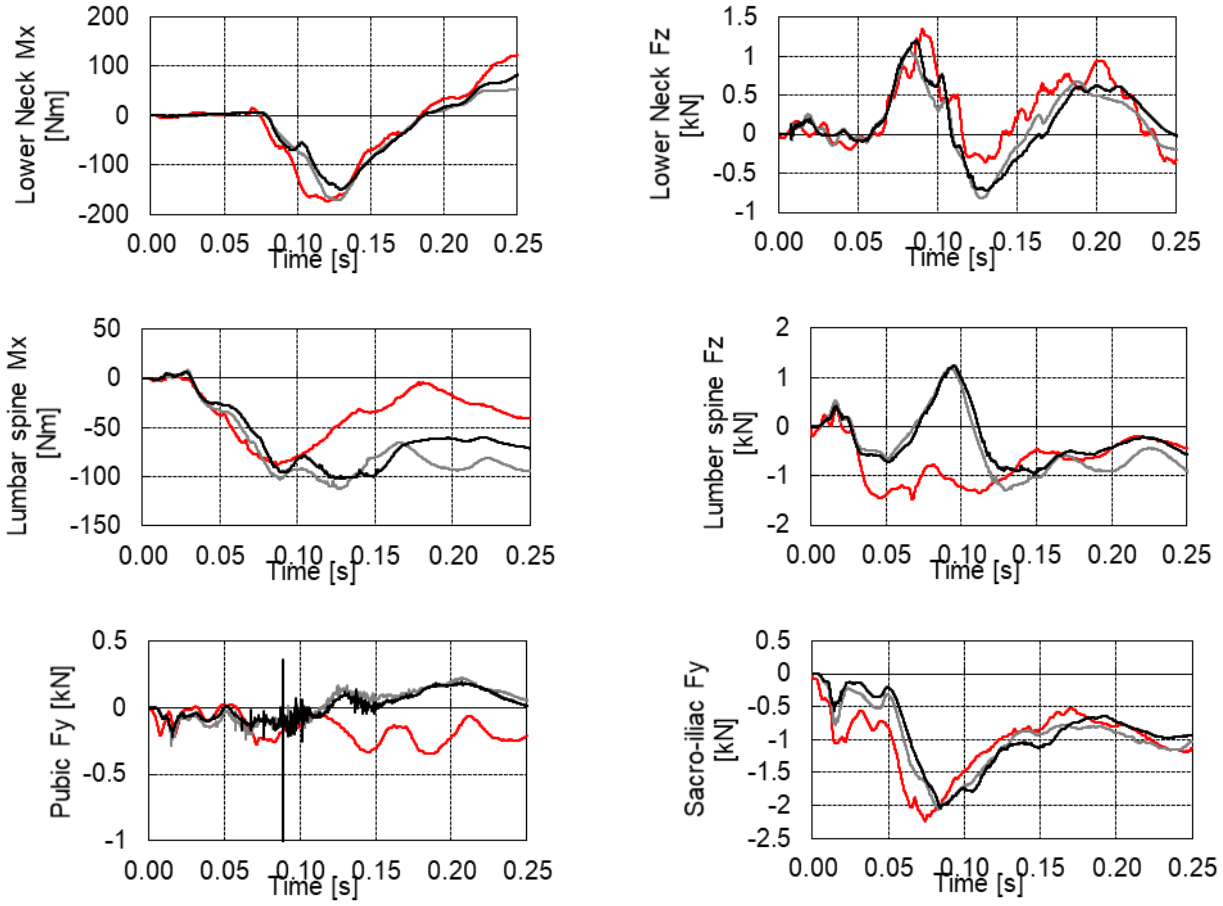

Figure 258 WS4_2 simulation (in red) compared with test data (in grey & black)

3.9.4 WS2_2 Simulation and Test Comparison

WS2_2 simulation used the SOTA DLPT belt only.

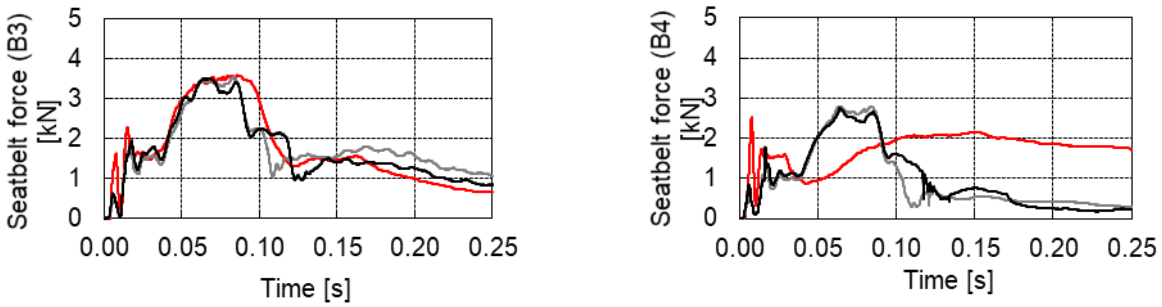

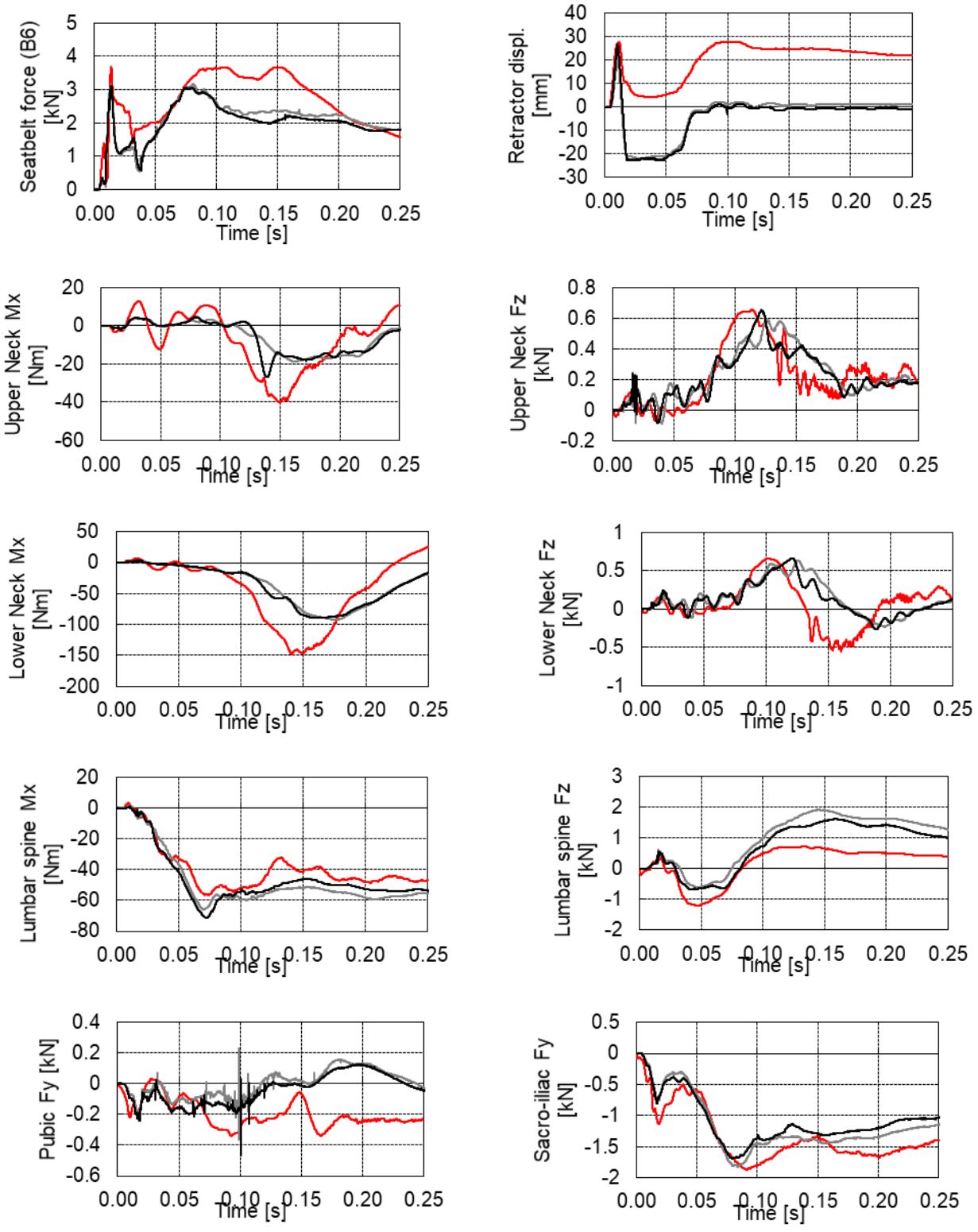

Figure 259 WS2_2 simulation (in red) compared with test data (in grey & black)

3.10 Madymo Simulation Results

3.10.1 WS3_2 Simulation and Test Comparison

The WS3_2 simulations used SOTA DLPT belt and seat side supports.

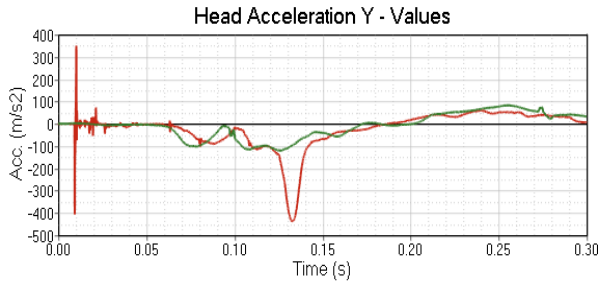

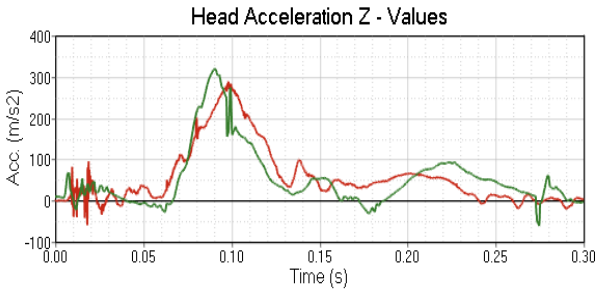

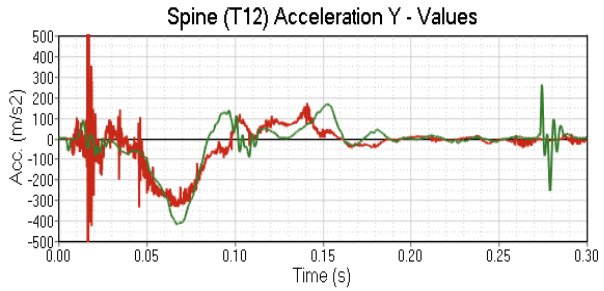

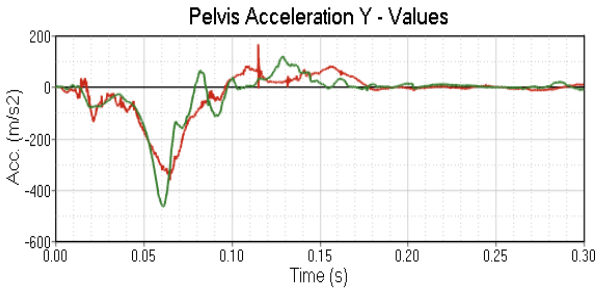

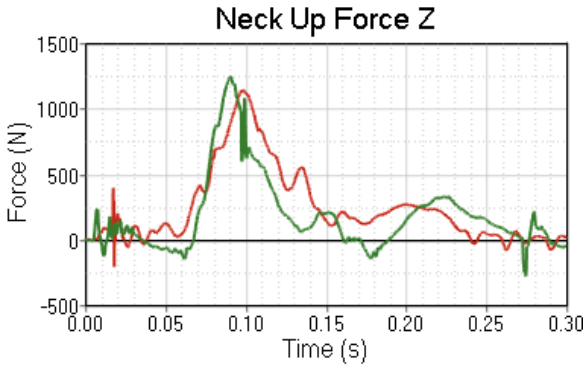

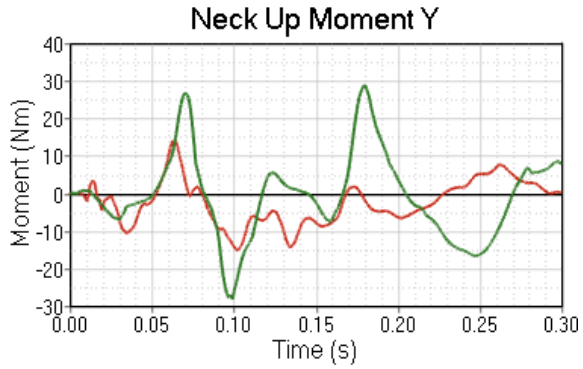

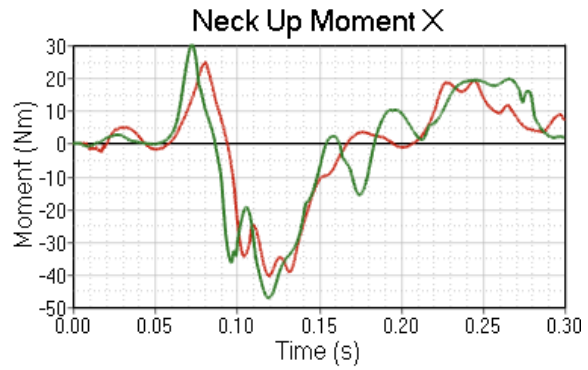

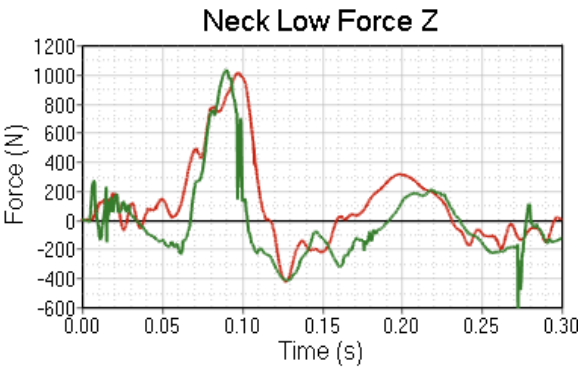

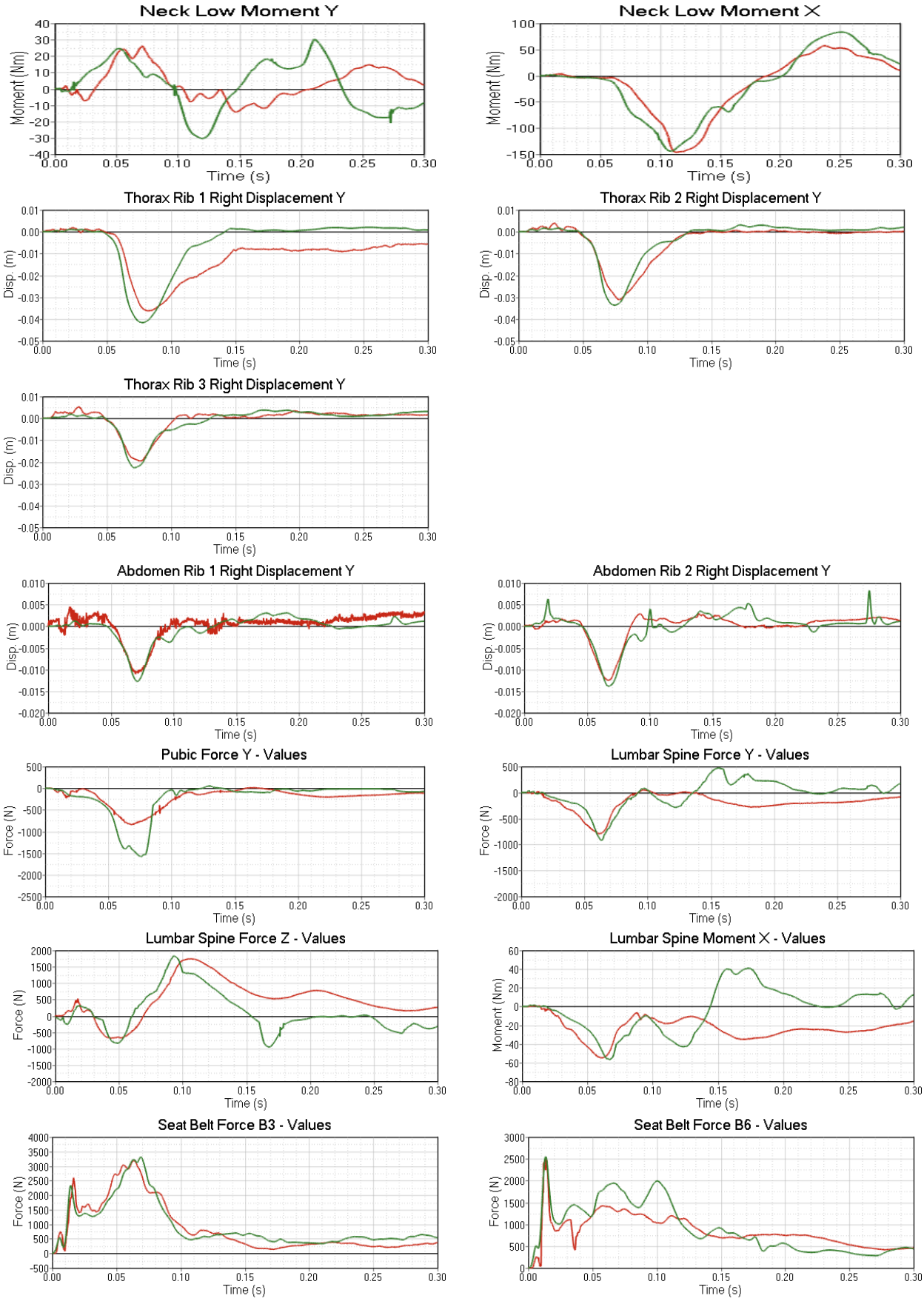

Figure 260 WS3_2 simulation (in green) compared with test data (in red)

3.10.2 WS5_2 Simulation and Test Comparison

The WS5_2 simulation used SOTA DLPT mounted inboard and seat side supports.

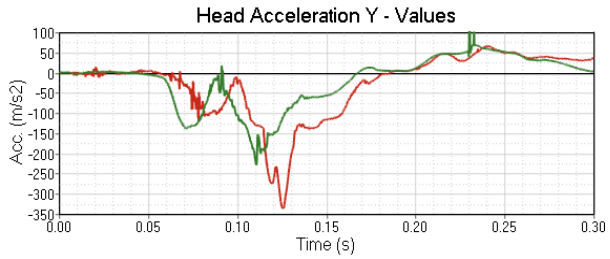

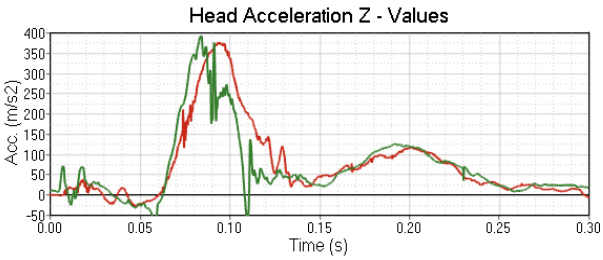

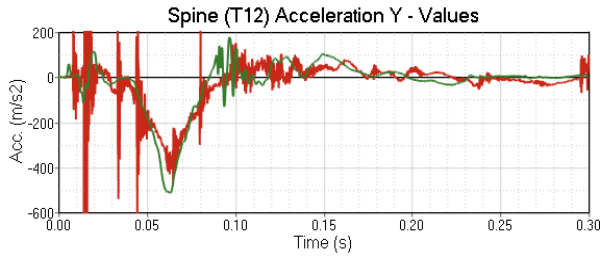

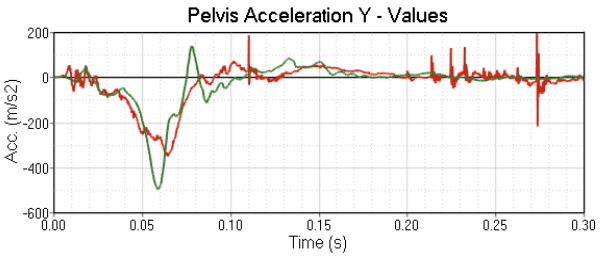

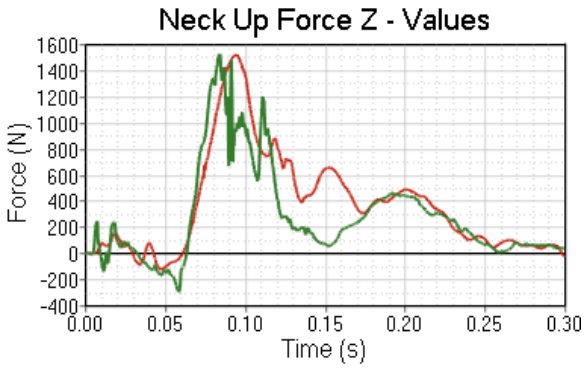

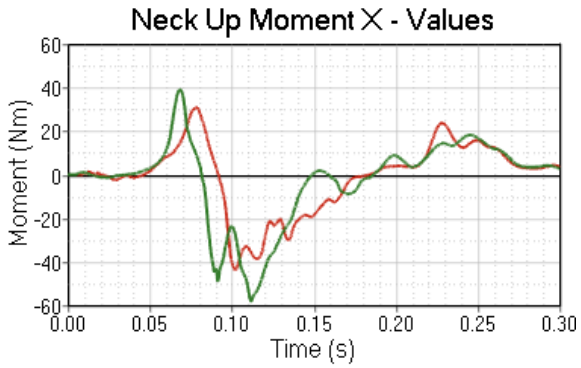

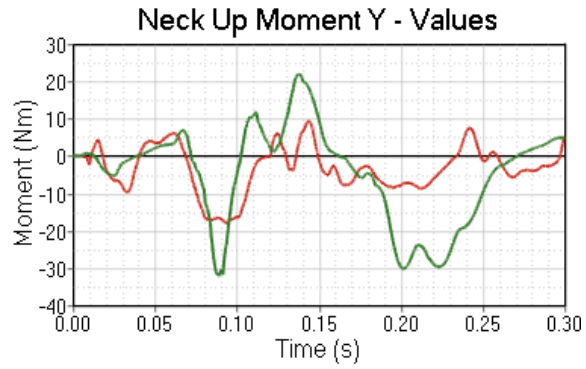

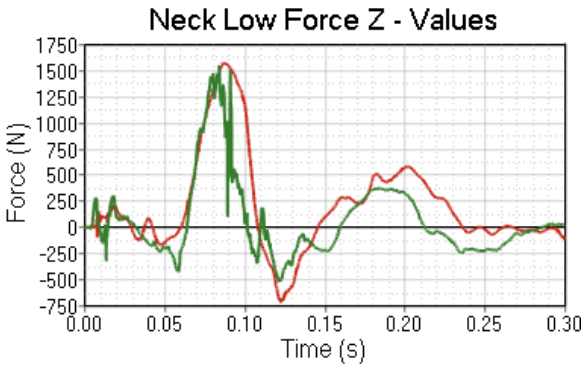

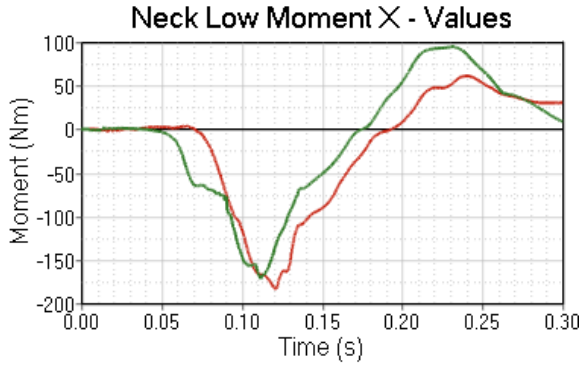
Neck Low Moment X - Values
Moment (Nm)
Time (s)

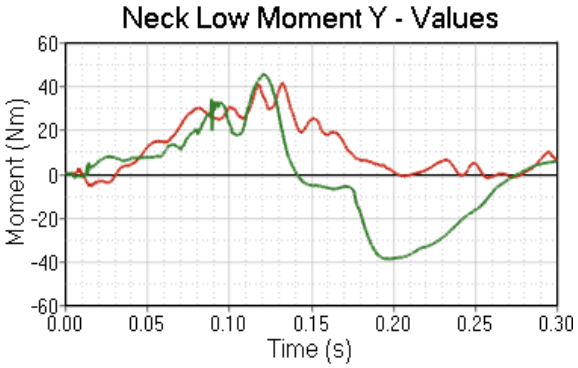
Neck Low Moment Y - Values
Moment (Nm)
Time (s)

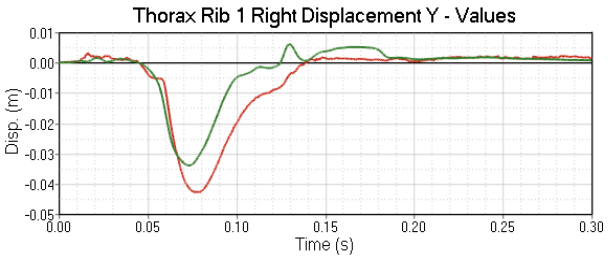
Thorax Rib 1 Right Displacement Y - Values
Disp. (m)
Time (s)

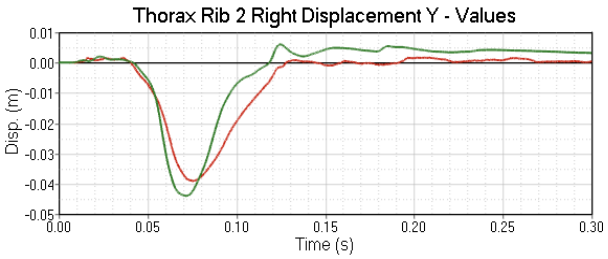
Thorax Rib 2 Right Displacement Y - Values
Disp. (m)
Time (s)

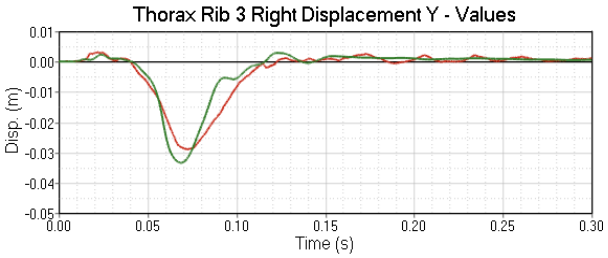
Thorax Rib 3 Right Displacement Y - Values
Disp. (m)
Time (s)

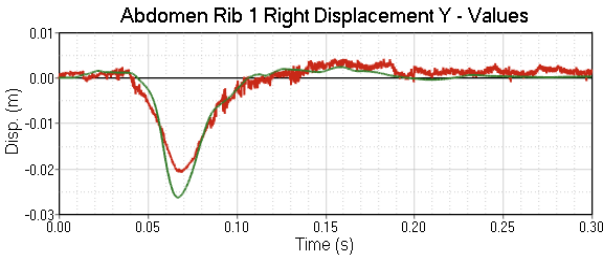
Abdomen Rib 1 Right Displacement Y - Values
Disp. (m)
Time (s)

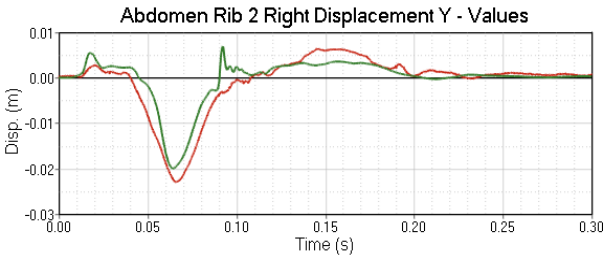
Abdomen Rib 2 Right Displacement Y - Values
Disp. (m)
Time (s)

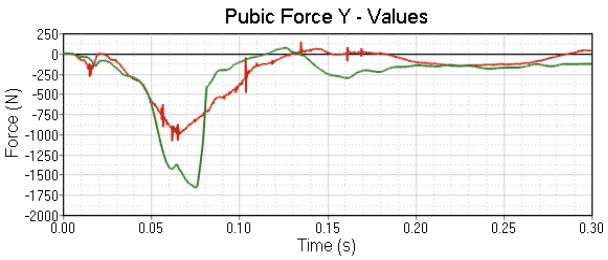
Pubic Force Y - Values
Force (N)
Time (s)

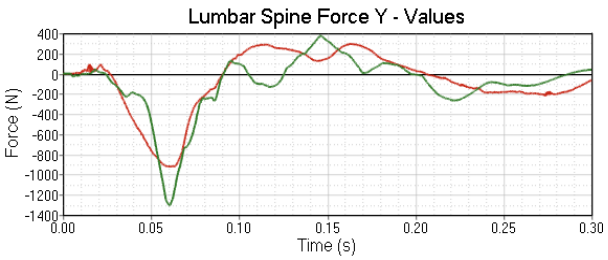
Lumbar Spine Force Y - Values
Force (N)
Time (s)

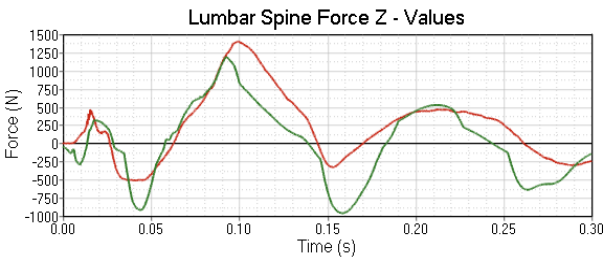
Lumbar Spine Force Z - Values
Force (N)
Time (s)

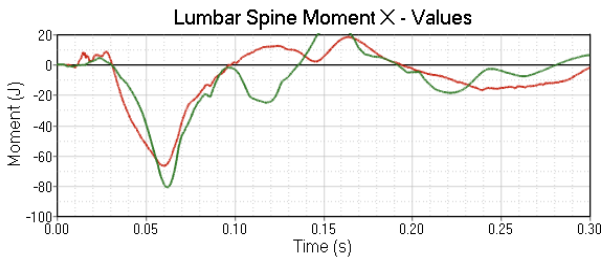
Lumbar Spine Moment X - Values
Moment (J)
Time (s)

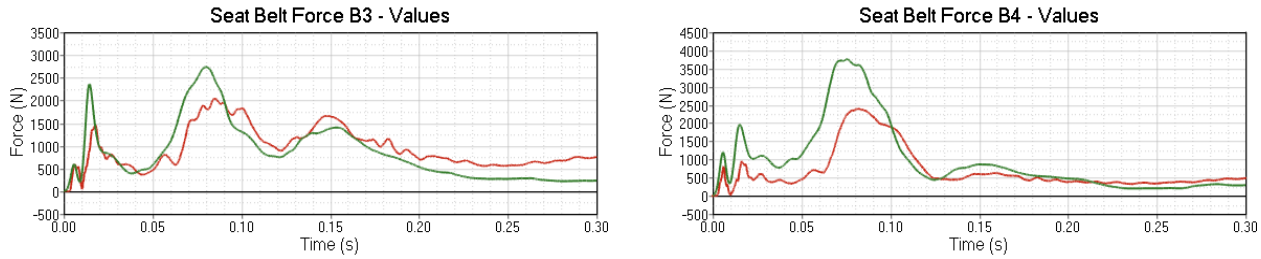

Figure 261 WS5_2 simulation (in green) compared with test data (in red)

*Belt force B6 data missing/corrupted: see Table 19

3.10.3 WS4_2 Simulation and Test Comparison

The WS4_2 simulation used SOTA DLPT belt mounted inboard.

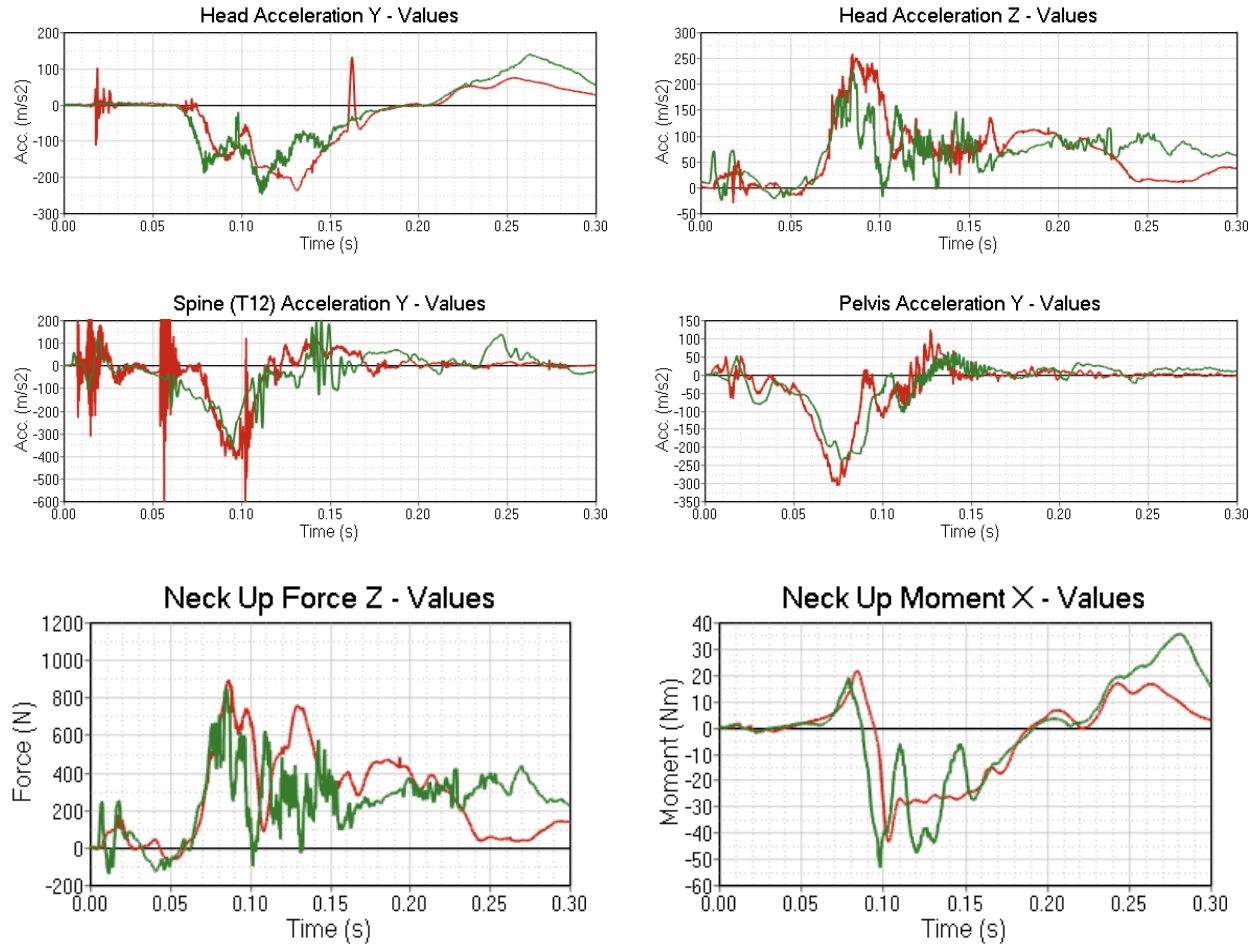

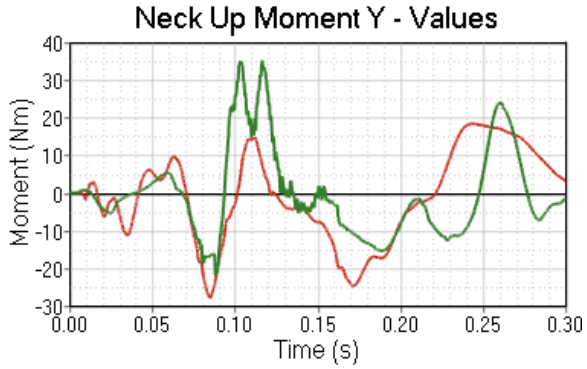
Neck Up Moment Y - Values
Moment (Nm)
Time (s)

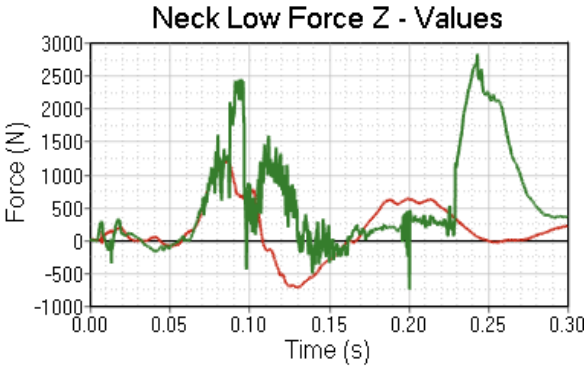
Neck Low Force Z - Values
Force (N)
Time (s)

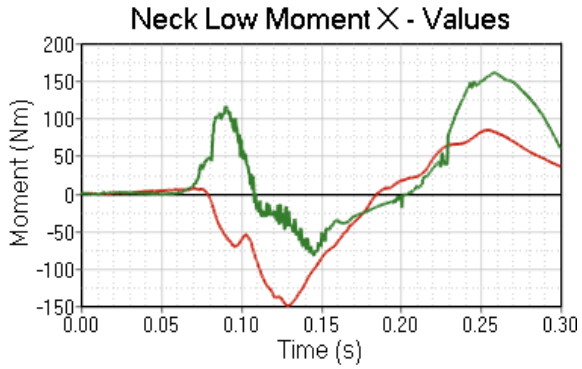
Neck Low Moment X - Values
Moment (Nm)
Time (s)

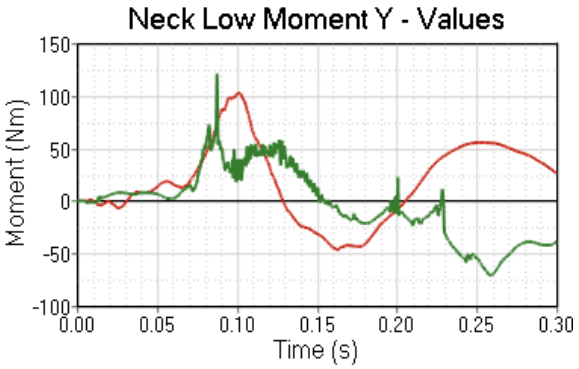
Neck Low Moment Y - Values
Moment (Nm)
Time (s)

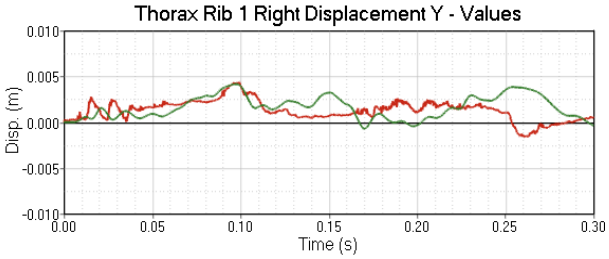
Thorax Rib 1 Right Displacement Y - Values
Disp. (m)
Time (s)

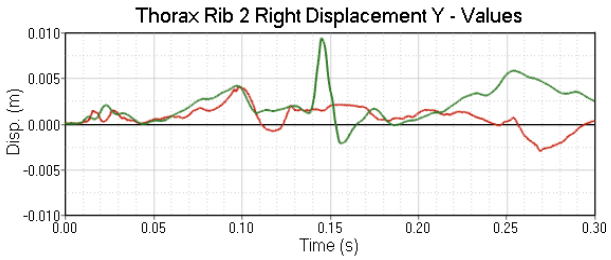
Thorax Rib 2 Right Displacement Y - Values
Disp. (m)
Time (s)

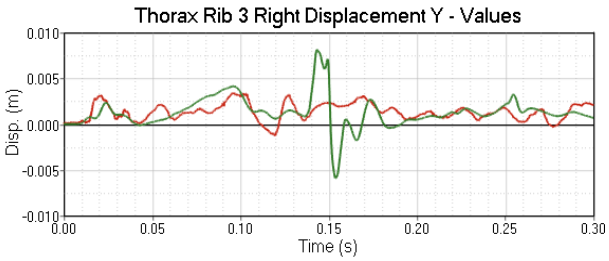
Thorax Rib 3 Right Displacement Y - Values
Disp. (m)
Time (s)

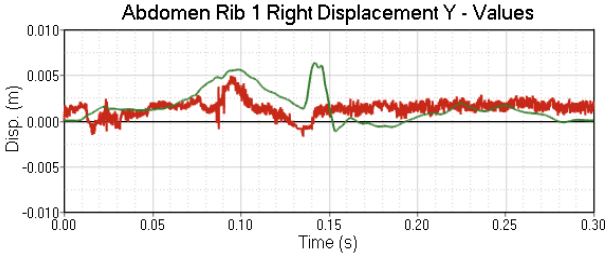
Abdomen Rib 1 Right Displacement Y - Values
Disp. (m)
Time (s)

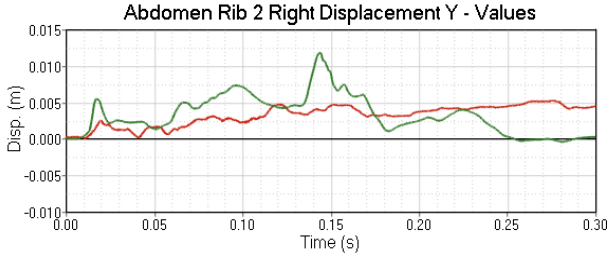
Abdomen Rib 2 Right Displacement Y - Values
Disp. (m)
Time (s)

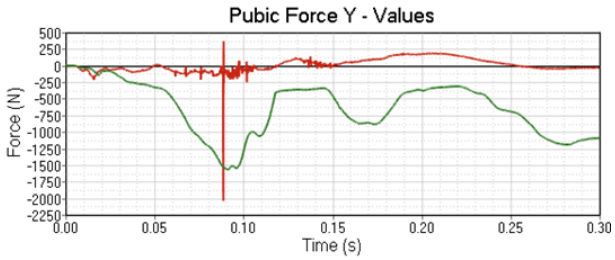
Pubic Force Y - Values
Force (N)
Time (s)

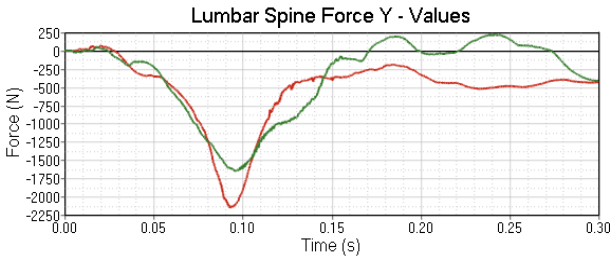
Lumbar Spine Force Y - Values
Force (N)
Time (s)

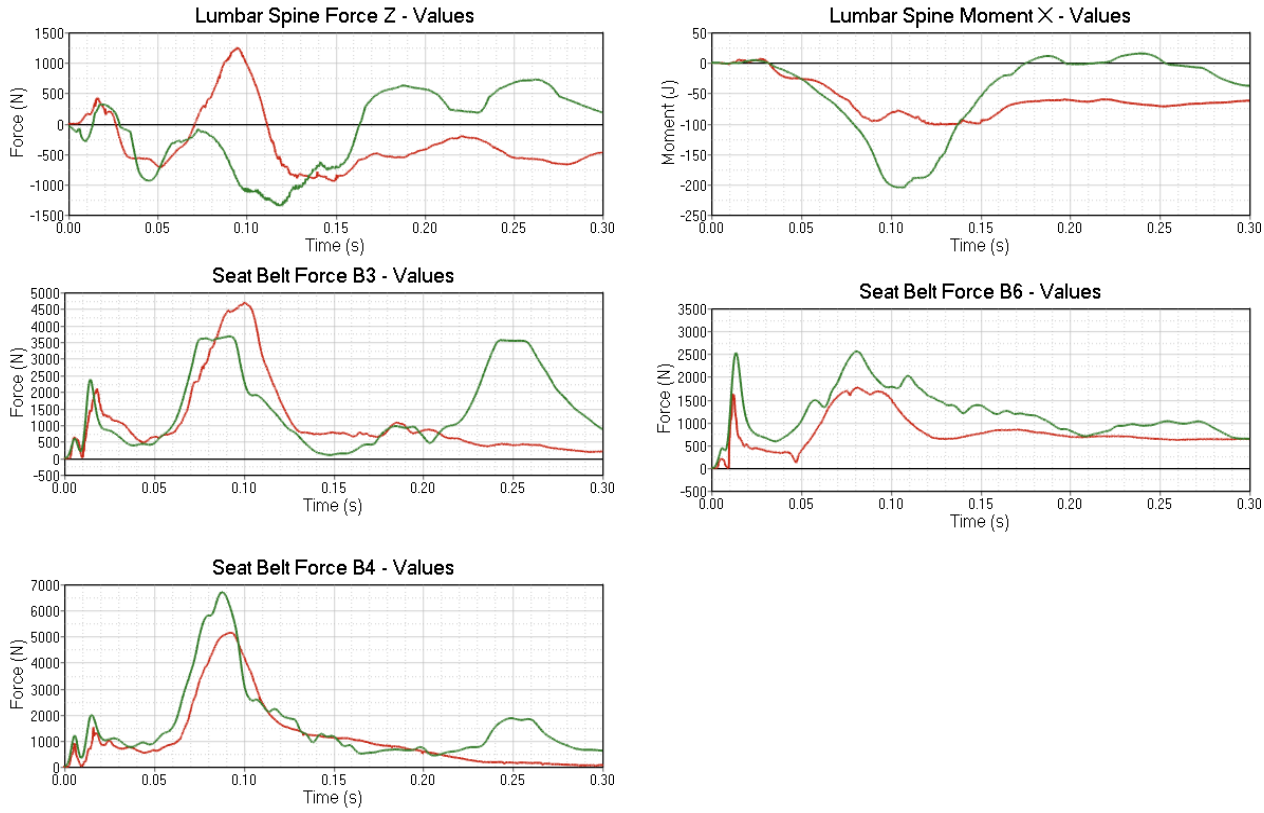

Figure 262 WS4_2 simulation (in green) compared with test data (in red)

3.10.4 WS2_2 Simulation and Test comparison

The WS2_2 used the SOTA DLPT belt only.

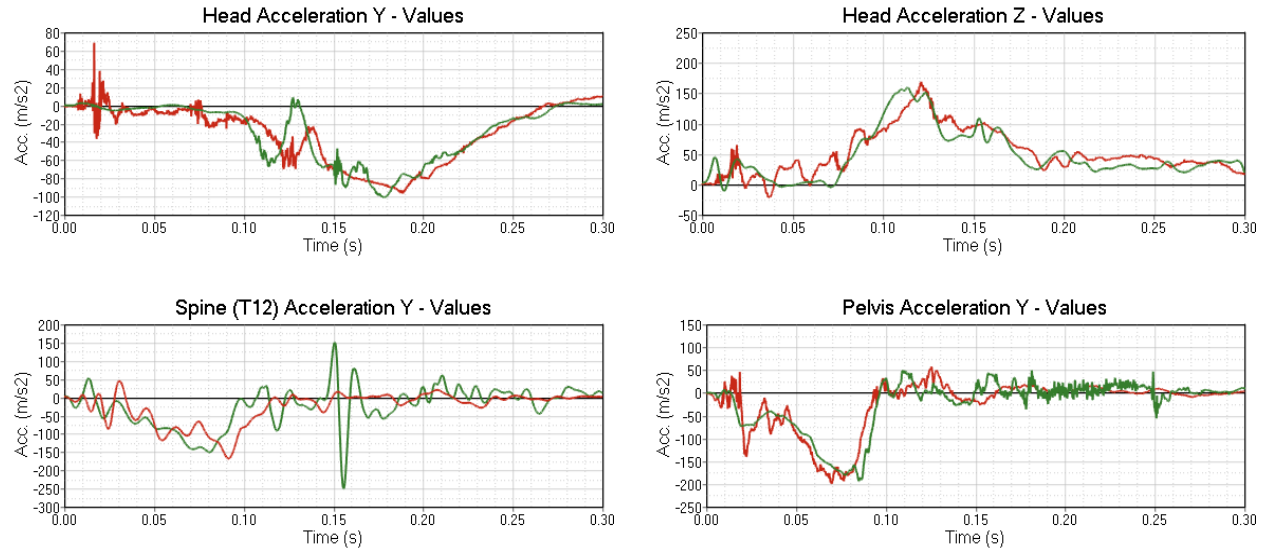

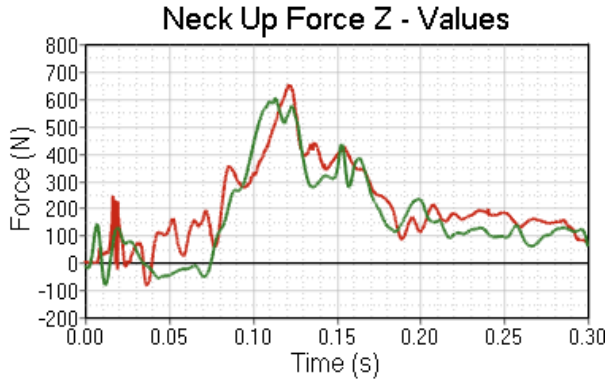
Neck Up Force Z - Values
Force (N)
Time (s)

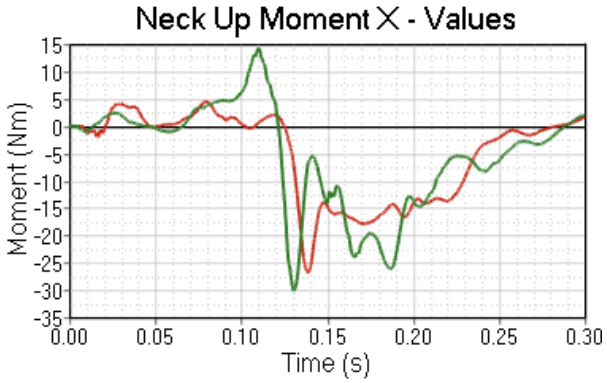
Neck Up Moment X - Values
Moment (Nm)
Time (s)

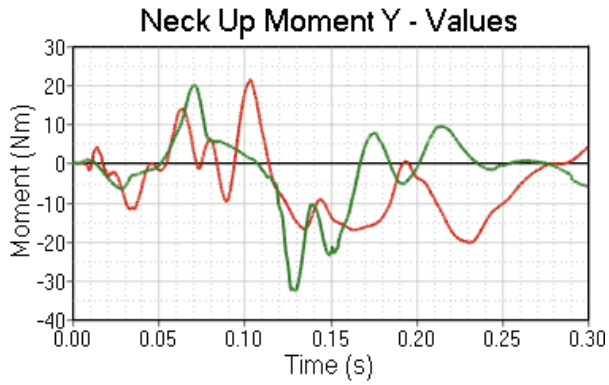
Neck Up Moment Y - Values
Moment (Nm)
Time (s)

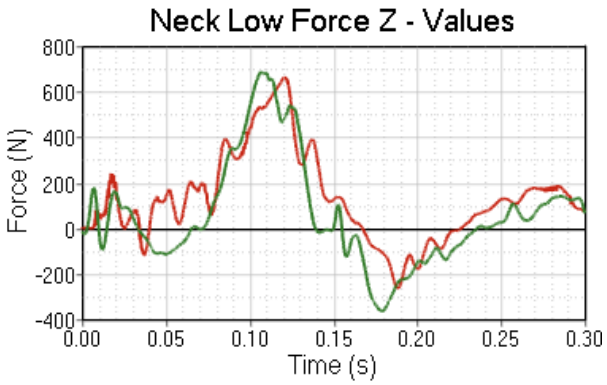
Neck Low Force Z - Values
Force (N)
Time (s)

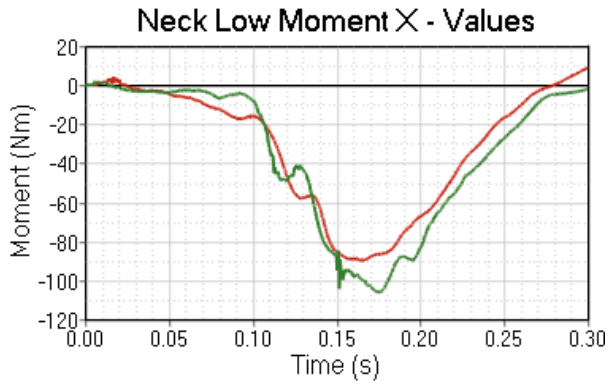
Neck Low Moment X - Values
Moment (Nm)
Time (s)

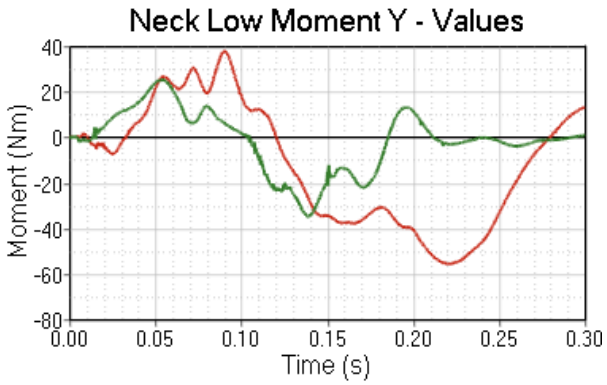
Neck Low Moment Y - Values
Moment (Nm)
Time (s)

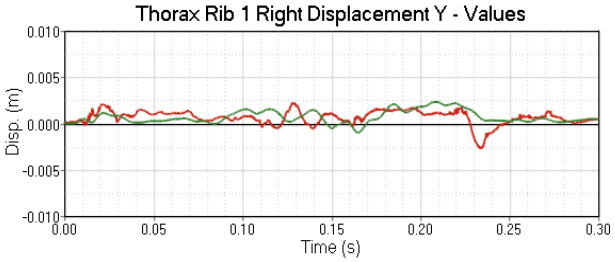
Thorax Rib 1 Right Displacement Y - Values
Disp. (m)
Time (s)

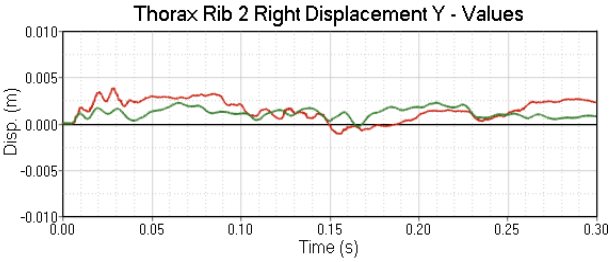
Thorax Rib 2 Right Displacement Y - Values
Disp. (m)
Time (s)

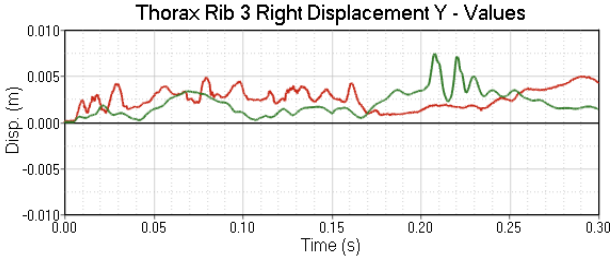
Thorax Rib 3 Right Displacement Y - Values
Disp. (m)
Time (s)

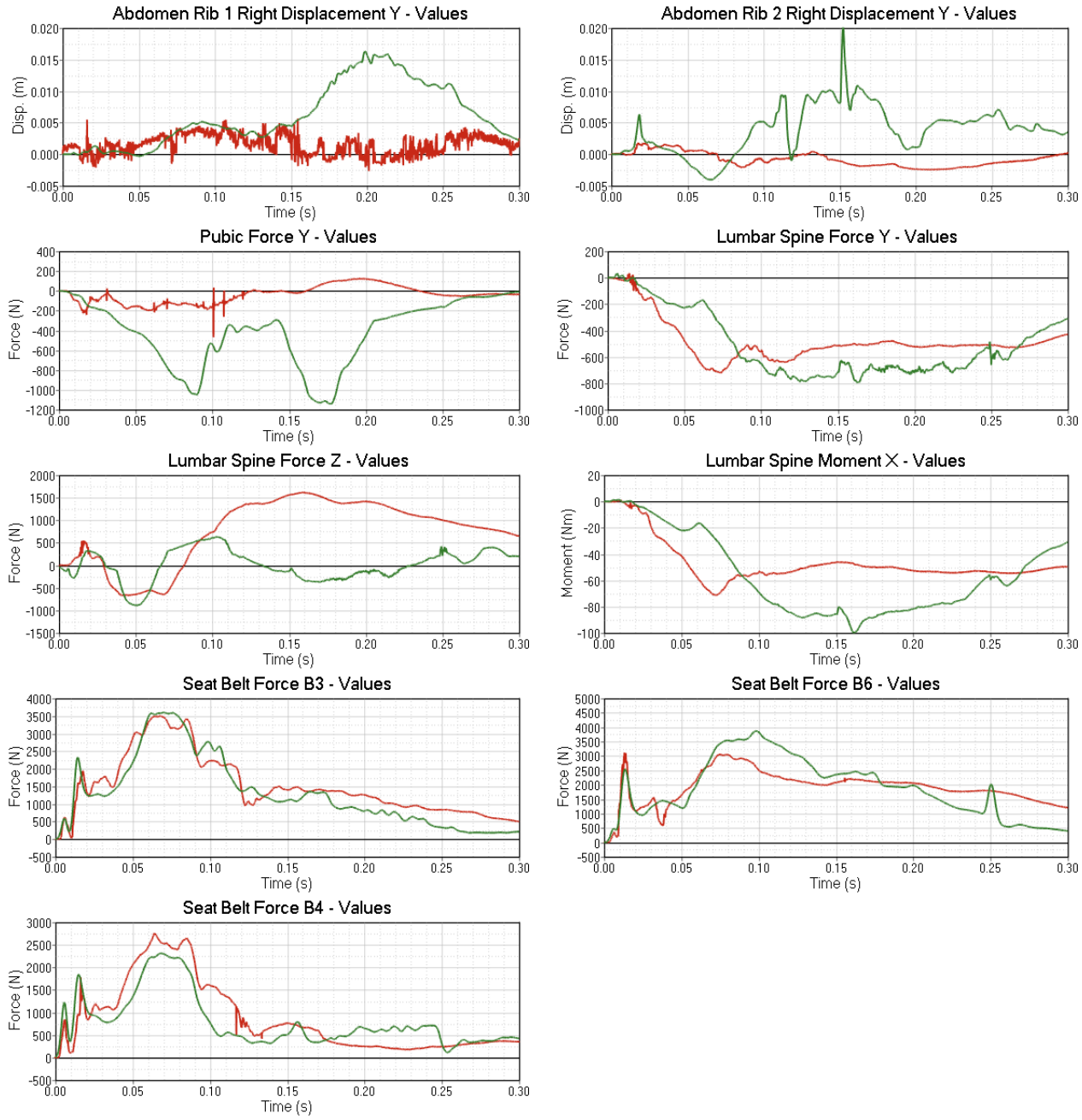

Figure 263 WS2_2 simulation (in green) compared with test data (in red)